

General Disclaimer

One or more of the Following Statements may affect this Document

- This document has been reproduced from the best copy furnished by the organizational source. It is being released in the interest of making available as much information as possible.
- This document may contain data, which exceeds the sheet parameters. It was furnished in this condition by the organizational source and is the best copy available.
- This document may contain tone-on-tone or color graphs, charts and/or pictures, which have been reproduced in black and white.
- This document is paginated as submitted by the original source.
- Portions of this document are not fully legible due to the historical nature of some of the material. However, it is the best reproduction available from the original submission.



ELECTRO-OPTICAL SYSTEMS, INC.
A XEROX COMPANY

300 NORTH HALSTEAD STREET, PASADENA, CALIFORNIA 91107 213/681-4671, 449-1230

FACILITY FORM 602

N 69-13470

(ACCESSION NUMBER)

463

(PAGES)

CR# 97923

(NASA CR OR TMX OR AD NUMBER)

(THRU)

1

(CODE)

03

(CATEGORY)

Final Report

ANALYSIS OF ELECTRIC PROPULSION ELECTRICAL POWER
CONDITIONING COMPONENT TECHNOLOGY

Prepared for
George C. Marshall Space Flight Center
National Aeronautics and Space Administration
Huntsville, Alabama 35812
Attention: Lawrence Garrison, Contracting Officer

Contract NAS 8-11257

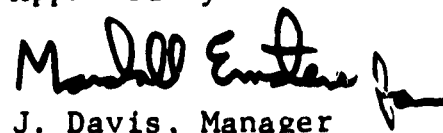
EOS Report 5400-Final

1 April 1968

Volume I: Data Bank

Prepared by
L. Klynn
P. Jalichandra
R. Shattuck

Approved by


J. Davis, Manager
Plasma System Division

PRECEDING PAGE BLANK NOT FILMED.

FOREWORD

The work described in this report was performed under the second follow-on to Contract NAS8-11257 for the National Aeronautics and Space Administration, George C. Marshall Space Flight Center. The studies and compilation were performed from January 1967 through December 1967.

First Year Program

The first year's program objectives involved preliminary investigations of the interface factors which significantly affect the power conditioning and control systems design approach. A comprehensive evaluation was made of current thruster development programs. The principle power conditioning requirements were established for these thrusters. The lithium-Hall arcjet and the cesium electron-bombardment thrusters were the most promising flight system candidates. Variable I_{sp} operational constraints were established for the two candidate thrusters. Conceptual power conditioning and control system block diagrams were delineated for promising thruster and powerplant candidates. This included the nuclear turboalternator as well as the in-pile nuclear thermionic powerplant. The power conditioning and control system specific mass and efficiency for the cesium electron-bombardment thruster was estimated to be 2.3 kg/kW and 91.9 percent with an ac power source and 3.1 kg/kW and 84.9 percent with a dc power source at a total power level of 1 MW. Below the 1 MW level, nuclear shielding was the principal power conditioning penalty. Above 1 MW, the secondary radiators were the principal penalty. The interface system for the lithium-Hall arcjet thruster was estimated to be 1.9 kg/kW at 95 percent efficiency with an ac power source and 1.5 kg/kW at 97 percent efficiency with a dc power source. A survey of the principal power conditioning components indicated three key power conditioning technology problem areas:

- a. Insufficient reliability data
- b. Low thermal and nuclear radiation tolerances
- c. Low power ratings and switching times for rectifiers and active switches

Second Year Program

The first year's work provided the foundation for continued and detailed analysis of various power conditioning and control system design approaches and resulting component requirements for promising powerplant and thruster candidates. The second year program tasks included:

- The establishment of interface requirements necessary for the fabrication and optimization of power conditioning and control systems.
- The establishment of a methodology for power conditioning and control design and analysis techniques.
- Survey and tabulation of key component characteristics.
- The selection of optimum power conditioning and control system design approaches for promising powerplant and thruster candidates.
- The analysis of power conditioning systems for a manned Mars electric propulsion mission.
- The identification of existing technical problem areas and future circuit and component development requirements.

The principal program objectives were directed at electric propulsion system levels greater than 1 MW using the in-pile nuclear thermionic powerplant.

Third Year Program

The first task of this program was to compile all data pertaining to electric propulsion into a Design Data Bank. The studies during the first and second years formed a strong basis for the data bank. The main topics delineated in the Design Data Bank were:

- Power source technology
- Electric thruster technology
- Power conditioning

Trends leading to future performance improvements were identified where possible. A format was selected such that annual updating would make the most recent data always available to mission planners.

Using the Design Data Bank as a foundation, power conditioning was studied for:

- 40-50 kW solar electric propulsion system
- 1-5 MW solar electric propulsion system
- 150 kW solar electric propulsion system

A solar electric propulsion system was designed for an unmanned Mars spacecraft. Optimization procedures were demonstrated on power conditioning for a 50 kW (1 AU) solar panel operating sixteen 2.5 kW Cesium Electron Bombardment Thrusters. Electric, magnetic, and thermodynamic interactions between various subsystems were investigated.

PRECEDING PAGE BLANK NOT FILMED.

TABLE OF CONTENTS

1. POWER SOURCE TECHNOLOGY	1-1
1.1 Performance Summary - An Overview	1-1
1.1.1 Summary of Solar Photovoltaic Array Technology	1-3
1.1.2 Summary of Nuclear System Technology	1-4
1.2 Solar Voltaic Power Sources	1-19
1.2.1 Solar Photovoltaic Cells	1-19
1.2.2 Solar Photovoltaic Panels	1-36
1.2.3 Solar Photovoltaic Array Concepts	1-62
1.2.4 Solar Array Temperature Characteristics	1-83
1.2.5 Solar Array Power Output versus Distance From the Sun for Various Missions	1-86
1.3 References and Bibliography for Section 1	1-92
1.3.1 References	1-92
1.3.2 Bibliography	1-94
2. ELECTRIC THRUSTER TECHNOLOGY	2-1
2.1 Cesium Electron Bombardment Ion Engine Systems	2-6
2.1.1 Introduction	2-6
2.1.2 Operation	2-8
2.1.3 Performance	2-13
2.1.4 Power Conditioning Requirements	2-35
2.1.5 System Considerations	2-53
2.1.6 Development Status	2-56
2.1.7 Conclusions	2-57
2.2 Mercury Electron Bombardment Engine	2-58
2.2.1 Summary	2-58
2.2.2 Introduction	2-58
2.2.3 Principles of Operation	2-60
2.2.4 Thruster Performance	2-64
2.2.5 Present Status	2-106

TABLE OF CONTENTS (contd)

2.2.6	Performance Predictions	2-122
2.2.7	Future Development Areas	2-126
2.2.8	Concluding Remarks	2-129
2.3	Contact Ion Thrusters	2-130
2.3.1	Introduction	2-130
2.3.2	Demonstrated Performance	2-134
2.3.3	Electrical Characteristics	2-146
2.4	Colloid Thrusters	2-153
2.4.1	Introduction	2-153
2.4.2	Parametric Performance	2-156
2.4.3	Thruster Status	2-182
2.4.4	System Considerations	2-187
2.5	MPD Arc Jet Engines	2-193
2.5.1	Introduction	2-193
2.5.2	Engine Mechanisms	2-193
2.5.3	Advantages of Alpha	2-198
2.5.4	Background and History	2-201
2.5.5	Current Development Status of the MPD Arc Jet	2-206
2.5.6	Projected Development of the MPD Arc Jet Engine and System	2-231
2.6	References and Bibliography for Section 2	2-241
2.6.1	References	2-241
2.6.2	Bibliography for Section 2	2-244
3.	POWER CONDITIONING AND CONTROL	3-1
3.1	Power Conditioning Electronics	3-1
3.1.1	Inverter-Converter Circuit Design	3-4
3.1.2	Voltage Transformation	3-42
3.1.3	Rectification	3-53
3.1.4	Power and Voltage Control	3-46
3.1.5	Filtering	3-50

TABLE OF CONTENTS (contd)

3.2	Converters	3-62
3.	Second-Breakdown Effects	3-63
3.2.2	Storage Time Effects	3-64
3.2.3	Transistors Considerations	3-68
3.2.4	Rectifier Considerations	3-72
3.2.5	Transformer Considerations	3-72
3.2.6	Circuit Selection	3-77
3.2.7	Overload and Short Circuit Protection	3-80
3.3	50 kHz Converter Design	3-82

PRECEDING PAGE BLANK NOT PAGE.

ILLUSTRATIONS

1	Specific Weight as a Function of Power for Various Power Sources	1-2
2	Temperature Range of Nuclear Space Power Systems	1-6
3	In-Pile Thermionic Reactor Designs	1-15
4	Comparison of In-Pile and Out-of-Pile Thermionic Reactor Characteristics	1-17
5	Out-of-Pile Thermionic Reactor	1-18
6	Theoretical Efficiency versus Semiconductor Band Gap	1-20
7	Electrical Characteristic Curves for Typical P/N Silicon Solar Cells, 1 x 2 cm at 25°C for Gridded and Nongridded Cells	1-22
8	Typical Electrical Characteristic Curves for P/N and N/P Silicon Solar Cells	1-25
9	Typical Conventional Solar Cell	1-28
10	Spectral Response of a Typical N/P Solar Cell in Relation to Incident Sunlight	1-29
11	Typical I-V Curve Limits for N/P Silicon Solar Cells Under Simulated Air Mass = 0 Conditions	1-31
12	N/P Solar Cell Radiation Degradation Factor, Proton Critical Flux versus Proton Energy	1-32
13	Typical Weights of Solar Cells and Contacts	1-38
14	Solar Cell Decay Rate Due to Meteoroid Impact	1-40
15	Range-Energy for Protons and Electrons in Quartz	1-45
16	Illustration of Current Technology	1-46
17	Two Types of Substrates in Current General Use	1-51
18	Silicon Photovoltaic Solar Array Weight Trends	1-54
19	Power Area versus Cell Efficiency for Various Cell Configurations	1-58
20	Typical Panel Structure	1-66
21	Five-Foot-Square Biconvex Demonstration Panel	1-67
22	EOS Configuration for 10 kW Solar Array	1-69
23	Boeing Box-Frame Solar Array	1-72
24	Hughes 50 ft ² Demonstration Rollup Solar Array	1-76

ILLUSTRATIONS (contd)

25	Ryan 50-Square-Foot Demonstration Rollup Solar Array	1-79
26	EOS Rollup Array Concept	1-81
27	Flat Panel Thermal Equilibrium Temperature	1-84
28	Thermal Equilibrium Temperatures for a Flat Oriented Solar Panel	1-85
29	Solar Array Power Output versus Distance from the Sun for a Venus Probe and Orbiter	1-87
30	Solar Array Power Output versus Distance from the Sun for a Jupiter Probe	1-88
31	Solar Array Power Output versus Distance from the Sun for a Mars Probe and Orbiter	1-89
32.	Voltage-Current Characteristic Curve for a 10-ohm-per-Centimeter, Non-P, 2 x 2 Centimeter, Solar Cell. Cell Efficiency = 11.3 percent	1-90
33	Electric Propulsion Operating Regimes	2-2
34	Power-to-Thrust Ratio versus Specific Impulse for Electric Propulsion Engines	2-3
35	Mass versus Power for Electric Propulsion Engines	2-5
36	Cesium Electron Bombardment Engine Schematic	2-9
37	Control Loops for Cesium Bombardment Engine Systems	2-11
38	Cesium Feed System	2-12
39	Permanent Magnet Engines of Thrust Levels 3.1×10^{-2} N, 4.5×10^{-3} N, 6.7×10^{-4} N, and 4.5×10^{-5} N	2-14
40	Thruster Mass versus Thrust	2-16
41	Thruster Volume versus Thrust	2-17
42	Mass Efficiency versus Thrust	2-18
43	Specific Impulse versus Thrust	2-20
44	Power-to-Thrust Ratio versus Specific Impulse	2-22
45	Overall Efficiency versus Specific Impulse	2-23
46	Zero-g Cesium Feed Systems	2-24
47	Feed System Power Requirements	2-25
48	Cesium Feed System Mass Performance	2-26
49	Feed System Volume versus Capacity	2-27
50	Neutralizer Weight versus Impulse	2-29

ILLUSTRATIONS (contd)

51	Neutralizer Volume versus Impulse	2-30
52	Neutralizer Anode Power	2-31
53	Neutralizer Heater Powers	2-32
54	Propellant Mass Requirements	2-33
55	Approximate Propellant Weight versus Impulse	2-34
56	Packaging Volume Efficiency	2-36
57	Engine System Component Volume versus Thrust	2-37
58	System Weight versus Thrust	2-38
59	System Power versus Thrust	2-39
60	Positive High Voltage Current versus Thrust	2-42
61	Positive High Voltage versus Thrust	2-43
62	Negative High Voltage versus Thrust	2-44
63	Arc Current versus Thrust	2-45
64	Arc Voltage versus Thrust	2-47
65	Negative High Voltage Current versus Thrust	2-48
66	Cathode Power Requirements	2-50
67	Electromagnet Power Requirements	2-51
68	Typical Mercury Electron Bombardment Ion Thruster	2-61
69	Mercury Boiler Propellant Reservoir	2-65
70	Gas-Pressurized, Positive Displacement Mercury Propellant Reservoir	2-66
71	High Voltage, High Pressure Isolator	2-71
72	Cutaway Schematic of Mercury Electron Bombardment Ion Thruster System	2-75
73	Enlarged View of a Mercury Hollow Cathode	2-78
74	Sputtering Damage Effect versus Energy	2-87
75	Plasma Bridge Type Mercury Neutralizer	2-90
76	Schematic of Mercury Electron Bombardment Ion Thruster System	2-95
77	Mercury Electron Bombardment Thruster Feed Power System versus Beam Current	2-98
78	Mercury Electron Bombardment Thruster Neutralizer System Power versus Beam Current	2-99

ILLUSTRATIONS (contd)

79	Thruster Mass as a Function of Thruster System Power	2-110
80	Thruster Mass versus Total Impulse (4.45×10^{-3} newtons thrust)	2-111
81	Thruster Mass versus Total Impulse (4.45×10^{-2} newtons thrust)	2-112
82	Thruster Mass versus Total Impulse (4.44×10^{-1} newtons thrust)	2-113
83	Thruster Size versus Thruster Power	2-114
84	Thruster Size versus Thruster Mass	2-115
85	Thrust as a Function of Thruster System Power	2-118
86	Power-to-Thrust Ratio versus Specific Impulse	2-119
87	Overall Efficiency versus Specific Impulse	2-121
88	Areas of Future Development of the Mercury Thruster System, with Schedule and Cost	2-128
89	Schematic of Contact Ion Thruster	2-131
90	Power-to-Thrust Ratios for Contact Ion Microthrusters	2-135
91	Contact Engine Weight (Without Propellant) versus Engine Thrust	2-138
92	Contact Engine Specific Weight versus Specific Impulse (no propellant weight included)	2-140
93	M1-R3 Endurance Test Parameters	2-142
94	Contact Engine Power versus Thrust, Showing Power Consumed by Various Engine Elements	2-148
95	Effect of Variation in Ionizer Power, $V+$, $V-$, Feed Power, and Neutralizer Power	2-149
96	Power-to-Thrust Ratio versus Specific Impulse	2-157
97	Ratio of Power Supply Plus Propellant Mass to Total Impulse versus I_{sp} for Solar Cells	2-158
98	Ratio of Power Supply Plus Propellant Mass to Total Impulse versus I_{sp} for Nuclear Power Supply	2-159
99	Predicted Thruster System Weight for East-West Stationkeeping of a Synchronous Satellite	2-161
100	Predicted Thruster System Weight for North-South Stationkeeping of a Synchronous Satellite	2-162
101	(q/m) versus Needle Voltage at Two Needle Temperatures	2-166

ILLUSTRATIONS (cont'd)

102	'q/m' versus Feed Pressure at Three Temperatures	2-167
103	'q/m' versus Feed Pressure at Four Voltage Settings	2-168
104	'q/m' versus Needle Temperatures	2-169
105	Plot of Particle Distribution Efficiency versus Specific Charge	2-170
106	Thrust versus M. This Plot Combines Temperature and Pressure Data	2-174
107	Thrust versus Needle Potential (V_n)	2-175
108	Mass Flow Rate versus Feed System Pressure	2-178
109	Mass Flow Rate versus Temperature	2-179
110	Mass Flow Rate versus Temperature for Various Voltages	2-180
111	Specific Impulse (I_{sp}) versus Feed Pressure at Three Voltage Settings and Two Temperature Settings	2-181
112	Deflection Angle and FWHM versus Deflection Voltage	2-184
113	Relationship of Thrust and Specific Impulse to Mass Flow Rate and Needle Voltage	2-188
114	Evolution of Alpha Concept	2-194
115	IAC-3 Thruster, Assembly Drawing	2-207
116	Ion Velocity versus Accelerating Potential	2-208
117	MPD Arc Jet Power-to-Thrust Ratio versus Specific Impulse	2-210
118	Thruster Model LAJ-AF-CG-2B with GAF-IV Feed	2-213
119	Block Diagram of MPD Arc Jet Power Supplies	2-217
120	MPD Thruster Model IAC-3	2-218
121	MPD Arc Jet Engine Power Requirements	2-220
122	Improvements in Efficiency and Operating Lifetime of ALPHA	2-236
123	Projected Minimum Performance of a Flight Test Model ALPHA Thruster	2-237
124	ALPHA System Block Diagram	2-238
125	ALPHA System Block Diagram - 2	2-239
126	ALPHA System Block Diagram - 3	2-240

ILLUSTRATIONS (contd)

127	Block Diagrams of Power Conditioning Electronics for DC Power Source	3-2
128	Block Diagram of Power Conditioning Electronics for AC Power Source	3-3
129	Basic Inverter Operation Diagram and Output Waveform	3-5
130	Comparison of Component ON-OFF Switching Characteristics	3-7
131	Transformer α versus Operating Frequency	3-8
132	Common Base and Common Collector Self-Excited Push-Pull Inverters	3-11
133	Common Emitter Self-Excited Push-Pull Inverters	3-14
134	Modified Common Emitter Self-Excited Push-Pull Inverter	3-16
135	Modified Jensen Type Self-Excited Push-Pull Inverter	3-17
136	Two-Stage Self-Excited Push-Pull Inverter	3-19
137	Push-Pull Inverter Power Stage	3-21
138	Polyphase DC-DC Converter Block Diagram	3-22
139	Modified Jensen Self-Excited Bridge Inverter	3-24
140	Two-Stage Self-Excited Hybrid Inverter	3-26
141	Basic Bridge Inverter Power Stage	3-27
142	Parallel Capacitor Commutated Inverters	3-31
143	Parallel Inverter Waveforms	3-32
144	Counter EMF Parallel Inverter	3-34
145	Basic Push-Pull Impulse Commutated Inverter	3-35
146	Modified Push-Pull Impulse Commutated Inverters	3-37
147	Push-Pull Inverter Circuit for Output Control	3-39
148	Impulse Commutated Bridge Inverters	3-40
149	Voltage Doubler Circuit	3-43
150	Typical Full-Wave Rectifier Circuits	3-44
151	Magnetic Control Circuits	3-47
152	Inverter Output Waveforms	3-56
153	Power Conditioning Output Filter Networks	3-57
154	Voltage Waveforms, Filtered and Unfiltered	3-59
155	Typical Two-Transformer Converter	3-65

ILLUSTRATIONS (contd)

156	Converter with Compensation for Storage Tube	3-67
157	Basic DC-DC Converter	3-69
158	Diagram of Selected Circuit	3-78
159	Efficiency versus Power Output	3-83
160	Representative 50 kHz Circuit	3-84
161	Output Voltage versus Input Voltage at 50 kHz	3-85
162	Output Voltage versus Output Power at 50 kHz	3-87
163	Efficiency versus Temperature at 100 Watts Output	3-88
164	Switching Frequency versus Temperature	3-89
165	High Frequency DC-DC Converters	3-90

PRECEDING PAGE BLANK NOT FILMED.

TABLES

I	Summary of Solar Array Features	1-5
II	Performance Characteristics of In-Pile Concepts	1-16
III	Table of Predicted Silicon Solar Cell Characteristics	1-34
IV	Pounds per kW as a Function of Coverglass Thickness	1-43
V	Array Area for 200-Watt System	1-52
VI-A	Solar Array Weight Breakdown as a Function of Coverglass Thickness for 8-Mil Solar Cells	1-57
VI-B	Solar Array Weight Breakdown as a Function of Coverglass Thickness for 12-Mil Solar Cells	1-57
VI-C	Solar Array Weight Breakdown as a Function of Coverglass Thickness for 4-Mil Solar Cells	1-57
VII	Coverglass Characteristics	1-60
VIII	Component Summation	1-61
IX	Typical Rigid Array Concepts	1-65
X	Projected Weight and Power Characteristics, 10.4 kW Array	1-70
XI	Typical Rollup Array Concepts	1-74
XII	Thruster System Performance	2-93
XIII	Thruster System Performance	2-94
XIV	Thruster System Power Supply Characteristics	2-97
XV	Telemetry Data Channels	2-101
XVI	Command Channels	2-102
XVII	2.5 Kilowatt Thruster System	2-124
XVIII	M1 Engine System Performance	2-136
XIX	Contact Ionization Thruster Endurance Tests	2-141
XX	M1-R3 Engine Data	2-143
XXI	Spray Characteristics of Various Propellants	2-164
XXII	Demonstrated Performance Parameters for Colloid Thrusters	2-177
XXIII	Thruster Control Commands	2-221
XXIV	Silicon Switching Power Transistors	3-70
XXV	Silicon Rectifier Diodes Fast Recovery Types	3-73

PRECEDING PAGE BLANK NOT FILMED.

TECHNICAL CONTRIBUTORS TO THE REPORT

Lee M. Klynn
Phijit Jalichandra
Russell Shattuck
James A. Wolters
Peter Ramirez, Jr.
Eugene H. Schraut
Gordon Sohl
Dr. Marshall Ernstene
Seymour Nelson
Dr. Rolf D. Buhler
Dr. Julius Perel
Arthur Y. Yahiku
John F. Mahoney
John Boyajian
Dr. Karl K. Knapp
Charles M. Hains
Sanford A. Friedlander
Verryl V. Fosnight

SECTION 1
POWER SOURCE TECHNOLOGY

This section discusses the electrical power systems which are relevant to electric propulsion. In order to be effective, the power systems should have the following characteristics:

- Power level ranging from 40 kW to 20 MW.
- Specific weight of 50 lb/kW as a minimum. A desirable goal will be 20 lb/kW or less.
- Operating time of 5000 hours as a minimum, or preferably 10000 hours and beyond.
- Available in the 1970-1985 period.

Because of the lifetime requirement, only the solar and nuclear reactor systems are capable of supplying this need.

1.1 PERFORMANCE SUMMARY - AN OVERVIEW

Figure 1 represents a summary of the specific weight performance of a wide variety of space power systems. These systems can be divided into two categories, i.e.

- a. Nuclear electric where a nuclear reactor is used to provide heat for energy conversion. The conversion efficiency is limited to a value less than the theoretical Carnot efficiency.
- b. Photovoltaic energy conversion where solar energy is converted directly into electricity. This type of system is not Carnot-efficiency limited.

The tentative conclusions, drawn within the framework of the previously described requirements, are the following:

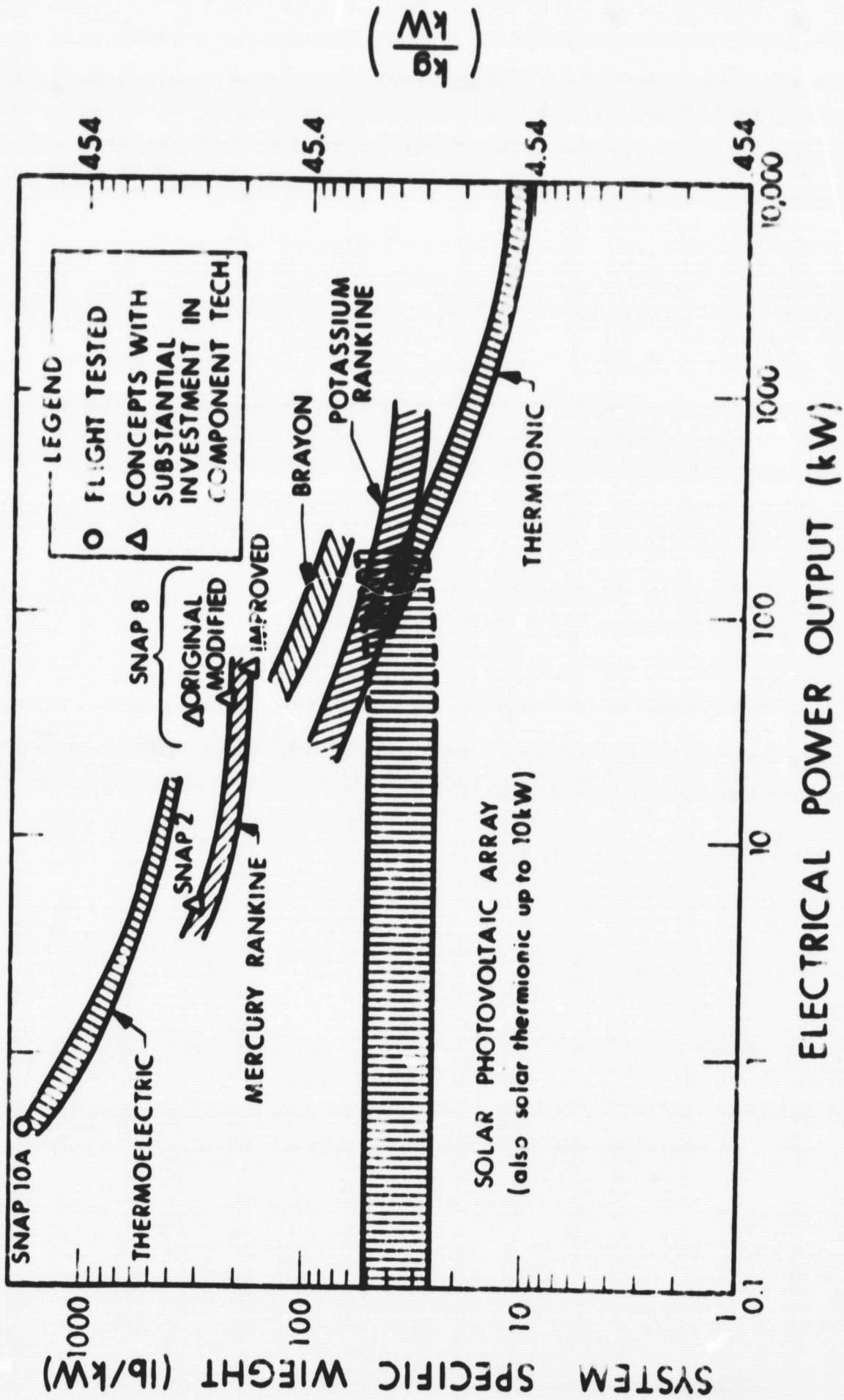


Figure 1. Specific Weight as a Function of Power for Various Power Sources

- Three types of power source, namely, the solar array, the nuclear potassium Rankine, and the nuclear thermionic are the leading candidates.
- For a 1970-75 unmanned electric propulsion mission, the power source requirement of 40-200 kW can be best served by the solar array.
- For a mission in the 1975-1985 period, the choice is narrowed down to either a nuclear potassium Rankine or thermionic system. The nuclear thermionic (in-pile or out-of-pile) certainly has a clear advantage. It offers a high performance potential at a large system size and high reliability because it does not require any moving parts.

In the following subsections, we will give a brief resume of the technology status, advantageous and disadvantageous features of the solar and nuclear systems. Additional information is contained in the documents listed in the bibliography, Subsection 1.3.2.

1.1.1 SUMMARY OF SOLAR PHOTOVOLTAIC ARRAY TECHNOLOGY

The specific weight of a flight-proven photovoltaic system at the present time (1967) is approximately 100 lb/kW. It is a work horse in the space power field due to its proven performance, long life, and high reliability. This is evidenced by the successful application in the Pioneer, Ranger, Mariner, Surveyor, and numerous classified and unclassified satellite programs. The arrays in the past programs have been limited to a size less than 2 kW. However, with an increase in booster capability, the application in the early 1970's for firm missions such as ATM, SIVB workshop, MOL, and MORL will call for the state-of-the-art array of a size up to 15 kW.

Current development programs throughout the industry have established a definite feasibility of the array performance of 25-50 lb/kW for a 1973-1975 mission. For example, Boeing is developing a 50 lb/kW system leading to a 50 kW Mars Mission. Electro-Optical Systems has already

demonstrated a 42 lb/kW panel and is now working in the Phase II effort toward a 27 lb/kW panel. Both the Boeing and EOS concepts employ a rigid-frame solar panel.

Concurrent with the above efforts, several roll-up array concepts are being developed by Fairchild-Hiller, Ryan Aeronautical Co., General Electric, and Hughes with a potential performance of 35 lb/kW. The development of roll-up arrays is timed for the mid 1970 application.

The advantageous and disadvantageous features of the photovoltaic system are summarized in Table I. Among the attractive features are its light weight and early availability, especially for a 40-200 kW size. For systems larger than 200 kW, it is anticipated that the specific weight will be increased due to the more complicated mechanisms and structural supports. Beyond this power range, the picture is not clear; more detailed and realistic conceptual study will be required.

1.1.2 SUMMARY OF NUCLEAR SYSTEM TECHNOLOGY

Since the heat-to-electricity conversion efficiency is limited to a fraction of the Carnot efficiency, the trend for the performance improvement of any nuclear system will be toward higher temperatures. The temperature ranges for various power conversion schemes are:

Thermoelectric	500-700 ^o C
Hg Rankine	650-750 ^o C
K Rankine	900-1200 ^o C
Brayton	650-1300 ^o C
Thermionic	1300-1800 ^o C

The temperature range of major components i.e. the reactor, power conversion, and heat rejection subsystems is depicted in Fig. 2.

TABLE I

Summary of Solar Array Features

Advantage

Disadvantage

- | | |
|--|---|
| 1. Offers 25-50 lb/kW performance | 1. Requires a large packaging volume. |
| 2. Flight-proven technology | 2. High production cost, especially for a large system. |
| 3. Low development cost | 3. For sizes greater than 200 kW, specific weight tends to increase due to complicated deployment mechanisms and structural supports. |
| 4. Early availability. 40-200 kW will be available in 1973-1975. | |

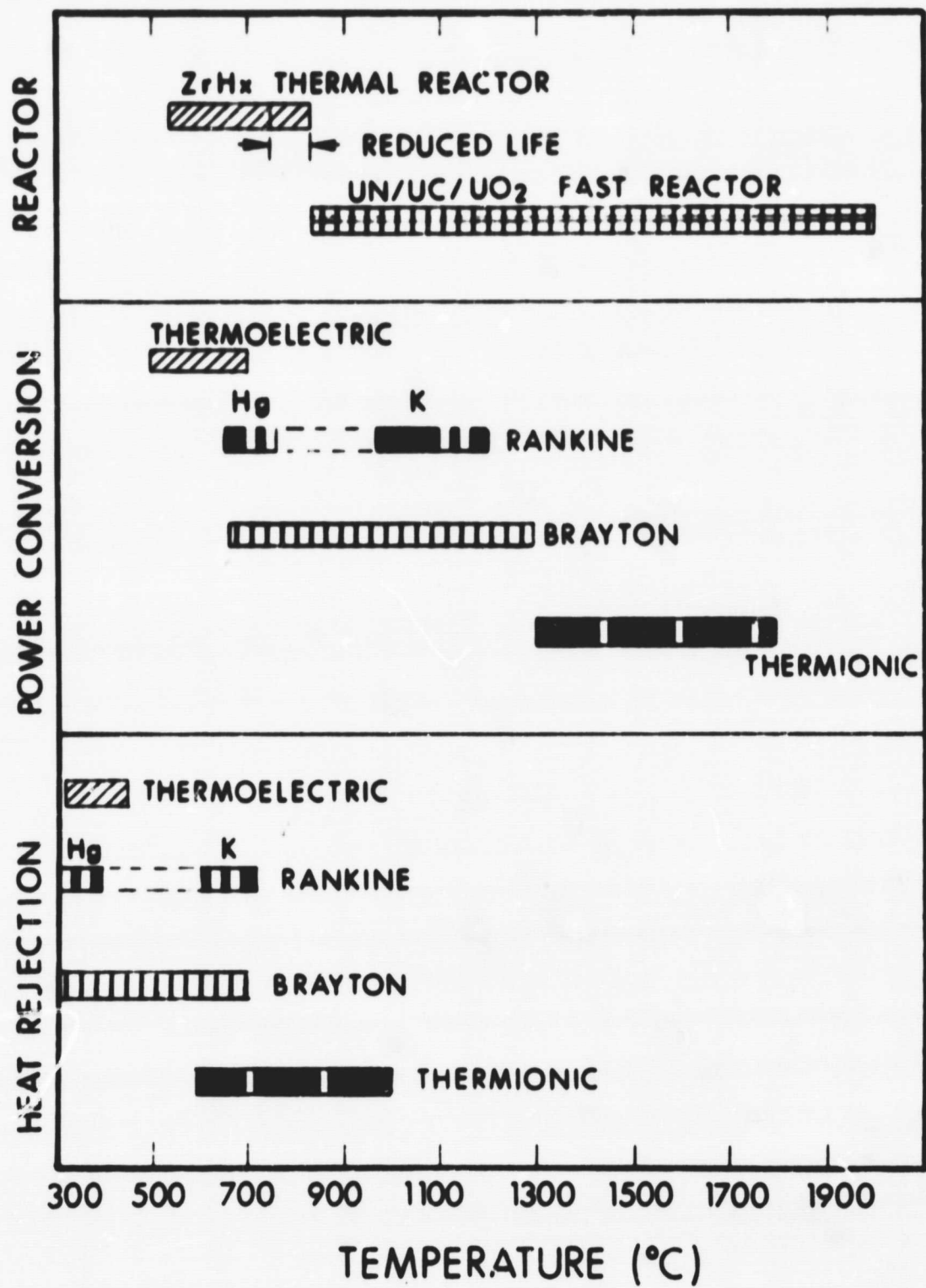


Figure 2. Temperature Range of Nuclear Space Power Systems

The specific weight of the nuclear systems shown in Fig. 1 includes an unmanned shadow shield which has the following typical characteristics.

- Neutron dose of 10^{11} - 10^{12} nvt
- Gamma dose of 10^6 - 10^7 rads
- Shield angle of 10-15 degrees

As a general rule, the shield accounts for 25-30% of the total system weight. This percentage will be increased to about 50-60% for the manned application whose typical dose tolerance is approximately 20 rem/year. This generalization does not apply to the 4π shielding requirement.

Not included in the system weight shown in Fig. 1 are the transmission line and power conditioning equipment. In general, the weights of these two subsystems are determined from the tradeoff with the power source weight itself. For a 50 lb/kW power plant, the optimum weight of the combined transmission line and power conditioning is about 7 to 10 lb/kW. This may be decreased to about 5 lb/kW for a high performance power plant, such as a large nuclear thermionic which has a specific weight of 10-15 lb/kW. The transmission and power conditioning efficiencies lie in the range of 95-99%.

For the electric propulsion application, the thermoelectric, mercury Rankine, and Brayton cycle systems will not meet the specific weight requirement. Therefore, detailed information for these systems will not be presented. We will, however, describe briefly the development of the zirconium hydride reactor system. The purpose is two-fold: to complete the nuclear picture for historical interest, and to serve as a prelude to discussion of the developmental problems unique to the Rankine turbo machinery.

1.1.2.1 Power Systems Utilizing SNAP Reactors

The zirconium hydride (ZrH_x) reactor has been developed by Atomics International under AEC sponsorship as a heat source for the SNAP program. The reactor has a temperature capability of $1300^{\circ}F$, although an operation at higher temperatures is possible, but with a lifetime less than 10,000 hours as intended. The temperature limitation is due to the problem of fuel swelling and the ability to retain hydrogen for neutron moderation. Two sizes of the zirconium hydride reactor have been evolved. The first one which has a thermal power capability up to 100 kW(t) was developed for the SNAP 10A/2 application. The second size which has a thermal rating of 600 kW(t) is being developed for the SNAP 8 mercury Rankine power conversion system.

The SNAP 10A is a thermoelectric system designed to operate at $1000^{\circ}F$ to produce 500 watts of power. NaK-78 is used to remove the reactor heat to the thermoelectric converter which consists of 2880 Si-Ge thermoelectric elements. The SNAP 10A has the distinction of being the first reactor power system in space. Although vast experience has been gained through an extensive development program culminating in the successful ground and flight tests, it has become obvious that the system is too heavy for any operational use. Present thermoelectric efforts are being directed toward the development of a $1300^{\circ}F$ Si-Ge converter which yields a higher efficiency and power output. Both the direct-radiating and compact converter concepts appear promising. Efforts are also being expended toward a SiGe/PbTe cascade system to further improve the system efficiency.

The SNAP 2 program involved the mating of a SNAP 2/10A reactor to a mercury Rankine engine to be operated at $1200^{\circ}F$ turbine inlet temperature. The rating for this system is 5 kW. The system employs two liquid-metal loops; NaK-78 is used to remove the reactor heat to the

boiler which converts liquid mercury into a super-heated vapor. The mercury turbine, alternator, mercury lubricated bearings, and mercury pump are integrated into a combined rotating unit (CRU).

In 1965 the SNAP 2 program was redirected toward providing basic information for the mercury Rankine engine technology. There is no question about the SNAP reactor capability but the same can not be stated about the power conversion equipment. The basic problem areas requiring solutions are:

- Seals and bearings of the CRU which can withstand high temperature operation and high speed (20,000-50,000 rpm)
- Acceptable startup procedures and restart capability
- Two-phase flow stability in the radiator-condenser in the zero-g environment - a phenomenon not well understood
- Inconsistent and somewhat unpredictable boiler performance believed to be caused by non-wetting conditions of mercury. The causes for non-wetting have been theorized but not confirmed conclusively by tests.

Among the problems cited above, the latter two are the most difficult and still remain to be solved. On the positive side, five CRU's have accumulated more than 20,000 hours of test time, with one CRU operated more than 6,600 hours. Because of the difficulties described, together with the absence in mission requirements, efforts in the program have dwindled down to almost nil.

The SNAP 8 mercury Rankine system has a design objective of producing 35 kW of electrical power at 1300^oF reactor outlet temperature. In comparison with the SNAP 2, the system is more complicated since it employs 4 fluid loops. It has a NaK loop for reactor heat removal, a Hg loop for power conversion, a second NaK loop for heat rejection, and finally, an organic loop for seal and bearing lubricants.

The development of the SNAP 8 system is being performed by two contractors; Atomics International for the zirconium hydride reactor under AEC and Aerojet General for the power conversion subsystem under Technical direction of NASA.

The SNAP-8 experimental reactor (S8ER) had accumulated 11,990 hours of operating time, of which 8,800 hours were at the design temperature of 1300°F and thermal power between 400 and 600 kW(t). Test results were considered satisfactory, although 80 percent of fuel elements were found to have cladding cracks when the core was disassembled. A critical evaluation of the cause has been completed and corrective actions are being implemented to the next reactor which will be put on test in the near future.

The objective of the power conversion system development is to demonstrate and improve the performance of major subsystem components. These include the following: Boiler, condenser, turbine-alternator, NaK pump-motor, Hg pump-motor, and lubricant pump-motor assemblies. The accumulated test time for these components varied from approximately 1000 to 8000 hours. However, one of the basic problems to be solved is the so called deconditioning (non-wetting) of the boiler.

The time table for the SNAP 8 availability is uncertain. This is partly due to the level of funding, but mostly due to the apparent system complexities involving various fluid loops and rotating parts. Recently, there has been an increasing trend toward the mating of the SNAP-8 reactor to a thermoelectric converter. By operating the converter at 1300°F inlet temperature, a four-fold improvement in performance can be achieved. Such a system, however, will have the maximum capability of about 20 kW(e) for a nominal thermal rating of 600 kW(t). For a larger electrical output the reactor must be operated at about 1400°F with a significant reduction in lifetime. An alternative to this solution will require development of an advanced zirconium hydride reactor with a thermal rating of 800-1200 kW(t) to extend the electrical output to the 40 kW range.

1.1.2.2 Brayton Cycle System

The technological advantages of the Brayton cycle are:

- Inherent simplicity of a single loop and a single phase working fluid.
- Noncorrosive properties of the inert gas working fluids such as helium, argon, krypton, xenon, or a mixture.
- The use of gaseous working fluid allows flexibility in regard to the heat source operating temperature. This flexibility is important because it permits the component improvement with increasing temperature to be done in a continuous fashion. The improved performance of the Rankine system must be done with a discrete increase in temperature e.g. 300°C in changing from mercury to potassium fluid.
- It has potentially high system efficiency, hence making it attractive in a 1-10 kW size where the cost of the isotopic heat source is at a premium.

The disadvantages of the Brayton cycle are:

- The cycle net performance is extremely sensitive to the performance of the major components. In a typical Brayton system, approximately 2/3 of the turbine mechanical output will be required to drive the compressor, leaving only 1/3 to do useful work. Thus, a small change in turbine or compressor work will result in a relative large change in the useful mechanical work.
- To compensate for the low gas cycle efficiency, when taking the power loss to compressor into account, the system must achieve a high Carnot efficiency by either operating at the high heat source temperature or low radiator temperature.

A low-radiator temperature approach is usually taken for a reactor Brayton cycle system. Since the reactor and shield weights are significant in the low power range the low radiator temperature will not introduce appreciable weight penalty. At high power levels, however, the radiator will dominate the system weight. For this reason, it is doubtful that a Brayton cycle system will be used beyond a 200 kW range.

The status of the Brayton cycle system is essentially of the early component development stage. Work in this area is being carried out mainly by Airesearch and NASA Lewis in-house efforts. These include: the rotating components, such as turbomachinery, generator, gas bearing and packaging; the heat transfer components such as the recuperator, gas-liquid heat exchanger and the liquid-filled radiator.

The heat sources for the Brayton cycle energy conversion system can be solar, isotopic, or reactor source. For the solar or isotopic system, the size will be limited to about 10 kW. The constraint on the solar power system is due to the difficulty in maintaining an accurate orientation of the solar concentrator. The constraint on the radio-isotopic system will be the isotope availability, cost, and the developing technology of the heat source itself. A program aiming at the development of a 2000^oF Pu-238 heat source suitable for the Brayton cycle application has just been initiated.

A nuclear Brayton cycle system utilizing the SNAP 8 reactor has been shown analytically to be competitive to other systems in the 20-30 kW range. In view of the more ready availability of the SNAP-8 thermoelectric system of a comparable size and specific weight performance it is doubtful if the SNAP-8 Brayton power system will ever be developed.

For a higher operating temperature required for a large system, the reactor will have to be a fast flux reactor using the UC or UO₂ fuel as indicated in Fig. 2. Several conceptual studies have been made to indicate the concept attractiveness but the mission requirements and hence a serious developmental effort are lacking.

1.1.2.3 Potassium Rankine Cycle Systems

The potassium Rankine concept is similar to the SNAP-8 mercury Rankine system with the exception that potassium is used in place of mercury as the turbine working fluid. The reactor outlet temperature for this system will be approximately 2200^oF. A fast flux reactor suitable for this temperature has not been developed. The development status of the power conversion components is not as far advanced as the SNAP-8. Aside from the 4-loop complexities of the concept, the problems associated with a higher temperature operation are:

- Use of refractory metals whose long-term engineering data are not abundant.
- Long-term material corrosion associated with the use of liquid metals.
- Long-term creep.
- Oxygen contamination of the liquid metal containment material.

In view of its high development risk, as weighed against the potential payoff in performance, it is doubtful that a potassium Rankine system will be developed for the electric propulsion application.

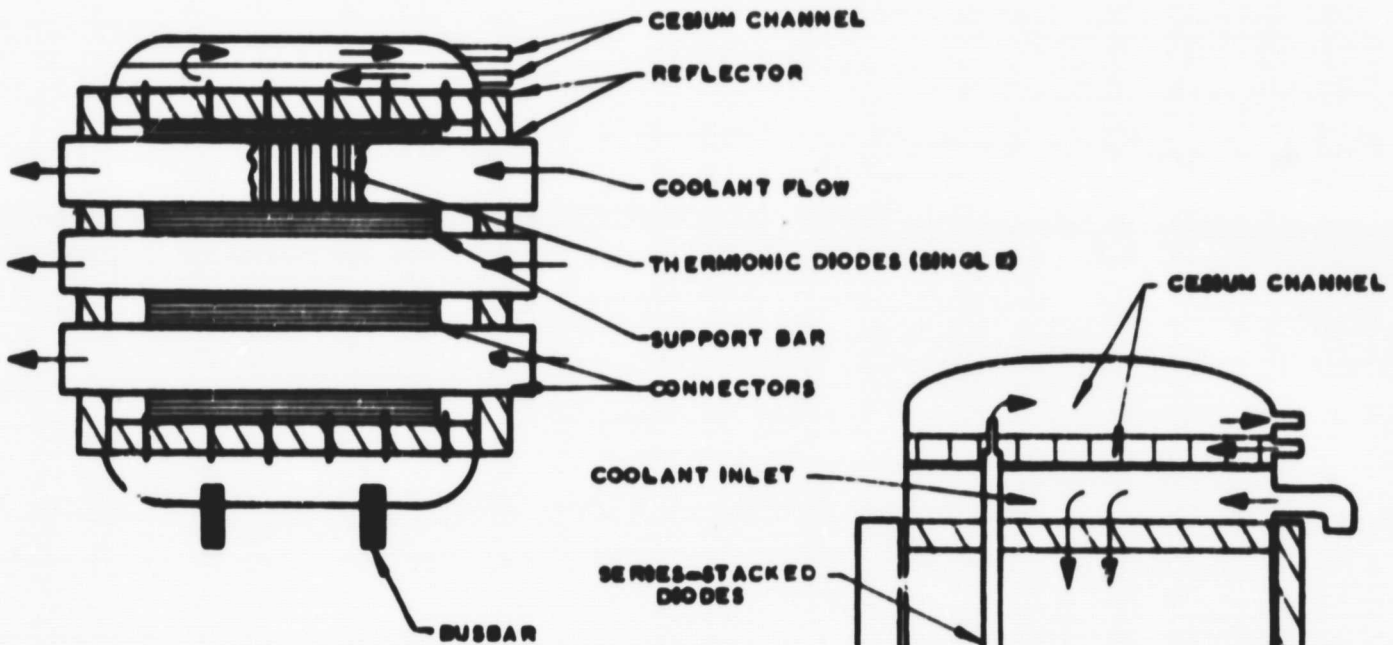
1.1.2.4 Nuclear Thermionic Systems

Among the various space power systems considered, the nuclear thermionic powerplant offers the most promise. Its specific weight varies from approximately 40 lb/kW for a small (50-100 kW) plant to 10-20 lb/kW for the megawatt size. In addition, the modestly concentrated development effort, if continued, will make this type of system available within approximately 10 years.

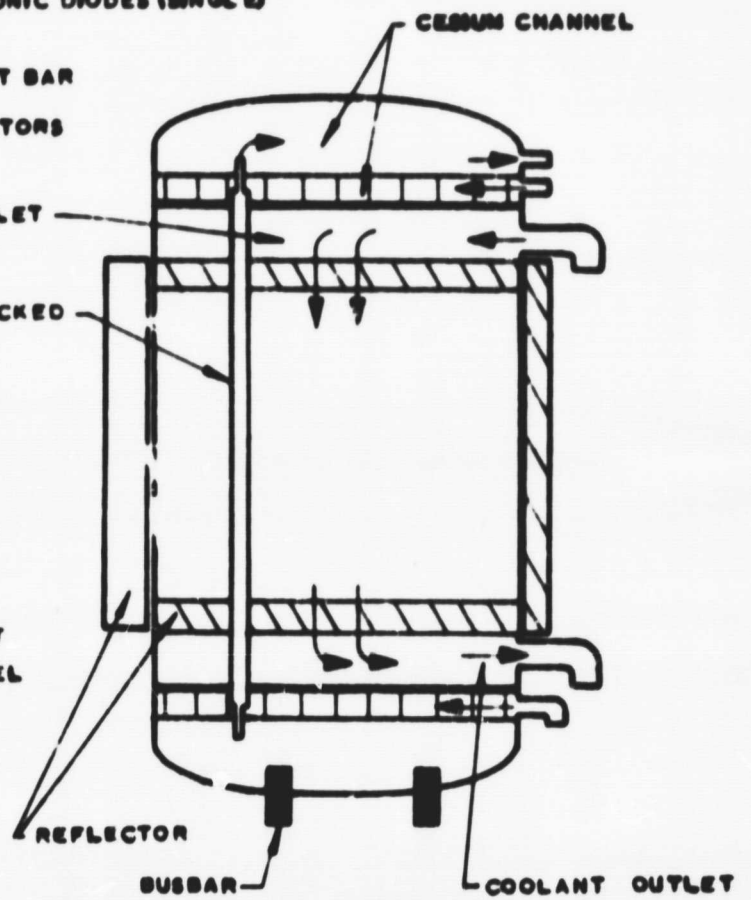
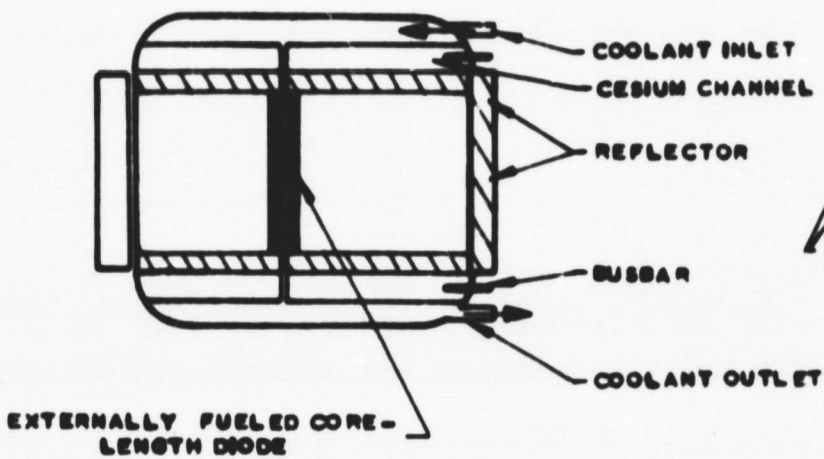
The present efforts have been concentrated primarily on the in-pile concept where the nuclear fuel and thermionic converter are integrated into a single reactor vessel. Three concepts, as shown in Fig. 3, have been proposed. The works in the flashlight, pancake, and externally fueled concepts are being carried out by General Electric, General Atomic and Westinghouse/Republic teams respectively. Much of these works is classified. The information reported in this document is based on the Pratt & Whitney and Douglas conceptual studies of the in-pile, flashlight concepts. The performance characteristics are shown in Table II and Fig. 4. They are, to a first approximation, representative of the in-pile powerplant.

For an out-of-pile concept, shown in Fig. 5, the reactor and thermionic converters are separated. Heat pipes are used to remove the reactor heat to the converters. Another set of heat pipes is used to remove the waste heat from the converter assembly to the vapor-fin radiator. The whole system is static requiring no moving parts. Since the concept is relatively new, the effort has not received as much attention as the in-pile concept. The out-of-pile performance characteristic shown in Fig. 4 is based on the EOS preliminary system conceptual study.

PANCAKE DESIGN



EXTERNALLY FUELED DESIGN



FLASHLIGHT DESIGN

Figure 3. In-Pile Thermionic Reactor Designs

TABLE II

PERFORMANCE CHARACTERISTICS OF IN-PILE CONCEPTS

PARAMETER	PRATT & WHITNEY	DOUGLAS
ELECTRIC OUTPUT, Mwe	3.25	5.51
FUEL MATERIAL	UC-ZrC	UO ₂ -W Cermet
MAX. FUEL TEMPERATURE, °C	1875	2290
EMITTER TEMP. °C	1750	1930
COOLANT INLET TEMP. (CONVERTER) °C	1060	970
RADIATOR AVE. TEMP. °C	960	870
POWER DENSITY, WATTS/Cm ²	4.4	6.2
CONVERTER EFF, %	12.1	16.3
SPACING, MILS	20	10
SPECIFIC WT. LB./Kwe	5.9	4.1
REACTOR	2.2	2.8
SHIELD (ELECTRONICS ONLY)	5.4	5.4
PRIMARY HEAT REJECTION	<u>13.5</u>	<u>12.3</u>
SUB TOTAL	5.2	5.5
POWER CONDITIONING	2.1	0.8
TRANSMISSION LINES	2.7	0.9
MISC. (STRUCTURAL SUPPORT, Etc.)	<u>10.0</u>	<u>7.2</u>
SUB TOTAL	23.4	19.4
TOTAL SPECIFIC WT., LB./Kwe		

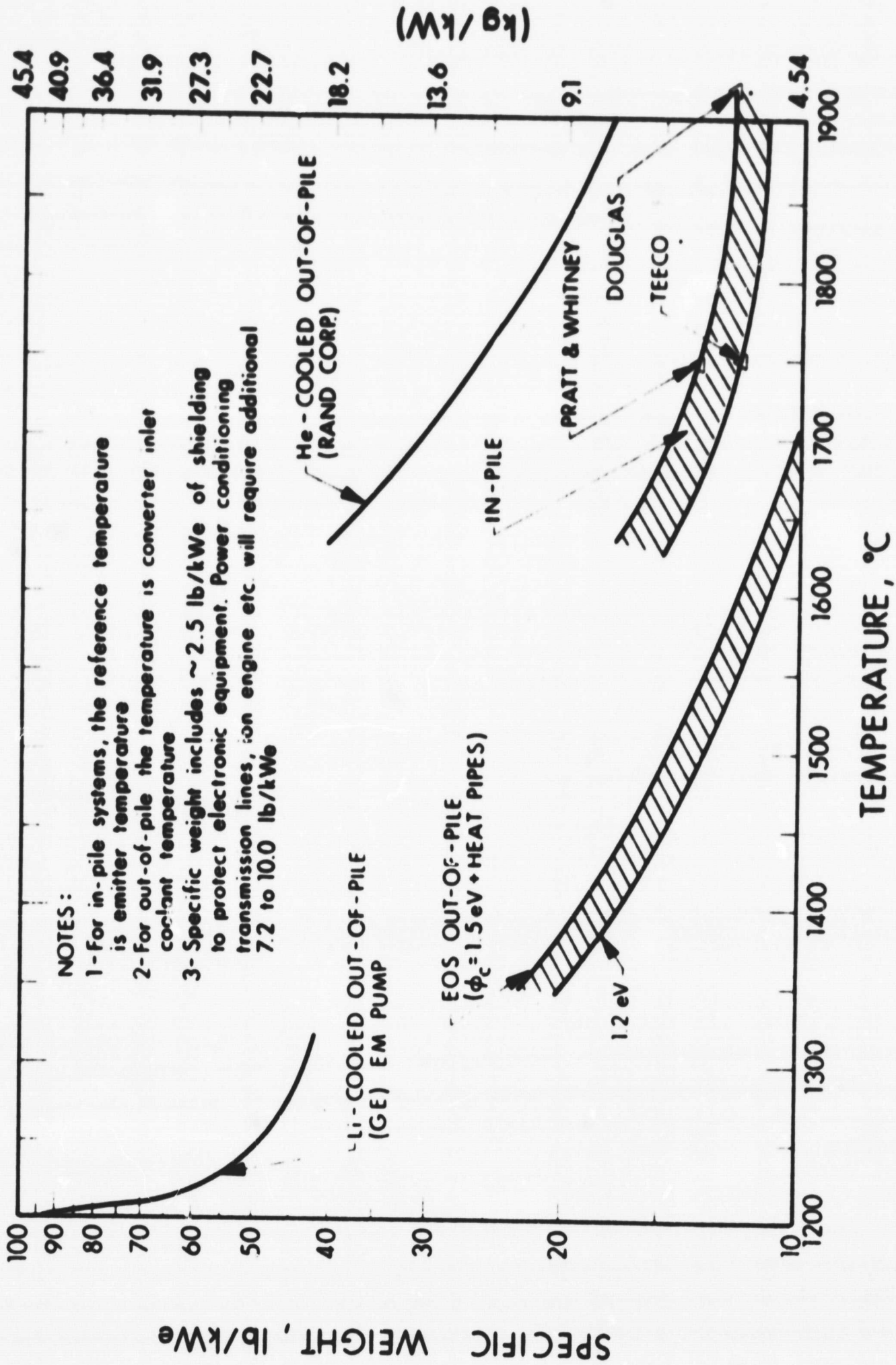


Figure 4. Comparison of In-Pile and Out-of-Pile Thermionic Reactor Characteristics

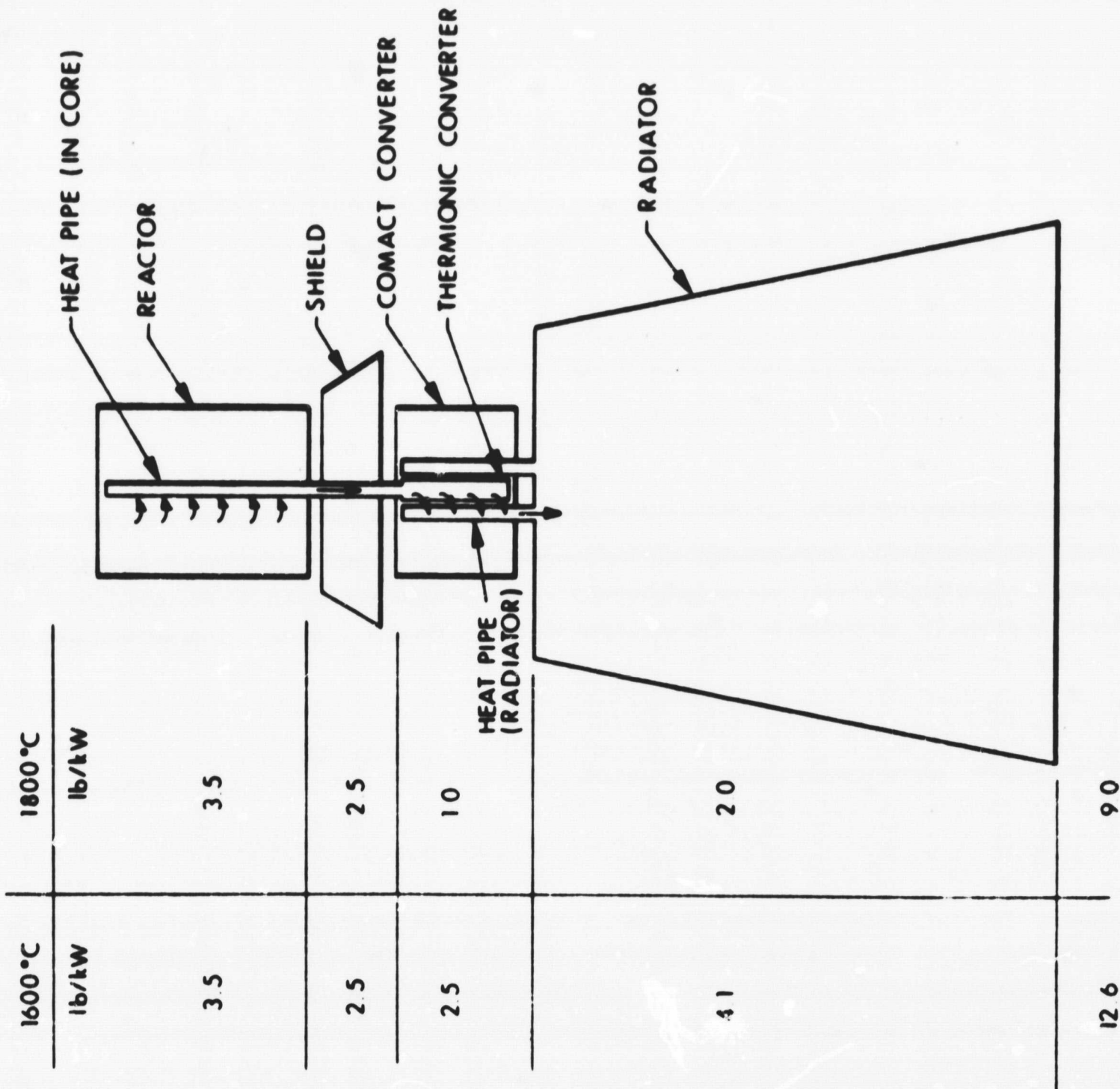


Figure 5. Out-of-Pile Thermionic Reactor

1.2 SOLAR VOLTAIC POWER SOURCES

1.2.1 SOLAR PHOTOVOLTAIC CELLS

1.2.1.1 Historical Background

Over one hundred years have passed since Becquerel, in 1839, first discovered that a voltage was developed when one electrode in an electrolyte solution was illuminated.^{1-1*} Forty years later, Adams and Day¹⁻² observed the effect in selenium. Investigation proceeded slowly into the 20th century with early solid state workers including Lange and Schottky doing work on selenium and cuprous oxide photovoltaic cells which eventually resulted in the photo-electric exposure meter. It was not until 1954 that a group of investigators at Radio Corporation of America demonstrated that practical efficiencies could be achieved in converting beta radiation into electrical energy using a silicon P/N junction photovoltaic cell.¹⁻³ Efficiencies up to 6% were obtained during this period using similar methods to produce electrical energy from sunlight. Also in 1954, 6% solar conversion efficiencies in cadmium sulphide P/N junctions were obtained.¹⁻⁴ Thus, practical conversion of electromagnetic radiation (light and beta rays) into electrical energy utilizing semiconductor junction materials has only been accomplished since 1954. Great strides have been made during the past 13 years in improving the efficiency and practicality of the conversion materials. Until now practically all spacecraft with mission durations greater than several days utilize photovoltaic power sources.

The great emphasis on the development of silicon for use in semiconductor electronic circuits has also aided the development of the photovoltaic energy conversion program. Figure 6, which shows the maximum

*References for Section 1 are located in Subsection 1.3.1.

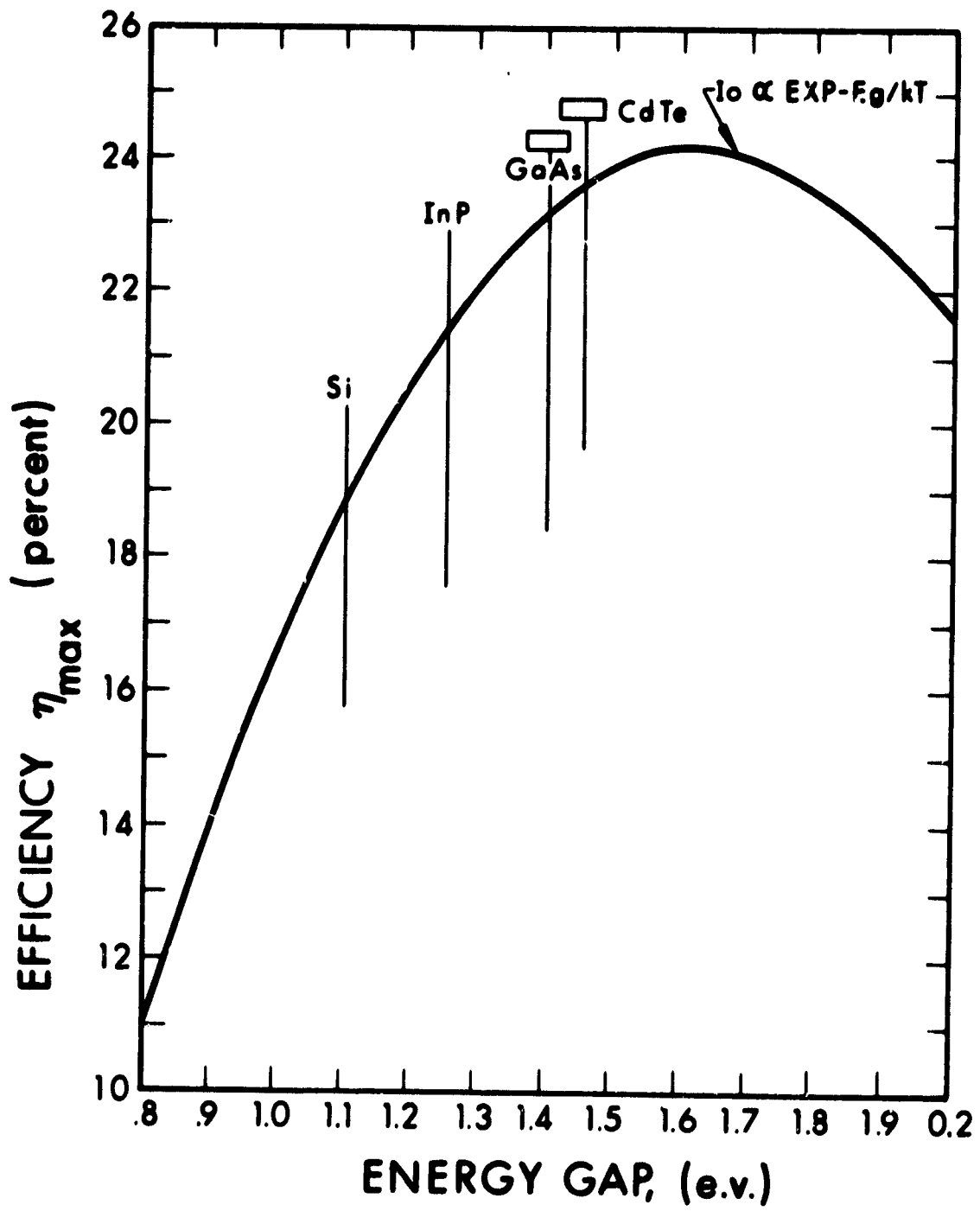


Figure 6. Theoretical Efficiency versus Semiconductor Band Gap

theoretical conversion efficiency as a function of semiconductor band gap, illustrates that silicon has a maximum attainable efficiency of 19%.¹⁻⁵ Although other materials, such as indium phosphide, gallium arsenide, and cadmium telluride, have higher maximum theoretical efficiencies, only silicon has received the effort necessary to produce practical quantities of high efficiency solar photovoltaic cells. Experimental quantities of gallium arsenide solar cells have been obtained in silicon solar cells, but the results have not been reproducible. Therefore, the history of the development of solar photovoltaic converters can actually be described in the development of silicon photovoltaic cells from 1954 to the present time. It is expected, however, that in the future, materials such as gallium arsenide and cadmium sulfide will receive the effort given to silicon previously and great advances should be made in improving the efficiency and economic feasibility of these compound type solar cells.

1.2.1.2 Developmental Trends - Silicon Solar Cells

The development of solar cells led first to a silicon wafer with a very thin surface layer (approximately 0.3 micron) doped with boron giving a P type semiconductor. The bulk of the wafer consisted of N type silicon which gave a P/N junction at the interface of the surface layer and base material. These early silicon solar cells had efficiencies of approximately 6% (at air mass = zero) and electrical characteristic curves similar to that shown in Fig. 7 for the non-grided solar cell.¹⁻⁶ Efforts to improve solar cell performance dealt with the factors limiting photovoltaic solar energy converter efficiency, which are:

- a. Reflection losses on the surface
- b. Incomplete absorption
- c. Utilization of only a part of the photon energy for the creation of electron hole pairs

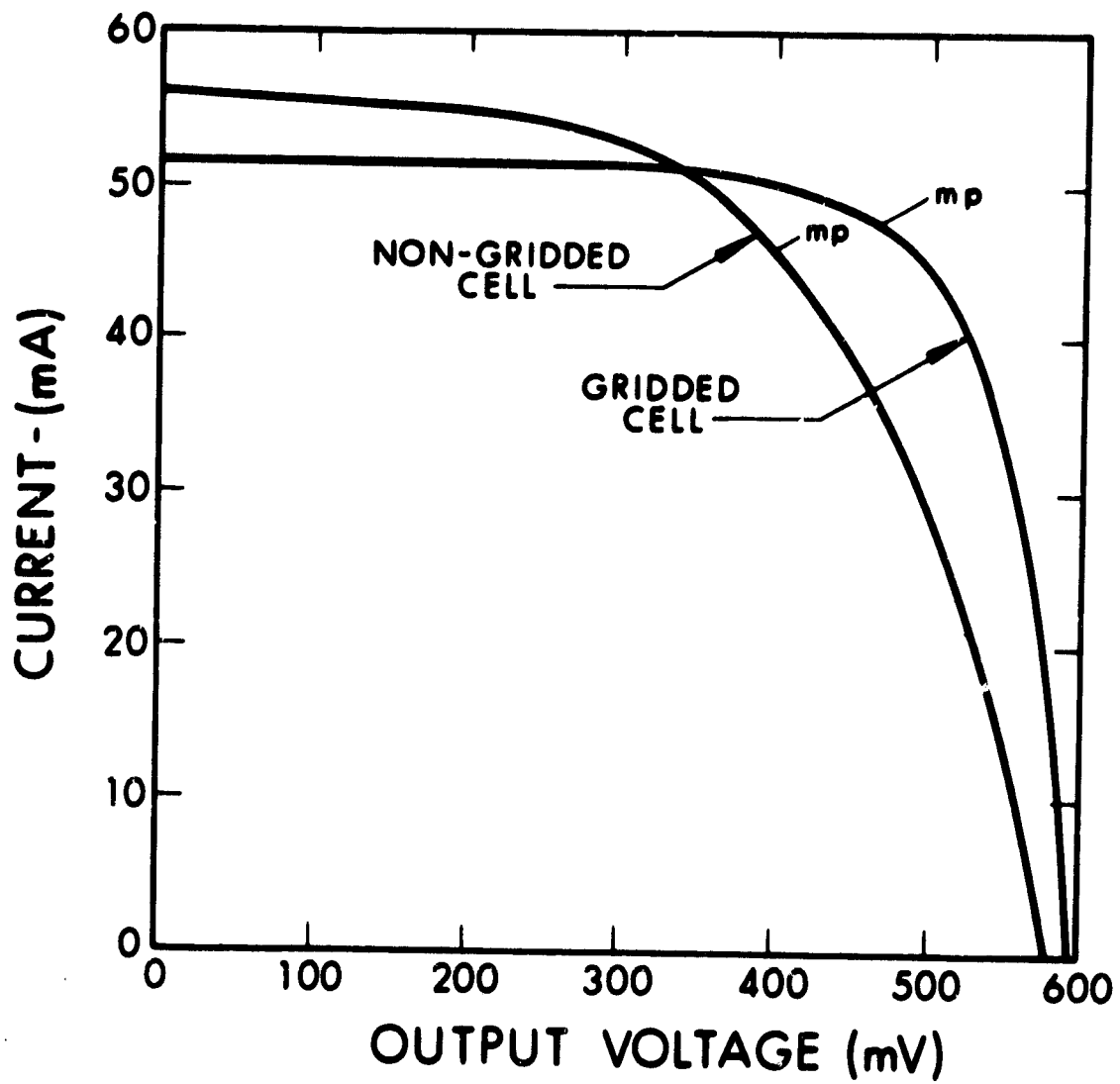


Figure 7. Electrical Characteristic Curves for Typical P/N Silicon Solar Cells, 1 x 2 cm at 25°C for Gridded and Nongridded Cells

- d. Incomplete collection of the electron hole pairs by diffusion to the P/N junction
- e. A voltage factor given by the ratio of open circuit voltage to energy gap potential difference
- f. A curve factor given by the ratio of maximum power point voltage times maximum power point current to open circuit voltage times short circuit current for an ideal P/N junction
- g. Additional degradation of the curve due to internal series resistance

All of the above factors reduce the maximum efficiency for silicon as shown on Fig. 6 (approximately 19%) down to 6% in the 1954-1960 time period. Items a, e, and f deal with the silicon cell as a macroscopic device while Items b, c, d, and g deal with the solar cell as a semiconductor material.

Various methods were attempted to minimize the factors limiting photovoltaic efficiency. Reflection losses were decreased by oxidizing the surface to form interference films or by coating the surface with special antireflection coatings. The curve factors were dealt with by optimizing the geometrical design of the solar cell in order to optimize the voltage and current outputs.

Various methods, utilizing known semiconductor properties, were attempted to increase the absorption of photons in the silicon solar cell. The concentration gradient cell¹⁻⁷ and ion implantation cell were two attempts either to vary the energy gap in the solar cell or to create a potential gradient in the cell to accelerate the carriers to the junction, thus effectively increasing their diffusion length. This increase in diffusion length reduced the carrier recombination before reaching the P/N junction and thus added to the output of the cell. The absorption of photons was also increased by making more perfect crystals and thus eliminating defects such as localized stresses in the silicon single crystals.

The collection efficiency, which is the ratio of electron hole pairs separated by the electric field of the P/N junction to the total number of electron hole pairs generated, as a function of the location of the pairs generated, the diffusion, and recombination by mobility and minority lifetimes. The optimum collection efficiency will be obtained if the layer between the light exposed surface and the P/N junction is as thin as possible and if at the same time the minority carrier diffusion length in the layer of opposite impurity type is as large as possible. Attempts were made to minimize the P layer thickness by controlling the doping temperature/time operation. The major difficulty in decreasing the thickness of the P layer is that the impurity concentration of the diffused P layer cannot be made sufficiently high in order to keep the series resistance of the P layer negligibly small for P layer thicknesses as thin as desirable for obtaining highest collection efficiency. In an effort to reduce the series resistance of solar cells with very thin P layers, the application of metallic grids, in 1962, over the P layer surface reduced the resistance of the P layer by lowering the length of the current path through the layer to the next connecting metallic line having low resistance. The effect of lowering the series resistance is so great that as much as a 20% increase in power was obtained from gridded cells as shown in Fig. 7.¹⁻⁶ The series resistance of cells with metallic grids has been lowered from values of many ohms to about 0.4 ohm.

The development of the N/P silicon solar cells by Mandelkorn at the USAERDL was a major accomplishment in the 1960 time period.¹⁻⁸ These solar cells were found to have superior radiation resistance compared to silicon P/N cells. Efficiencies obtained with these N/P converters were comparable to those obtained with the best P/N solar cells. Figure 8 shows electrical characteristics for equivalent efficiency P/N and N/P silicon solar cells. These are typical of production quantities of their particular type for the early 1960's and indicate that

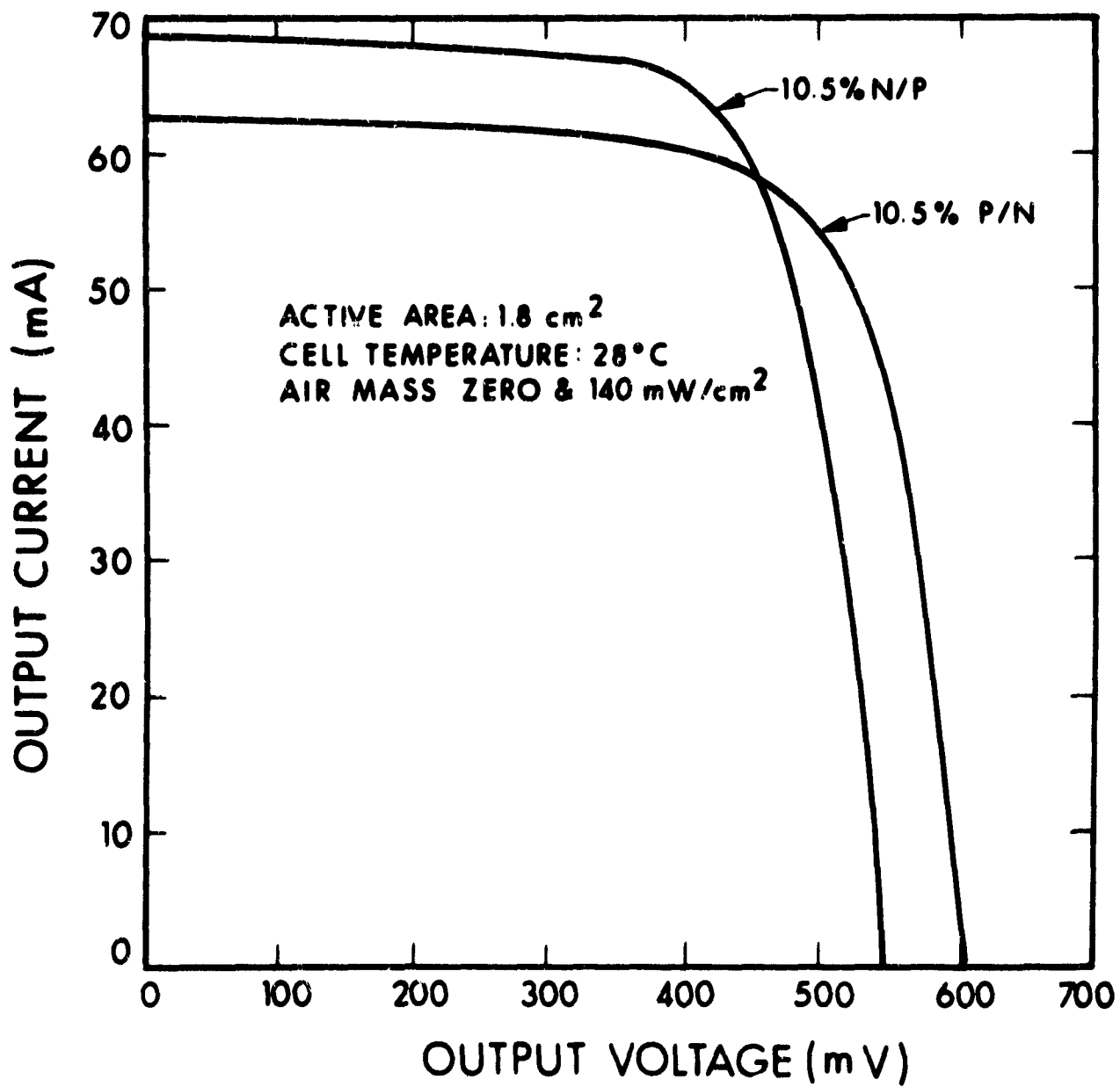


Figure 8. Typical Electrical Characteristic Curves for P/N and N/P Silicon Solar Cells

N/P silicon solar cell technology is equal to that of the P/N silicon solar cell technology. Because of the advantages of the N/P silicon solar cell, the industry converted completely to the production of high efficiency, high radiation resistance N/P silicon solar cells and discontinued production of P/N cells. The cost of N/P silicon solar cells, being only 10% higher than that for equivalent P/N cells, was not deemed sufficient cause for keeping P/N cells in production.

Other developmental trends in the early 1960's were the attempts to increase the size of the basic silicon solar cell converter in order to minimize handling and cost and maximize power per unit area. The original solar cells produced in the 1954-1960 time period were generally 1 x 2 cm with the P strip accounting for 5 to 10% of the total cell area. Larger solar cells of either 2 x 2 or 3 x 3 cm would reduce the area utilized for the top contact to a maximum of 5%. Although most solar power supplies utilized on the early spacecraft were fabricated from 1 x 2 cm solar cells, the 2 x 2 cm cell is coming into general use for application on solar photovoltaic power supplies. Larger area cells are under development but breakage losses have tended to make these cells uneconomical at this time.

The concern of spacecraft designers over system weight led solar cell manufacturers to examine the possibility of decreasing the overall thickness of the silicon cell with the possibility of maximizing power to weight ratios. Original solar cells were from 18 to 30 mils in thickness. Progress was made in the development of a 12 mil, high efficiency silicon solar cell of either P/N or N/P type. However, it was found, under subsequent investigation, that decreasing the solar cell thickness below 12 mils led to a severe degradation in the cell efficiency. Except for special instances, the 12 mil silicon solar cell is the optimum cell for use on spaceborne solar photovoltaic power supplies. Research is continuing, however, into the improvement of efficiency of thin solar cells.

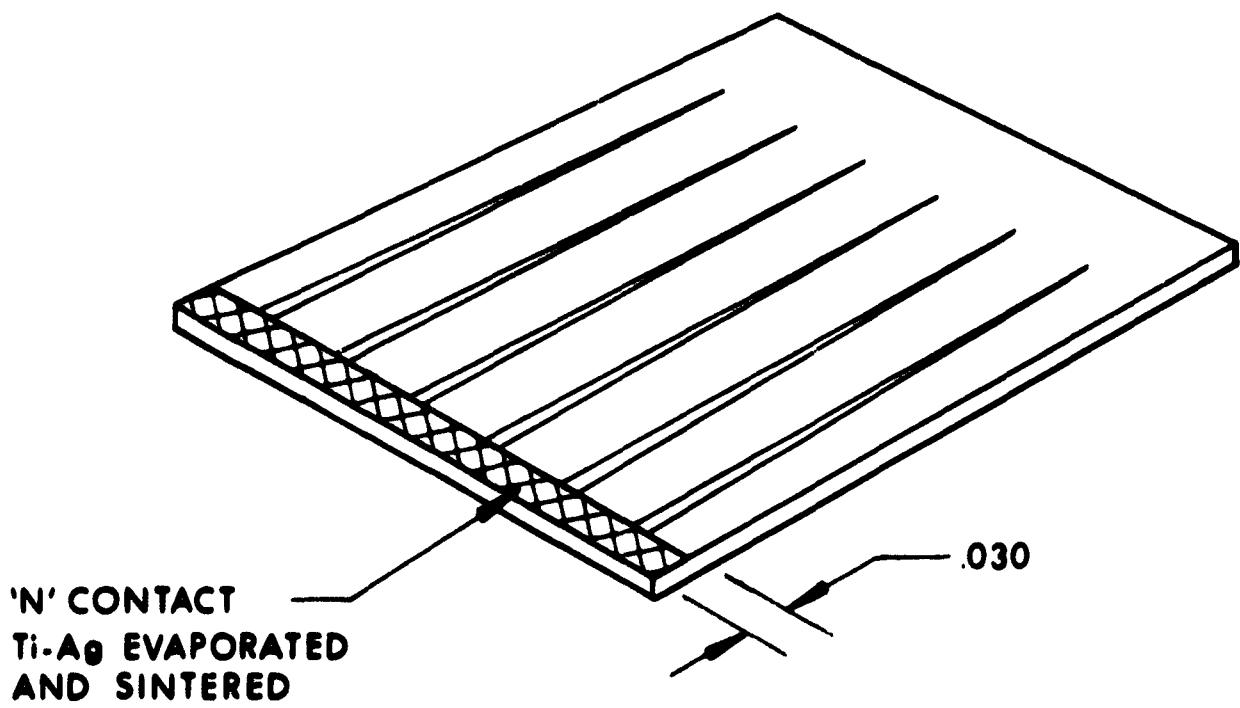
1.2.1.3 Current Technology - Silicon Solar Cells

Long-life satellites and probes have been almost exclusively dependent upon the solar cell for power. Even if no improvements are made in the presently available silicon solar cell, it will probably dominate the space power field for at least five more years. Approximately two million solar cells are being delivered per year to various users under NASA and Air Force contracts. Before 1963 most cells were of the boron diffused P/N variety, but the phosphorous diffused N/P cells are presently the only cells being used except in specific instances requiring the higher voltages of the P/N cell. The discussion in this section will therefore be limited to the present state of the art of silicon N/P solar cells.

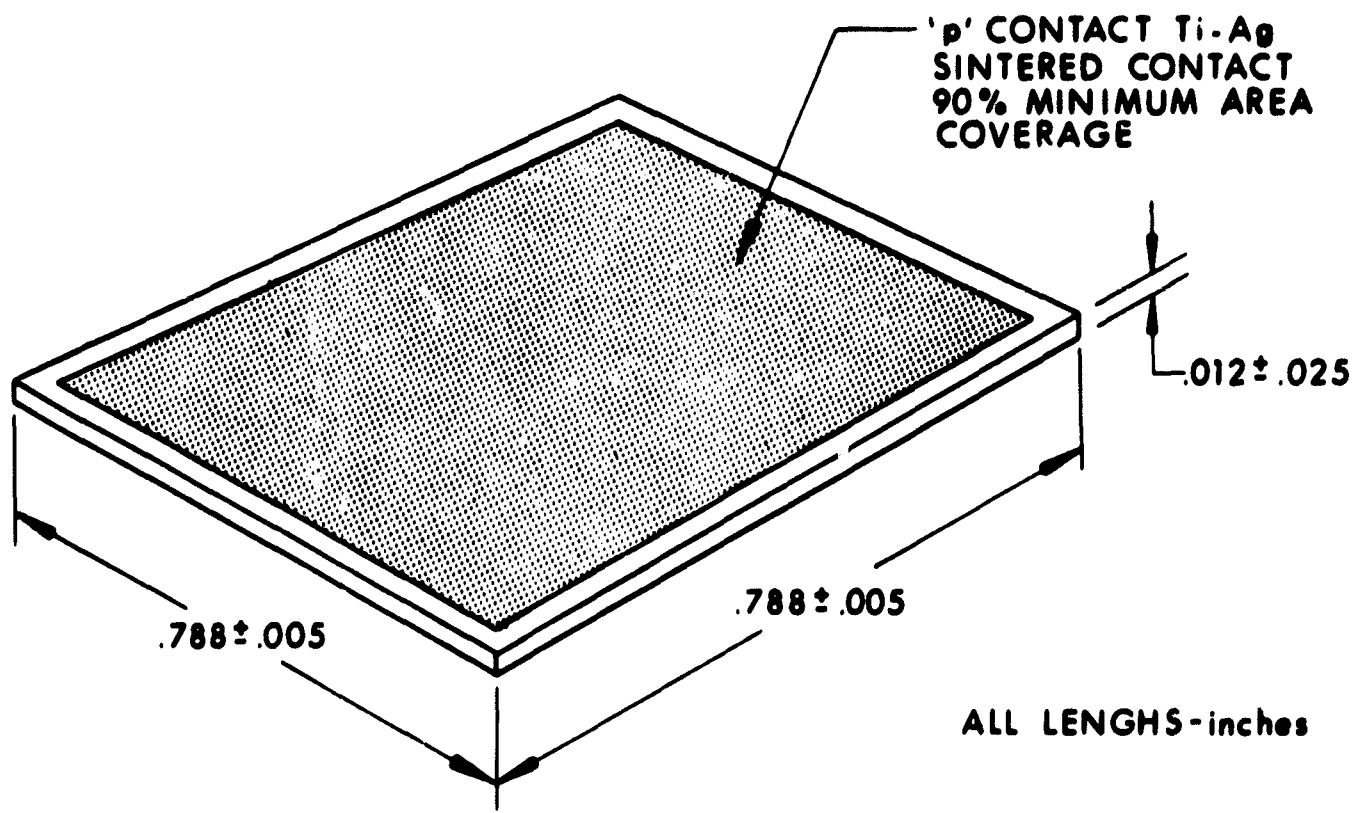
The silicon solar cell presently available in production quantities is 12 mils thick, 1 x 2 or 2 x 2 cm, with a soldered sintered silver-titanium ohmic contact (Fig. 9). The specific weight of the cell is approximately 0.12 gram/cm², and the average space efficiency is 10.5%. The typical cost for solar cells ranges from \$10 per cell for 2 x 2 cm, 11.3% efficient, to \$4 per cell for the same size at 10.5% efficiency. (All efficiencies stated in this report will be at air mass zero, 28°C and 140 mW/cm² unless otherwise stated.)

General Properties of Silicon N/P Solar Cells

A typical N/P solar cell operated between 0.37 micron and 1.1 microns. The spectrum outside this range is either reflected from the surface, transmitted through the cell without creating electron hole pairs, or reradiated from the cell as heat. Figure 10 shows the spectral response of a typical N/P silicon solar cell in relation to the spectrum of incident sunlight.



ACTIVE SURFACE OF SOLAR CELL



BOTTOM SIDE OF SOLAR CELL

Figure 9. Typical Conventional Solar Cell

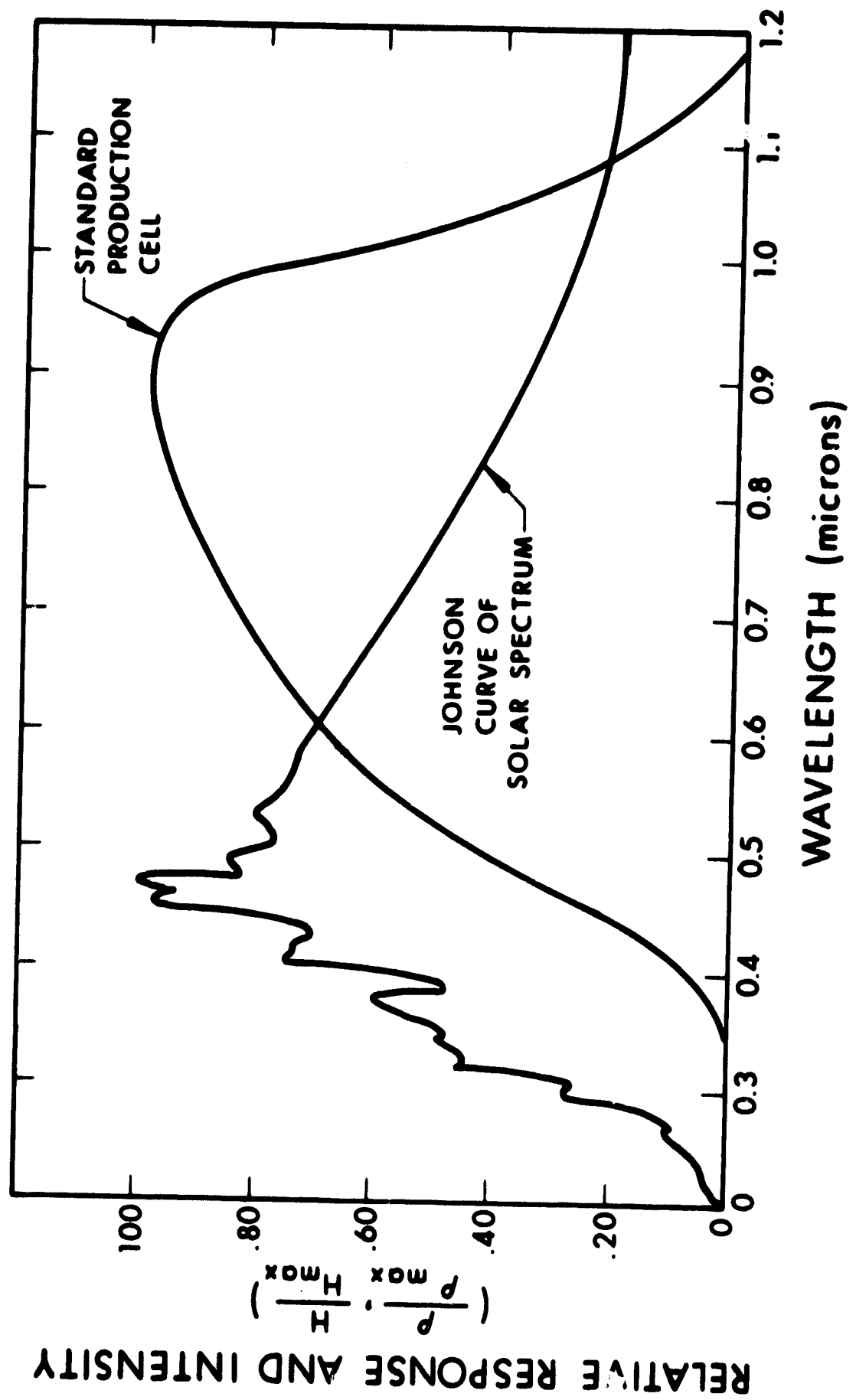


Figure 10. Spectral Response of a Typical N/P Solar Cell in Relation to Incident Sunlight

The electrical characteristic curve of a typical N/P silicon solar cell under simulated air mass zero conditions is shown in Fig. 11. The curves show the typical limits at various temperatures encountered in the operation of solar cells in space.

It can be seen that the open circuit voltage per cell ranges from approximately 0.55 volt at 25°C to 0.39 volt at 100°C. The efficiency of the solar cell will affect the curve by increasing the current at the maximum power point and slightly changing the voltage at the maximum power point. The voltage of a solar cell can be assumed to be independent of the efficiency of the cells and the impinging solar intensity but is very dependent upon the cell temperature and internal series resistance. The cell current is a direct function of the solar intensity and cell efficiency and is relatively independent of the cell temperature and internal series resistance.

The degradation due to particulate radiation bombardment within the Van Allen belt can be severe in silicon solar cells. The original P/N silicon solar cell was severely degraded by the space radiation environment and the development of the N/P solar cell has brought about the advantage of the N/P cell in this respect.

The N/P solar cell is less affected by radiation bombardment due to the difference in the minority carrier in the bulk of material which for N/P material is electrons. The degradation due to particulate radiation is a function of the protection given the solar cells by glass coverslides and the critical flux. The critical flux is defined as the integrated particle flux necessary to cause a 25% decrease in the initial output power of a solar cell. The critical flux as a function of proton energy is shown in Fig. 12, and a value of 1×10^{11} P/cm² for protons between 4 and 20 meV is typically used in calculations to determine percent power degradation. The power degradation (Q) due to

TYPICAL I-V CURVE LIMITS FOR
N/P SILICON SOLAR CELLS,
UNDER SIMULATED AIR MASS=0
CONDITIONS.

CELL ACTIVE AREA 1.8 CM²

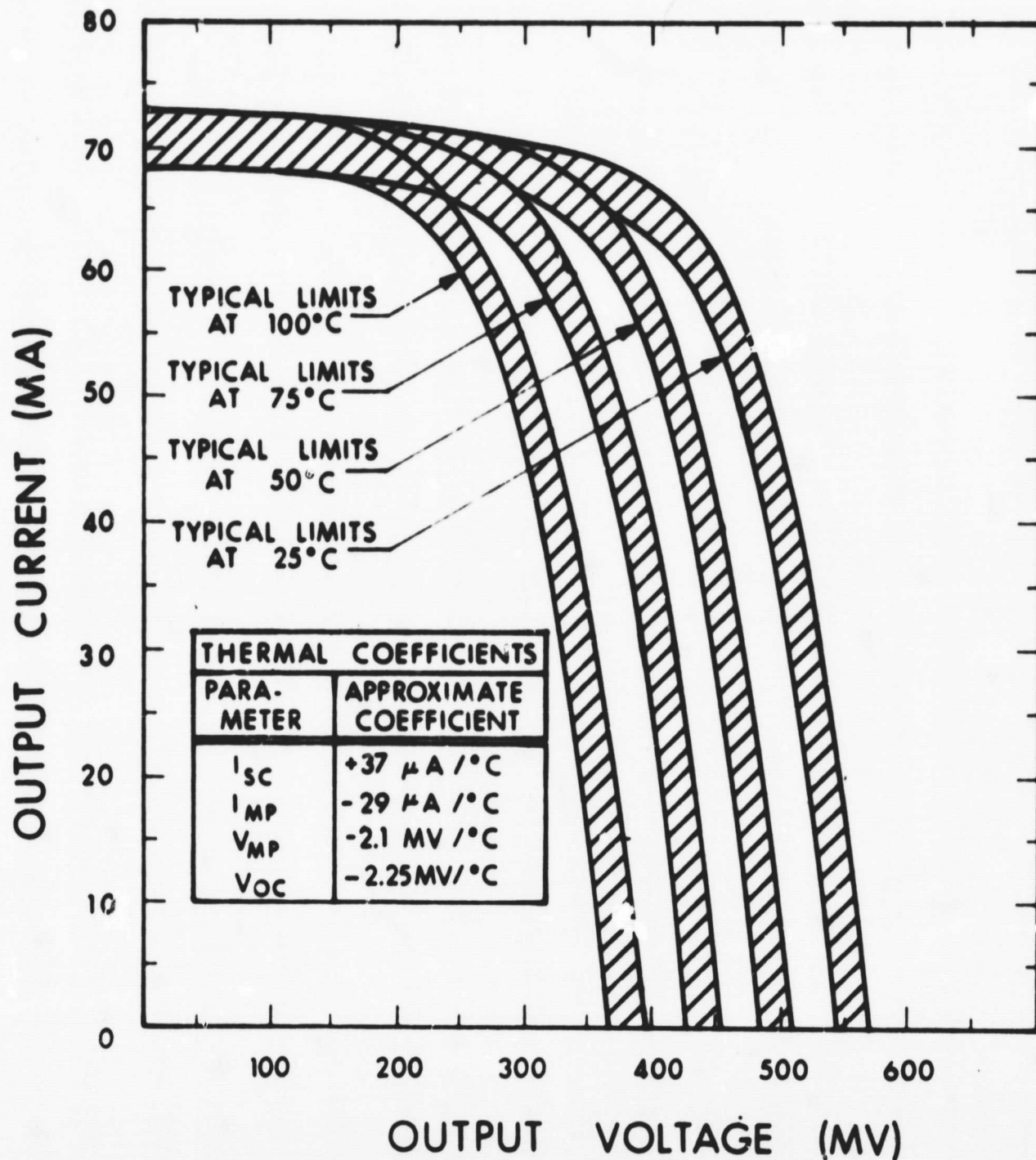


Figure 11. Typical I-V Curve Limits for N/P Silicon Solar Cells Under Simulated Air Mass = 0 Conditions

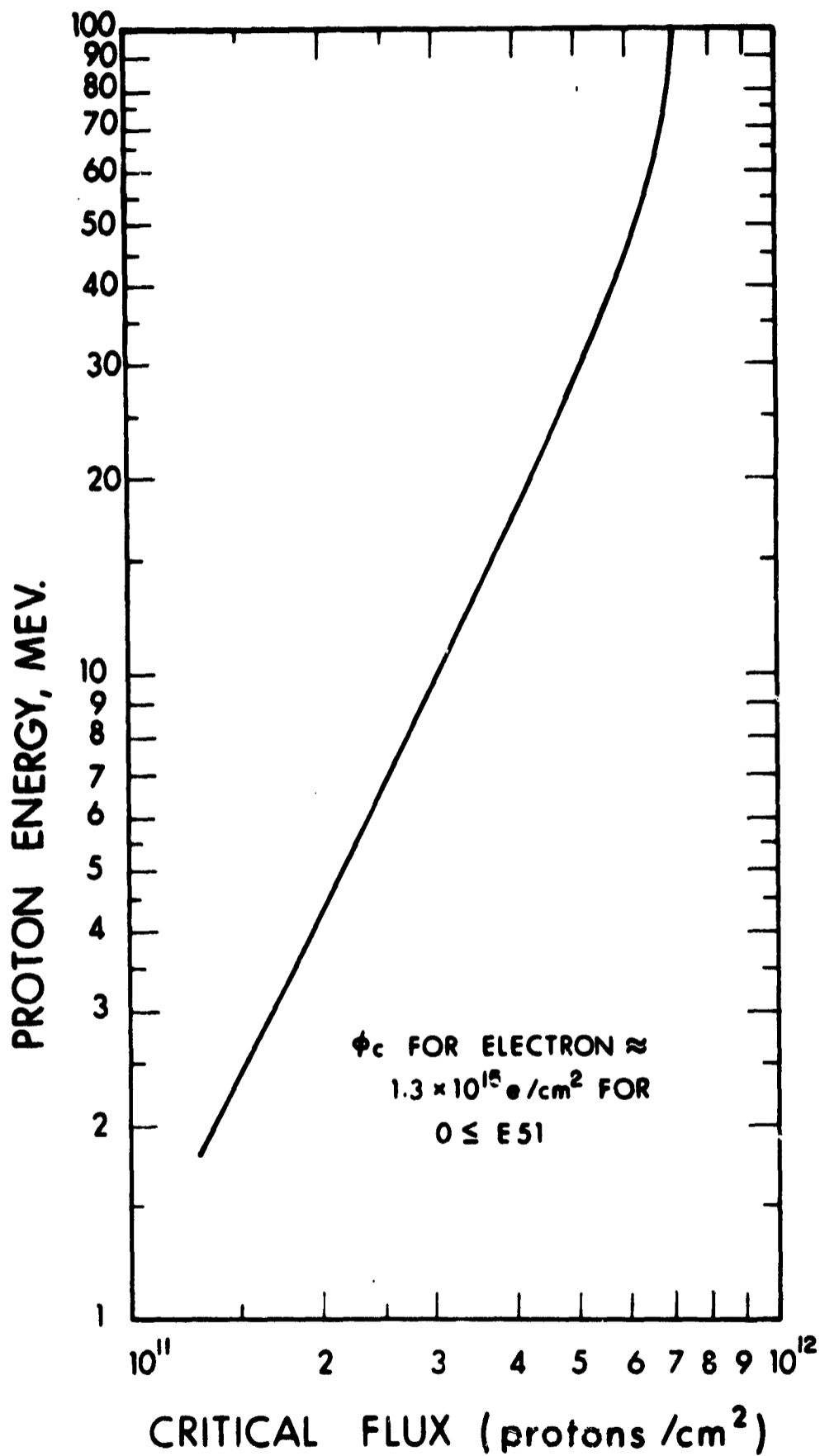


Figure 12. N/P Solar Cell Radiation Degradation Factor, Proton Critical Flux versus Proton Energy

particulate radiation is determined by using the following equation, which was derived using empirical analysis¹⁻⁹ of experimentally obtained radiation damage. The equation for percent power remaining versus integrated flux is

$$Q = 1 - \sqrt[7/9]{\left(\frac{\phi}{\phi_c}\right)^{1/2}} + 1^{-1/2}$$

where Q = percent power remaining

ϕ = integrated flux

ϕ_c = critical flux to reduce cell power output 25%

The radiation resistance of N/P solar cells can be improved by incorporating a potential field within the bulk of the cell which accelerates electron hole pairs to the P/N junction, thus neutralizing the effect of radiation bombardment which decreases the lifetime, τ , or diffusion length. Drift field and ion implantation cells which incorporate potential fields in the cell are presently under investigation, but results to present do not indicate startling improvements in radiation resistance.¹⁻¹⁰ Improvements of up to 20% in radiation resistance have been made, but this does not presently warrant the selection of these cells for use on space power supplies, since the efficiencies are not yet as good as the standard N/P solar cells.

1.2.1.4 Projected Technology - Silicon Solar Cells

Table III shows the predicted silicon solar cell characteristics from the present to the 1985 time period. It is readily apparent that no major advances are expected in silicon solar cell efficiencies beyond that which is presently available in 1967. The relative improvement in efficiency for thin solar cells (less than 12 mils thick) will exceed that obtained during the next 20 years for the thicker cells but not to an extent that could be classified as an outstanding improvement.¹⁻¹¹

TABLE III

TABLE OF PREDICTED SILICON SOLAR CELL CHARACTERISTICS

	<u>Present (1967)</u>	<u>1975</u>	<u>1985</u>
Type	N or P	N or P drift field	N or P drift field
Ohmic contact	Top soldered	Same or wraparound Ag-Ti	Same or wraparound Ag-Ti
	Silver-titanium	or Ce-Ti	or Ce-Ti
Thickness	12 mils	12, 8 mils	12, 8, 4 mils
Weight*	0.12 gm/cm ²	0.12 gm/cm ²	0.12 gm/cm ²
Base resistivity	1-10 ohm-cm	1-25 ohm-cm	1-25 ohm-cm
Size	1 cm x 2 cm	Same; also: 3 cm x 3 cm	Same; also: 1 cm x 30 cm
	2 cm x 2 cm	1 cm x 13 cm	2 cm x 30 cm
		2 cm x 13 cm	3 cm x 30 cm
Power output at 55°C for 12 mil cell	13.1 mW/cm ²	14.1 mW/cm ²	14.6 mW/cm ²
Total cell efficiency at 28°C (average) production	10.5% (12 mils) 0.5% (8 mils) 7.5% (4 mils)	11.5% (12 mils) 10.3% (8 mils) 8.5% (4 mils)	11.7% (12 mils) 11.0% (8 mils) 9.5% (4 mils)
Cost/cm ²	\$ 2.00/cm ²	\$ 1.75/cm ²	\$ 1.50/cm ²

* Based on 12 mil nominal thickness

The efficiency of the 4 mil cells should be expected to be improved from 7.5% available at the present time to approximately 9.5% in 1985 or about a 25% increase in efficiency¹⁻¹¹. Other expected improvements in silicon solar cell technology during the next 20 years will be the enlargement of the basic cell size to a maximum of approximately 3 cm to 30 cm (90-100 cm²) and a projected lowering of bare cell costs from \$2/cm² at present to approximately \$1.50/cm² in the 1985 time period. It is also expected that some improvements will be made in increasing the radiation resistance of N/P silicon solar cells by changing the dopant material used to obtain the P material, improving the drift field cells presently in development, or by changing the material used in the contacts to the solar cell.

In summary, it is expected that the N/P silicon solar cell producing approximately 11 watts/ft² over long durations in the moderately severe areas of the Van Allen belt. This power will be produced at a cell cost of approximately \$100 per watt. The silicon solar cell will continue to be the prime source of electrical power in space for missions requiring power up to approximately 50 kW, since the solar cell is a proven piece of space hardware capable of supplying reliable power at reasonable cost and specific weights.

1.2.2 SOLAR PHOTOVOLTAIC PANELS

1.2.2.1 Historical Background

The specific power capability of solar array systems has continued to grow over the years since 1958 when it was first employed as a power source for a spacecraft. This spacecraft (Vanguard) is still in orbit, the solar panel are still providing power, in this case, unfortunately, to operate its milliwatt beacon transmitter. Since that time, the power requirements for spacecraft have increased and in most cases the specific power capability of solar arrays has managed to keep in step. The development of the larger power arrays primarily has been the result of development in the manufacturing techniques associated with lightweight structure fabrication and the development of engineering technology associated with handling and working with the cells. To date only silicon solar cells have been utilized in a solar cell array.

It should be noted that since the advent of gridded solar cells in 1960, the actual air mass zero conversion efficiency has improved little; however, the specific power capability of the array itself (watt/lb) has continued to show improvement.

The early solar photovoltaic systems were either body-mounted on the skin of the satellite or extended on booms on non-oriented or semioriented paddles. Only in a few instances were the solar panels oriented toward the sun. The power requirements in the beginning of the space program were limited as was the area and weight allotments for the solar array. The basic structures used on early spacecraft for mounting the solar cells were heavy (approx. 2 lbs/sq ft) but great efforts were being made to develop extremely lightweight structures for the expected larger power photovoltaic systems.

The first lightweight structures were generally of aluminum honeycomb with either aluminum or fiberglass facing sheets which led to a specific weight of the total array of approximately 1.2 lbs/sq ft, without critically affecting structural rigidity.

The advancement of knowledge concerning the radiation environment encountered in earth orbital missions led to the optimization of the cover glass design for solar cells in order to minimize system weights. Early satellites generally utilized extremely thick (60-70 mils of quartz) cover glasses in order to limit the degradation due to Van Allen particle bombardment. The reduction in coverglass thickness due to the improved radiation resistance offered by the N/P silicon solar cells.

1.2.2.2 Critical Subsystems

The complete solar array consists of many subsystems integrated into a reliable lightweight package. The most critical of the array subsystems are discussed in the following sections.

Silicon Cells

The choice of the type of solar cell obviously seriously affects the overall photovoltaic array with respect to weight, area, power reliability and cost.

The choice of the thickness of solar cells can vary from 18 mils as used on the Ranger and Mariner spacecraft to 12 mils presently being used on Surveyor, IMP, etc, to thinner solar cells (8 mils, 4 mils, etc.) which are being projected for use on future spacecraft. The density of the silicon cell is 2.66 grams/cm³ and the specific weight for the present 12-mil soldered solar cells is 0.12 grams per cm². Figure 13 shows cell weight versus cell thickness for the types of cell contacts (i.e. solder and solderless). The specific weight for a typical solar cells

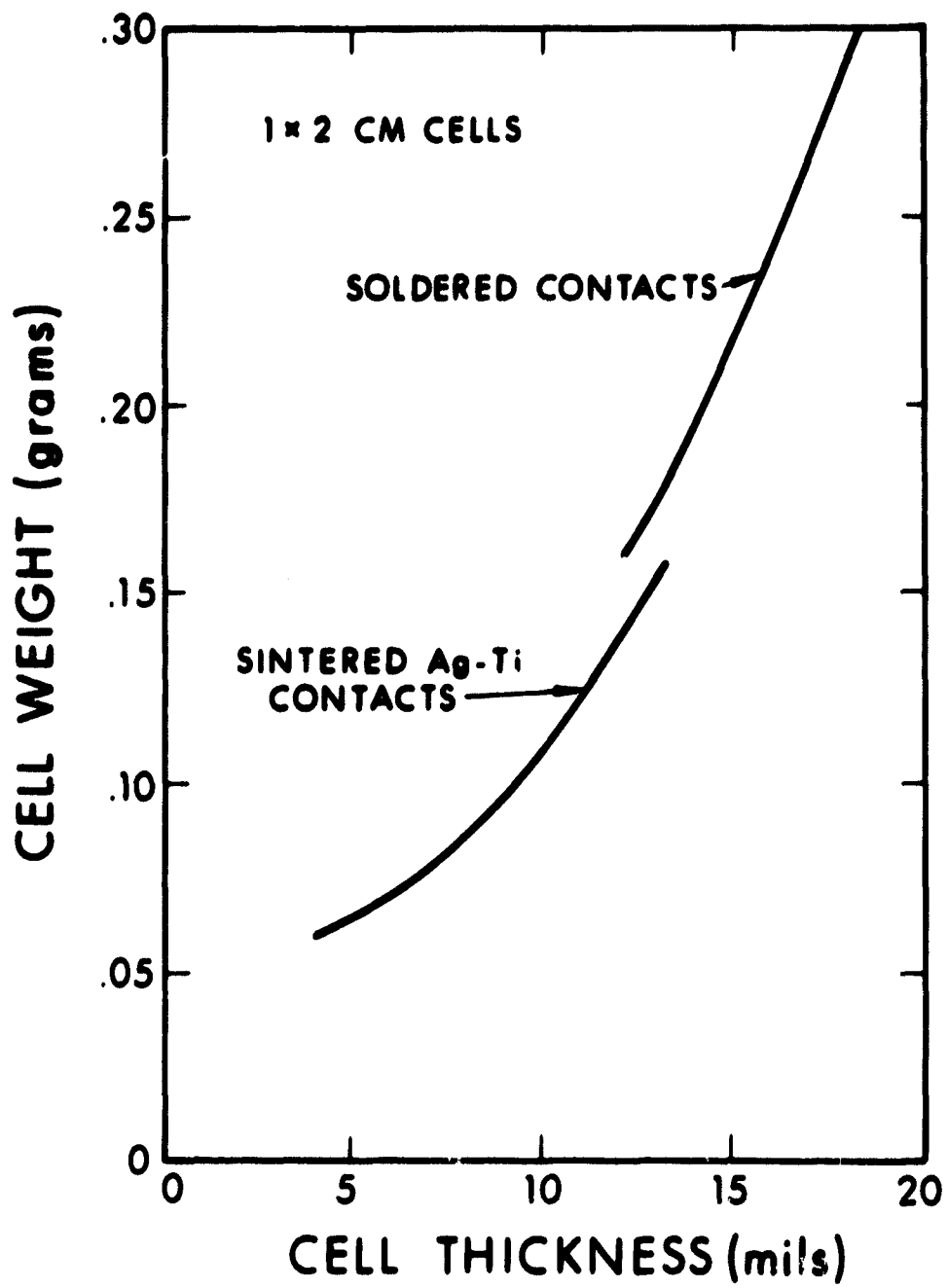


Figure 13. Typical Weights of Solar Cells and Contacts

of present design is 0.22 lbs/sq ft (or approximately 20 percent of the total array weight depending on the overall array size).

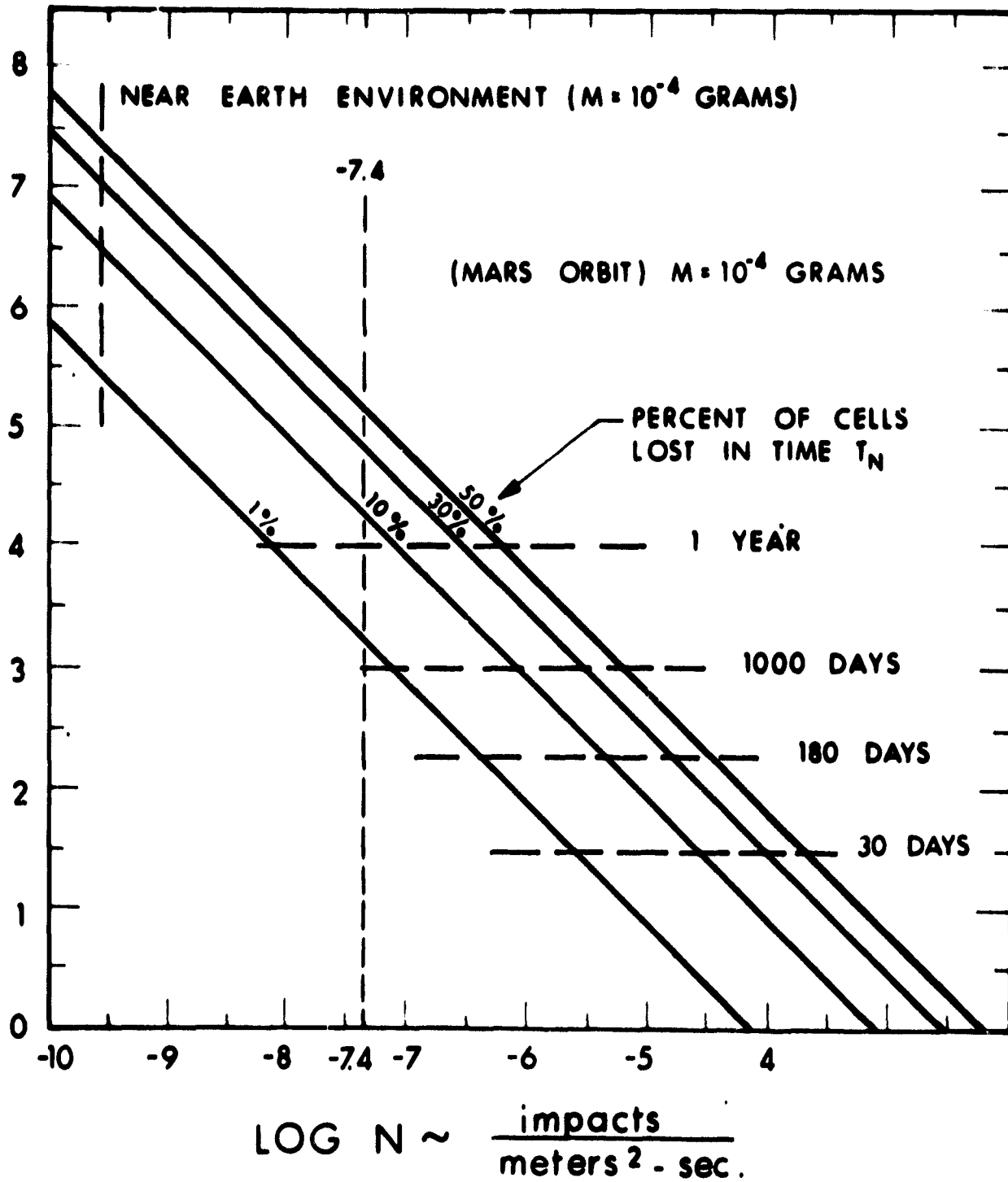
The total array area is inversely proportional to the solar cell efficiency and present designs indicate a value of approximately 10 watts per sq ft in space at 1 A.U. which for a 50-kilowatt oriented array gives a total area of approximately 5000 sq ft. The area for non-oriented array gives as much as 4 to 5 times greater than the oriented array area.

In the same manner that cell efficiency affects array area, power output is also affected by the cell efficiency. The specific power output is watts per sq ft and watts/lb are a function of both the cell efficiency, and cell thickness. Since the efficiency of solar cells is directly related to the thickness of the cell, a trade-off must be made in the design of solar arrays to optimize array weight as a function of array area in order to meet the requirements of maximum specific powers.

The reliability of solar cell operation in the space environment has become a proven fact and with proper design, reliabilities of 0.9999 can be achieved. The reliability of the solar array is dependent upon many factors that affect the use of the solar cells. The incorporation of the cell into an electrical submodule affects reliability as does the incorporation of the submodule into the entire electrical circuits.

The degradation effects of meteoroid bombardment on solar cells is generally very small as shown in Fig. 14. This figure relates solar cell losses as a function of bombardment time, assuming one cell is lost per impact. This is generally assumed to be a worst case since micro-meteoroid impacting a surface will only damage a small area of the impacted surface. In the case of an impact on a solar cell, a small segment of the active area will be lost but the cell should still be

LOG T_n = LOG TIME TO FAIL N% OF CELLS ~ DAYS



1 CELL LOST/IMPACT
 SOLAR CELL DECAY RATE DUE TO METEOROID IMPACT

Figure 14. Solar Cell Decay Rate Dur to Meteoroid Impact

capable of producing usable power. The impact of a large micrometeoroid or meteoroid will cause catastrophic failure in a cell or in the entire array, but the probability of this occurrence is so small as to be assumed to be zero. As shown in Fig. 14, it would require over ten years in orbit to lose one percent of the total cells on the array (i.e., assuming, pessimistically that one cell is lost per impact). This loss is readily accounted for in the 10 percent over-sizing allowed for in the array design. It can therefore be assumed that power degradation, during the time period of the mission, due to meteoroid bombardment is negligible.

Figure 14 is derived using a near-Earth micrometeoroid model of:

$$\log N_E = -13.8 - \log M$$

where N_E = number of particles/m² sec. of mass M grams and greater at a distance of 1 AU from the sun (i.e., near-earth-space).

This model was obtained from the Jet Propulsion Laboratory as part of the Voyager program environmental predictions.

The cost of the silicon solar cell is the most important factor affecting the total cost of the overall photovoltaic array. The cell costs range from \$2.00 per cm² for presently available silicon cells, to a future predicted cost of \$1.50 per cm² in 1985. This gives a cost of approximately \$1800 per square foot which for large areas such as a 50 kilowatt oriented array would mean a total cell cost of approximately \$9 000,000. It can be seen that in the case of non-oriented arrays, this cell cost could go up to as much as 50 million dollars.

Solar Cell Filters

The primary purposes of putting a transparent coverslide on a solar cell are to reduce the temperature of the solar cell by increasing the effective α/ϵ ratio and to reduce the effect of particulate radiation on the solar cell. Each of these parameters will be discussed in the following paragraphs.

Table IV summarizes the results when different coatings are used on the coverglass. All systems calculations assume the use of a coverglass with 415 millimicron blue and anti-reflective (AR) coatings. The important effect obtained when using the coverglass as a thermal control surface is to lower overall cell temperature which effectively increases the solar cell output.

The density of the quartz coverslide is 2.66 grams/cm^3 . Thus a 6-mil quartz coverslide weighs 0.071 lbs/sq ft, any other thickness quartz coverslide can be scaled up or down from this number.

The other use of coverslides on solar cells is the protection of the solar cell from particulate radiation bombardment. In very intense radiation fields, the only way to obtain long life from a solar cell is to protect it with a transparent coverslide material. Of the three coverslide materials in general use, the best for protection against particulate radiation is sapphire, however, this material is quite expensive and is not generally in use in current solar array designs. The next best material is quartz or fused silica which offers very good radiation protection compared to glass or microsheet which discolors under heavy radiation flux. The discoloring of glass is due to the formation of "F" centers or color centers in the bulk glass material which is generally due to the existence of impurities in the glass such as sodium atoms. The ability of a quartz coverslide to protect a solar

TABLE IV

POUNDS PER kW AS A FUNCTION OF COVERGLASS THICKNESS

100.0 sq ft/kW for 10.3 percent solar cell, 8 mils thick for 0 degradation at 50°C

<u>Coverglass Thickness (mils)</u>	<u>Pound/Kilowatt</u>
6	43
12	50
20	61
30	73
45	92
60	111

89 sq ft/kW for 11.5 percent solar cell, 12 mils thick for 0 percent degradation at 50°C

6	42.7
12	49
20	59
30	69
45	86
60	103

121 sq ft/kW for 8.5 percent silicon solar cell, for 0 percent degradation at 50°C

6	46.6
12	55
20	68
30	83
45	106
60	129

cell is typically shown in the range-energy curve for quartz. This curve shows the minimum energy that will penetrate a quartz coverslide. Figure 15 gives the range-energy for protons and electrons in quartz. As can be seen, the 6-mil quartz coverslide will stop all protons with energies less than 4.5 meV and all electrons with energies less than 200 keV. Curves in Fig. 15 can be summarized in the following equation:

$$\begin{aligned} \text{Electron shielding level } E &= 1.5 \times r^{0.698} \\ \text{Proton shielding level } E &= 28.6 \times r^{0.558} \end{aligned}$$

The present state-of-the-art coverglass used to protect a cell from radiation is bonded to the cell with approximately 2 mils of adhesive (see Fig. 16). In the case of a spacecraft operating outside the earth's to protect the cell from low energy proton damage. It is felt that cover glass can be reduced safely to 3 mils or perhaps slightly less to guard the cells against low energy protons, but have been maintained at 6 mils to minimize coverglass attrition during panel fabrication. Promising programs are presently being conducted in the solar cell industry which will permit deposition of glass directly on the surface of solar cells thereby eliminating the requirements for cells-glass adhesives. Available test data indicates that up to 2 mils of glass can be deposited directly on the cell with only a 3 percent decrease in the power producing capability of the cell. Twenty mils of glass have been deposited on a solar cell with a 9 percent decrease in the power producing capability. Work accomplished at Lockheed Missiles and Space Division on an organic-metallic coating has indicated that 2 mils of this coating is equivalent in radiation protection to 20 mils of quartz but further development is necessary before these results are firmly established. The use of integrated coverglass for low altitude earth-orbiting missions will greatly reduce the weight, complexity, and cost in fabricating a solar photovoltaic array. With proper designs, the integrated coverglass thickness can be minimized to a point where it no longer becomes a major portion of the total array weight.

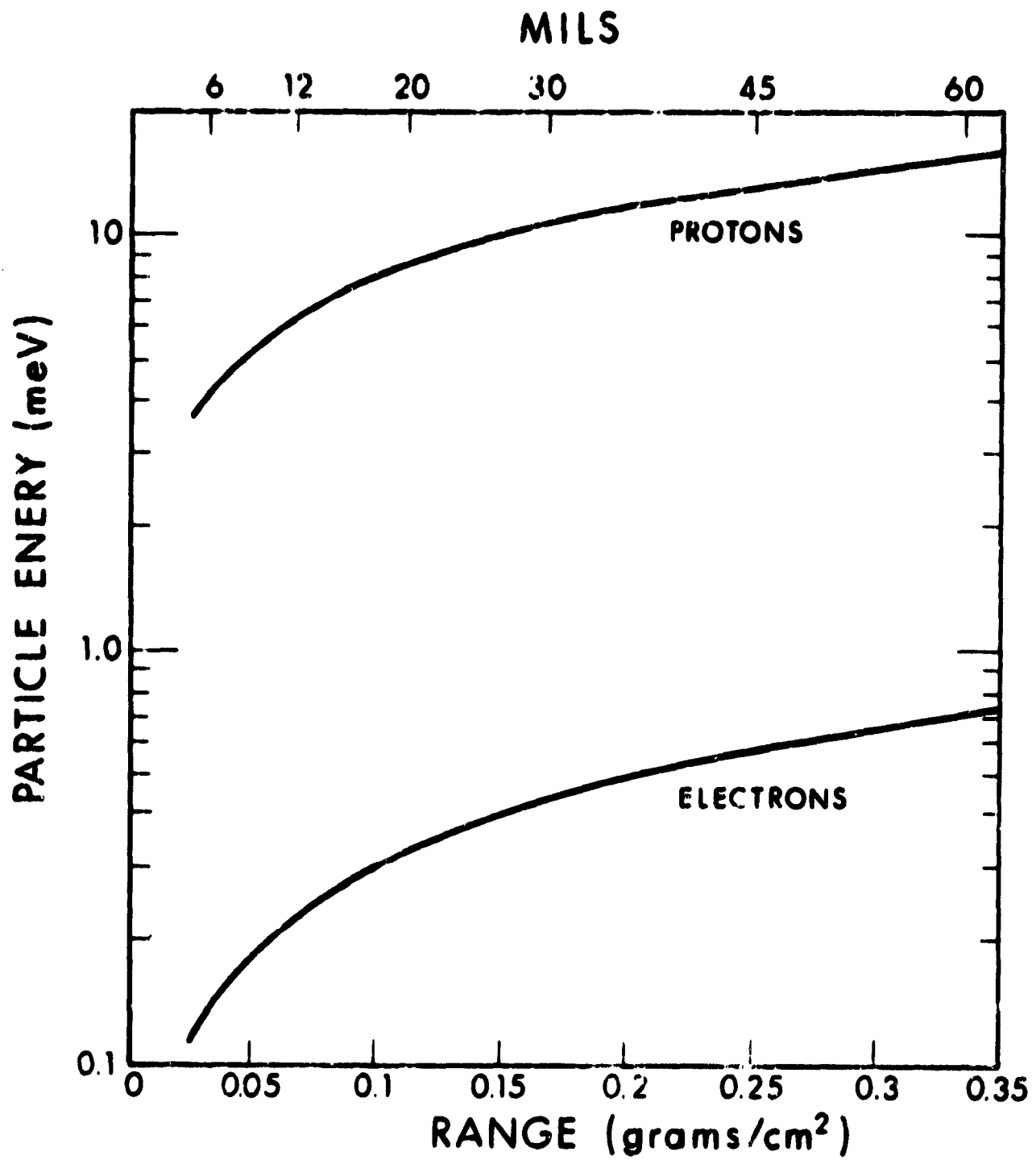
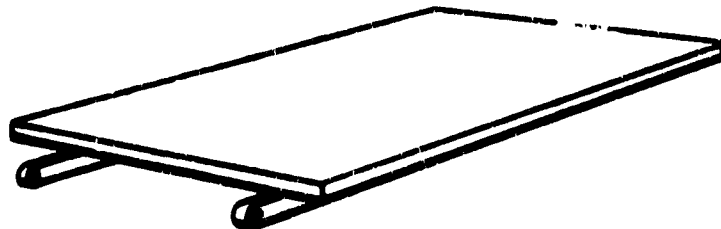
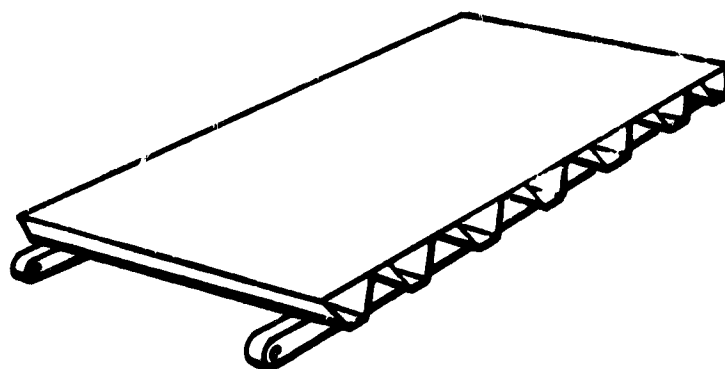


Figure 15. Range-Energy for Protons and Electrons in Quartz

TYPES OF SUBSTRATE USED IN 1966



HONEYCOMB



CORRUGATED
SHEETMETAL

Figure 16. Illustration of Current Technology

Adhesives

Two types of adhesives are used on a solar photovoltaic array; one for securing the coverslide to the solar cell (except in the case of integrated coverglass) and another to bond the cell assembly to the substrate (see Fig. 16). The critical adhesive in most earth-orbiting missions is the coverslide adhesive which must be capable of withstanding the space environment, i.e., vacuum, temperature, particulate radiation and ultra-violet radiation, without degrading the performance of the solar cell. Coverglass adhesives fall into two general classes: 1) silicone adhesives, and 2) clear epoxies. In both cases, the adhesives are sensitive to uv radiation and will discolor if not protected by a uv reflecting coating on the coverglass. It is expected that the coverglass adhesive will assume a role of minor importance when the integrated coverglass becomes an established production technique.

As in the case of the coverglass adhesives, the adhesives used to bond the solar cell assembly to the substrate fall into two classes: 1) silicone adhesives and 2) epoxy adhesives.

The silicone adhesives are generally room temperature vulcanizing (RTV) which gives some degree of flexibility under extreme temperature variations encountered as the satellite enters and leaves occultation. The epoxy adhesives are more rigid and are generally applicable to solar arrays that encounter minimum temperature variations during the mission lifetime. In all cases, adhesives used on solar cell assemblies have been proven by actual use in space and a wide variety are available depending on the particular mission and its requirements.

Interconnections - Bus Bars

Interconnection design involves parallel and series connection between solar cells. A wide variety of configuration for interconnections have been used in flight solar panels. In general, the interconnections used to date have involved assembly steps in which hand-soldering

was performed close to or on cells. Techniques are being developed to automate solar cell submodule fabrication and this procedure should be available industry wide by 1970.

Many materials have been used for interconnections on various flight spacecraft; some of which were titanium, silver, copper, molybdenum and kovar. Each of these materials has advantages and disadvantages. The materials are usually gold or silver plated to decrease resistivity and increase solderability. The factors to be considered in interconnector design include:

1. Thermal expansion compatibility
2. Thermal conduction
3. Solderability
4. Electrical resistance
5. Applicability of automated assembly techniques
6. Mechanical springback interaction with cells
7. Weight
8. Reliability (see Section on Solar Cell Reliability)
9. Compatibility for use with different thickness solar cells

Typical bus bar weight including solder, is approximately 0.03 lbs/sq ft which is a small part of the total array weight.

Insulation

The solar cell assemblies must be adequately insulated from the substrate in order to prevent electrical short circuits which could degrade the performance of the solar array. Typical insulations that have been used on flight spacecraft have included fiberglass or mylar sheeting between the substrate core and solar cell adhesive and organic or inorganic dielectrics sprayed or hand painted on the substrate skin. In many cases, the insulation is also used as a thermal control surface; therefore it should not degrade in the space environment. It has been found experimentally that inorganic paints or dielectrics are much more resistant to uv degradation than organic coatings and thus

for missions where critical thermal control is required, inorganic coatings should be used.

Array Substrate and Framework

It has been questioned whether present technology can support the design of rigidized lightweight solar cell substrates larger than those of OAO and NIMBUS (236 sq ft and 48 sq ft, respectively). Yet the requirement for larger, more powerful arrays is continuing, such as for the electric propulsion missions. There are studies presently programmed to evaluate the feasibility of fabricating solar arrays capable of producing many kilowatts of electrical power with a specific weight of 50 lbs/kW(e) or less. These solar arrays, if developed, would require several thousand square feet of area. Orientation to normal incidence sunlight is a requirement to minimize weight.

The structural, thermal, guidance, and communications problems associated with integration of such large arrays into a spacecraft would require a design that can employ fabrication techniques and materials not previously used in array fabrication. Structures being investigated presently include: flat, rigid panels hinged together by various methods; semi-rigid structures and completely flexible structures. The following paragraphs discuss lightweight, rigid structures suitable for use as substrates for large area photovoltaic systems.

The lightweight rigid substrate must support the solar cells, wiring and other equipment and be strong enough to support its own weight during launch and possible orbital maneuvers. The substrate and substrate frame are designed to provide a definite separation of the fundamental frequencies from the natural frequencies of the attitude control system. A typical substrate and frame structure that has been proven in space use is the one used for the Mariner vehicle. This structure allowed a low temperature operation through good thermal

design which improved the cell efficiency and increased the power level. This type of structure has proven to be very light and has a high stiffness/weight ratio.

The flat rigid substrates which are presently being used generally consist of an aluminum honeycomb structure with an aluminum, titanium, or fiberglass facing sheet. Figure 17 illustrates two types of substrates in present use. They are the honey comb structure, typical of 770 program and corrugated sheetmetal, typical of Mariner and Ranger.

Solar Photovoltaic Array Configuration

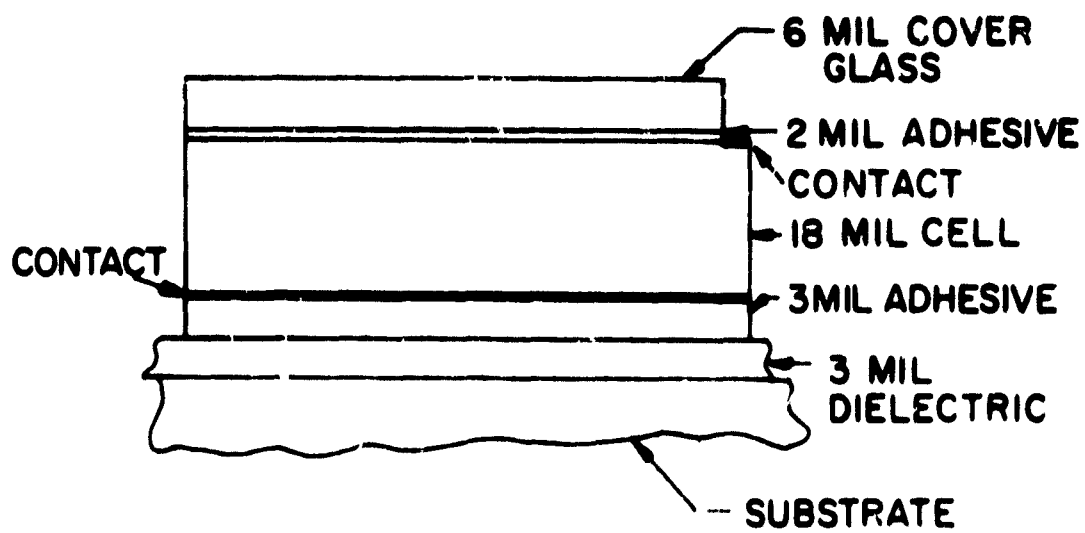
In considering various solar array configurations, several basic patterns and designs may be chosen. These include:

- a. Sun-oriented solar array
- b. Semisun-oriented array
- c. Nonoriented, body-mounted solar array
- d. Non-oriented paddles

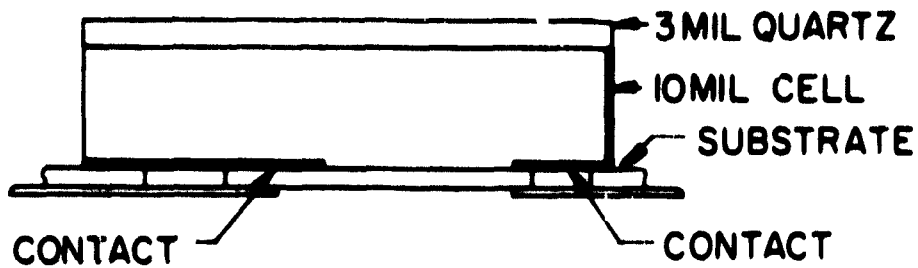
The sun-oriented, flat panel, has size and weight advantages; however, some critical areas exist in its integration with the vehicle.

Since the vehicle attitude control system may be used to aim the antenna system, a separate positioning system would be required for the solar array. Thus, bearings would be needed to allow rotation of the array, and slip rings, for a rotary transformer would be required for power transfer.

The semioriented and nonoriented paddles, have been used on many spacecraft such as IMP, OAO, Explorer XII, etc., and have proven quite feasible. A major problem area with the use of paddles is shadowing of portions of the solar array by other paddles or the spacecraft itself. Two electrical means are available to minimize these losses.



B. TYPICAL "CELL STACKS" IN CURRENT SOLAR PANELS



C. ADVANCED CELL STACK USING "WRAP-AROUND CELL"

**Figure 17. Two Types of Substrates in Current General Use
 (Note: Wrap-around Contacts Give 4 Percent Greater Active Area.)**

The cells may be arranged to insure that only small sections are lost to shadowing, or switching mechanisms can be used to take shadowed sections out of the electrical circuit.

The nonoriented, body-mounted array has been successful in the Syncom series and Early Bird satellites. The major problem with this array is low utilization of the total solar cell active area and possible temperature variations across the array. However, for low power outputs, this array is the simplest to incorporate into a space vehicle. Assuming 10 watts per sq ft for an oriented array, a nonoriented, body-mounted structure requires approximately five times the total area of the oriented array, or equivalently the specific power is 2 watts per sq ft. For a 200 watt system, 100 sq ft of surface area is required. Table V summarizes the area required to supply 200 watts using a sun-oriented, a nonoriented paddle array, and a nonoriented body-mounted array.

TABLE V
ARRAY AREA FOR 200-WATT SYSTEM

	Sun-Oriented Panel	Nonoriented Paddle	Nonoriented, Body-Mounted Array
Area	20 sq ft	65 sq ft	100 sq ft

1.2.2.3 Current Technology

The silicon solar cell power system is the only long-term power source which has been actually demonstrated in space. In this section, the developments' status and design characteristics of present solar power systems are discussed. Advanced developments which will offer weight and cost advantages will be discussed in the next section.

The technology of photovoltaic system design and fabrication has been continuously improved since the launching of the first spacecrafts. Appreciable weight reductions have been accomplished and much more is expected in the future. At present, only the 1 x 1 cm, and 2 x 2 cm silicon cell are in use on solar photovoltaic arrays. The 2 x 2 cm cell is becoming more common and most photovoltaic systems to be used in the late 1960's will incorporate the 2 x 2 cm cell.

The most advanced oriented solar cell panels that have been built up to the present time are those for the Mariner, Ranger, and Surveyor vehicles. The Ranger and Mariner panels are rectangles, approximately 2.5 ft x 5.5 ft with 6-mil coverslides and the panel weighs 1.5 lbs per sq ft (21 lbs total) including substructure, adhesives, cells, coverslides, wiring and attachment brackets. The Surveyor panel is approximately 9 ft² with 6-mil coverslides and the panel weighs about 8.5 lbs or a specific weight of 0.94 lb/ft². During the next several years, solar panel specific weights will be reduced appreciably, even for much larger panels. A weight figure of 1.0 lb/ft² is a reasonable estimate of the obtainable state-of-the-art in the next five years for the larger panels which will be used in multi-kilowatt systems. For long duration missions operating in the Van Allen belt, the weight of thicker coverslides must be included which would therefore increase the specific weight of the photovoltaic array. The state-of-the-art 1967 for solar photovoltaic arrays, both panels, paddle and body-mounted arrays for a large number of flight spacecraft indicates an array of specific weight from 0.7 lbs (Explorer XII 15.3 ft²) at a minimum to 1.6 lb/ft² (for NIMBUS B, 48 ft²). These values are typical of the practical state-of-the-art obtainable in the 1960-1970 time period.

The specific weight of both the entire solar array and its components is decreasing and the expected trends are shown in Fig. 18. The lower curve shows the specific weight of the substrate/frame and it can be seen that in 1962 the state of the art was approximately 1.2 lb/ft² (Ranger).

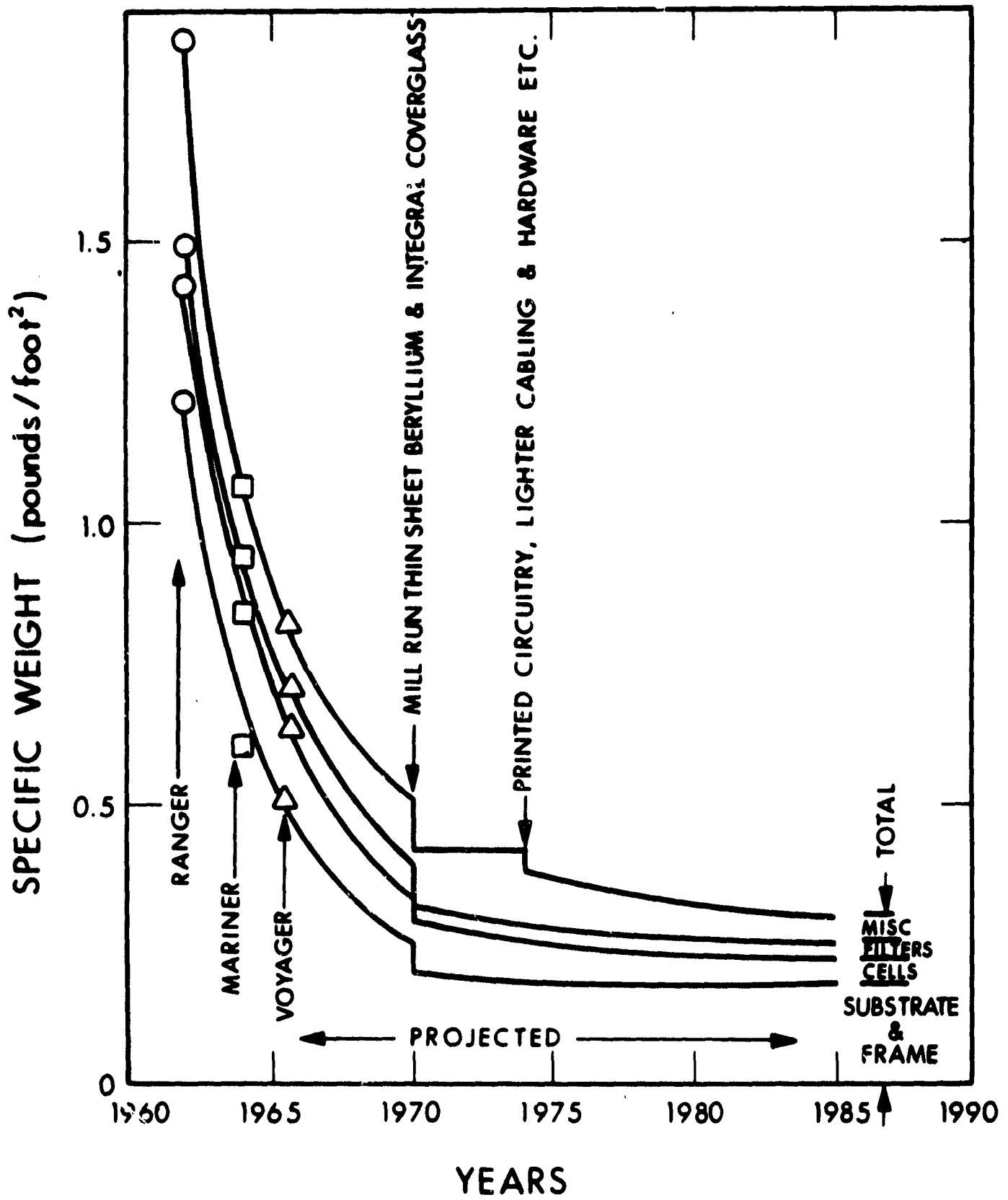


Figure 18. Silicon Photovoltaic Solar Array Weight Trends

Specific weights have been decreasing until at the present time a specific weight of 0.5 lb/ft^2 is obtainable (Voyager). The specific weight of the substrate/frame is also expected to decrease as newer substrate designs are introduced. A step-decrease in weight is predicted in the early 70's when beryllium substrates and beryllium structures are expected to be used extensively. The specific weight of the substrate/frame should then level out to a minimum value of approximately 0.18 lb/ft^2 .

The second curve shows the expected decrease in solar cell specific weight as increased efficiency thin cells are developed. The probable minimum practical thickness for silicon solar cells is 4-mils which gives a specific weight of 0.045 lb/ft^2 .

The third curve shows the expected decrease in coverglass weight after 1970 when integrated coverglasses become items of standard use. Before 1970, the minimum coverglass thickness is 6-mils of SiO_2 which gives minimum radiation protection but practical thermal control. The thin (2-mils or less) integrated coverglass will give the same thermal control and indications from Lockheed (see Sec. 3.2.2.2) are that radiation protection using organic-metallic filters is superior to that of much thicker coverglass. The expected minimum specific weight for coverglass will be approximately 0.02 lb/ft^2 .

The top curve shows the expected trend in total array specific weight including such items as adhesives, bus bar, solder, paints, hardware, cabling, etc. The specific weight of these miscellaneous items, taken as a group, is shown to decrease uniformly from a maximum value of 0.32 lb/ft^2 in 1962 to approximately 0.13 lb/ft^2 obtainable at present. The specific weight is then expected to remain fairly constant until the use of integrated cover-glasses eliminates the need for coverglass adhesives. Improvements are also expected in decreasing hardware requirements and minimizing cabling weights by improved designs. The expected minimum total array specific weight after 1980 is 0.25 lb/ft^2 .

1.2.2.4 Projected Technology

The development of lightweight rigid structures incorporated into large area, lightweight photovoltaic systems will continue into the 1970-1985 time period with improvements in decreasing structural weight and improving cell performance over that which has been obtained in the 1960-1970 time period.

The development of new, lightweight, rigid structures such as the follow-core electroformed beryllium substrates, lightweight honeycomb made of titanium, or beryllium, etc., would aid appreciably in decreasing array weight without detracting from array reliability. The specific weight of the new structures will decrease from approximately .3 - .5 lbs/ft² to 0.15 - 0.30 lb/ft². Yet, the panels will demonstrate the same structural rigidity and strength as that obtainable from the heavier substrates used at present. Table VI A, B, and C illustrates a projected solar array weight breakdown as a function of coverglass thickness for 4-mil, 8-mil and 12-mil solar cells in the 1970-1985 time period. It can be seen, depending on the coverglass thickness, which is a function of orbital attitude and inclination (location within the Van Allen belt), the total array specific weight without attachments or deployment mechanisms, ranges from a minimum of 0.385 lbs/ft² utilizing 4-mil solar cells and a standard 6-mil coverglass to 1.16 lbs/ft² for a 12-mil solar cell utilizing a 60-mil coverglass. Table VI A, B, and C shows the lb/kW as a function of coverglass thickness utilizing 4, 8 or 12-mil solar cells with the efficiencies shown in the Tables. The minimum specific power that can be practically obtained utilizing conventional fabrication techniques presently in use, is 43 lbs/kW. However, the continued advancement of developments now in the experimental stage such as integrated coverglasses, and large area or thin cells will lead to specific weights much less than that obtainable utilizing conventional fabrication techniques. The curves shown in Fig. 19 illustrate the performance

TABLE VI-A SOLAR ARRAY WEIGHT BREAKDOWN AS A FUNCTION OF COVERGLASS THICKNESS FOR 8-MIL SOLAR CELLS

Coverglass Thickness (mils)	6	12	20	30	45	60
Coverglass Weight (lb/ft ²)	0.07	0.14	0.24	0.35	0.53	0.70
Solar Cell Weight	"	"	0.20	"	"	"
Adhesives Weight	"	"	0.02	"	"	"
Bus Bar and Solder Weight	"	"	0.03	"	"	"
Cabling and Hardware Weight	"	"	0.05	"	"	"
Dielectric and Paint Weight	"	"	0.03	"	"	"
Substrate Weight	<u>0.14</u>	<u>0.14</u>	<u>0.15</u>	<u>0.16</u>	<u>0.17</u>	<u>0.19</u>
TOTAL	0.43	0.50	0.61	0.73	0.92	1.11

TABLE VI-B SOLAR ARRAY WEIGHT BREAKDOWN AS A FUNCTION OF COVERGLASS THICKNESS FOR 12-MIL SOLAR CELLS

Coverglass Thickness (mils)	6	12	20	30	45	60
Coverglass Weight (lb/ft ²)	0.07	0.14	0.24	0.35	0.53	0.70
Solar Cell Weight	"	"	0.14	"	"	"
Adhesives Weight	"	"	0.02	"	"	"
Bus Bar and Solder Weight	"	"	0.03	"	"	"
Cabling and Hardware Weight	"	"	0.05	"	"	"
Dielectric and Paint Weight	"	"	0.03	"	"	"
Substrate Weight	<u>0.14</u>	<u>0.14</u>	<u>0.15</u>	<u>0.16</u>	<u>0.17</u>	<u>0.19</u>
TOTAL	0.48	0.55	0.66	0.78	0.97	1.16

TABLE VI-C SOLAR ARRAY WEIGHT BREAKDOWN AS A FUNCTION OF COVERGLASS THICKNESS FOR 4-MIL SOLAR CELLS

Coverglass Thickness (mils)	6	12	20	30	45	60
Coverglass Weight (lb/ft ²)	0.07	0.14	0.24	0.35	0.53	0.70
Solar Cell Weight	"	"	0.045	"	"	"
Adhesives Weight	"	"	0.02	"	"	"
Bus Bar and Solder Weight	"	"	0.03	"	"	"
Cabling and Hardware Weight	"	"	0.05	"	"	"
Dielectric and Paint Weight	"	"	0.03	"	"	"
Substrate Weight	<u>0.14</u>	<u>0.14</u>	<u>0.15</u>	<u>0.16</u>	<u>0.17</u>	<u>0.19</u>
TOTAL	0.385	0.455	0.565	0.685	0.875	1.065

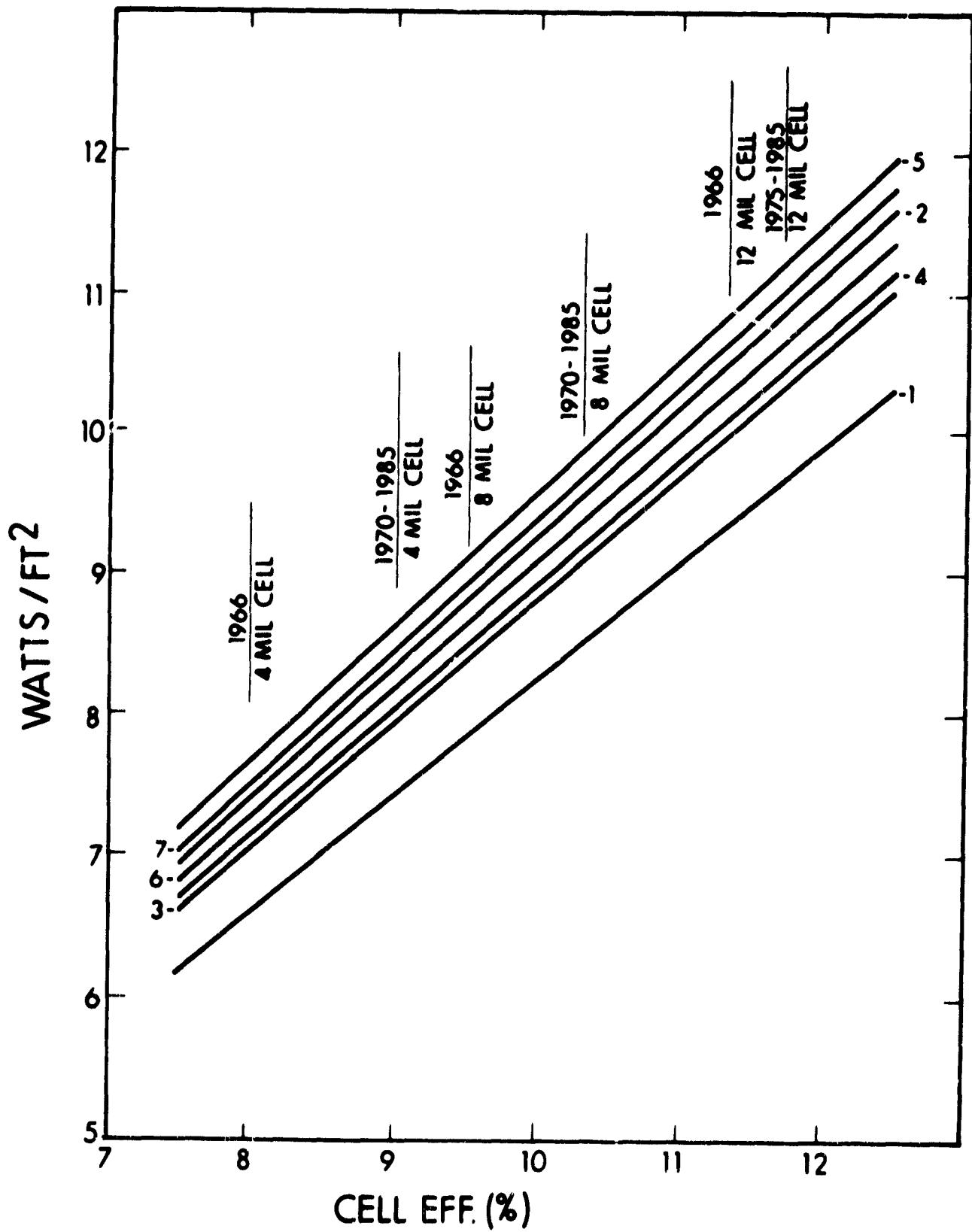


Figure 19. Power Area versus Cell Efficiency for Various Cell Configurations

to be expected using various combinations of cells and coverglasses. These curves take into consideration the type of coverglass, efficiency of solar cell, assembly and filter loss, and changes in packing factor. The parameters for each curve are summarized in Table VII. The 4-mil and 8-mil cells will require improvement even greater than that expected in order to successfully compete with the 12-mil solar cells in terms of watts/sq ft output power.

Although 12-mil solar cells have a higher power output per square foot, it can be seen from Table VIII that the 3 x 3 cm 4-mil cell with wrap-around contacts and integrated coverglass will provide the lightest weight per kW of any of the configurations considered. However, it is questionable at this time whether 4-mil cells will be available even in the 1970-1985 time period in the 3 x 3 cm size due to their extremely delicate nature. Assuming that 4-mil cells will not be available in the 3 x 3 cm size, during any period of this study, examination of Fig. 19 and Table VIII indicates the optimum cell/coverglass configuration to be a 3 x 3 cm 8-mil wrap-around solar cell with one-mil integrated coverglass. This configuration will give 28.7 lb/kW and produce 9.7 watts/sq ft in the 1970-1985 time period.

In conclusion, it is projected that the state-of-the-art of photovoltaic power systems utilizing high efficiency silicon solar cells and lightweight rigid structures will be capable of 25 lbs/kW and 10 watts/sq ft. This means that for a multi-kilowatt array producing, for example 10 kW electrical power, the photovoltaic array will weigh 250 lbs and have an area of 1,000 sq ft. These weights and areas will be well within the boost and envelope capabilities of the launch vehicles expected to be used in the 1970-1985 time period. It can also be expected that solar photovoltaic arrays supplying up to 50 kW electrical power will be capable of being placed in orbit without undue restrictions on other components of the spacecraft.

TABLE VII
COVERGLASS CHARACTERISTICS

<u>Cells and Modifications</u>	<u>α</u>	<u>ϵ</u>	<u>α/ϵ</u>	<u>T*</u>	<u>% Power of Power at 28°C</u>	<u>% Power Gain from Bare Cell</u>
Ideal cell	0.70	1.00	0.70	28°C	100	-
Bare cell	0.935	0.368	2.54	85°C	777	-
Cell with $\approx 1.11_{\mu}$ SiO coating	0.874	0.642	1.36	63°C	86%	4.3%
Cell with 0.006 inch glass and A-R coating	0.813	0.835]	0.974	46°C	92%	15.8%
Cell with 0.006 inch glass, 415 m μ blue and A-R coatings	0.81	0.835	0.97	46°C	92%	8.5%
Cell with 0.006 inch glass, 415 m μ blue, 1.15 μ red and A-R coatings	0.70	0.835	0.84	35°C	96%	11.2%

*Assuming a rear surface emissivity of 0.9 radiating to space.

TABLE VIII
COMPONENT SUMMATION

(4) Curve	Cell Size (cm)	Cell Thickness (mils)	Cell Contact	Filter	Filter Thickness (mils)	Filter Loss	Other Losses	Cells /ft ²	Packing Factor (percent)	lb/kt 1965	(1) lb/kt 1970
1	2 x 2	12 8 4	Conventional	Conventional	6	0.96	0.90	205.05	88.9	42.6 44.7 45.7	41.5 1.2 -0.6
2	2 x 2	12 8 4	Wrap-around	"	4	0.96	0.90	218.43	94.6	37.2 38.3 38.5	35.6 35.3 34.2
3	2 x 2	12 8 4	"	Integrated	1	0.913	0.90	218.43	94.6	35.2 35.7 35.0	34.0 33.0 31.1
4	3 x 3	12 8 4	Conventional	Conventional	4	0.96	0.90	98.50	95.4	36.3 37.0 36.4	35.0 34.1 32.4
5	3 x 3	12 8 4	Wrap-around	"	4	0.96	0.90	100.12	96.9	34.3 34.9 34.3	33.1 32.1 30.5
6	3 x 3	12	"	Inte- grated (1966)	1	0.913	0.90	100.12	96.9	32.2	31.2
7	3 x 3	12	"	Inte- grated (1970) (1985)	1	0.94	0.90	100.12	96.9	32.1 30.7 31.2	29.6 27.4 30.1
		8 4								31.1 29.8	28.7 26.5

NOTES:

- (1) Weights include cell, filter, filter adhesive, cell adhesive, solder, bus bar, dielectric, paint, cabling, and electrical hardware.
- (2) Weights do not include mechanisms, substrate, frame or struts.
- (3) 0.1212 lbs/ft² allowed for dielectric, paint, cabling and electrical hardware.
- (4) Reference H3. 16.

1.2.3 SOLAR PHOTOVOLTAIC ARRAY CONCEPTS

This section discusses the photovoltaic power sources which are applicable to solar electric propulsion. The discussion will be limited to the power systems which have a specific weight of 50 lb/kW or less. Power systems which do not presently meet the above criterion but are potentially capable of yielding the 50 lb/kW performance will also be discussed.

1.2.3.1 Status of Development

1.2.3.1.1 Array Concept

There are two array concepts which are suitable for the electric propulsion application. The first consists of rigid-frame solar panels which are folded together to form a launch package. Once in orbit the panels are deployed in an accordion fashion. The advantageous features of this concept are: (1) demonstrated experience from a design, fabrication, and flight-proven hardware standpoint; (2) superior structural characteristics in terms of withstanding retromaneuver and/or artificial g loads. The main disadvantage is the large packaging volume required. For this reason the array size will be limited to approximately 50 kW for the Centaur class of launch vehicle.

The second approach is to employ a rollup solar array. For this concept the solar cells are mounted on a flexible substrate. In a stowed position the array is rolled in layers forming a cylindrical body. Deployment is effected by extending mechanisms which may be extending booms, scissors mechanism, or the substrate itself. The main advantage of the concept is its extremely compact volume. It is thus conceivable to speak about a megawatt size solar array. The problems of this concept lie in the areas of insufficient operating experience and the structural dynamic characteristics.

1.2.3.1.2 Power System Size

The development status of the solar array may be categorized according to the power system size as follows:

- Flight proven hardware - up to approximately 1 kW
- Detail conceptual design - 20 to 50 kW
- Paper study - 1 to 5 MW

A rigid frame array which is flight-proven up to approximately 1 kW size has been studied conceptually up to 50 kW. Several arrays of approximately 50 square feet have been fabricated for demonstration purposes. (A demonstration panel normally consists of mock-up cells mounted on substrate with deployment mechanism. The primary purpose is to demonstrate feasibility in deployment and structural integrity of the concept.) The rollup array has been studied conceptually up to 20 kW.

1.2.3.1.3 Areas Requiring Further Development

Based on the above discussion it is clear that a detailed conceptual design should be performed for the megawatt size array, with particular emphasis on the rollup concept. The primary objective will be to obtain the performance characteristics and parametric data. The conceptual study should include the following:

- Detailed system layout
- Study of deployment and retraction techniques
- Packaging study
- Structural analysis with particular emphasis on dynamic characteristics associated with launch, retromaneuver and artificial g load requirements.
- Manufacturing techniques to reduce array cost to manageable level.

1.2.3.2 Rigid Frame Solar Arrays

Two rigid array concepts are capable of meeting the 50 lb/kW (or less) requirement. These are the biconvex, electroformed concept developed by EOS and the box-frame approach being developed by Boeing (see Table IX).

1.2.3.2.1 EOS Biconvex Array (Ref. 1-12)

42 lb/kW Solar Panel

Approximately a year ago EOS initiated, under NASA sponsorship, a lightweight solar panel development program. Under this program a demonstration panel was produced which has a specific weight of 42 lb/kW. The demonstration solar panel confirmed the soundness of the EOS curved-shell, electroformed structure concept. The concept has a performance potential of 27 lb/kW. A second year follow-on effort is being directed toward that goal.

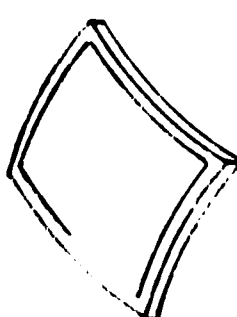
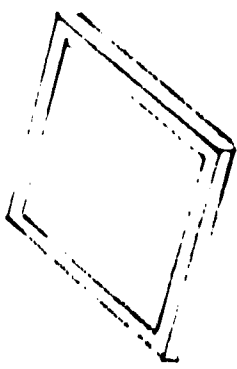
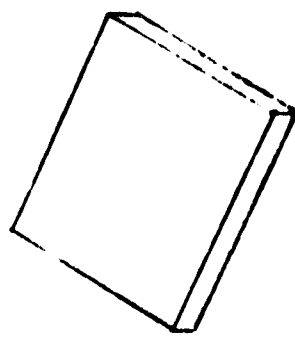
The basic structure of the panel consists of an electroformed nickel hollow-core substrate held in a biconvex position by an aluminum frame. Covering the hollow-core structure is a sheet of fiber glass upon which the solar cells are placed. Figure 20 shows a typical panel construction. Figure 21 is a photograph showing the demonstration panel with partial mounting of solar cells and anodized aluminum blanks to simulate the active cells.

10 kW Power System Conceptual Design

A conceptual design of a 10 kW power system was made to evaluate the effects of system component interaction. Such interaction affects the optimum size of the solar panel module, deployment mechanisms and

TABLE IX

TYPICAL RIGID ARRAY CONCEPTS

ORGANIZATION	SKETCH	WORK DESCRIPTION	SPECIFIC WEIGHT	DEPLOYMENT MECHANISM	COMMENTS
EOS		Electroformed Nickel Substrate with Aluminum Frame	19 $\frac{\text{kg}}{\text{kW}}$ 42 $\frac{\text{lb}}{\text{kW}}$	Hinges, Springs, and Latches Alternate Mechanisms are Scissors or Lazy Tongues etc.	Potential 27 $\frac{\text{lb.}}{\text{kW}}$ 12 $\frac{\text{kg/kW}}$ Requires Large Packaging Volume.
BOEING		Beryllium Frame with Fiber Glass Substrate	18-23 $\frac{\text{kg}}{\text{kW}}$ 40-50 $\frac{\text{lb}}{\text{kW}}$	Same as Above	Potential 40 $\frac{\text{lb.}}{\text{kW}}$ 18 $\frac{\text{kg/kW}}$ Requires Large Packaging Volume.
EOS LOCKHEED ELECTRONICS HUGHES TRW AND OTHERS		Aluminum Honeycomb Substrate	45 $\frac{\text{kg}}{\text{kW}}$ 100 $\frac{\text{lb}}{\text{kW}}$	Same as Above	Proven Hardware.

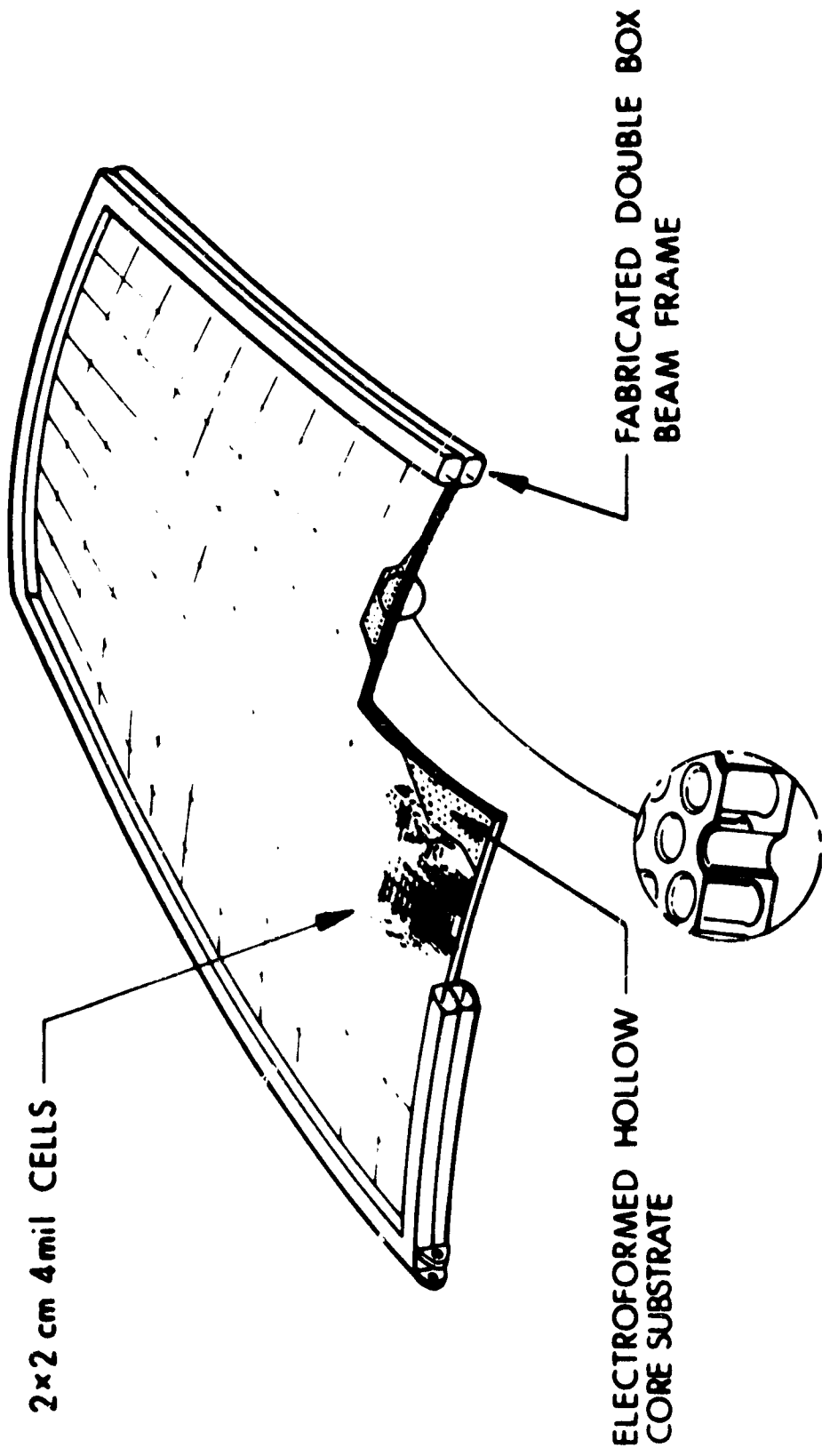


Figure 20. Typical Panel Structure

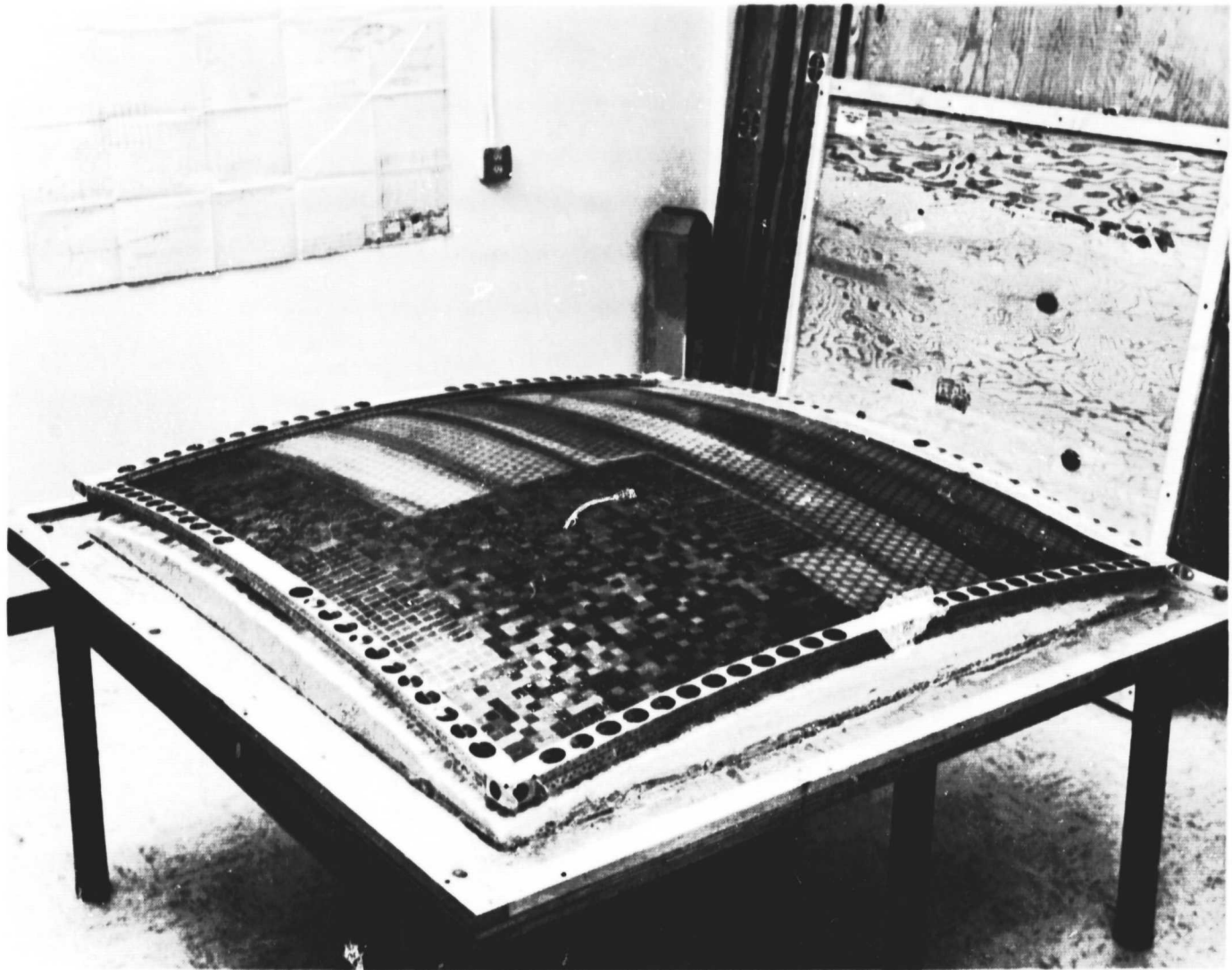


Figure 21. Five-Foot-Square Biconvex Demonstration Panel

method of array deployment and the array packaging problem. The 10 kW array is capable of tolerating the environment of an Atlas/Centaur vehicle and can be stowed within a shroud similar to the OAO. This conceptual study has resulted in the selection of a 5-foot-square panel as the optimum size. The array overall specific weight is determined to be 42 lb/kW, including the electrical cabling and deployment mechanisms. The configuration of this power system (suitable for Jupiter flyby mission) is shown in Fig. 22.

27 lb/kW Solar Panel

The weight of the solar array which was described previously can be further reduced to 27 lb/kW level if the following design modifications and technology advances are made:

- Use of electroformed aluminum hollow-core as the substrate structure.
- Use of beryllium as the panel frame material.
- Development of 4-mil solar cells with 1-mil integrated cover glass capable of producing 10 W/ft² at standard conditions.
- Incorporation of major electrical cables into the frame design so that this material serves the dual purpose of conducting current and adding to the structural strength.
- Incorporation of thermal control surfaces into the metallic substrate by anodizing.
- Use of better production techniques to decrease the adhesive weight.

In summary, the technology developed for the 42 lb/kW panel can be further improved to yield a 27 lb/kW system. The required development effort will be relatively modest. The estimate of the advanced solar arrays incorporating all the improvement outlined above is shown in comparison with the current solar arrays in Table X.

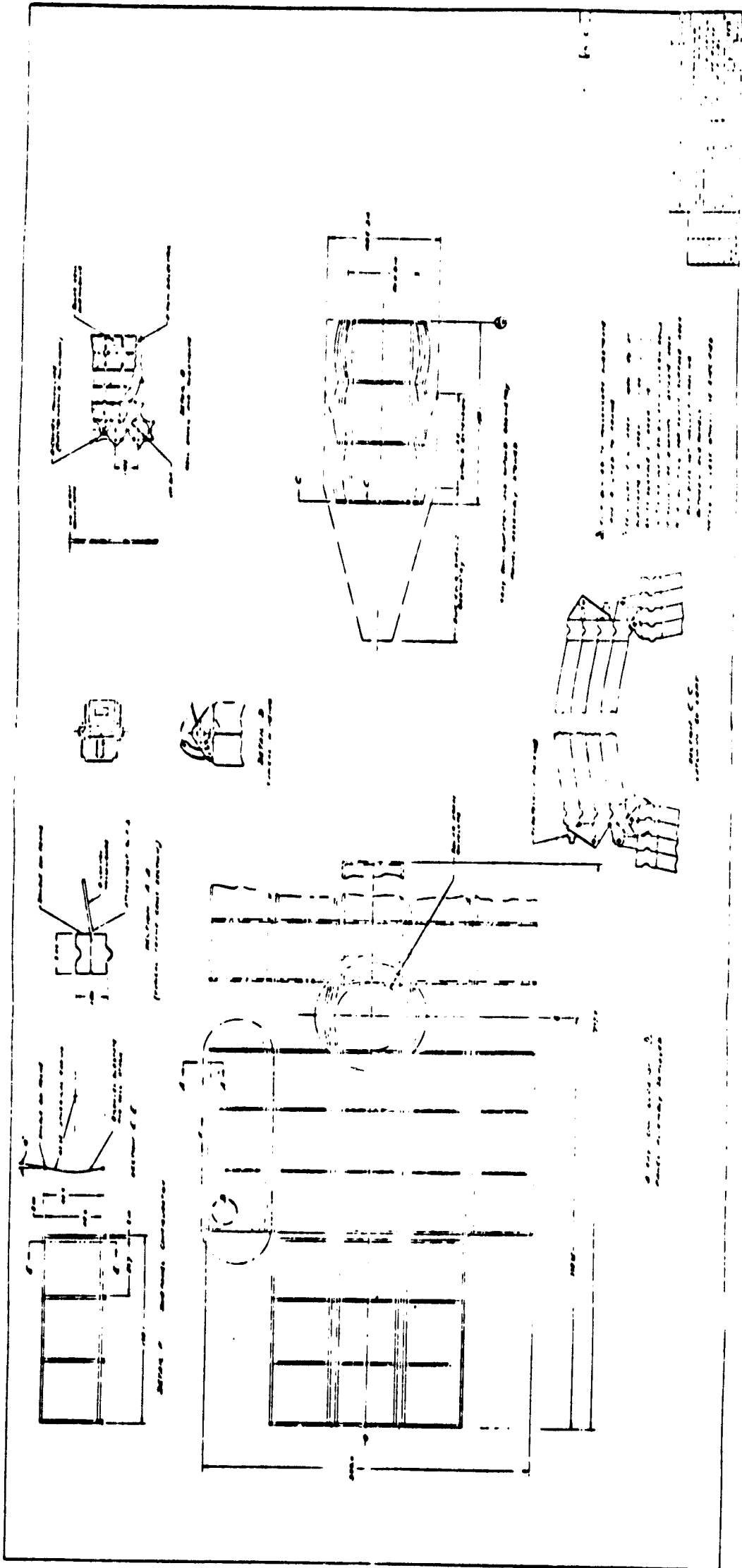


Figure 22. EOS Configuration for 10 kW Solar Array

TABLE X

PROJECTED WEIGHT AND POWER CHARACTERISTICS, 10.4 kW ARRAY

Item	Description	Demonstration Panel Design		Array Design	
		lb/ft ²	lb	lb/ft ²	lb
Cover glass	3-mil microsheet 2 x 2 cm	0.0394	41.0		
	1-mil integral cover glass 2 x 2 cm			0.0131	13.7
Filter adhesive	2-mil RTV-602	0.0096	10.0		
	None			- - -	- -
Solar cell	4-mil conventional contact 2 x 2 cm	0.0530	55.1		
	4-mil wraparound contact 2 x 2 cm			0.0530	55.1
Interconnector	Bus bar and solder	0.0200	20.8		
	Printed circuit back-contact			0.0100	10.4
Cell adhesive	4-mil RTV-40	0.0207	22.8		
	Same			0.0207	22.8
Dielectric	1-mil H-film	0.0072	7.9		
	Same			0.0072	7.9
Dielectric adhesive	2-mil RTV-40 18% of area	0.0037	4.1		
	Same			0.0037	4.1
Thermal control paint	3-mil laminar X-500	0.0240	29.7		
	None, anodized substrate			- - -	- -
Cabling and hardware	Separate cable bundles	0.0228	28.2		
	Major cabling incorporated in frames			0.0050	6.2
Mechanisms	For deployment	0.0376	46.7		
				0.0376	46.7
Substrate	2-mil electroformed nickel	0.0664	73.0		
	Electroformed aluminum alloy			0.0464	51.1
Frame	10-mil aluminum box beam	0.0815	101.0		
	Beryllium frame			0.0538	66.7
Total	lb	440.3		285.0	
Specific power	W/ft ²	10		10	
Array power	W	10,400		10,400	
Weight/power	lb/kW	42.4		27.4	

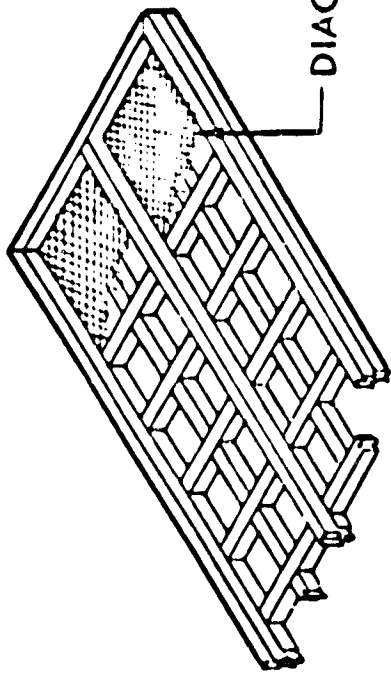
1.2.3.2.2 Boeing Box-Frame Array Concept (Ref. 1-3 and 1-14)

The work performed by Boeing on large area photovoltaic arrays has an objective of achieving a power system capable of producing 48 kW at 50 lb/kW. A typical subpanel consists of thin-walled, double-box-section beryllium frames and single-box-section intercostals. The matrix substrate of pretensioned fiber glass tape is bonded between the frames and to the intercostals. The solar cell modules, consisting of coverglasses, cells, and interconnectors, are then bonded to the substrate. The backs of the cells, covered with a thermal control coating, reject heat directly to space. The individual subpanels are joined together by hinges and latches. The main subpanels deploy when the rotary drive unit retracts a cable which imparts a turning moment about the pulleys and hinges. As each subpanel reaches the fully deployed position, hinge latches are locked.

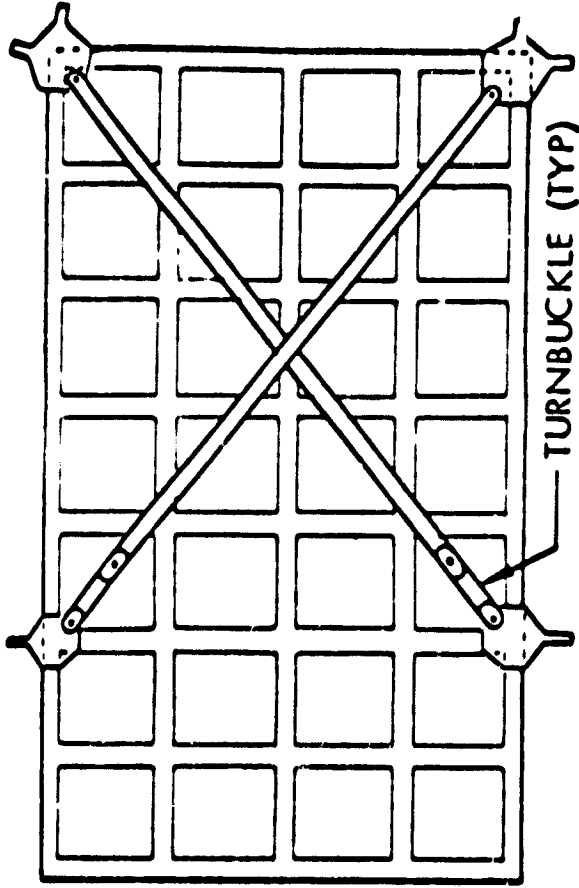
Figure 23 shows a second generation panel which incorporated the necessary changes and improvements determined during the study. This includes: orientation of fiber glass tapes at 45° with respect to the frame; addition of beryllium diagonal bracing; and provision of shear ties and stack clamping for shear transfer between stowed subpanels in the launch mode. Other improvements are: replacement of twisted wire cables with flat aluminum or copper conductors; replacement of back-connected cells by standard front-connected ones; and replacement of 4-mil coverglass with 3-mil covers. The specific weight breakdown is shown in the tabulation below:

● Cell modules	12.3
● Structure	15.1
● Adhesive and thermal coatings	4.4
● Mechanisms	3.8
● Buses	<u>3.2</u>
Total	38.8 lb/kW

REDUCED DEFLECTION



DIAGONAL SUBSTRATE

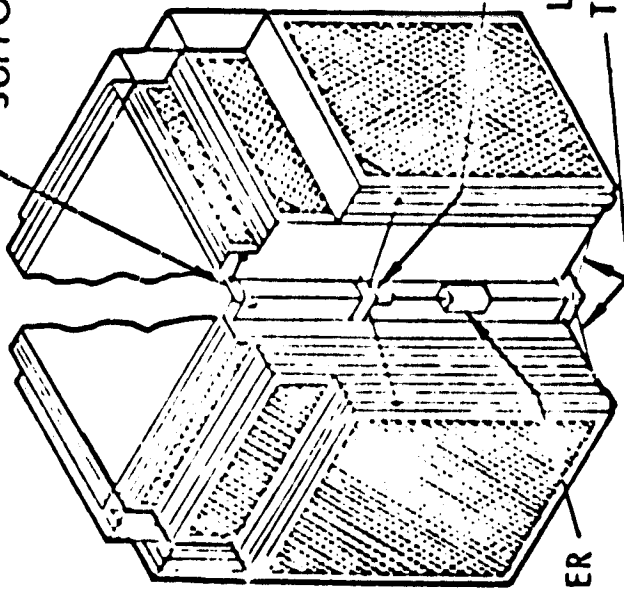


TURNBUCKLE (TYP)

DARK SIDE SUBPANEL 1

DIAGONAL STRUT

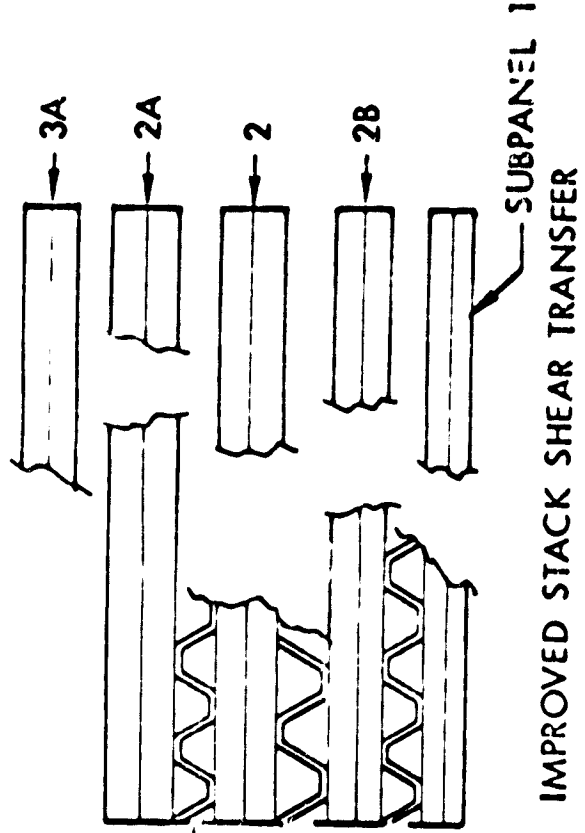
ADDITIONAL SUPPORT TIE



PIN PULLER

UPPER RELEASE PIN

LOWER TENSION TIE RODS



SHEAR TIE (ENLARGED)

IMPROVED STACK SHEAR TRANSFER

SUBPANEL 1

Figure 23. Boeing Box-Frame Solar Array

1.2.3.3 Rollup Solar Arrays

Existing rollup array concepts, either demonstrated or paper study, are summarized in Table XI. All these concepts have the following common features:

- Deployment mechanisms
- Means for solar panel protection during launch, including takeup rolls, cushion pad, casing, etc.
- Structural support
- Substrate
- Electrical components, including solar cell stacks, dielectric, and wiring.



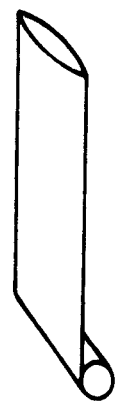
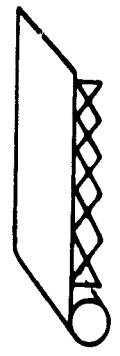

It is therefore possible to synthesize new concepts different from those shown in Table XI. The following paragraph describes some of the array concepts proposed by the industry.

1.2.3.3.1 Hughes Rollup Array Concept (Refs. 1-15 and 1-16)

A rollup solar array concept has been proposed by Hughes. Conceptual designs and analyses have been made on 20 kW power systems to determine the concept feasibility. A 50 square foot demonstration panel has been fabricated for verification of the design procedure and limited environmental tests.

The basic concept employs dendritic solar cells, 1 x 30 cm, bonded to a flexible substrate which supports the cells and associated wiring. In the stowed condition, the array is rolled up together with a thin, protective cushion. The rollup assembly is enclosed in an external shell which provides radial pressure of approximately 0.6 psi. The interwound foam cushion transfers the applied pressure uniformly to the array substrate and prevents any relative motion between substrate

TABLE XI
TYPICAL ROLLUP ARRAY CONCEPTS

Organization	Sketch	Word Description	Specific Weight	Deployment Mechanisms	Comments
Hughes		Extendable booms with fiber glass substrate (dendritic cells)	18 kg/kW (40 lb/kW)	Drive motor De Haviland or Hunter spring booms. (Uses takeup spools for cushion sheets)	Design for 0.003g load. Demonstration model has been built
Ryan		Extendable booms with fiber glass substrate (Uses small silicone pads for cushioning)	36 kg/kW (80 lb/kW)	Drive motor, titanium booms	Design for 0.2g load. Demonstration model has been built
EOS		Substrate itself is the boom	23 kg/kW (50 lb/kW or less)	Sprocket drive with motor. Also takeup spool.	Design for 0.2g load
Fairchild - Miller		Scissors booms with fiber glass substrate	37 kg/kW (82 lb/kW)	Scissors or lazy tongs	"g" load is not indicated. Demonstration model has been built.
Goodyear and Others		Inflatable substrate with chemical injection for stiffening	Not available	Inflation of internal tubes followed by chemical injection	Not retractable

layers and the storage drum during launch environments. Theoretical calculation has indicated that this design will withstand a 60g acceleration without any relative substrate layer movement.

Two types of deployment booms are considered. One is the DeHaviland device with six nested elements. The other is the Hunter spring which is wound at an angle to the boom axis such that when released the spring forms a long conical tube. The deployment scheme relies on the positive action of the extending booms. As the array is being deployed, the foam cushion will be rolled up on a takeup spool. Figure 24 shows the demonstration rollup array in the deployed condition.

The demonstration array has been put through a limited environmental test (such as temperature shocks ranging from -250 to +250°F). The rate of change applied was 50°F per minute.

A conceptual design was made for a 20 kW array to evaluate the potentiality of the demonstration panel in terms of a large system. The array is designed to withstand 0.003g perpendicular to the surface and 0.003 rad/sec² rotation about the principal axis. The weight breakdown for the 20 kW system, based on 10 W/ft² 50°C temperature, and 95 percent packing factor, is listed below.

● Panels (0.168 lb/ft ²)	16.8 lb/kW
● Deployment mechanisms	12.5 lb/kW
● Drums	3.0 lb/kW
● Cushions	1.7 lb/kW
● Covers	1.2 lb/kW
● Takeup spools	0.7 lb/kW
● Rewind mechanism	0.5 lb/kW
● Structure	1.2 lb/kW
● Bus bars	0.6 lb/kW
	<hr/>
Total	38.2 lb/kW

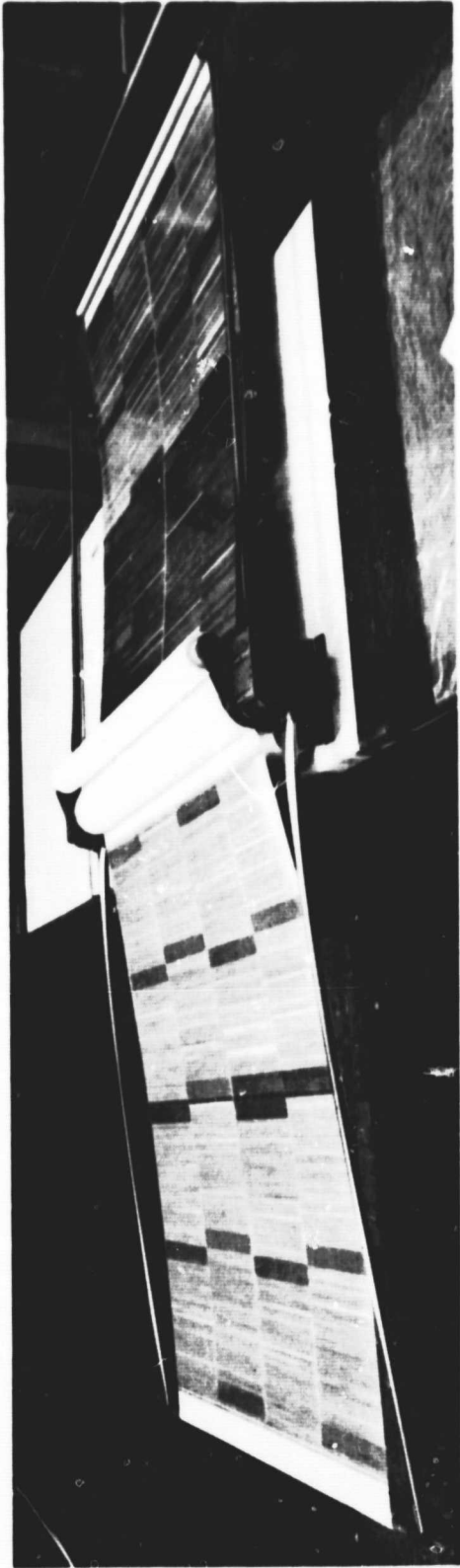


Figure 24. Hughes 50 ft² Demonstration Rollup Solar Array

1.2.3.3.2 Ryan Rollup Array Concept (Ref. 1-17)

A different rollup array approach was taken by Ryan Aeronautical Company. The basic idea of mounting solar cells on a flexible substrate stretched between two extendable booms is the same as with the Hughes approach. The main differences are in the design of the boom and its deployment mechanism, and in the approach of separation and cushioning of substrate layers during the stowed condition.

The array concept has as an objective a power system which has a solar array area of 200 square feet. The array is to be compatible with the Atlas/Centaur vehicle environments as well as with a hypothetical spacecraft similar to the one for a 1969 Mars mission. A 50 square foot demonstration array (without solar cells and wiring) was fabricated. It consists of four 55.8 x 36.6 inch modular panels. The calculated existing specific power is 12.5 W/lb, with a potential growth to 14.5 W/lb (70 lb/kW).

The Ryan boom is made of two titanium ribbons seam-welded together at the two edges. The array is designed to be deployed and retracted many times for purposes of checkout, retromaneuver, etc. When retracted, the boom which has a near circular shape is depressed to a flat surface by a guide sleeve and spring-loaded rollers. As the direction of the storage drum is reversed the pressure on the beam is removed and the beam returns to its original shape. The power required for the drive motor is approximately 10W.

The basic substrate material, selected to withstand the heat sterilization requirement for Mars landing mission, is epoxy-impregnated fiber glass cloth. The substrate thickness is 3 mils; the edge is built up to a thickness of 12 mils. The ends of each substrate are provided with piano-type hinges which permit modules to be easily replaced.

The substrate layer separation and cushioning are provided by half-inch-diameter silicone foam rubber pads mounted on the back surface of the substrate. The pads are faced with 2-mil Teflon sheets. The demonstration array in a deployed position is shown in Fig. 25. The weight breakdown for existing and future arrays is listed below.

	<u>Existing</u>	<u>Future</u>
• Beams	4.9	4.8
• Substrate	2.3	2.3
• Support structure	15.9	12.5
• Mount provision	2.0	--
• Solar cells and wiring	<u>15.0</u>	<u>15.0</u>
• Totals	40.1 lb	34.6 lb
Specific power	12.5 W/lb	14.5 W/lb
Specific weight	80.0 lb/kW	70.0 lb/kW

1.2.3.3.3 EOS Rollup Array Concept

The basic feature of the array concept lies in the use of curved-shell substrates to provide structural stiffness without any assistance of extending booms. This approach departs from other concepts which rely on the booms to provide the required moment of inertia. The Hughes concept, for example, employs De Havilland booms in arriving at the specific power performance of 40 lb/kW, but offering only 0.003g resistance to acceleration. The Ryan approach employs stiffer booms to meet the 0.2g requirement. However, its specific weight is increased to 80 lb/kW.

The stiffness property of a curved shell is well known. This property is derived from the fact the section moment of inertia of a thin, flat structure can be enhanced significantly by providing edgewise restraints to force the structure into a curved surface. The main problem is to devise a means of providing these edge restraints.

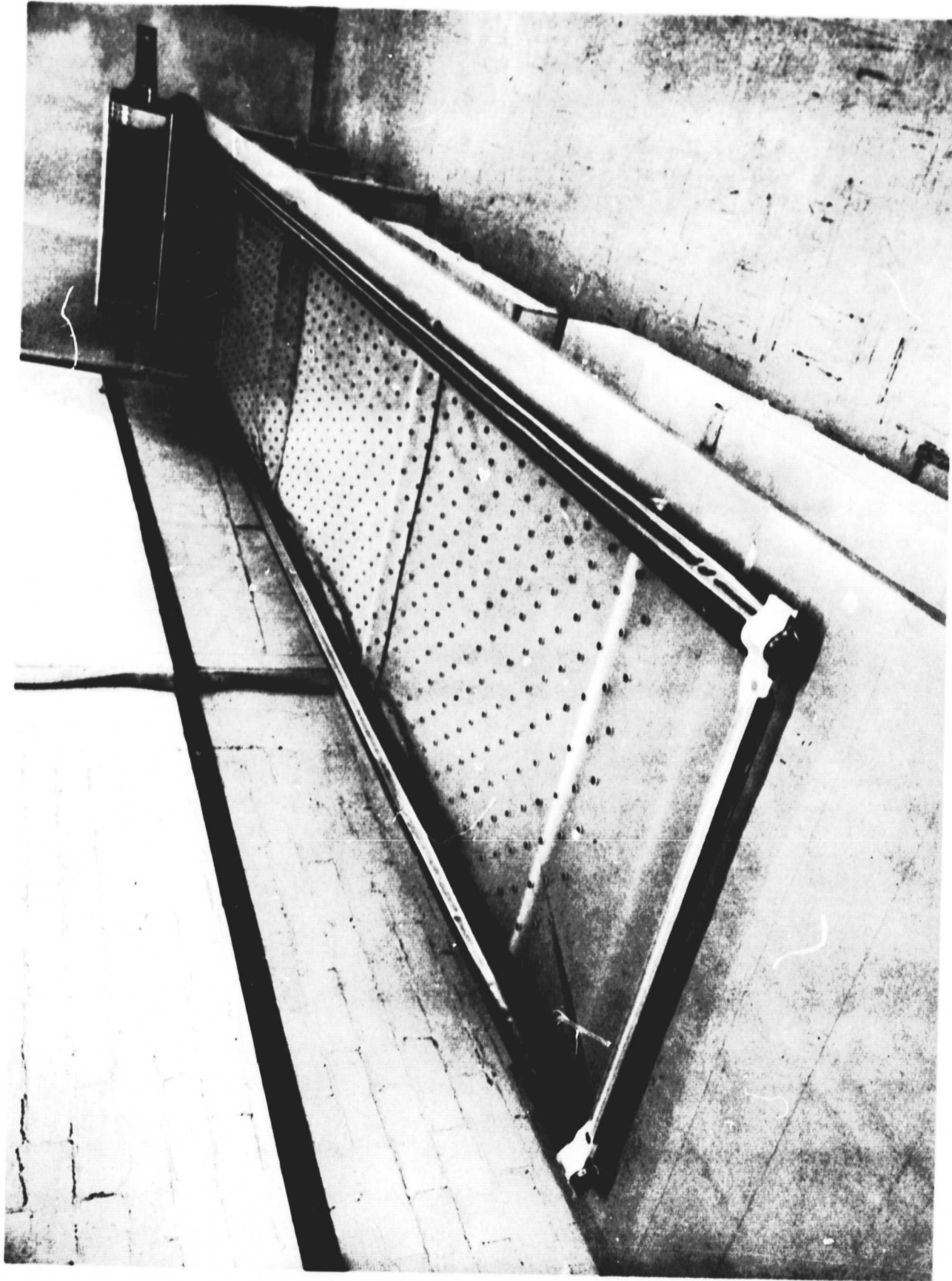


Figure 25. Ryan 50-Square-Foot Demonstration Rollup Solar Array

Figure 26 illustrates a rollup array concept which utilizes the curved-shell approach. The array substrate consists of two beryllium sheets of approximately 7 mils in thickness. The two sheets are bonded together at the edges. Small rectangular holes are provided along the edge in the same manner as a photographic film. These holes fit over a sprocket drive which serves to deploy and retract the solar array.

The deployment mechanism consists of a drive motor, a cushion take-up spool, the sprocket drive, two guide rollers, and tension wires spaced at approximately 18 inches apart.

In the undeployed configuration, the two substrate sheets and the wires lie flat in the untensioned mode. (The far end of the array which is left beyond the guide rollers is an exception. This portion is left in the string-and-bow configuration to facilitate deployment.) Upon command, the sprocket drive which is chained to the motor shaft will start to feed the array through the guide rollers, and the cushion pad will be taken up simultaneously. The guide rollers are positioned in such a way that the two substrate sheets bow slightly. The angle formed between the sheets will be approximately 10° . At this angle, the ratio of the plan-form to the curved surface will be about 0.98. Final selection of the subtended angle will be determined from trade studies since a large angle will result in a stiffer structure and less weight but the power output per unit area will also be less.

The two beryllium sheets are kept in the bow shape by tension wires. There are two approaches which appear to be attractive for keeping the wires under tension. The approach is to use one continuous piece of wire which is threaded diagonally through flexible eye bolts attached to the array edge. As the array is deployed the slack of the wire will be taken up by a take-up spool which is geared at an appropriate ratio to the sprocket drive. The second approach is to use individual tension

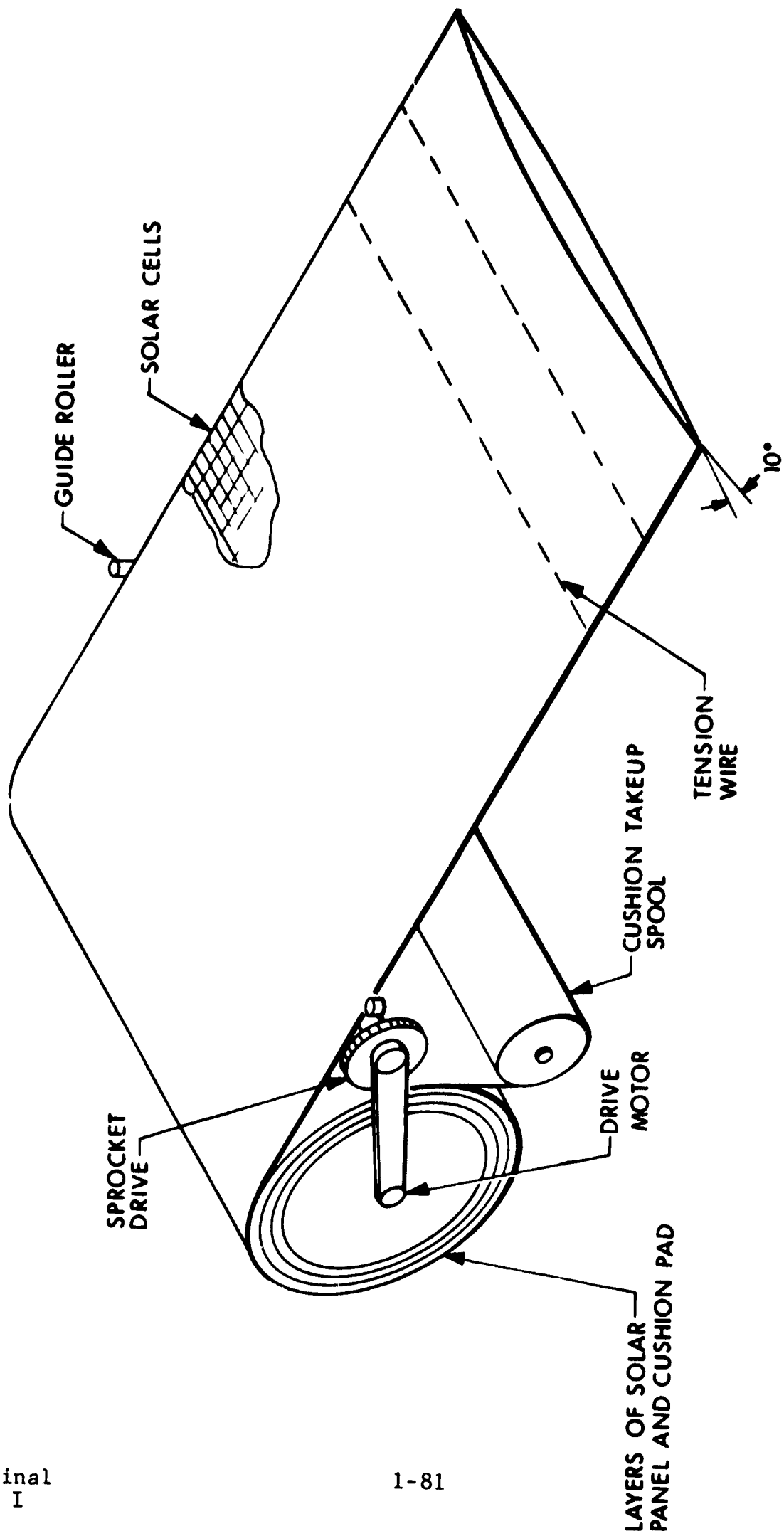


Figure 26. EOS Rollup Array Concept

wires. Each wire has one end permanently tied to the array edge with the other end free. As the array is fed past the roller a mechanism grasps the free end and pulls the wire in tension. The tension wire is held in place with latching spring mechanism. During retraction mode, the process is reversed.

Solar cell stacks and associated wiring will be mounted on a fiber glass sheet which is bonded to the front beryllium sheet (sun side). The back (shadow side) beryllium skin will have lightening holes for weight reduction and temperature control purposes. The system weight estimate is summarized below.

● Solar cell stack including dielectric cells, wiring, etc.	20.0
● Substrate 0.007 beryllium	13.3
● Cushions	1.7
● Drums and takeup spools	3.5
● Motor, sprockets, drive chain, guide rollers and tension wires	<u>5.0</u>
● Total	43.5 lb/kW

1.2.4 SOLAR ARRAY TEMPERATURE CHARACTERISTICS

The equilibrium temperature of a solar panel is an important parameter in the determination of power output of the array. Figures 27 and 28 show equilibrium temperatures for flat oriented solar panels for a specific case typical of a solar panel and for a general array design, respectively.

The panel temperatures were calculated as a function of solar intensity using the following assumptions:

- a. The panel is a flat plate with both sides radiating to cold space.
- b. There is no adjacent spacecraft to block the panel radiation.
- c. The panel has "perfect conduction"(isothermal).
- d. * $\frac{\alpha}{\epsilon_T + \epsilon_B} \approx 0.50$ $\frac{\alpha(1 - \eta K_F)}{\epsilon_T + \epsilon_B} \approx 0.45$

*Specific conditions used to obtain Fig. 27.

General Equation

$$\alpha S \cos\beta = \sigma(\epsilon_T + \epsilon_B) T^4 + P/A \quad (1)$$

$$P/A = \eta K_F \alpha S \cos\beta \quad (2)$$

Combining Eqs. 1 and 2

$$T = \left[\frac{\alpha S \cos\beta (1 - \eta K_F)^{-1/4}}{\sigma (\epsilon_T + \epsilon_B)} \right] \quad (3)$$

Assume

$$\frac{\alpha}{\epsilon_T + \epsilon_B} \approx 0.50 \quad (4)$$

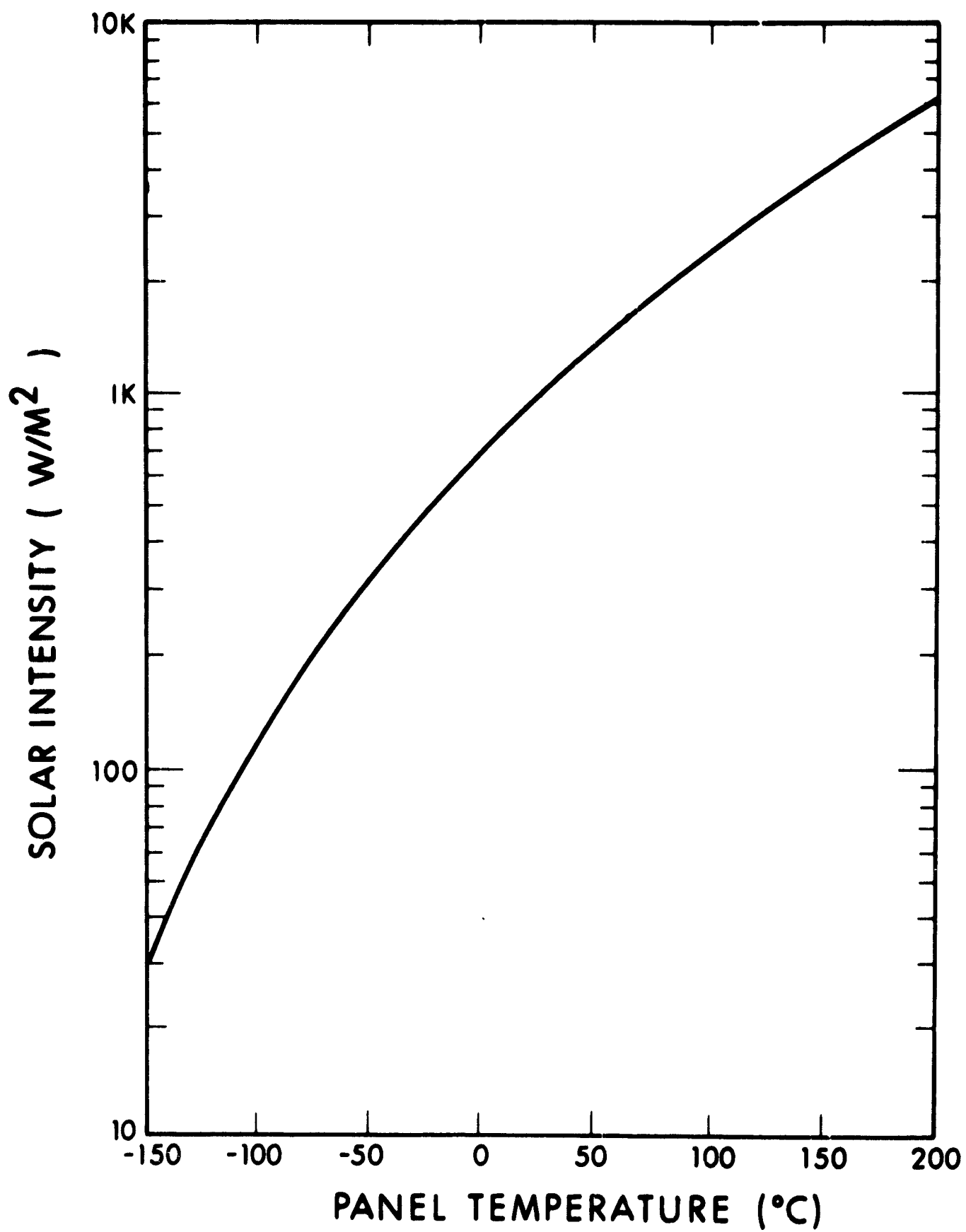


Figure 27. Flat Panel Thermal Equilibrium Temperature

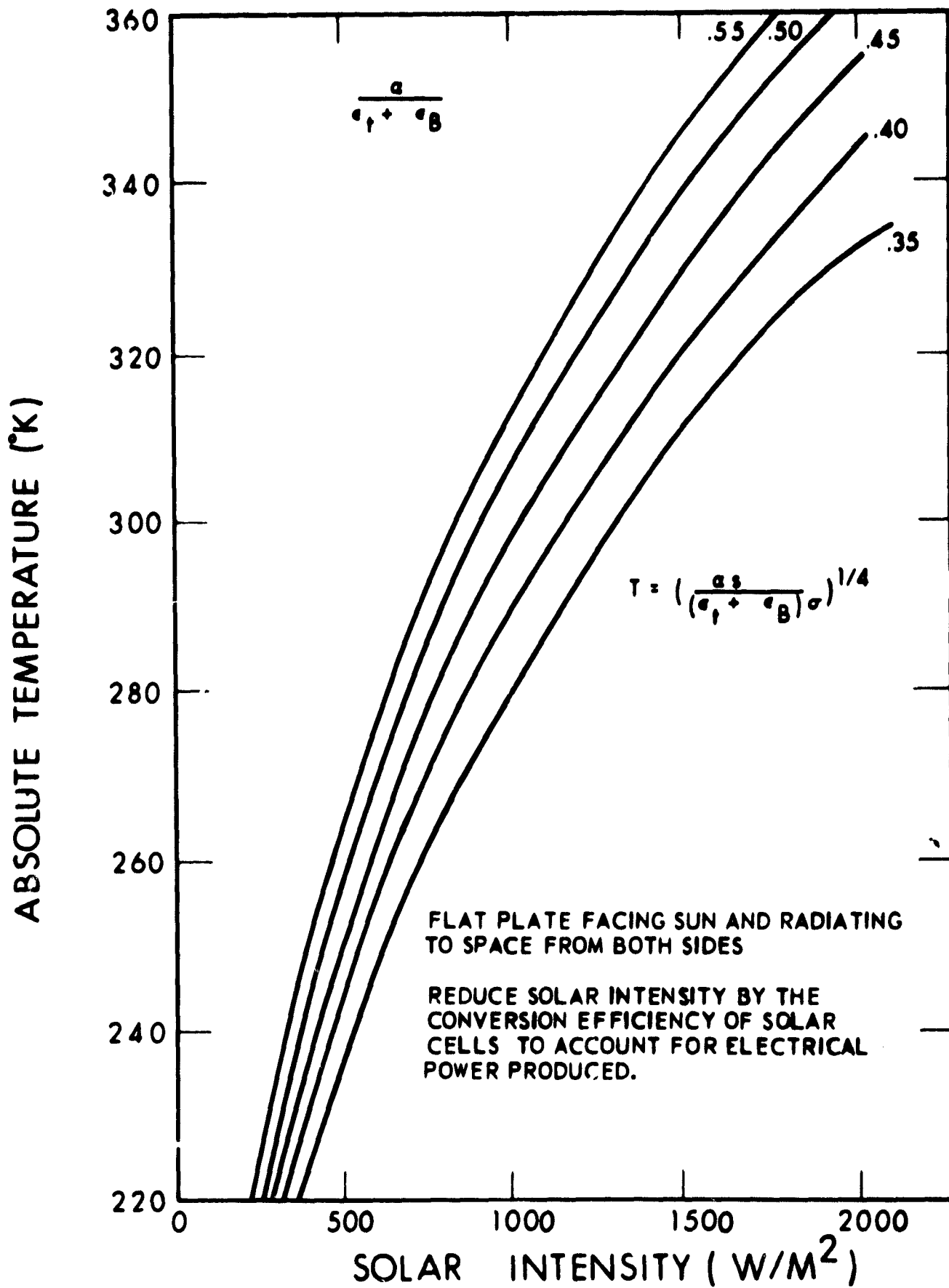


Figure 28. Thermal Equilibrium Temperatures for a Flat Oriented Solar Panel

then

$$\frac{\alpha (1 - \eta K_F)}{\epsilon_T + \epsilon_B} = 0.45 \quad (5)$$

Combining Eqs. 3 and 5

$$T = \left(\frac{0.45 S}{\sigma} \right)^{1/4} \quad (6)$$

- where
- α = solar absorptivity
 - S = solar radiation (MW/cm^2)
 - σ = Stefan-Boltzmann constant = $5.67 \cdot 10^{-9}$
 - ϵ_T = emissivity of panel top surface
 - ϵ_B = emissivity of panel bottom surface
 - T = panel temperature ($^{\circ}$ Kelvin)
 - P = electrical power output (watts)
 - A = panel area (ft^2)
 - η = solar cell efficiency
 - K_F = solar cell packing factor
 - β = incident light angle from normal to the panel (degrees)

1.2.5 SOLAR ARRAY POWER OUTPUT VERSUS DISTANCE FROM THE SUN FOR VARIOUS MISSIONS

Figures 29, 30, and 31 illustrate variations in solar array power output for three missions under consideration, using Fig. 32 as the basic solar cell E-I characteristic curve. The missions are a Mars Probe and Orbiter, a Jupiter Probe, and a Venus Probe and Orbiter. The Mars Probe and Orbiter and the Venus Probe and Orbiter assume a 50 kilowatt array at one AU while the Jupiter Probe assumes a 14 kilowatt array at one AU. The change in power is due to temperature, intensity, and radiation degradation variations during the mission duration. However, since the launch period is the 1975 year,

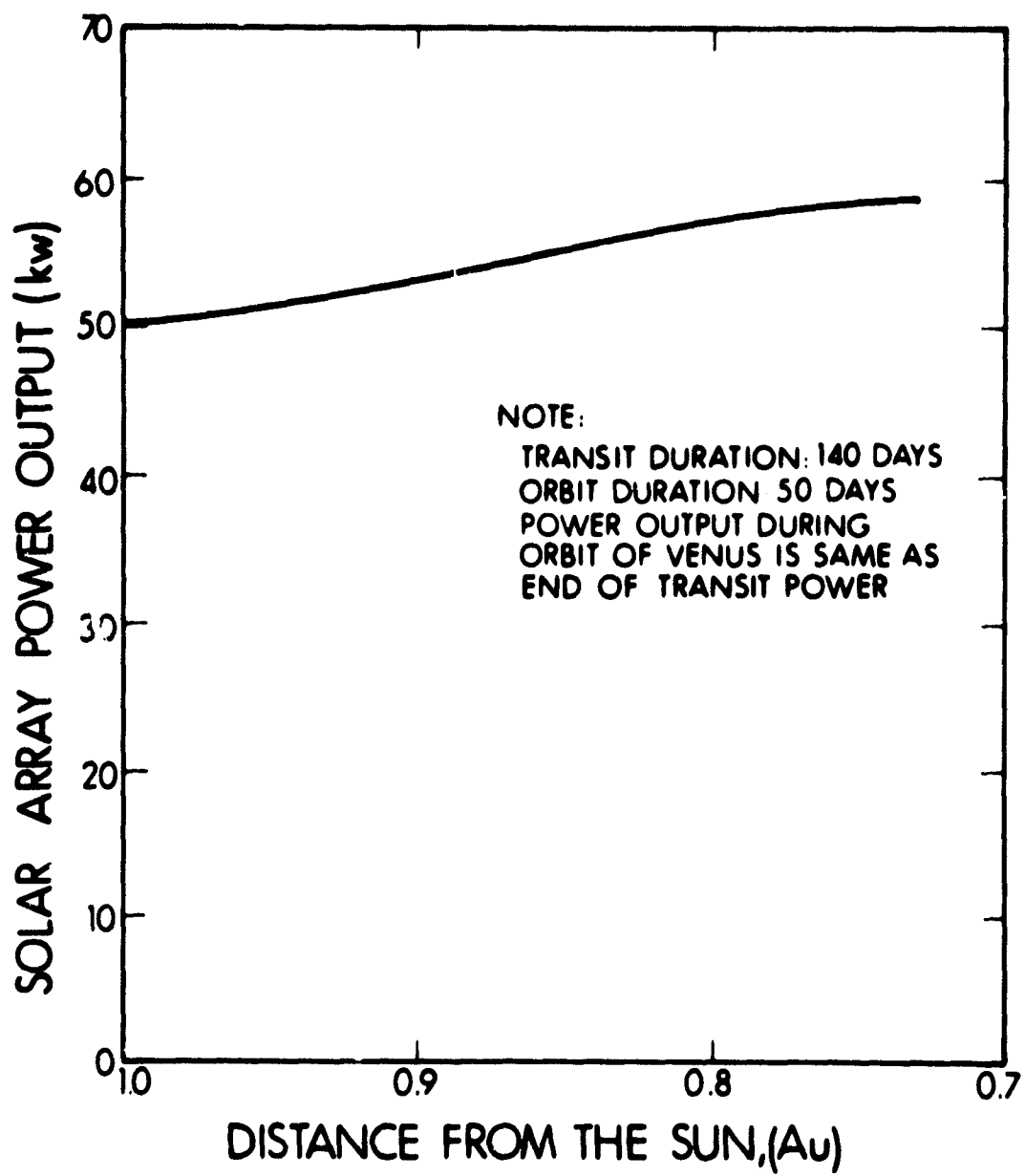


Figure 29. Solar Array Power Output versus Distance from the Sun for a Venus Probe and Orbiter

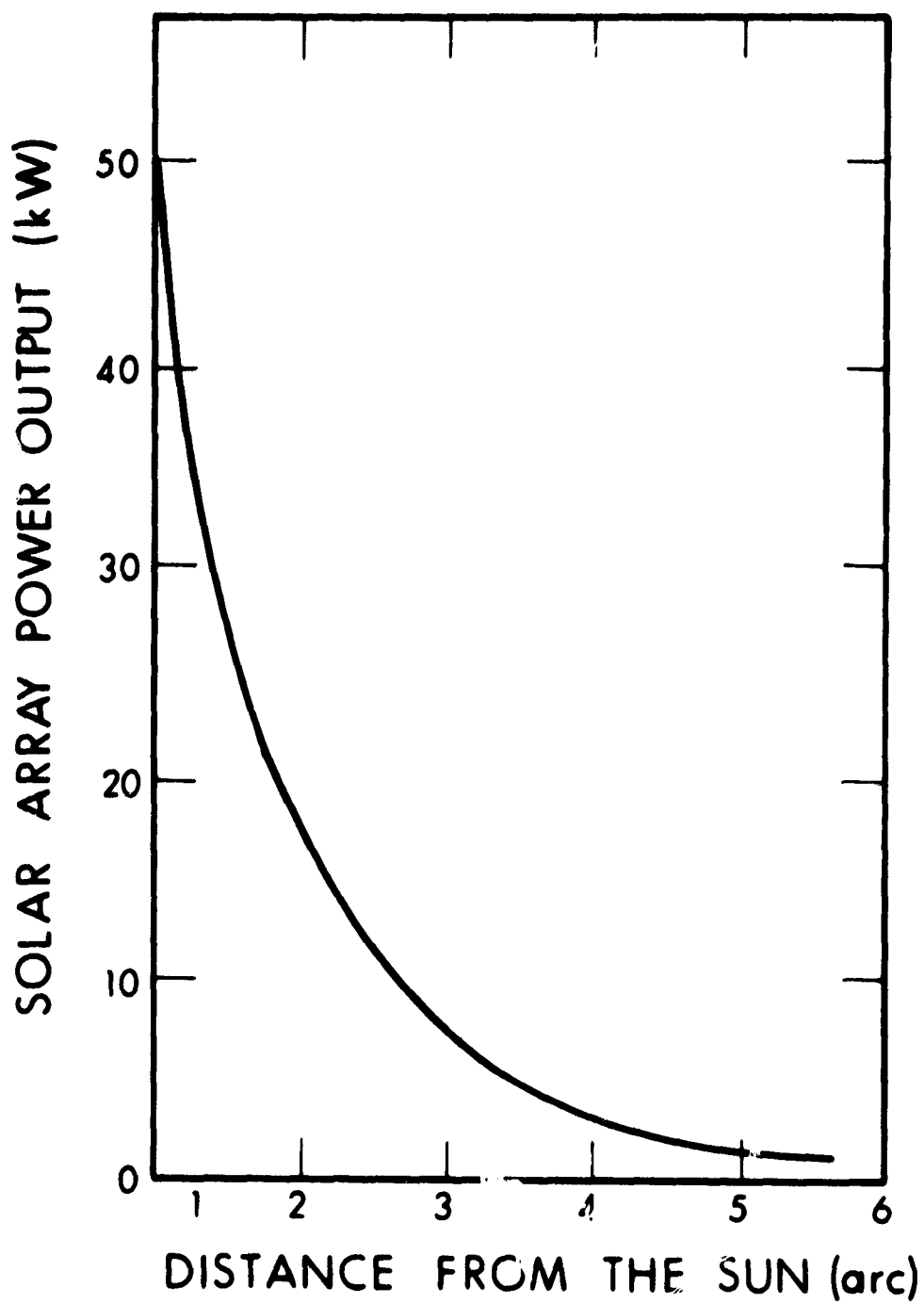


Figure 30. Solar Array Power Output versus Distance from the Sun for a Jupiter Probe

NOTE: TRANSIT TIME: 270 DAYS
ORBIT TIME: 50 DAYS
POWER OUTPUT IN MARS
ORBIT IS SAME AS POWER
OUTPUT AT 1.67 AU.
(END OF TRANSIT)

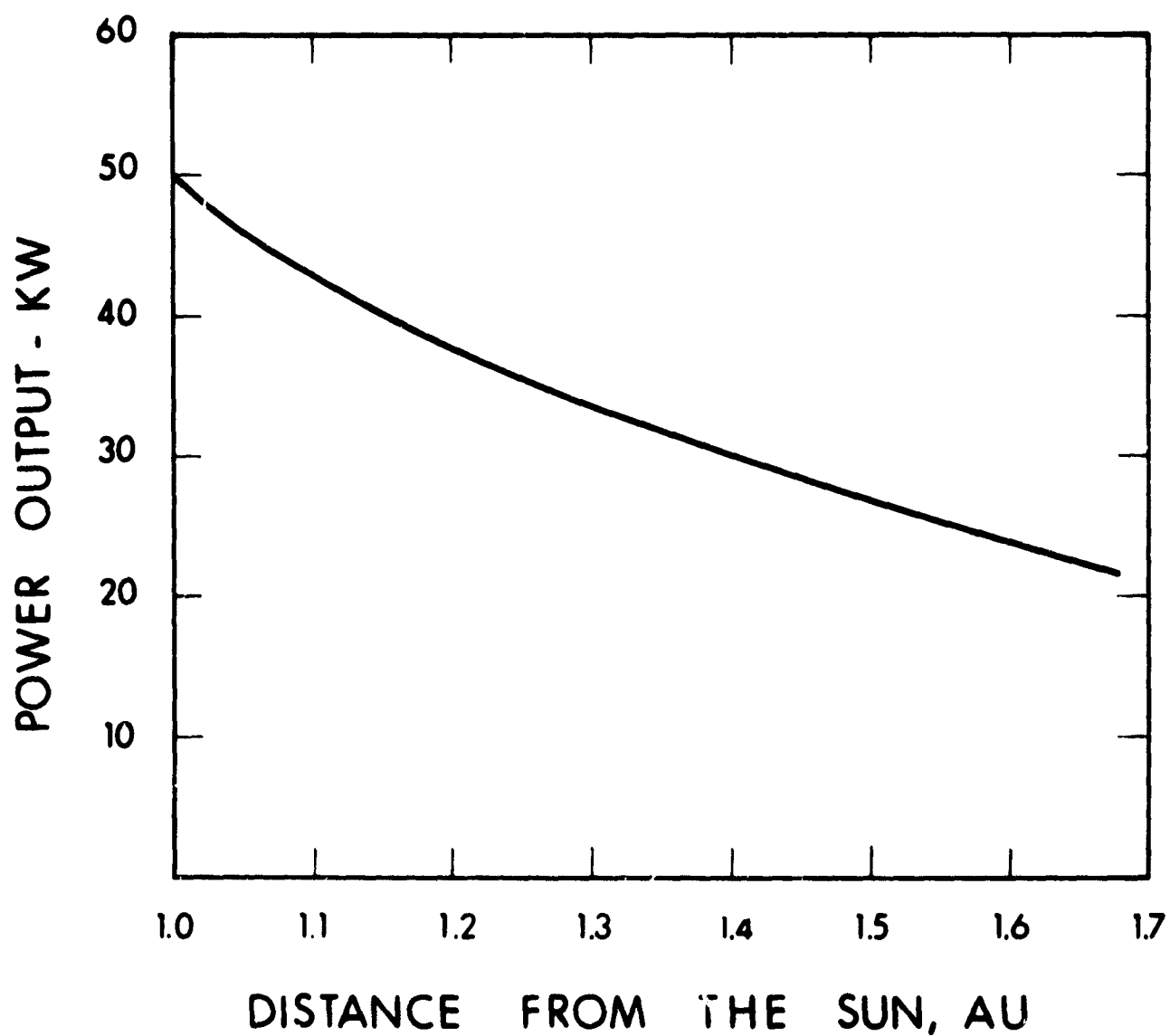


Figure 31. Solar Array Power Output versus Distance from the Sun for a Mars Probe and Orbiter

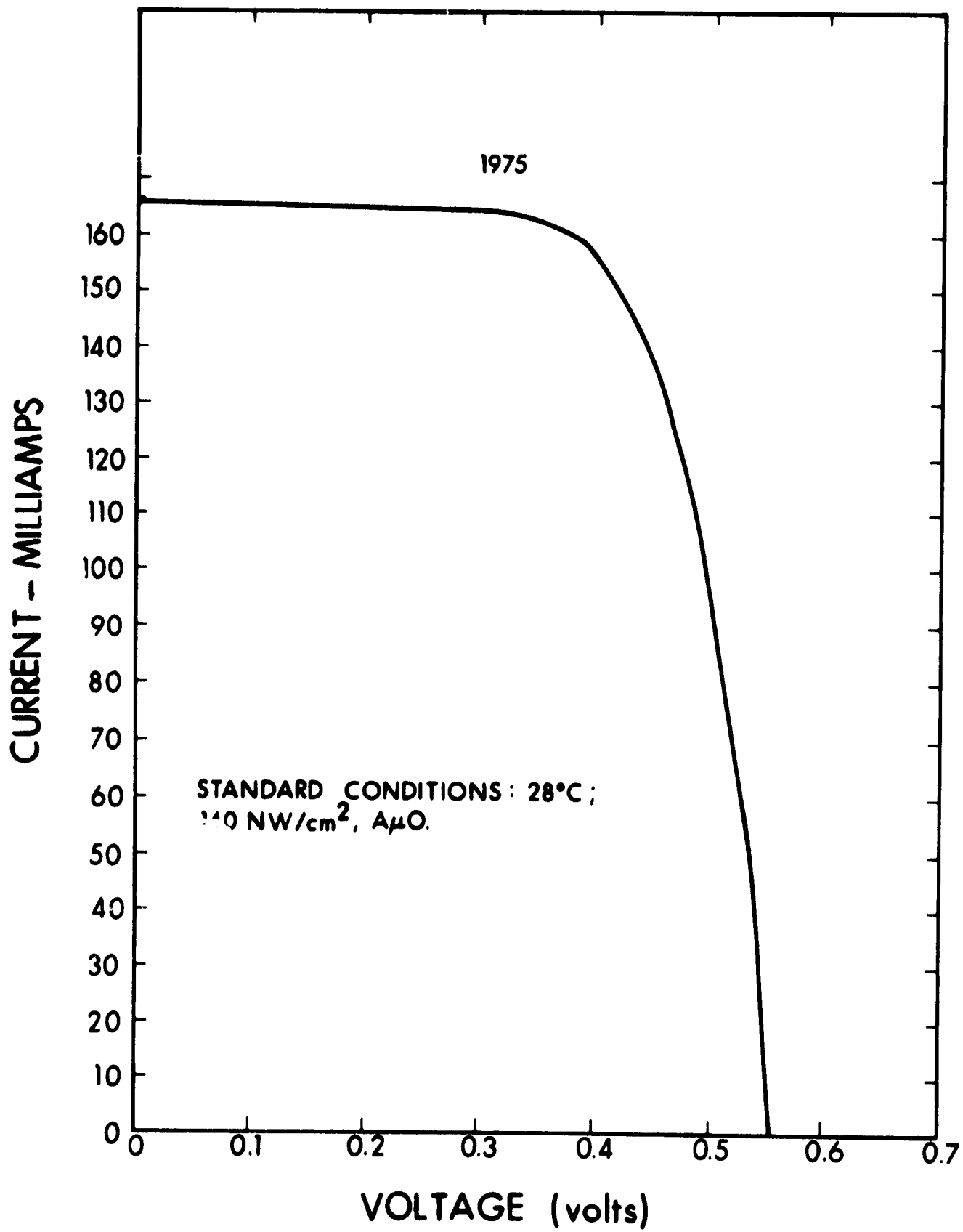


Figure 32. Voltage-Current Characteristic Curve for a 10-ohm-per-Centimeter, Non-P, 2 x 2 Centimeter, Solar Cell. Cell Efficiency = 11.3 Percent

radiation degradation can be assumed to be negligible since this is the period of minimum solar flare activity. The curves then basically show the effects of variation in temperature and intensity on solar array power output.

The Venus Probe and Orbiter solar array will increase in power from 50 kilowatts at earth to approximately 59 kilowatts at Venus encounter and orbit. The transit period from earth to Venus was assumed to be 140 days while the orbit duration was assumed to be 50 days. The power output during orbit will be constant, being that of the power at encounter. The power output of the Jupiter Probe will vary from 14 kilowatts at earth to approximately 400 watts at Jupiter encounter. The variation in the Mars Probe solar array power output is from 50 kilowatts at one AU to approximately 22 kilowatts at Mars encounter and orbit. The transit time was assumed to be 270 days to Mars with an orbit time of 50 days. The power output during orbit will be the same as that of Mars encounter.

1.3 REFERENCES AND BIBLIOGRAPHY FOR SECTION 1

1.3.1 REFERENCES

- 1-1. E. Becquerel, "On Electrical Effects under the Influence of Solar Radiation", Compt. Rend, Vol. 9, p. 561, 1839
- 1-2. W. J. Adams and R. E. Day, "The Action of Light on Selenium", Proceedings Royal Society, Vol. A-25, p. 113, 1877
- 1-3. P. Rappaport, "The Electronic Voltaic Effect in P-N Junctions Inducted by Beta Particle Bombardment", Physical Review, Vol. 93, p. 246, January 1954
- 1-4. D. C. Reynolds, et al, "Photovoltaic Effect in Cadmium Sulphite", Physical Review, Vol. 93, p. 533, October 1954.
- 1-5. P. Rappaport, "The Photovoltaic Effect and its Utilization", RCA Review, Vol. 20, No. 3, September 1959
- 1-6. M. Wolf, "The Present State of the Art of Photovoltaic Solar Energy Conversion", Solar Energy, Vol. 5, No. 3, p. 83, July-September 1961.
- 1-7. M. Wolf, "Drift Field in Photovoltaic Solar Energy Converter Cells", Proceedings of the IEEE, Vol. 51, No. 5, May 1963
- 1-8. J. Mandelkorn, et al, "Comparison of P-N and N-P Silicon Solar Cells", Proceedings 15th Annual Power Sources Conference, p. 42-45, May 1960.
- 1-9. Hoffman Company and Heliotek Corporation Solar Cell Data Books Compendium of Solar Cell Properties
- 1-10. S. A. Friedlander, "A Parametric Study of Proton and Electron Damage to Solar Cells in Space", Hughes Aircraft Technical Report, December 1963.
- 1-11. P.H. Fang, "Current Status of Drift Field Solar Cells", N64-29163, NASA-Goddard Space Flight Center, June 1964
- 1-12. "Development of Lightweight Rigid Solar Panel" EOS Report 7027-IDR, 18 May 1966
- 1-13. "Fabrication Feasibility Study of a 20 Watt Per Pound Solar Cell Array" Boeing Report No. D2-23942-5, 19 November 1965

- 1-14. "Large Area Solar Array Design Progress" Baseline Evaluation Review, 20 December 1966, The Boeing Company
- 1-15. "Recent Developments in Large Area Solar Cell Arrays" Kenneth A. Ray, Proc. Fifth Photovoltaic Specialists Conference, Goddard Space Flight Center, 18 October 1965
- 1-16. "Flexible Integrated Solar Cell Array Industry Presentation" Hughes Aircraft Space System Division, 29 September 1966
- 1-17. "Design, Fabrication and Demonstration of a Deployable Large Area Solar Cell Array Structure for Interplanetary Space Probes" Technical Presentation by Ryan Aeronautical Company, 15 March 1967

1.3.2 BIBLIOGRAPHY

A. Nuclear Thermoelectric

1. "Nuclear Space Power Systems", H. M. Dieckamp of Atomics International, Sept. 1964.
2. "Reactor-Thermoelectric Power Systems for Unmanned Satellite Applications", J. D. Gylfe and R. E. Wimmer, Intersociety Energy Conversion Engineering Conference, Sept. 1966.
3. "Advanced-SNAP-Reactor Thermoelectric Space Power Systems, G. S. Budney, Power and Propulsion Systems Technology.

B. Nuclear Rankine Turboelectric

1. "Nuclear Space Power Systems", H. M. Dieckamp of Atomics International, Sept. 1964.
2. "SNAP Mercury Rankine Program", R. L. Wallerstedt and J. J. Owens, Intersociety Energy Conversion Engineering Conference, Sept. 1966.
3. "Potassium Rankine-Cycle Power Plants from 10 kW to 1000 kW", R. A. Rackley and E. A. Mock, Intersociety Energy Conversion Engineering Conference, Sept. 1966.
4. "SNAP-8 Development Status", Henry O. Slone, Space Power Systems Advanced Technology Conference NASA SP-131 Aug. 1966.
5. "Potassium Rankine System Materials Technology", Louis Rosenblum et al, Space Power Systems Advanced Technology Conference NASA SP-131, Aug. 1966.
6. "Potassium Rankine Systems Technology", Robert E. English et al, Space Power Systems Advanced Technology Conference, NASA SP-131, Aug. 1966.
7. "SNAP-8 - A Technical Assessment" J. N. Hodgson et al, Intersociety Energy Conversion Engineering Conference, Aug. 1967.

C. Nuclear Brayton Cycle

1. "Brayton Cycle Technology", Warner L. Stewart et al, Space Power Systems Advanced Technology Conference, NASA SP-131, Aug. 1966.
2. "Reactor-Powered Brayton Cycle for Large Space Stations", Anthony Pictsch, Intersociety Energy Conversion Engineering Conference, Aug. 1967.
3. "Nuclear Brayton Cycle Powerplants for Space Applications", S. I. Freedman et al, Intersociety Energy Conversion Engineering Conference, Aug. 1967.

D. Nuclear Thermionic System

1. "Review of Industry-Proposed In-Pile Thermionic Space Reactors", J. P. Davis et al, JPL Tech. Memo No. 33-262, Oct. 1965.
2. "Parametric Studies Report, Advanced Nuclear Electric Power Generator System Study Thermionic Nuclear Space Power Plant", Report PWA-2240 Pratt & Whitney, July 1963.
3. "Out-of-Pile Nuclear Thermionic Power System" unpublished data by EOS, 1967.

SECTION 2

ELECTRIC THRUSTER TECHNOLOGY

The phrase, electric propulsion, brings to mind a great variety of propulsion devices. At some time during the past 10 years it seems that every possible means to increase the energy of a storable propellant and exhaust it from a vehicle to provide thrust has been explored. The devices that have survived the exploratory research are the purely thermal resistojet and arcjet, the electrostatic colloid and ion engine and combination thermal/electromagnetic system known as the magnetoplasmadynamic arcjet.

These various systems have found certain preferred operating areas in which their application is most promising. These regimes are shown in Fig. 33. In reality, there are no real boundaries to the regimes, but engineering facts have established most of the nominal limits. Successful operation of any of these thrusters outside these limits will require breakthroughs in materials, propellants, propellant storage methods, power supplies and a host of other technologies.

The most generally useful formulation of thruster performance is in terms of power-to-thrust ratio and specific impulse. Such a formulation measures the efficiency, thrust and propellant mass required by any given thruster. For very high energy missions (high total impulse) the thrusters of serious interest are the cesium and mercury bombardment thrusters, the cesium contact thruster and the MPD arcjet. The performance (1967) of these four types are displayed in Fig. 34.

The most advanced of the four is the cesium bombardment thruster. It has the best performance, yields the lowest system mass and has demonstrated the best long-term reliability and reproducibility.

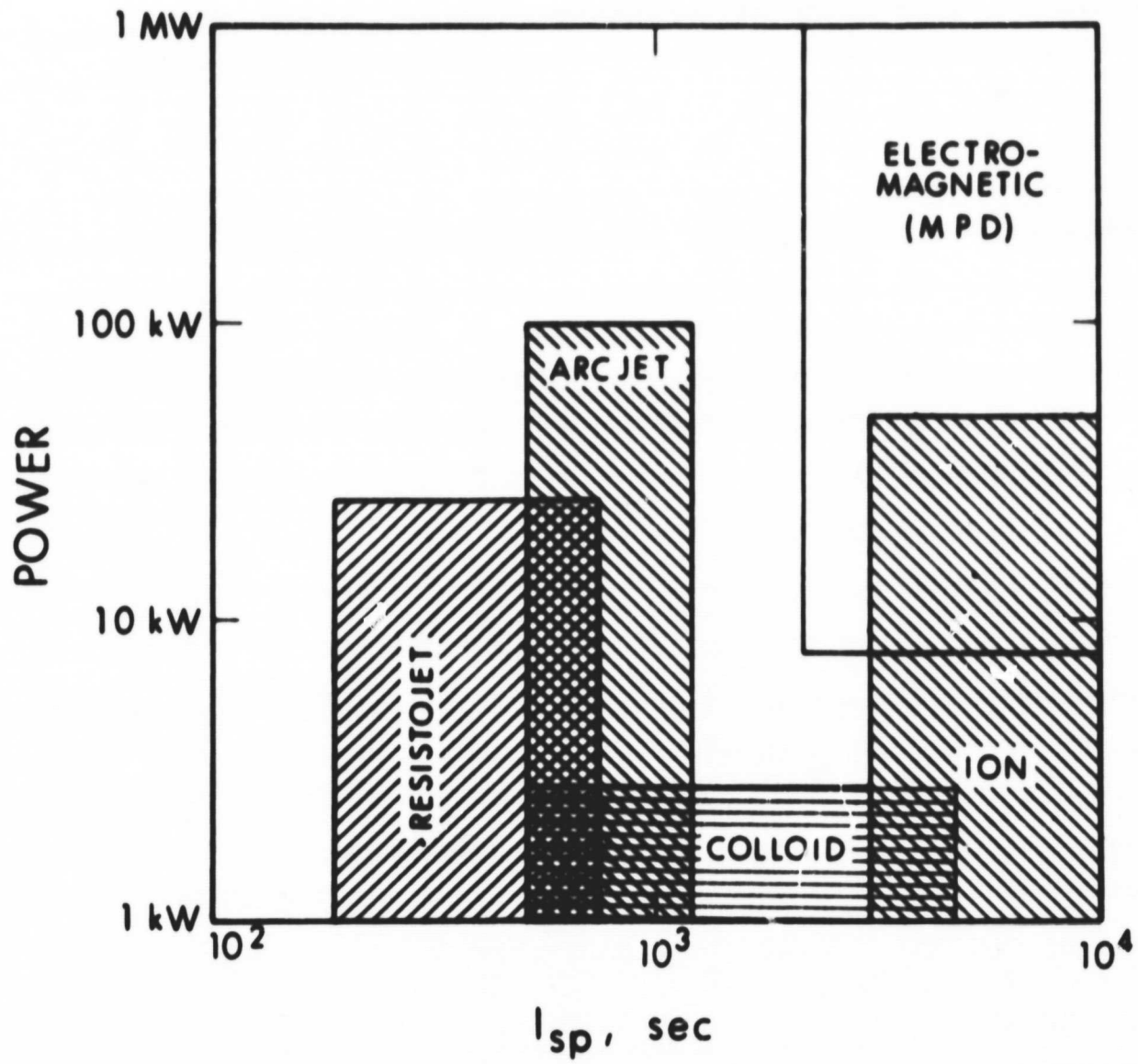


Figure 33. Electric Propulsion Operating Regimes

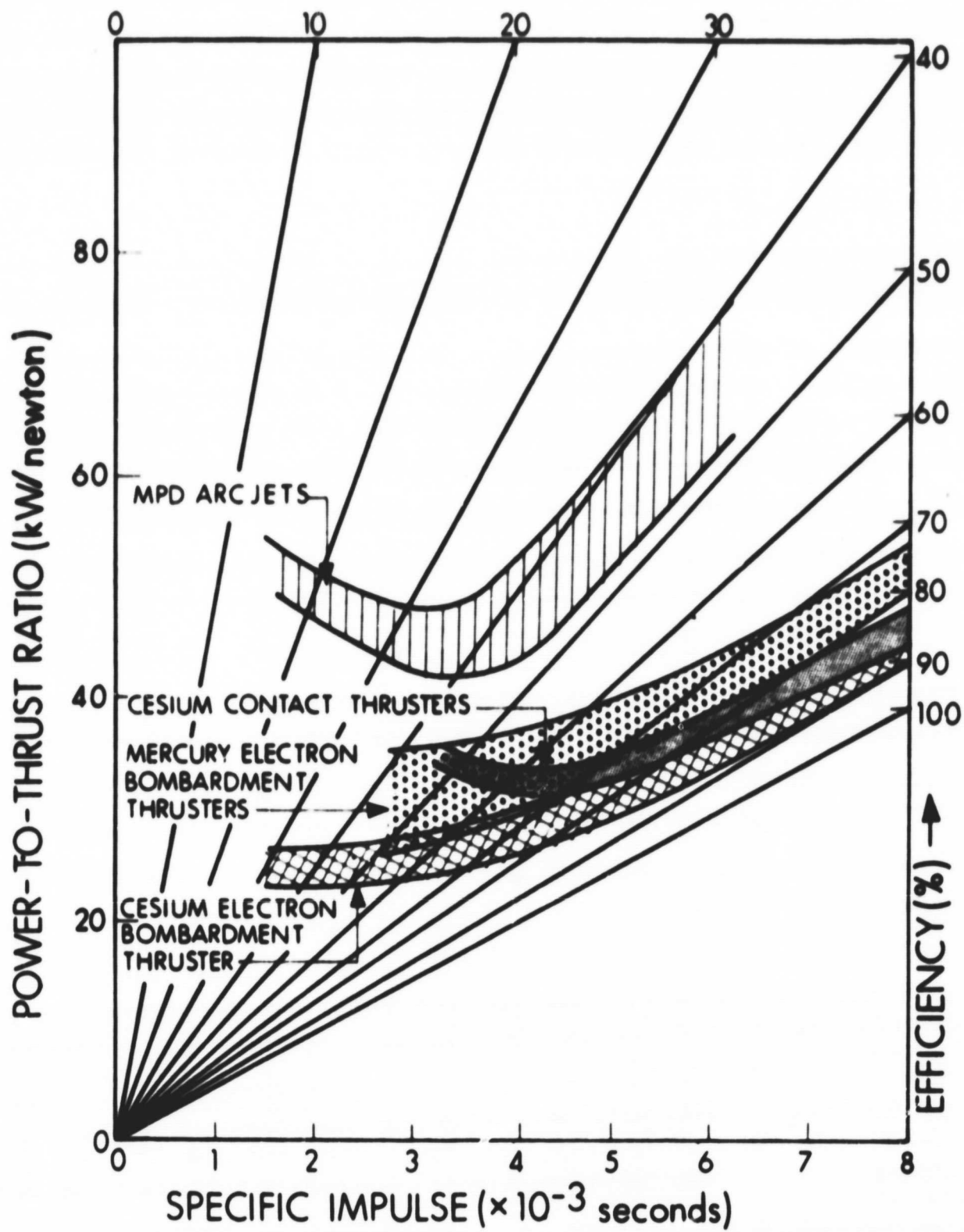


Figure 34. Power-to-Thrust Ratio versus Specific Impulse for Electric Propulsion Engines

From a long range viewpoint the MPD arcjet is probably the most promising. At present, its performance is not as good as the other types but its potential advantages are high thrust density, ruggedness and simplicity. Given time and development effort it should be the best choice for prime electric propulsion.

The mass of the two bombardment ion thrusters is shown in Figure 35. These data are for thrusters that exist. It should be mentioned that the mercury thrusters have not received much mass reduction attention to date and the mass should ultimately be reduced considerably. Because of its inherent higher magnetic field, it will probably not be built any lighter than twice the mass of the corresponding cesium bombardment thruster.

The MPD arcjet shown on the curve indicates a constant mass irrespective of the power level. This results from the rather massive components that are required. Since this thruster is still in a laboratory status further improvements are to be expected but are difficult to speculate about at present.

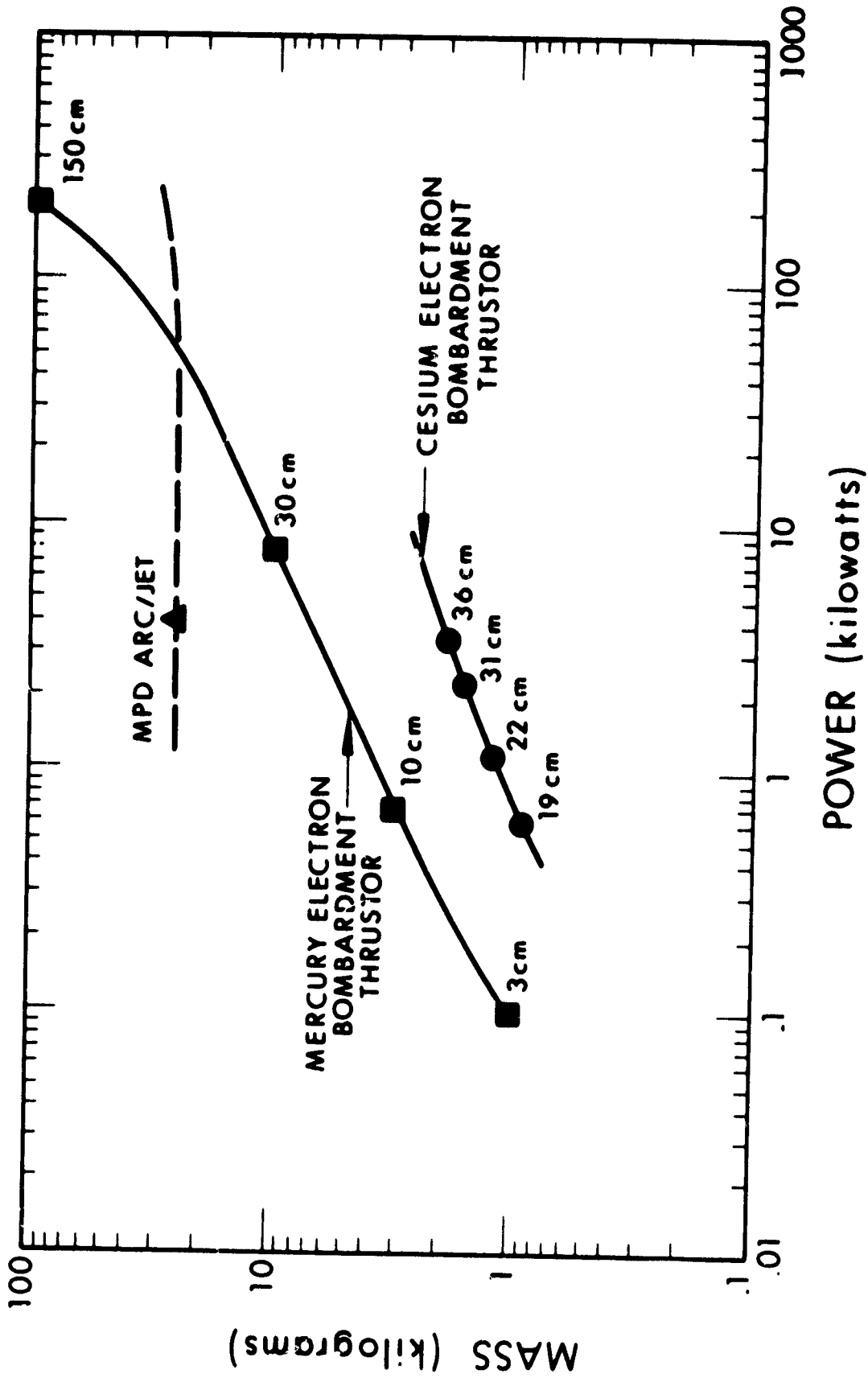


Figure 35. Mass versus Power for Electric Propulsion Engines

2.1 CESIUM ELECTRON BOMBARDMENT ION ENGINE SYSTEMS

2.1.1 INTRODUCTION

Cesium electron bombardment ion engine systems are comprised of a fuel reservoir and feed system, an engine, a neutralizer, and power conditioning and controls. Power conditioning and controls will be discussed in a separate section.

The use of cesium in a bombardment ion engine system offers a very high efficiency. The ionization potential of cesium is the lowest known and its density is relatively high. This results in a high ratio of accelerating energy to accelerating energy plus ionization energy, or power efficiency. Due to its low ionization potential and large ionization cross section, a large fraction of the propellant is ionized, thus the mass utilization efficiency is high. The product of power and mass efficiencies, or overall engine efficiency, is therefore very high.

Additional advantages accrue from the use of cesium. It is easily handled by static zero-g feed systems, it allows the use of a cesiated tantalum cathode with its attendant long lifetime, and its characteristics in the discharge allow the use of weak magnetic fields with a resulting low engine weight. The cesium plasma bridge neutralizer used with these systems is the most efficiency and long-lived neutralizer developed to date.

In this analysis, two principal objectives were taken. The first was to characterize engine system volume, mass, and power. The second objective was to describe in some detail the interfaces between this system and its power conditioning and the spacecraft.

In search for a common parameter upon which to characterize the propulsion system, the most immediate candidate is thrust level. If a specific impulse can be assumed, then thrust level determines engine size, mass, and electrical operating characteristics. The feed system is sized on the basis of the total impulse. Again, if a specific impulse can be assumed, then the feed system size and mass can be characterized as a function of the product of thrust and time. The neutralizer can also be characterized as a function of the emission-thrust-time product. Assuming certain general packaging characteristics, it is then possible to find the propulsion system size, mass, and power as a function of thrust and time.

A large number of curves were generated in order to arrive at the final system parameters. These curves were derived from experimental data and known scaling relations. For example, feed system masses are known for a number of lightweight Zero-g systems. The principal feed system mass is the reservoir. The mass of this reservoir with a constant skin thickness should be proportional to the two-thirds power of the capacity. Practical feed systems are somewhat more efficient at larger capacities, however, and the mass is better approximated as the volume to the 0.6 power. In addition, certain fixed mass associated with the vaporizer and flanges must be considered. In this manner, the example curve was derived. Similar detail was included in the generation of all the remaining curves. It was not felt appropriate to include such great detail in this report, so the curves are discussed only where they might appear questionable.

As discussed in Section 2.1.6, considerable performance improvement is expected in the near future. Such improvements were not considered in the generation of the data included herein. While this dates the enclosed material, it allows more accurate detail. Minor inaccuracies

in detail will be absorbed in the final values for size, mass, and power so these final values may be considered as very accurate norms. Details of the integration of the propulsion system into each spacecraft will modify these overall values beyond the range of error inherent in the results presented.

2.1.2 OPERATION

2.1.2.1 Engine

A schematic of a cesium electron-bombardment ion engine system is shown in Fig. 36. Cesium propellant is introduced as a vapor through the cathode, is ionized in the discharge chamber, and is accelerated through the electrodes to high exhaust velocities. Within the chamber the cesium vapor is bombarded by electrons passing from the cathode to the anode. The paths of these electrons are increased by applying an axial magnetic field. This increases the probability of ionization and results in a significant reduction in discharge power and an increase in mass utilization.

The electrons are emitted from the cesiated tantalum surface within the cathode. Such a surface is capable of emitting currents of one ampere per square centimeter at temperatures as low as 600° centigrade. The tantalum surface is cesiated by the propellant flow. Prior to starting, the cathode is heated externally. Once the discharge has been initiated, the cathode emitter is maintained at operating temperature by ion bombardment from the plasma, radiation from the plasma, and other second order effects. With the discharge on, the external heating power is removed and the cathode runs in an autocathode mode.

When an ion arrives at the screen electrode, it is accelerated by the electric field between the screen and accelerator electrodes to

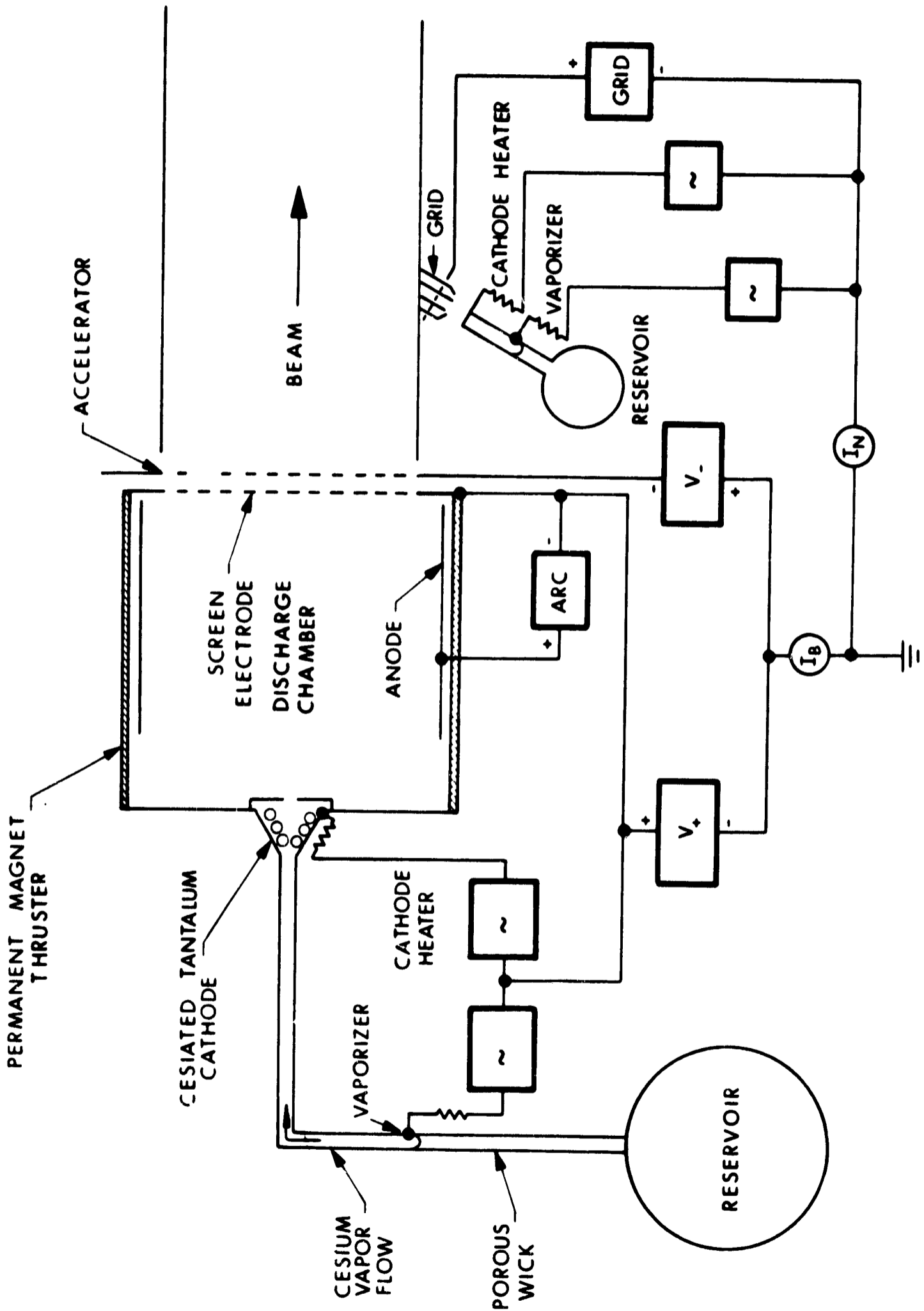


Figure 36. Cesium Electron Bombardment Engine Schematic

a high exhaust velocity. The accelerator electrode is biased negative to prevent the passage of electrons from the exhaust to the source.

2.1.2.2 Control

Two control loops used with this engine are shown in Fig. 37. The first is a feed control loop. The exhaust beam current is measured at the power supplies and compared with a reference. The error between the reference and the beam is amplified and used to drive the cesium vaporizer. This results in precise beam current control. The second control loop senses a small increase in beam current resulting from a small increase in discharge power and adjusts the discharge power up or down to operate at the point where maximum engine efficiency is achieved. This control (Section 2.1.4.3) is unique to the cesium electron bombardment ion engine.

2.1.2.3 Feed System

The cesium feed system, shown schematically in Fig. 38, represents a simple yet effective solution to the problems of phase separation and flow control in zero gravity. By properly designing a network of tapered cells into the propellant reservoir, the liquid cesium is pumped by surface tension forces to the feed line. At the feed line, a wick draws the cesium from the reservoir. At the free end of the wick a heater is used to evaporate the cesium in a controlled flow to the engine. Increasing or decreasing the heat to this vaporizer effects rapid and accurate flow control.

2.1.2.4 Neutralizer

The cesium discharge neutralizer consists of a miniature cesium feed system, a cathode similar to the engine autocathode, and a sustaining

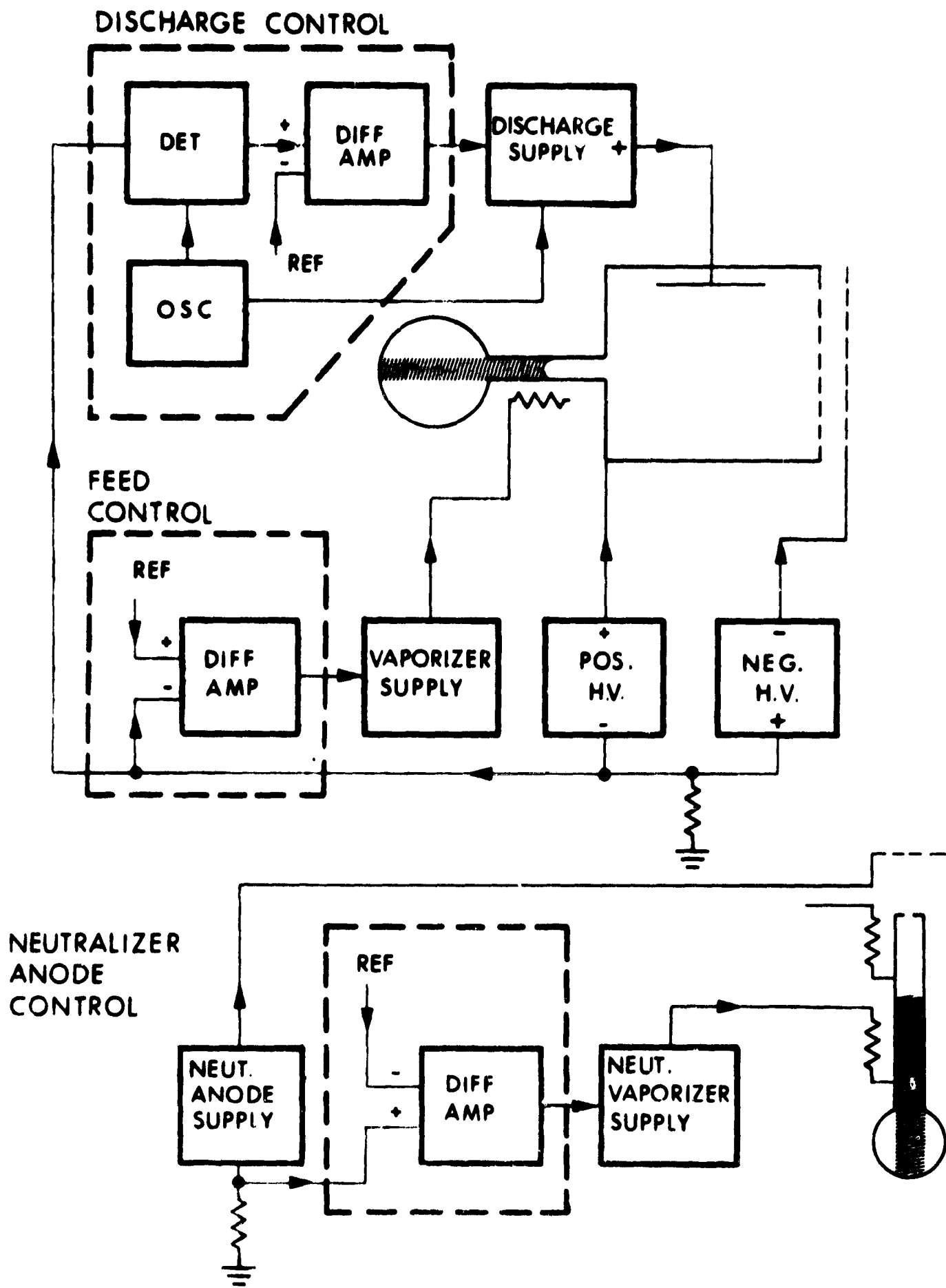


Figure 37. Control Loops for Cesium Bombardment Engine Systems

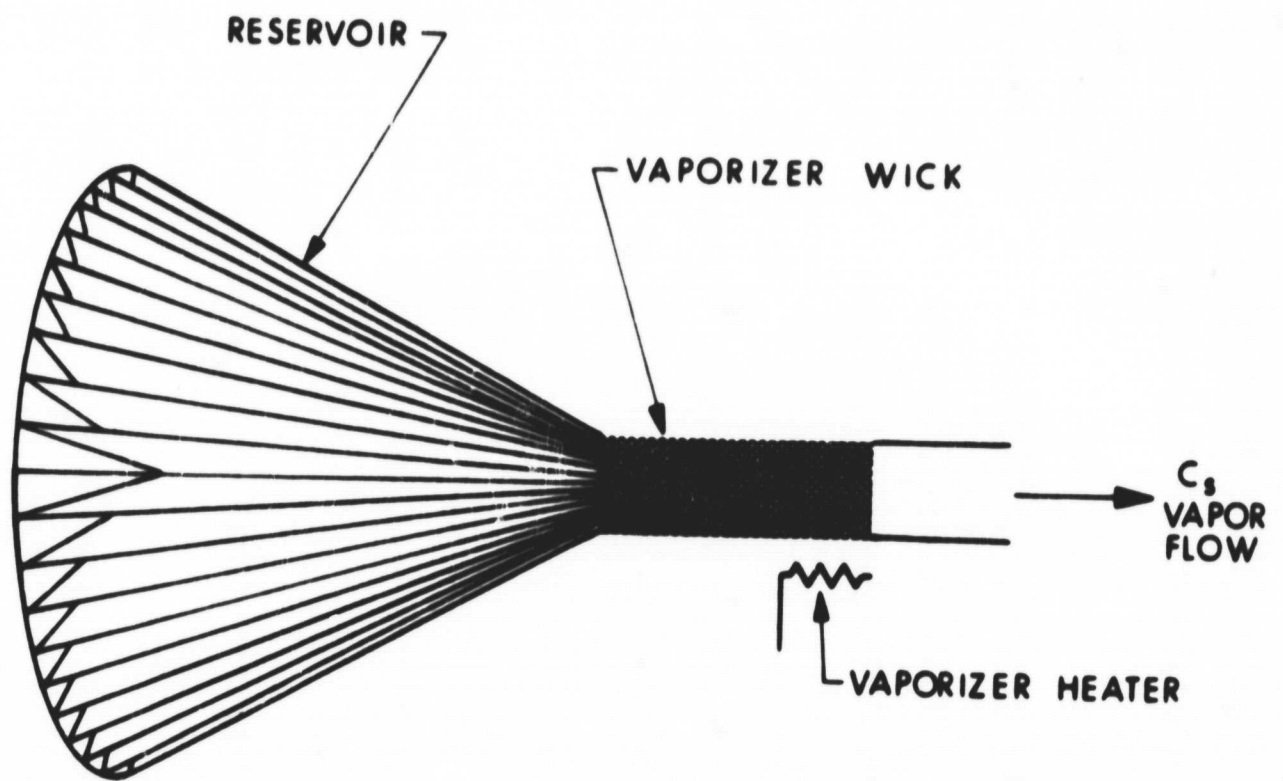


Figure 38. Cesium Feed System

anode electrode. A dc bias is applied to the sustainer and the cathode is heated electrically. The vaporizer of the miniature feed system is then heated until a discharge is initiated between the cathode and sustainer electrode. Vaporizer power is regulated to maintain a pre-determined current to the sustainer electrode as indicated in Fig. 37. With this discharge established, a conductive plasma bridges the space between the neutralizer and the exhaust ion beam. As a result, electrons are conducted into the beam at very low voltages while the neutralizer may be located far enough out of the beam to prevent degradation due to ion bombardment.

2.1.2.5 Lifetime

Two cesium electron bombardment ion engine systems have been life-tested. Both systems consumed a total power of 1 kilowatt and generated approximately 30 millinewtons of thrust. The specific impulse for both tests was 5,000 seconds. In these tests, the 9 kg and 18 kilogram zero-g feed systems used ran to cesium exhaustion. The engines performed as designed and the neutralizers operated throughout both tests. The tests ran for 3700 hours and 8100 hours respectively, and the tests indicate that lifetimes of 2 to 5 years are to be expected.

2.1.3 PERFORMANCE

This section describes the performance achieved to date with the major ion engine subsystems.

2.1.3.1 Engine

Cesium electron bombardment ion engines have been built and operated at thrust levels from a few micronewtons to 45 millinewtons. Figure 39 shows engines of a permanent magnet variety which span the thrust range from 12×10^{-6} newton to 45 millinewtons.

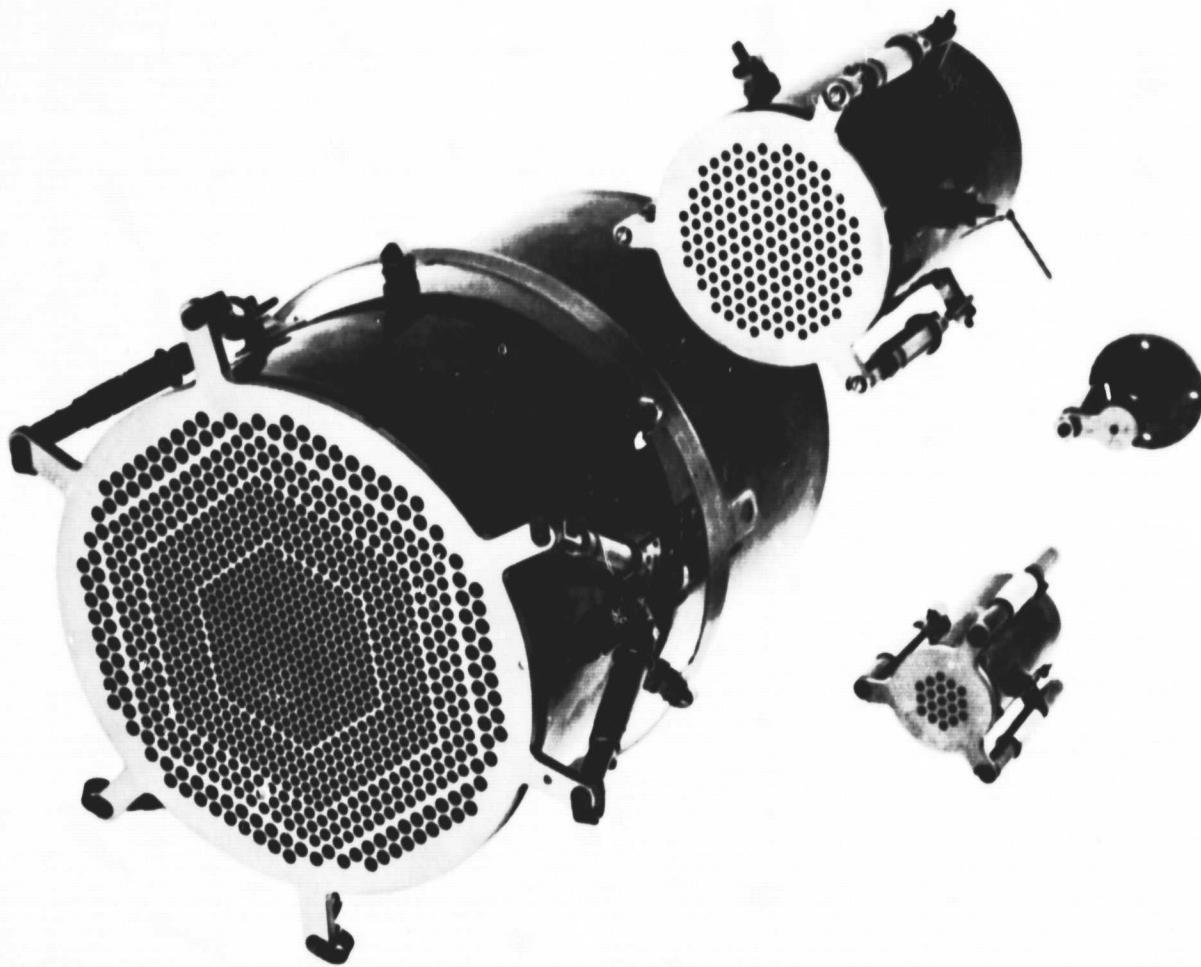


Figure 39. Permanent Magnet Engines of Thrust Levels 3.1×10^{-2} N, 4.5×10^{-3} N, 6.7×10^{-4} N, and 4.5×10^{-5} N

Mass

Mass performance of cesium engines has been well established and is shown as a function of thrust in Fig. 40. Weight is a function of thrust because thrust determines the beam current and the effective electrode area which is required. The thruster mass is one of the least significant masses of a cesium ion engine system especially when permanent magnet engines are used.

Volume

Thrust level also determines the overall engine volume. This volume shown in Fig. 41 includes the necessary space which must be left around the engine to provide high voltage isolation. It includes the volume occupied by the discharge chamber, cathode, electrodes and the electrode support insulators.

Mass Utilization

A great deal of performance data has been obtained for cesium thrusters. This performance has been verified in life tests where no significant reduction in efficiency has been found. The first characteristic considered here is the mass utilization efficiency. This is shown in Fig. 42 as a function of thrust. The mass efficiency is reduced at low thrust due to the smaller discharge chambers required and resultant increase in the ratio of surface area to volume within the thruster. Knowledge of the mass utilization efficiency allows computation of the required propellant mass from the total mission impulse requirement and thruster specific impulse. Only very small margins are required since the mass utilization efficiencies have been verified over long periods in a number of life tests. Comparisons of the total calculated cesium expelled to

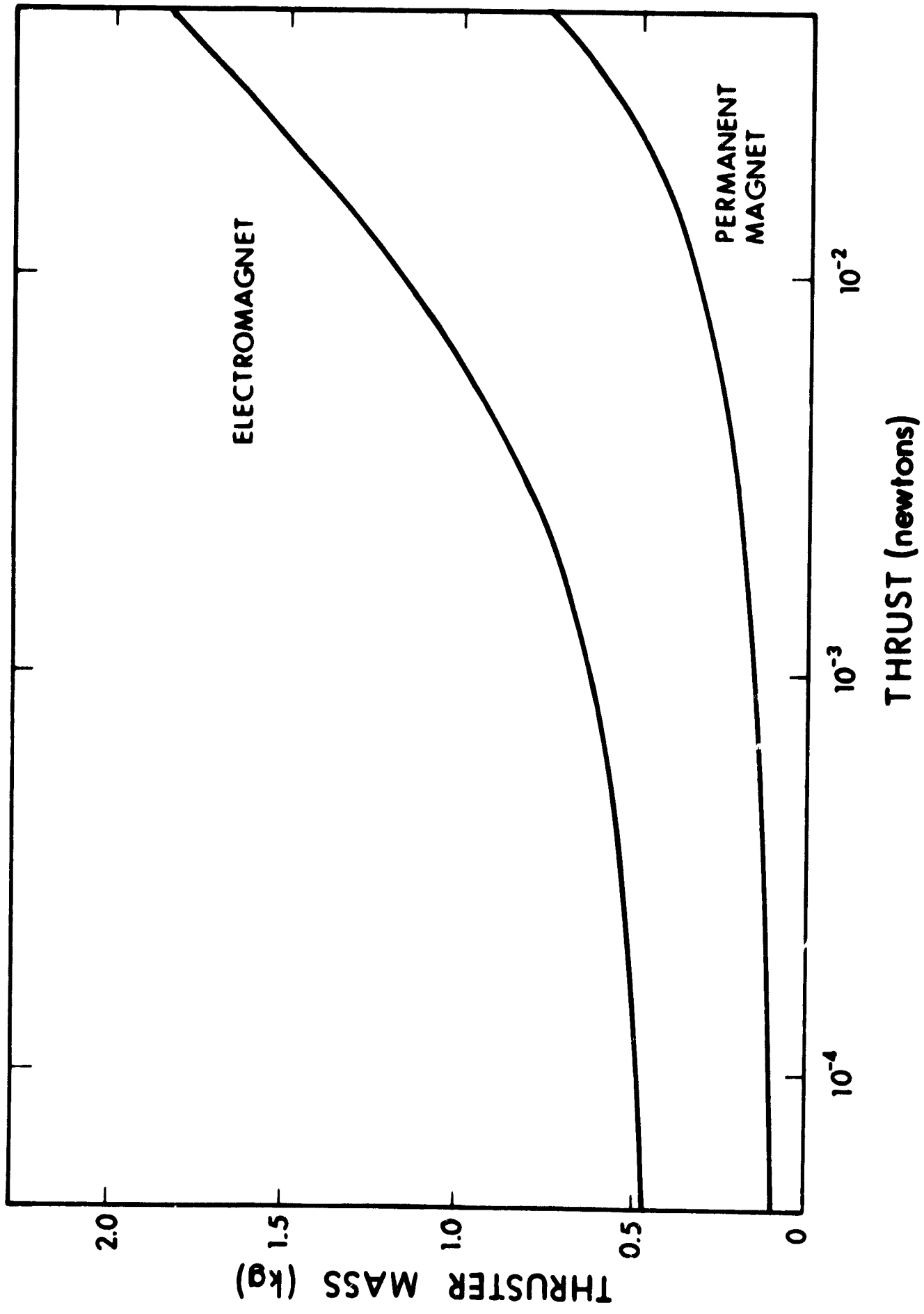


Figure 40. Thruster Mass versus Thrust

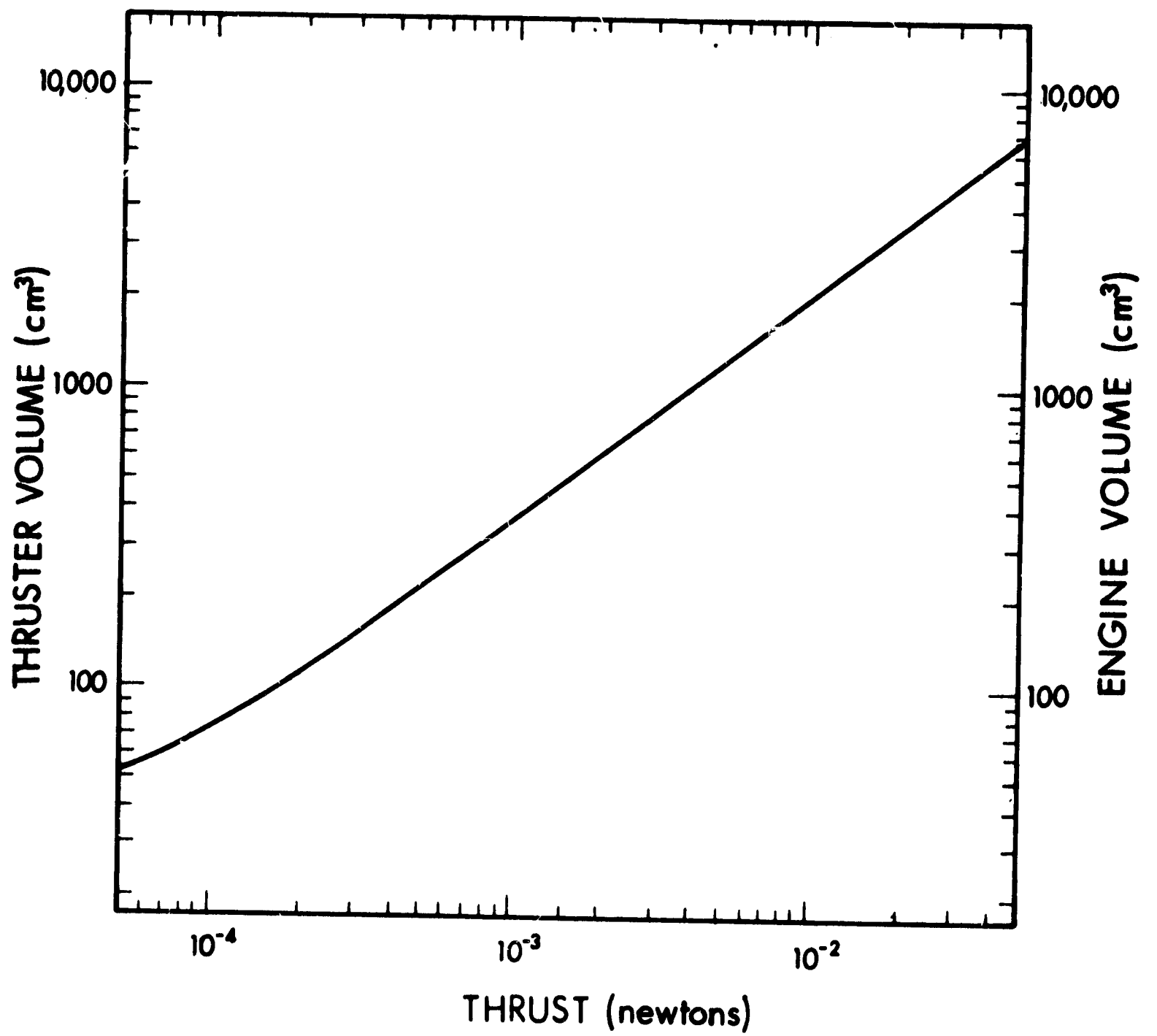


Figure 41. Thruster Volume versus Thrust

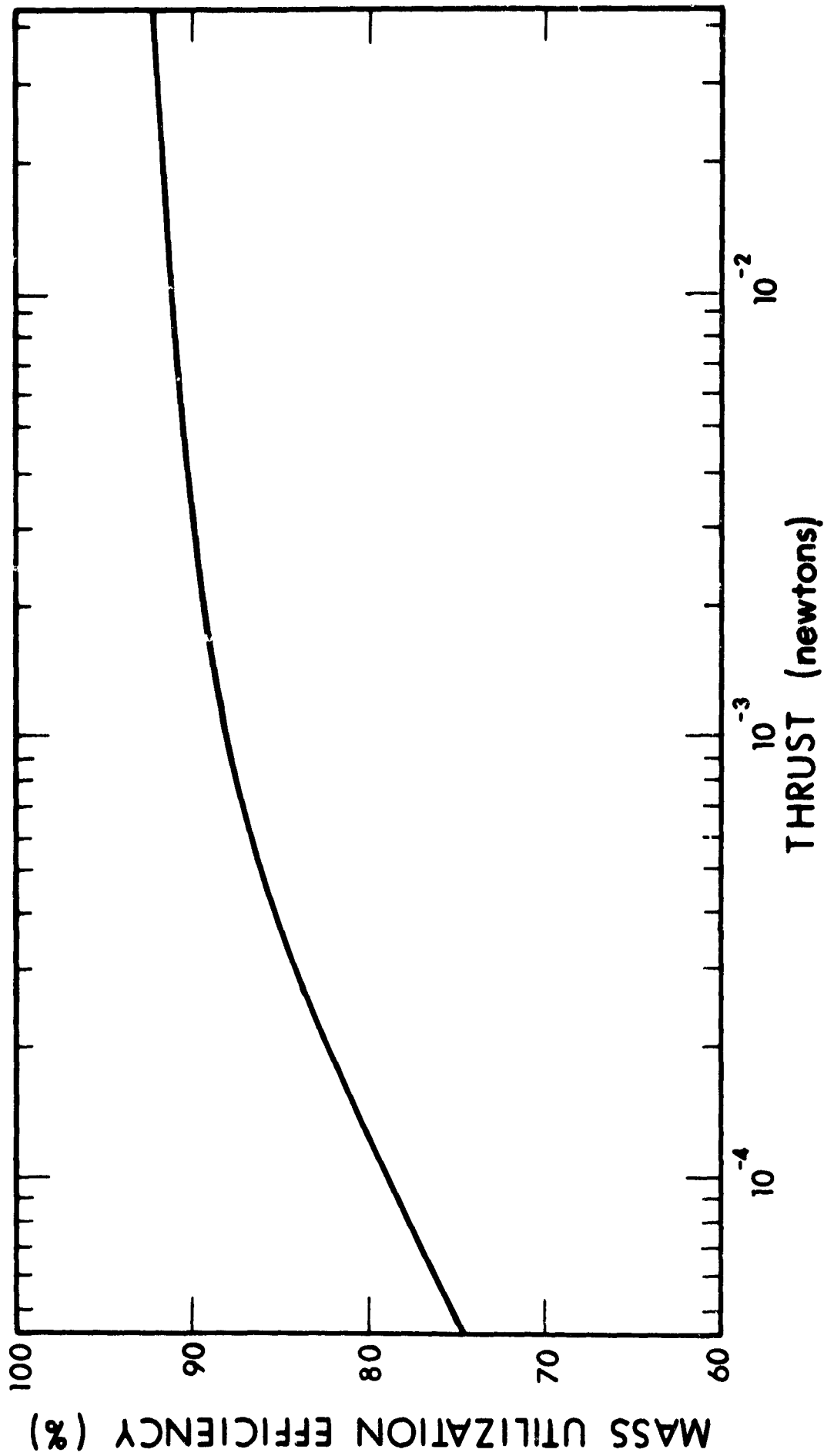


Figure 42. Mass Efficiency versus Thrust

the measured mass change of the reservoir, have been in agreement with the estimated mass efficiency to within 1 percent.

Specific Impulse

For low thrust ion engines, the small total fuel mass required reduces the importance of specific impulse. Such systems are normally considered for power-limited satellite applications, so specific impulse is determined by the point at which the minimum thruster power is realized. For high thrust missions where significant spacecraft design parameters are affected by the efficiency versus specific impulse characteristic of the engine, specific impulse cannot be ignored.

The specific impulse is determined by the mass utilization efficiency and accelerated ion energies. The ion energies are determined by the net accelerating potential which can be accurately approximated by the positive high voltage potential applied to the ion source. No doubly charged ions are observed with cesium electron bombardment ion engines, so the average exhaust velocity can be computed as the product of the mass efficiency and the ideal exhaust velocity.

The change of power efficiency with specific impulse is not very great, so specific impulse can be generalized. Figure 43 shows the resulting specific impulse as a function of thrust level. The ideal specific impulse is that corresponding to the ion velocities uncorrected for the mass utilization efficiency.

Power Efficiency

For thrust levels well in excess of 4.5 millinewtons, thruster efficiency is not strongly dependent upon size and the performance of cesium bombardment engines can be characterized by a power-to-thrust ratio

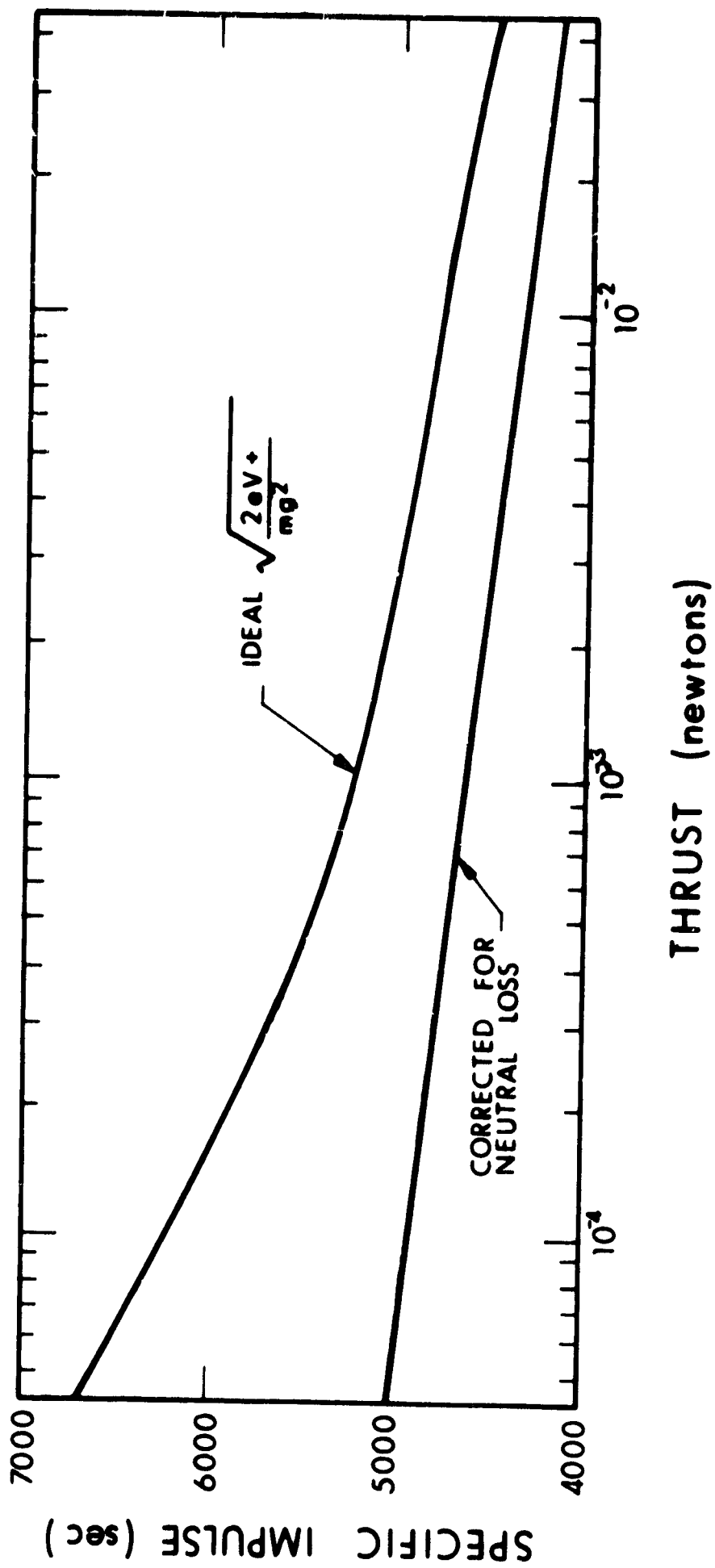


Figure 43. Specific Impulse versus Thrust

versus specific impulse curve as shown in Fig. 44. Another curve used to define this performance is the overall engine efficiency versus specific impulse as shown in Fig. 45. Detailed engine power requirements will be presented and discussed in Subsection 2.1.4.

2.1.3.2 Feed System

Zero-g cesium feed systems have been built and operated with capacities ranging from 0.05 kg to 18 kg. Propellant tankage masses have ranged from 100 percent of the fuel mass for the smallest feed systems to 10 percent for lightweight 2.3 kg feed systems, and 15 percent for large systems which were not designed to be especially mass efficient. Flight qualified cesium feed systems can be built with a mass in the neighborhood of 10 percent of their cesium mass capacity. Two typical feed systems are shown in Fig. 46. These feed systems have capacities of 0.25 kg and 18 kg. The larger system has a laboratory valve atop its vaporizer and the small feed system has a neutralizer attached.

Power requirements for these zero-g feed systems range from 3 watts to 10 watts as shown in Fig. 47. The power required depends upon the response speed necessary. Heat shielding can be used to minimize the power requirement. Most systems built to date have had response times on the order of 30 to 60 seconds. The mass performance expected from cesium zero-g feed systems is shown in Fig. 48. The data are presented as a function of fuel mass since this determines the overall size of the feed system. Feed system volume is shown in Fig. 49.

2.1.3.3 Neutralizer

The principal mass of the cesium discharge neutralizer is the feed system and cesium mass. The cesium mass is determined by the mission duration and the emission current or thrust level. These neutralizers

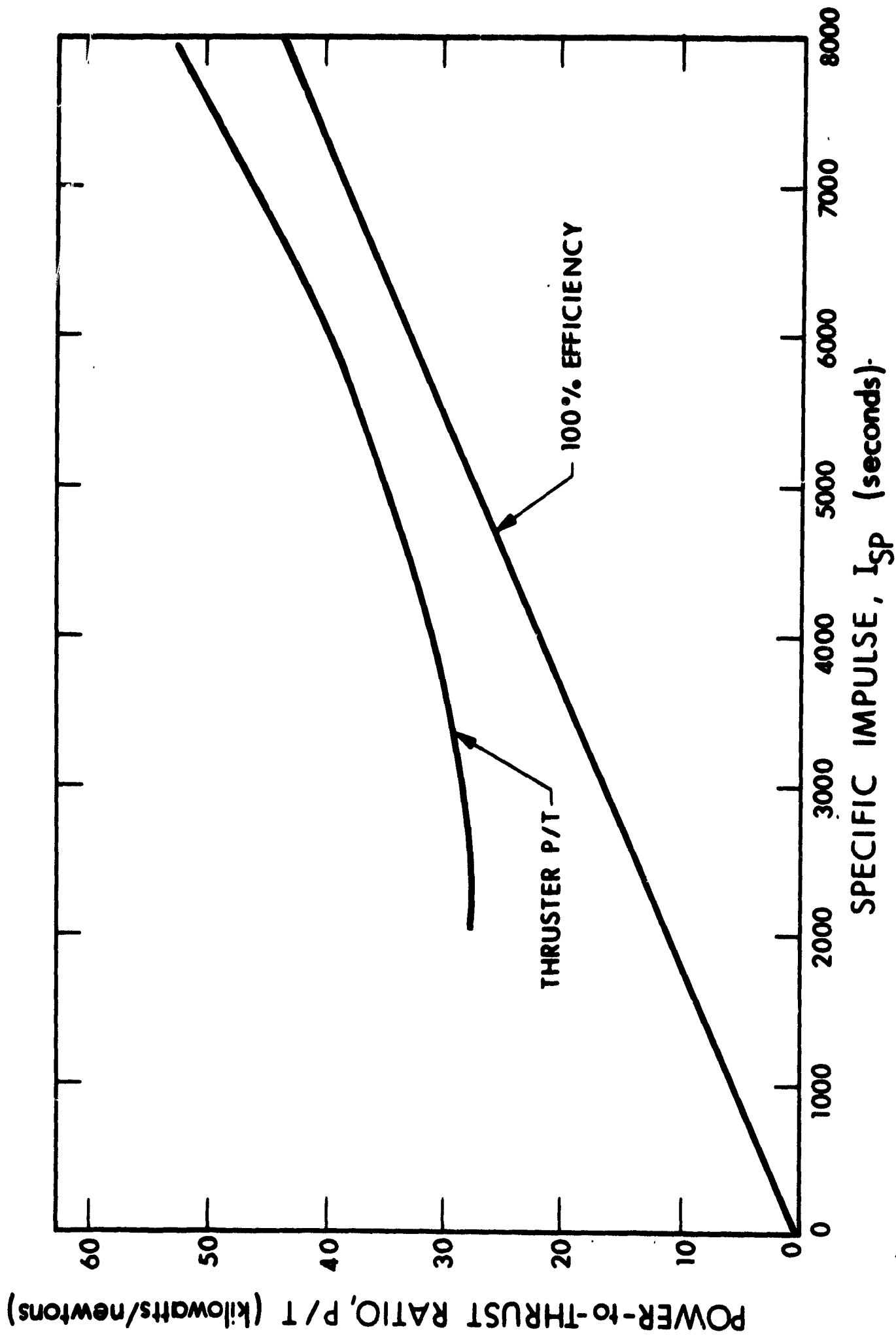


Figure 44. Power-to-Thrust Ratio versus Specific Impulse

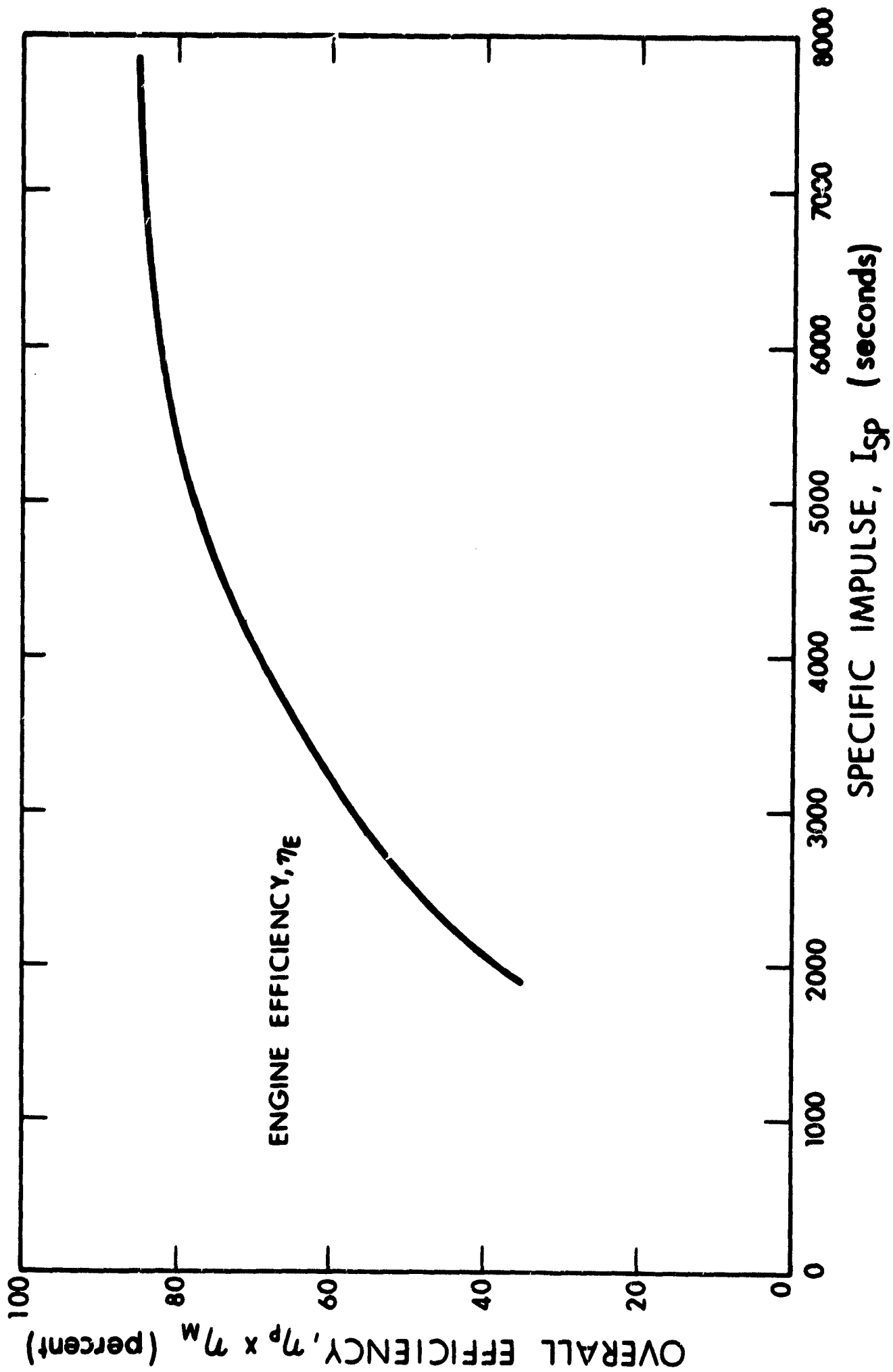


Figure 45. Overall Efficiency versus Specific Impulse

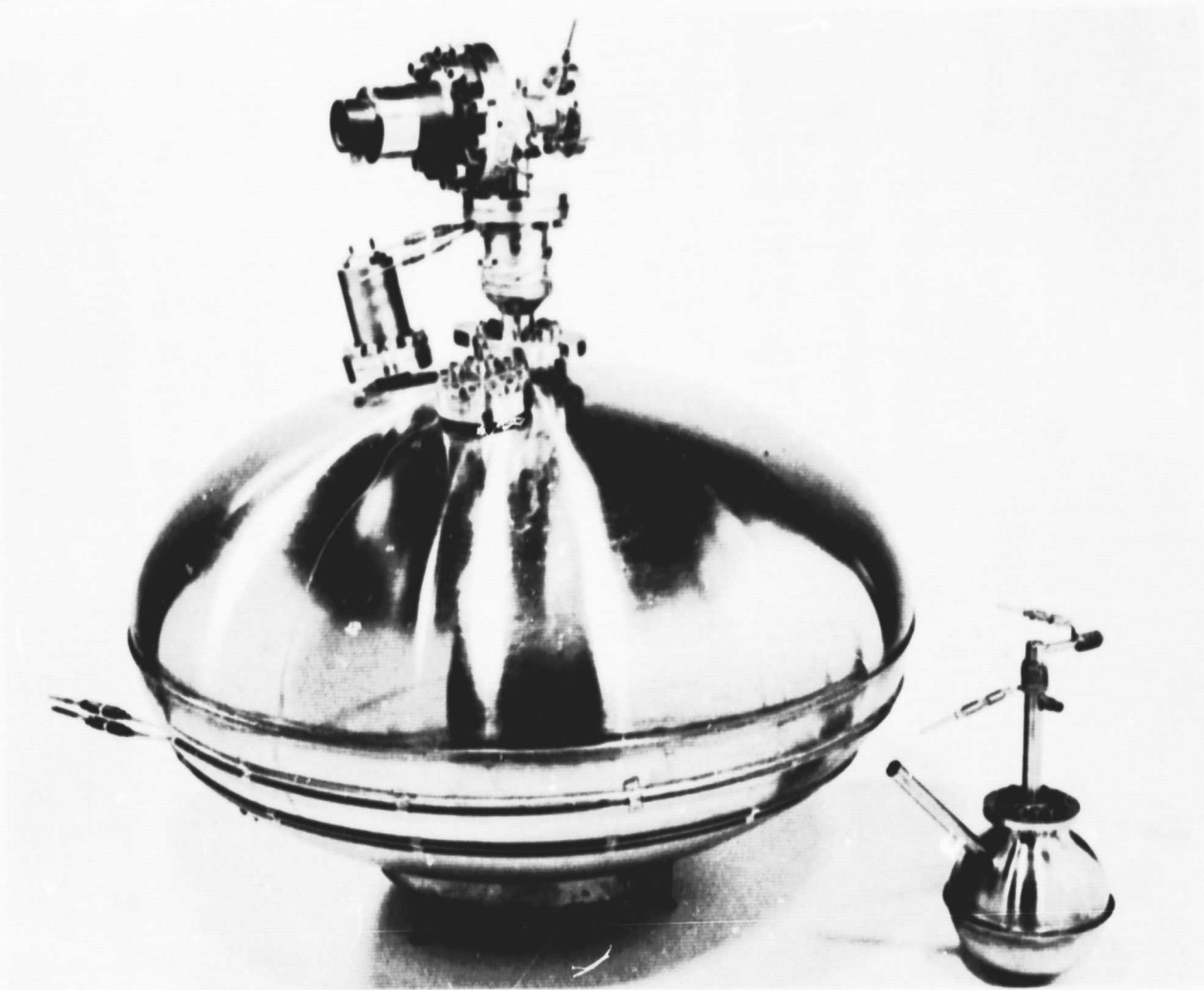


Figure 46. Zero-g Cesium Feed Systems

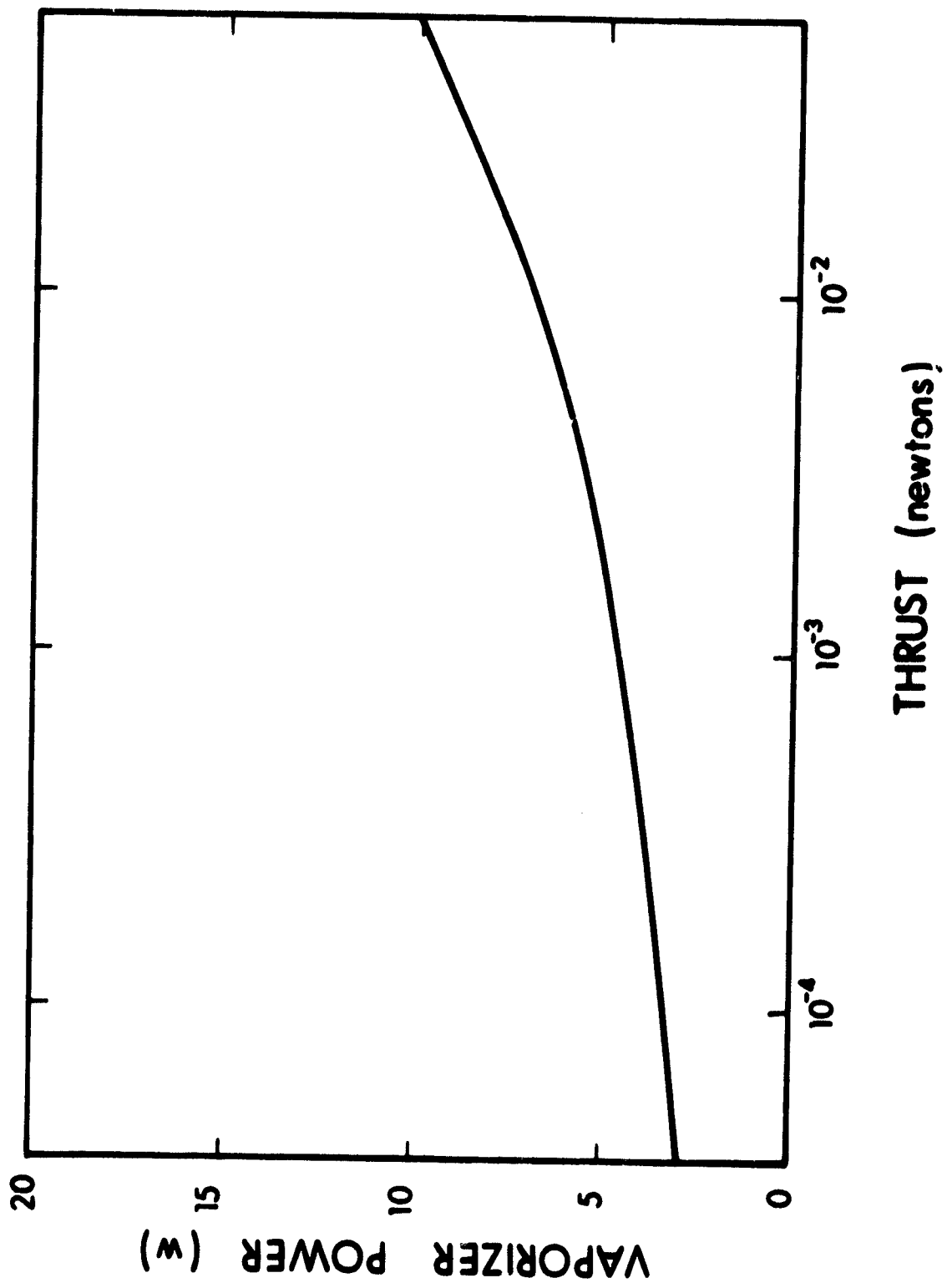


Figure 47. Feed System Power Requirements

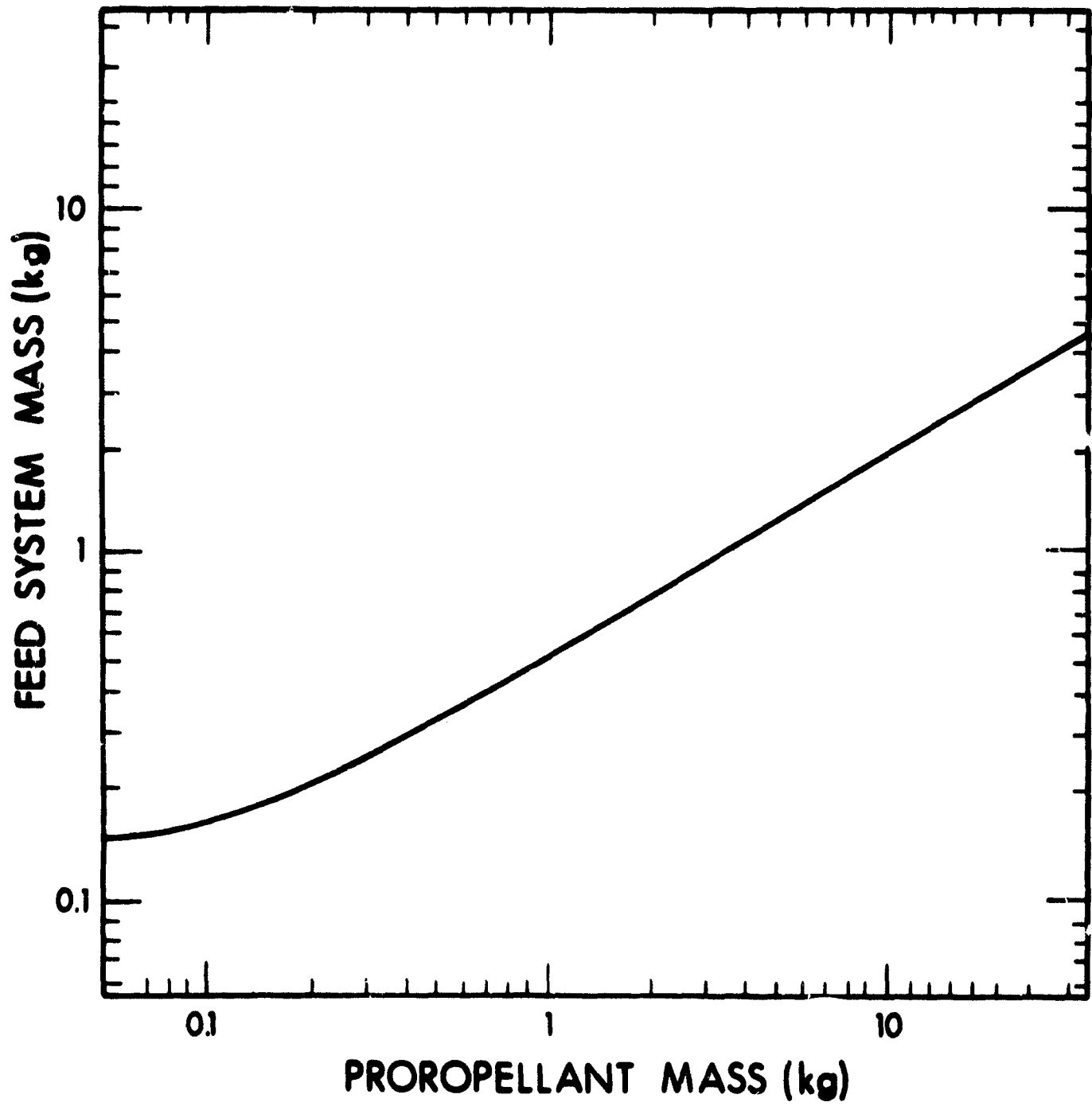


Figure 48. Cesium Feed System Mass Performance

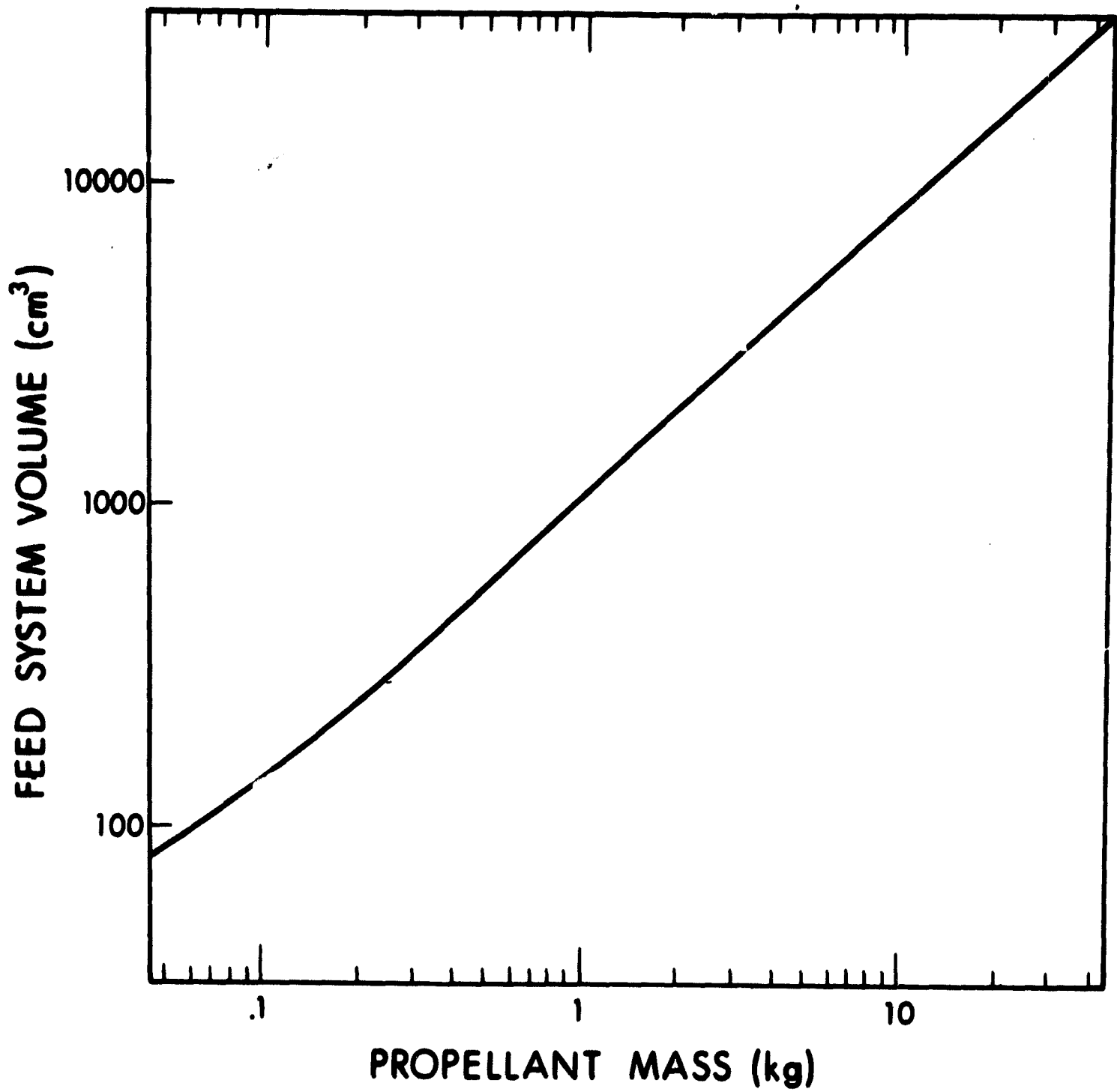


Figure 49. Feed System Volume versus Capacity

require a minimum cesium flowrate at low thrust levels and approximately 1 percent of the engine flowrate at high thrust levels. In the range of interest between 4×10^{-5} and 5×10^{-7} newtons thrust, the neutralizer mass is relatively independent of the product of thrust and time except near 5×10^{-2} newtons thrust, where the mass becomes proportional to this product. Volume is determined by the neutralizer mass since the mass is primarily cesium. Neutralizer mass and volume are shown in Figs. 50 and 51, respectively.

Neutralizer power consumption is nearly independent of the thrust level. Neutralizer anode, cathode, and vaporizer powers are plotted as a function of thrust level in Figs. 52 and 53.

2.1.3.4 Propellant Requirements

The total propellant mass required is determined by the product of thrust and time divided by specific impulse. Figure 54 shows curves of propellant weight versus thrust for different mission times. These curves were drawn using the specific impulse corrected for mass efficiency from Fig. 43. The dotted line in Fig. 54 corresponds to a curve for constant specific impulse. As can be seen, the effect on total mass of assuming a constant specific impulse is very small. If this assumption is made, a single curve for propellant mass as a function of the product of thrust and mission time can be drawn as shown in Fig. 55.

2.1.3.5 System Volume

To the sum of engine, feed system, and neutralizer volumes one must add additional space since the components do not necessarily mesh in a clean physical package. This packaging volume is shown in

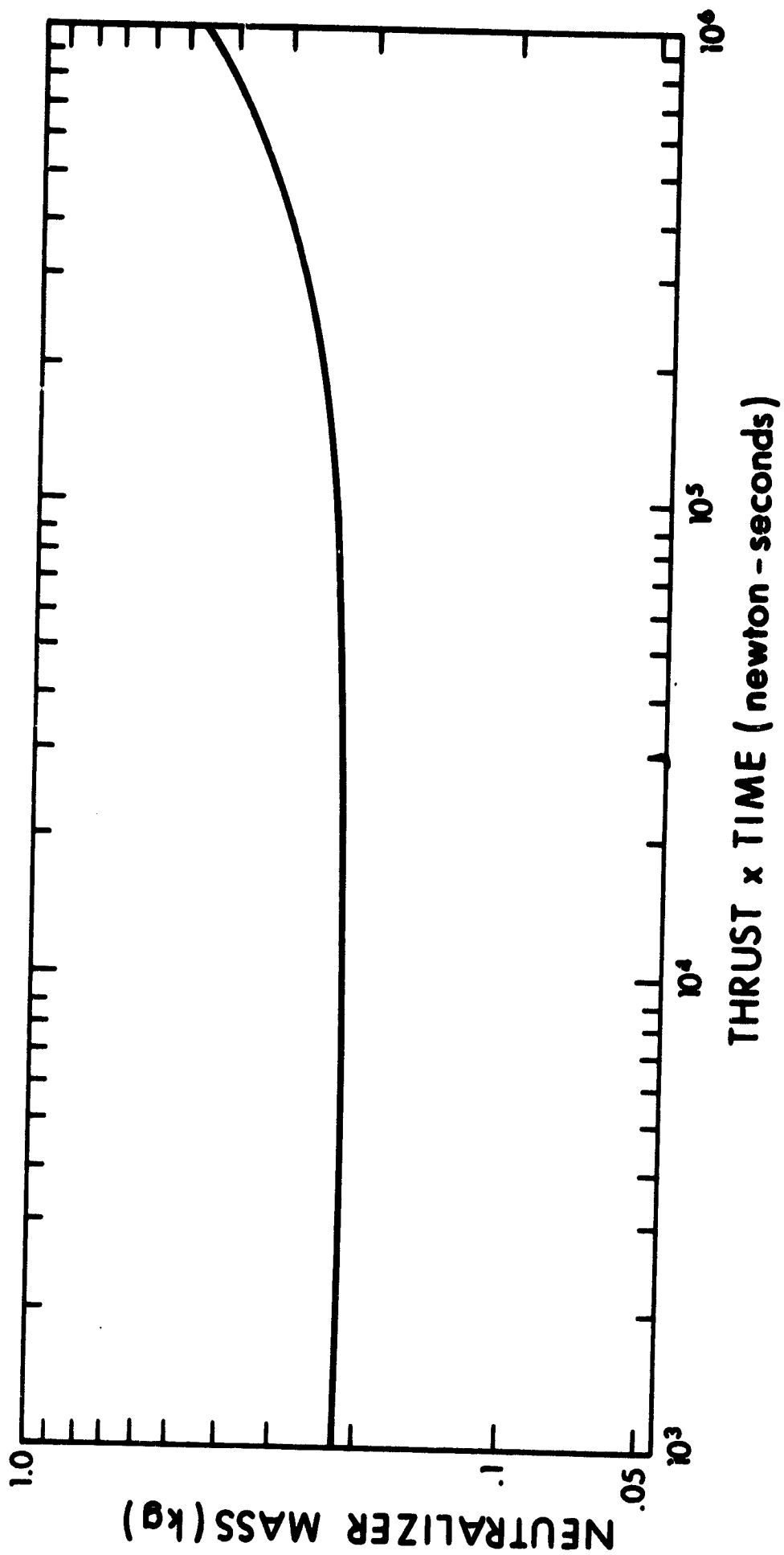


Figure 50. Neutralizer Weight versus Impulse

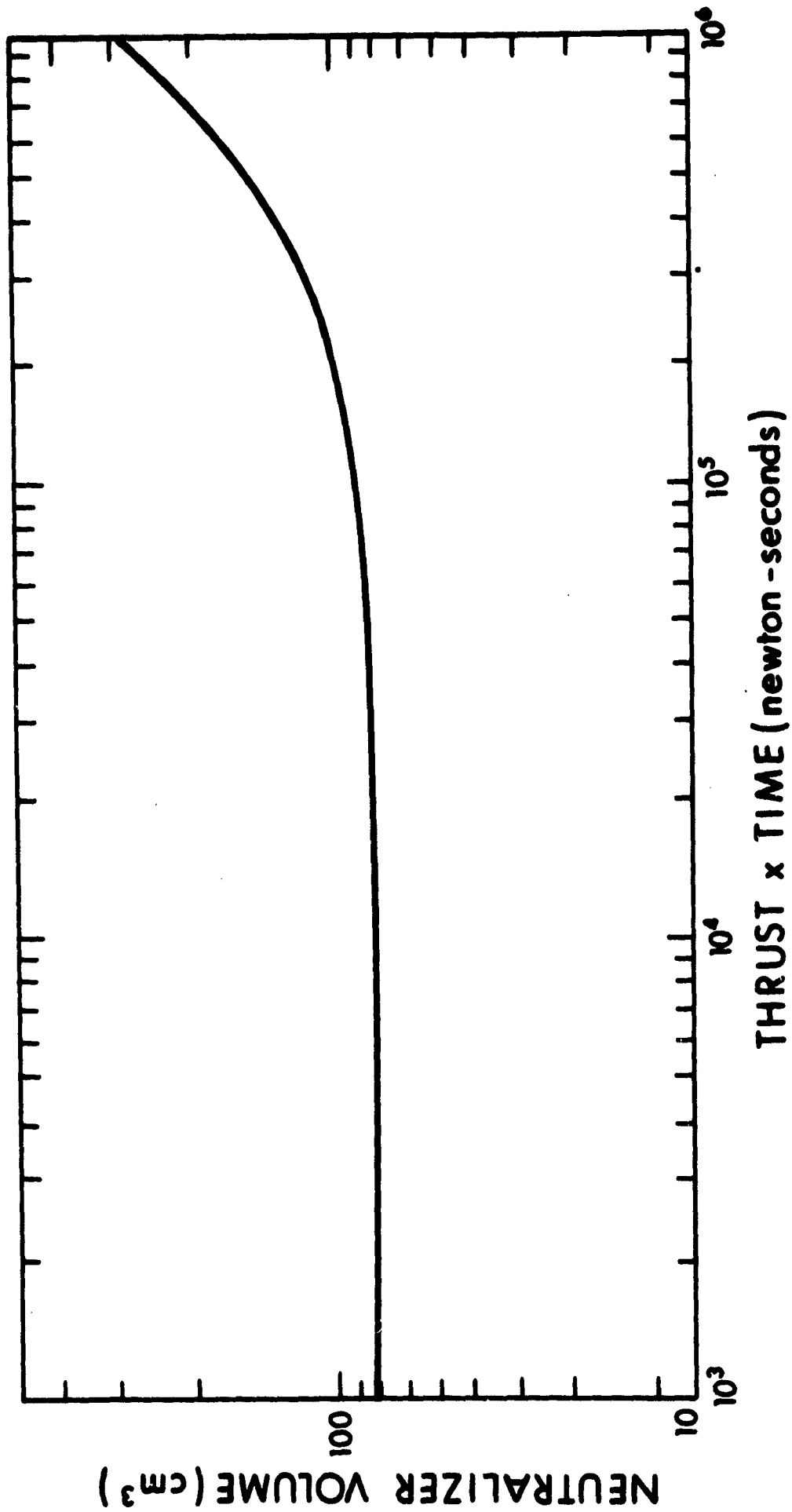
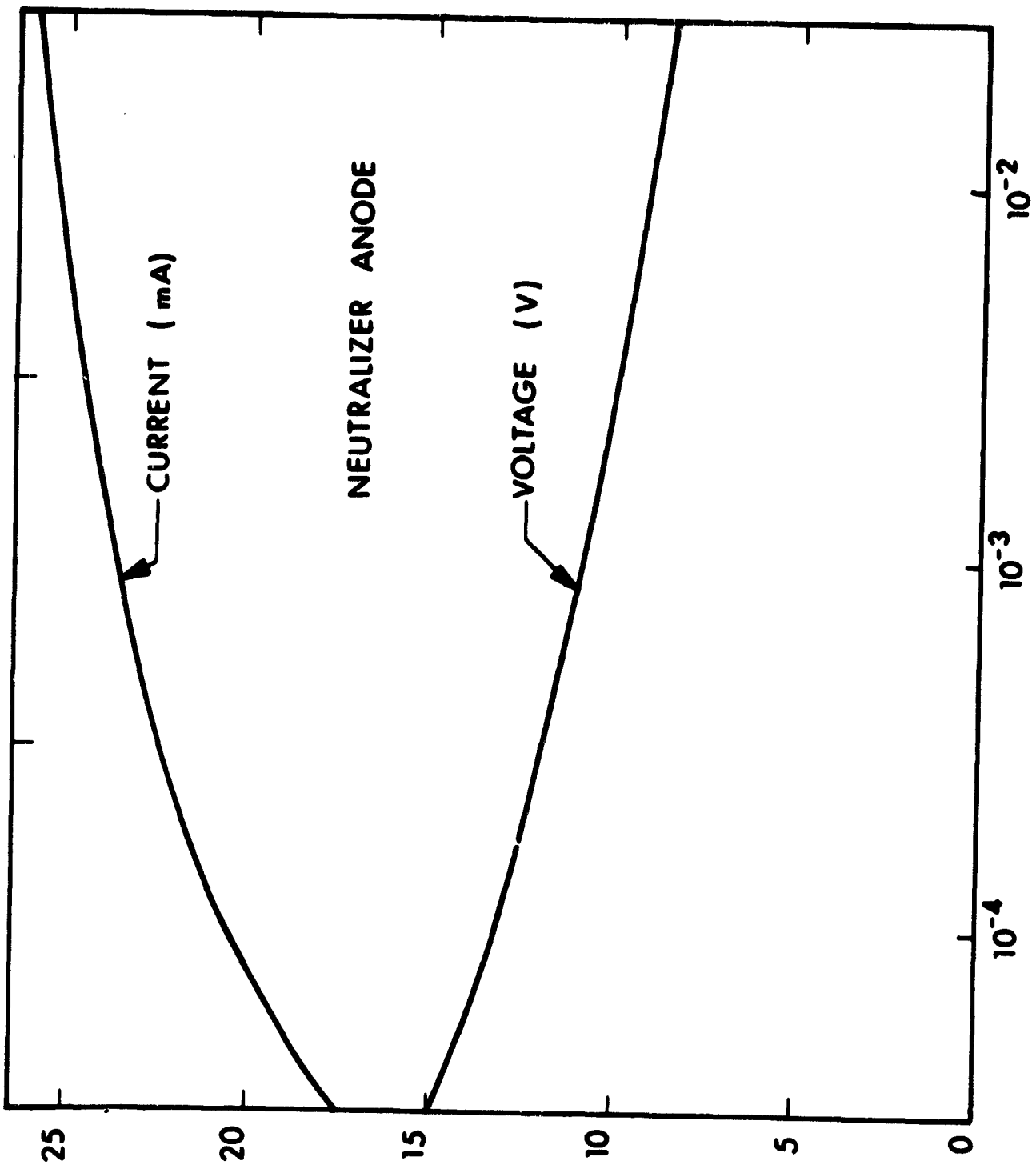


Figure 51. Neutralizer Volume versus Impulse



THRUST (newtons)

Figure 52. Neutralizer Anode Power

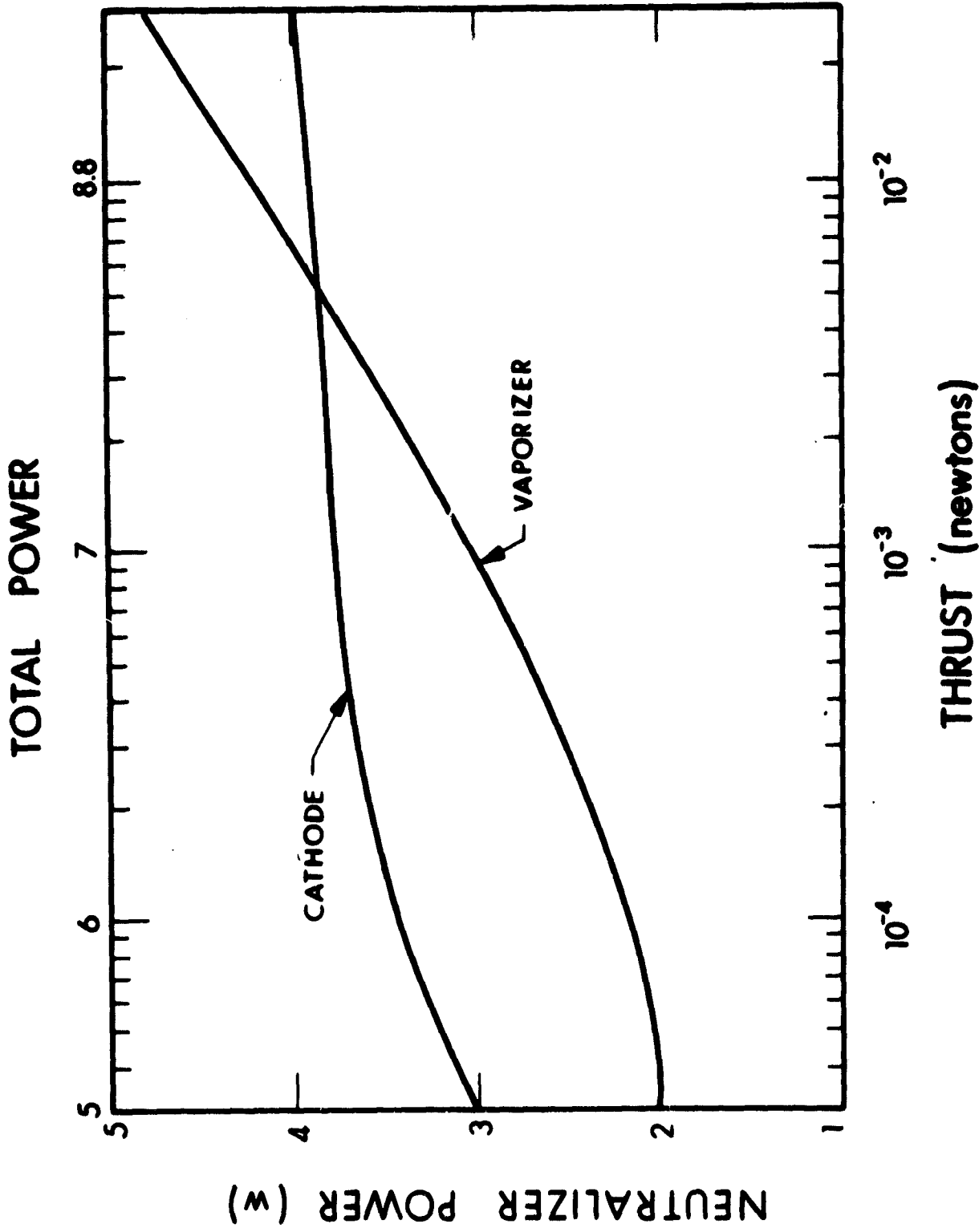


Figure 53. Neutralizer Heater Powers

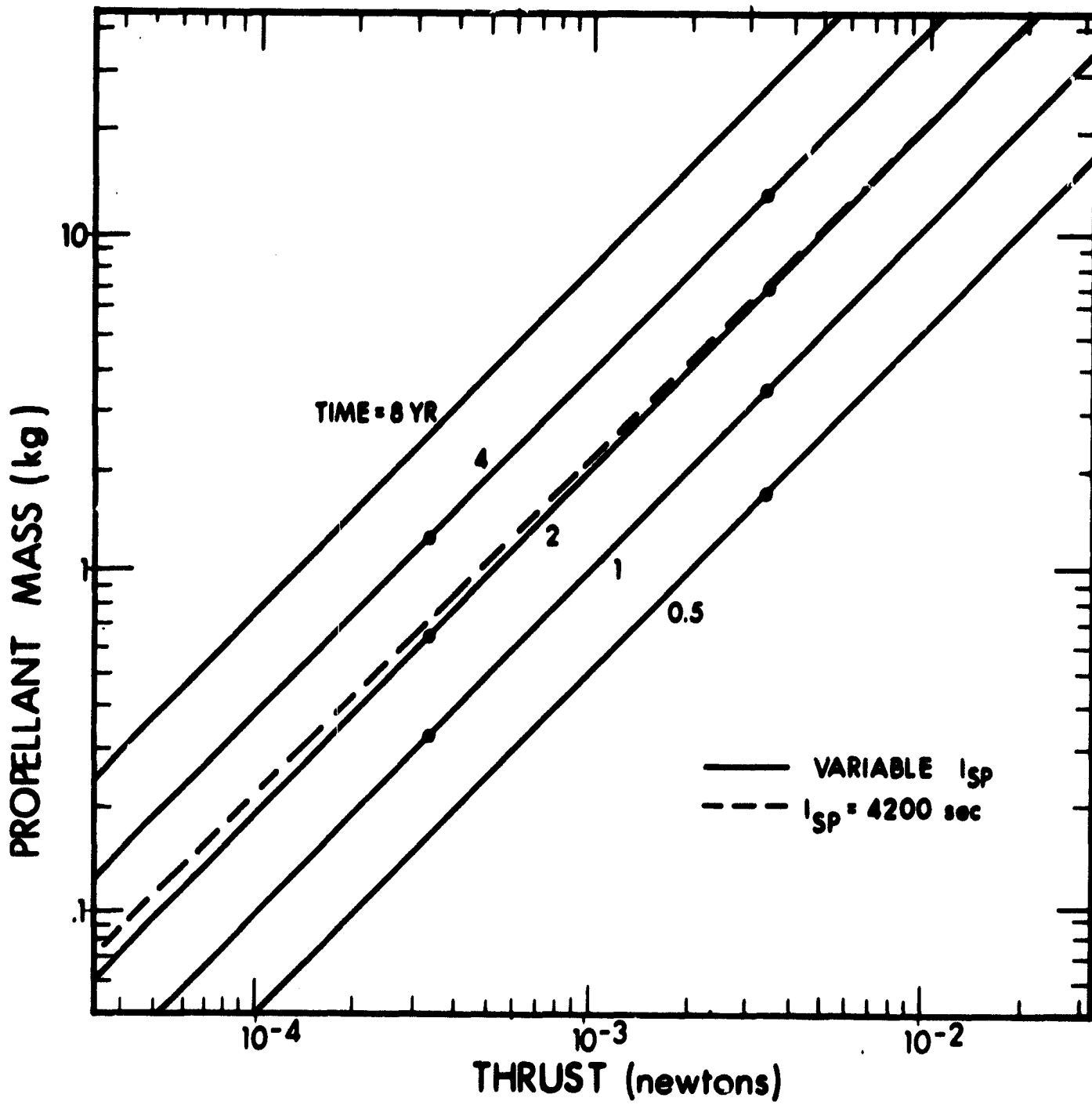


Figure 54. Propellant Mass Requirements

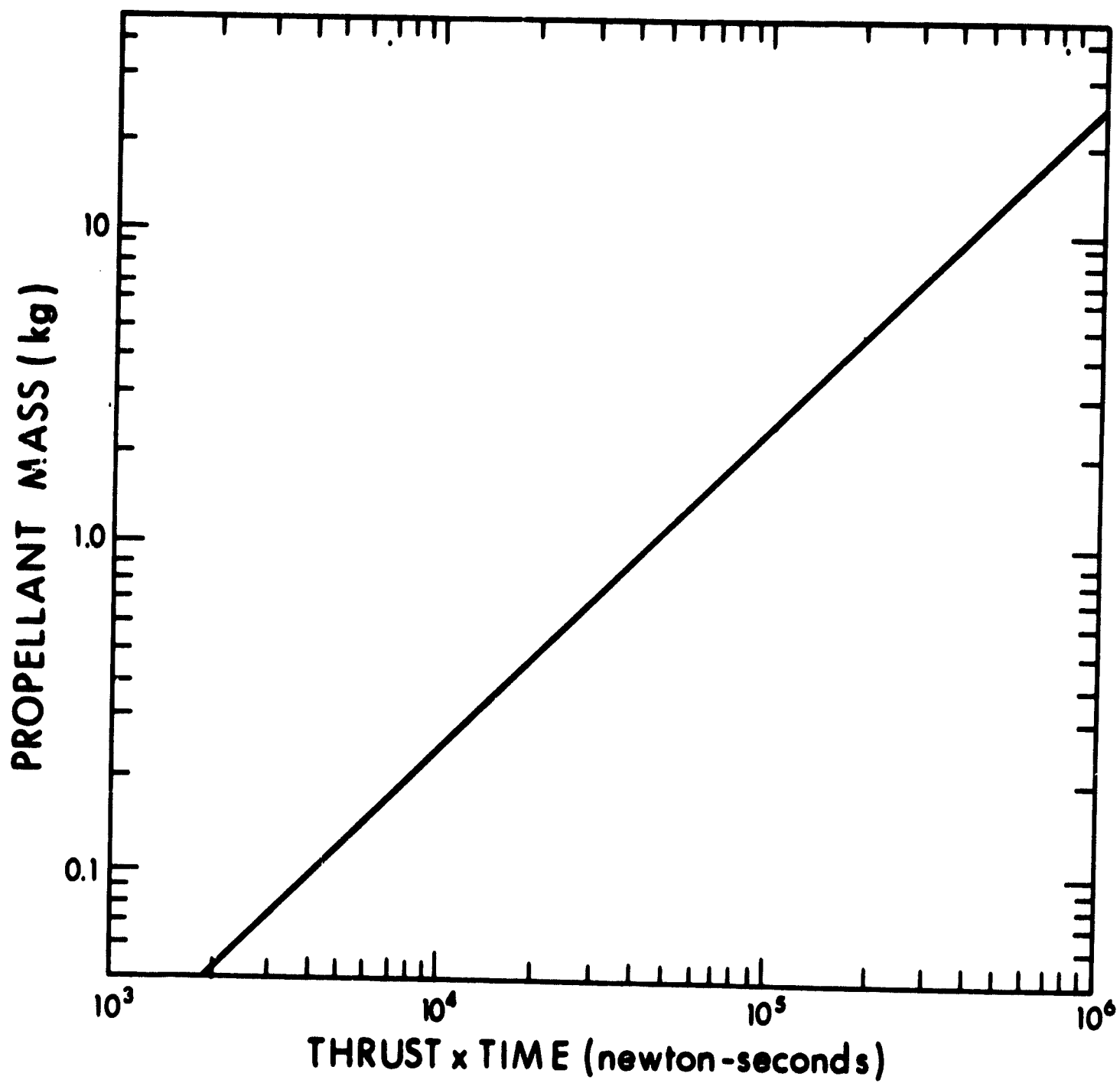


Figure 55. Approximate Propellant Weight versus Impulse

Fig. 56 as a function of the component volumes. This assumes the system is packaged effectively in a right circular cylinder of approximately two-to-one length-to-diameter ratio. Since the component volumes are determined by both thrust and mission time, the overall system volume is presented in Fig. 57 as a function of thrust for various mission durations.

2.1.3.6 System Mass

System mass performance is somewhat more difficult to predict. In this analysis, we have assumed three components for the packaging mass over and above the mass of the engine, propellant, feed system, and neutralizer. This mass consists of a fixed mass of 0.3 pounds, plus 10 percent of the component mass, plus a mass proportional to the overall package area of 0.01 pounds per square inch. These weights, added to the subsystem mass, yield a set of curves of system mass versus thrust for different mission times. This set of curves is shown in Fig. 58.

2.1.3.7 Power

Adding the engine powers from Subsection 2.1.4 to the neutralizer and feed system powers, the overall system power as a function of thrust is shown in Fig. 59.

2.1.4 POWER CONDITIONING REQUIREMENTS

A maximum of nine engine, feed systems, and neutralizer loads must be provided with appropriate powers. These loads can accept dc and/or ac depending upon the nature of the load function. The function of each load will be described first, followed by definition of the specific load requirements for various system operating levels.

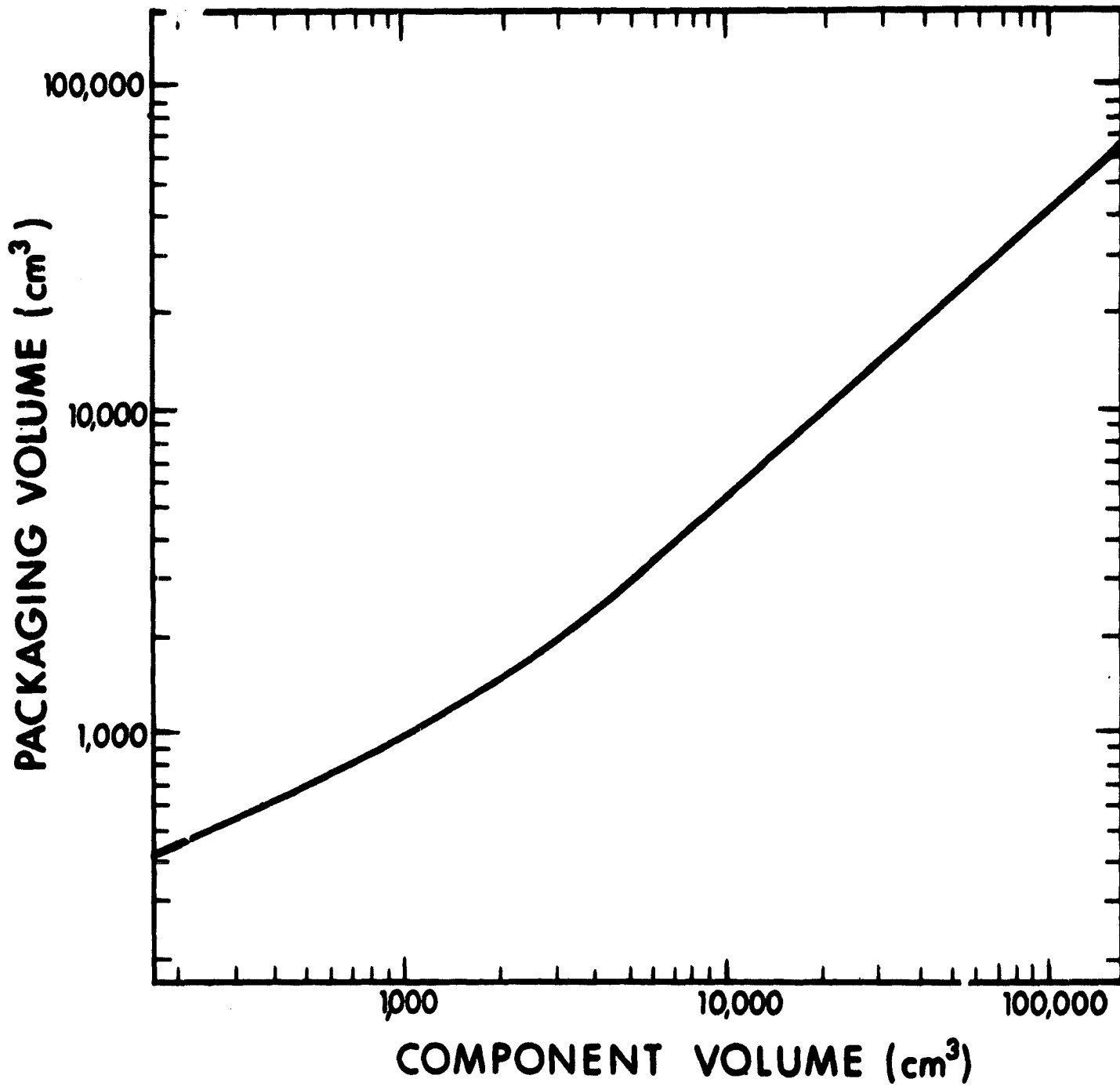


Figure 56. Packaging Volume Efficiency

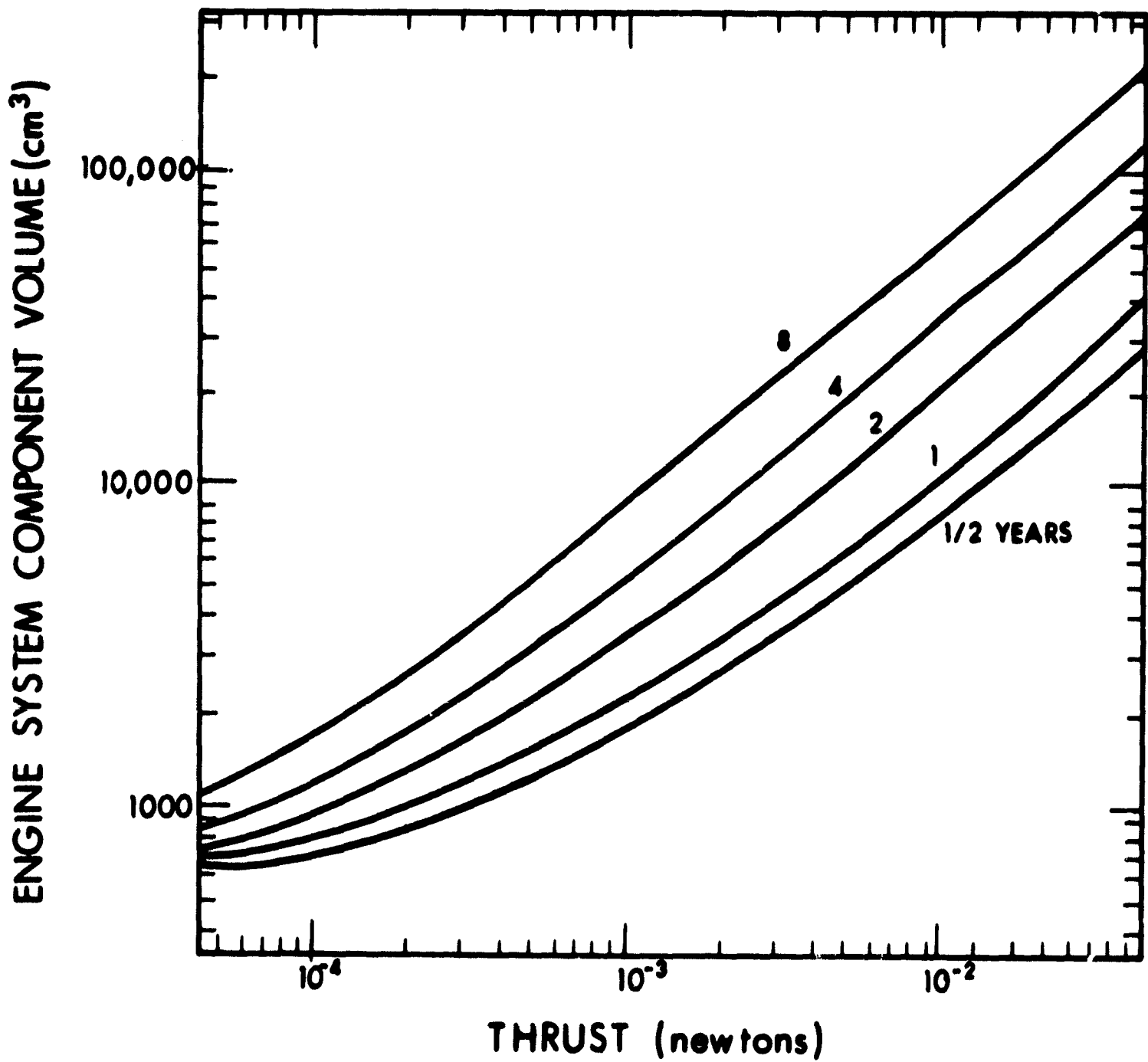


Figure 57. Engine System Component Volume versus Thrust

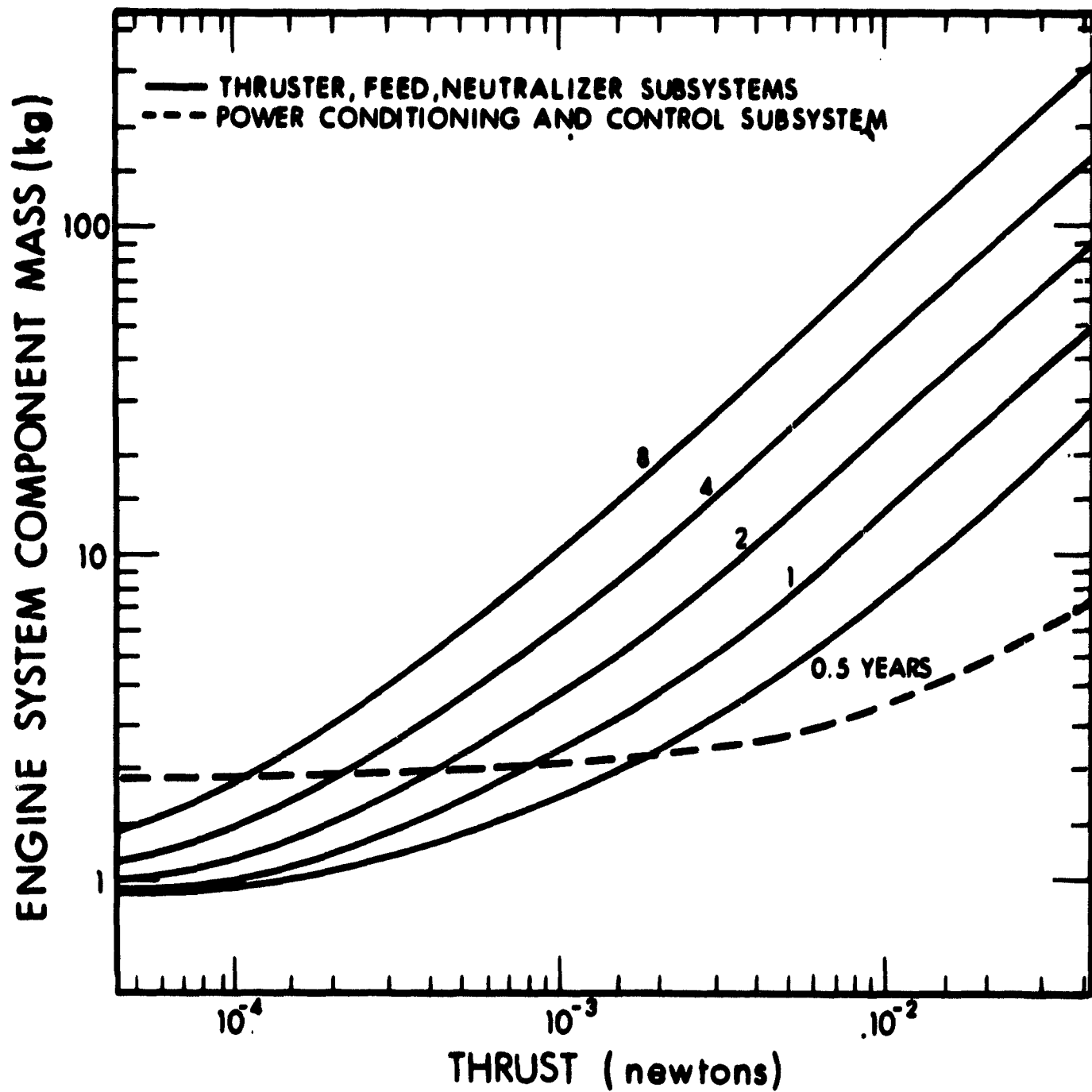


Figure 58. System Weight versus Thrust

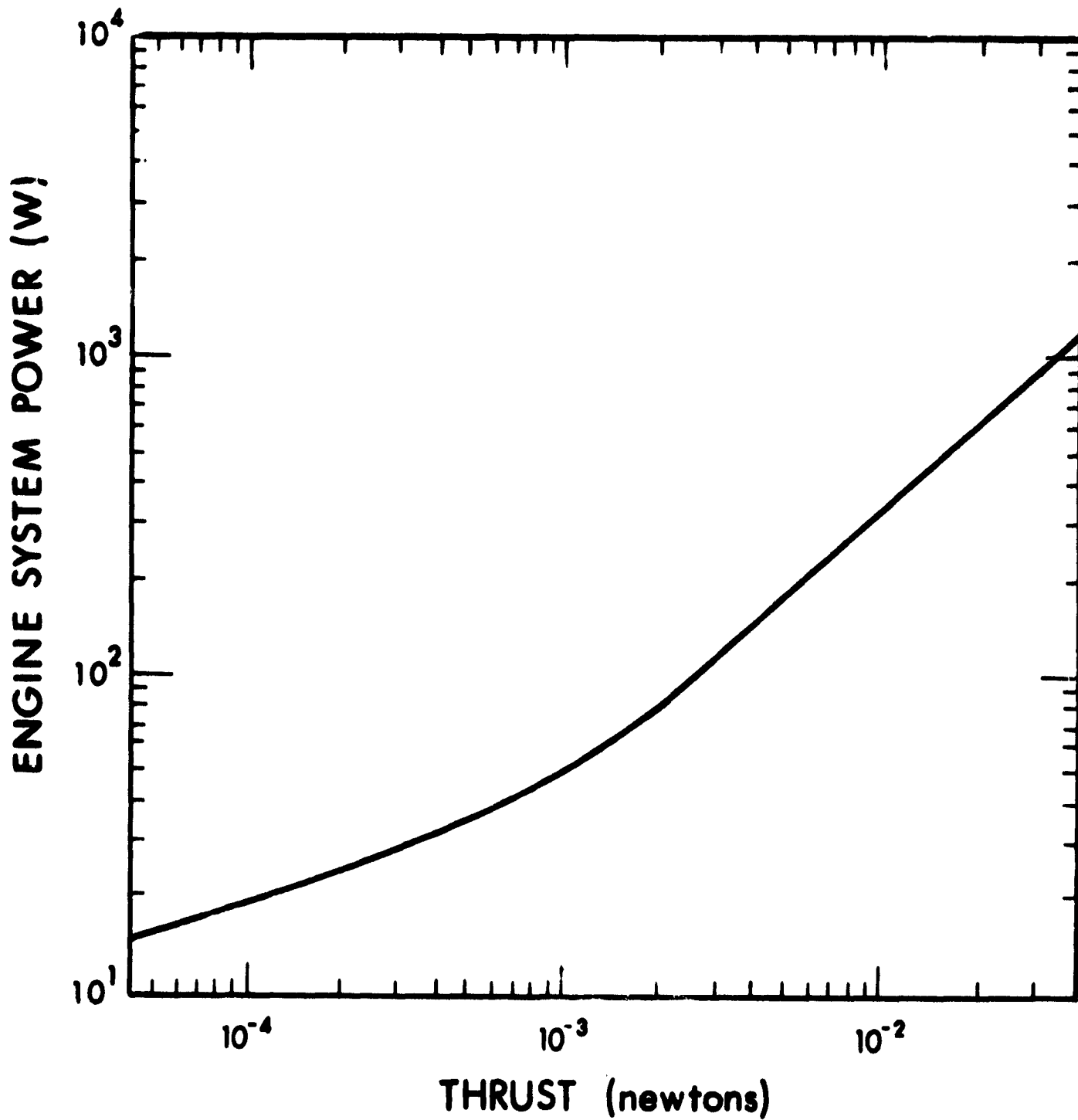


Figure 59. System Power versus Thrust

2.1.4 1 Positive High Voltage

The major portion of the power for thrusters above 4 millinewtons thrust is supplied in the form of positive high voltage power. This supply maintains the source at a positive potential with respect to ground and provides the source of energy for ion beam acceleration. The load for this supply is the ion beam current plus any stray drain currents between ground and the source or the accelerating electrode and the source. With adequate care taken to prevent stray currents from ground to the source, the ion beam current is computed as the difference between the currents to the source supplied by this power supply and the current to the accelerating electrode as shown in Fig. 37.

The power from this supply is the only power which is converted to useful ion beam energy. For high thrust engines, and specifically high efficiency engines, this supply handles the major portion of the electrical power. The positive high voltage supply must satisfy three requirements. First, the supply must be protected against overload caused by breakdowns, This requires a momentary power turnoff to clear faults. Second, when the power supply is turned on, the engine plasma appears as a very low impedance between the high voltage power supply output and ground or the accelerating electrode. As a result, high transient currents must be delivered during the turnon period without triggering the overload cycle. Finally, the positive high voltage must never fall below about 75 percent of the nominal working voltage. This restriction on ripple level is required because bombardment engines always operate space-charge limited. Momentary loss of high voltages will allow the plasma within the engine to extrude into the gap between electrodes. This results in high currents which can trigger the overload circuit.

The current drain on the positive high voltage power supply is primarily determined by the thrust level. Thrust is proportional to the product of ion beam current and the square root of the positive high voltage. The positive high voltage is determined as a function of thrust by the specific impulse data of Fig. 43. The ion beam current is therefore a function of thrust alone. A drain current between the accelerator and positive supply must be added to the beam current. The resultant positive high voltage supply current is shown as a function of thrust in Fig. 60.

The positive high voltage used in this determination is shown as a function of thrust in Fig. 61.

2.1.4.2 Negative High Voltage

The second power supply and the only other high voltage power supply is the negative accelerator bias supply. This supply provides the bias required to establish a negative barrier to reflect electrons from the exhaust beam. This barrier prevents electron backstreaming from the exhaust beam to the source which would result in a power loss. Again, overload protection, turn-on surge current capability, and limited ripple are requirements for this supply.

The barrier voltage required to prevent electron backstreaming depends upon the positive high voltage and is shown as a function of thrust in Fig. 62. The current drain on this supply ranges from 10 percent of the positive high voltage current at low thrust levels to the order of 1 percent at high thrust levels. This current is shown in Fig. 63.

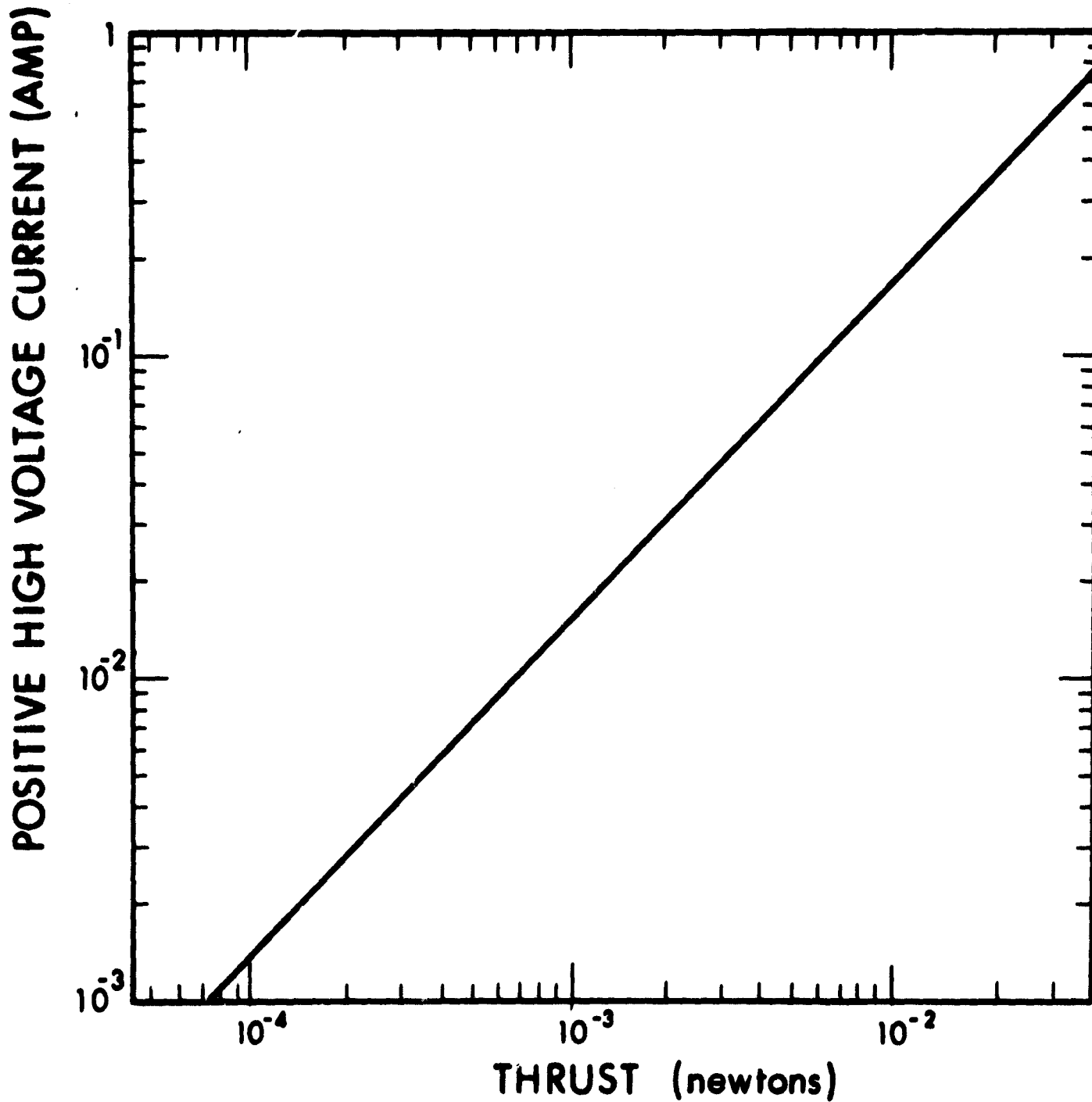


Figure 60. Positive High Voltage Current versus Thrust

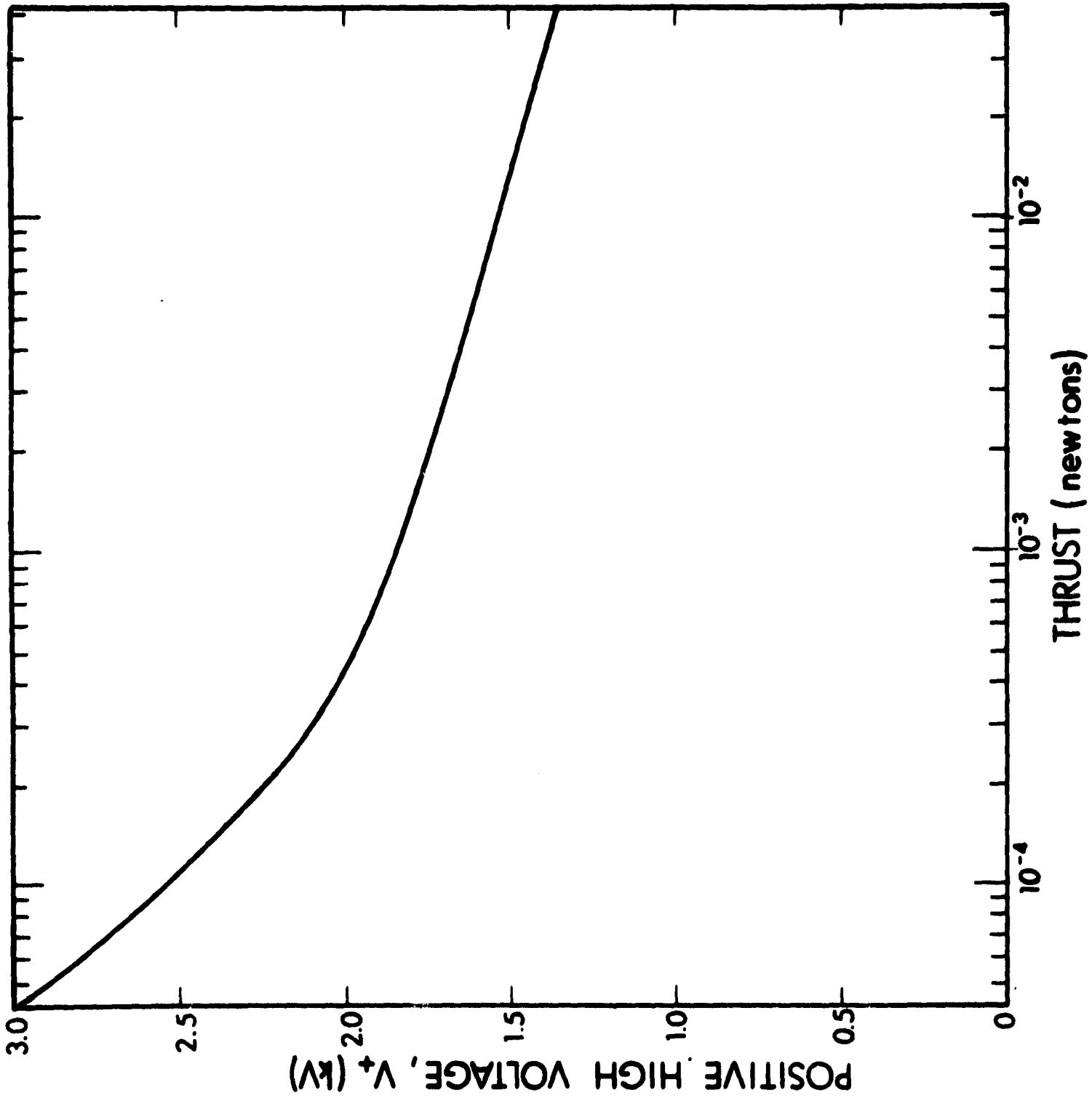


Figure 61. Positive High Voltage versus Thrust

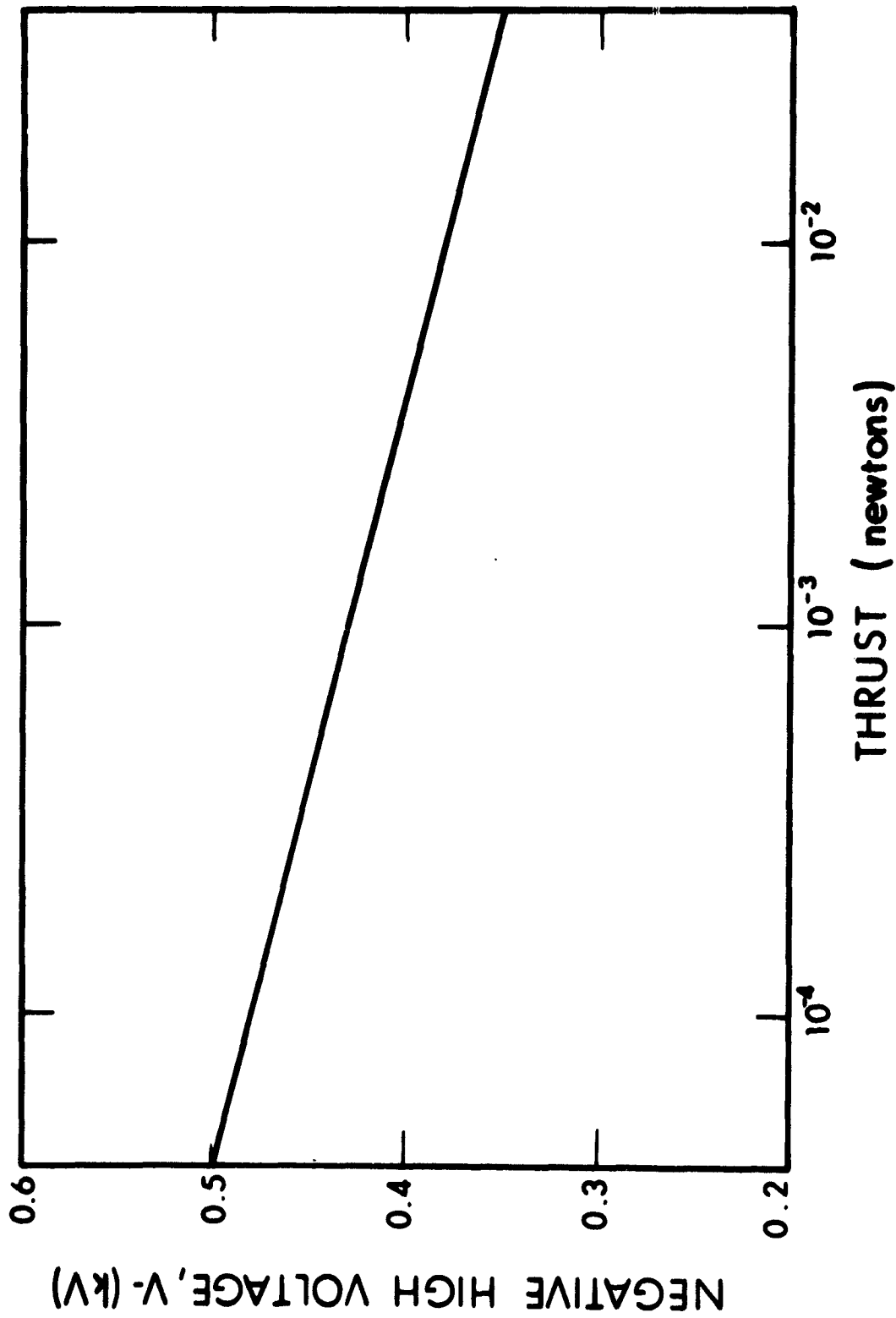


Figure 62. Negative High Voltage versus Thrust

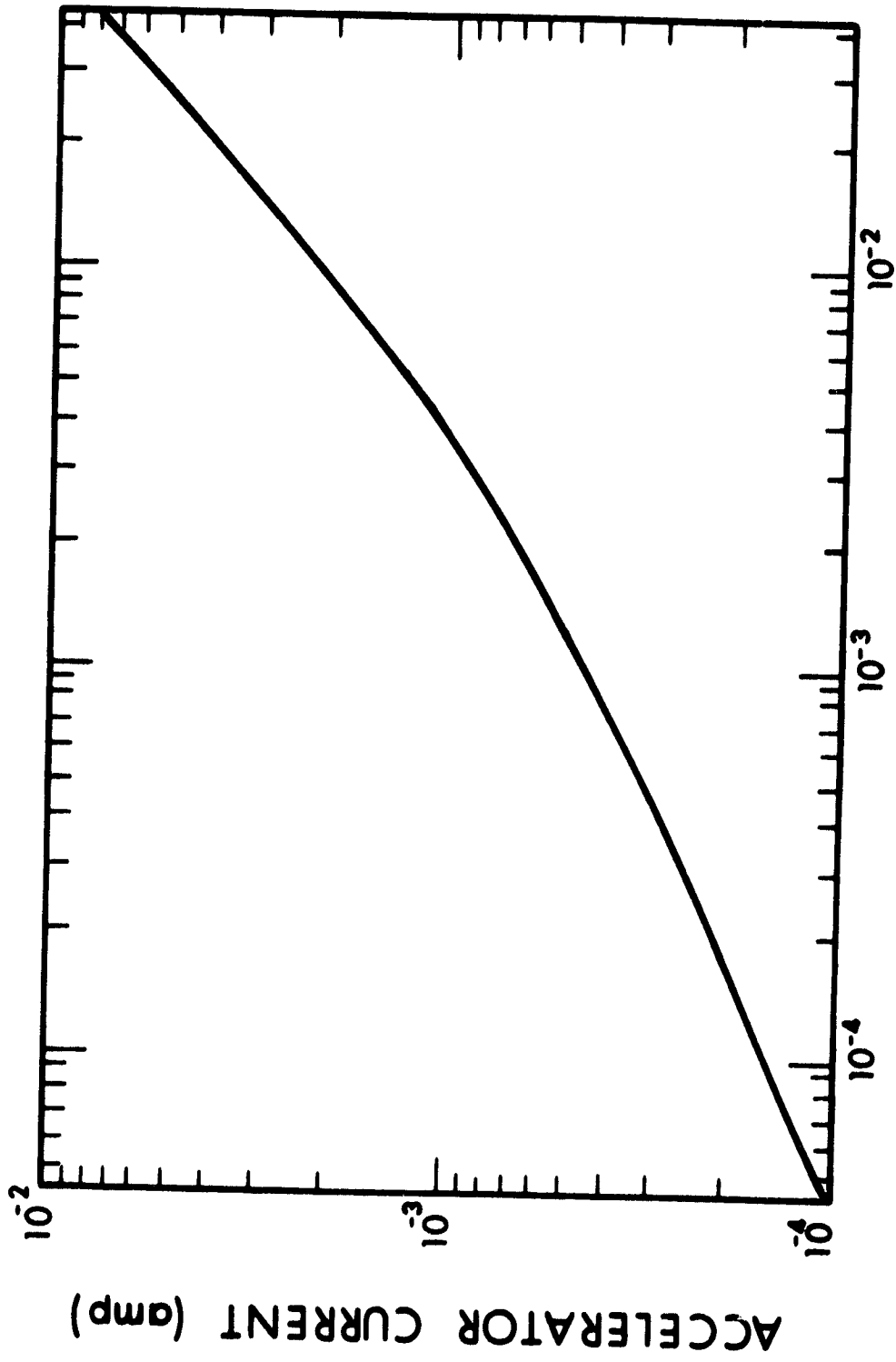


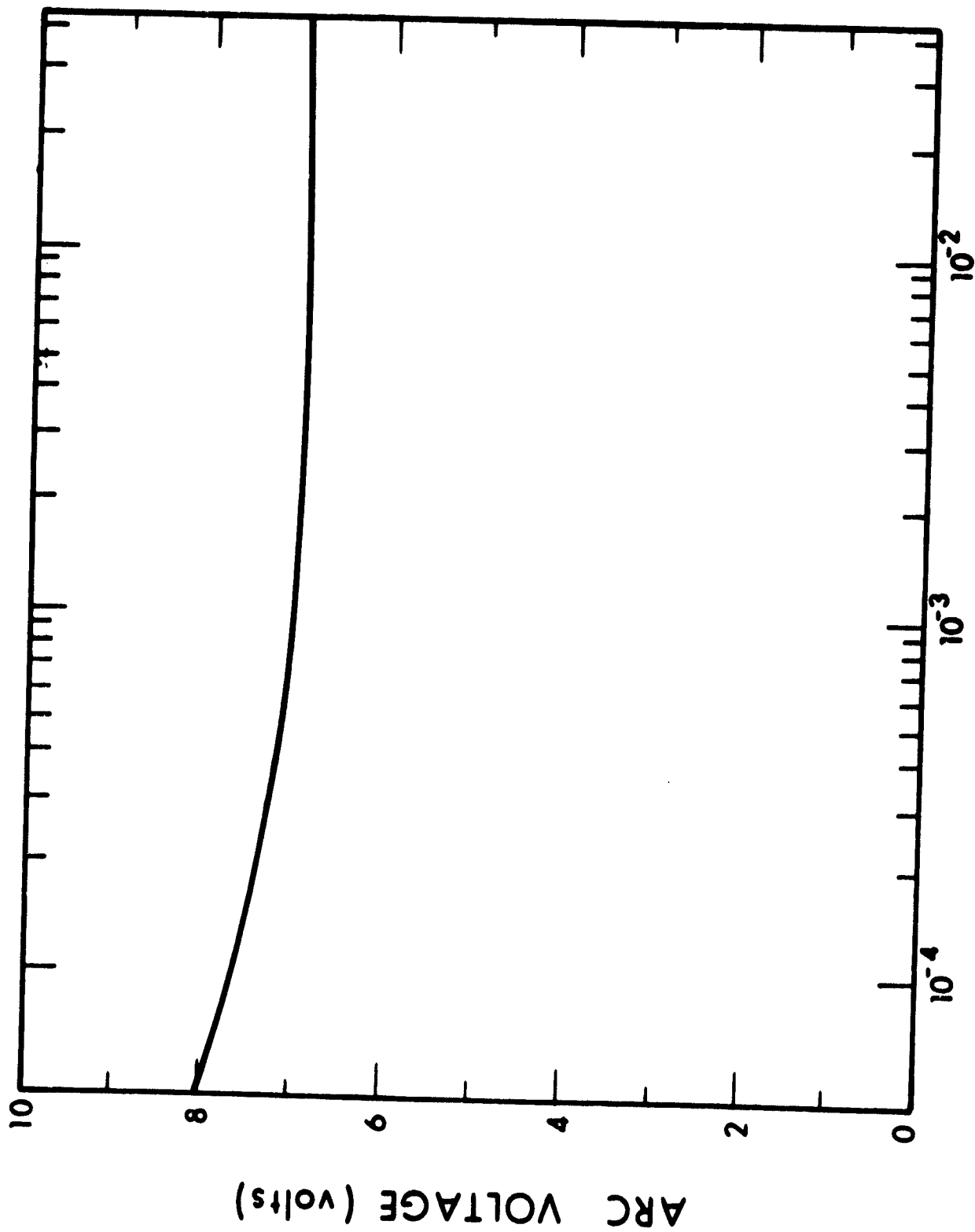
Figure 63. Arc Current versus Thrust

2.1.4.3 Discharge Power

This supply provides the voltage and current necessary to sustain the discharge in the engine. This supply is biased at high voltage (V_+) and its output current is normally limited to protect the supply. The discharge power supply output is controlled by a feedback control loop as shown in Fig. 37. This control circuitry modulates the discharge power and senses the magnitude of the resultant modulation on the ion beam current. High beam modulations indicate that the addition of a small amount of discharge power will result in a high beam current increase. In this case, the control increases the average discharge power. The control effectively maximizes the overall source efficiency.

If a dc discharge power supply is used the current ripple must be limited to approximately 10 percent of the average current level. When alternating current power is supplied to the engine (when multiple anodes are used in a self-rectifying discharge configuration) inductive filtering must be used in the center tap return line to the cathode to achieve 10 percent discharge current filtering.

The discharge voltage is nearly the same for all cesium electron bombardment ion engines. A slight increase in voltage is observed at the low thrust level. Discharge voltage is shown as a function of thrust in Fig. 64. The discharge current is a function of the ion beam current which in turn is a function of thrust level, so the discharge current is also shown as a function of thrust in Fig. 65.



THRUST (newtons)

Figure 64. Arc Voltage versus Thrust

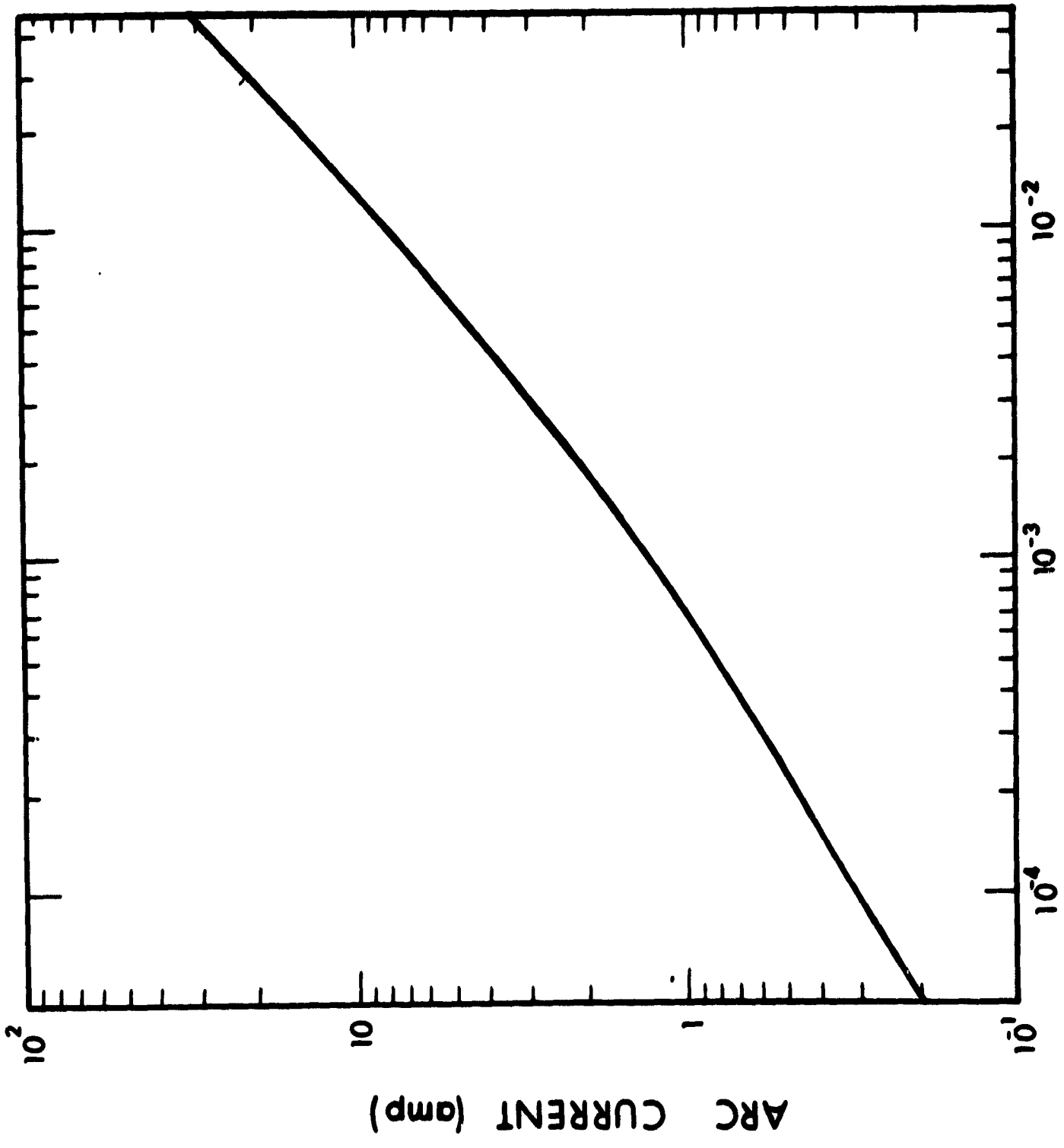


Figure 65. Negative High Voltage Current versus Thrust

2.1.4.4 Cathode Power

Cathode power is required for large engines only during startup. For smaller engines, it may be required continuously. The cathode power serves to bring the cathode to temperatures adequate for electron emission and, if necessary, to maintain the cathode at such temperatures. Since the power delivered is converted entirely into thermal energy, any waveform may be accepted. The power supply must be isolated at positive high voltage and must be capable of being turned off for auto-cathode operation. Both preheat and steady-state cathode power levels are shown in Fig. 66.

2.1.4.5 Magnet Power

A magnet power supply is required when spacecraft constraints preclude the use of permanent magnet materials. This is a low voltage dc power supply, again isolated at the positive high voltage potential. Regulation and filtering to within 5 percent is the generally established requirement for this supply. This power is shown in Fig. 67.

2.1.4.6 Feed System Power

The feed system requires only one power supply. This is the vaporizer power shown earlier. As in the case of the cathode power supply, all the electrical energy is converted to thermal energy so almost any waveform is acceptable. The vaporizer power must be controllable in order to effect feedback control of the cesium flowrate. This supply is also isolated at the positive high voltage potential.

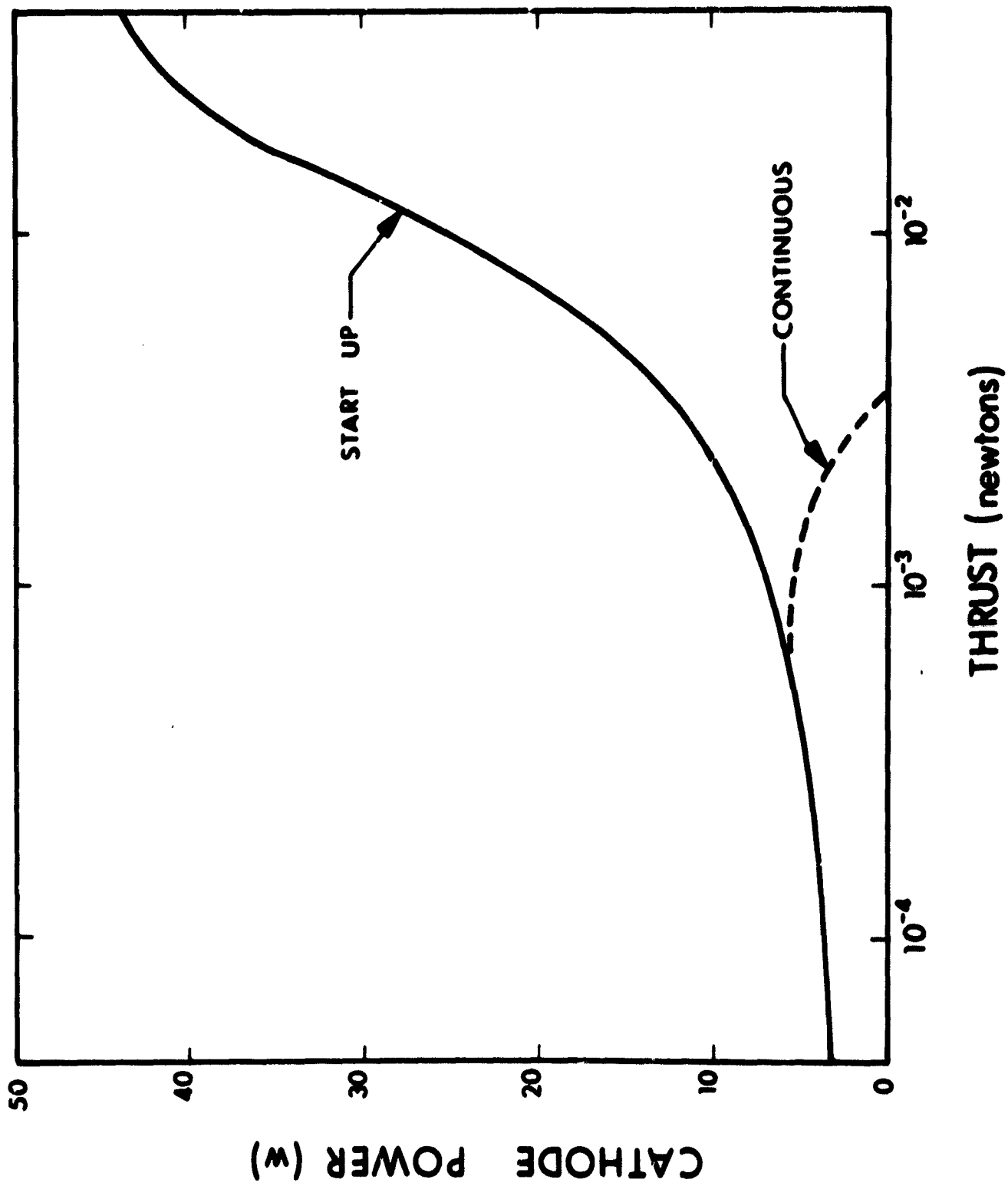


Figure 66. Cathode Power Requirements

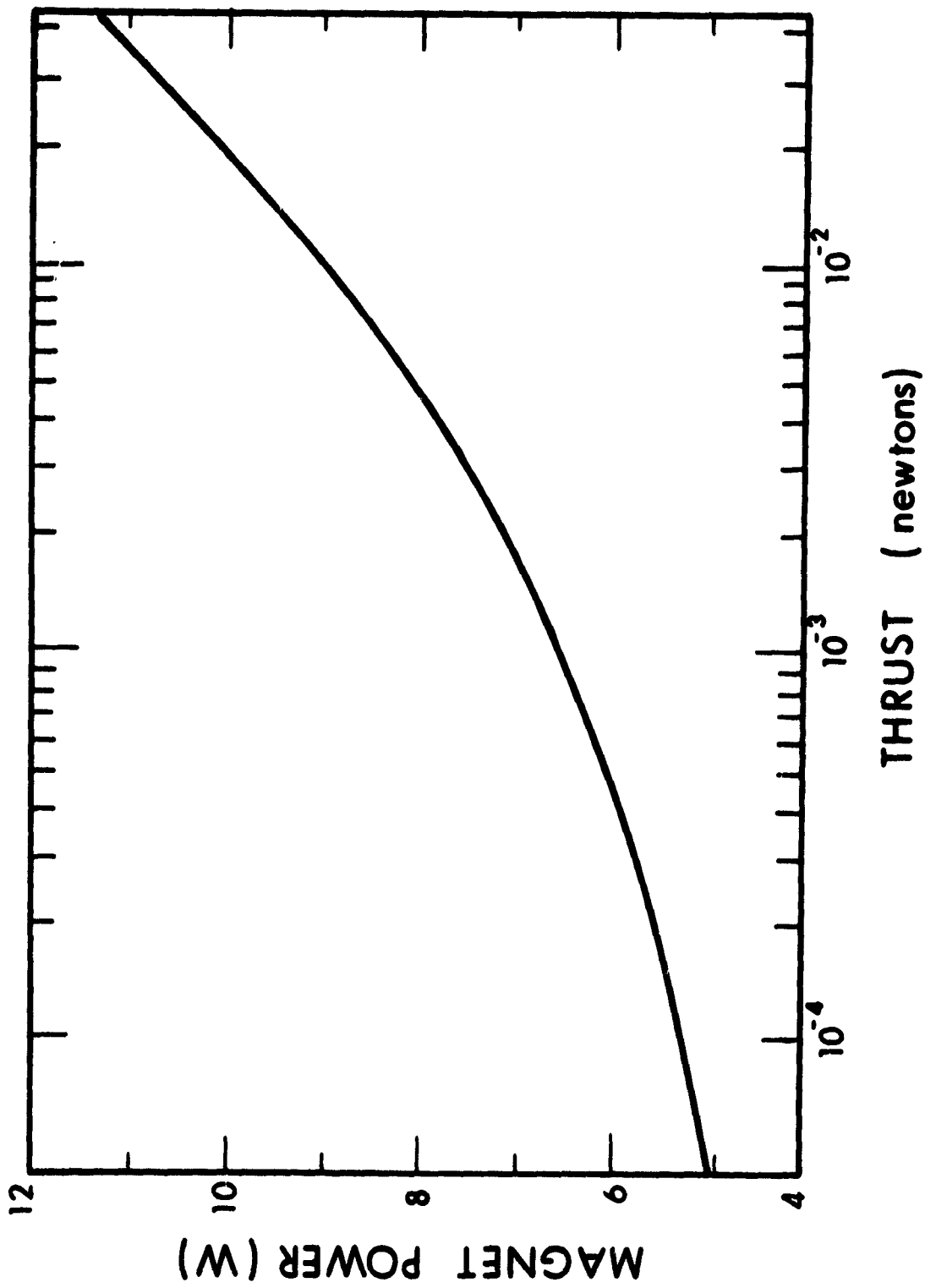


Figure 67. Electromagnet Power Requirements

2.1.4.7 Neutralizer Power

Three neutralizer power supplies are required. The first of these is the neutralizer anode power. As described earlier, this dc bias supply is used to establish a discharge from the neutralizer. A no-load voltage on the order of 100 volts is required in low thrust applications where low flowrates make the discharge difficult to initiate. This positive supply is referenced to the neutralizer common potential at ground. Ripple must be limited to ± 50 percent.

The second neutralizer power is the power required to bring the neutralizer cathode to operating temperature. As a heater supply, any waveform may be used. The power need not be controlled unless this function is combined with the neutralizer vaporizer supply. This supply is also referenced to neutralizer common.

The last neutralizer power supply is that which powers the neutralizer vaporizer. This vaporizer supply must have a controllable power output referenced to neutralizer common. The output power is controlled as a function of the neutralizer anode potential or current in order to effect operation at the minimum reliable cesium flowrate. This supply can have any convenient output waveform.

2.1.4.8 Pre-heater

One additional supply used in some applications is a pre-heater supply. This supply powers a heater located in such a position as to bring the ion engine and its electrodes to a temperature above the cesium dewpoint at operating flowrates. This supply delivers power during initial startup only. It can be referenced to ground, and can use any convenient waveform.

2.1.4.9 Impedances

The voltage and current for each of the power supplies have been shown as a function of thrust level. In the case of the cathode power, vaporizer power, neutralizer cathode power and neutralizer vaporizer power, only the total power is shown. These loads can be varied conveniently between impedances of 1 to 10 ohms. The body heater would be designed to utilize the maximum available pre-heat power and could be designed to operate with any impedance from 1 ohm to a few tens of ohms.

2.1.5 SYSTEM CONSIDERATIONS

2.1.5.1 Response

Typical turn-on times required for cesium bombardment engine systems are on the order of 15 to 30 minutes. This response can be enhanced through specific designs or through utilization of a standby mode of operation where the thruster is kept at temperatures adequate to allow immediate turn-on.

Turnoff response is instantaneous. No problems have been encountered in turning off cesium bombardment engines by simply removing all power. Subsequent re-starts are unaffected by this mode of shutdown.

2.1.5.2 Thrust Vector Alignment

Thrust vector alignment accuracy is within 2° of the thruster axis for conventional ion engines. The use of well-controlled fabrication, assembly and alignment processes can yield thrust vector accuracies on the order of $1/2$ to 1° . Thrust vector alignment

depends principally upon the alignment accuracy achieved between the two electrodes and $1/2^\circ$ thrust vector alignment requires that this electrode alignment be maintained to within 0.001 inches after launch.

Thrust deflection has been demonstrated on cesium bombardment micro-thrusters. Deflection angles of $\pm 5^\circ$ can be obtained. The techniques established for thrust vectoring can be applied to any cesium bombardment ion engine and used in conjunction with the spacecraft attitude control system to cancel thrust vector alignment errors.

2.1.5.3 Clearance

Ion beam exhaust profiles from cesium electron bombardment ion engines have been measured by probing the exhaust and examination of the erosion caused by ion beam impingement on vacuum tank walls throughout long tests. Approximately 90 percent of the ion beam falls within a cone of 10° half-angle, while 99 percent of the beam falls within a 20° half-angle cone. Negligible ion flux is detected beyond a half-angle of 30° .

When this type of engine is integrated with a spacecraft, care must be taken to prevent projection of any spacecraft components within a 30° half-angle cone about the thruster axis. This will prevent erosion through sputtering, and deposition of cesium on spacecraft surfaces. In order to sustain a monolayer cesium surface coverage on a spacecraft component, that component must be located well within a half-angle cone of 20° about the thruster axis.

2.1.5.4 Electrical

Commands must be provided to the power conditioning system to effect desired operating modes of the engine. The three basic modes are thruster system off, standby, and on. Thus, operation of the ion

engine system can be effected through the use of only three commands. Additional commands are required if throttling and thrust vectoring are used.

Telemetry is desirable on any spacecraft system to provide diagnostic information for analysis of failures in flight. Specific performance measurements can also be made to allow ground command modification of the thruster system operating levels. Telemetry can range anywhere from simply the ion beam current up to a complete compliment of a dozen or more diagnostic channels as have been used on ion engine flight tests.

2.1.5.5 Thermal

The thermal interface for the cesium electron bombardment ion engine system presents somewhat unique problems to the spacecraft designer. First of all, the ion engine may not necessarily be operated in a continuous mode. This requires that the thermal control measures used be sufficient to maintain reasonable temperatures under both full power dissipation and zero power dissipation conditions. Fortunately, the engine feed system and neutralizer operate at relatively high temperatures and are not severely affected by cold storage temperatures. Thermal stabilization can be achieved by closely coupling solar energy to the system, forcing the total power variation between full load and no load to be negligible, or by coupling the ion engine system to the spacecraft with a specific thermal impedance. In either case, the effect is to reduce the ratio of maximum to minimum power radiation from the ion engine system.

The power conditioning may be packaged either with the engine, which minimizes the spacecraft high voltage wiring, or in a remote location. Remote operation of the power conditioning unit removes all electronic components from the environment which is established for the ion

engine. This allows wider temperature variations on the ion engine hardware. A thermal interface must be carefully designed for each application.

2.1.6 DEVELOPMENT STATUS

Cesium electron bombardment ion engines have been developed to a high level of efficiency. This high efficiency has been demonstrated as both repeatable and predictable. Nearly identical high performance has been achieved on life tests of 4,000 and 8,000 hours of 3×10^{-2} newton engine systems, including feed system engine and neutralizer. Research is presently under way to identify ways to increase efficiency. One of the principal techniques which is promising from the standpoint of efficiency improvement is scaling from the low millipound level to the 0.11 newton level. The reduction in wall area to volume ratio for the discharge chamber and reduction of cathode losses (present even in the autocathode configuration) is expected to reduce overall system losses by as much as 50 percent.

Other opportunities present themselves for improving engine efficiency. Cathode design is being studied to reduce the cathode power. While the cathode in many cesium engines operates in an autocathode mode, 50 percent or more of the discharge power can be dissipated in maintaining emission temperatures. In addition to reducing autocathode losses, new magnetic field configurations used in mercury electron bombardment ion engines may be used to further increase engine efficiency.

While there is every reason to believe that significant efficiency improvements will be made, such projections have not been used in this study. The effect of such improvements will be realized in a reduction of the power for any given thrust. It does not appear

unreasonable to assume that the discharge and cathode powers shown in this analysis may be reduced by 50 percent within the next few years.

2.1.7 CONCLUSIONS

The cesium electron-bombardment ion engine system is one of the most efficient, high specific impulse electric propulsion systems available. A high degree of confidence has been established. This confidence could only be enhanced through additional ground testing and flight testing. Improvements in efficiency will come with time. Future areas of emphasis include research to more fully understand the details of ionization mechanisms, development of thruster systems for specific applications, and ground and space life testing. Even with the existing level of performance, established in 1964, this thruster system is one of the most efficient, high-specific-impulse propulsion systems.

2.2 MERCURY ELECTRON BOMBARDMENT ENGINE

2.2.1 SUMMARY

The objective of this survey is to present the current status of the mercury electron-bombardment ion thruster systems as a component of potential electric propulsion systems for mission application. Descriptions have been given regarding the results of investigations to date as well as the major development problem areas of the thruster system and subsystems.

Future desired development areas have been outlined to indicate where potential thruster system performance gains may be achieved.

In addition to the tables of data and performance figures which have been given to fully describe the present state of the art for mercury thruster systems, a 2.5-kilowatt system has been designed and presented as a mercury thruster system example which includes developments to date and the expected near-term improvements which can be predicted with a high degree of confidence.

An exhaustive bibliography is included which may be referred to for detailed analyses in particular areas.

2.2.2 INTRODUCTION

The objective of this particular discussion on thruster systems is to give the present status (as of 1967) of the mercury electron-bombardment ion thruster system as a component of an electric propulsion system, to describe the major investigations and development problems to date of the thruster system and its subsystems, and to discuss future development and projected system performance.

The term "thruster system" as used throughout is defined to include (a) the thruster, (b) the feed system, and (c) the neutralizer system. The feed system can be broken down into its subsystems which are the propellant storage reservoir, transfer line, vaporizer, and isolator. The neutralizer system can also be broken down into its subsystems; the propellant storage reservoir, transfer line, vaporizer, neutralizer cathode, and keeper electrode.

Although the performance and electrical requirements of the thruster system are extensively discussed in the following subsections, the detailed presentation and discussion of the power-conditioning requirements are discussed elsewhere. Only generalized schematics and block diagrams have been presented here to indicate the function and magnitude of the specific power requirements of the thruster system.

The first subsection of this discussion is devoted to the operating principles of the mercury electron-bombardment ion thruster system.

The next subsection presents the current status and a detailed discussion of the level of development of the mercury thruster system. Numerous tables and figures have been included to fully illustrate its performance and capability.

A representative 20-centimeter diameter mercury thruster system has been defined which operates with 2.5 kilowatts of input power and produces 0.74 newton of thrust at 5000 seconds specific impulse. This particular thruster system incorporates developments in thruster technology to date as well as future potential developments. This thruster system may be used to illustrate the projected performance for future mission considerations. Further, the system selected has been designed to take advantage of new, and yet realistic, improvements in many of the thruster subsystems.

Future development areas are outlined and discussed briefly to indicate those areas where improvements could result in the greatest gains to thruster system performance, reliability, and lifetime.

Finally, concluding remarks are given which summarize the extensive investigations to date as well as the contents of the present effort. A level of development is described from this survey which is used to identify the state of the art for mercury, electron-bombardment ion thruster systems.

2.2.3 PRINCIPLES OF OPERATION

A typical mercury, electron-bombardment ion thruster is shown in Fig. 68. Although the present discussion is of mercury propellants, this particular thruster design can produce thrust with a variety of propellants including cesium, argon, nitrogen, and hydrogen. The basic phenomenon of electron-bombardment ionization is the feature of this particular thrust device which permits the use of such a variety of propellants.

The operation of this thruster, which is described below, is common for any of the propellants listed. Mercury, however, is preferable from a thruster system consideration because of its high atomic weight, minimum storage volume, and high thrust density.

The propellant, usually in the liquid state, is stored in a reservoir. The reservoir is required to contain the propellant and dispense it in the liquid state to the transfer line or feed line. The propellant is delivered to a vaporizer which is located at the end of the transfer line. Vaporization occurs by contact of the liquid propellant with a hot porous plug or vaporizer which is located in the transfer line. The vaporizer regulates the flow of propellant through it by utilizing porous plugs with specified permeability and cross section area. When

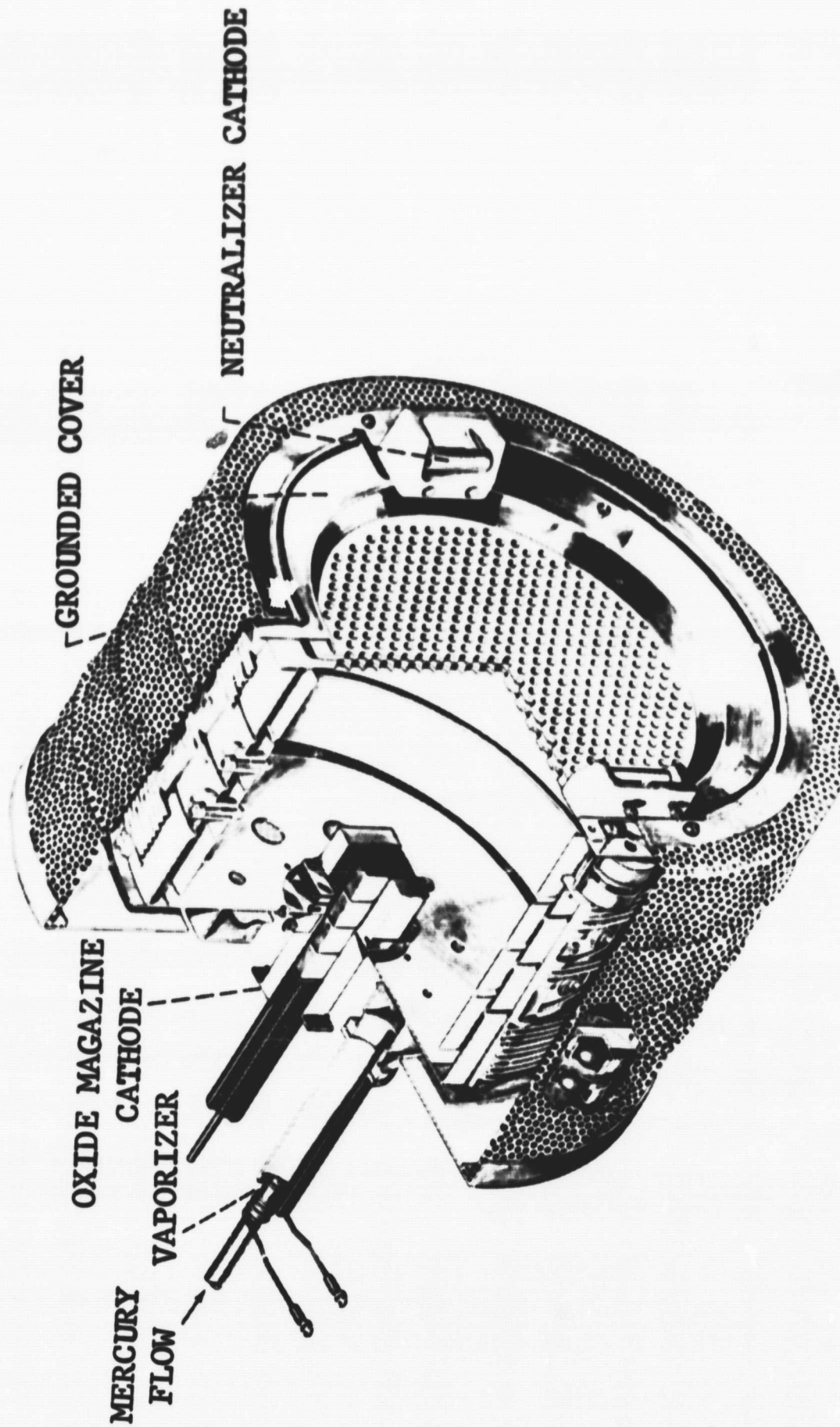


Figure 68. Typical Mercury Electron Bombardment Ion Thruster

the plug is maintained at some predetermined temperature by heating the section of transfer line containing it, then vapor will be delivered through the plug at a known flow rate. The vaporizer plug also serves to separate the liquid and vapor phases of the propellant to ensure that liquid does not migrate downstream of the vaporizer to the isolator or ionization chamber where electrical breakdown and shorting could occur.

An electrical insulating device, the isolator, is utilized downstream of the vaporizer to physically connect the vaporizer to the vapor distribution system. The incorporation of the isolator allows the feed system reservoir-vaporizer and thruster proper to be maintained at separate potentials. This feature is particularly useful when two or more thrusters operating at different voltages or specific impulse values are used or when the thruster and neutralizer are fueled from a common reservoir. The primary reason for this approach is the realization of substantial weight saving accrued when one, rather than several, reservoirs are used.

The vapor is then distributed and introduced into the thruster ionization chamber. Present thruster designs utilize a vapor distributor system which introduces vapor directly into the ionization chamber and also into the thruster hollow cathode (see Subsection 2.2.4.2.2).

The propellant vapor is ionized in the ionization chamber by means of electron bombardment. Electrons are supplied by the hollow cathode which is located on the axis at the rear of the thruster. A simple thermionic emitter would suffice except that lifetime and efficiency considerations prohibit their use. These electrons are attracted to the cylindrical anode because of the potential drop which exists between the cathode and anode.

The orbital paths of the electrons are contained within the anode diameter and lengthened by the application of an axial magnetic field surrounding the ionization chamber and anode. This magnetic field, which can be supplied by either electromagnets or permanent magnets, increases the residence time of the electrons in the ionization chamber by preventing their direct migration to the anode and, thus, enhances the probability of the electrons striking and ionizing propellant atoms. Further, the magnetic field diverges slightly toward the screen end of the ionization chamber. This field divergence acts upon the electron motions which, in turn, act upon the ions that have been formed by electron-bombardment collisions to direct the ions toward the extraction system at the downstream end of the ionization chamber. The ions thus formed are subsequently focused and accelerated from the chamber by the acceleration system. The acceleration system consists of two electrodes: one screen electrode attached to the downstream end of the ionization chamber and one accelerator electrode mounted a specified distance or gap downstream of the screen electrode by peripheral standoff insulators. Both electrodes have a similar pattern of apertures in them through which the ions are focused and accelerated to form many individual positive ion beams downstream of the accelerator electrode.

Neutralization of the individual ion beams is then effected by the addition of low-energy electrons from a neutralizer system. Although a simple thermionic electron emitter would suffice for supplying these electrons, for reasons of efficiency and lifetime (similar to the requirements for the thruster cathode) a "plasma-bridge" type neutralizer system incorporates a propellant reservoir, vaporizer, and hollow cathode device which operates in a manner very similar to those components in the thruster. Neutralization, which is necessary for the successful operation of all electrostatic thrusters, requires both current neutralization of the ion beam (equal magnitude of positive and negative currents) and also charge neutralization of the ion beam (equal number densities of ions and electrons in the exhaust beam).

2.2.4 THRUSTER PERFORMANCE

This subsection describes and discusses the major subsystems of the thruster system. Each subsystem will be briefly described from a historic point of view. The trend of development efforts to date will be discussed and data will be shown to indicate the present level of performance for each subsystem. The entire thruster system will be described under Subsection 2.2.4.5, Power and Control.

2.2.4.1 Feed System

The following subsections describe the components comprising the feed system which are the reservoir, transfer line, vaporizer, and isolator. The specific designs of components discussed were chosen because they represent state of the art and the most likely designs to receive serious mission application considerations. Other feed system designs not discussed here may be found in the literature listed in the bibliography.

2.2.4.1.1 Reservoir

The feed or propellant system has undergone the greatest physical change of all the subsystems since inception of the mercury thruster system in 1959. The feed system has evolved from a simple boiler or electrically heated cavity of liquid mercury to the gas-pressurized, positive-displacement systems which exist today. Examples of these two types of feed systems are shown in Figs. 69 and 70, respectively.

The major reasons for the development of the mercury reservoir to the present gas-pressurized, positive-displacement design include: (a) reduction of auxiliary power to dispense propellant from the reservoir, (b) minimum use of moving components, and (c) development of a reservoir design of minimum weight, volume, and structural complexity.

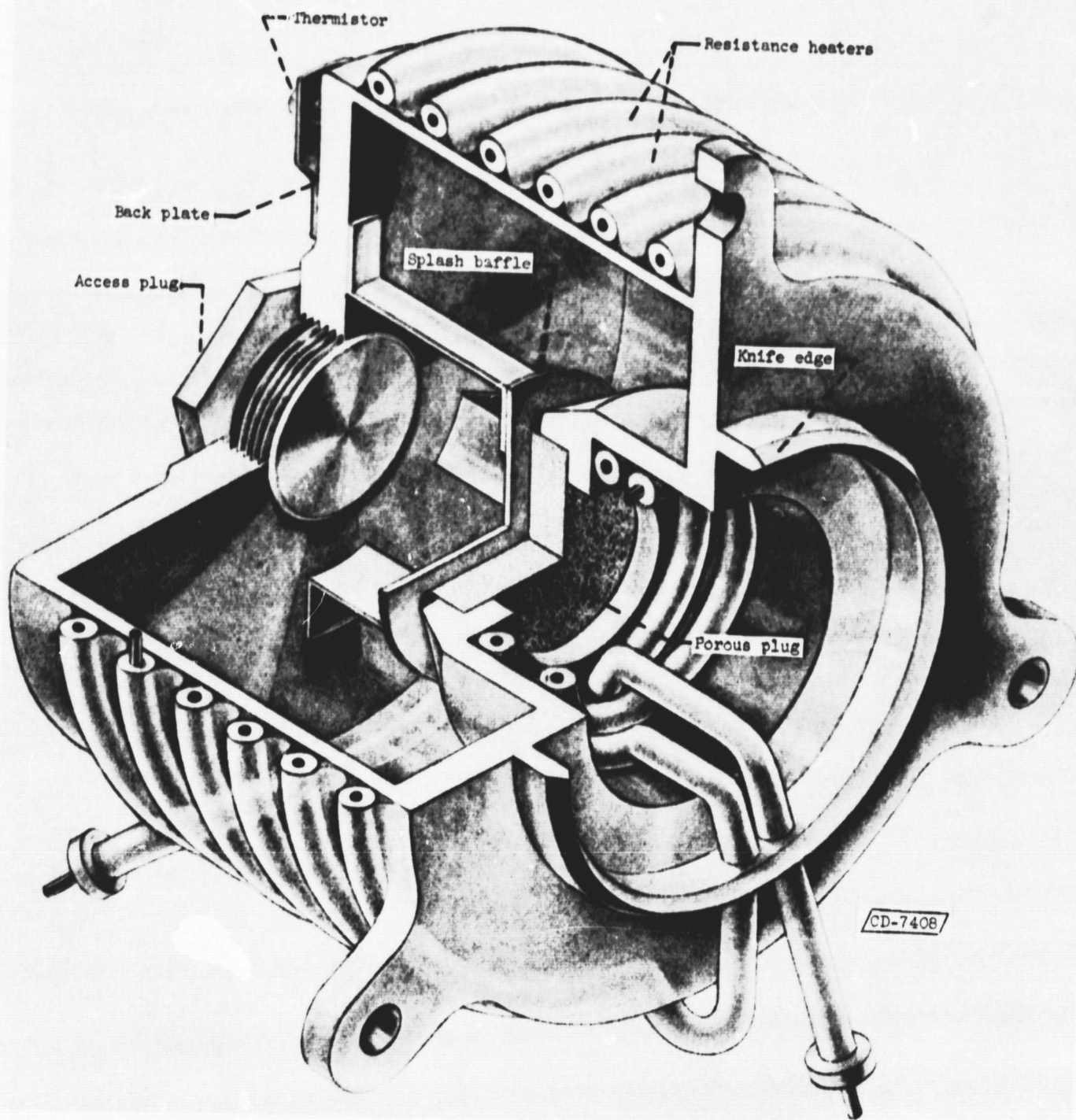


Figure 69. Mercury Boiler Propellant Reservoir

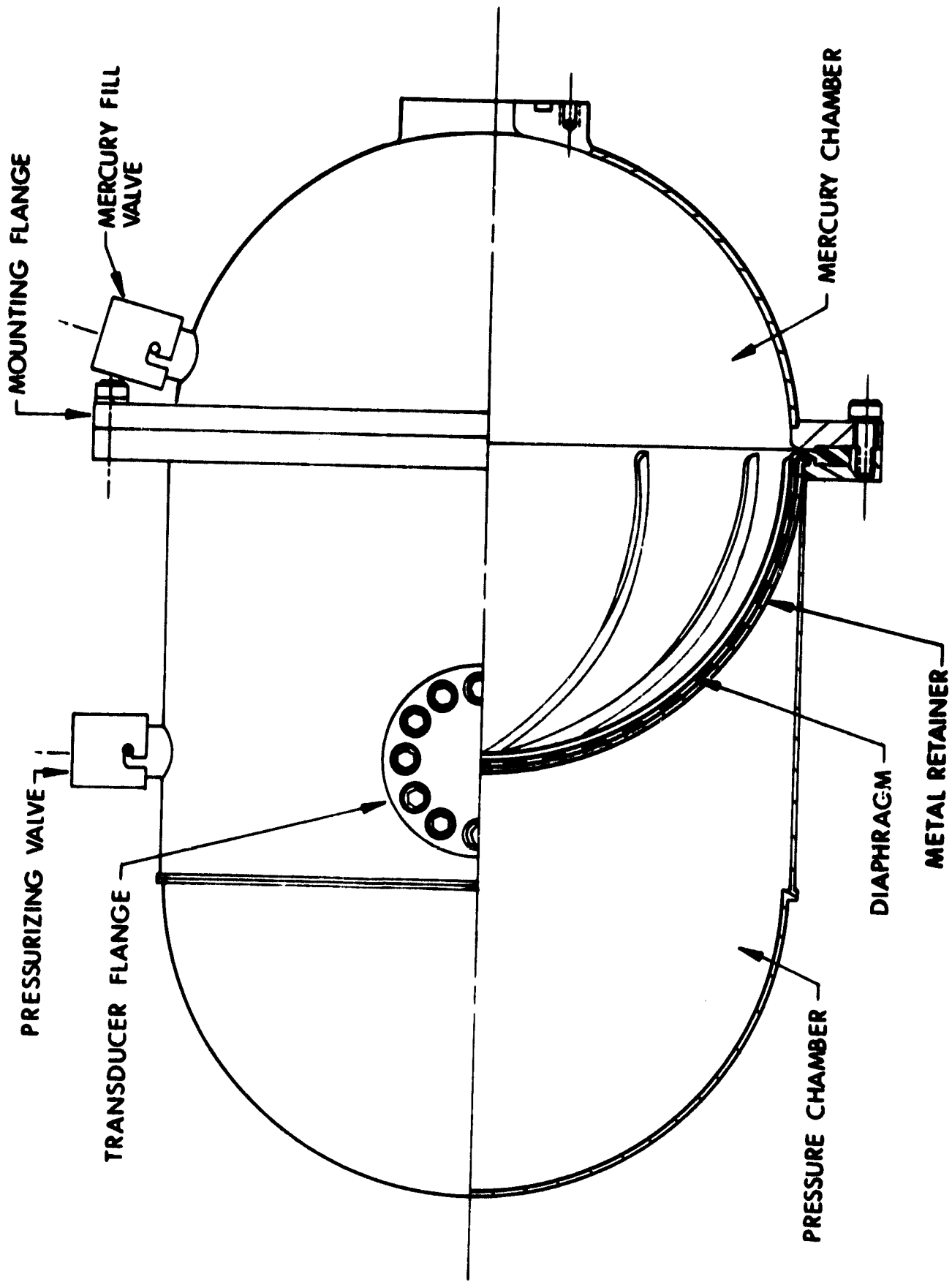


Figure 70. Gas-Pressurized, Positive Displacement Mercury Propellant Reservoir

Although all of the above objectives cannot be totally satisfied in a single design, a design can be developed which incorporates many of the desirable features. The design shown in Fig. 70 is such a design. This reservoir does not require auxiliary power to dispense the liquid propellant. Rather, the propellant is expelled from the reservoir by gas-pressurized bladder system. A moving part, the bladder, is incorporated in this design. However, suitable materials such as butyl rubbers or rolling metal bladders can be utilized which exhibit the required lifetimes and cycles in similar devices.

The physical design and shape of this reservoir is of minimum weight and volume. The gas reservoir, however, adds weight and volume that is not used to store propellant. Also, the structural complexity of this reservoir design requires special tooling and fabricating techniques in order that reproducible and structurally sound systems can be built.

Nitrogen gas is used to force the liquid mercury into the transfer. Argon gas or other nonreactive gases could also be used. The gas is contained in a chamber behind the liquid mercury reservoir and separated from it by a bladder. The bladder is constrained to eliminate possible sloshing of the mercury or rupture of the bladder during launch or other violent motions of the reservoir by a perforated metal retainer. The nitrogen gas is nominally maintained at a pressure of 2 atmospheres which is sufficient to permit gas expansion into the mercury reservoir as the mercury volume decreases during operation and yet adequate to maintain sufficient pressure to expel all of the mercury. Tests have shown that this reservoir is capable of reproducibly discharging more than 99 percent of the mercury from the reservoir.

Although minor contamination problems have been encountered with the use of certain of the butyl rubber bladders in the positive-displacement reservoirs, specially treated rubbers as well as any other of several

available materials including metals can be utilized to eliminate any contamination. The mercury should be triple-distilled grade and special care should also be used in handling, since the contamination problems originate at this interface in the reservoir. No materials problems have been observed with the basic structure of the reservoir. Several of the 300 series stainless steels have been quite satisfactory.

2.2.4.1.2 Transfer Line

The transfer line is simply a tube or line used for the transfer of liquid mercury from the pressurized reservoir to the vaporizer. This line is usually quite small in diameter (nominally 0.250 centimeter), since it delivers liquid mercury rather than vapor.

Material considerations of the transfer line include only the requirement that fabrication problems are minimized. Since the vaporizer plug is a refractory material, normally tungsten, the line and flange must also be refractory. This allows straightforward electron beam welding techniques to be utilized.

Sealing the flange to the reservoir is affected with a rubber O-ring. This ring is highly reliable in producing a tight seal and is compatible with liquid mercury. High temperatures which might affect rubber O-rings are not encountered; nominal operating temperatures of this flange area are less than 50°C. A similar rubber O-ring, the outer rib of the bladder, is used to seal the reservoir domes together.

2.2.4.1.3 Vaporizer

The vaporizer is a porous tungsten plug, usually about 0.63 centimeter in diameter, that is beam welded into a slightly enlarged section of tube near the downstream end of the transfer line. Porous tungsten

material is used which has transmission coefficients similar to the materials used for ionizer materials in cesium, contact-ionization ion thrusters. Average bulk density is about 70 percent that of solid tungsten and the average pore diameter is about 5 microns.

During thruster operation, the vaporizer plug is heated to about 300°C by a swaged tantalum heater coil that is brazed to the transfer line section containing the plug. Laboratory tests utilizing thermocouples to monitor the vaporizer temperature, as well as periodic weight measurements of the mercury in the reservoir indicate that mercury vapor flow can be determined from temperature readings to within 5 percent of the actual value.

Although a description has been given on the vaporizer, it should be noted that a vaporizer is not utilized in the mercury electron-bombardment ion thruster when it incorporates a liquid-mercury pool cathode. This cathode uses liquid mercury directly from a pressurized reservoir as described in Subsections 2.2.4.1.1 and 2.2.4.1.2. This cathode is described further in Subsection 2.2.4.2.2, Cathode.

2.2.4.1.4 Isolator

Electrical isolation of the feed system and the thruster is an important part of the present system design. The features of an isolator are apparent when considering future missions. Isolation allows a common propellant reservoir to be utilized by several thrusters. This concept eliminates the problem of electrical coupling between thrusters as when thrusters are not operating at the same specific impulse or positive, high voltage values. The common reservoir feature is desirable because of weight and cost savings. Further, the common reservoir utilizing isolation eliminates the electrical problems introduced when one or more thrusters of an array are not operating due to command or failure.

The concept of a common reservoir is desirable to also provide propellant to a single thruster and neutralizer system. This feature, however, has not been seriously considered because of the present small weight fraction of the neutralizer reservoir as compared to the thruster reservoir and because of the longer transfer line needed for the neutralizer which may require auxiliary heating.

The isolator designs required to electrically separate the feed system from the thruster, although straightforward in nature, are complicated by the following technical considerations:

- a. Isolation devices tend to be large and heavy.
- b. Isolators, without extensive design analysis, need to be heated to prevent condensation of mercury vapor and subsequent electrical breakdown problems.
- c. Technological problems involved in fabricating isolator devices lead to the use of exotic materials and techniques.

Although the efforts to date concerning isolators have not been extensive, a satisfactory design has been developed and evaluated. An example of this isolator design is shown in Fig. 71. The design is a high-pressure isolator which is necessary due to the use of hollow cathodes. These hollow cathodes maintain a steady-state pressure level in the isolator region of 5 to 50 millimeters of mercury. Isolator designs used with oxide-type cathodes only attain steady-state pressure levels of about 0.05 millimeters of mercury pressure.

Isolators are usually fabricated of ceramics such as boron nitride or Lucalox (high density alumina) and have mounting flanges at each end made of metals, such as Inconel, which are structurally compatible with the ceramics. Metal screens are used at each end and, frequently, throughout the length of the isolator to prevent electrical arcing across the entire isolator length and to define the mercury plasma boundary at the downstream end.

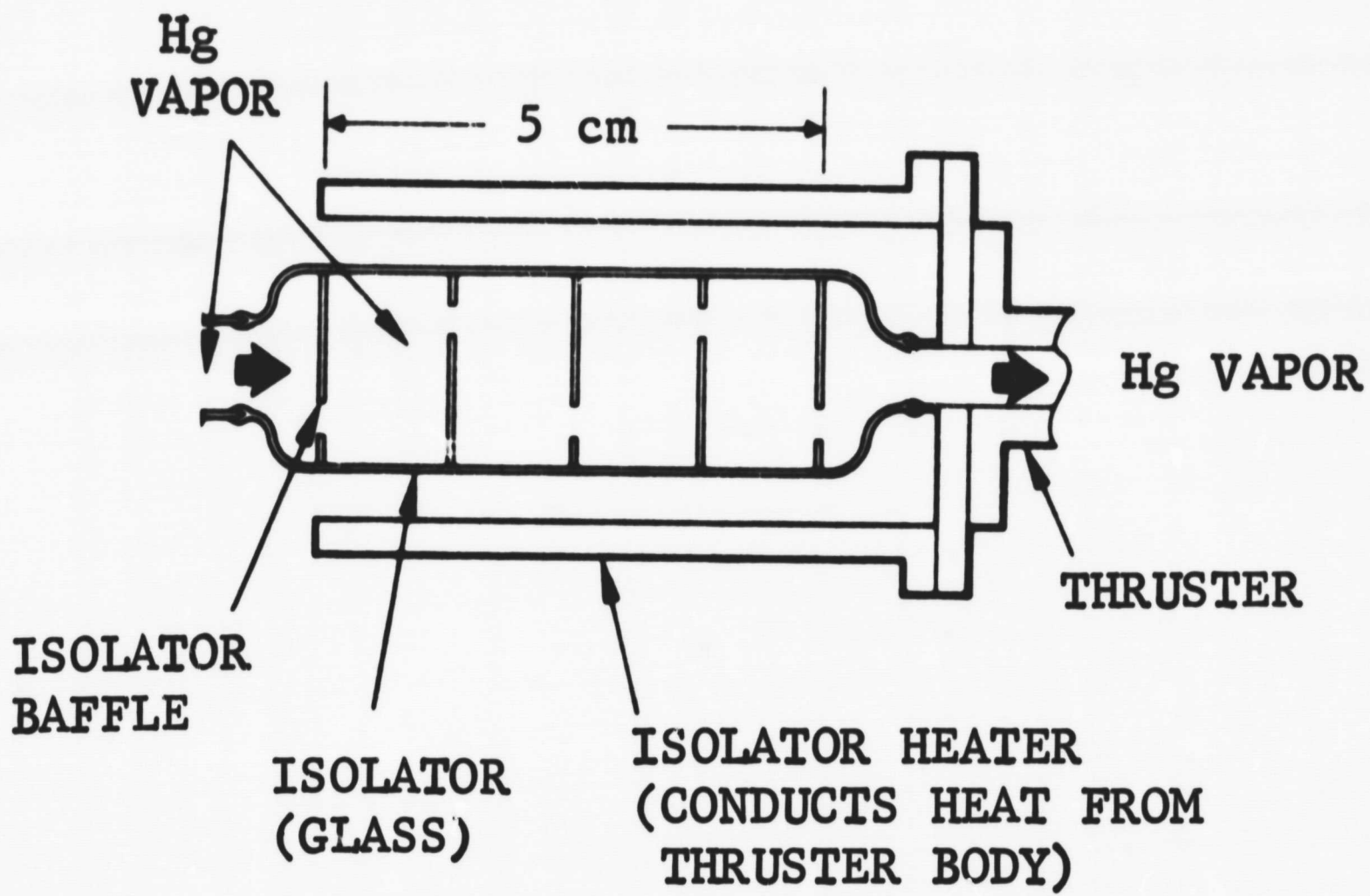


Figure 71. High Voltage, High Pressure Isolator

High-pressure isolators, such as the design shown in Fig. 71, are about 5 centimeters in length and have an inner diameter of 1.25 centimeters. Low-pressure isolators are about twice as large (2.5 centimeter inner diameter).

It is possible to design the isolator such that heat conducted from the thruster is utilized to maintain the isolator temperature at about 300°C where mercury condensation will not occur. This design task, however, is extremely difficult when hollow cathodes are used due to the requirement that only a small portion of the total mercury vapor flow is through the hollow cathode. A heater wrapped around the isolator body is used together with conduction and radiation of heat from the thruster to maintain the isolator above the condensation temperature of mercury vapor at its particular operating pressure.

2.2.4.2 Ionization

The ionization process in the mercury electron-bombardment ion thruster is described in the following subsections. Specific reference is made to the vapor distribution system, cathode, ionization chamber, and magnetic field. These thruster components are discussed from the point of view that they represent the best available designs and technology. The particular components discussed at length have been designed for the Space Electric Rocket Test II (SERT II) that incorporates state-of-the-art hardware. Other potential components are mentioned briefly. Specific details of these may be obtained by checking the publication listed in the bibliography.

2.2.4.2.1 Vapor Distribution System

Investigators have dealt with the techniques of delivering mercury vapor into the ionization chamber. Although many designs have been

generated, the similarity among them is that the basic considerations were (a) what type of cathode was utilized and (b) what was the performance of that particular cathode. In short, vapor distribution systems to date have been specifically treated for a given thruster design.

A few investigations, however, have treated the general problem of how to introduce mercury vapor into the ionization chamber. Innovations such as radial flow (introducing vapor into the chamber through the periphery of the chamber itself), reverse flow (introducing vapor near the screen electrode and directing it toward the cathode upstream of the electrode), and axial flow (various combinations of introducing vapor at the upstream plane of the thruster and allowing it to flow parallel to the axis of the thruster) are the concepts that have received major emphasis.

Although the conclusions reached from the above-mentioned concepts of vapor distribution cannot be generalized, they do indicate trends when combined with particular types of thruster cathodes. The general result of most studies, where cathode-type considerations are minimized, is that the vapor distribution system should be of the axial flow design or a modification of the same.

Typical axial flow designs introduce propellant vapor into the thruster from the vaporizer by utilizing a manifold. The manifold is connected directly to the isolator and is of such a design that it delivers vapor to the cathode backplate, the plate forming the rear plane of the ionization chamber of the thruster. The backplate, usually considered to be a component of the vapor distribution system, permits vapor flow into the chamber through a ring of holes radially displaced outward from the thruster axis. The location and specific hole sizes are determined experimentally and are not highly critical. The holes are

equal in size despite the fact that vapor may be introduced into the manifold from the vaporizer at a specific point. Experiments with similar hole sizes have shown that the vapor is distributed rapidly and evenly to all holes at the vapor temperatures and pressures of interest. The holes are faced with fine metal screens that define the plasma at the plane of the backplate. These screens are designed to prevent arcing or electrical breakdown from occurring through the conducting vapor to feed system surfaces.

The previous discussion of vapor distribution systems is based upon a thruster design that utilizes an oxide type of cathode. The most promising design, as shown in Fig. 72, however, incorporates a plasma-bridge type cathode device or hollow cathode that requires mercury vapor flow through it for proper operation. The hollow cathode is a highly efficient electron emitter when compared to the oxide cathodes that have been considered. The primary reason for this is that hollow cathode operation is sustained with a minimum energy requirement by means of a low-pressure mercury discharge. The use of the hollow cathode requires incorporation of a transfer line for mercury vapor between the isolator and the hollow cathode. Proper operation of the hollow cathode is obtained when only about 10 percent of the total vapor flow passes through the hollow cathode tip. The remainder of the flow is, therefore, required to expand through a series of holes drilled in the transfer line upstream of the hollow cathode. This flow is distributed to the holes in the backplate as described above for delivery into the ionization chamber.

The backplate and manifold are made of mild steel to complete the magnetic field circuit when permanent magnets are used. Nonmagnetic stainless steel is used, however, when the magnetic field is provided by an electromagnet. The major reason for using the same material, whether permanent magnets or electromagnets are used, is to minimize the fabrication and materials problems involved in mating the manifold to the backplate. The transfer line attached to the hollow cathode is tantalum and is nominally 0.320-centimeter diameter tubing.

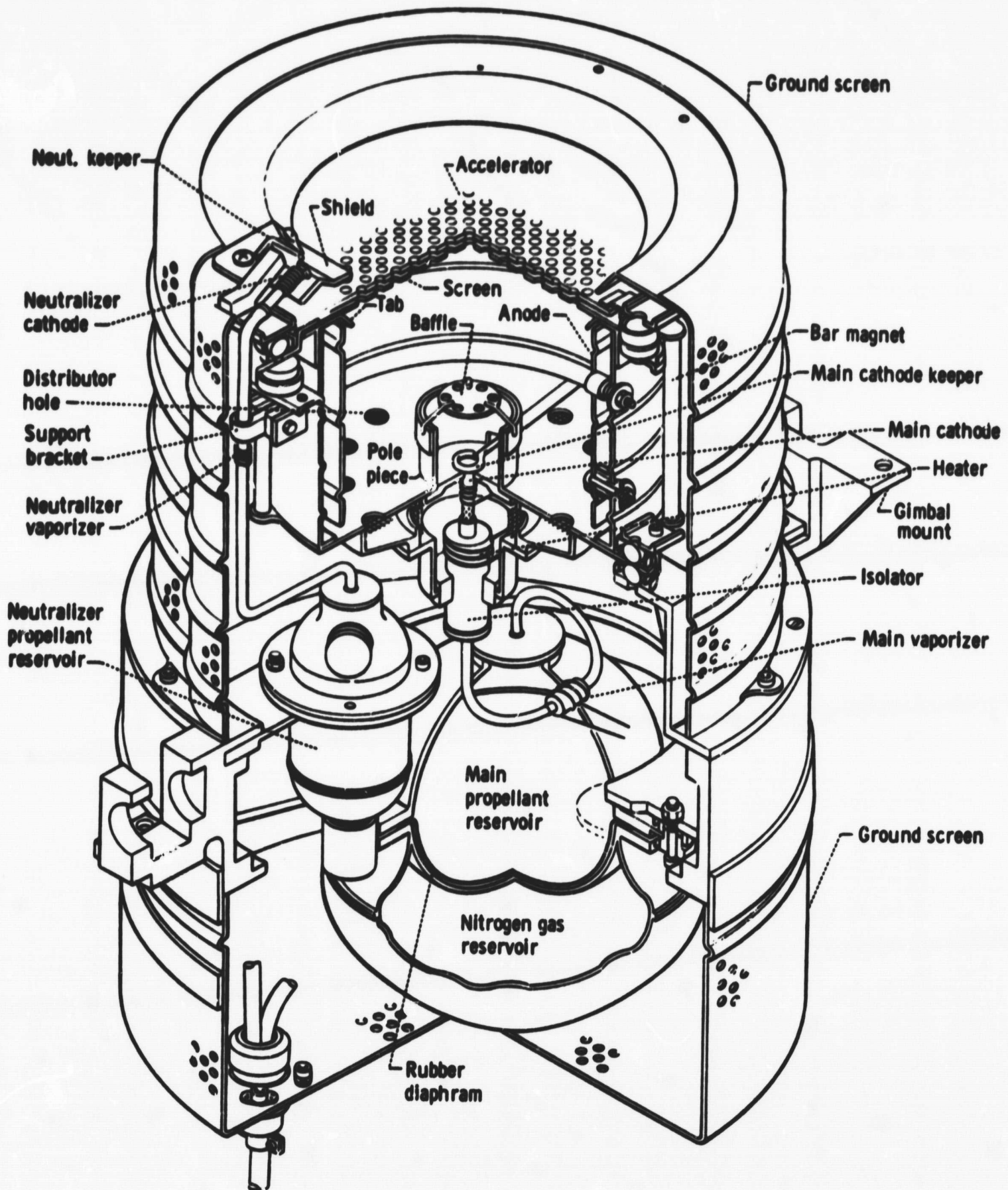


Figure 72. Cutaway Schematic of Mercury Electron Bombardment Ion Thruster System

2.2.4.2.2 Cathode

A survey of the mercury thruster systems would certainly not be complete without a discussion of thruster cathodes. To date, these electron emitters have been the major obstacle to the extensive "system" studies and extended duration testing which are required prior to the system applications. The cathode, as well as neutralizer, emitters have both been plagued by many similar problems including:

- a. Excessive power requirements
- b. Difficulty of fabrication and handling
- c. Short lifetimes (a few hundred or thousand hours)
- d. Unreproducible operating characteristics
- e. Increasing and unstable power requirements versus operating time

All of the above drawbacks have been experienced at one time or another with most of the electron emitters that have ranged in type from the straightforward refractory metal ribbon or wire to miscellaneous oxide impregnated and dispenser cathodes.

A novel electron emitter, however, was conceived which used a cesium plasma. Called the "plasma-bridge" electron emitter, this device was subsequently developed, using mercury propellant, into what is commonly termed the mercury hollow cathode.

Most of the past work with emitters other than the hollow-cathode type have involved attempts to improve performance. Thruster performance increases were only minor and the improvements to the overall thruster system lifetime were small. Recent work with hollow cathodes, however, shows that substantial improvements can be made, i.e., small emitter heating power, increased lifetime, increased propellant utilization and reproducibility, and stable, long-term operation.

A hollow cathode is shown in the sketch in Fig. 73. The present design of this cathode design is identical to the plasma-bridge type emitter or cathode of the neutralizer system. The body of the hollow cathode is fabricated from a 0.32-centimeter diameter tantalum tube with a 1-centimeter thick disc of 2 percent thoriaated tungsten welded into the end of the tube. This disc, the orifice plate, has a tapered hole cut through it (0.03-centimeter diameter end and 0.02-centimeter diameter inside). The major reason for such a thick orifice plate is due to lifetime considerations. This plate is sputtered by ions originating within the ionization chamber at nominal energies of 30 to 40 electron volts. The main reason for the shape of the hole in the orifice plate is due to the use of laser cutting techniques.

The cathode is indirectly heated by a tungsten-rhenium heater coil wrapped around the cathode body and affixed in place and insulated by flame-sprayed alumina. Additional thermal shielding is provided by wrapping the cathode with layers of tantalum foil. The reasons for using the flame-sprayed heater design and layers of radiation shielding are to reduce thermal power losses and to minimize the steady-state heating power requirements of the cathode.

An insert, a coil of 0.001-centimeter thick tantalum foil which is coated with approximately a 0.002-centimeter thick layer of barium carbonate, is placed inside the cathode tube immediately behind the orifice plate. The coil insert is formed in such a manner that a small cavity in the coil exists opposite the hole in the orifice plate.

A keeper or holding electrode is employed during hollow cathode operation. The keeper electrode is utilized to facilitate hollow cathode startup and to maintain the cathode discharge during steady-state operation of the thruster. The function of the keeper during steady-state operation is not clearly understood. Experiments with the keeper,

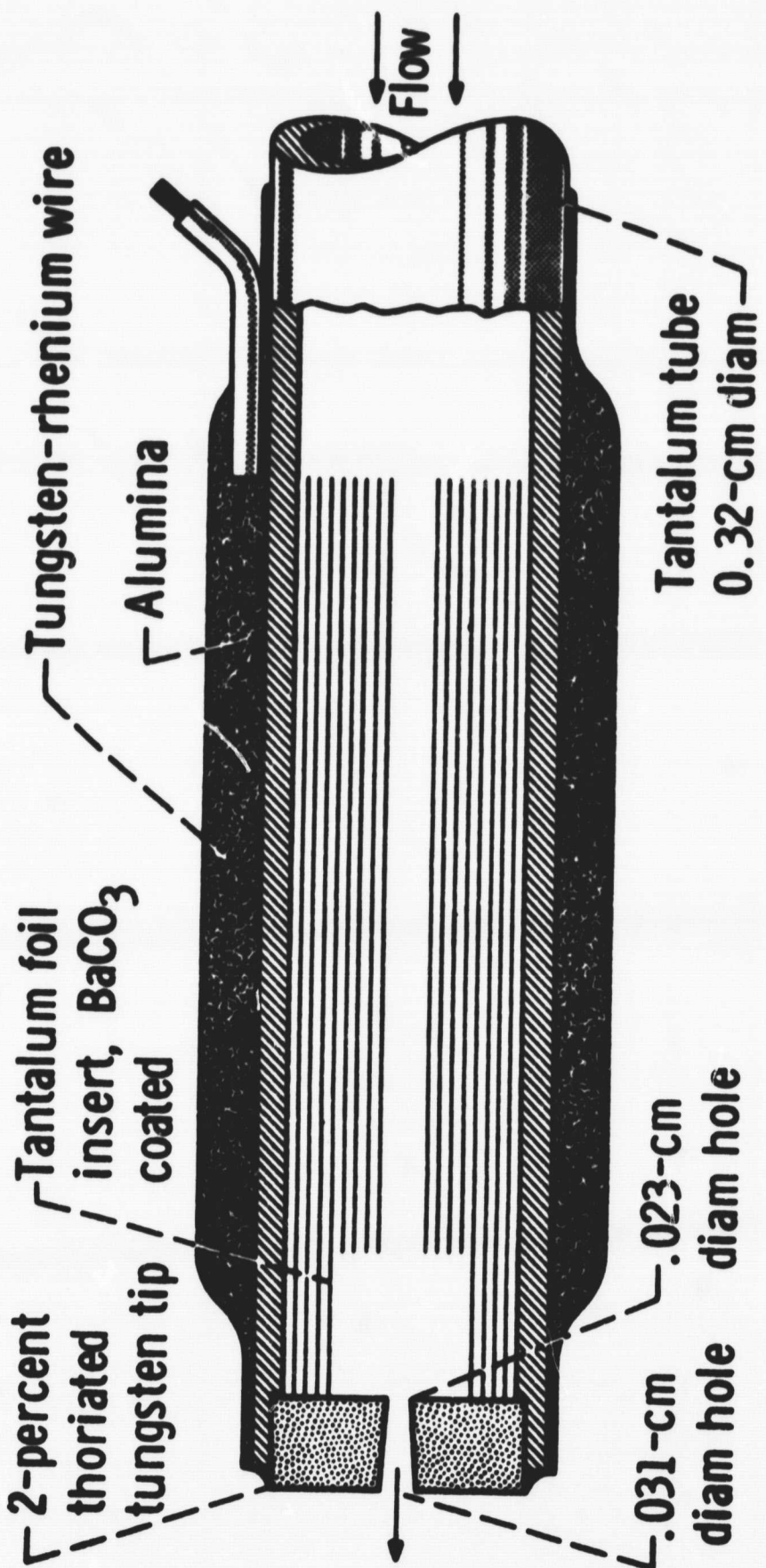


Figure 73. Enlarged View of a Mercury Hollow Cathode

however, have shown that at keeper currents less than 0.2 ampere the discharge becomes unstable, while at currents greater than 0.8 ampere excessive power to the keeper electrode lowers the overall thruster efficiency. Nominal starting characteristics of the keeper electrode are 300 volts at 0 ampere. The keeper electrode will maintain the hollow-cathode discharge with no voltage applied to the thruster anode at 30 volts and 0.5 ampere. When the anode supply is activated and the thruster is operating in a steady-state manner, the characteristics of the keeper are 12 volts and 0.5 ampere. The preceding discussion refers to a thruster which produces about a 0.250-ampere ion beam. The keeper electrode nominally a ring with an inside diameter of 0.60 centimeter of 0.150-centimeter diameter tantalum wire placed 0.20 centimeter downstream of the plane of the end of the orifice plate. An alumina plate attached to the backplate is used to position the hollow cathode, support the keeper electrode, minimize thermal conduction away from the cathode, and reduce leakage of mercury vapor from the manifold into the ionization chamber near the hollow cathode.

Another requirement when using the hollow cathode is a small cylindrical cavity which extends into the ionization chamber from the backplate. This structure is commonly called the cathode pole piece since it is made of magnetic, mild steel material when permanent magnets are used to provide the magnetic field. When an electromagnet is used to provide the magnetic field, the backplate and cathode pole piece are made from nonmagnetic stainless steel. The cathode pole piece is nominally 6.0 centimeters in diameter, 3.2 centimeters in length, and mounted on the axis of the thruster extending downstream from the backplate. The reason for using the pole piece is to provide the proper magnetic field shape in the vicinity of the cathode. A baffle, usually a 2.5-centimeter diameter stainless steel disc, is mounted about 0.125 centimeter downstream of the pole piece and attached to it by means of several small supporting struts. Another reason for using the pole piece and

the baffle is to optimize the environment required for maintaining an efficient discharge from the hollow cathode. The primary reason for the use of a baffle is the necessity of controlling the coupling voltage between the hollow cathode and the thruster anode. The exact function of the cathode pole piece is not clearly understood. It has been determined experimentally, however, that the hollow cathode operation is most efficient and that the overall thruster performance is best when the pole piece configuration described above is used.

Minor problems of lifetime have been encountered during thruster testing with hollow cathodes. The area of greatest concern has been erosion of the cathode orifice plate by ions formed within the ion chamber and cathode pole piece cavity. These ions have energies up to 30 or 40 electron volts, and, therefore, are energetic enough to sputter surfaces which attract them. The sputtering problem, however, is not serious. Continued work in this area should result in increasing the life of the hollow cathode to values greater than several thousands of hours.

Continued efforts with the hollow-cathode development should also reduce and/or eliminate present difficulties in the areas of fabrication, the use of multiple-reservoir feed systems, and excessive heating power and vapor flow requirements.

Another type of thruster cathode design, the liquid mercury-pool cathode has been extensively developed and tested. Although this particular cathode type requires close thermal control to maintain operational stability, it potentially has the features of low power requirement, high propellant utilization, and long life. The major reason that this particular cathode has not been considered in the present thruster is due to the fact that it is an experimental device only and, as a result, is not of such a design as to merit further consideration.

2.2.4.2.3 Ionization Chamber and Anode

The ionization chamber geometry, also illustrated in Fig. 72, includes the cathode and screen pole pieces, the cathode, and the anode. The ionization chamber is the region where mercury vapor ionization occurs via electron-bombardment collisions.

Previous investigations have revealed the fact that the particular anode and chamber geometry and size can be experimentally determined. Further, the anode and chamber designs are a function of: (a) the power required for thruster discharge initiation and steady-state operation, (b) anode and ionization chamber ion-recombination losses, (c) thruster weight and size, and (d) arc current requirements.

The geometry shown in Fig. 72 with the anode length equal to roughly two-thirds of the length of the ionization chamber and mounted at the downstream end of the thruster has been experimentally determined to be the optimum configuration. This chamber geometry, however, does not refer to the 50-centimeter and 150-centimeter diameter thrusters because these particular thrusters use more than one cathode.

It is obvious that the general shape of the ionization chamber is based upon the physical properties of the mercury plasma formed in the chamber. This shape is, in large measure, determined by the type of vapor distribution system, the electron emission characteristics of the cathode, the ion residence time in the chamber, and the shape and intensity of the magnetic field. Although the anode is commonly fabricated from a nonmagnetic stainless steel, it can be made from any good electrically conducting material such as copper or aluminum. Anode designs for flight-type thrusters would normally consider aluminum because of the attractive weight advantage it has over any of the other candidate materials.

The ionization chamber is simply a cylinder of nonmagnetic stainless steel with provisions for mounting of the backplate and screen electrode. When an electromagnet is used, the magnet coil is wound directly upon the outer chamber surface. The use of permanent magnet rods, however, requires special mounting brackets and the incorporation of a screen pole piece of magnetic, mild steel (see Subsection 2.2.4.2.4).

An advanced design of permanent magnet-type thruster utilizes permanent magnet sheet material to form the actual ionization chamber shell. This design has obvious potential in that considerable weight and fabrication steps can be eliminated. Special care, however, must be exercised with this design due to the critical requirements for magnetization of the shell. In addition, the concept of the magnetic shell does not appear to offer sufficient weight advantages over electromagnets for thruster sizes larger than 50 centimeters in diameter. The permanent magnet, however, does eliminate the need for the power as required with an electromagnet. The proper design of thruster, therefore, can only be determined after the size and predicted performance level have been selected and the necessary tradeoff studies performed to select the magnetic field type.

2.2.4.2.4 Magnetic Field

Several brief discussions of the magnetic field have already been made in the preceding subsections. The main reason for this is due to the fact that the magnetic field requirements, whether electromagnet or permanent magnet, dictate the design of the thruster and manifold.

The study of the magnetic field design requirements including type, strength, orientation, and degree of divergence has been performed to date with the following major objectives:

- a. Minimum arc power requirement per ion (eV/ion)
- b. Minimum magnetic field current and power for electromagnets
- c. Minimum weight and volume
- d. Ease of fabrication and assembly

The design of thruster which typifies state of the art for thruster sizes up to about 50 centimeters in diameter is shown schematically in Fig. 72. This particular design utilizes eight permanent magnet (Alnico V) rods equally spaced around the ionization chamber to provide the necessary magnetic field. The field lines are constrained to follow the pole pieces and the cathode and screen pole pieces to optimally shape the magnetic field.

The cathode pole piece has previously been discussed in Subsection 2.2.4.2.2. The screen pole piece is a magnetic mild steel collar located between the anode and the screen electrode and is of similar diameter to that of the chamber. The particular shape of the screen pole piece is such that the magnetic field lines located in the vicinity of the anode prevent electrons supplied from the cathode from traveling directly to it. The specific shape of the screen pole piece, as well as that of the cathode pole piece, has been determined experimentally.

The procedure in defining the correct permanent magnet field has been to match the characteristics or field shape obtained with electromagnets. Although the field lines provided by electromagnets are quite different from those of permanent magnets, good approximations of the electromagnet fields have been obtained by proper iterations of the design of the pole pieces and permanent magnet shape, weight, and method of attachment.

Investigations have revealed that for mercury electron-bombardment thruster sizes up to 50 centimeters in diameter, the necessary magnetic

field can be provided by the use of permanent magnets. Although most effort to date has been with the use of permanent magnet rods, the feasibility of using sheet or shell magnets as described in Subsection 2.2.4.2.3 has been demonstrated in the cesium electron-bombardment thrusters. The major reason for considering the use of permanent magnets is obvious. They eliminate the power, control, and isolation requirements of electromagnets. Another advantage is that the weight of permanent magnets is usually less than that for electromagnets.

2.2.4.3 Acceleration

The acceleration system in the electron-bombardment types of thrusters consists of a screen electrode and an accelerator electrode. The screen electrode is usually securely attached to the ionization chamber end and is at the same potential as the chamber. This is a high positive potential normally a few thousand volts which determines the value of specific impulse for the thruster. The accelerator electrode is biased to a high negative potential primarily to obtain optimum focusing of ions from the ionization chamber. The negative potential also prevents the backstreaming of electrons downstream of the electrodes from entering the thruster which could result in erroneous data and difficulty of control.

The main function of the acceleration system is to focus, extract, and accelerate the ions formed in the ionization chamber into a well defined beam of ions downstream of the accelerator electrode. The electrodes are usually flat metal plates into which a hexagonal array of small apertures have been drilled. Typical electrode geometries for thrusters larger than 10 centimeters in diameter include an array of about 1000 apertures within the anode diameter of the electrodes. These apertures are sized such that the open area of the electrode or area of apertures only is in the range of 65 to 75 percent of the total area of the

electrode. This value of open or transmission area of the electrodes is an indication of the qualitative and quantitative capability of the system to extract and accelerate ions. These high-transmission electrodes, when properly designed, are definitely superior to those designs with small open area (about 50 percent). These electrodes have historically been made from molybdenum or other similar materials that are fairly resistant to sputtering damage.

The electrodes do, however, undergo sputtering damage from two sources: (1) ions that are extracted from the ionization chamber and are poorly focused will impinge on the electrodes during their transit through the acceleration system (primary ion sputtering) and (2) ions that are formed downstream of the accelerator electrode by charge-exchange collisions and are focused back onto the accelerator electrode (charge-exchange ion sputtering). The sputtering damage caused by primary ions can be largely eliminated by proper and careful design of the screen electrode. The upstream surface of the screen electrode defines the plasma from which the ions are extracted and, therefore, the efficiency with which they are accelerated through the entire system. Proper design of this screen electrode can result in minimum primary ion interception by the electrodes as well as optimum ion extraction and thruster performance.

The sputtering damage of the accelerator electrode by charge-exchange ions is a strong function of the propellant utilization of the thruster. This is the case because the un-ionized or neutral propellant atoms are those which undergo charge-exchange reactions with ions downstream of the accelerator electrode and are then attracted to that electrode. Increasing the propellant utilization will, therefore, reduce the sputtering damage caused by charge-exchange ions. The damage caused by charge-exchanged ions can also be reduced with lower values of the accelerator electrode potential (smaller values of the high-negative potential). The sputtering damage effect versus energy can be seen by

referring to Fig. 74. This figure gives the sputtering yield of atoms per impinging mercury ion versus the impinging ion energy for several materials. The figure also shows that the choice of electrode material can affect the sputtering damage incurred by the electrode.

In the past, both electrodes have been fabricated from either molybdenum or stainless steel. Because of the structural and thermal properties, molybdenum continues to be used for the screen electrode. Aluminum, however, has replaced other materials for the accelerator electrode due to its low weight and low sputtering yield.

The electrode thicknesses, of 0.075 and 0.150 centimeter for the screen and accelerator electrodes, respectively, with an accelerating gap between them of 0.250 centimeter, are representative of the acceleration systems in the range of thruster sizes from 10 to 50 centimeters in diameter. Thruster sizes not included in this range have slightly different acceleration system geometries.

Work on improving thruster lifetime has been performed by various organizations because the accelerator electrode receives minor direct interception of primary ions due to improper focusing and experiences major sputtering damage due to the charge-exchange ions. This particular work has, in addition to the use of different materials, involved the use or consideration of exotic materials (i.e., beryllium, ceramics, and bimetallic types) and the consideration of electrode protection by coating the basic electrode metal with a low sputtering yield of liquid metal or other insulating material. One effort has even considered the use of replaceable electrodes either entirely or by the use of wire electrodes which are continuously replaced across the end of the thruster.

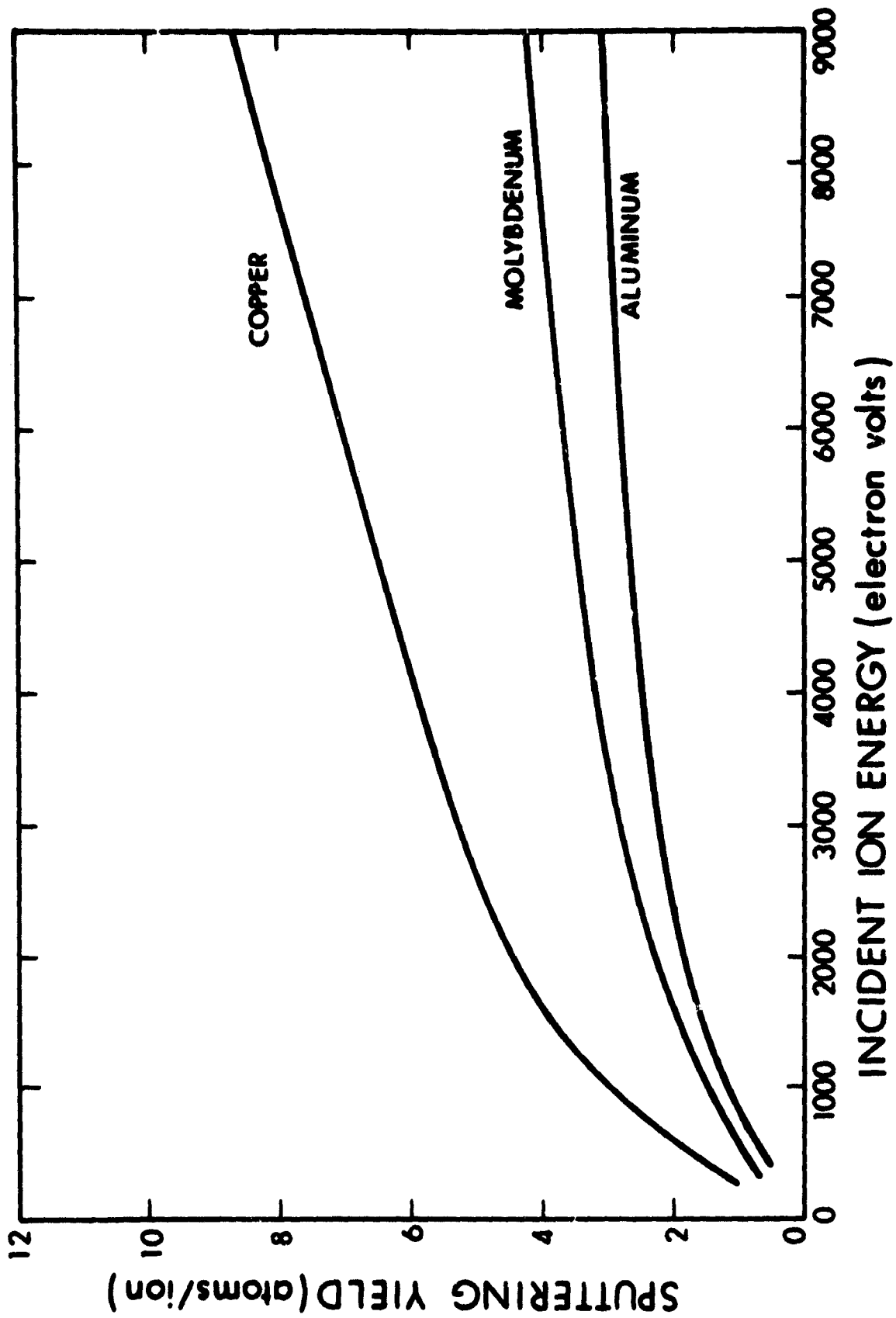


Figure 74. Sputtering Damage Effect versus Energy

Although only a modest level of effort has been performed to theoretically determine the correct electrode geometries and resultant performances, most effort has been of a "cut-and-try" nature. This has been a necessary method because of the relatively unknown conditions in the ionization chamber from which the ions are extracted. Experimental work has, however, resulted in accelerator system designs of sufficient merit and potential that they have not been a deterrent to thruster operation, good performance, and long life.

Other factors which affect the acceleration system design and the thruster system performance and efficiency include the desired value of specific impulse and thrust for a given thruster size as well as the method and degree of post-acceleration ion beam neutralization. Because these factors are of importance in the design and operation of the acceleration system, they will be discussed separately under their respective subsections.

2.2.4.4 Neutralization

The need to neutralize the ion beam produced by the thruster is obvious. Without the addition of electrons, the individual beams of ions would be repelled back toward the acceleration system by the positive, space-charge buildup of ions immediately downstream of the thruster. This space-charge buildup occurs in an extremely short period of time (nanoseconds to microseconds).

It is therefore imperative that effective and complete neutralization occurs when the thruster is producing and accelerating ions for purposes of generating thrust. Many types of neutralizer systems have been investigated to determine which types are satisfactory. Although the primary requirement is to provide both current and charge neutralization of the ion beam, several other factors are equally important in the determination of the correct type of neutralizer. These factors include the lifetime, efficiency, and complexity of the neutralization system.

The difficulties experienced in selection criteria of neutralizers are exactly the same as those encountered in the selection of cathodes for the thruster. Both the neutralizer and thruster cathodes must be good electron emitters. Although this is an obvious requirement, a good electron emitter is not synonymous with lifetime, efficiency, and simplicity or complexity. Emitter investigations in the past have dealt with many types including refractory or wire, dispenser, impregnated, and oxide. Each of these types of emitters is attractive from an electron emission standpoint. All of them, however, are unattractive from either an efficiency, lifetime, or fabrication viewpoint.

The neutralizer cathode problem has been resolved by the use of the hollow cathode, as is also true of the thruster cathode. The use of the hollow cathode as a neutralizer electron emitter, however, preceded its incorporation into the thruster. Initial investigations with the hollow cathode neutralizer followed the successful demonstration of a similar type of cathode which operated with cesium propellant. This particular device was termed a cesium "plasma-bridge" type neutralizer and utilized a propellant reservoir and vaporizer separate from those components in the thruster. A schematic of the mercury plasma-bridge neutralizer is shown in Fig. 75.

The work with mercury propellant has resulted in a plasma-bridge neutralizer cathode which also has a separate propellant reservoir and vaporizer. The mercury neutralizer, however, also incorporates a neutralizer anode or keeper electrode. This keeper performs the function of maintaining the neutralizer cathode discharge during startup, low beam, and steady-state operation of the thruster. This function is very similar to that of the thruster cathode keeper electrode.

The neutralizer is usually located immediately downstream of the thruster and adjacent to the beam (2 centimeters downstream of the accelerator

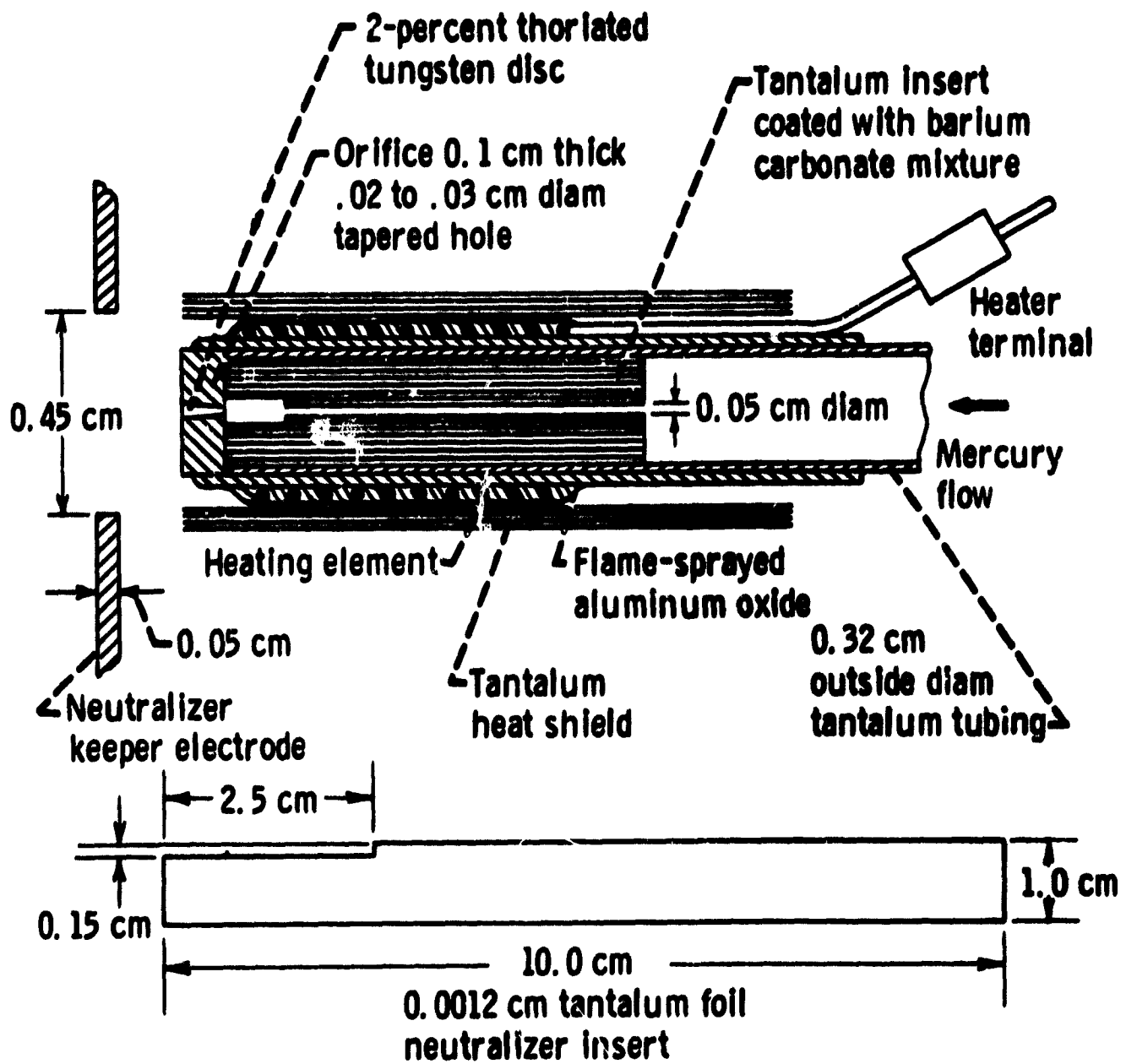


Figure 75. Plasma Bridge Type Mercury Neutralizer

electrode and 2 centimeters radially outward from the edge of the accelerator electrode aperture pattern). This position is selected as a compromise between the lowest "coupling" voltage between the neutralizer cathode and ion beam and the least damage to the neutralizer system resulting from primary ion interception and charge-exchange sputtering. The value of the coupling voltage is significant not so much because it reduces the net accelerating voltage of the ions by the amount of the coupling voltage, but because the coupling voltage represents the maximum energy of ions that can form between the neutralizer cathode and ion beam and strike the cathode. Any resultant sputtering damage would directly influence the operating lifetime and, perhaps, the performance of the neutralizer system.

The position of the neutralizer cathode is, therefore, a tradeoff of neutralizer cathode lifetime versus efficiency or power required to provide electrons to the ion beam as a function of coupling voltage. Proper placement of the neutralizer, however, is possible such that lifetimes necessary for near-term missions are feasible with this type of device.

As mentioned above, the mercury plasma-bridge neutralizer requires a propellant reservoir and vaporizer. Present designs incorporate this particular neutralizer system into the thruster system with a separate propellant reservoir and vaporizer for the neutralizer and a separate propellant reservoir and vaporizer for the thruster. Although this fact means added weight for the neutralizer and thus, the thruster system, the contribution of the neutralizer system weight to the total thruster system represents less than 5 percent of the total thruster system dry weight for thrusters required to produce more than about 10^5 newton-seconds total impulse.

2.2.4.5 Power and Control

The preceding sections have dealt with the basic operation of the thruster system and state of the art components. This section will be devoted to a general presentation of the power and control requirements. In addition, tables and figures of data will be given which include thruster system performance for various thruster sizes. This data has been extrapolated to the curves of Subsection 2.2.5 to indicate the general range of performance by utilizing the best features from all of the existing thruster system investigations.

Tables XII and XIII list specific thruster system performance parameters, calculated performance values, and other data of interest which are normally presented to fully describe the capability of a given system. These data which have been taken from tests that were not necessarily "performance optimized," are listed for a range of existing thruster sizes from 5 to 20 centimeters in diameter. Also, included in the listing is the limited data available on the 50- and 150-centimeter diameter thrusters. These data are necessarily limited due to the lack of extensive test investigations and system considerations.

The electrical schematic of the mercury electron bombardment ion thruster system is shown in Fig. 76. Note that the bias supply has been included only for reference to ground testing techniques. The specific power supplies utilized have been noted as to whether ac or dc type power is needed. The general range of each power supply has not been given. This voltage-current capability for individual supplies is best determined by reference to a particular thruster system design and size. This is the case because any two thrusters will seldom have the same operating characteristics.

TABLE XII

THRUSTER SYSTEM PERFORMANCE

Thruster System Parameter	Thruster Diameter, centimeters				
	5	5	10	10	15
Assumed mission time, hours	1000	1000	1000	1000	1000
Thrust, newtons	2.9×10^{-3}	2.9×10^{-3}	3.0×10^{-2}	1.3×10^{-2}	2.8×10^{-2}
Specific impulse, seconds	4050	3020	4000	4000	4180
Positive high voltage, kilovolts	4.000	4.000	2.500	2.500	3.000
Negative high voltage, kilovolts	1.000	1.000	2.000	1.000	2.000
Beam current, amperes	0.023	0.023	0.290	0.125	0.250
Beam power, watts	92	92	725	313	750
Drain power, watts	6	1	10	7	15
Magnet power, watts	8	0	180	36	0
Arc power, watts	22	13	250	76	76
Cathode-keeper power, watts	19	16	220	72	21
Feed system power, watts	9	9	10	9	8
Neutralizer system power, watts	15	15	200	0	25
Total thruster power, watts	156	131	1595	513	870
Thruster system power, watts	171	146	1595	513	895
Thruster mass efficiency, percent	66	48	80	80	86
System mass efficiency, percent	66	48	80	80	81
Thruster overall efficiency, percent	39	34	42	49	74
System overall efficiency, percent	36	30	36	49	0.68
System power-to-thrust, kilowatts/newton	59	50	53.6	39.4	32
System propellant mass, kilograms	0.35	0.48	2.71	1.17	2.30
Thruster mass, kilograms	2.30	1.40	4.22	4.22	3.80
Neutralizer system mass, kilograms	0.01	0.01	0.02	0.02	0.02
Total tankage mass, kilograms	0.02	0.02	0.14	0.06	0.12
Thruster system mass, kilograms	2.33	1.43	4.38	4.30	3.94
System mass (loaded), kilograms	2.68	2.91	7.09	5.47	6.24
Cathode-neutralizer type	oxide	oxide	Ta ribbon	Ta ribbon	hollow

TABLE XIII

THRUSTER SYSTEM PERFORMANCE

Thruster System Parameter	Thruster Diameter, centimeters				
	15	20	20	50	150
Assumed mission time, hours	1000	1000	1000	1000	1000
Thrust, newtons	2.8 x 10 ⁻²	5.9 x 10 ⁻²	4.3 x 10 ⁻²	5.6 x 10 ⁻¹	3.0
Specific impulse, seconds	4380	5000	5500	8900	8150
Positive high voltage, kilovolts	3.000	3.900	3.900	10.000	9000
Negative high voltage, kilovolts	1.8000	1.160	1.100	5.000	5000
Beam current, amperes	0.250	0.460	0.300	2.8	15.7
Beam power, watts	750	1800	1170	28,000	141,000
Drain power, watts	14	12	10	525	----*
Magnet power, watts	0	0	0	600	----*
Arc power, watts	54	250	165	700	----*
Cathode-keeper power, watts	60	110	100	900	----*
Feed system power, watts	15	28	25	150	----*
Neutralizer system power, watts	25	0	0	0	----*
Total thruster power, watts	893	2200	1470	30,675	175,000
Thruster system power, watts	918	2200	1470	30,875	175,000
Thruster mass efficiency, percent	85	80	88	90	87
System mass efficiency, percent	80	80	88	90	87
Thruster overall efficiency, percent	71	66	70	81	70
System overall efficiency, percent	65	66	70	81	70
System power-to-thrust, kilowatts/newton	33	37.3	34.2	55	58
System propellant mass, kilograms	2.34	4.30	2.55	23.30	135
Thruster mass, kilograms	5.60	5.44	5.44	21.80	102
Neutralizer system mass, kilograms	0.02	0	0	0	0
Total tankage mass, kilograms	0.12	0.22	0.13	1.17	3
Thruster system mass, kilograms	5.74	5.66	5.57	22.97	105
System mass (loaded), kilograms	8.08	9.96	8.12	46.27	240
Cathode-neutralizer type	oxide	oxide	oxide	oxide	oxide

*Not available

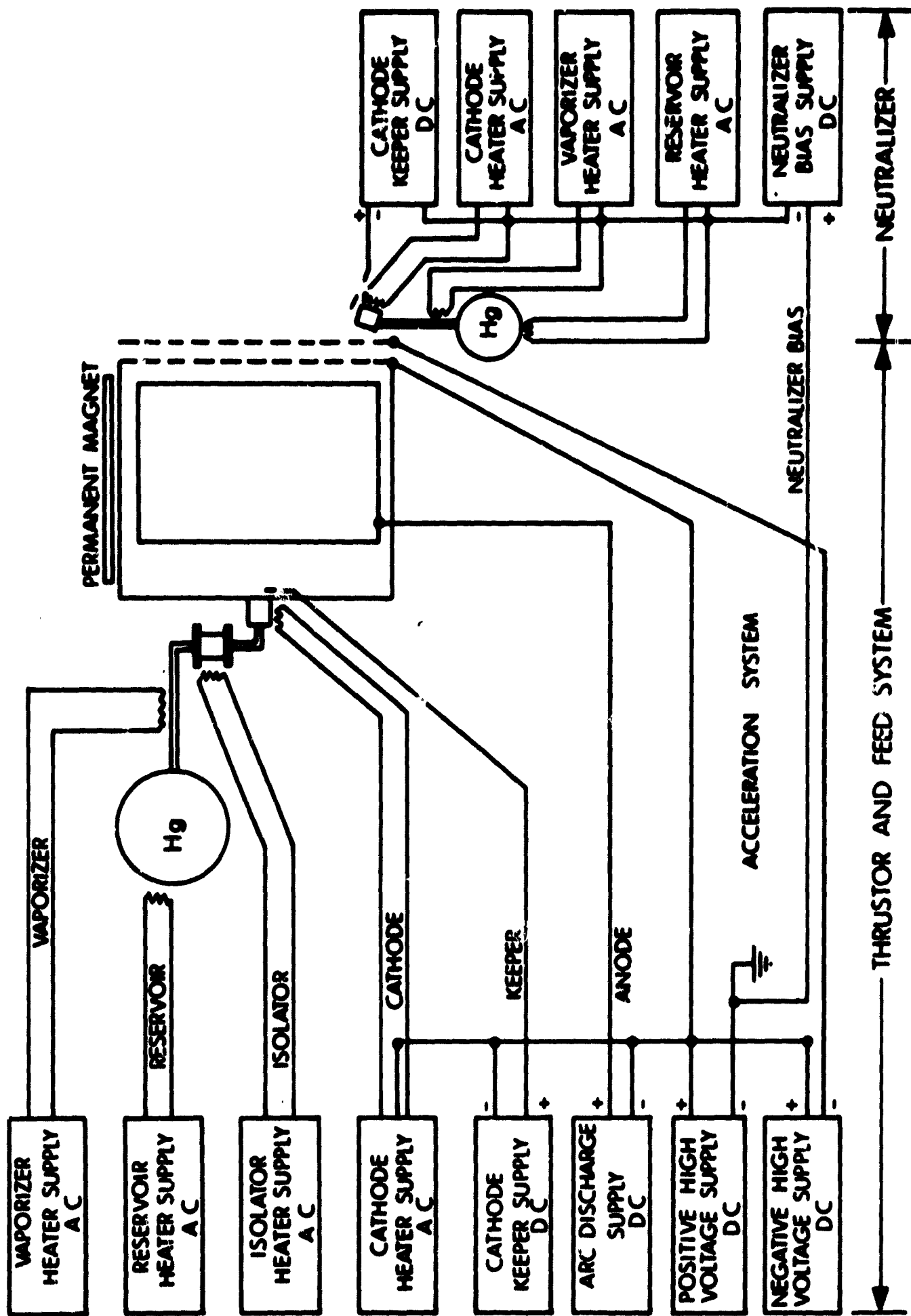


Figure 76. Schematic of Mercury Electron Bombardment Ion Thruster System

General power supply characteristics, as shown in Table XIV, however, can be discussed. The ac power supplies are required to supply only heating power and are usually low voltage-low current supplies. Included in this category are the power supplies required for the reservoirs, vaporizers, and cathodes. The next general category of power supplies are the low voltage-low current dc power requirements which include the keeper electrodes, thruster anode, and, if applicable, the thruster electromagnet. The remaining supply requirement is the high voltage-low current dc supplies required for the high positive and high negative accelerating voltages.

Table XIV lists the power supplies and the restrictions on each in terms of high voltage isolation, regulation, and control.

The types of controls necessary to operate the thruster system in a steady-state mode include the following:

- a. A beam-control loop to sense the actual beam current and compare this value with a predetermined or preset value. This loop regulates the thruster vaporizer power and thus temperature as required to provide the proper flow rate and maintain the level of beam current.
- b. A neutralizer control loop to sense the voltage level at a preset value of current of the keeper electrode. Deviations from the proper voltage are sensed and utilized to control the neutralizer vaporizer power and temperature as required to provide the proper coupling potential between the neutralizer and the ion beam by varying the flow rate.

Related to these two control loops is the requirement for thruster and neutralizer system vaporizer powers. These two particular power requirements have been defined during development of many of the mercury thruster systems to be directly related to the beam current output of the thruster. This relationship has been plotted in Figs. 77 and 78 which show thruster feed system power versus beam current and

TABLE XIV
THRUSTER SYSTEM POWER SUPPLY CHARACTERISTICS

<u>Power Supply</u>	<u>H.V. Isolation</u>	<u>Regulation or Control</u>
Thruster:		
Reservoir	No	Temperature, 50°C ± 20°C
Vaporizer	No	Flow rate, function of beam current
Isolator	No	Temperature, 300°C ± 50°C
Cathode	Yes	Temperature, 1200°C ± 100°C
Keeper	Yes	Constant voltage
Anode	Yes	Constant voltage
Screen	Yes	Current limited
Accelerator	Yes	Current limited
Turn-on	Yes	Automatic sequencing
Turn-off	Yes	Total power removal
Neutralizer:		
Reservoir	No	Temperature, 50°C ± 20°C
Vaporizer	No	Flow rate, function of beam voltage
Cathode	No	Temperature, 1200°C ± 100°C
Keeper	No	Constant voltage
Bias	No	Constant voltage
Turn-on	No	Automatic sequencing
Turn-off	No	Total power removal

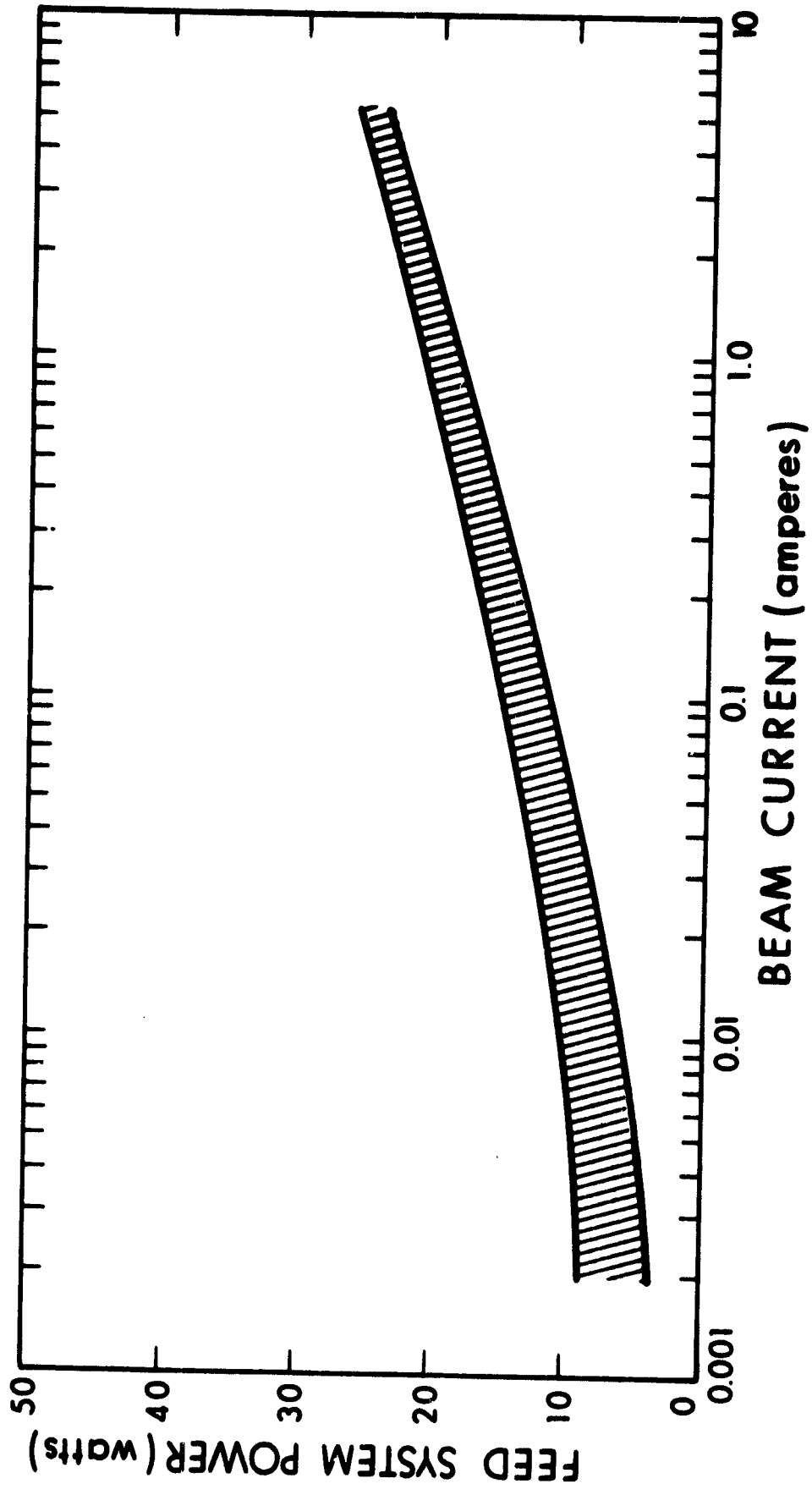


Figure 77. Mercury Electron Bombardment Thruster Feed Power System versus Beam Current

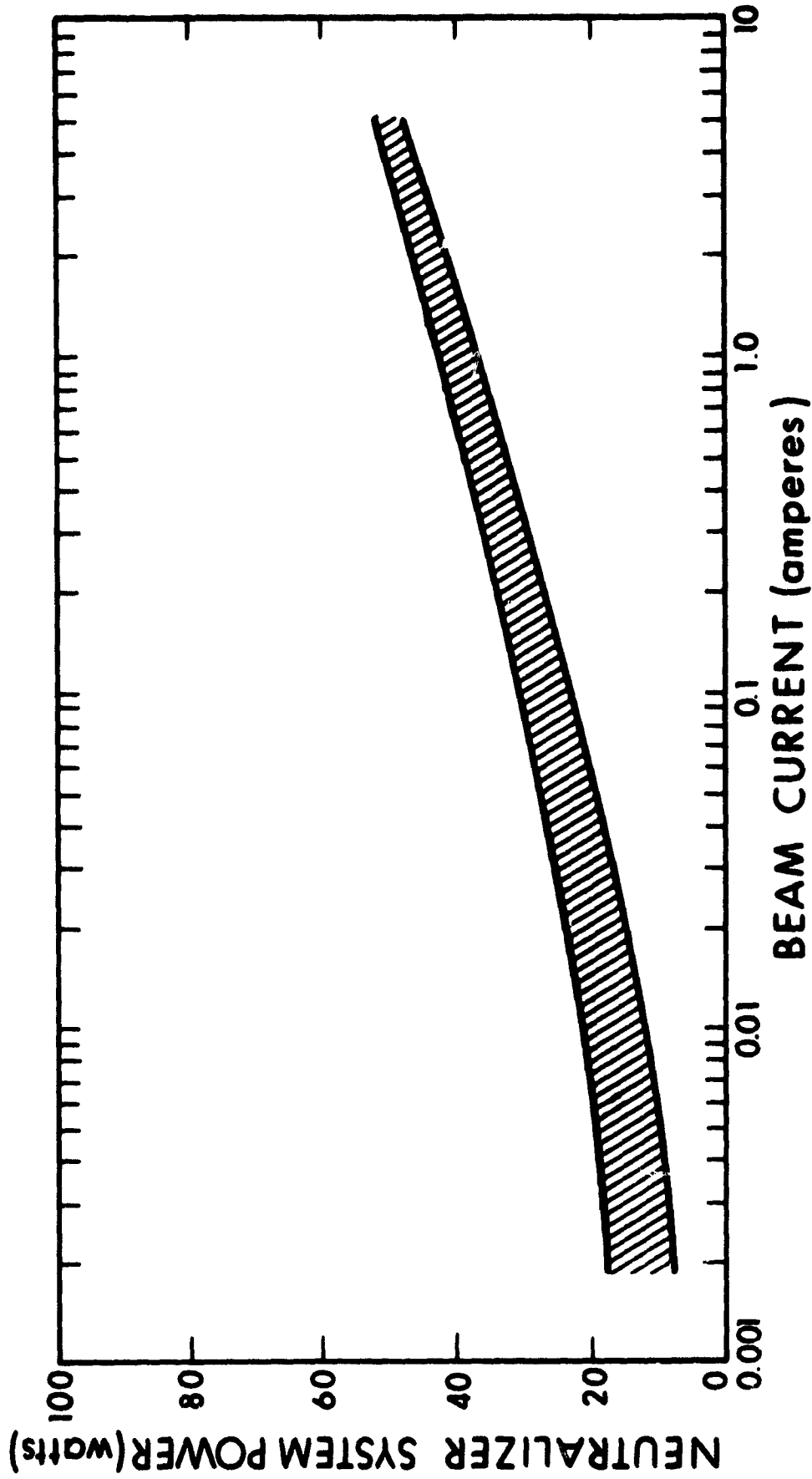


Figure 78. Mercury Electron Bombardment Thruster Neutralizer System Power versus Beam Current

neutralizer system power versus beam current, respectively. In the case of the thruster, the feed system power represents only the thruster vaporizer power, whereas with the neutralizer system, the neutralizer system power includes the vaporizer, cathode, and keeper electrode power requirements.

A thruster arc control loop was previously incorporated into the thruster when the various types of oxide cathodes were used. The loop was designed to adjust the cathode emission by varying the cathode heater power in order to match a preset value of thruster arc current when the thruster arc voltage was held constant (the use of the word arc in this instance is synonymous with anode or discharge). This particular control loop is not used, however, when thrusters are run with hollow cathodes due to the predictable emission characteristics.

It is possible to operate the thruster system in a "hands-off" mode by utilizing the above-mentioned control loops as required for a specific system design. A list of desirable telemetry and command channels necessary for three different degrees of system analysis are presented in Tables XV and XVI, respectively. It can be seen that minimum to maximum quantities of data can be obtained when the flexibility of communication channels selected for a particular mission is exercised. The actual number of channels chosen, however, is based upon the degree of analysis desired, the weight and power requirement as well as the complexity of command channels, and the particular mission.

The need for command channels is based upon the degree of control desired in analyzing and/or correcting thruster system performance while it is in space. It should be noted that the commands listed as "necessary" are required to optimize thruster system performance while those listed as "desired" give the investigator the additional capability of thruster system performance mapping and detailed study.

TABLE XV
TELEMETRY DATA CHANNELS

<u>Data or Parameter</u>	<u>Minimum Data</u>	<u>Nominal Data</u>	<u>Research Data</u>
Current:			
Thruster Reservoir	-	-	-
Thruster Vaporizer	-	✓	✓
Thruster Isolator	-	✓	✓
Thruster Cathode	-	✓	✓
Thruster Keeper	✓	✓	✓
Thruster Anode	✓	✓	✓
Thruster Screen	✓	✓	✓
Thruster Accelerator	✓	✓	✓
Neutralizer Reservoir	-	-	-
Neutralizer Vaporizer	-	✓	✓
Neutralizer Cathode	-	✓	✓
Neutralizer Keeper	✓	✓	✓
Neutralizer Emission	✓	✓	✓
Voltage:			
Thruster Reservoir	-	-	-
Thruster Vaporizer	-	-	✓
Thruster Cathode	-	-	✓
Thruster Isolator	-	-	✓
Thruster Keeper	✓	✓	✓
Thruster Anode	✓	✓	✓
Thruster Screen	✓	✓	✓
Thruster Accelerator	✓	✓	✓
Neutralizer Accelerator	-	-	-
Neutralizer Vaporizer	-	-	✓
Neutralizer Cathode	-	-	✓
Neutralizer Keeper	✓	✓	✓
Neutralizer Bias	✓	✓	✓
Temperature:			
Thruster Reservoir	-	-	✓
Thruster Vaporizer	-	✓	✓
Thruster Isolator	✓	✓	✓
Thruster Cathode	-	✓	✓
Thruster Anode	-	-	✓
Thruster Chamber	-	-	✓
Neutralizer Reservoir	-	-	✓
Neutralizer Vaporizer	-	-	✓
Neutralizer Cathode	-	✓	✓
Pressure:			
Thruster Reservoir	-	-	✓
Neutralizer Reservoir	-	-	✓

TABLE XVI
COMMAND CHANNELS

<u>Power Supply</u>	<u>Necessary Command</u>	<u>Desirable Command</u>	<u>Parameter Affected</u>
Thruster:			
Reservoir	No	Yes	Temperature
Vaporizer	No	No	--
Isolator	No	Yes	Temperature
Cathode	No	Yes	Temperature
Keeper	Yes	Yes	Voltage
Anode	Yes	Yes	Voltage
Screen	No	Yes	Voltage
Accelerator	No	Yes	Voltage
Turn-on/off	Yes	Yes	Power
Neutralizer:			
Reservoir	No	Yes	Temperature
Vaporizer	No	No	--
Cathode	No	Yes	Temperature
Keeper	Yes	Yes	Voltage
Bias	Yes	Yes	Voltage
Turn-on/off	Yes	Yes	Power

An important command function is that of thruster and neutralizer turn-on and turn-off. It is clear that the start up sequencing of both must be completely automatic and must also be precisely timed such that the thruster is not allowed to emit ions prior to the emission of electrons. Without complete neutralization of any portion of the beam, several complications result. These include:

- a. When any value of thrust is being produced by the thruster, incomplete neutralization of this beam will result in an excess of ions emitted which leave the spacecraft negative. When this occurs, the ions are repelled due to the ion space-charge buildup which prevents the thruster from producing thrust. The order of time required for reversal is nanoseconds. In addition, the beam will rapidly assume the high positive potential of the screen, and the spacecraft will assume a high negative potential (screen) which will attract the ions and prevent further emission of them from the thruster. Because there is a slight time delay, however, the spacecraft will assume a potential which is positive with respect to the local space potential.
- b. The current and charge emission of electrons in excess of the current and charge emission of ions will cause the spacecraft to assume a potential which is negative with respect to the local space potential. Excess electron emission, however, will not lead to the results described above.

From the preceding discussion, it is obvious that the magnitude (current and charge) of emissions from the neutralizer and from the thruster must be synchronized. Since operation of the neutralizer is mandatory, some means must be chosen to either rapidly increase its emission when only partial neutralization is occurring or the thruster must be rapidly throttled back or turned off until the neutralizer emission capability is regained. It is known, however, that rapid increase in the neutralizer emission is extremely difficult because of the thermal response of the neutralizer system. It is also difficult to rapidly throttle down the thruster because of the same types of thermal response considerations in the thruster. It is necessary, therefore, to turn off the thruster when the ion beam is not being completely neutralized.

The requirement for turn-off of the thruster must also be automatic because of the intolerable time delays involved in sensing the problem and commanding turn-off from the earth. One potential method of determining the degree of neutralization is with the use of a probe. This probe would measure the potential of the beam, and thus the spacecraft potential, and compare this value to the space potential in the vicinity of the spacecraft. The nominal spacecraft potential is defined above is usually a few volts positive. If, however, total neutralization is not occurring, the spacecraft potential as indicated by the probe would rapidly rise to a potential value approximately equal to the positive high voltage of the screen electrode power supply. This screen voltage will normally be of the order of a few thousand volts as dictated by the specific impulse. The rapid rise of the beam potential (space potential in the vicinity of the probe) or the magnitude of that potential could be utilized to provide the signal required to turn off the thruster.

Another method which could be utilized to turn off the thruster system would be to take advantage of the fact that a poorly neutralized or unneutralized beam would partially be reflected back onto the acceleration system which would result in overloads to the two high voltage supplies. This fact could be combined with an overload number counter which would limit high voltage cycles to a predetermined number. After this number of cycles (say five or ten) is reached, a signal caused by that fact could be used to turn off the thruster.

This latter method of sensing partial or no neutralization is not desirable because it does not prove that turn-off of the thruster was caused by a failure or inadequacy of the neutralizer system. The high voltage supplies will normally cycle when overloads due to any cause are sensed. These causes may include the flaking of metal from between the electrodes, the presence of any foreign metal which could short out either high voltage supply, and micrometeorite impact on or near the electrodes.

Although the use of a potential probe would measure the exact effectiveness of the neutralizer system, it is undesirable because of the need to provide additional design as well as cost, components, weight, and volume to the spacecraft.

In addition to the general discussion above, various investigations and development work with the mercury thruster systems have resulted in reduction of power-conditioning and control requirements. These include the following:

- a. The incorporation of permanent-magnet type magnetic fields which obviate the need for any type of power supply and regulation.
- b. Reduction of thruster and neutralizer cathode heater requirements. Previously the oxide cathodes required up to 100 watts heating power at about 50 amperes current. Present hollow-cathode type designs require less than 20 watts heating power at about 3 amperes current.
- c. Examination of the ionization chamber operation using alternating current directly for the discharge.

These as well as other areas discussed in Subsection 2.2.7 will continue to be investigated and the benefits will chiefly be seen in reducing the power-conditioning restrictions and control requirements.

2.2.5 PRESENT STATUS

The following section will be used to present and describe those thruster system parameters and calculations which are of interest to mission planners. The basic system design evolved in the preceding sections and typified by the SERT II mercury, electron-bombardment ion thruster system will be used as the basis for these parameters. All of the values presented below represent realistic and attainable ones that have been selected to define the present state of the art for mercury thruster systems.

Numerous figures have been included that are representative of present and expected near-term system performance. Consideration has been given to the potential improvements in many of the subsystems and components. These improvements are included in the figures and represent the extrapolated performance values based upon the expected performance for the next generation of thruster systems.

2.2.5.1 Durability

Durability for thruster systems includes the reliability and lifetime capabilities of all subsystems and components. The primary consideration here is whether or not the thruster system is capable of performing a given mission. Although the ultimate performance in terms of time for a system is a function of component lifetime, the reliability and durability are equally important as they apply to the total system.

The following discussion will be limited to lifetime, reliability, and durability as they pertain to the thruster system and subsystems and components. Specific limitations and potential problem areas will be selected. It has been assumed that those components are areas that

have been omitted from this discussion meet the necessary requirements of lifetime, reliability, and durability for near-term missions. Near-term missions are defined as those potential unmanned missions which will take place from the present to 1975. These will primarily be scientific, reconnaissance, and communication satellites having orbits about the earth up to synchronous altitudes and lifetimes up to a maximum of five years. Nominal lifetimes, however, may be significantly shorter. This is particularly true when consideration is made of the thrust system requirements which indicates small duty cycles even for the five-year missions. Thus, the average lifetime requirements for the near-term missions appear to be limited to about two years.

For the mercury electron-bombardment ion thruster system, the thruster and neutralizer cathodes have historically been the life-limiting components of the total system. Introduction of the hollow-cathode type emitters and keeper electrodes has increased the efficiency and reproducibility of operation for the thruster and neutralizer system. Very long lifetimes, however, are still a problem with these emitters because of the mercury discharge voltages. The arc voltage of about 35 volts is sufficiently high that ion sputtering of the cathode continues to be a problem. This problem has been reduced from the magnitudes incurred with the former oxide cathode designs by the fact that the discharge voltage has been reduced (from 50 volts with oxide cathodes) and that the thruster geometry has been modified to result in reduced cathode sputtering.

Although the lifetimes of the emitter systems are limited at present to less than one year, continued efforts in this area can result in greater lifetimes; lifetimes that are adequate for the near-term missions presently being planned.

The ultimate life-limiting component in the mercury system as well as any of the electrostatic devices is the accelerator electrode. Since this electrode is sputtered by ions formed downstream of the thruster by charge-exchange collisions, the effective damage can be reduced. Factors that are capable of reducing this damage include; (a) use of materials of low sputtering yield, (b) reduction of the neutral mercury flow out of the thruster (increased propellant utilization), (c) electrode designs which minimize the effective erosion, and (d) thicker electrodes. All of these factors can result in reducing the damage and, therefore, increasing the life of the electrode. At this time, however, the erosion of the accelerator electrode is sufficiently small that lifetimes greater than those required for near-term missions exists.

Minor materials problems such as bladder and vaporizer materials have been encountered in the past. These have been eliminated through the use of both improved designs and material substitutions.

Although the thruster system has several areas where improvements in lifetime can be made, it does have adequate potential for near-term missions. Continued development in these several areas to eliminate or reduce the present limitations, however, will greatly increase the usefulness and capability of the mercury thruster systems.

Reliability and durability are obviously necessary to the successful application of any system in space. Little direct concern, however, is made of these requirements in this discussion because of the present status and future capability of the mercury system. Suffice it to say that complete qualification and environmental evaluation are necessary prior to the application and use of any system in space.

2.2.5.2 Mass

Near-term mission requirements emphasize the following parameters in order of decreasing importance; reliability, durability, lifetime, power-to-thrust ratio, efficiency, mass, and size. Although the mass is not of prime concern for these missions, it becomes, increasingly, the pacing factor for missions of longer duration and greater distances from earth.

System mass can be traded directly for system power and, thus, performance. This relationship can be seen in Fig. 79. Shown is the thruster mass only as a function of power of the thruster system. Figures 80, 81, and 82 show the effect of total thruster system weight on performance capability in terms of total impulse. These figures present three thruster system sizes (4.45×10^{-3} , 4.45×10^{-2} , and 4.45×10^{-1} newtons thrust) or the effect of different levels of thrust upon total impulse. It is seen that for larger values of total impulse, the percentage of system dry mass is smaller. Also, the higher the thrust of the systems for a given mission length, the smaller is the percentage of system dry mass.

2.2.5.3. Size

Thruster size is only of minor importance. Size is, however, a consideration used to define the basic system volume requirements.

As seen in Figs. 83 and 84, thruster size can be related to the total thruster system power and thruster mass, respectively. A given size of thruster will have a certain mass. However, the power is obviously a function of the desired specific impulse and thrust and, therefore, each size of thruster can operate within a range of available power or over a range of specific impulse.

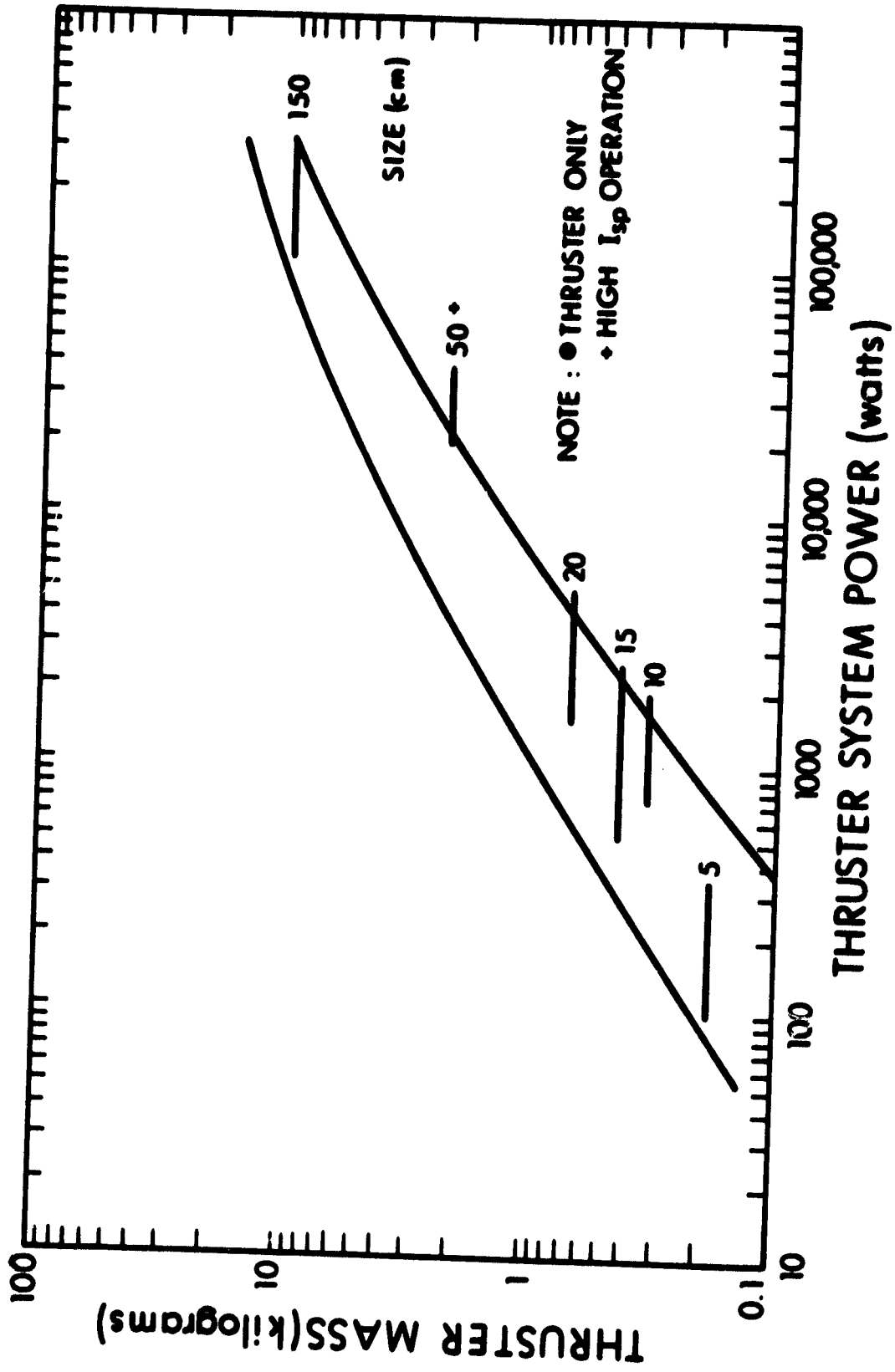


Figure 79. Thruster Mass as a Function of Thruster System Power

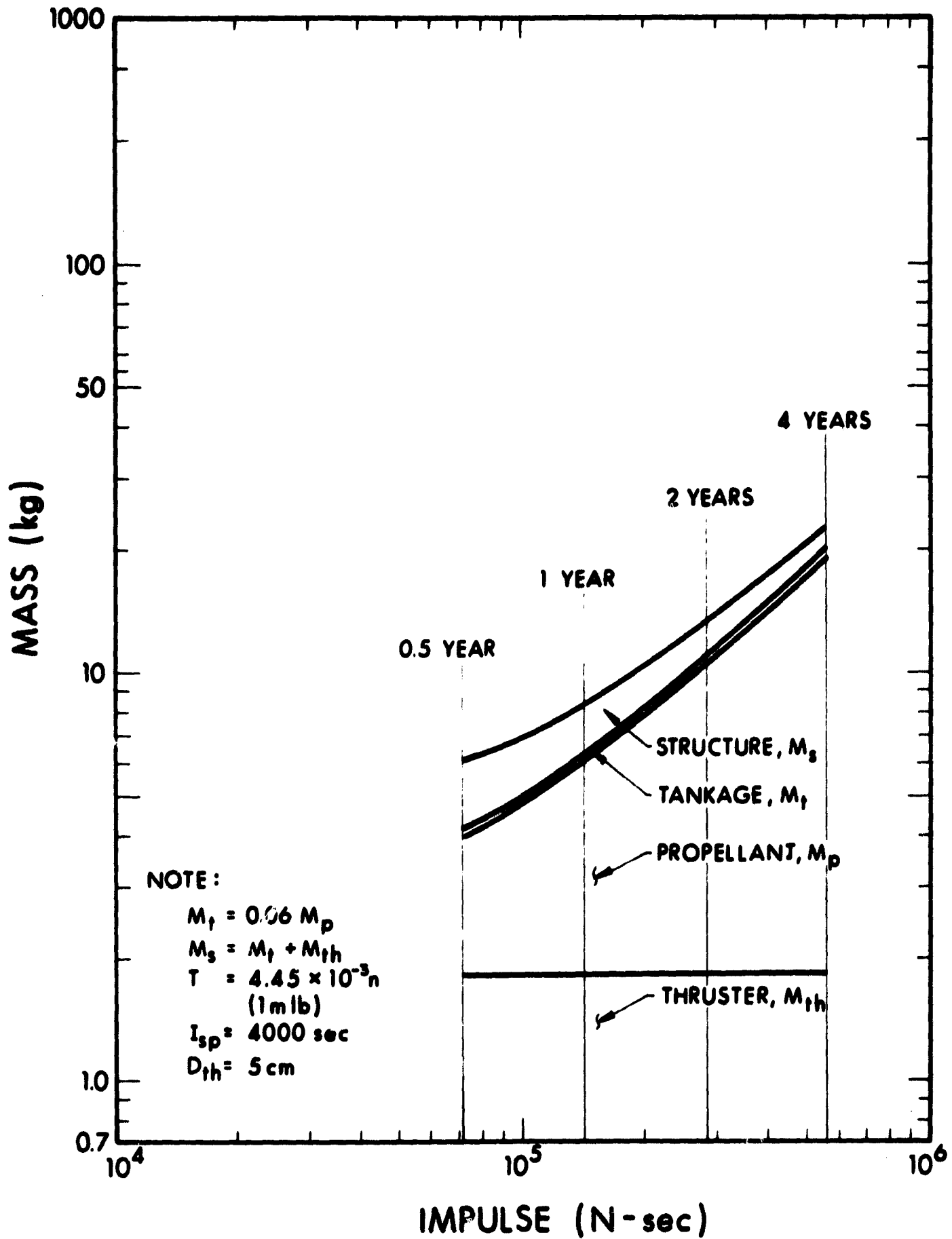


Figure 80. Thruster Mass versus Total Impulse (4.45×10^{-3} newtons thrust)

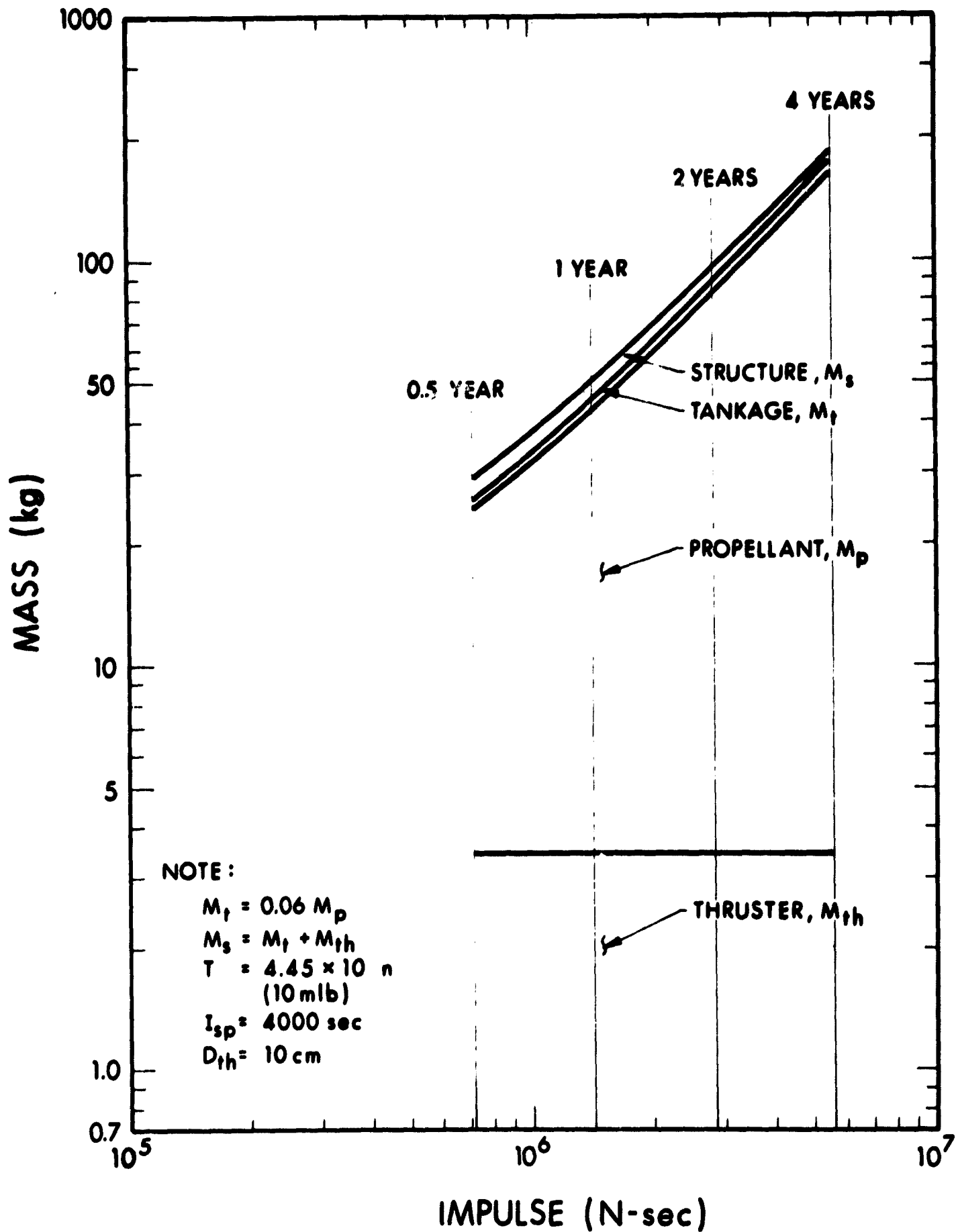


Figure 81. Thruster Mass versus Total Impulse (4.45×10^{-2} newtons thrust)

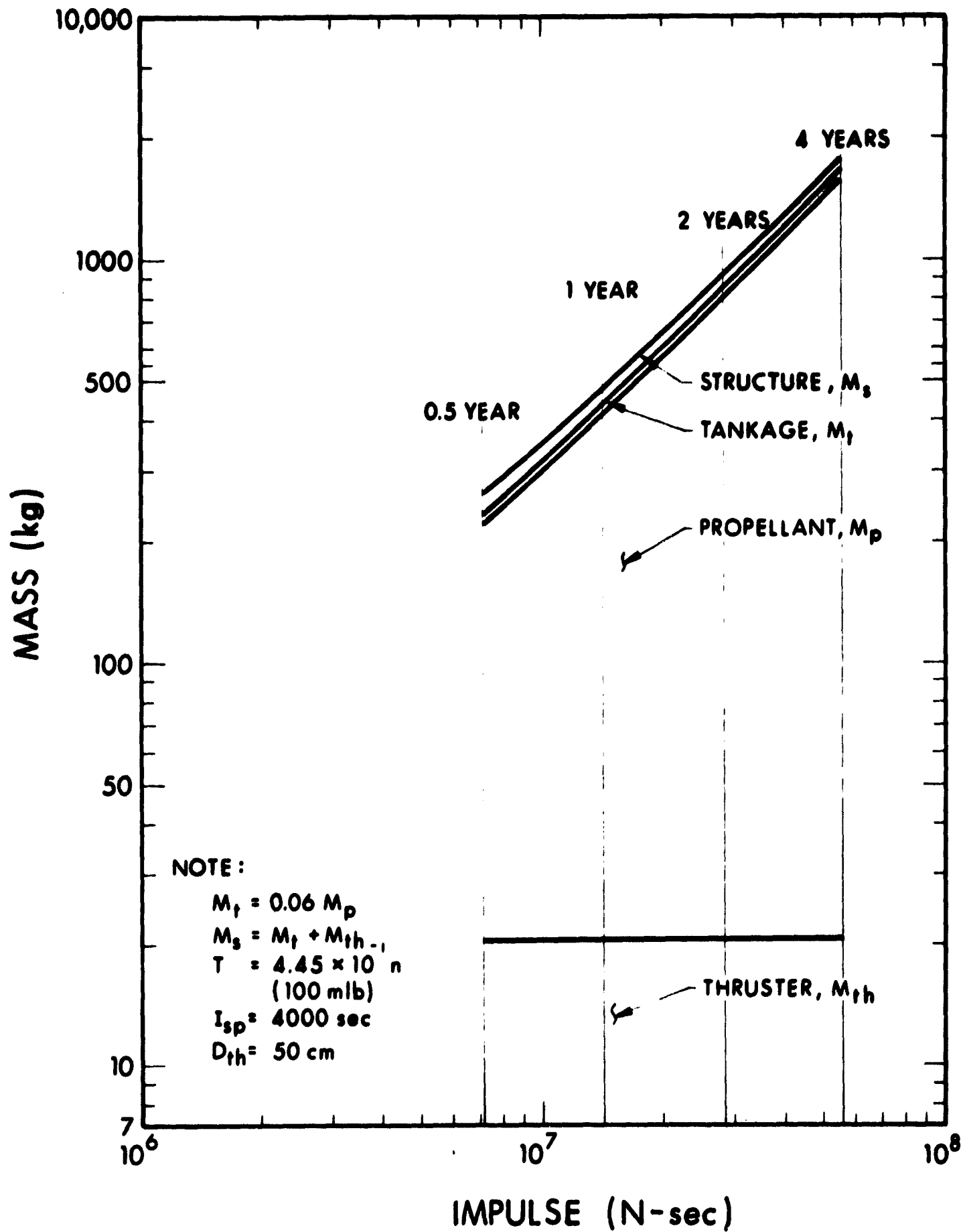


Figure 82. Thruster Mass versus Total Impulse (4.44×10^{-1} newtons thrust)

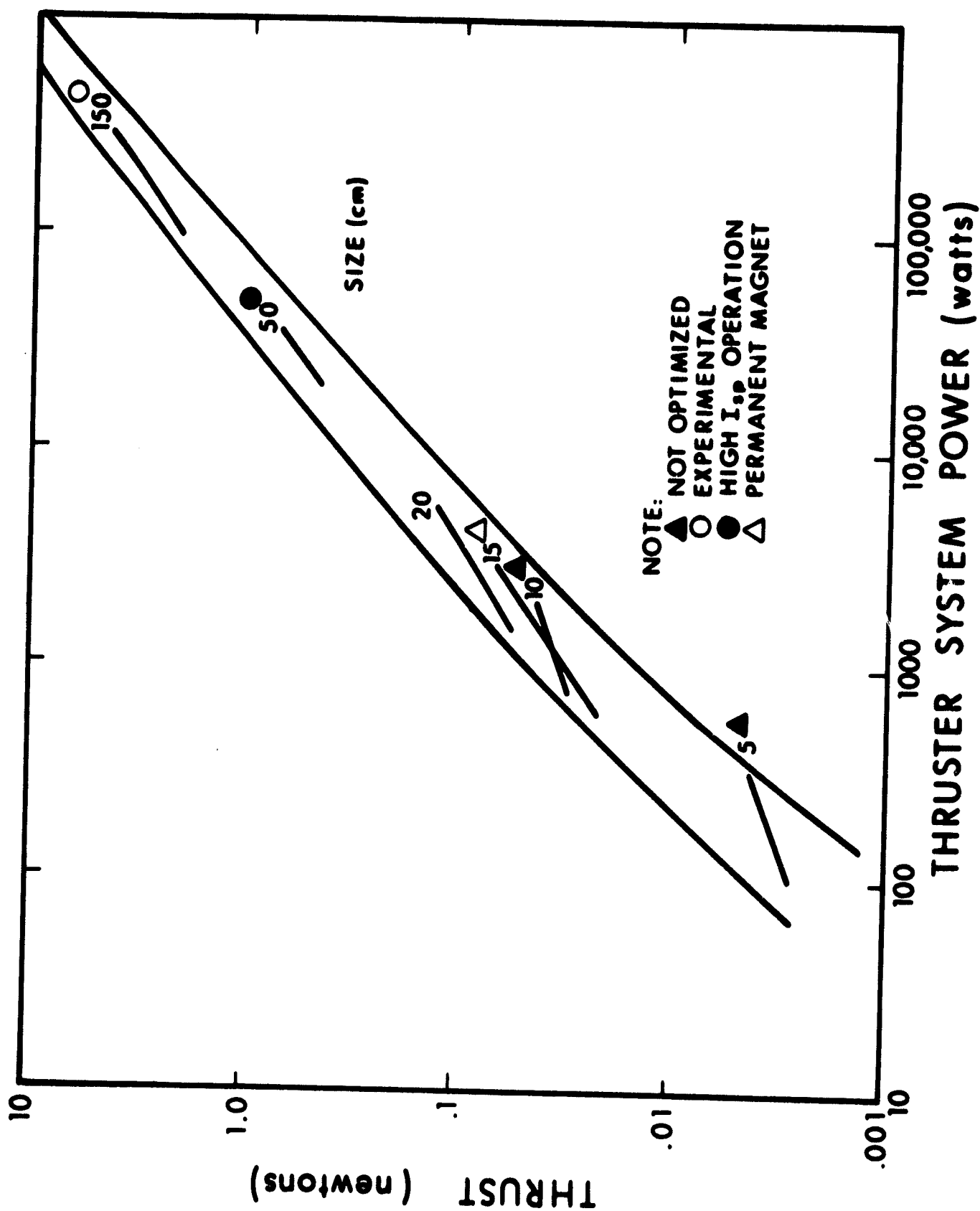
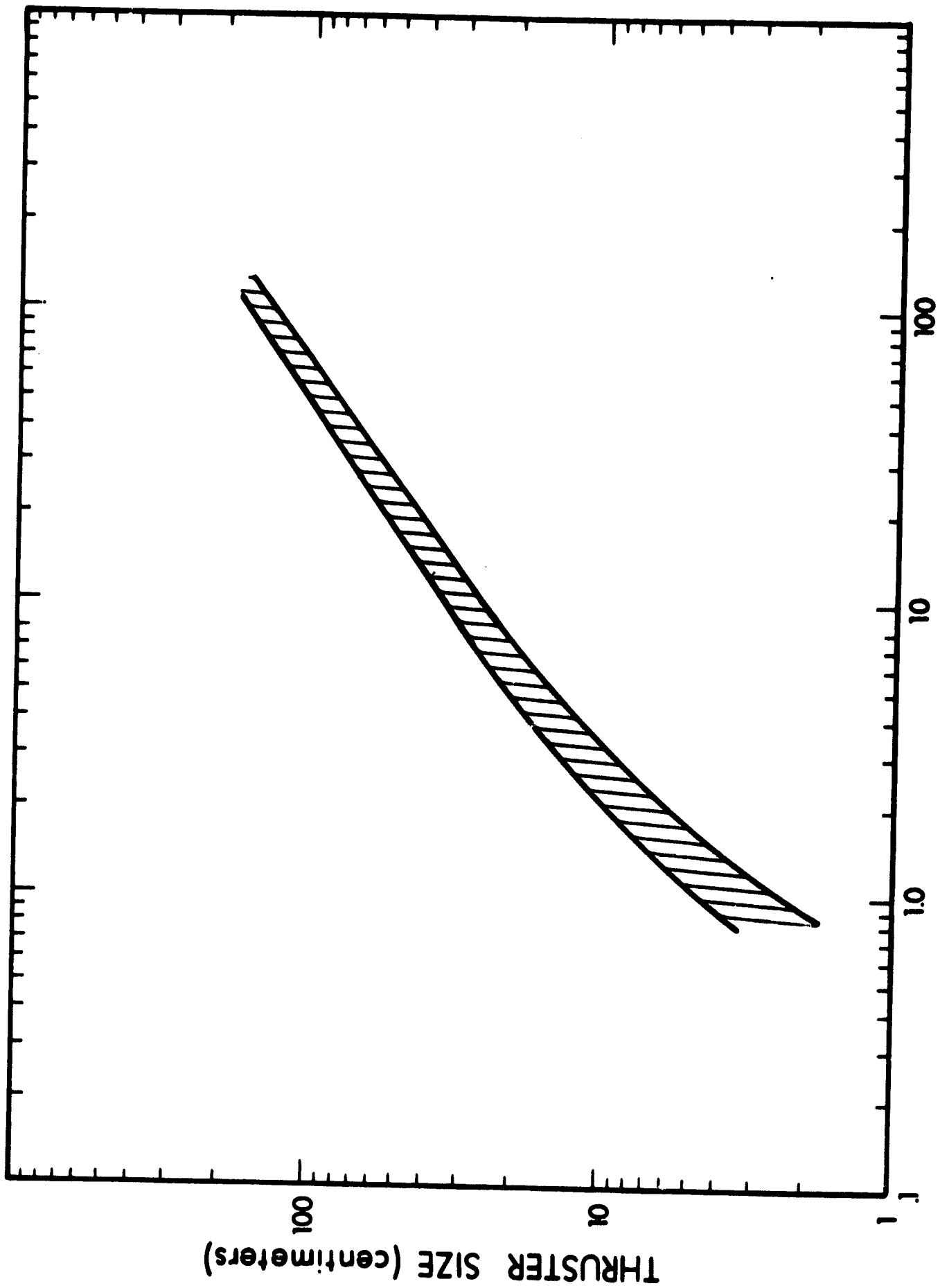


Figure 83. Thruster Size versus Thruster Power



THRUSTER MASS(kilograms)

Figure 84. Thruster Size versus Thruster Mass

The thruster size is normally represented by the anode diameter. For mercury thrusters, the anode diameter should be multiplied by about 1.3 to arrive at the overall thruster diameter. No consideration in this thruster envelope has been made for the neutralizer system since it can be mounted either to the thruster or to the spacecraft structure. The only requirement for location and mounting of the neutralizer is that the relative position with respect to the ion beam is maintained.

2.2.5.4 Clustering - Scaling

Considerable effort and experimentation has occurred in the area of the clustering and the scaling of thrusters.

In particular, work has resulted in the evaluation of an array of three 20-centimeter-diameter mercury thrusters and of an array of nine 20-centimeter-diameter thrusters. In each of these investigations, the groups of thrusters were operated and particular attention was given to the electrical and magnetic interactions between and among them. The effects of magnetic field interactions can be minimized by the use of permanent magnets and pole pieces which define the field lines within the thruster with use of pole pieces. Although the majority of electrical interactions can be eliminated by the incorporation of effective shielding techniques, it is apparent that the greatest difficulty from thruster interactions is due to the types of controls used to operate individual thrusters and groups of thrusters. This is because common power supplies are ordinarily utilized to power more than one thruster or similar functions in many thrusters.

Thrusters utilizing mercury propellant have been fabricated, tested, and evaluated ranging in size from 5 to 150 centimeters in diameter. It is worth mentioning here that despite the lack of detailed scaling laws which would aid in design of thrusters of different size than

those previously built, this lack is not critical. It remains that the best guidelines for defining and designing a new thruster depend upon the following:

- a. Specific application which defines thrust, power level, weight, and size.
- b. Experienced and capable personnel who are familiar with the design of thrusters and their operating characteristics.

In addition to the conventional thruster design shown in Fig. 68, two bidirectional thruster designs have been investigated. One of these thrusts in two directions 180 degrees apart while the other thrusts in two directions 90 degrees apart. Excessive fuel loss through the dormant electrode system in either thruster design is prevented by utilizing very small apertures in the accelerator electrodes. Although neither of these thruster designs has been extensively investigated or found to be particularly efficient, they do represent unique techniques for obtaining thrust vectoring.

2.2.5.5 Thrust

Thrust capability of any system is a requirement defined for a specific mission. Whatever power, size, mass, and other requirements are dictated for the particular system are a result of the desired thrust.

Although the thrust is a direct function of power as noted in Fig. 85, it is also a function of specific impulse. This is seen in Fig. 86 which shows the range of power-to-thrust versus specific impulse for the mercury thruster system. Other variables, such as thruster size and system mass, are only an indirect function of thrust. Their effect of system definition can be visualized by referring to all of the curves shown in Figs. 79 through 86.

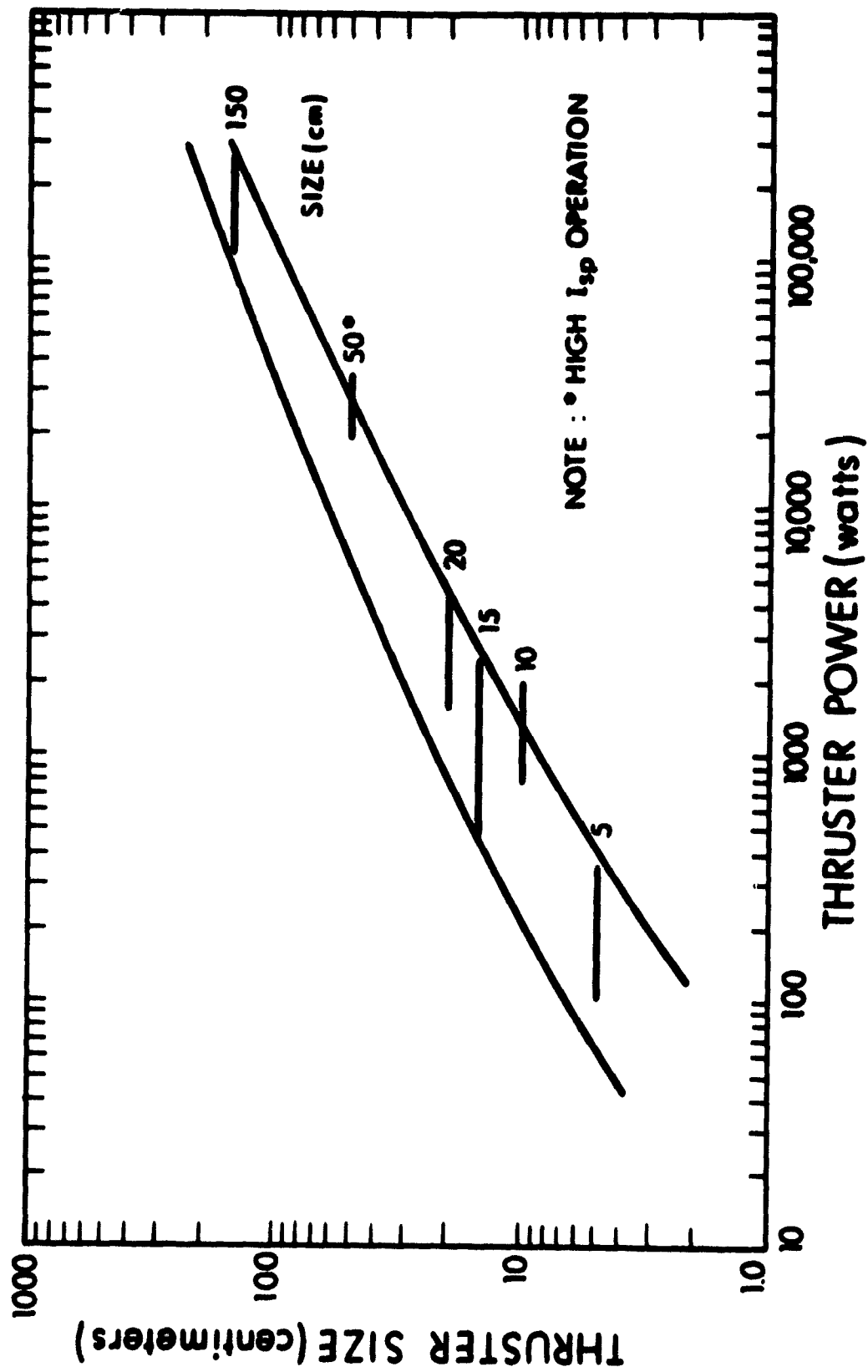


Figure 85. Thrust as a Function of Thruster System Power

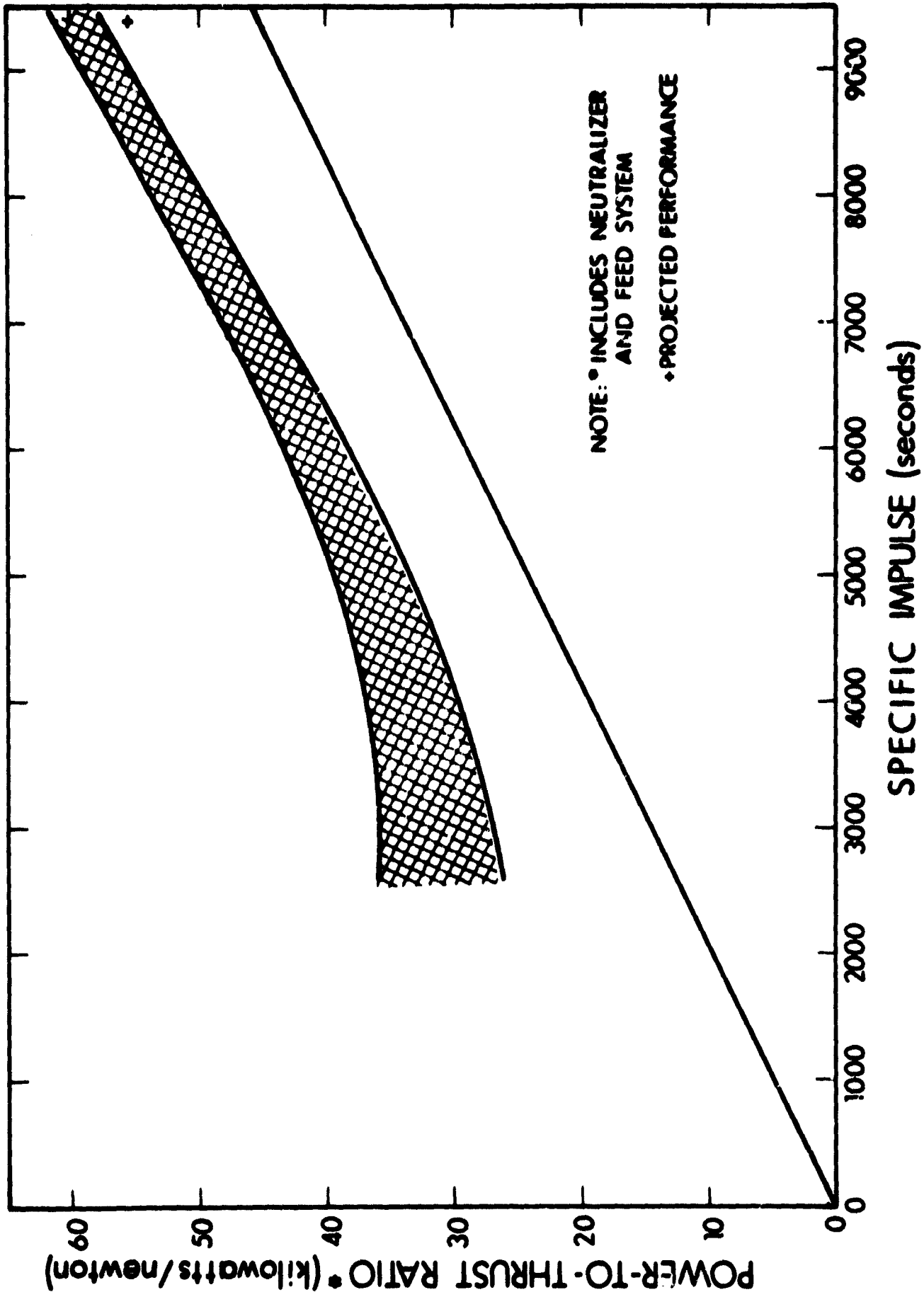


Figure 86. Power-to-Thrust Ratio versus Specific Impulse

2.2.5 6 Specific Impulse

Specific impulse, perhaps the most familiar "figure of merit" for all classes of thrusters, is the measure of the amount of thrust produced by a given rate of flow of the propellant and is directly proportional to the ejection velocity.

The specific impulse when corrected due to incomplete ionization of the propellant, is the accepted basis for thruster performance comparisons and is termed the "effective" specific impulse. In all of the curves and data presented, the effective specific impulse is implied whenever specific impulse is given.

The two most frequently used curves which indicate the performance and merit of thrusters are the power-to-thrust ratio and overall efficiency. These are plotted as a function of specific impulse in Figs. 86 and 87, respectively. It should be noted here that although these curves show the performance range for the mercury thrusters, they do not show such other important considerations such as size, mass, or durability. These additional considerations can only be obtained after the particular mission, specific impulse, and thrust requirements have been selected. To describe at this point the necessary development and definition of a specific thruster system would only result in a review of the previous discussions and a review of history. It is more important to realize, however, that the application and design of any system does not begin until the specific mission requirements and timetable for development are provided. It is then the task of experienced and qualified personnel to design, fabricate, evaluate, and qualify the candidate thruster system.

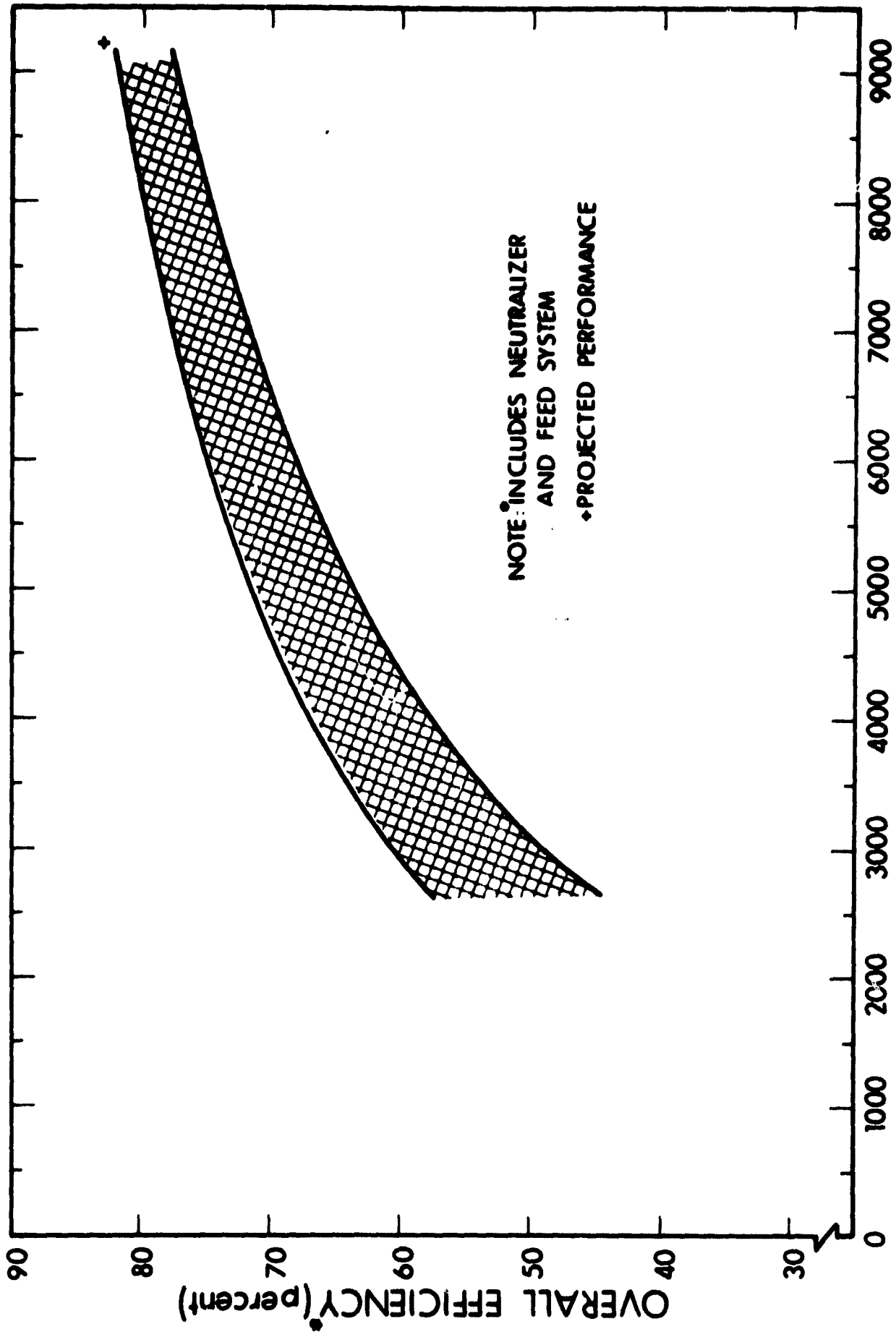


Figure 87. Overall Efficiency versus Specific Impulse

2.2.6 PERFORMANCE PREDICTIONS

This section includes a general discussion of the expected performance of the mercury electron-bombardment ion thruster system. It is difficult to classify and categorize completely this information and, as a result, only an outline of the potential system improvements will be presented. These improvements have been developed and evolved since the introduction of the mercury ion source as a thrust-producing device in 1959 and represent the present and near-term improvements affecting thruster system performance and capability. Greatest of these, which are also described in other sections are:

- a. Improvement of thruster and neutralizer electron emitters or cathodes which require minimum power and are long-lived.
- b. Design and development of ion acceleration systems matched to ionization chamber characteristics to give efficient ion extraction and minimum accelerator electrode erosion.
- c. Increase of propellant utilization via increased ionization chamber efficiency, optimum propellant introduction and distribution methods, and efficient electron emitters.
- d. Design and utilization of divergent magnetic fields which, for a given thrust and specific impulse, yield maximum ionization chamber performance.
- e. Development and application of permanent magnet thruster configurations which perform as well as electromagnet designs and require no power.
- f. More sophisticated thruster systems and test techniques which involve at least preliminary investigation and development of the following advanced subsystems:
 - (1) "Zero-gravity" type feed systems including the gas-pressurized, positive-displacement systems
 - (2) High perveance (performance) electrode acceleration systems
 - (3) Breadboard and flight power-conditioning equipment
 - (4) Longer and larger volume vacuum facilities with greater pumping speeds
 - (5) Extensive measurement and data-recording systems

Representative data, summarized in Tables XII and XIII, from various thrusters have been reviewed and utilized in the presentation of the above mentioned Figs. 79 through 87.

These curves provide a starting point for mission planners desiring to utilize mercury thruster systems. The curves presented in Figs. 79 through 87 have been taken from original investigations given in the bibliography. Although the curves show the specific operating characteristics and potential of various thruster systems and subsystems, they have been purposely generalized and extrapolated such that performance capabilities and ranges are suggested in heretofore uninvestigated areas.

2.2.6.1 2.5 Kilowatt Thruster System

To illustrate the expected thruster system performance for near-term applications, a 2.5 kilowatt mercury thruster has been chosen to illustrate the potential and performance obtainable with the mercury thruster system.

Table XVII gives the approximate values and performance calculations for this system. The mission requirements for this particular thruster include a specific impulse of 5000 seconds, 2.5 kilowatts of power to operate the system, and a mission lifetime of 2 years.

Although this system indicates near-term performance, it should be stressed that these values are approximate. The ultimate capability is obviously based upon the development and qualification of such a system.

TABLE XVII
2.5 KILOWATT THRUSTER SYSTEM

<u>Thruster Parameter</u>	<u>Value</u>
Input power, watts	2,500
Thruster power, watts	2,465
Neutralizer power, watts	35
System mass efficiency, percent	79
System overall efficiency percent	69
Power-to-thrust ratio, kilowatts/newton	34
Specific impulse, seconds	5,000
Thrust, newtons	0.74
Positive high voltage, volts	3,600
Negative high voltage, volts	2,000
Beam current, amperes	0.6
Thruster system weight, kilograms	10
System specific weight, kilogram/kilowatt	4
Propellant weight, kilograms	100
Mission time, hours	17,500

Several features of this particular thruster system, however, are noteworthy and applicable to most of the projected mercury thruster systems under consideration for near-term missions. These features include the following:

- a. A gas-pressurized, positive-displacement feed system reservoir capable of "zero-gravity" operation
- b. An isolator device to "electrically" isolate the feed system from the thruster
- c. A hollow-cathode type electron emitter in the thruster and neutralizer system
- d. Permanent-magnet type magnetic field
- e. Neutralizer system mounted to or separate from the thruster
- f. Control loops to provide completely automatic operation of the thruster system
- g. Structural design of the thruster to produce a durable, lightweight system

As illustrated by the large bibliography for missions for electric thrusters, there has not been a lack of effort in the areas of missions, mission requirements, and related mercury thruster system development. To date, however, serious use of electric propulsion has not occurred because of the low confidence level in electric thrusters in general and in mercury electric thrusters in particular. This lack of confidence is expressed in the following areas of greatest concern to mission planners:

- a. Lack of adequate life test data which would reveal the capability of electric thrusters to operate reliably in space without experiencing major changes in operating characteristics for periods of time greater than a few thousand hours.
- b. Lack of substantiated data that small thrust (less than 5×10^{-3} newtons thrust) mercury thruster systems can be designed and qualified that have:
 - (1) Long life
 - (2) Durable and reliable components and subsystems

- (3) Moderate levels of efficiency
 - (4) Thrust vectoring and throttling response
 - (5) Simple packaging in small volumes at minimum weight
- c. Electrical space power capability that would allow mission planners to meaningfully design prime thrust missions utilizing electric propulsion.

Although these facts exist, many mission analyses have recently been made which utilize electric propulsion in one particular area where it is capable of performing the near-term missions. These missions, for the most part, require microthrust capability for use in station keeping and attitude control of various spacecraft platforms. One of the reasons that such types of applications are now being considered is due to the development of techniques which allow the fabrication of lightweight solar cell arrays (18 kilograms per kilowatt is now state of the art for these power sources). The recent development of these arrays means that microthrust systems can be designed with minimum weight and power requirements for the entire thrust system including thruster system propellant, power-conditioning and control equipment, and power source.

2.2.7 FUTURE DEVELOPMENT AREAS

The mercury thruster system as described in the preceding sections is quite capable of performing the thrust activities of most near-term missions. There are several areas, however, where new or continued development and investigation could result in improved performance and capability. In addition, areas of thrust and performance not covered by the present mercury thruster system investigations should be included.

Development of the components and subsystems, as outlined below, could result in improved systems and competitive performance.

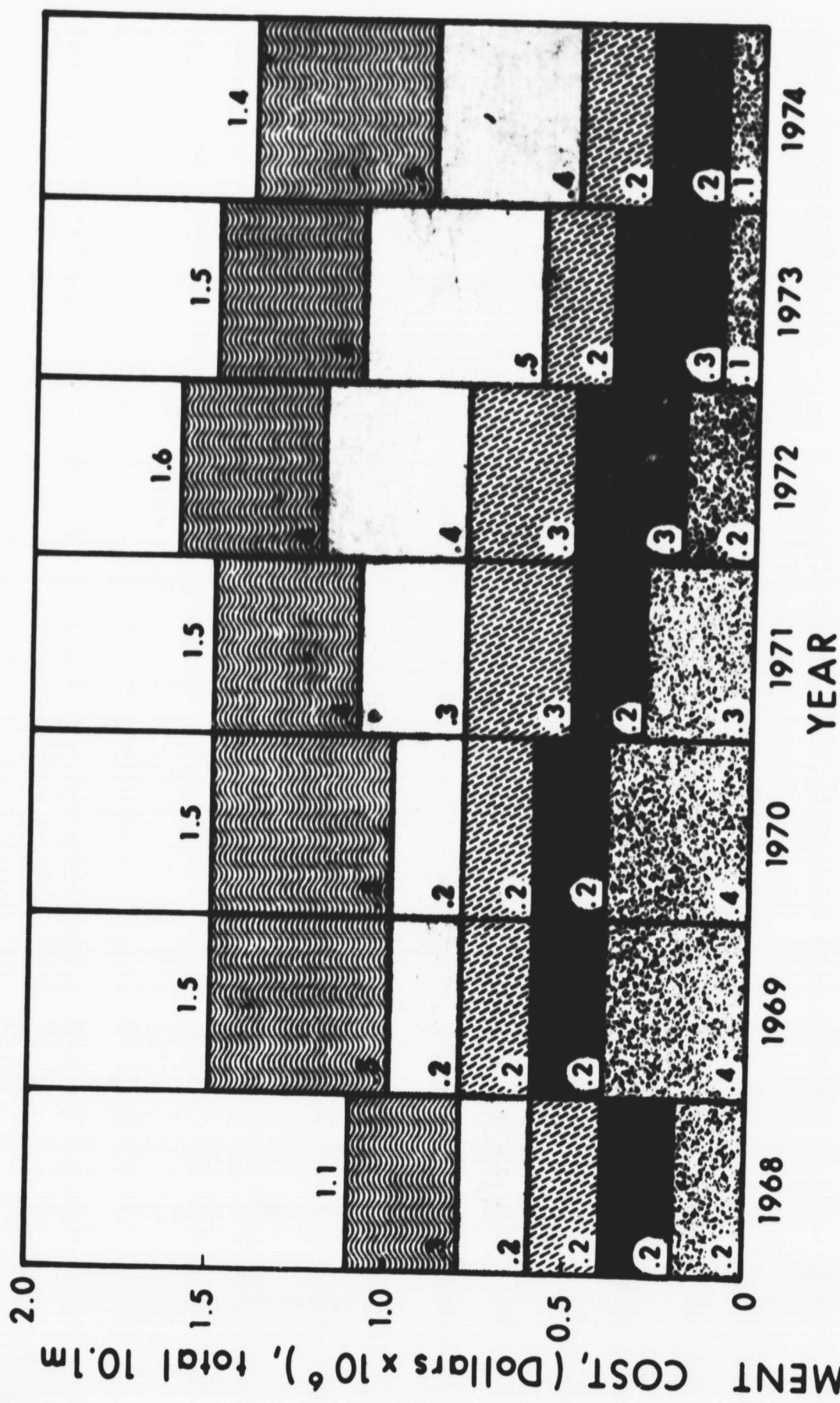
- a. Electron emitters for the thruster and neutralizer that are efficient, long-lived, and easily fabricated
- b. Higher perveance acceleration systems
- c. Lighter weight, structurally sufficient component designs
- d. Lightweight permanent magnet designs
- e. Consideration of an ac-operated discharge which could eliminate dc rectifier losses and possibly reduce the cathode sputtering

General areas of development where potential benefit may occur include:

- a. Development of mercury microthruster systems
- b. Use of a single reservoir concept for each thruster and neutralizer or for more than one thruster system
- c. Development of feed systems not dependent upon pressurized gas
- d. Use of unitized, one-piece construction for such items as the ionization chamber, propellant reservoir, and system support structure
- e. Extensive thruster "system analyses" oriented toward potential applications

Although the exact nature and results of the above-outlined areas of improvements cannot be predicted, these areas are, in general, representative of those areas which could produce the improvements necessary for thruster systems beyond the present near-term missions. The future development of the mercury thruster systems will be in two major areas: One will be the investigation and development of very small thrust systems (microthruster systems), and the other will be the optimization and refinement of present thruster systems from a systems application point of view.

Figure 88 presents the general areas of future development, schedule, and costs that are required to bring the status of the mercury thruster system to the "application" level in the period beyond about 1975.



- SYMBOL** **DEVELOPMENT AREA DESCRIPTION**
- ELECTRON EMITTER STUDY (EFFICIENCY, LIFE, STRUCTURE)
 - FEED SYSTEM STUDY (MECHANISM, CONCEPT, STRUCTURE)
 - THRUSTER DEVELOPMENT (ACCELERATION, FIELD, STRUCTURE)
 - P/C INTERFACE (A.C. ARC, ELECTRICAL DESIGN, CONTROL)
 - MICROTHRUSTER SYSTEMS (TOTAL SYSTEM INCLUDING P/C)

Figure 88. Areas of Future Development of the Mercury Thruster System, with Schedule and Cost

2.2.8 CONCLUDING REMARKS

The objective of this subsection has been to present the current status of the mercury electron-bombardment ion thruster systems and to predict performance in terms of potential near-term missions.

Although research and investigation into the efforts that have been performed with the mercury thruster do not include extensive system considerations, the discussion has been presented from the "system" point of view. Descriptions have been given regarding the results of investigations to date as well as the anticipated thruster system performance.

Curves of reported performance are presented and extrapolated, where necessary, to indicate the potential performance and capability of the mercury thruster system. In addition to this state of the art discussion, a 2.5-kilowatt system has been offered as an example of a system incorporating both the developments to date and the anticipated near-term improvements which can be predicted with a high degree of confidence.

Included in this report is an extensive bibliography of the investigations of the mercury thruster system since 1960. This collection provided the basis for the conclusions contained herein and is intended to provide the detailed analysis in particular areas not covered in this report.

2.3 CONTACT ION THRUSTERS

2.3.1 INTRODUCTION

2.3.1.1 Description

An ion engine consists of a positive ion source supplied with propellant from a feed system, a set of accelerating electrodes to eject the ions in a thrust-producing beam, and a neutralizer to add electrons to the departing ions so the thruster and spacecraft remain neutral. The contact ionization thruster depends for its operation on the ability of hot tungsten (1100°C) to ionize cesium that evaporates from it. Sintered porous tungsten serves as the ionizer. Cesium vapor diffuses through the tungsten and evaporates as ions from its outer surface. Ionization is produced since the 3.7 volt ionization potential is well below the 4.5 volt work function of tungsten. Other ionizer materials with even higher work functions have been investigated, but the most stable and efficient porous ionizers are being built of tungsten.

As shown in the accompanying sketch (Figure 89), the ionizer is heated electrically. Thermal radiation from the ionizer is the major power loss, so the structure is heavily heat shielded.

An accelerating electrode, biased negative, is positioned in front of the ionizer. This serves two purposes: it applies a strong electric field at the ion source, helping to overcome space charge limitations, and it blocks neutralizing electrons from flowing upstream to bombard the ionizer. A neutralizer and a feed system complete the ion thruster. These will be described later, along with other subsystems.

The useful range of contact engines is very broad. Thrusters have been built with nominal operating thrusts from 4.5×10^{-5} newtons to 0.45 newtons. The corresponding input power ranges from 15 watts to 20

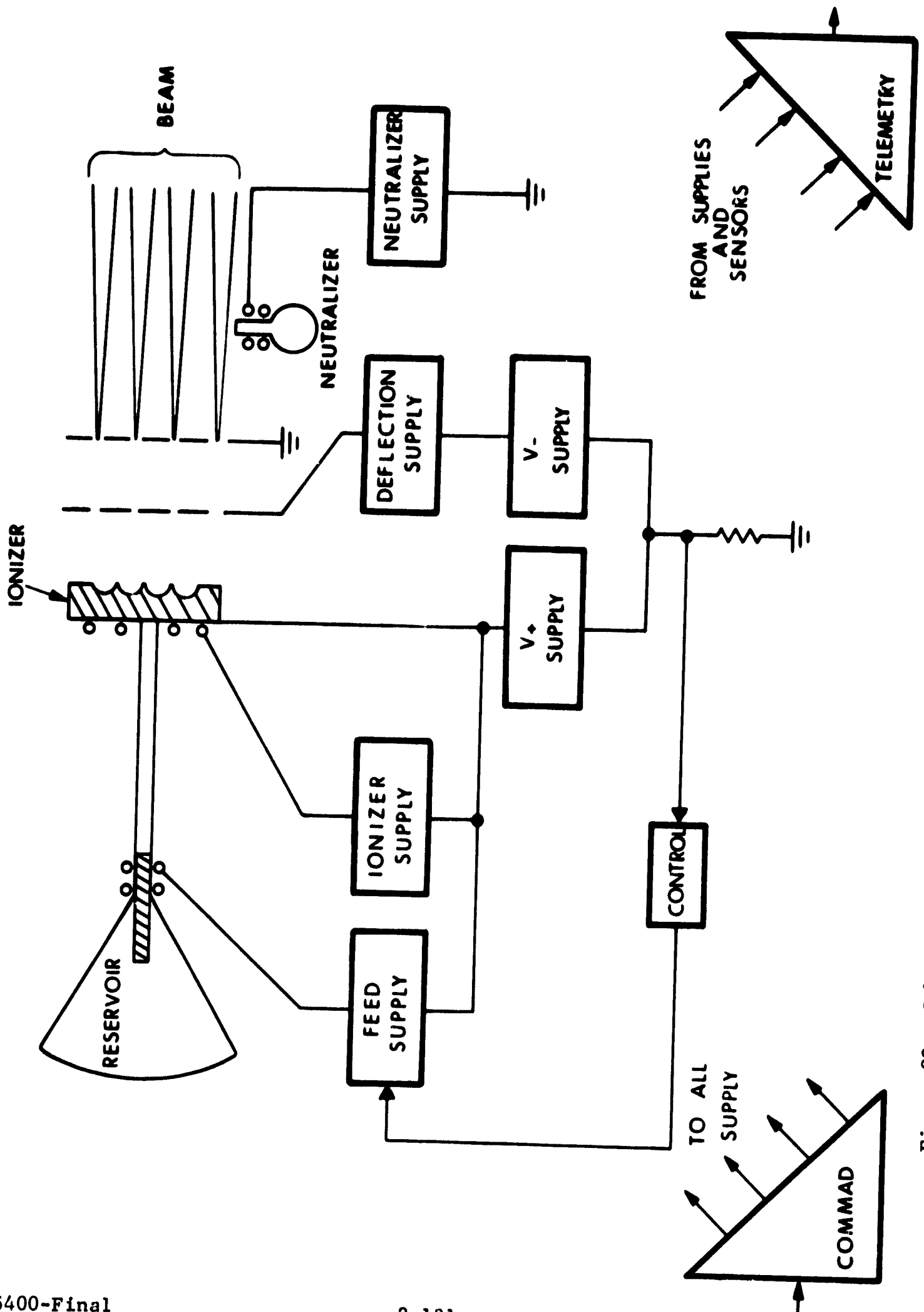


Figure 89. Schematic of Contact Ion Thruster

kilowatts. The performance of contact ion thrusters is not as good as bombardment thrusters, and large tungsten contact ionizers are very expensive and difficult to construct. At the present time, contact thrusters may be attractive only for satellite control (requiring thrust below a few millipounds), and not for prime propulsion. At these levels their use may be dictated by their special capabilities, such as beam vector control or throttleability. These performance features are discussed in a later section.

The history of contact engine development extends back further than any other type of electric thruster. Contact ionization of cesium was first pointed out as being extremely efficient by Irving Langmuir. Development of such sources for propulsion began in 1957. Most of the development of these engines has been conducted at Electro-Optical Systems, Hughes Research Laboratories, TRW Systems and NASA-Lewis Research Center. Contact engines research has been supported by the Air Force Aero Propulsion Laboratory and by NASA Lewis Research Center. Supporting research has been conducted at a variety of laboratories. Contact engines were tested in ballistic flights by the Air Force in 1962 and 1964 and by NASA in 1964. In 1965, the Air Force flew a contact engine as an auxiliary experiment in the SNAP 10-A nuclear reactor test. NASA Goddard Space Flight Center has purchased contact microthrusters to perform east-west station keeping on forthcoming ATS flights.

2.3.1.2 Subsystems

Figure 89 shows a contact engine and the power sources for its operation. There are at least five sources:

V_+ , which biases the source and supplies the ion current and power.

V_- , which biases the accelerator

Ionizer, which heats the ionizer

Feed, which supplies the cesium; this may be more than one supply if there are valves, etc. to be powered.

Neutralizer, which heats the neutralizer to supply electrons; these may be more than one heater, and there may be neutralizer bias supplies.

Other supplies may be required, such as deflection bias supplies if the engine is equipped for beam vectoring. In addition in a complete contact engine system there are command circuits and telemetry circuits to control and activate these supplies.

The system can be divided into subsystems in various ways. A logical way according to operation of the ion engine would be

- a. Feed (including its power supply)
- b. Ionizer (including its heater supply)
- c. Accelerator (including the V_+ , V_- , and deflection supplies)
- d. Neutralizer (including its supply or supplies)
- e. Control and Telemetry

These subsystems are interrelated. A signal from the V_+ and V_- supplies must be used to control the feed rate, for example. The control and telemetry subsystem obviously interacts with all of the others.

Subsystems can also be defined according to the technologies involved in developing and fabricating them. From this point of view, the division is:

- a. Ion Thruster
- b. Power Supplies
- c. Command and Telemetry

The latter two are closely related and frequently are studied together. Thus, on the ATS microthruster system, there is a Thruster Subsystem and a Control Logic/Power Conditioning Subsystem.

The cesium feed and neutralizer elements are very similar to those required by cesium bombardment engines, and a discussion of them is contained in Section 2.1 of this document.

2.3.2 DEMONSTRATED PERFORMANCE

2.3.2.1 Performance

The most significant performance measure for the contact engine (or for any electrostatic engine) is the power/thrust ratio. This is shown as a function of specific impulse in Figure 90 for a high performance contact engine, the EOS "M1" engine and the ATS microthruster. Power here includes all engine power: neutralizer and feed system as well as ionizer and beam power. Efficiency of the M1 engine is plotted in Table XVIII.

Two reservations must be considered in extrapolating these data. First, the curve is different for engines of different size. The curve in the figure is for a fairly large engine, capable of producing 0.1 newton. The data are valid for all engines of this design above about 1 mlb, since peripheral heat losses are small in these larger engines. Losses and useful beam power both scale directly with ionizer size. But below 5×10^{-3} newton the losses become more significant. The power figure chosen for each engine is an optimal one, near the minimum of the P/T versus I_{sp} curve.

The second caution in considering engine power is that this power is closely related to engine life. Favorable power/thrust ratio demands

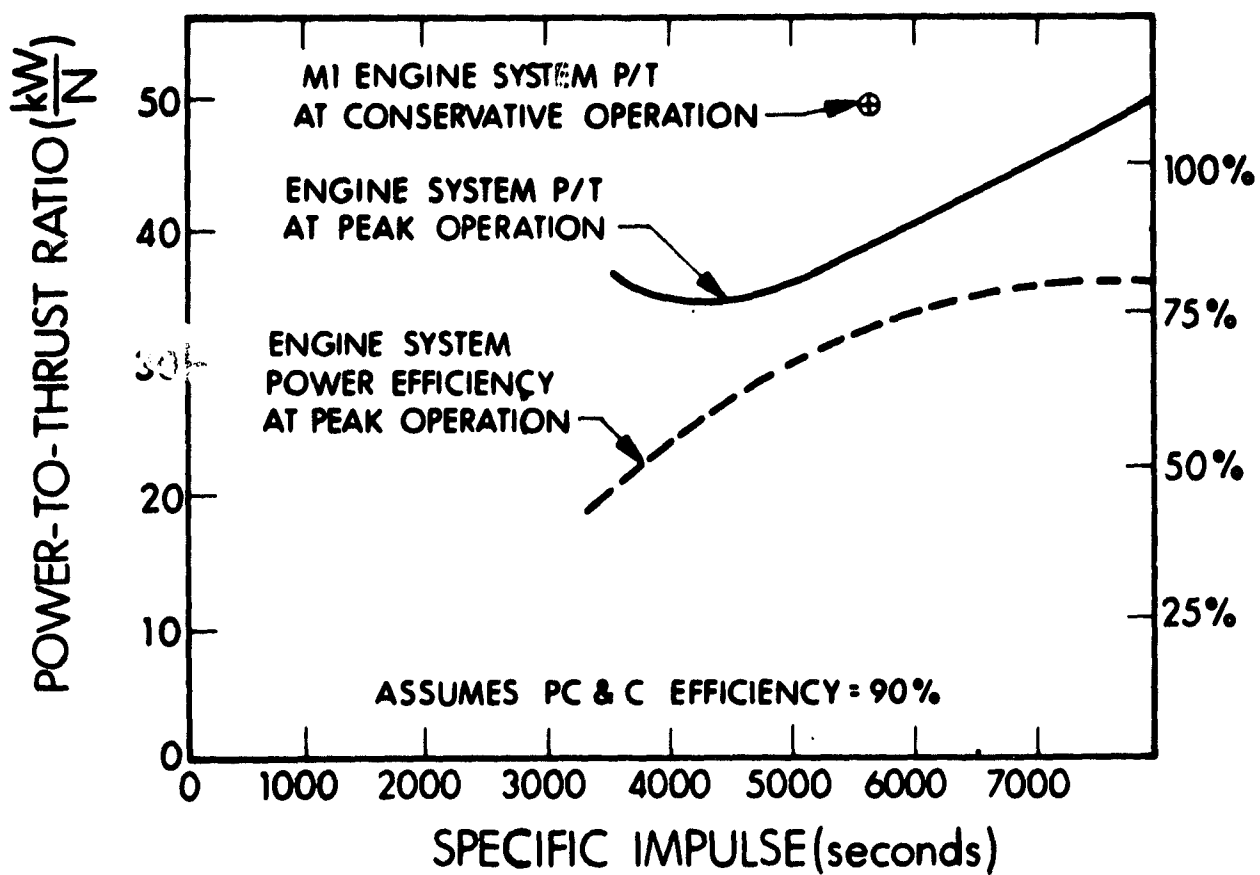
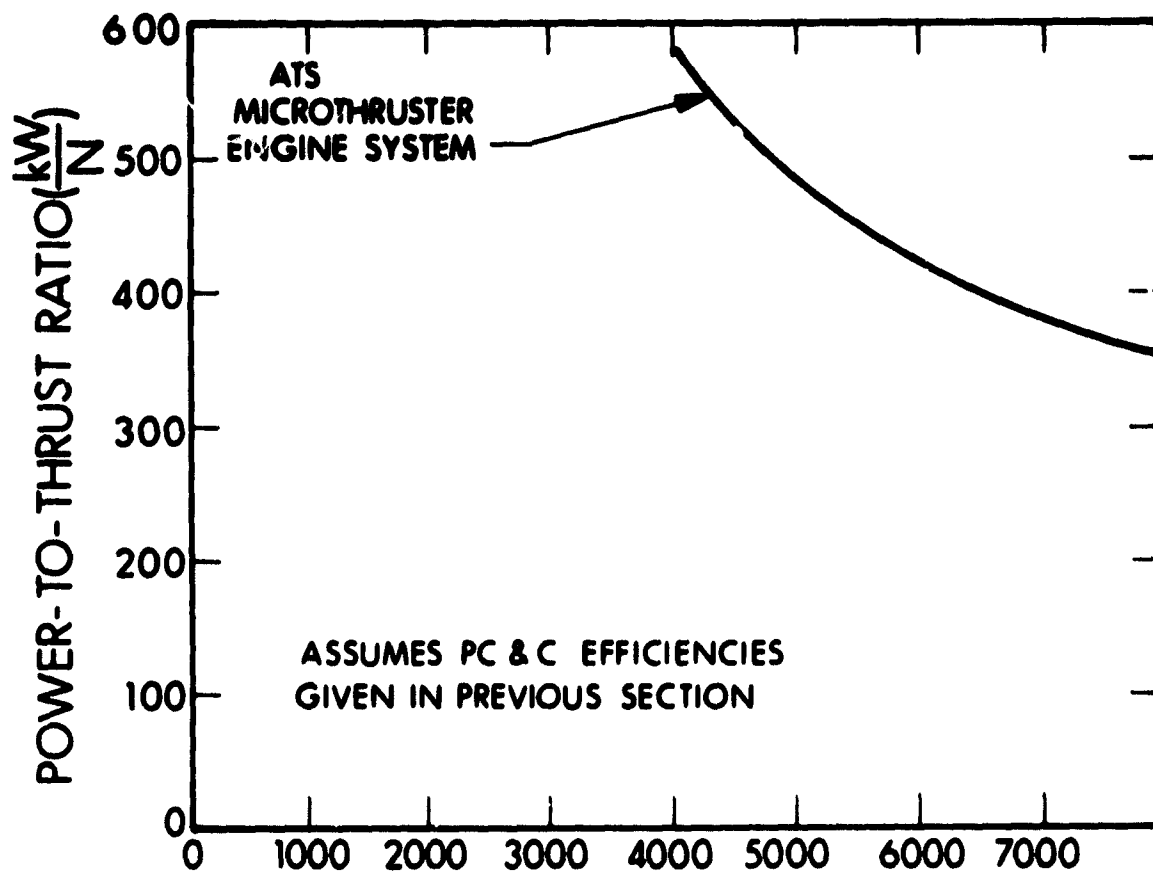


Figure 90. Power-to-Thrust Ratios for Contact Ion Microthrusters

TABLE XVIII
M1 ENGINE SYSTEM PERFORMANCE*

Specific Impulse, sec	Beam Current, mA	Thrust, N x 10 ³	Ionizer Power, W	Total Power, W**	Power/ Thrust, kW/N	Efficiency, Percent
3460	505	23.5	340	790	37.3	51
3880	565	29.7	340	948	35.5	60
5500	895	66.5	340	2262	37.8	79
6730	920	84.0	340	3208	44.4	86
7780	920	97.0	340	4124	47.3	90
8690	920	109.0	340	5036	51.6	92

* Thrust and specific impulse corrected for 7V beam potential.

** Assumes power conditioning efficiency is 90%.

high ionizer current density. This increases sputtering damage and other wear-out mechanisms. For the present state of the art in large tungsten ionizers, this tradeoff can be exemplified as follows:

for P/T = 39 kW/N, life ~ 1000 hours
for P/T = 45 kW/N, life ~ 10,000 hours

2.3.2.2 Weight

Two well-established contact engines provide weight estimates. The first is the EOS M1 engine, which operated typically at 23×10^{-3} newtons with a 1 kW input. (This is the engine which at peak performance gave 6.7×10^{-2} newtons for 2.26 kW, with reduced lifetime as mentioned above). It weighed 4.1 pounds, including neutralizer and mounting structure but not including cesium supply. The other engine is the ATS microthruster. This operates at 10^{-4} newtons while consuming 17 watts. Its mass is 1.1 kilograms, of which cesium supply is a negligible part. Thus, contact engines seem to have a weight-to-thrust profile as in Fig. 91. Below about 4.5×10^{-3} newtons the mass is mostly structure and heat shielding, and does not scale with thrust.

The current from a contact engine is limited either by ionizer or perveance considerations. For a given current the thrust depends on the accelerating voltage, and hence thrust varies with specific impulse. Therefore, the ratio of mass to thrust, or mass to power, also varies. Figure 92 shows the "specific mass" (mass/power) for the M1 engine at peak performance. Note that for microthrusters the beam power is a small part of the total power, so this strong variation with specific impulse does not occur. The ATS microthruster consumes about 15 watts with no beam; at full beam, this rises only to 17 watts.

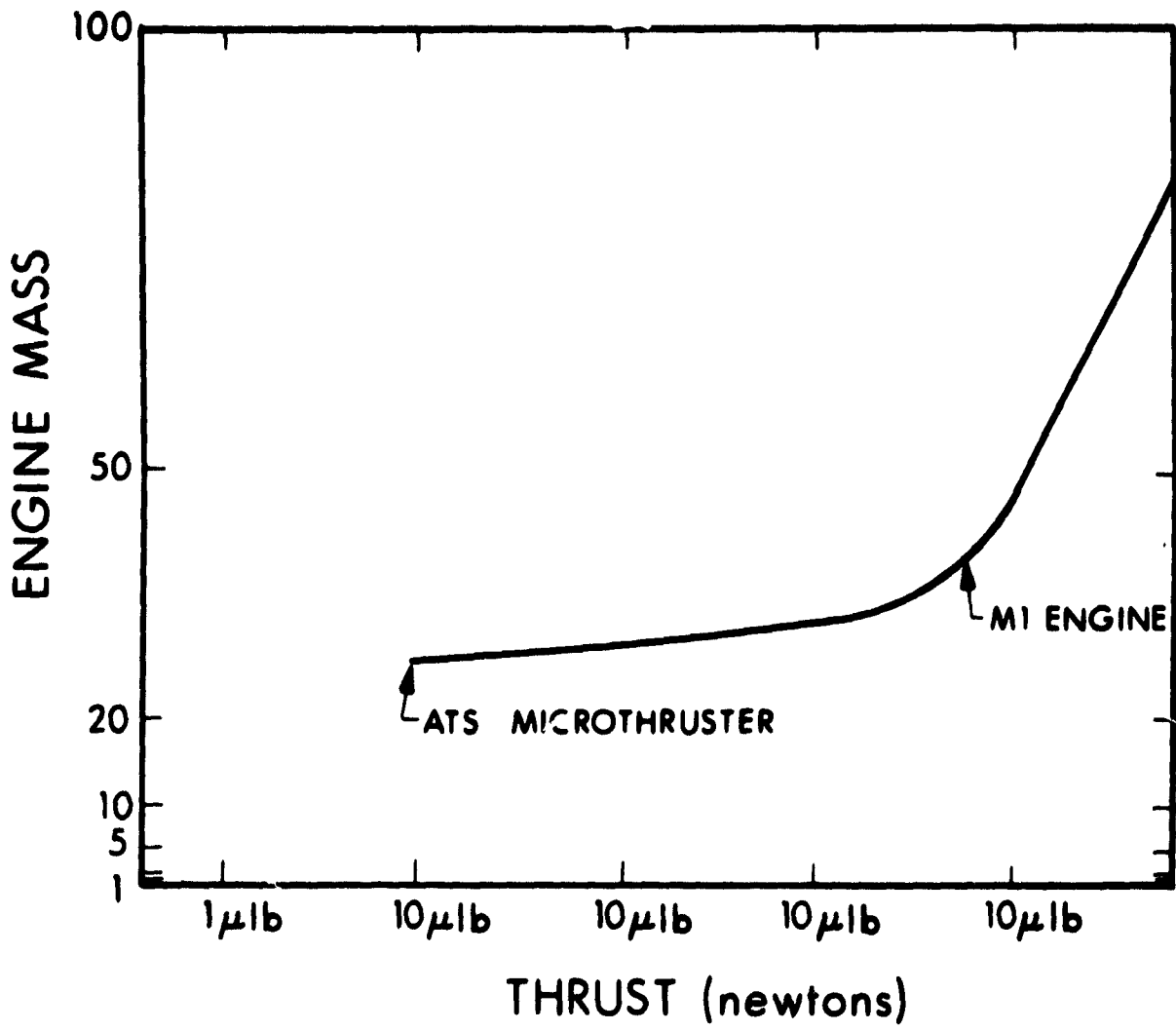


Figure 91. Contact Engine Weight (Without Propellant) versus Engine Thrust'

2.3.2.3 Life

The subject of lifetime has already been touched upon. Because they must operate at high current density to be efficient, contact ion engines have an inherent lifetime limitation due to electrode erosion from ion sputtering. Even with "perfect" ion optics and focusing, with no ions from the contact ionizer ever striking the electrode, sputtering still takes place from slow ions generated by charge exchange scattering. This process can be reduced by the use of a sacrificial electrode which attracts the ions and is sputtered without degrading the overall optics, or by clever design of the optics themselves; the latter is the usual course.

Endurance tests of large contact ion engines are summarized in Table XIX. The most significant was the 2284-hour test of engine M1-R3. This was the longest test of a contact engine ever reported. At the close of the run, electrodes were in good condition and appeared able to continue for several thousand hours. When test objectives of 2000 hours had been met, it was decided to learn as much as possible by allowing the engine to continue operating until a failure occurred. The neutralizer cesium supply was exhausted at 2100 hours and subsequent testing was unneutralized. A graphic record of run parameters appears in Fig. 93. Table XX shows run data.

The run ended when the ionizer heater failed at its input terminal. This connection was made by crimping a tantalum rod to the tantalum center conductor of the heater. The joint was supported by an alumina sleeve. The tantalum center conductor had melted and some of the alumina had fused, indicating a very high temperature. A hot spot could have occurred for several reasons: The crimp connection could have become loose, tantalum could have evaporated from the heater wire, or tantalum could have reduced the alumina, effectively decreasing the diameter of the heater. Ionizer heater data indicated that the heater resistance

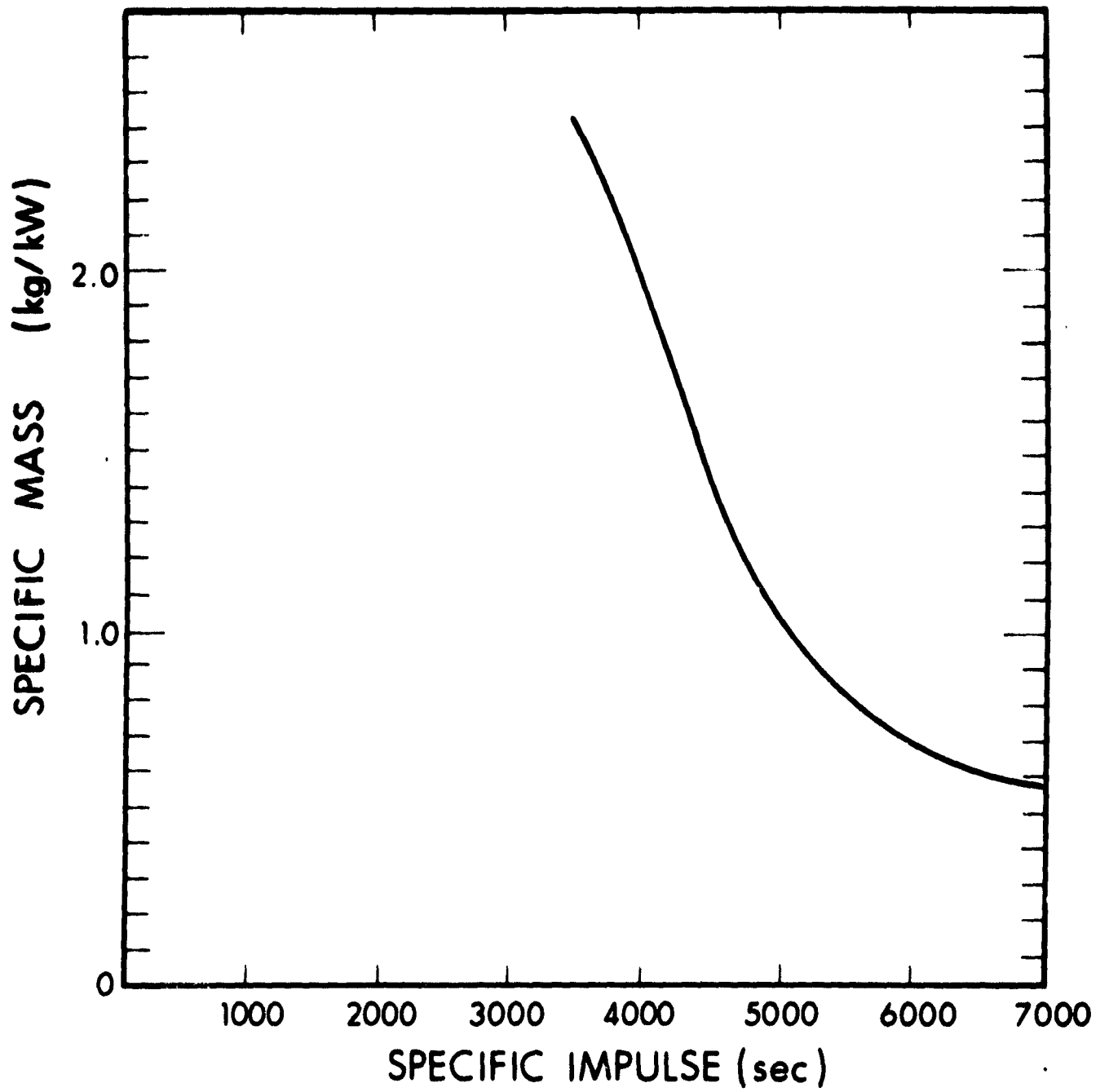


Figure 92. Contact Engine Specific Weight versus Specific Impulse (no propellant weight included)

TABLE XIX

CONTACT IONIZATION THRUSTER ENDURANCE TESTS

<u>Thruster Tested</u>	<u>Start Date</u>	<u>Isp (sec)</u>	<u>Thrust (Nx10⁶)</u>	<u>Total* Power (watts)</u>	<u>P/T (kW/N)</u>	<u>Duration (hours)</u>	<u>Cause of Termination</u>
M1-R1	10 Feb 65	5900	46	1800	39	587	Vaporizer heater failure
M1-6	30 Aug 65	6150	25	1150	46	392	Vacuum failure
M1-8	2 Dec 65	5500	23	990	44	263	Vaporizer leak
M1-R2	3 Sep 65	6150	26	1218	47	776	Ionizer heater failure
M1-R3	29 Nov 65	5500	23	1005	44	2284	Ionizer heater failure
M1-10**	10 May 66	5500	23	995	44	1000	Test goals achieved

* Operating plasma bridge neutralizer power included.

** With flight-type power conditioning operating in vacuum.

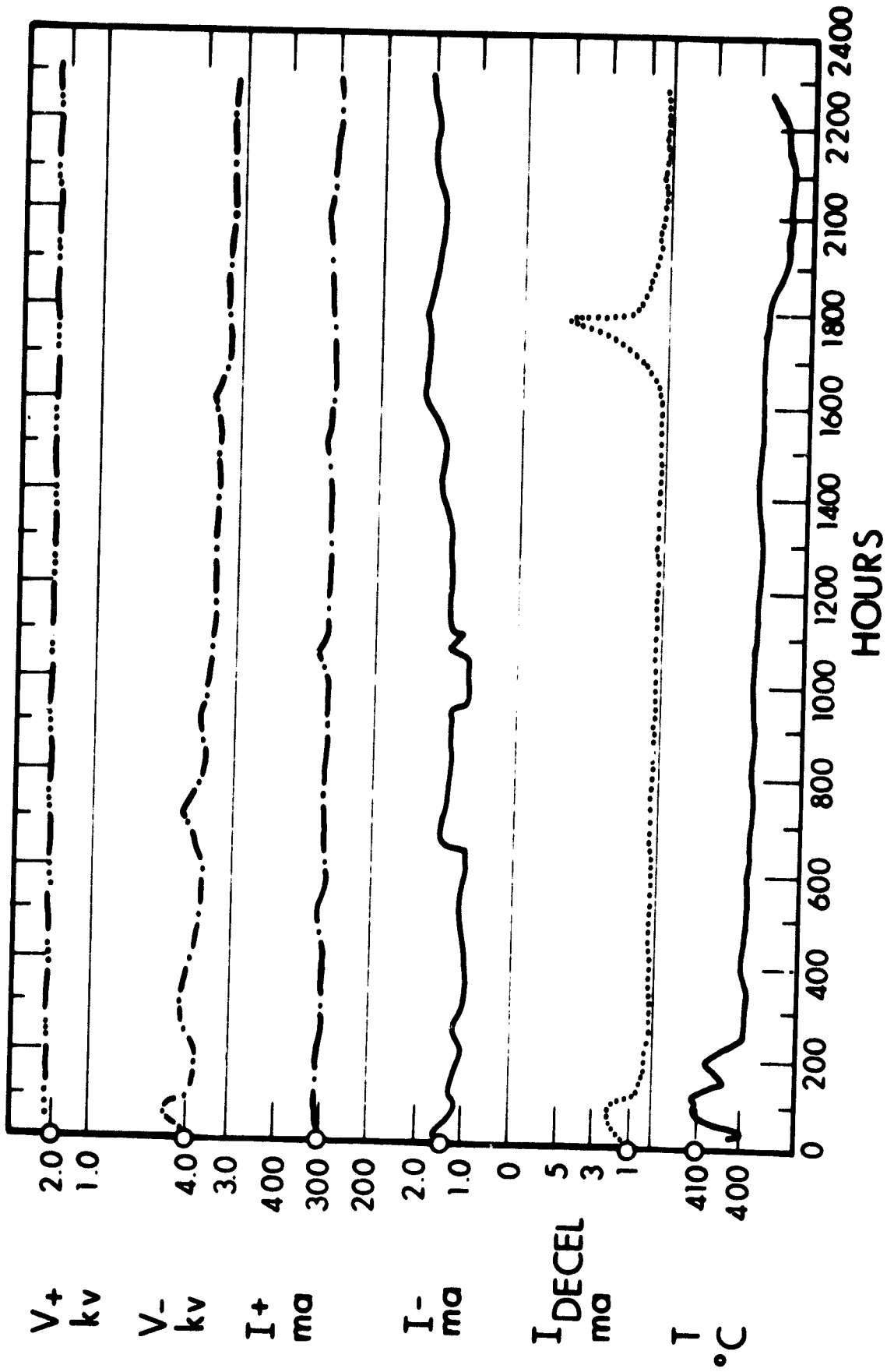


Figure 93. M1-R3 Endurance Test Parameters

TABLE XX
M1-R3 ENGINE DATA

Run Hours	V_+	I_+	V_-	I_-	I_{decel}	$I_{\text{neutralizer}}$	P_{ionizer}	P_{thruster}	T	P/T
	kV	mA	kV	mA	mA	mA	W	W	N	W/N
0	1.9	310	4.6	1.4	0.5	297	382	988	0.023	43
200	2.0	304	3.7	1.0	0.4	280	378	1000	0.023	44
400	2.0	308	3.8	1.0	0.2	285	380	1005	0.023	44
600	2.0	303	3.6	1.0	0.3	270	380	1000	0.023	44
800	2.0	302	3.6	1.4	0.3	278	385	1010	0.023	44
1000	2.0	300	3.5	1.0	0.2	270	385	1018	0.022	45
1200	2.0	302	3.4	1.5	0.3	265	385	1007	0.023	44
1400	2.0	305	3.5	1.7	0.2	275	395	1026	0.023	44
1600	2.1	301	3.6	2.0	0.5	280	383	1024	0.023	45
1800	2.0	310	3.2	2.2	2.1	290	390	1025	0.023	44
2000	2.1	309	3.2	1.8	0.5	290	382	1022	0.024	44
2200	2.1	300	3.3	1.9	0.2	*	390	1011	0.023	45

* Neutralizer cesium supply exhausted at 2100 hours.

was increasing slowly with the run time, which would indicate that one or more of the mechanisms was in process. Resistance data did not predict that failure was imminent, however.

The accelerator electrode experienced some early erosion around its edges due to beam former misalignment, but after the first 100 hours the erosion was progressing very slowly. Daily photographs were taken after 200 hours of operation and it is difficult to detect change throughout the remaining 1400 hours of the run. The decelerator electrode suffered somewhat more heavy erosion at the beginning of the run but by 100 hours this erosion had stopped. There was very little ionizer erosion.

The run of M1-6 was ended by a vacuum failure which badly oxidized the ionizer. The failure was caused by liquid nitrogen dripping on a gate valve, because the nitrogen controller had a faulty relay. A gasket in the valve froze and opened a large vacuum leak. This typifies the complicated problems involved in keeping facilities running for thousands of hours. The test of M1-R2 ended when the ionizer heater failed and the test of M1-8 ended when the vaporizer tube developed a leak.

The amount of cesium used during the 2283-hour test of M1-R3 was 3.42 ± 0.01 kg, found from comparing the weights of the cesium reservoir before and after the test. The average ion beam for the test was 302 ± 2 mA, corresponding to a cesium use of 3.43 ± 0.03 kg. These figures indicate an ionization efficiency of 98.6 percent or better.

Sections were taken from the accelerator and decelerator electrodes. If erosion is extrapolated linearly, which is conservative, the worst web would be severed in 21,500 hours, or ten times the present test. Such extrapolation is useful chiefly in that it does not predict imminent failure.

This test, together with briefer tests of M1 engines operating at higher current density, established a tradeoff of efficiency versus lifetime for this design of contact engine. Insofar as lifetime is established by basic electrode erosion, and for conventional spherical-tungsten ionizers as used here, the tradeoff is as follows:

for P/T = 39 kW/N, Life ~ 1,000 hours;
for P/T = 45 kW/N, Life ~ 10,000 hours.

There is little experimental information on the life of contact microthrusters. They generally run at current density below that for large thrusters, so their lifetime should be greater. One microthruster test ran 3000 hours, and the test ended only because cesium was exhausted. Further investigation of microthruster system life will be made later under Contract AF 33(615)-67-C-1854.

2.3.2.4 Pulse and Turn-On Considerations

The contact engine is not well suited for providing brief thrusting periods. There are two reasons for this. First, the ionizer represents a considerable thermal mass, which requires some time to heat up. This is aggravated by the fact that the ionizer is heavily heat-shielded for efficiency, and so is not usually designed to be overdriven for rapid heating. Second, thrust cannot be modulated by the obvious means of turning on and off high voltage, since cesium "flooding" of the ionizer occurs.

Typical turn on times from a cold start for present-day contact engines are 1 hour for the M1 4.5×10^{-2} newton engine and 10 minutes for the ATS microthruster. Most of this is spent heating the ionizer. The buildup of thrust is faster, controlled by the response of the cesium feed system vaporizer. Depending on the specific design of the vaporizer

this response time is between 10 seconds and one minute. The same time constant is typical for termination of thrust.

The power profile during turn-on depends on the engine size. Typically, the ionizer is turned on first, and this represents about 20 percent of the power for a large engine or 60 percent for a microthruster. This power level is held until the ionizer reaches full temperature. During this heat-up either current limiting or power limiting must be used, for the ionizer heater resistance changes by several hundred percent. After the ionizer is hot, the high voltage and vaporizer supplies are energized. The neutralizer is turned on with the ionizer. When the engine is turned off, all power may be removed simultaneously. It is preferable, however, to first de-energize the vaporizer and let the beam decay before removing high voltage and ionizer power.

2.3.3 Electrical Characteristics

This section describes the electrical power, controls, and telemetry appropriate to a contact ion engine. Thruster power requirements have already been touched on in the discussion of Section 2.3.2

2.3.3.1 Power

Power inputs for a contact engine are in the following categories:

Ionizer heat:	ac or dc heater power. 5W to several kW. Isolated.
Beam (V_+):	+dc, 1 to 5 kV, 1 mA to several amperes.
Accelerator (V_-):	-dc, 100 V to 5 kV, 10 μ A to several mA.
Feed:	ac or dc heater power. Several watts. Isolated.
Neutralizer:	ac or dc heater power. Several watts.

Feed system power and neutralizer power are discussed further in the section on Bombardment Ion Engines. These elements are virtually identical for the cesium contact and cesium bombardment engines.

Figure 94 shows how power requirements vary with contact engine size. A typical specific impulse of 5500 seconds was chosen. Total power is similar to that shown earlier, in connection with engine characteristics

As discussed under "pulse and turn-on" considerations, the ionizer must be heated before the rest of the engine is turned on. The ionizer heater supply must be current - or power - regulated during the heat-up period. High voltage and feed system vaporizer are turned on after the ionizer reaches full temperature. The neutralizer may be turned on at any time during the start-up. It is most commonly energized when the ionizer begins heating.

Regulation of the various power supplies is not critical. Characteristics appear in Figure 95. It is perhaps most important for the ionizer heater supply to deliver sufficient power. A drop of 1 percent in heater voltage lowers temperature by 1/2 percent or about 7 degrees. Since ionizers are customarily operated 20 to 50 degrees hotter than necessary, regulation to a few percent is sufficient. For the high voltage, regulation is less important. A 1 percent change in V_+ varies the specific impulse and the thrust by 1/2 percent. Changes in V_- show no effect, unless they are so gross as to defocus the beam or cause space charge problems. These seldom appear within 10 percent of the desired V_- . The neutralizer heater, like the ionizer, must simply keep the device hot enough. Temperature is seldom set close to the minimum level, since this engine element consumes so little power. (This may not be strictly true for a thermionic neutralizer filament on a microthruster. Here the temperature is kept as low as possible, while still providing adequate emission, to prolong filament life.)

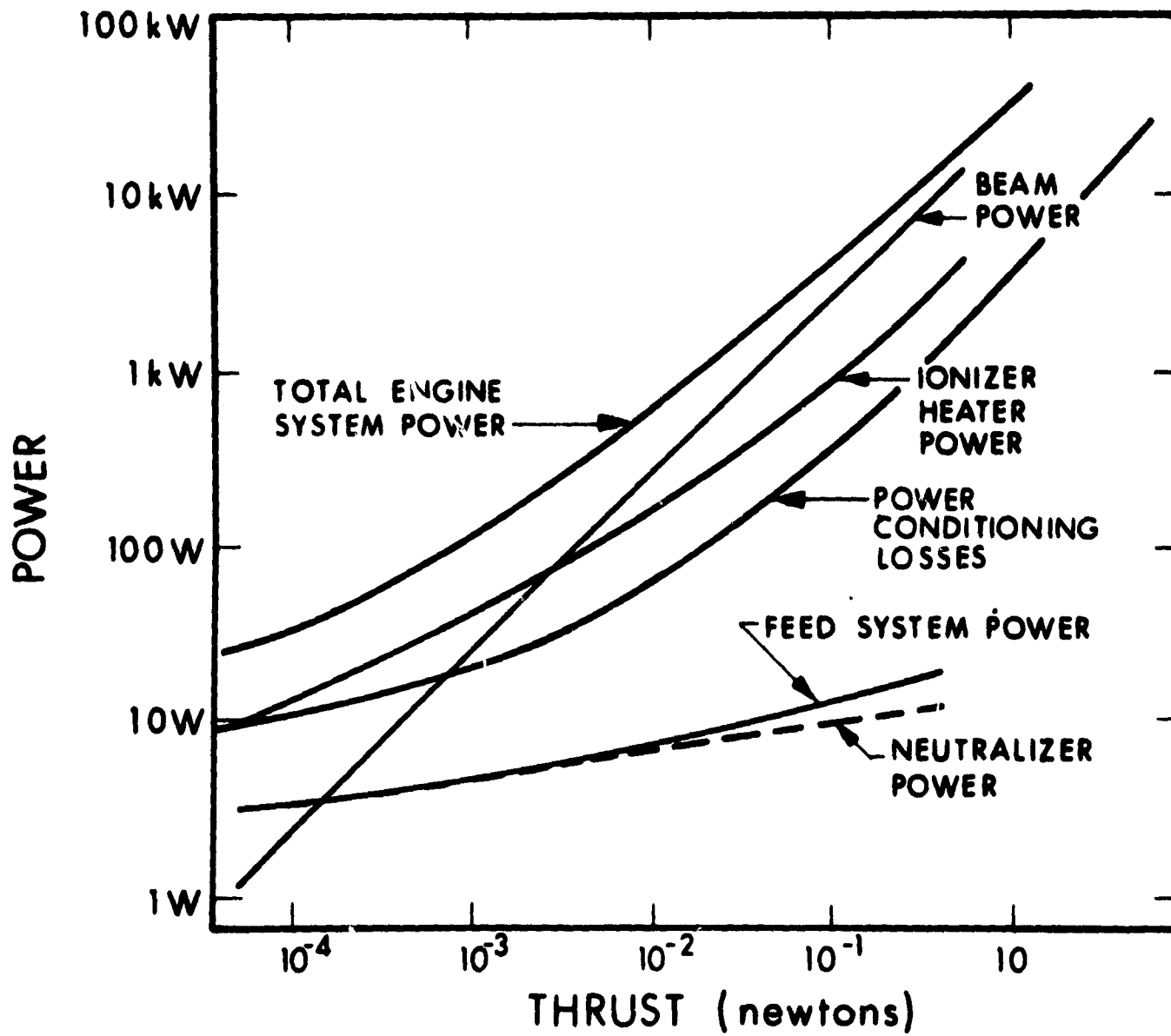


Figure 94. Contact Engine Power versus Thrust, Showing Power Consumed by Various Engine Elements

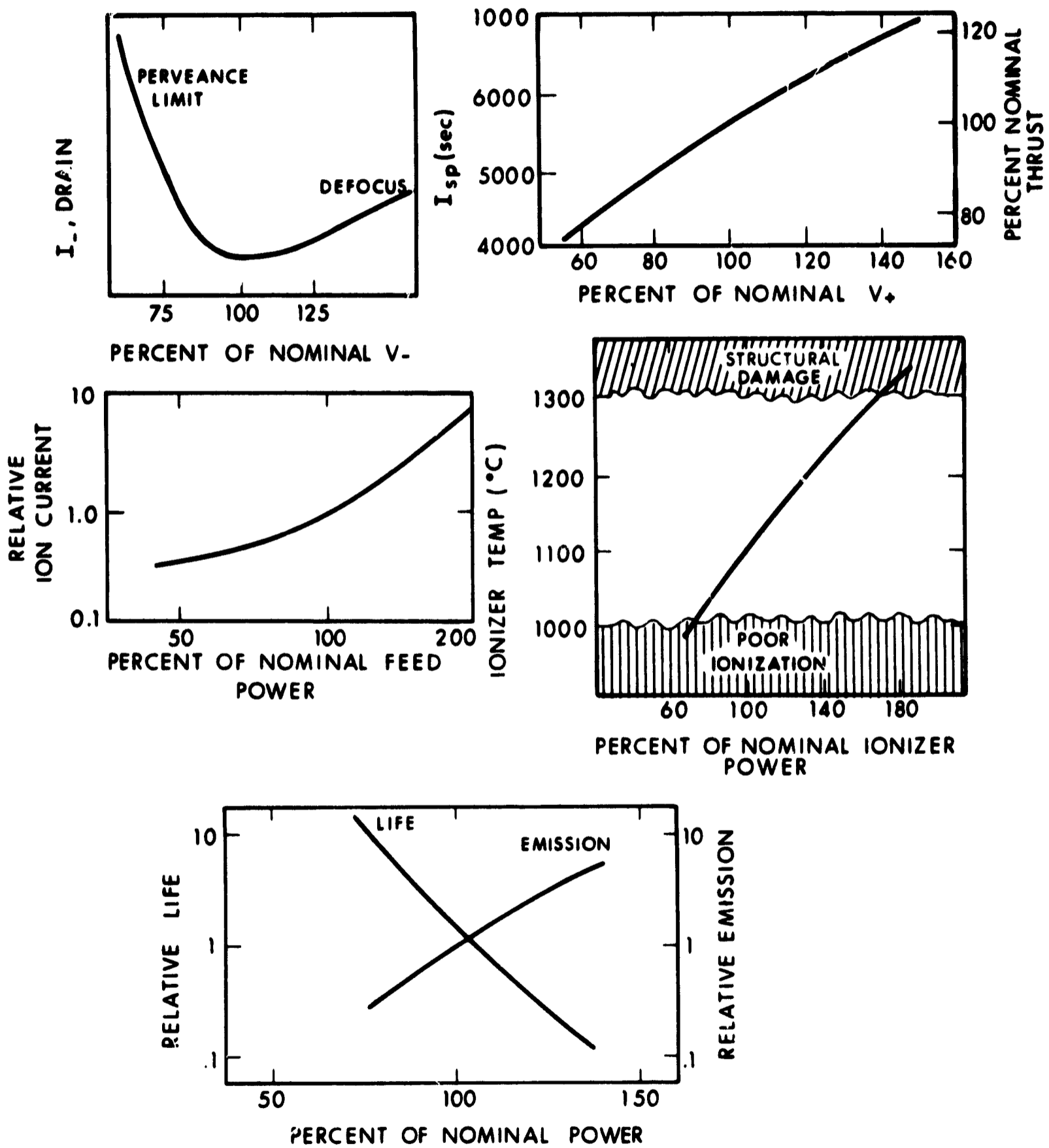


Figure 95. Effect of Variation in Ionizer Power, V_+ , V_- , Feed Power, and Neutralizer Power

The feed system vaporizer supply, finally, is "unregulated" in that it is part of a control loop. Beam current is sensed, and vaporizer power adjusted to give the desired beam.

Allowable ripple on the dc supplies for a contact engine has never been well defined. V_+ ripple will vary thrust and specific impulse. Unless V_+ or V_- ripple is great enough to cause defocusing or space change problems, there should be no bad effect. The ion engine heaters (ionizer, neutralizer, and vaporizer) can run equally well on ac or on dc.

2.3.3.2 Controls and Commands

Controls and commands for a contact ion engine can be categorized according to the role of the engine in its mission. An operational engine system requires few commands. An experimental system requires more commands for diagnostic operation and to investigate peculiarities of engine behavior.

A qualified, operational system would use the following commands and controls:

- a. System on/off
- b. Thrust Level
- c. Thrust Direction (if beam is vectored).

For an experimental device, it is appropriate to have separate commands for each element, so that operations can be closely controlled. These additional commands might be used:

- a. Ionizer heater on/off
- b. High voltage on/off
- c. Neutralizer on/off
- d. Feed on/off (i.e., idle thrust level)

As for active controls on ion engine operation, very few are needed. Present systems include only one control loop. This regulates vaporizer power to maintain desired ion beam. Beam current is sensed, either by measuring I_+ or, more accurately, by measuring $(I_+ - I_-)$. This is compared to a desired reference level. The difference signal is amplified and used to power the vaporizer. This loop has one long time constant (the thermal response of the vaporizer) and so should be inherently stable. Other loops have been investigated in the past (regulating ionizer temperature to keep the neutral efflux or drain current at some low level, for instance) but it is quite satisfactory and much simpler to simply pre-set ionizer power. The same is true of other engine inputs.

2.3.3.3 Telemetry

An operational contact engine system requires little telemetry. Minimum requirements are probably I_+ and I_- . I_+ (beam current) is used to indicate the thrust being produced, assuming that voltage supplies are functioning properly and that neutralization is adequate. I_- (accelerator drain current) is the most sensitive indication of healthy engine operation. Almost nothing can go seriously wrong with a contact engine without increasing drains.

For more thorough diagnosis of engine operation, the following telemetry indications are useful:

- a. V_+ and V_- . These show whether voltage supplies are indeed functioning properly.
- b. Ionizer heater current (or power). This shows whether the ionizer is healthy. It is much easier to measure and telemeter current than ionize temperature, and the same information is provided.

- c. Neutralizer emission. This indicates whether the neutralizer is performing satisfactorily.
- d. Neutralizer heater current (or power). This helps to diagnose any problem with the neutralizer.
- e. Thrust status. This confirms that the electronic command circuitry is carrying out the desired function.
- f. Thrust vector status. This provides similar configuration of beam direction if the system is equipped for beam deflection. For deflection in various directions, this may require 2 or 3 telemetry channels.
- g. Input power (or current and voltage). This indicates generally satisfactory system performance. It may require 2 channels.
- h. Temperatures. One or more channels may profitably be used to monitor critical temperature points in the electronics or engine. Engine monitoring is difficult because most of the hardware is at high voltage.
- i. Beam potential (or spacecraft potential). This indicates the adequacy of neutralization. It requires extra equipment: either a beam probe or a potential meter (field meter) for the spacecraft.

2.4 COLLOID THRUSTERS

2.4.1 INTRODUCTION

2.4.1.1 Introductory Remarks

The production of charged liquid droplets has been investigated for almost a century. During the present decade this phenomenon was recognized as a source of charged particles with potential application as an electrostatic space thruster. Subsequently, it has been shown to be not only a feasible concept which is competitive with other types of thrusters, but a system that should outperform them.

The generation of charged liquid droplets is accomplished by the application of an intense electric field to a liquid propellant at the tip of an emitter of small radius of curvature. Both positive and negative particles are generated by a variety of propellant liquids, emitter shapes, and materials. The characteristics of generated and accelerated charged particle beams are examined by current measuring techniques such as time-of-flight (TOF) analysis, retarding potential analysis, neutral particle detection devices, and visual observation.

The charged particle thruster is unique in that it is the only electro-static propulsion system in which the energy required to generate charged particles is negligibly small. Both surface ionization and electron bombardment ion thrusters expend a relatively large amount of energy in just ionizing the propellant.

The charged particle thruster has a potential efficiency of greater than 90 percent in the very low and very high specific impulse ranges. At very low specific impulses, large particles with

uniform low charge-to-mass ratios (specific charge) may be used while Cs^+ or HSO_4^- ions may be electrostatically sprayed to produce very high specific impulse beams. In the intermediate specific impulse range (500-3000 sec), the efficiency of present charged particle thrusters is degraded by the production of particles having a wide spread of charge-to-mass ratios. The formation of nonuniform charge-to-mass ratio droplets when operating in the 10^3 to 10^5 C/kg range is typical of all propellants investigated so far.

New propellants being developed give hope for considerably better efficiencies. Even with the present efficiencies, however, the best charged particle systems are more efficient than the best ion engines up to a specific impulse of approximately 3000 sec (nominal 5 kV accelerating potential), and again are more efficient in the Cs^+ ion mode around 7000 sec.

Besides efficiency, such factors as startup time and standby power requirements are important considerations in thruster systems. Versions of the charged particle thruster utilizing capillary feed systems require no standby power and have startup times under a millisecond, allowing pulsed operation without power penalties. Even where pressure regulated or pump type feed systems are used, the startup time would be only a few seconds.

2.4.1.2 Brief Historical Background

In 1952, H. Preston-Thomas^{2-1*} discussed the electrostatic acceleration of charged colloidal particles as a possible means of space propulsion. In 1957, theoretical papers were presented on performance characteristics of both liquid and solid charged particles. A program was initiated in 1958 by Aerojet-General on an experimental and theoretical investigation of charged colloid propulsion. Although solid particles were initially

*References and bibliography for Section 2 are located in Subsection 2.6.

considered, the investigation was directed toward liquid drop generation encouraged by reports in the literature on the electrical atomization of liquids. This work under the direction of R. D. Schultz²⁻² was subsequently supported by AFOSR with ARPA funds. This work concentrated on the generation of particles at specific charges of about 10^2 C/kg accelerated by 100 kV to obtain specific impulses of greater than 1000 seconds.

Around 1959 AFAPL initiated some inhouse investigations in liquid drop spraying. R. Hunter analyzed some of the propulsion characteristics of a heavy charged particle beam having a specific charge spread.²⁻³ This work developed into an inhouse experimental study and contractual studies with C. Hendricks at the University of Illinois²⁻⁴ and with TRW Systems (S.T.L.).²⁻⁵ The work of Hendricks was aimed at theoretical and experimental research on the charged particle generating mechanisms. The work at TRW, eventually under E. Cori, was a research and development program aimed ultimately toward a heavy charged particle thruster for space propulsion.²⁻⁶

In 1961, M. W. Hoffman of Los Alamos reported on generating liquid gallium droplets which ranged in size from 2 to 100μ using a high pressure feed.²⁻⁷

D. Gignoux and H. Anton of Cosmic Inc. reported in 1961 on a technique employing a rotating nozzle to vary the feed rate to the cylinder rime and generate charged liquid droplets.²⁻⁸ They have continued this work under sponsorship of NASA Lewis up to about 1965. Their recent work includes the testing of octoil and glycerol up to voltages of 60 kV at currents up to 1 mA.²⁻⁹

Work continued at AFAPL with investigations of negative particles and the bipolar concept (electrodeless thruster) by Hunter in 1964.²⁻¹⁰

L. A. Cox at High Voltage Engineering used the condensation technique to generate charged particles (1961-1963?).

D. Golden and C. T. Norgren at NASA Lewis made experimental and theoretical studies of colloid thrusters (1962-1965).²⁻¹¹

TRW is developing a microthruster for a flight test in the near future. They have tested a bipolar thruster and linear slit configurations. Thrust vectoring was investigated and the energy losses at the emitter tips were examined.²⁻¹² An extensive single needle parametric study was conducted.²⁻¹³

EOS initiated colloid studies early in 1966 and then went on contract with AFAPL in the middle of the year. They studied thruster scaling laws, and liquid metal spray (obtaining a high efficiency Cs thruster). Linear slit geometries and various needle shapes and materials were examined in addition to various propellants. Energy loss at the needle tips was studied. A 73 needle bipolar thruster was tested for over 50 hours to obtain 3.5×10^{-4} N and 5.5×10^{-4} N thrust at 4.5 kW/N.^{2-14,2-15} Needle rows, focusing techniques and deflection studies were made recently.

2.4.2 PARAMETRIC PERFORMANCE

2.4.2.1 Parametric Relations

Parametric relations are shown in Figs. 96 through 98 to serve as a basis for mission application studies. In Fig. 96 power to thrust ratio is shown as a function of specific impulse. Straight lines corresponding to constant efficiencies of 50, 60, 70, 80, 90, and 100 percent are shown. The shaded region is where colloid thrusters typically operate.

Figures 97 and 98 were obtained from Reference 2-16 and show the ratio of propellant plus power supply mass to total impulse for a solar cell power supply with a specific mass of 25 kg/kW and a SNAP 10-A nuclear

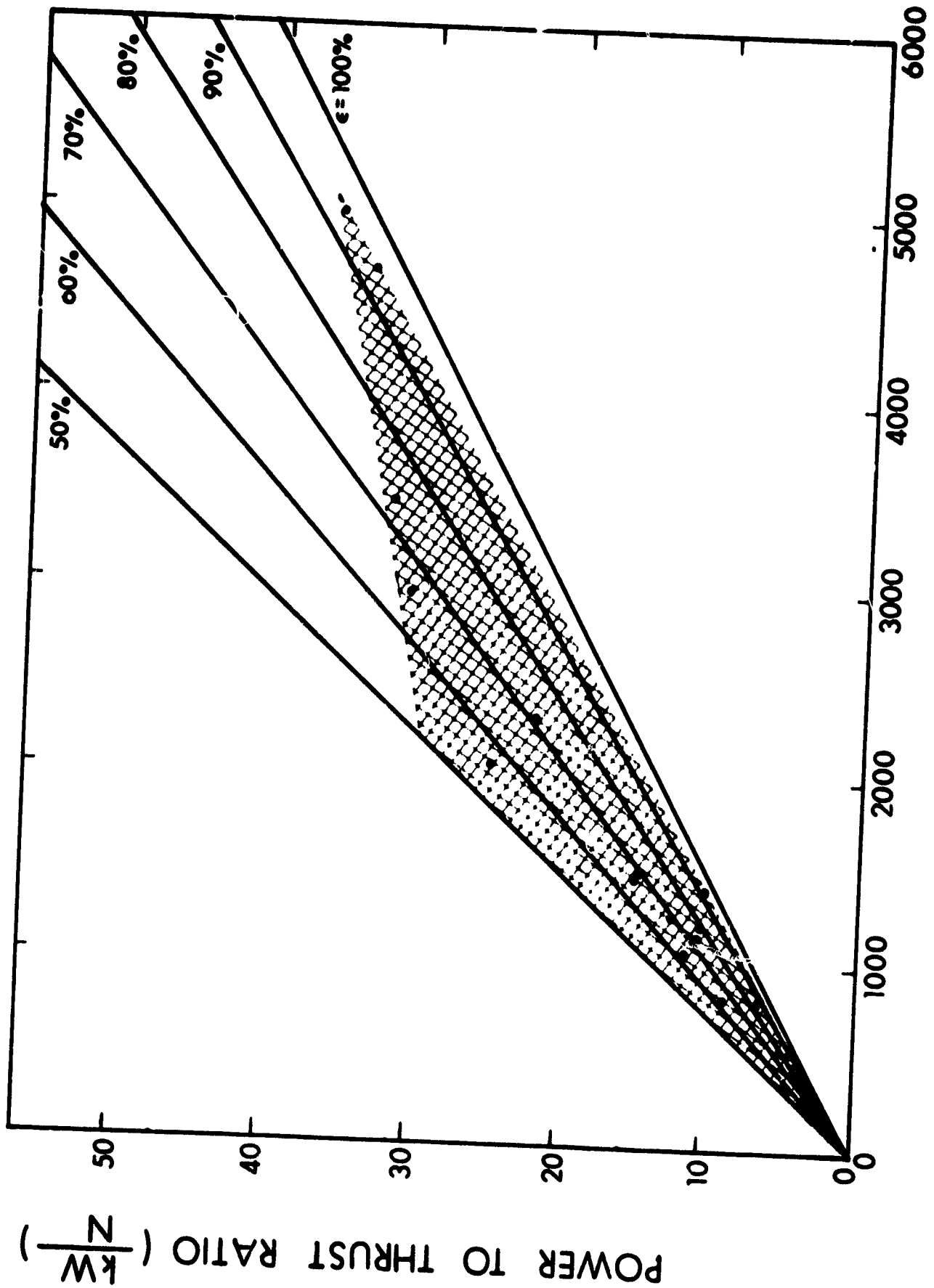


Figure 96. Power-to-Thrust Ratio versus Specific Impulse

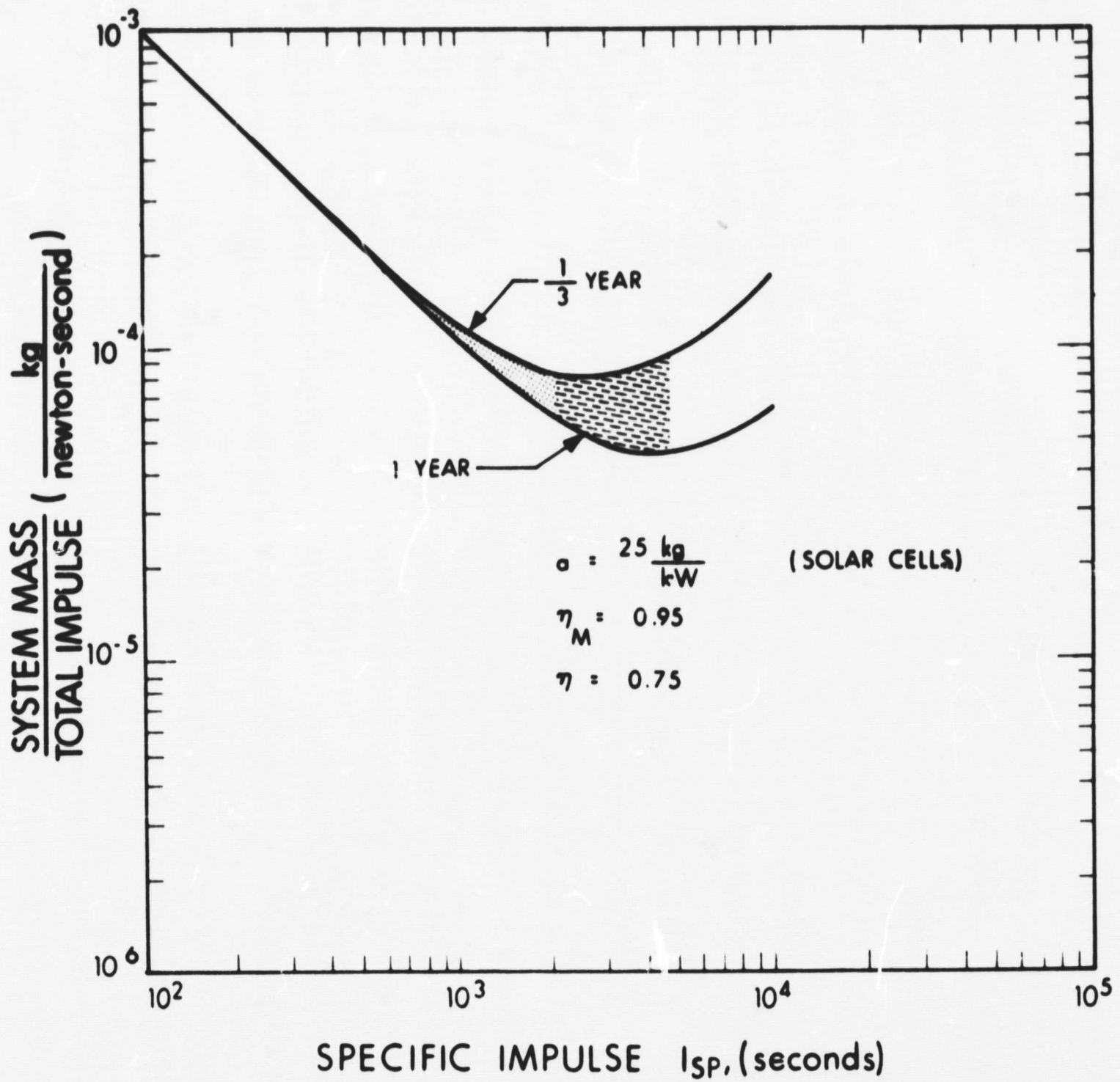


Figure 97. Ratio of Power Supply Plus Propellant Mass to Total Impulse versus I_{sp} for Solar Cells

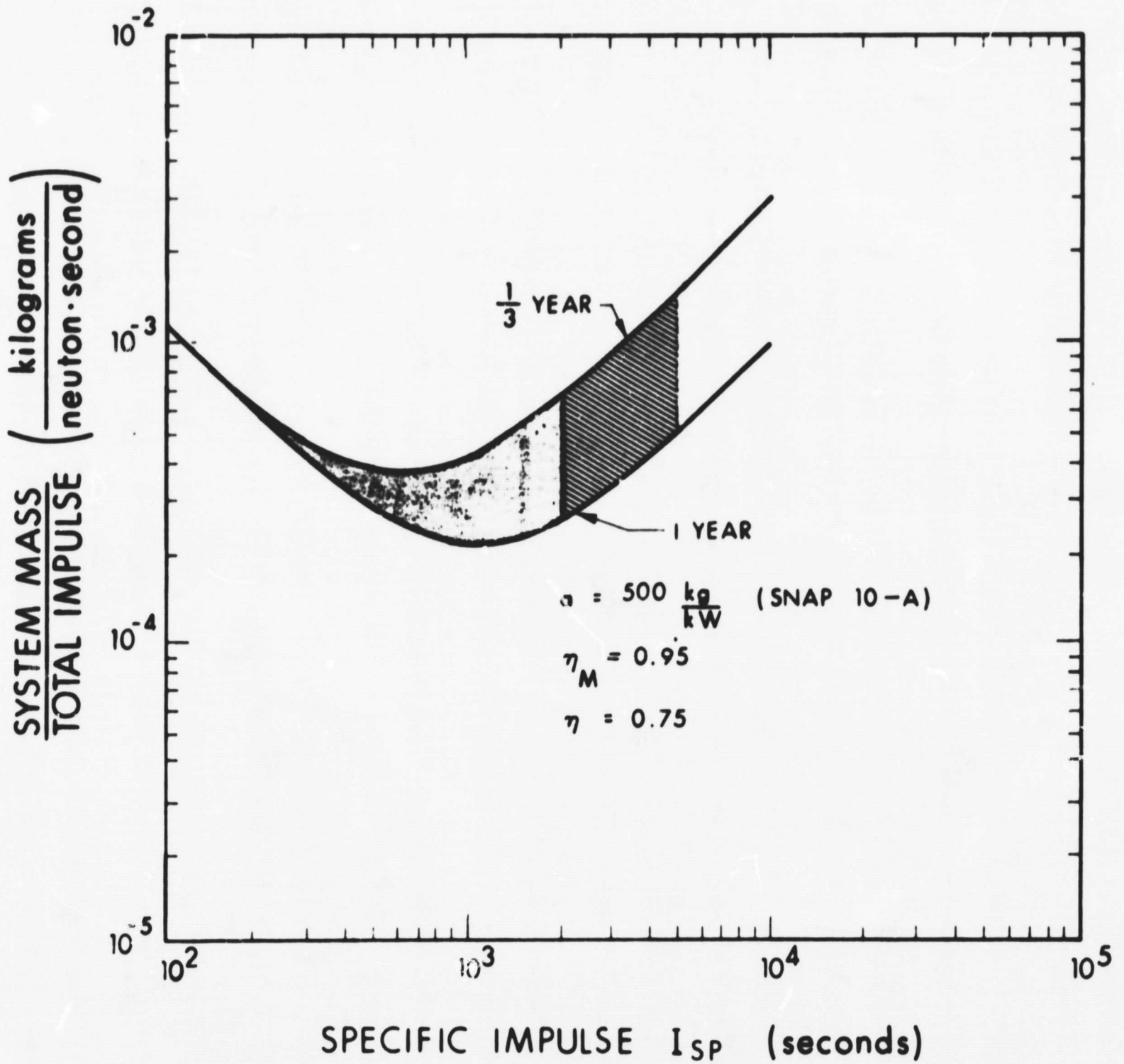


Figure 98. Ratio of Power Supply Plus Propellant Mass to Total Impulse versus I_{sp} for Nuclear Power Supply

power supply with a specific mass of 500 kg/kW respectively. In both cases the mass utilization efficiency is assumed to be 0.95 and the overall efficiency is assumed to be 0.75. Missions corresponding to durations of 1/3 and 1 year are indicated by the solid curve. The shaded area represents the predicted capabilities of colloid thrusters without post acceleration. The lined area represents the capability assuming post acceleration up to 100,000 volts.

The following is a discussion on the application of colloid thruster for east-west and north-south stationkeeping of synchronous satellite.²⁻¹²

One of the most promising applications for the electrostatic thruster is east-west stationkeeping of a gravity-gradient-stabilized synchronous satellite. For a 454 kg satellite, a thrust level of the order of 50 micronewtons would be required. Shown in Fig. 99 is a comparison of thruster system mass as a function of total impulse for a flight-type cesium contact thruster²⁻¹⁷ and a colloid thruster. In order to obtain these curves, a value of 91 kg/kW was used for the solar cell power source. A total impulse of about 4540 newton-seconds corresponds to about a 5 year satellite life. From this curve, it is clear that a colloid thruster operating at a specific impulse of 1000 seconds can potentially offer a significant mass advantage over the cesium contact thruster for east-west stationkeeping. The reason for this is due mainly to the relatively low power required for the colloid thruster (5 watts) as compared to the cesium contact thruster (20 watts).

Another mission of considerable interest is that of north-south stationkeeping for a synchronous satellite. For this mission, a 454 kg satellite would require a thrust level of about 1.3 millinewtons on a thruster duty cycle of about 50 percent. Shown in Fig. 100 is a comparison of projected thruster system weight as a function of total impulse for the colloid, cesium contact and cesium bombardment thruster systems. The data for the cesium contact and cesium bombardment

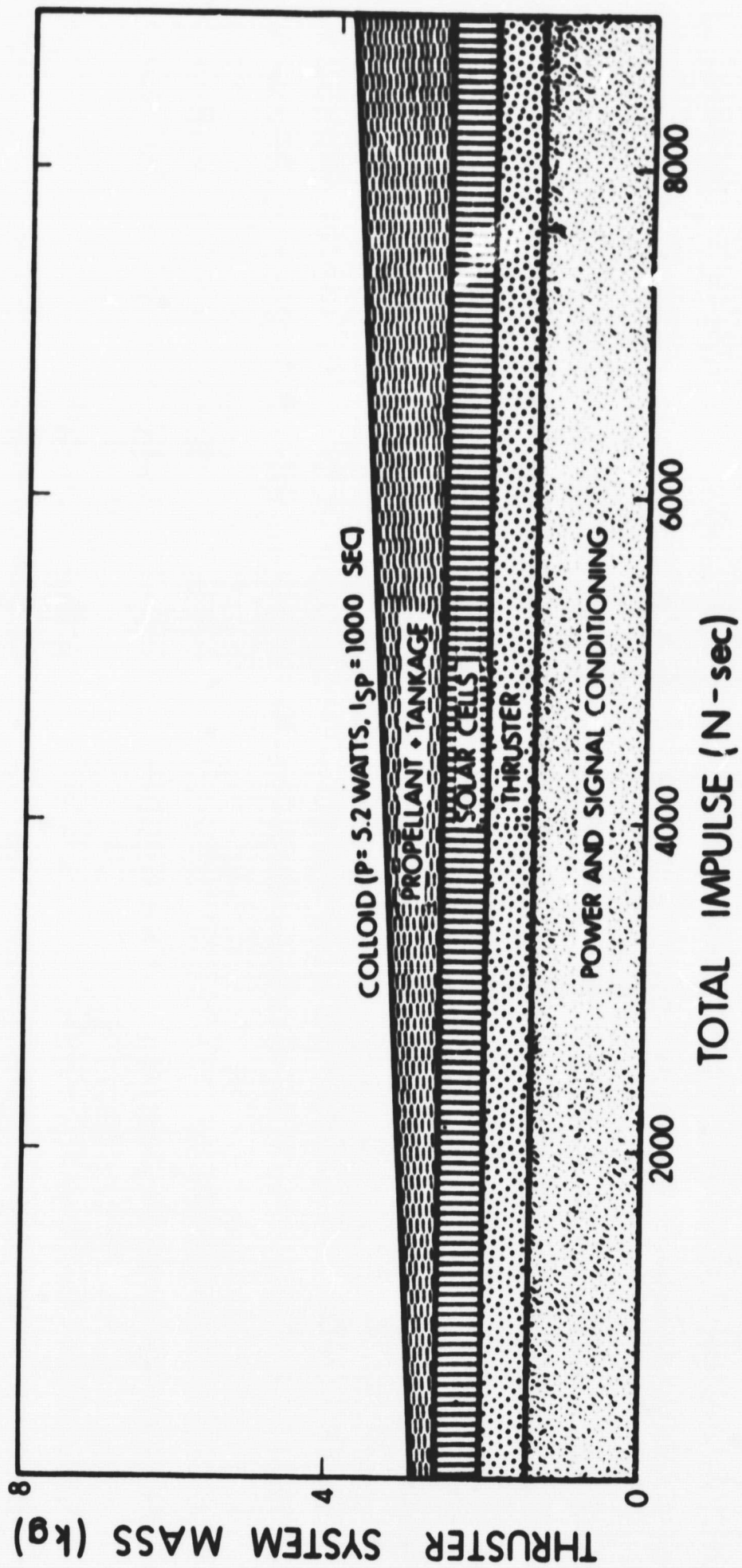


Figure 99. Predicted Thruster System Weight for East-West Stationkeeping of a Synchronous Satellite

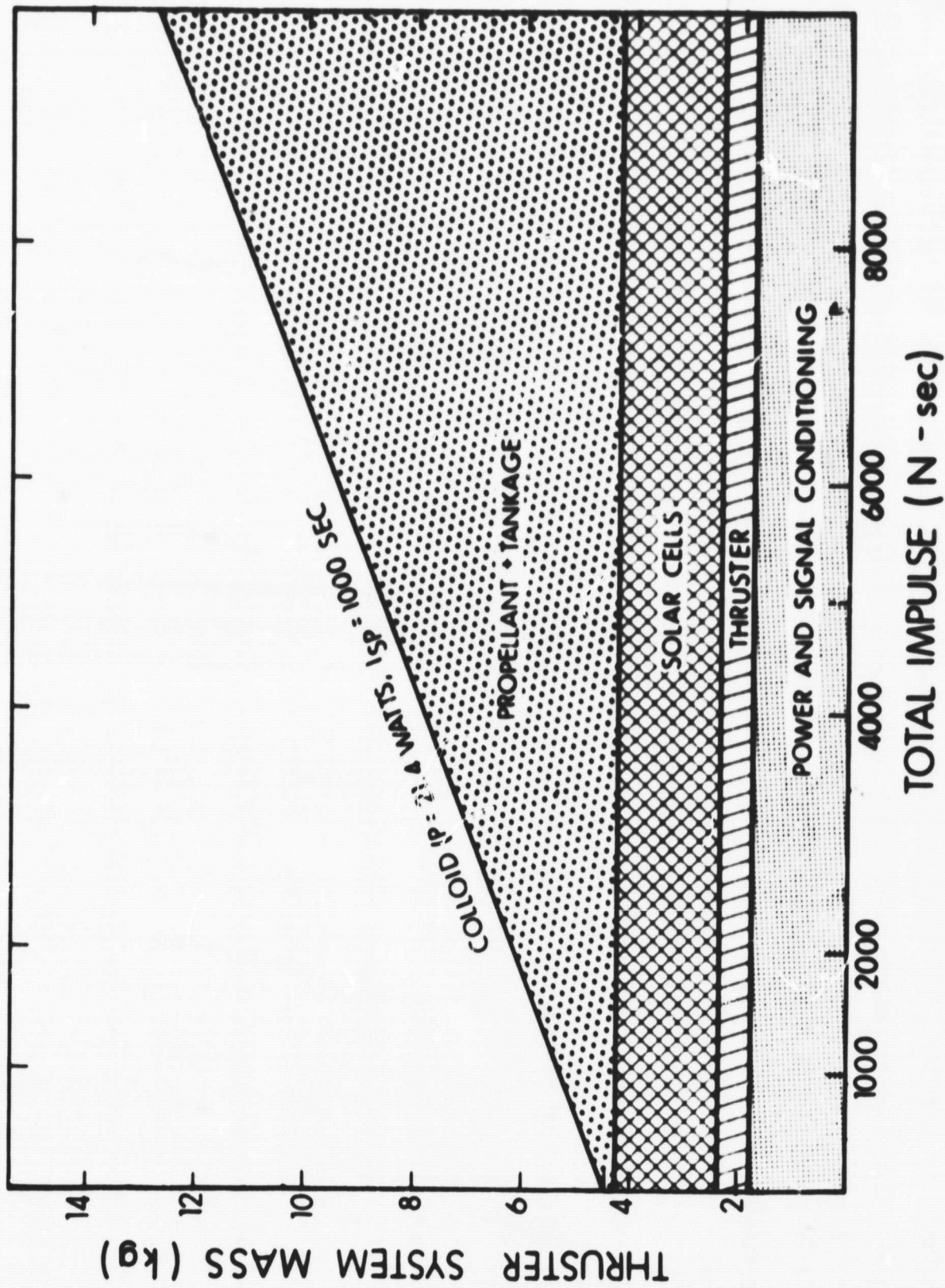


Figure 100. Predicted Thruster System Weight for North-South Stationkeeping of a Synchronous Satellite

was extrapolated from References 2-18 and 2-19 respectively. As can be seen from Fig. 100, the colloid thruster offers a significant weight and power advantage over the other thruster systems, below total impulse values of about 10^5 newton-seconds. A total impulse of 10^5 newton-seconds corresponds to a maximum satellite life of about 4 years for a north-south stationkeeping operation on a 454 kg satellite. Therefore even at the higher thrust levels (i.e., greater than 45 micro-newtons) the colloid thruster can offer significant mass savings for reasonably long satellite lifetimes.

2.4.2.2 Charge-to-Mass Ratio

The hydrodynamic spraying of charged droplets from a capillary emitter generally results in the emission of a broad range of specific charge. Mean charge-to-mass ratios from approximately 4×10^1 to 7.2×10^5 C/kg have been obtained. This range has been produced by a wide variety of working fluids with a large range of electrical conductivities. Table XXI is a summary of spray characteristics of different propellants tested (Ref. 2-15). Investigations of other working fluids for a colloid thruster have been made and charge-to-mass ratios obtained fall within the range given above (Ref. 2-16).

Parameters used to vary charge-to-mass ratio in laboratory experiments are emitter geometry and potential, mass flow rate of the propellant fluid, and fluid conductivity. In general, the charge-to-mass ratio is dependent on emitter potential and fluid conductivity in an increasing fashion. A more extensive range of charge-to-mass ratio is achieved for a given solvent by varying fluid conductivity in addition to varying emitter potential (Table XXI). The charge-to-mass ratio of droplets is observed to decrease with increasing mass flow rates.

TABLE XXI

SPRAY CHARACTERISTICS OF VARIOUS PROPELLANTS

Propellant (Polarity of Voltage)	Conductivity σ ($\Omega^{-1} \text{ cm}^{-1}$)	Mean Charge- to-Mass Ratio $\langle q/m \rangle$ (C/kg)	Specific Impulse I_{sp} (sec)	Distribution Efficiency ϵ_s (Ratio)	Thrust T (μN)
20 g TEAC/100 ml Oleic Acid (Positive and Negative)	1.2×10^{-4}	41 to 430	79 to 257	0.30 to >0.95	7.5 to 65.8
20 g TEAC/100 ml Glycerol (Negative)	3.0×10^{-4}	1.9×10^3 to 1.8×10^4	425 to 1245	0.62 to 0.80	3.7 to 35.4
20 g NaI/100 ml Glycerol (Positive)	3.85×10^{-4}	3.25×10^3 to 1.34×10^5	340 to 3430	0.45 to 0.85	0.4 to 18.3
2 ml H_2SO_4 /100 ml Glycerol (Negative)	6.0×10^{-4}	1.4×10^3 to 5.1×10^3	420 to 780	0.77 to 0.82	13.7 to 83.2
10 ml H_2SO_4 /100 ml Glycerol (Negative)	1.96×10^{-3}	4.08×10^4 to 4.30×10^4	1455	0.63 to 0.66	17.1 to 18.8
93.8 percent H_2SO_4 (Negative)	8.1×10^{-1}	3.69×10^5 to 4.45×10^5	4680 to 5100	>0.90	33 to 46
Liquid Cesium (Positive)	2.7×10^4	5.7×10^5 7.2×10^5	4050 to 10,000	>0.95	0.38 to 27.4

Unlike other electrical propulsion systems (for example, the electron bombardment and contact ionization engines), the average charge-to-mass ratio of particles generated by the electrohydrodynamic process varies in a complicated manner with nearly any change in other engine parameters. A series of experiment curves illustrating the dependence of charge-to-mass ratio on emitter voltage, feed pressures (directly proportional to mass flow) and temperature for a FcCl_3 /glycerol propellant fluid are given in Figures 101 to 104 (Paf. 2-13).

This data was taken utilizing a single emitter and exemplifies the general behavior and trends for organic solvent doped with conductive salts. The charge-to-mass ratio increases with increasing voltage and decreases with increasing feed rate and temperature.

This dependence of charge-to-mass ratio on other thruster parameters and the broad range available makes research in this area more complex but in no way detracts from the overall unique versatility of the colloid thruster concept.

The charge-to-mass ratio distribution efficiencies, a measure of the charge-to-mass ratio spread in a particle beam, are used in determining one important aspect of thruster efficiencies. A mixture of ions (high specific charge particles) with heavier multimolecular particles are present in a typical beam. While ideal emission consists of particles with the same charge-to-mass ratio, this is not readily obtainable in present spraying processes. One exception was the electrostatic spraying of liquid cesium in which over 95 percent singly charged ions are emitted. The general trend is for specific charge efficiency to decrease with increasing emitter potential (2 to 10 kV range) and mass flow rates (30 to 760 torr range).

Some interesting features concerning the charge-to-mass ratio efficiencies of a charged particle beam are illustrated in Figure 105. The charge-to-mass ratio efficiencies versus average specific charge are

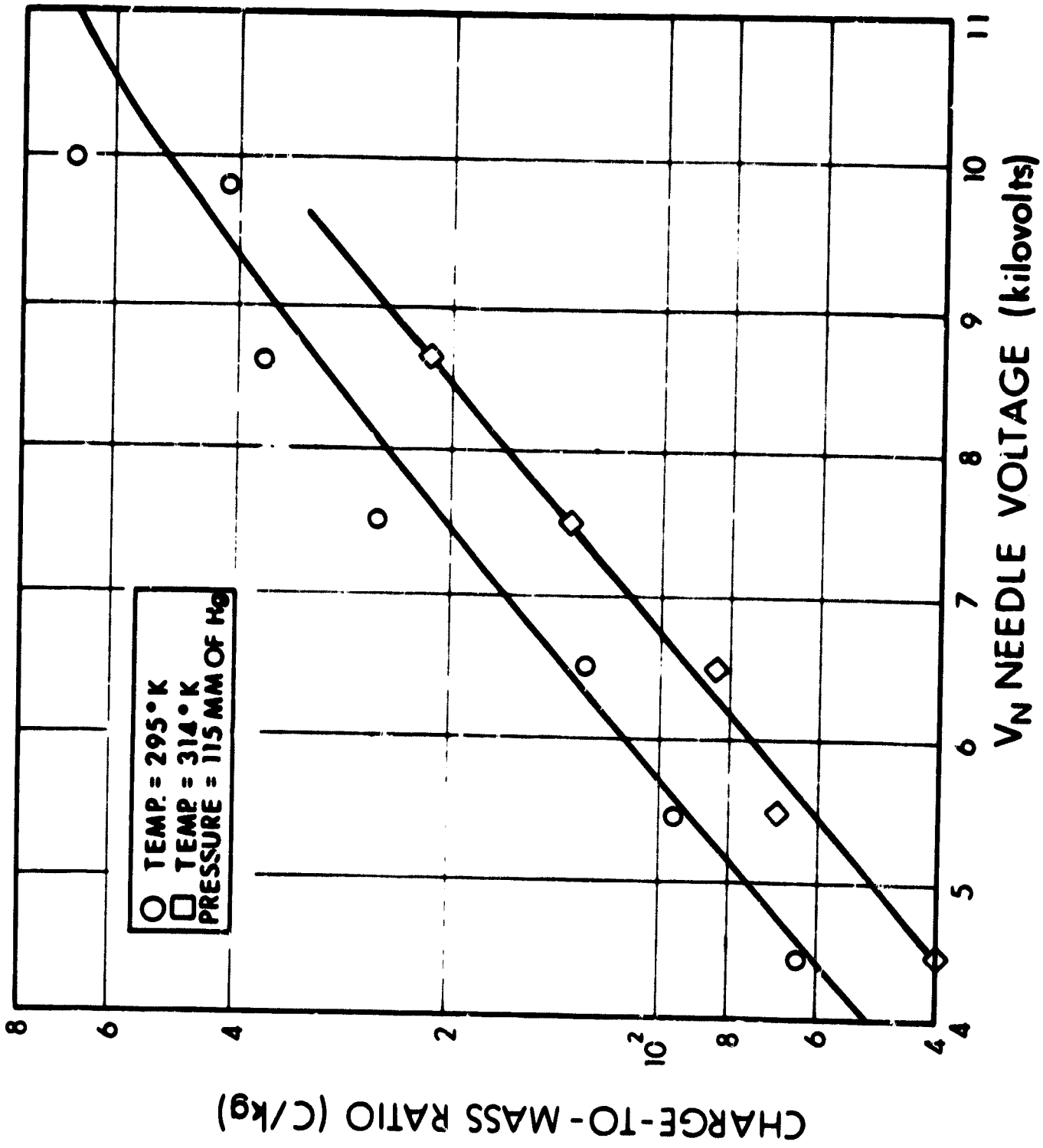


Figure 101. $\langle q/m \rangle$ versus Needle Voltage at Two Needle Temperatures

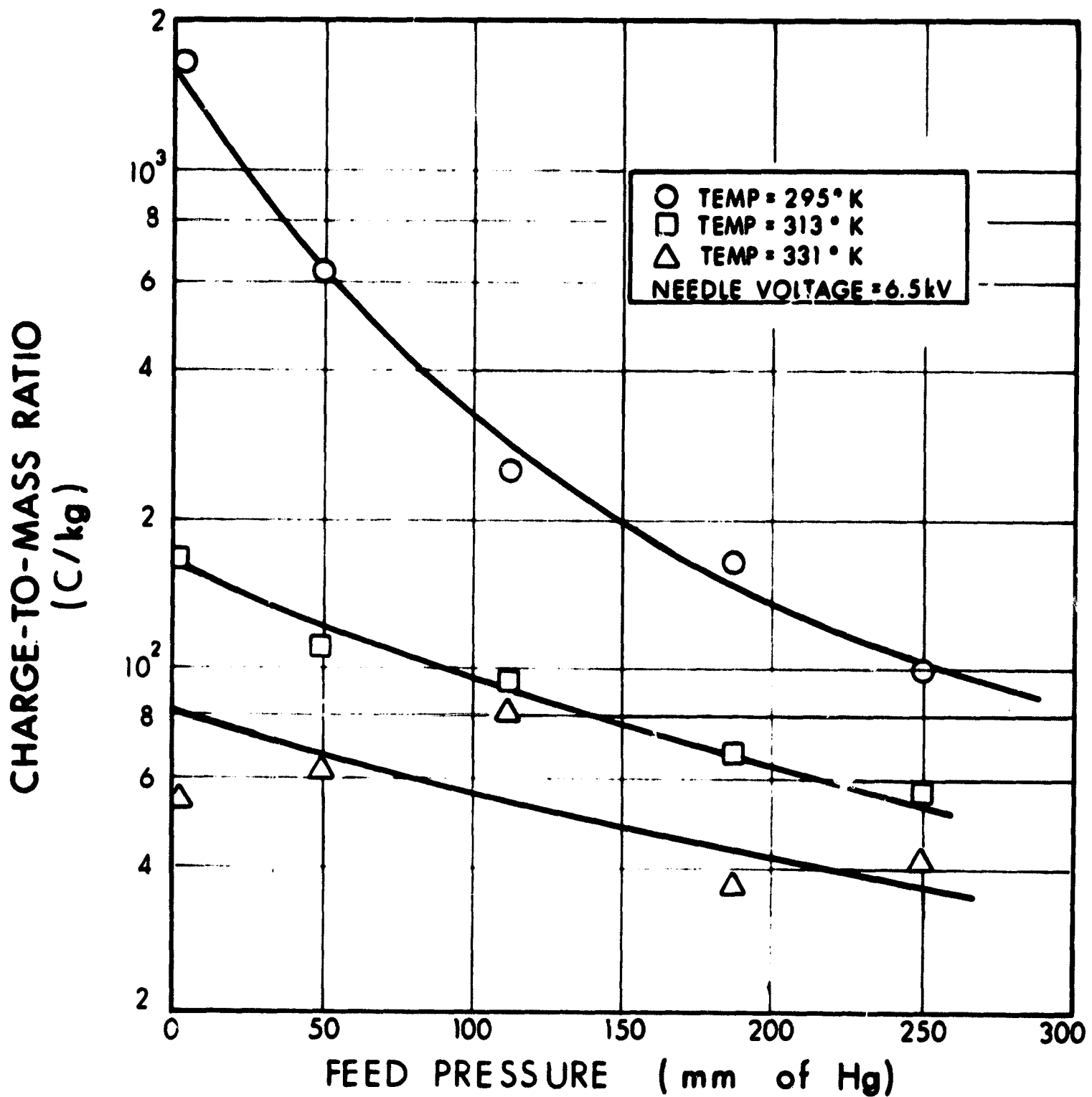


Figure 102. $\langle q/m \rangle$ versus Feed Pressure at Three Temperatures

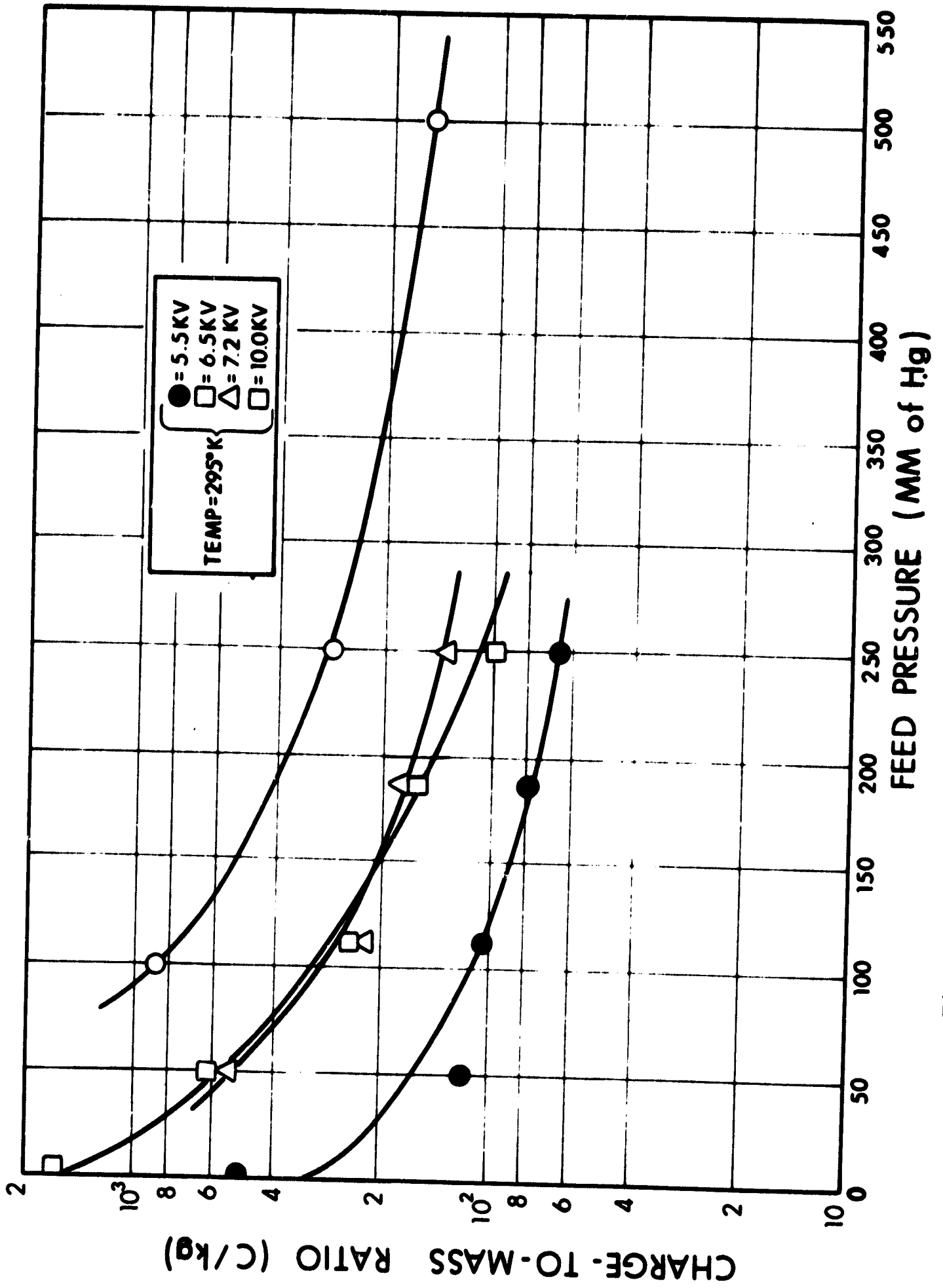


Figure 103. $\langle q/m \rangle$ versus Feed Pressure at Four Voltage Settings

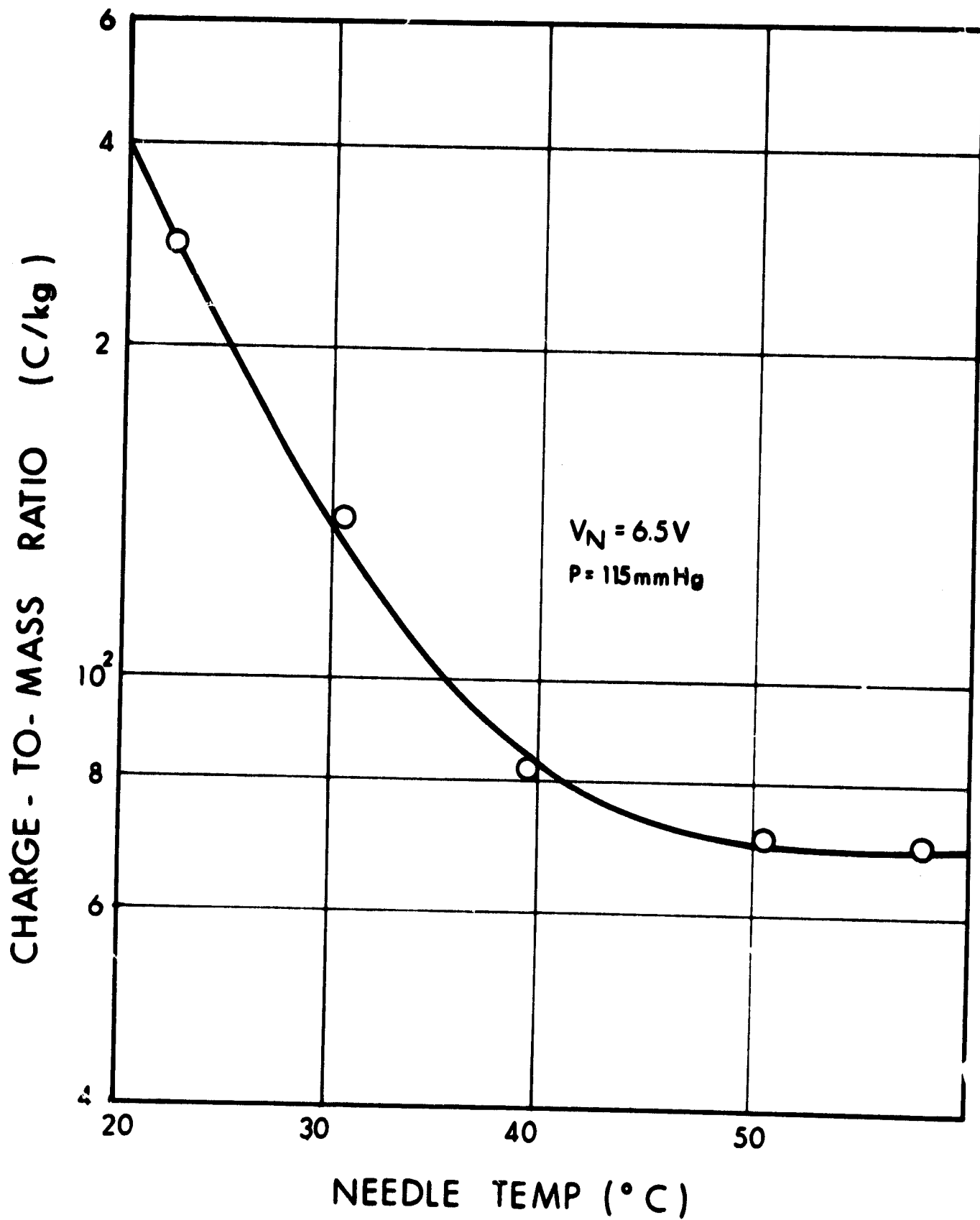


Figure 104. $\langle q/m \rangle$ versus Needle Temperatures

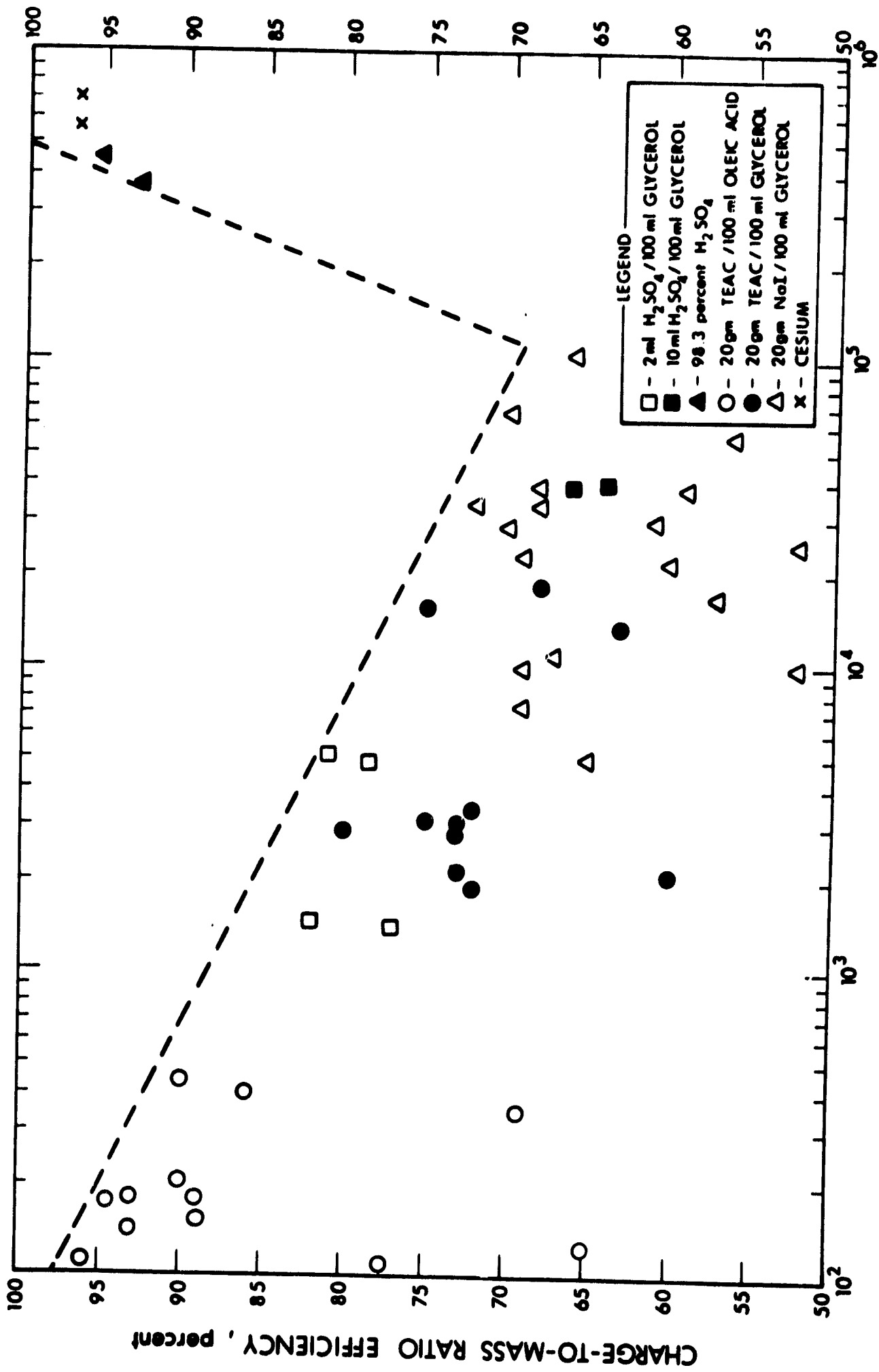


Figure 105. Plot of Particle Distribution Efficiency versus Specific Charge

plotted for a variety of fluids tested. As the average charge-to-mass ratio increases over the range from 10^2 C/kg to 10^5 C/kg, there is a definite trend for efficiencies to decrease. Propellant studies by other investigators have produced similar results in showing a decrease in efficiency with increasing charge-to-mass ratio (Ref. 12). The reason for the particularly high efficiencies for charge-to-mass ratios greater than 10^5 C/kg is that particles are ionic and therefore are stable. For cesium, greater than 95 percent of the beam was observed to consist of singly charged ions.

2.4.2.3 Power, Thrust, Power-to-Thrust Ratio, and Charge-to-Mass Ratio Distribution

The colloid thruster system differs uniquely from other electrical propulsion systems in that the fields used to accelerate the charged particles also provide the energy for particle generation. For a bipolar scheme, incorporating both negative and positive particle generation accomplishing neutralization, the power input is nearly just the power supply voltage times the beam current.

The great advantage of colloid thruster devices over those of other electrical propulsion systems is they can operate more efficiently at specific impulses less than 5000 sec. Electrical efficiency for propulsion systems is defined by,

$$\text{Thruster Efficiency} = \frac{\text{Beam Power}}{\text{Power Input}}$$

The charged particle beam generated from colloid emitter sources is characterized by a spread in charge-to-mass ratio. An ideal colloid source would produce a beam of particles with identical charge-to-mass ratios (very nearly approximated by liquid cesium propellant). The presence of a charge-to-mass ratio distribution is responsible for a beam power loss and has been shown to be expressible in efficiency terms as (Ref. 2-3).

$$\epsilon = \frac{\langle q/m^{1/2} \rangle^2}{\langle q/m \rangle}$$

This term is appropriately termed the beam power efficiency associated with the spread in particle charge-to-mass ratios. Neglecting other sources of energy losses, the overall thruster efficiency is represented then, by the beam power efficiency. There are, however, other processes that occur along with the generation and acceleration that consume energy and these must be included in the overall thruster system efficiency. These processes do not contribute toward total thrust and involve particle interaction near the emitter tip, neutral mass emission and beam angular spread.

The thrust produced by an ideal, monoenergetic beam of positively charged particles is

$$T = \frac{d(m_+ v)}{dt}$$

where m_+ is the mass of propellant contributing to the thrust and v is the velocity of the charged particles. Hence the thrust is given by

$$T = \dot{m}_+ v.$$

The total Kinetic energy in the beam is

$$\frac{m_+ v^2}{2} = q V$$

where q is the charge on a particle and V is the accelerating potential.

The Kinetic power in the beam is

$$i_B V = \frac{i_B}{q/m_+} \frac{v^2}{2}$$

where i_B is the beam current

Since

$$\frac{i_B}{q/m_+} = \dot{m}_+$$

and using

$$V = \frac{T}{\dot{m}_+}$$

the ideal beam power becomes

$$i_B V = \frac{T^2}{2\dot{m}_+}$$

The effect of neutrals on reducing the thrust levels for an ideal thruster can be determined if we let \dot{m} , the total mass flow in the beam be

$$\dot{m} = \dot{m}_+ + \dot{m}_n$$

where \dot{m}_n represents the mass flow of neutrals then

$$T^2 = 2 (\dot{m} - \dot{m}_n)^2 \frac{q}{m_+} V$$

and

$$T = (2V)^{1/2} \left(\frac{q}{m_+}\right)^{1/2} (\dot{m} - \dot{m}_n)$$

Figures 106 and 107 illustrate how thrust varies with mass flow and voltage for a single needle.²⁻¹³ This demonstrated performance will be of value when determining which parameters to control for system operation.

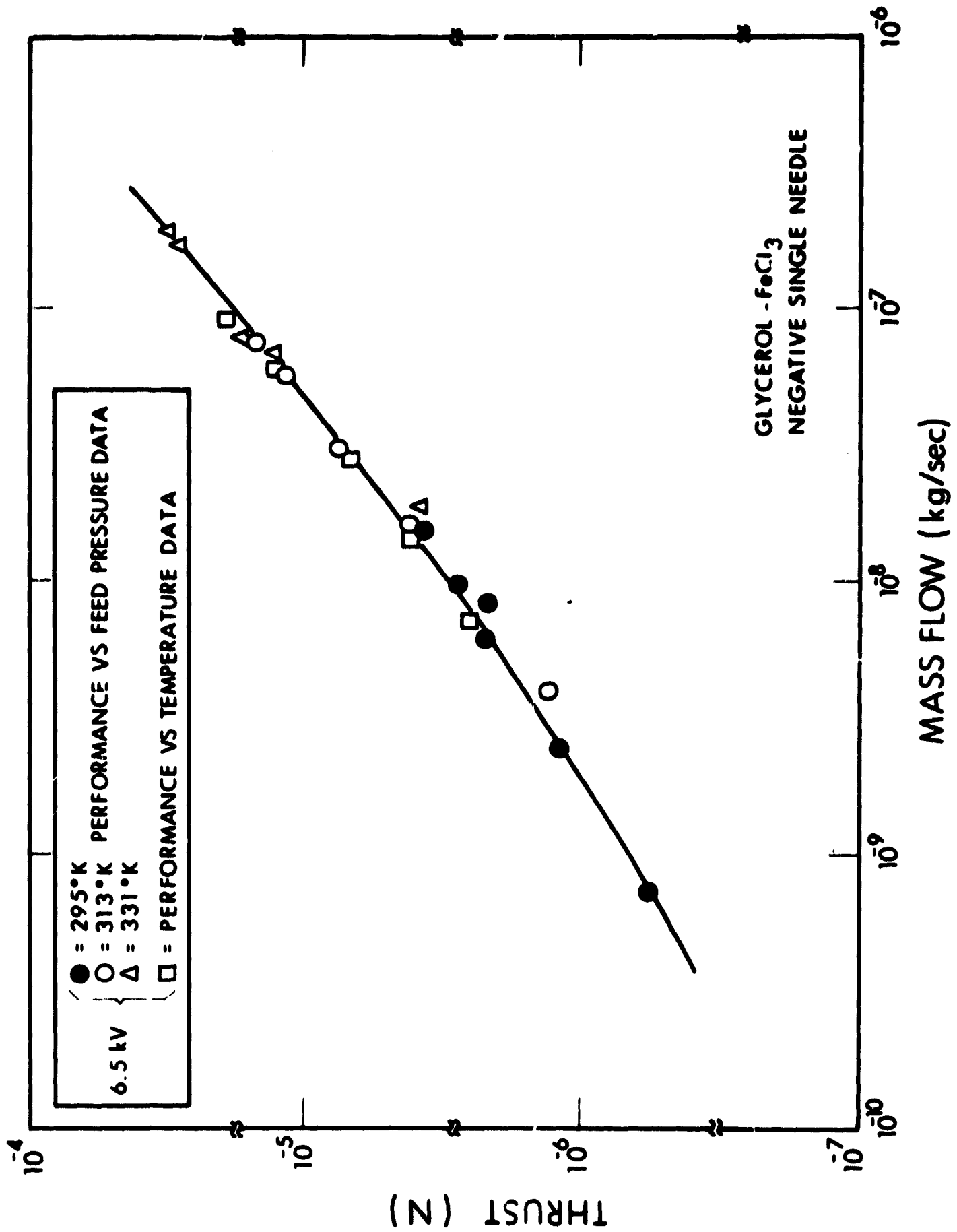


Figure 106. Thrust versus \dot{M} . This Plot Combines Temperature and Pressure Data

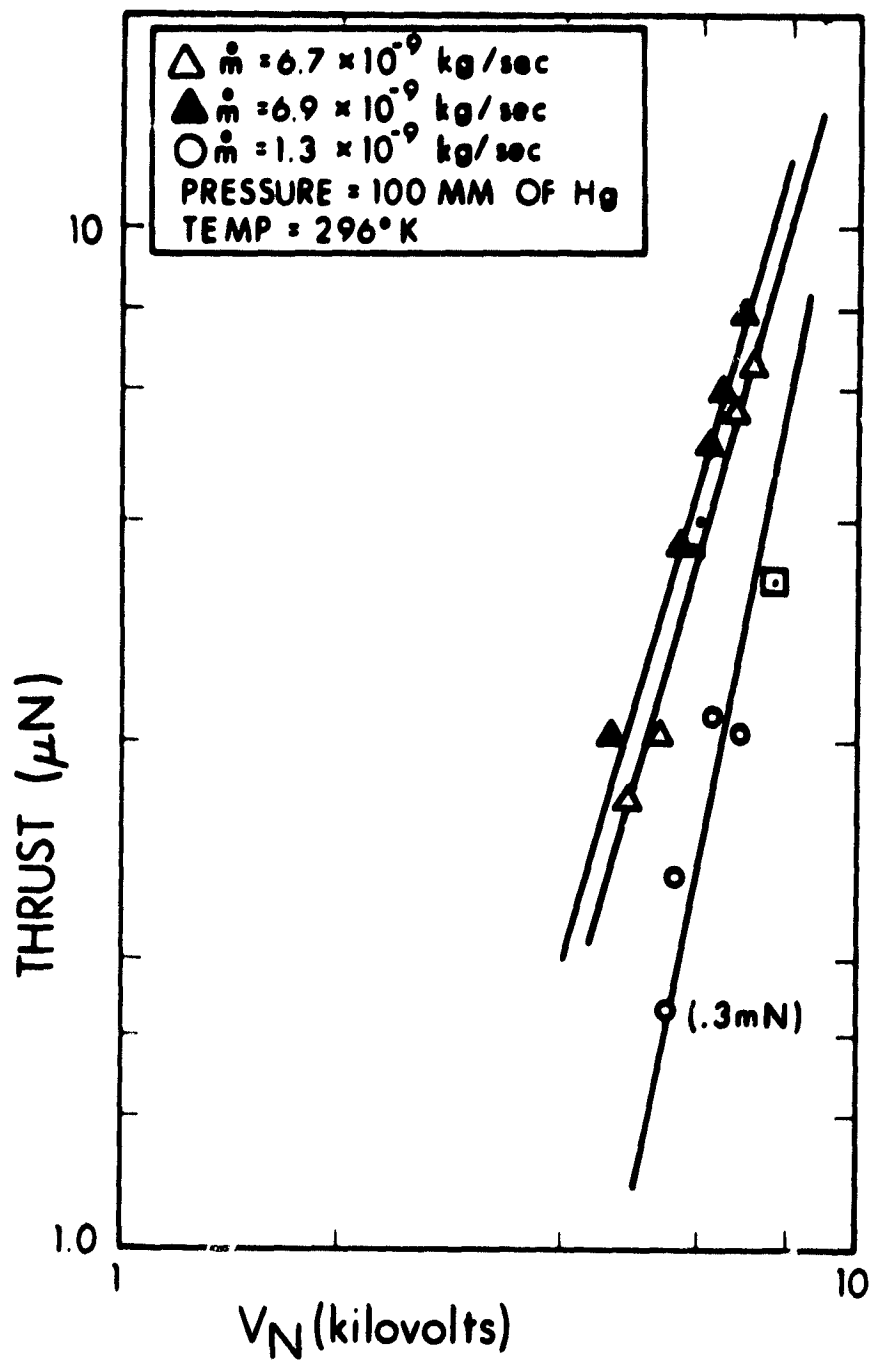


Figure 107. Thrust versus Needle Potential (V_n)

The performance characteristics of laboratory colloid thrusters have been investigated and Table XXII lists some thruster parameters determined from published data.^{2-12,2-14}

2.4.2.4 Mass Flow Rate

The rate at which propellant mass is utilized in a colloid thruster system influences the manner in which thruster parameters, such as thrust and specific impulse, may vary. The problem, then has been to determine which parameters control the rate of mass expenditure and the quantitative nature of their dependence. Once this has been established the effects of mass flow rate on thruster parameters can be studied via these control parameters. Combining an understanding of control and thruster parameters, a flight feed system can be ultimately designed.

Control parameters used to vary mass flow in the laboratory are feed pressure and temperature. Mass flow rates as a function of these parameters have been measured and the results are illustrated in Figures 108 through 110. These mass flows were measured using an emitter with a 0.10 mm diameter bore. Useful information can be obtained from these plots as follows:

- a. Mass flow rate varies linearly with feed pressure.
- b. There is an exponential dependence of mass flow on temperature. This is a result of the viscosity of the propellant and its dependence on temperature in this range.
- c. Mass flow remains constant with emitter potential insofar as increases in emitter potential do not indirectly produce temperature rises.

Additional experimental investigation is needed to determine the effects of mass flow on thruster parameters. Data isolating upper and lower limits on thrusts and specific impulses achievable for given mass flows and propellant types are needed. Figure 106 in Section 2.4.2.3 shows how thrust varies with mass flow for a single needle. Figure 111

TABLE XVII
DEMONSTRATED PERFORMANCE PARAMETERS
FOR COLLOID THRUSTERS

<u>Thruster Type</u>	<u>I_{sp} (sec)</u>	<u>T (μN)</u>	<u>P/T (kW/N)</u>	<u>Reference</u>
36 Needle Single Polarity	587 to 691	574 to 735	3.7 to 4.3	12
73 Needle Bipolar	500 to 750	356 to 557	4.4	14
60 Needle Single Polarity	763 to 840	494 to 618	5.3 to 5.8	12
36 Needle Single Polarity	1024 to 1212	392 to 533	5.3 to 5.8	12

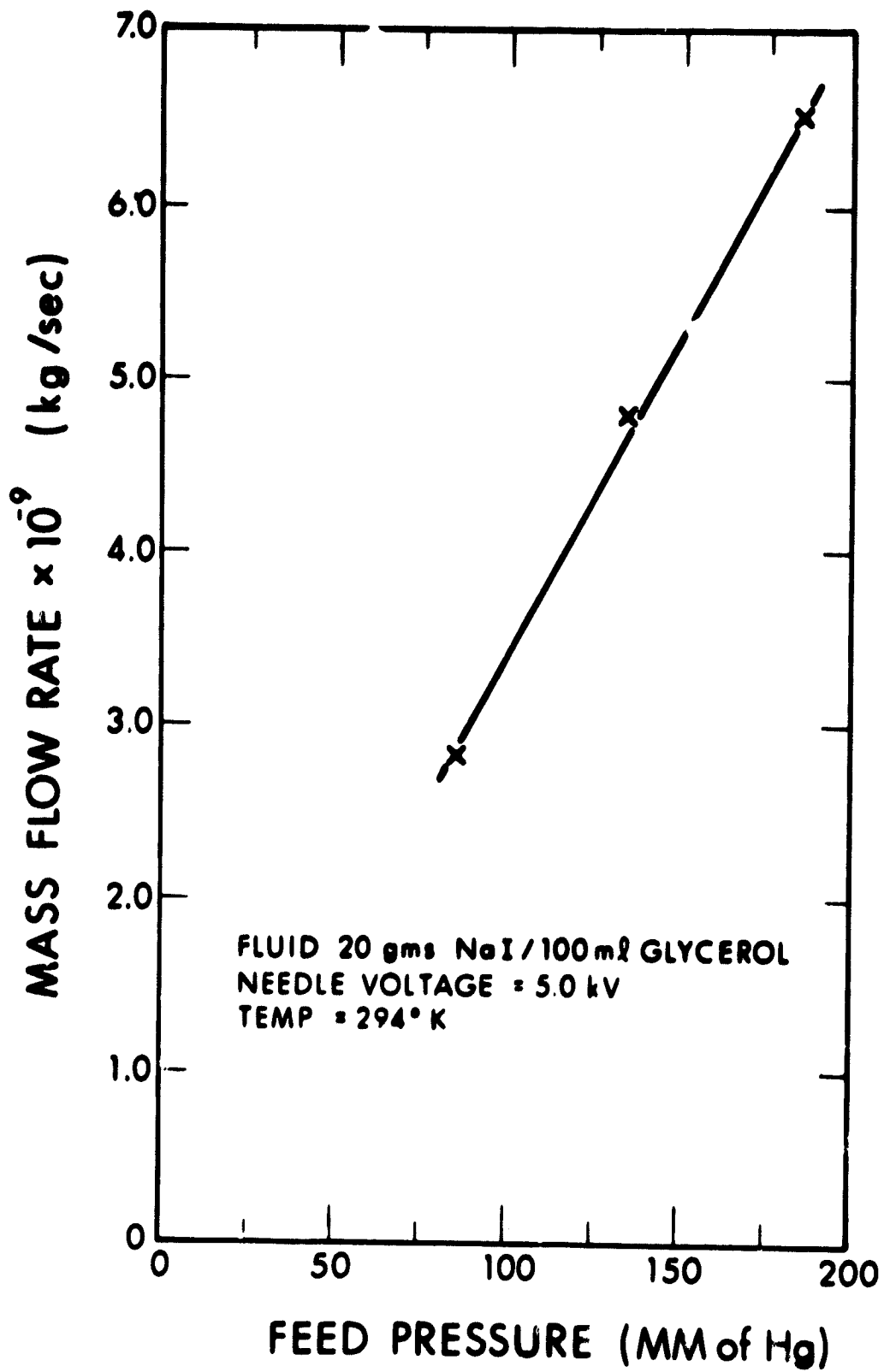


Figure 108. Mass Flow Rate versus Feed System Pressure

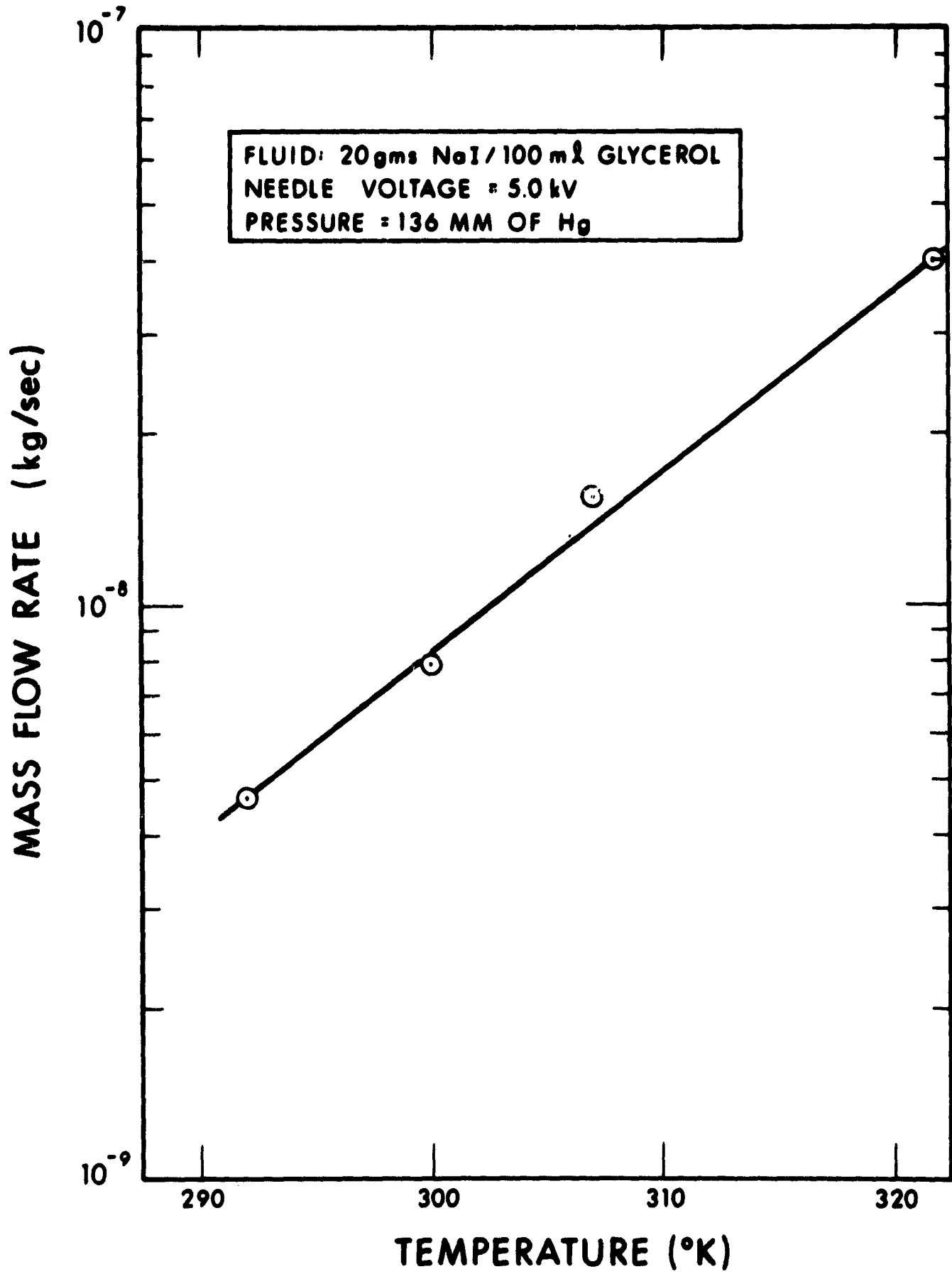


Figure 109. Mass Flow Rate versus Temperature

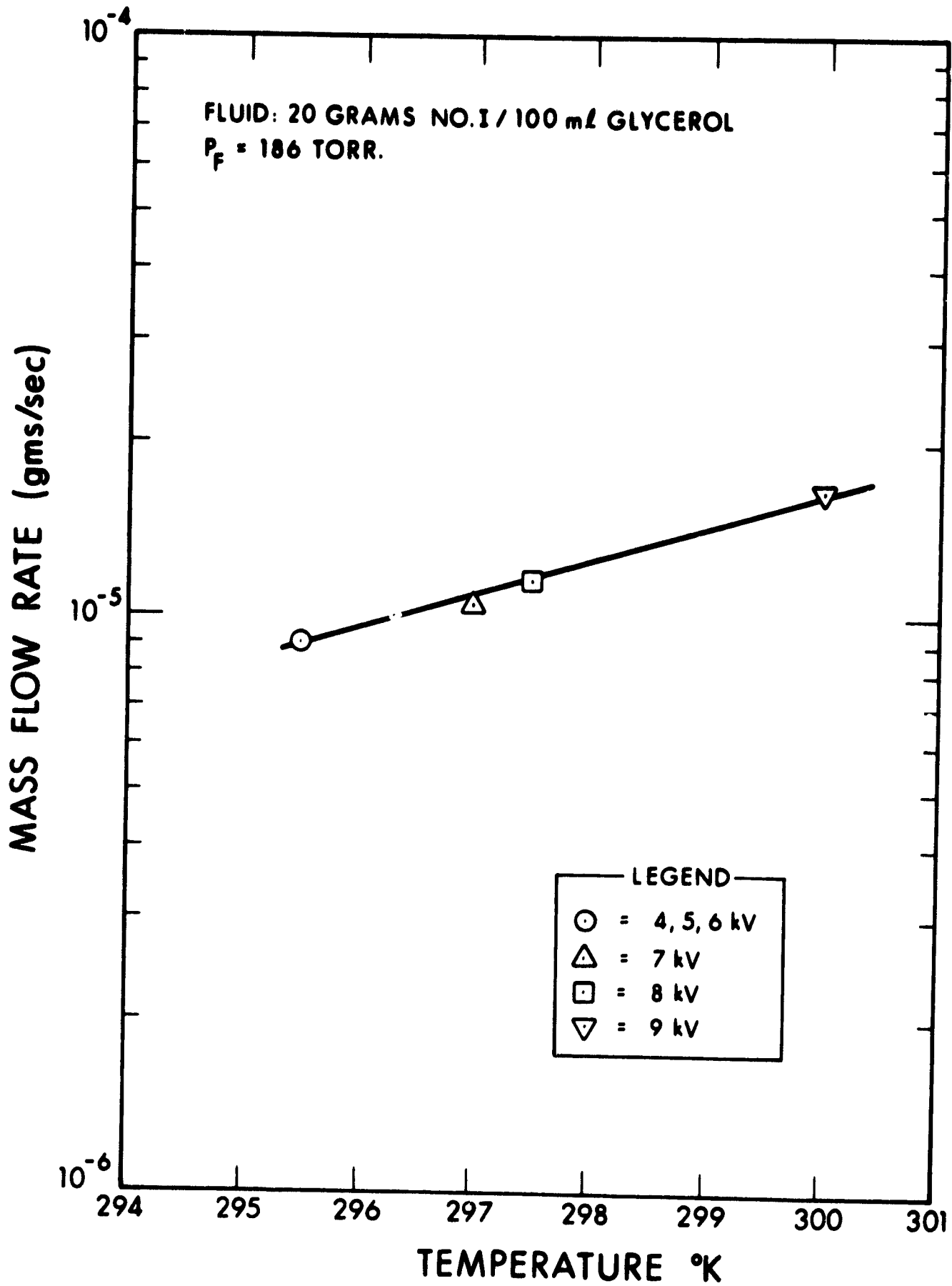


Figure 110. Mass Flow Rate versus Temperature for Various Voltages

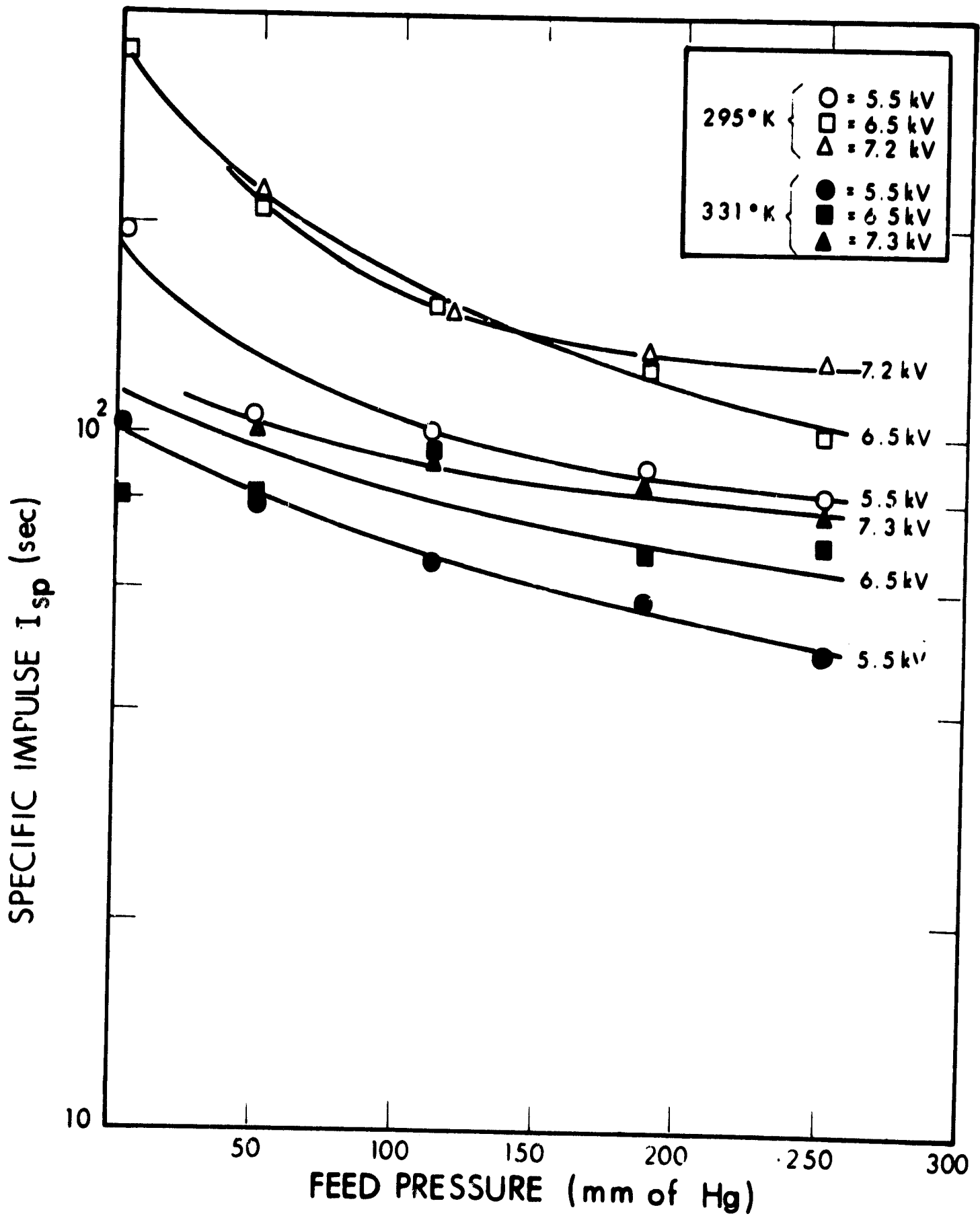


Figure 111. Specific Impulse (I_{sp}) versus Feed Pressure at Three Voltage Settings and Two temperature Settings

shows the effect of varying mass flow on specific impulses. This plot is a good example of the complexity involved when there is an interaction of many thruster variables. The decrease in specific impulse with increasing pressure is a result of lowering the average charge-to-mass ratio of the generated charged droplets. Increasing mass flow has the property of reducing charge-to-mass ratios.

2.4.3 THRUSTER STATUS

2.4.3.1 Electrical Characteristics of Thrusters

To examine the electrical characteristics of a heavy charged particle thruster specified operational requirements will be assumed. The following parameters are required of the thruster.

Specific Impulse	10^3 sec
Thrust	0.89 millinewtons
Voltage	6 kV

Assume further that the following are the operating characteristics of the thruster at the parameters specified above:

Total Efficiency	~ 50 percent
Mean Charge-to-Mass Ratio	10^4 C/kg
Mass Efficiency	90 percent

At this mean charge-to-mass ratio, efficiencies and the required parameters the following are obtained:

Beam Current	800 μ A
Power in	9 W
Power to Thrust	10 kW/N
Mass Flow Rate	8×10^{-8} kg/sec

At a reasonable value of $5\mu\text{A}/\text{emitter}$, 160 emitters would be required to produce the total current.

For a bipolar system the above characteristics are complete since no neutralizer is required. To include a neutralizer several more watts would be required. The disadvantage of the bipolar system is in the two feed and control systems.

2.4.3.2 Vector Control

Electrostatic control of thrust vector has been demonstrated experimentally.

The best results have been obtained by first focusing the beam of charged particles and then deflecting the beam with a pair of deflecting plates which also serve as the extractor. Figure 112 shows how the deflection angle, θ , and the full width at half maximum (FWHM) varies with deflection voltage, V . The deflection was found to be very linear with voltage up to at least 30 degrees. It was seen that the FWHM of 10 degrees remain nearly constant throughout the range of deflection.

2.4.3.3 Life and Life Test

Duration runs discussed below show that thrusters can operate for over 1000 hours with little degradation. Emission efficiency decreases with erosion of emitter tip shape, but operation can nevertheless be maintained in spite of severe erosion. Complete destruction of the emitter tip shape does not stop operation. If the emitter is sealed over or clogged by deposition, emission of course ceases. Erosion of the emitter may in fact prevent clogging and maintain operation although degrade performance.

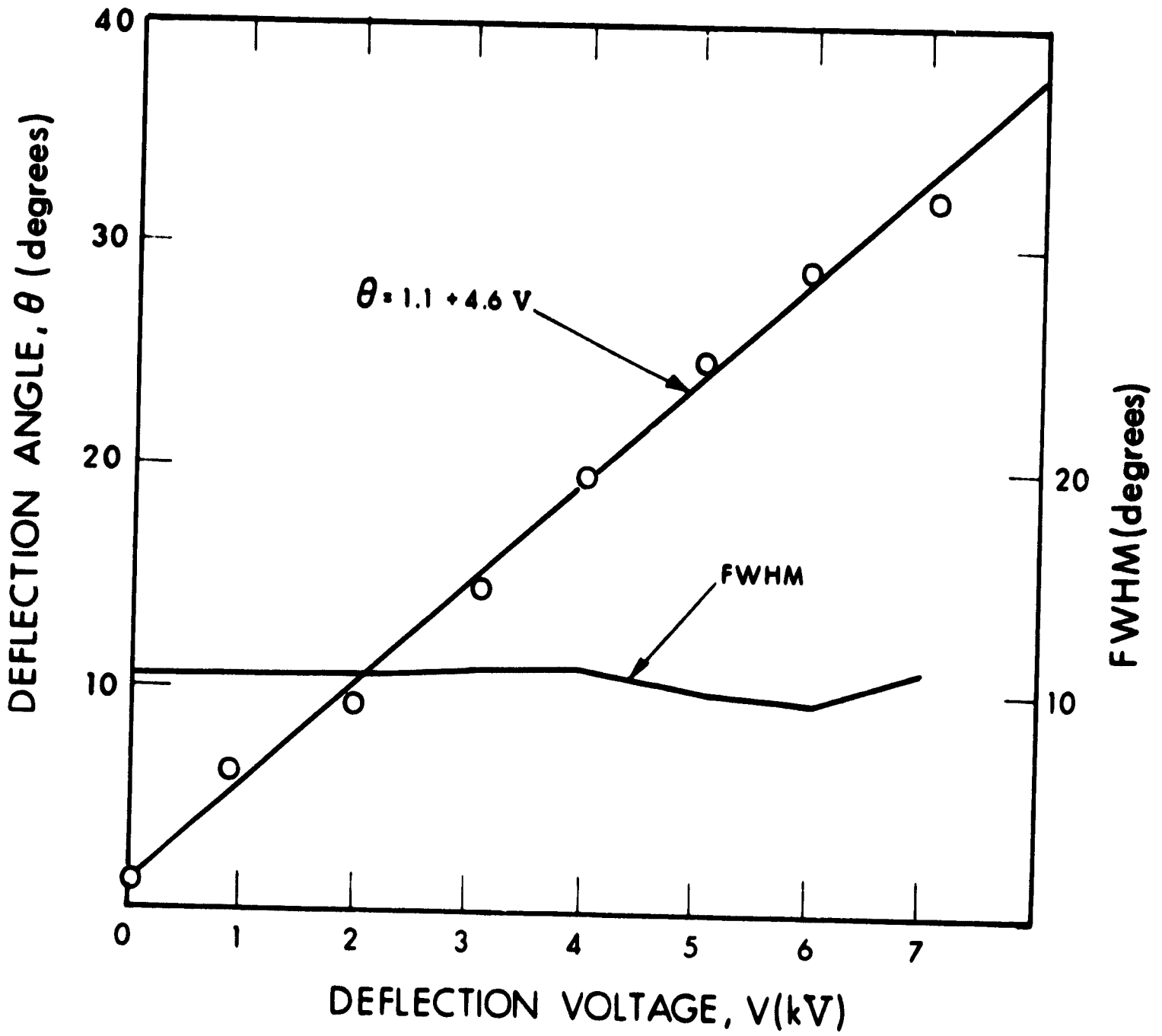


Figure 112. Deflection Angle and FWHM versus Deflection Voltage

Performance of several thousand to ten thousand hours can be anticipated in the future although little work has been done in this direction. Propellants should be selected to minimize deposition and operation limited to good stable modes minimizing erosion due to discharges at the emitter tips.

Several bipolar thrusters have been operated continuously for over 50 hours. As an example a thruster with 37 positive emitters and 36 negative emitters was operated continuously for over 53 hours.^{2-14,2-15} The operating voltages were +4.4kV and -5.8kV. The average currents over a 50 hour period were +150 μ A and -154 μ A with a thrust of 0.36 millinewtons. This produced a power to thrust ratio of 4.4 kW/N. During the entire run, only a minimum of adjustment of the feed system pressure was required to maintain the emitter current balance and a constant thrust level. The fact that no significant drop in current level was observed during the 50 hours of operation is an excellent indication that a run of this duration is not effected by deterioration of the emitters. The needle tips when examined after the test showed very little erosion resulting from this run.

After 50 hours had elapsed the thrust level was increased to 0.55 millinewtons by increasing the feed pressure and adjusting the emitter voltages to maintain a reasonably balanced emitter currents. The emitter currents and voltage were +215 μ A at +4.18kV and -240 μ A at -5.8kV. The power to thrust ratio remained at 4.4 kW/N.

The mass flowrate was not measured directly, therefore, the specific impulse is not known. However, based on results of single needle tests it is estimated that the specific impulse was between 450 and 700 seconds.

Longer life tests have been conducted with positive colloid thrusters. A thruster module developed for a flight microthruster system has

accumulated 1500 hours of operation, of which 820 hours were continuous, at a specific impulse in the 800 seconds range with no apparent sign of degradation (Ref. 2-12).

2.4.3.4 Development Areas

The colloid thruster as a functional reality has made many advances. More and refined diagnostic techniques are needed to support experimental development and to provide the theoretical groundwork for understanding the mechanisms of particle generations and energy losses.

More experimental research is needed in the area of developing a flight feed system for controlling propellant mass flow rates. This will involve a closer study of mass flow effects on thrust and specific impulse and the choice of suitable controls. Various schemes for a workable feed system have been examined and a more extensive analysis of proposed alternatives is necessary. Presently a reliable, light-weight positive pressure feed system that consumes very little power is being considered. Mechanical means for providing pressure to a propellant reservoir by using a spring loaded device has been considered (Ref. 2-20). Conversion of thermal energy, utilizing the increase in vapor pressure of a suitable material producing pressure, for mechanical displacement of a propellant fluid has also been considered.

Single emitter studies utilizing small bore capillary tubing have produced maximum currents on the order of 25₁A for common experimental propellants. (Highly conductive fluids such as H₂SO₄ and liquid metals produce much more but are intrinsically high specific impulse devices.) To achieve operational thrust levels then, colloid thrusters based on single needles must by necessity contain large arrays of needles. This introduces a fabrication problem as mass production techniques on such small work places have not been developed.

Experimental studies in the propellant area have been limited to organic solvents doped with conductive salts and liquid metals. Motivation behind propellant studies have been aimed at producing charge droplet beams with more efficient spread in charge-to-mass ratios and also in achieving desired limits in charge-to-mass ratios. Studies in source configurations have not provided any encouraging results in altering specific charge efficiencies. Fluid research, however, remains an important area for development.

Another area for development is in the direction of producing sources of higher thrust density. The present approach is to replace needle emitters with slit geometrics or closely spaced needles to simulate slits. Calculations have shown that the slit geometry using closely spaced needles will produce 2 to 3 times the current density over that of needle geometries.

2.4.4 SYSTEM CONSIDERATIONS

2.4.4.1 Control System

The performance of colloid thrusters can be varied over a wide range of thrust and specific impulse by controlling the mass flow rate and needle voltage. Thrust increases with increasing mass flow rate and needle voltage while specific impulse decreases needle voltage. Figure 113 shows a typical example of how thrust and specific impulse are related to mass flow rate and needle voltage.

The design of a flexible system requires feedback information to control the mass flow rate and needle voltage. The feedback information available are the beam current, needle voltage, and thrust obtained from the orbital path of the satellite. If the current versus needle voltage characteristics are known for different mass flow rates then the above information

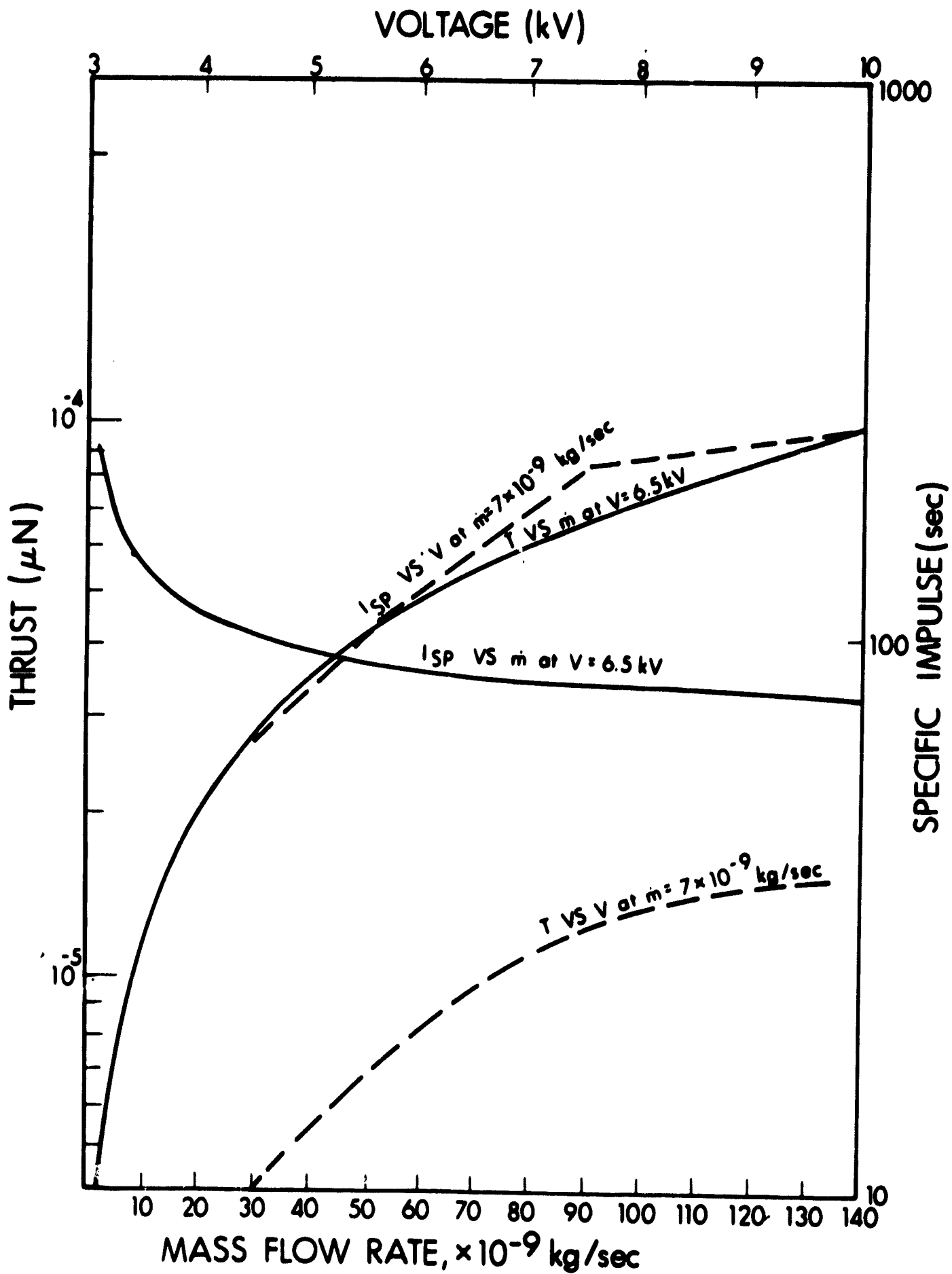


Figure 113. Relationship of Thrust and Specific Impulse to Mass Flow Rate and Needle Voltage

will be sufficient to determine specific impulse and power to thrust ratios. The voltage and mass flow rate can then be adjusted accordingly to obtain the desired performance.

2.4.4.2 Feed System

Three basic approaches are available for a flight reliable feed system. The classification of these system types are:

- a. Positive Displacement System
- b. Positive Pressure System
- c. Capillary Feed System

The various physical means of implementing any one of these systems may depend on the choice of control parameters and propellant fluid. Clearly the design problem is optimizing operation utilizing a knowledge of parameters involved.

The present state-of-the-art for colloid thrusters precludes the use of capillary feed systems except for the possible use of liquid metals which in turn generally produces ions. Since capillary feed systems are essentially self-sustaining, they are ideal for spraying of liquid metals at high currents with no applied external pressure. Instead of producing heavy droplets, liquid metals generate higher efficiency ion beams with high specific impulses. Until suitable accel-decel mechanisms are developed colloid thrusters using liquid metal propellants will remain outside the useful colloid range of 700-1500 sec. Organic solvents such as glycerol, a common colloid thruster propellant, have been fed by capillary means but this method is seriously limited by the lack of control and low current emission. One advantage of a capillary feed system is that it eliminates the need for valves or pressure regulators. For liquid metal feed systems the technology of surface tension feed systems is a highly developed one.

A positive displacement system differs essentially from a positive pressure system in that the volume of fluid displaced remains constant, not the pressure. For example, small changes in system volume due to temperature variations or accumulative plugging will result in pressure changes. Additional feedback controls would be needed for changing the rate of displacement to maintain constant pressure. For this reason, a positive pressure system seems at present to be a more favorable choice for controlling propellant feed. One advantage of the positive displacement system is that it determines the mass flow rate of propellant fluid accurately.

An example of a positive pressure feed system, developed by TRW Systems, involves the use of a spring loaded device in conjunction with a shut off valve (Ref. 2-12). The spring applies a constant pressure to a diaphragm housing the propellant fluid and compensates for changes in system volume. This is a simple device and is adaptable to any compatible fluid requiring only changes in spring pressure. This system has the disadvantage of making it necessary to pre-select a given level of pressure for operation.

Another approach, is to replace the spring concept with a medium whose pressure can vary. Briefly, a material whose vapor pressure varies with temperature in a desired range can be utilized to provide the force necessary to displace a diaphragm. A number of suitable organic and inorganic materials are available with the proper vapor pressure characteristics. Suitable choice depends on the feed pressure range, minimum variation with changes in ambient temperature and the propellant fluid itself. Basically, a system using this principle has the feed pressure controlled by temperature. At this time a simple on-off valve seems desirable over check valves and flow regulators due to acceleration forces in a mission vehicle. These forces can result in premature fluid displacements and leaks. A disadvantage in a system of this type is that a temperature control requires additional power.

In any feed system selected, certain universal requirements are to be met by the choice of control propellant. These are low vapor pressure and non-corrosiveness. A minimum amount of stored propellant for long missions requires low vapor pressure. That the propellant be non-corrosive is self-explanatory.

2.4.4.3 Neutralization

The use of a bipolar thruster configuration provides neutralization while thrust is produced by both the positive and negative particles. Neutralization is assured by the emission equal positive and negative currents. Good efficiency operation is obtained by matching the specific charge of the two polarity beams. If the charge-to-mass ratio differs greatly between the two polarities, the lower charge-to-mass ratio particles will provide most of the thrust while the other provides the neutralization current. Assuming for simplicity a very narrow charge-to-mass ratio distribution and that the accelerating voltage and the emitted currents are the same for both polarities, the fraction of the total thrust provided by the negative particle is

$$\frac{T_-}{T} = (1 + k^{1/2})^{-1},$$

where k is the ratio of the charge-to-mass ratios $(q/m)_- / (q/m)_+$. When the charge-to-mass ratios are equal the contributions to the thrust are equal. For a 10 percent or greater contribution to the thrust by the negative beam the charge-to-mass ratios should be within two orders of magnitude of each other. This is not a very stringent requirement since less than one order of magnitude difference can readily be achieved which in turn provides better than a 25 percent contribution.

For operation of a single polarity positive emission an electron emission neutralizer can be used. The power for a neutralizer emitting hundreds of μ A of electrons is several watts. This is in the power consumption range of a thruster operating at a couple of μ lb. It could be advantageous to use a negative emitter to neutralize even with a mismatch of the charge-to-mass ratios ($k > 100$).

2.4.4.4 Telemetry

For a bipolar colloid thruster (no external neutralization required) operating with an extractor electrode and a temperature controlled feed system, the following telemetry signals should be provided for minimum operation:

- a. Positive and negative voltages
- b. Positive and negative currents
- c. Feed system control temperature

In addition to these signals, a failure diagnostic operation should include signals for the extractor current, temperature of thruster housing or extractor, and signals indicating on and off status of any feed system valve.

For maximum research conditions it would be desirable to have additional instrumentation in the form of thermocouples to examine the temperatures developed near the positive and negative needles and transducers to determine mechanical durability of a system during launching operations. Although suitable mass flow detectors for these low flow rates have not been developed to date, it would be advantageous to receive telemetry data on this parameter. This would be important in analyzing the operational characteristics such as specific impulse and thrust.

2.5 MPD ARC JET ENGINES

2.5.1 INTRODUCTION

The magnetoplasmadynamic (MPD) arc jet is an electromagnetic engine for space propulsion under development in several laboratories. The following discussion is based on the EOS MPD arc jet which is referred to as ALPHA (Alkali Plasma Hall Accelerator). The evolution of the ALPHA thruster is shown in Fig. 114.

The ALPHA engine is a unique type of MPD arc jet thruster. In this device an axisymmetric arc discharge is maintained between an anode and a buffered cathode in the presence of solenoidal magnetic field. Lithium or an alternate alkali metal is used as the propellant. The propellant is vaporized and injected through an annular slot in the anode into the "interaction zone," characterized by nearly parallel magnetic flux lines. Here the propellant is ionized by electron-atom collisions. The resultant electrically neutral plasma then flows through a region of diverging magnetic flux lines, designated the "electromagnetic nozzle," where it is accelerated to produce thrust. A brief and somewhat simplified explanation of the acceleration mechanism is presented in the following subsection. A more complete discussion appears in Ref. 2-21.

2.5.2 ENGINE MECHANISMS

An electromagnetic thruster may accelerate particles in any or all of the following different ways:

1. By gas dynamic thrust,

$$F_1 = \int p \, dA;$$

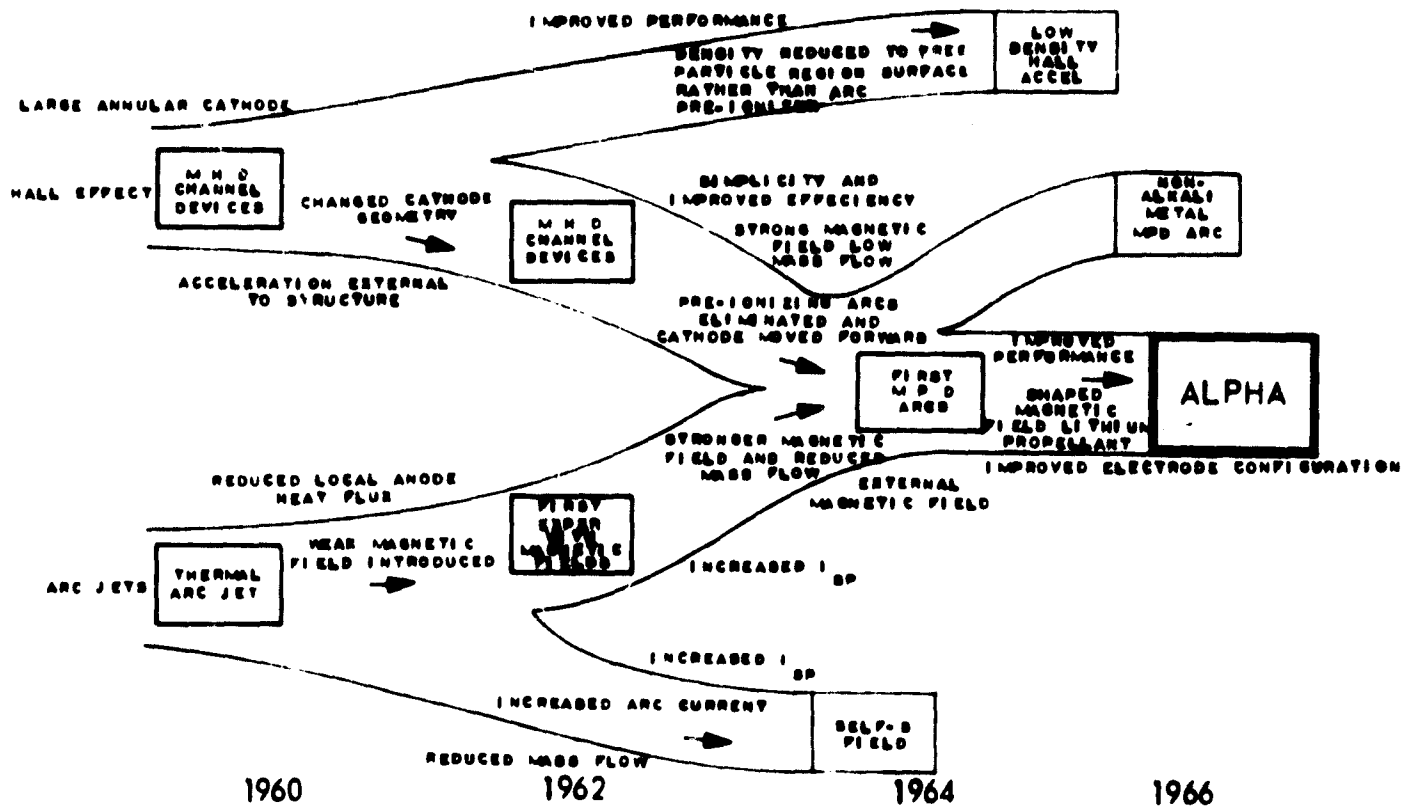


Figure 114. Evolution of Alpha Concept

2. By self-magnetic field thrust,

$$F_2 = \frac{\mu_0 I^2}{4\pi} \left(\frac{3}{4} + \ln \frac{A_a}{A_c} \right); \text{ and}$$

3. By Hall current interaction, wherein the thrust,

$$F_3 = \dot{m}_a \sqrt{\frac{2 Z e V_{AD}}{m_a}},$$

is obtained by accelerating the propellant ions through the potential drop between the anode and the downstream plasma.

Definitions:

$F_1, F_2,$ and F_3 = force (N)

p = pressure (N/m^2)

A = area (m^2)

μ_0 = permeability of free space = $4\pi \times \frac{10^7 W}{\text{amp}^2/\text{meter}}$

I = current

\ln = log

$\frac{A_a}{A_c}$ = cross section ratio

\dot{m} = mass flow rate (kg/sec)

Z = mean degree of ionization

e = electronic charge (C)

m_a = mass of an atom (kg)

V_{AD} = potential drop, anode-to-downstream plasma (V)

In ALPHA, the Hall mechanism predominates. This mechanism can be described in either of the following two equivalent ways:

- a. A neutral plasma is accelerated by the Lorentz force due to the interaction of an azimuthal Hall current with the radial component of the applied magnetic field.
- b. Ions are electrostatically accelerated in the electric field through the electrons which are trapped in an applied magnetic field.

An axial component of the electric field accelerates the ions in the downstream direction and causes an equal magnitude reaction upon the electrons in the upstream direction. This upstream force upon the electrons is balanced by a downstream Lorentz ($\vec{j} \times \vec{B}$) magnetic force. In the thruster, the net acceleration force upon the plasma is primarily due to a Lorentz force and is proportional to the product of an azimuthal Hall current and the radial component of an applied magnetic field.

The plasma in the region downstream of the electrodes consists of several distinguishable zones. About the axis is a highly luminous cathode jet. From diagnostic studies it has been found that this jet carries (conventional) current to the cathode. Surrounding the cathode jet is an anode sheath which carries the current away from the anode. Also there is a downstream zone in which there is no current and which consists of a neutral beam of accelerated plasma. The structure of the plasma, which is easily visible to an observer, is helpful in explaining the mechanisms.

The primary purpose of the cathode jet is to act as a virtual cathode. Very large electron energies occur in the cathode jet; it is the only place where excitation of ions is visible. The electron energy can support a potential drop from the cathode end of the cathode jet into the downstream zone, providing some acceleration of the ions in the cathode jet. Energy dissipated by currents in the cathode jet appears mostly in the electrons. This in turn provides ionization power, some beam kinetic power, and electrode losses.

In the anode sheath region, ions are formed by electron-atom collisions. These collisions occur most frequently near the anode, where electron energies are large. Ions formed in this region accelerate in the electric fields toward the downstream zone. The energy they achieve is determined primarily from the anode-to-downstream plasma potential drop, V_{AD} .

From a functional standpoint, the volume of plasma may be divided into two regions: the energy addition or interaction region, where the arc currents flow, and the expansion region or electromagnetic nozzle, where the particle energy is transformed into beam kinetic energy. In the interaction region the propellant is injected at the anode and mostly ionized where the electric potential is close to the anode potential. The ions move radially inward and eventually join up with electrons from the cathode jet. This motion represents a current of magnitude $Z |e| \dot{m}_{Li}/m_a$, and the ions acquire an energy equal to $Z |e| V_{AD}$. As the ions move radially inward the $j_r B_z$ force spins the ions in the azimuthal direction. This motion establishes the potential V_{AD} , which is determined by

$$V_{AD} = \int_{R_1}^{R_A} V_{\theta} B_z dr.$$

The difference between the arc current and $Z |e| \dot{m}_{Li}/m_a$ represents the amount of electron current which flows across the magnetic field lines. The power represented by $\left[1 - (Z |e| \dot{m}_{Li}/m_a) \right] V_{AD}$ goes into ionization, radiation and anode losses and is not recoverable as beam kinetic power.

The power loss in the virtual cathode, given by IV_{CD} , is also dissipated by electron conduction and goes entirely into losses, e.g., cathode power loss, radiation, and ionization of material in the cathode jet.

The electromagnetic nozzle is the region of diverging magnetic field in which the plasma is accelerated axially. If sufficient energy per particle has been introduced to the plasma, the electromagnetic nozzle can convert this energy to axial kinetic energy in a manner similar to the energy conversion process in a solid wall nozzle. The electromagnetic nozzle in ALPHA is distinguished from a "pure" magnetic nozzle in that there exists a strong radial electric field. The ions gyrate in the cyclotron direction and rotate about the axis of symmetry in the anti-cyclotron direction, the net motion being a hypocycloidal trajectory. The pure magnetic nozzle, by contrast, has no radial electric fields; the ions simply rotate about the magnetic flux lines in the cyclotron direction, the energy conversion process being essentially the inverse of a reflection at a magnetic mirror.

2.5.3 ADVANTAGES OF ALPHA

The chief advantages of ALPHA over other types of electric propulsion system are discussed below, roughly in the order of their importance.

2.5.3.1 Thrust Density

The fact that ALPHA can produce thrust densities 100 to 1000 times greater than other types of high performance electric thruster is certainly its single most significant advantage. The importance of this advantage tends to increase with increasing power level. Generally speaking, the more ambitious the mission contemplated, the higher the requisite thrust and electrical power. Even at moderate thrust and power levels, however, a space charge limited thruster such as an ion engine must actually comprise a matrix of many separate thrusters. The required area of this array is usually rather large for most applications beyond the microthruster regime. Moreover, it tends to scale linearly with thrust or power, since scaling beyond a few kilowatts would be achieved by merely adding more thruster units. The

difficulties in fabricating, packaging, deploying and maneuvering such huge arrays are well known. Indeed, these difficulties are at least partially responsible for the sustained widespread interest in developing the technology of the MPD arc jet thruster. Not only is the latter extremely compact, but more significantly, its size is a relatively insensitive function of thrust or power.

2.5.3.2 Specific Impulse Range

Competitive types of electric thruster, as well as ALPHA, are capable of performing efficiently at high specific impulse (I_{sp}). ALPHA, however, is unique (at least among those thrusters likely to be operational within the next decade) in that it can perform with relatively high efficiency even at I_{sp} values as low as 1500 seconds. The efficiencies of alternate types of engine are so low in the I_{sp} range between 1500 and 3500 seconds that most of this range is, from a practical standpoint, inaccessible to them. However, largely as a result of the projected state-of-the-art of electrical powerplant technology, it happens that the optimum I_{sp} for a wide variety of astronautic missions contemplated for the next decade lies precisely within this I_{sp} range.

2.5.3.3 Power Conditioning

An MPD arc jet characteristically requires dc power at about 100 volts. Consequently, it needs much simpler and less massive power conditioning equipment than thrusters requiring thousands of volts. Indeed, for many applications, especially those where the primary power is provided by solar panels, the necessity of transformers may be entirely obviated by matching the electrical power output directly to the thruster (arc and magnet) inputs. Such rudimentary power conditioning as will be required would therefore consist mostly of the indispensable but relatively lightweight switching equipment and logic circuitry needed for thruster control.

2.5.3.4 Mechanical Construction

An MPD arc jet is not the only type of high performance electric thruster having no moving parts. The ALPHA, however, has very few parts altogether. Basically, it consists of an anode, a buffered cathode, a magnet and a simple feed system. Moreover, each component is itself strikingly simple, mechanically rugged, and relatively free of critical tolerances. While it is certainly possible that an actual flight configuration ALPHA thruster might incorporate a number of features which increase the sophistication of the device at the price of added complexity, it is nevertheless unlikely that any of the intrinsic ruggedness of the engine components would have to be sacrificed.

2.5.3.5 Versatility

Though lithium or an alternate alkali metal is preferred (in order to minimize frozen flow losses), ALPHA can be operated with almost any propellant. Also, the thrust can be throttled and the I_{sp} may be varied during a mission. The flexibility of the thruster is remarkable in another respect: It is capable of operating in a nested sequence of different modes and so provide a type of reliability otherwise unattainable. Thus, it can function as a Hall current accelerator, an electrothermal arc jet (should its magnet system fail), a resistojet or cold gas thruster (should the arc jet fail too), and even, with appropriate choice of propellant, as a mono-or bi-propellant chemical rocket.

Finally, since ALPHA offers a unique combination of uncluttered geometry with virtually unlimited variety in the choice of propellant, it is possible to imagine a hybrid chemical/electric thruster with several interesting applications. One could thus have a single thruster capable of operating in the "electric mode" at high I_{sp} for extended periods of time, but which could also operate in the "chemical mode" at relatively low I_{sp} whenever short bursts of high thrust are desired. This feature

might be valuable for missions requiring electric propulsion for a heliocentric trajectory followed by chemical propulsion for a braking maneuver to effect planetary capture. Another potential application might be a geocentric "patrol" mission (electric mode) with "inspection" or "evasive" capability (chemical mode). Of course the same types of mission could also be performed with another ALPHA variant: a hybrid MPD arc jet/thermal arc jet thruster. Here too the device would function primarily as a steady state ALPHA engine, but could also deliver short bursts of relatively high thrust.

2.5.4 BACKGROUND AND HISTORY

2.5.4.1 Fundamental Problems

Present steady-state electromagnetic accelerators have evolved through experiments which fused arc jet technology and Hall current acceleration schemes. The history of this process is shown schematically in Fig. 114. Since engine development took place without having a well-developed theoretical foundation on which to build, the research into these devices has been difficult and open to criticism from many quarters. In particular, a number of important questions concerning the physical feasibility of the device were raised. First, thrust and mass flow measurements indicated that exhaust velocities were being obtained which were higher than could be generated by accelerating singly-charged ions through the arc potential. The possibility that this "anomalous" velocity could be achieved was questioned. Second, some measurements were made which indicated that the ambient gas in the test chamber was being recirculated by the accelerator discharge. Arguments were then advanced that this was probably happening in all of the tests where good performance had been reported. Some strength was added to these arguments by the fact that this phenomenon could be invoked to explain the "anomalous" behavior. Third, most groups that have tested MPD arc jet thrusters have found that at one time or another discharges occurred between the vacuum tank and the electrodes. ^{2-22 through 2-24}

Some people then argued that such discharges might perhaps be essential to the operation of the engine and that once this discharge path was eliminated, either by using an insulated tank or a very large tank, then the engine would be forced to operate in an entirely different discharge mode. Because of this possible extraneous discharge path, it was also argued that any performance measurements made to date might be greatly in error. Beyond those scientific feasibility problems, a number of engineering questions were raised. Many doubted that a low power loss, accurate and reliable feed system could ever be developed for supplying lithium propellant to the engine. Later, once electric propulsion appeared to be wedded to a solar cell power source for many years to come, the possible contamination of solar cell surfaces by lithium or other alkali metals was used as an argument to rule out any MPD thrusters using alkali metal propellants.

2.5.4.2 MPD Arc Jet Program at EOS

Despite the foregoing problems, an MPD arc jet propulsion system has been developed that has shown impressive gains in performance over the past three years.

The main technical goals of the program are attainment of an overall efficiency of 50% over the entire I_{sp} range from 1500 to 6000 seconds and the demonstration of an engine operating lifetime of 500 hours. Significant technological steps which led to the present status include

- a. Development of technology for the routine handling of alkali metals.
- b. Development of vacuum test chamber techniques.

Establishing that engine operating characteristics or performance are not a function of test chamber pressure if the pressure is kept below 1 micron (10^{-3} torr). Measurements were made down to pressures as low as 2×10^{-7} torr. 2-22

c. Developing instrumentation including:

- (1) Pressure transducers and high temperature thermocouples compatible with lithium
- (2) High sensitivity thrust balance
- (3) Local calorimetric energy flux probe for use in a condensible medium
- (4) Total beam energy segmented calorimeter
- (5) Optical phototracer velocity measurement technique
- (6) Three-dimensional Hall effect, magnetic field and current density probe
- (7) Spectroscopic Doppler axial and azimuthal velocity measurement techniques.

A number of the foregoing diagnostic techniques, such as particle velocity measurements in the exhaust beam using spectroscopy and time of flight measurements phenomenological theory, were developed in which an important new concept, the "effective mass", was postulated, 2-25 through 2-28. The measurements and theory clarified the problems associated with "entrained mass" and developed criteria to determine when gas recirculation is likely to occur.

- d. Wall Effects. Tests were conducted in tanks of various shapes and sizes with the same engine operating at the same mass flow, arc current and magnet current. Identical performance was achieved. Other tests were conducted in which a target was placed so as to intersect the exhaust beam. When the targets were situated close to the engine (less than 2 ft away) arcing to the target was observed. When this occurred, measurements of thrust, arc voltage, etc., were unsteady and unreliable. By moving the target downstream (more than 3 ft from the cathode tip) the arcing to the target could be stopped (i.e., no attachment points could be seen on the target, voltage between target and anode became steady, and all other instrumentation became steady). These tests indicate that the size of the vacuum tank can affect the discharge path but that once the tank becomes large enough, no interference between the discharge and the tank walls occurs.
- e. Attainment of 100-Hour Thruster Lifetime. The successful completion in January 1967 of an endurance test exceeding 110 hours (100 hours of uninterrupted operation with lithium) was an important milestone for the ALPHA program. This test resulted in no discernible erosion or other damage to the anode, and remarkably little erosion of the cathode and buffer (virtually all of which occurred during several preliminary startups and shutdowns). Before-and-after photographs are shown in Refs. 2-27 and 2-28.

- f. Lithium Feed System Development. Two types of lithium feed systems were developed during the ALPHA program. The earlier one was a bellows-operated device (Refs. 2-25 and 2-29). The mechanical complexity of this type of system posed formidable engineering difficulties in calibration and operation for extended periods of time. It nevertheless represented a great step forward in the overall program inasmuch as it demonstrated that lithium could be stored, heated and transferred in a manner useful for thruster applications.

The second type of lithium feed system was developed to circumvent some of the intrinsic disadvantages of the bellows device. The new system, a gas-actuated feed, underwent an evolution of its own (Refs. 2-22, 2-27, and 2-28) and is still being used. The key feature of this device is the pressurization of the lithium reservoir by argon, the latter constituting the "driver gas" whose pressure regulation serves to control the mass flow rate of lithium vapor through a sonic orifice inside the anode. The chief advantages of the gas-actuated feed system are its mechanical and functional simplicity and the regenerative economies afforded by using some of the waste heat in the anode (which would otherwise have to be radiated away) to vaporize the molten lithium enroute from the reservoir to the injection slot within the anode.

2.5.4.3 Component and Overall System Design Improvements

- a. Design of Electrodes and Insulators for Structural Integrity. Learning how to build and cool thruster components and how to put them together so as to be capable of withstanding conditions in the vicinity of the arc discharge was a gradual and painstaking process. Many problems involving heat transfer, fabrication and joining techniques for high-temperature materials compatible with alkali metals, and of course, optimum configuration, all had to be solved during the course of thruster development.
- b. Introduction of the Buffer and Buffer Gas. Early in the program a decision was made to accept the penalties associated with the introduction of a "buffer" as a separate new component of the arc head. This decision represents an important milestone because it marks a transition to relatively stable and efficient arc operation with greatly reduced cathode erosion. Essentially, a buffer is a metal enclosure surrounding the cylindrical cathode along most of its length and terminating near the (generally conical) cathode tip. A steady flow of "buffer gas" (which may be thought of as a secondary propellant) is maintained within the thin annular region between the

cathode and the buffer. This gas (usually hydrogen) flows downstream past the cathode tip, where it is finally injected into the arc discharge region. Its mass flow rate is kept below 10% of that of the lithium "primary propellant". Although the buffer and buffer gas actually perform several functions, the main one is to increase the pressure at the cathode tip, thereby promoting stable "point attachment" of the arc. Without buffering, the arc was found to attach sometimes at a diffuse spot and sometimes at a point, and to shift erratically between the two modes. The "diffuse attachment" mode proved to be highly undesirable because of excessive power loss to the cathode and erosion of cathode material.

- c. Improvement of the Magnetic Field Configuration. The configuration of the applied magnetic field has undergone a gradual evolution, partly due to trial-and-error experimentation guided by intuitive judgement and partly as a consequence of predictions based on the analysis of acceleration mechanisms. Each improvement in the field shape has resulted in some reduction in the required magnet power and a corresponding increase in overall thruster efficiency. While none of these modifications can be considered particularly dramatic, the more salient developments included the addition of a second electromagnet, thus extending the magnetic nozzle further downstream of the anode, and the discovery of the importance of the gradient of the magnetic induction at the axial location of the cathode tip. No attempt was made to optimize the electromagnets themselves. It was recognized at the outset that, once the optimum field configuration could be determined, it would then be a straightforward matter to design the best magnet to generate the desired field. Hence it was decided to defer (to a future advanced development program phase) the realization of performance improvements deriving exclusively from the optimization of solenoid construction, and to concentrate instead upon studying the interactions between the geometry of the applied magnetic field and the efficiency of the accelerator.
- d. Radiation-Cooling of the Anode. One of the more important milestones of the program was the removal of the anode's dependence upon a convective cooling loop. This was done by conducting most of the anode heat into an adjacent graphite radiator, and by conducting the rest into the vaporizer, where it is largely absorbed by the lithium propellant. Despite some difficulties introduced by the resultant coupling of the maximum propellant flow rate to the arc current, this technique has worked out quite well.

- e. Development of IAC. The most recent series of thruster design embodies several modifications aimed at reducing power losses and increasing the arc voltage (so as to provide a greater potential drop through which to accelerate the ions). Several such "IAC" (Isolated Anode Configuration) thrusters have been successfully tested. The new design is characterized by the isolation of the anode from the cathode-buffer assembly by physical separation and by removal of insulator material. This change was motivated by the finding from tests of earlier model thrusters that a substantial amount of heat was being conducted across the insulator from the anode into the buffer and showing up as a temperature rise in the buffer coolant. A second feature of the IAC is the integration of the "hot-liner" inside the downstream magnet housing with the anode itself. The reason for this stems from the finding that previously much more heat was lost to the hot-liner than was lost to the anode. Since the two components always tended to operate at very nearly the same potential anyway, it was deemed practical to combine them into a single unit and thereby facilitate heat conduction from the liner into the anode, thus increasing the heat available for vaporizing lithium. A third feature of the IAC is the increased ratio of the diameter of the anode to that of the cathode-buffer assembly. (Analysis had indicated that the maximum arc potential should be a sensitive function of this ratio.) Finally, a component designated the "plasma isolator" has been incorporated into the IAC design. This device consists of a number of concentric rings, each of which is electrically insulated from adjacent rings as well as from the vacuum chamber and other support structure. This provides a means of mechanically supporting the cathode-buffer assembly without shorting out the radial potential gradients in the plasma. Another function of the plasma isolator is to intercept back-scattered particles, particularly ions gyrating upstream along magnetic flux lines.

2.5.5 CURRENT DEVELOPMENT STATUS OF THE MPD ARC JET

2.5.5.1 Engine Characteristics and Performance

The best performance to date has been achieved with IAC-type thrusters. Figure 115 is a typical drawing of model IAC-3. (Recent data from prior tests are tabulated and plotted in Ref. 2-28.) The arc voltage versus ion velocity is shown in Fig. 116, and the power-to-thrust ratio is

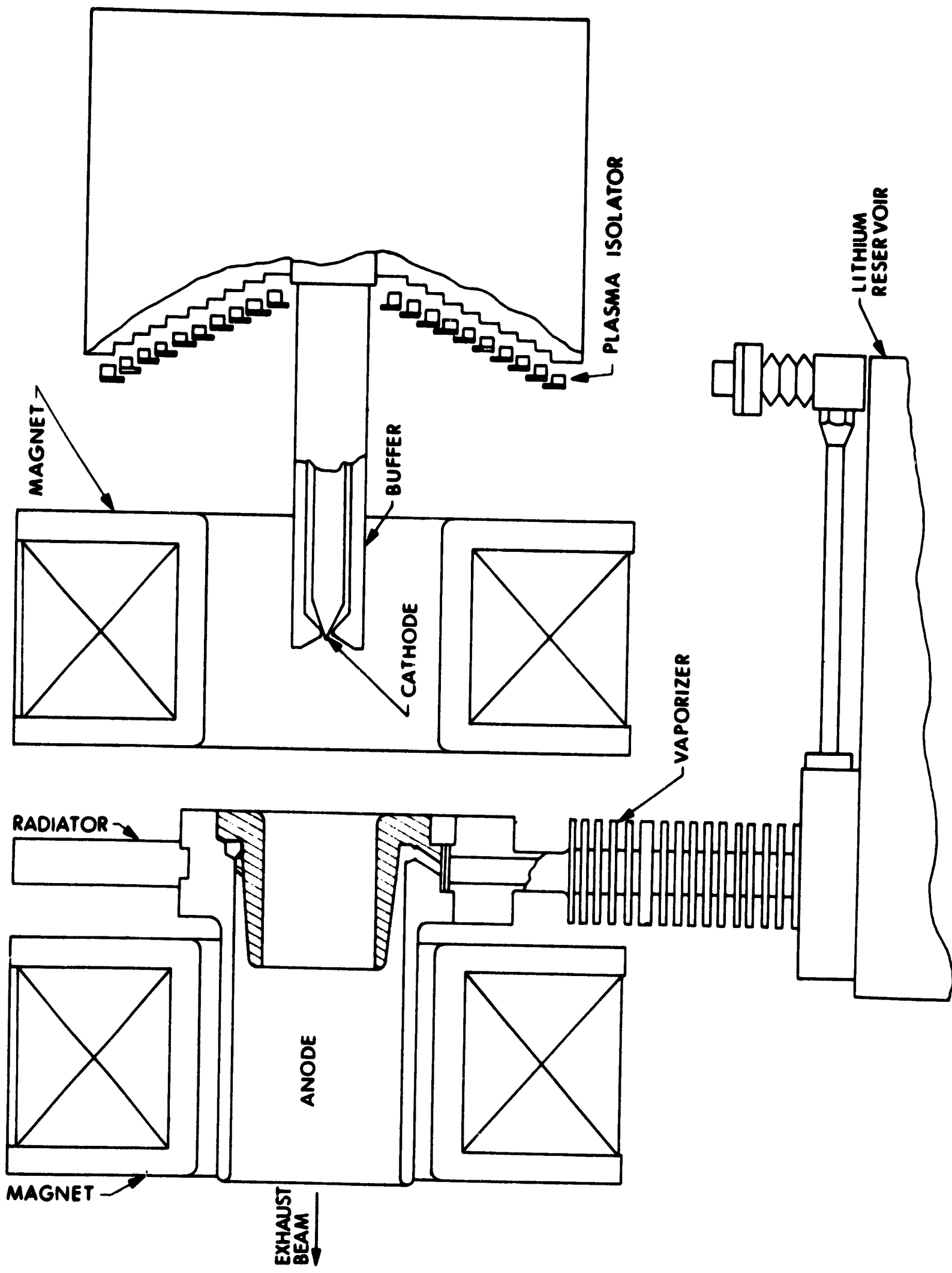


Figure 115. IAC-3 Thruster, Assembly Drawing

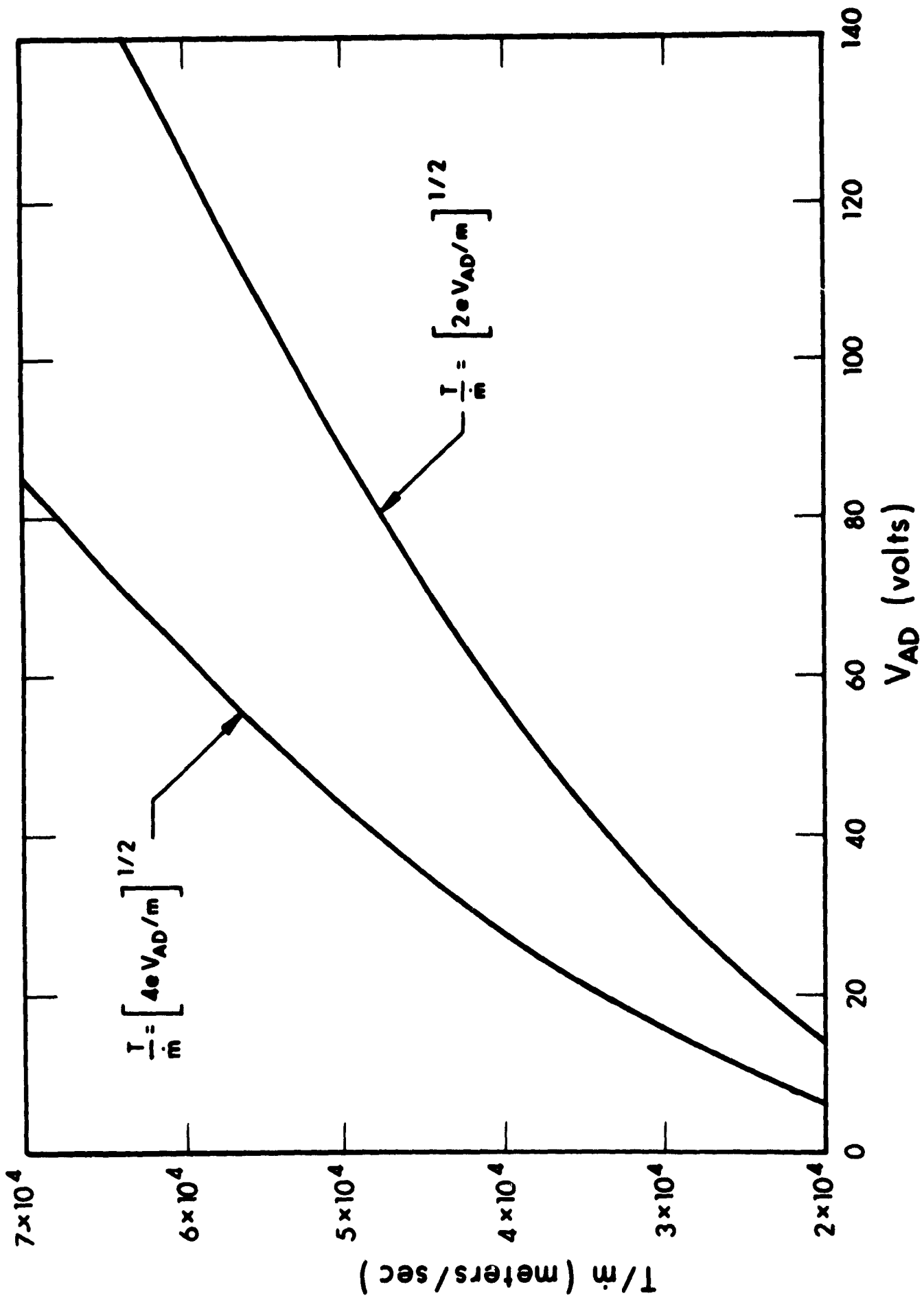


Figure 116. Ion Velocity versus Accelerating Potential

plotted as a function of specific impulse in Fig. 117. It is seen that thrust efficiencies (values of beam kinetic power divided by arc power) as high as 51% and overall efficiencies (values of beam kinetic power divided by arc plus magnet power) as high as 44% have been measured. The values reported for magnet power, incidentally, are those for the actual magnets used. No attempt has yet been made to construct and use optimized magnets. When this is finally done, it is anticipated that the required magnet power will drop appreciably. The thermal efficiency, defined as $1 - (\text{power loss to the electrodes}/\text{arc power})$, reached as high as 68%. Slightly higher values (over 70%) had occasionally been recorded in earlier runs. For the IAC tests, the arc power was typically 20-30 kW, and the lithium mass flow rate was usually 10-13 mg/sec. The thrust and specific impulse for the most part varied between 0.44 and 0.59 newtons and 3000 and 4000 sec, respectively.

The power per unit thrust (P/T) generally exceeded the best (i.e., minimum) values attained in pre-IAC tests, due mostly to operation at somewhat higher specific impulse. In the test of the IAC-1 thruster (Run 901), for example, the minimum values of P_{arc}/T and $(P_{\text{arc}} + P_{\text{magnet}})/T$ were 209 and 250 kW/lb, respectively. This compares with minima of 168 and 208 kW/lb obtained earlier in 1967 in a test (Run 736) of the thruster configuration designated LAJ-AF-CG-2C, GAF-V-2.

In evaluating the performance achieved with ALPHA engines, it should be borne in mind that primary emphasis in the test program has been placed upon checking out new ideas, correlating measurements with theory, and in general attempting to further the understanding of the acceleration mechanisms and their interactions. Seldom have two consecutive tests been made with identical thrusters; continual design modification has been the rule rather than the exception. It is therefore clear that the current development status of ALPHA has not

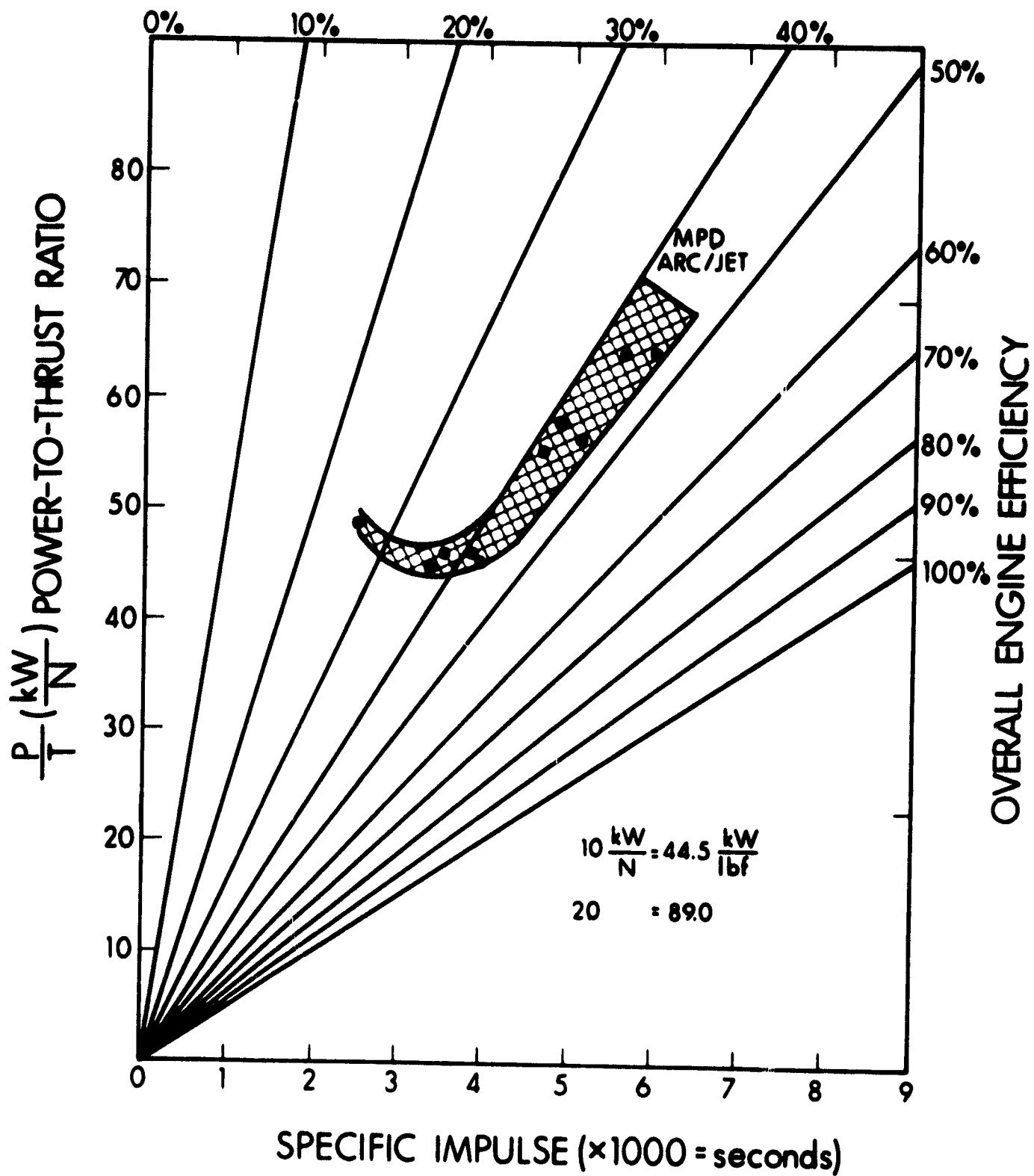


Figure 117. MPD Arc Jet Power-to-Thrust Ratio versus Specific Impulse

yet arrived at the point where a specific design has been "frozen", so that efforts may thenceforth be concentrated upon refining it in order to extract the maximum possible performance.

It is appropriate to consider some of the characteristics of recent laboratory model thrusters other than gross performance data. This will serve to bracket the more important "system" aspects of recent thruster configurations with respect to earlier models on the one hand and with respect to goals for the immediate future on the other.

The longest endurance test of an ALPHA thruster occurred at the beginning of 1967 (Run 732). The total elapsed time of arc jet operation was 111 hours, 26 seconds, of which 110 hours, 13 seconds were with lithium propellant, and over 100 hours were uninterrupted. Termination of the run was voluntary, and the electrodes evidenced little or no discernible erosion. This test was conducted with thruster model LAJ-AF-CG-2B, GAF-IV-1 (see Fig. 118). It is worth noting that more recent designs, especially IAC-2 and IAC-3 (see Fig. 115), are much less "cluttered" in the immediate vicinity of the arc discharge, and more significantly, most of the (boron nitride) insulator material has been removed. Past experience has shown that the insulators tend to be the components most susceptible to erosion and cracking. For these reasons it is felt that the prognosis for greatly extending the demonstrated thruster lifetime in the near future is highly encouraging. A 500 hour life test is scheduled for next year. However, there does not appear to be any technical reason why tests of much longer duration could not be attempted earlier if it were considered useful to do so.

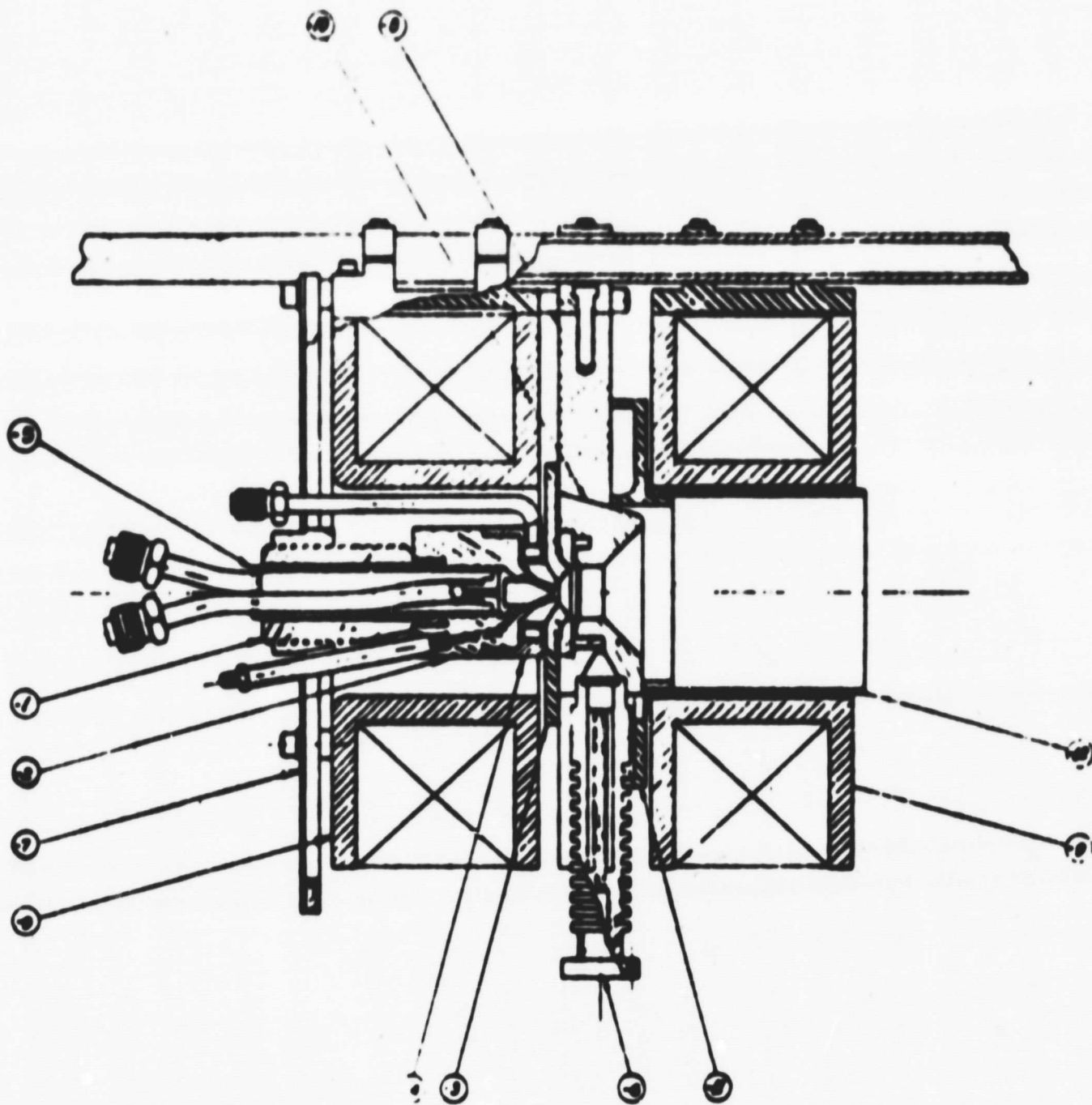
The present feed system design and its relationship to past and projected developments is another significant aspect of the current status of ALPHA. As mentioned previously, the undesirable consequences of attaching the lithium vaporizer directly to the anode proved troublesome

because of the concomitant coupling of the maximum propellant flow rate to the arc current. The practical significance of this coupling was that it tended to limit operation to relatively low flow rates. Extrapolations from plots of measured thrust per unit arc current and other test data, as well as analysis, had indicated that the thruster would function at higher efficiency if the propellant mass flow could be increased. This was finally accomplished by redesigning the anode and the vaporizer and paying particular attention to the heat conduction path from the former to the latter. Several other difficulties with the gas-actuated feed system were encountered. Some of these proved sufficiently recalcitrant to necessitate significant detours in the ALPHA program. The most serious ones were:

- a. The problems of anode cracking due to excessive thermal stress during temperature cycling.
- b. The frustrations of repeatedly unsuccessful attempts to obtain a leak-tight seal at the anode/vaporizer braze joint.
- c. The subtleties of mass flow rate calibration.

All of these problems have finally been solved, and the present feed system design is considered satisfactory for laboratory test purposes. In order to test an ALPHA engine in space, it will, of course, be necessary to have a feed system capable of operating under zero-gravity conditions. It is unlikely, however, that this next step in feed system development will entail any radical departures from the technology of the present gas-actuated feed. Instead, it is more probable that zero-g capability will be provided simply by using capillary forces to collect the propellant in the reservoir, rather than gravity. Once collected, however, pressure forces would still be used to drive the propellant into the vaporizer.

The radiation cooling of the arc head components is another area in which the present development status has already advanced to a point where relatively little additional work will be required to pass from the laboratory test phase to flight hardware. For more than a year, thruster



		O 501		
1	12	-500	NOY LINED	MOLT TUNGSTEN
1	11	-500	MAGNET INSULATOR	BORON NITRIDE
1	10	-500	ANODE	TUNGSTEN
0	0	001	ELECTROMAGNET	COBALT IRON
1	0	000	RADIATOR	GRAPHITE
1	7	-500	SEEDING PLATE	316 STAINLESS
1	0	-500	VAPORIZER	MOLYBDENUM
1	0	-500	CATHODE ASSEMBLY	TUNGSTEN CARBIDE
1	0	-500	SHIELD ASSEMBLY	
1	0	-500	SHIELD INSULATOR	BORON NITRIDE
1	0	-500	CATHODE	
1	0	-500	NOZZLE	

Figure 118. Thruster Model LAJ-AF-CG-2B with GAF-IV Feed

designs have incorporated a graphite radiator surrounding the anode. Several features and implications of the radiation cooling of the anode should be emphasized: First, the thermal power which must be dissipated from the anode has usually been equal to or greater than the sum of the cathode and buffer power losses. Second, the anode radiator has always been of rather moderate dimensions (see Fig. 118 and the thruster assembly drawings in Ref. 2-28); indeed, the maximum dimension is about equal to the magnet diameter. Finally, this radiator has proven to be so effective in laboratory tests, that occasionally steps had to be taken to decrease its effectiveness in order to keep the anode sufficiently hot to permit adequate heat conduction to the vaporizer! The meaning of these considerations is clear: The apprehension has been expressed in some quarters that a flight model ALPHA thruster is likely to require so much surface area to radiate waste heat that one of its biggest advantages over the ion engine, viz., its enormously higher thrust density, would effectively be forfeit. This apprehension is entirely groundless.

The IAC-3 design (Fig. 115) represents the present state of the art, not so much by virtue of the fact that it happens to be the most recent one, but because it is itself admittedly transitional, in the same sense that the entire program is approaching the threshold of an advanced development phase. In the IAC-3 model, for example, an important step has been taken toward the radiation-cooling of the cathode and buffer. These components are now fabricated of thoriated tungsten throughout most of their length. At least five times as much heat is radiated away as is conducted toward the isolator region, where the copper construction and water cooling loops begin. The reason why complete radiation cooling of the cathode and buffer was not attempted in this design is simply that it was desired to utilize the isolator from the preceding (IAC-2) model, and this isolator required water cooling anyway. The next step, which is the total elimination of all plumbing connections between the arc head and the laboratory environment, is scheduled for the near future.

Other features of a flight model ALPHA thruster which have not yet been incorporated into a laboratory test model include optimized radiation-cooled magnets, components designed specifically for minimum weight, and power conditioning equipment. Present plans call for the design, fabrication and testing of high-efficiency radiation-cooled electromagnets by early March 1968. Component weight reduction and the development of power conditioning equipment have not been considered appropriate tasks under past or present research contracts. Consequently, work in these areas has been deferred until the advent of an advanced development program specifically oriented toward a flight test. Neither effort, however, is considered likely to comprise a major fraction of such a program, since the requisite engineering appears to be rather straightforward.

Current Typical MPD Arc Jet Summary

1. PROPELLANT: Lithium
2. BUFFER GAS: Hydrogen (also used for cold gas attitude control system and for propellant feed pressurization)
3. THRUSTOR SIZE AND WEIGHT: 0.5 ft³; 100 lb
4. MAGNET TYPE: Radiation-cooled electromagnets (Bitter solenoids)
5. NUMBER OF MAGNETS: 2
6. ELECTRODES: Anode, cathode and buffer, all fabricated of thoriated tungsten and radiation cooled
7. FEED SYSTEM: Composite capillary and gas-actuated (hydrogen gas pressurization) zero-gravity type feed. Lithium vapor injected into arc discharge region through annular slot in anode. Heat for lithium vaporization conducted from anode during steady-state operation, but preheated via umbilical prior to booster launch, and via on-board power from lift-off until arc initiation. Lithium vapor flow rate metered by a sonic orifice inside anode.

8. ARC POWER INPUT: 3.7 kW
9. ARC VOLTAGE: 61.7V
10. ARC CURRENT: 60A
11. MAGNET POWER INPUT: 300W
12. MAGNET VOLTAGE: 5V
13. MAGNET CURRENT: 60A
14. THRUST LEVEL: 26.7 millipound
15. POWER-TO-THRUST RATIO: 150 kW/lb (including magnet power)
16. SPECIFIC IMPULSE: A single operating point will be selected in the range of 3000-4000 sec
17. OVERALL THRUSTER EFFICIENCY: 50% (beam kinetic power/total power input to thruster)

2.5.5.2 Power Conditioning and Control

The power conditioning and control for MPD arc jet engines cannot be precisely stated until a flight type engine configuration has been established. This section will discuss the power conditioning and control requirements for flight modified laboratory engine.

A block diagram of the MPD arc jet power supplies is shown in Fig. 119. The diagram shows that the engine requires four power supplies for operation and one or two power supplies for control. This very likely will not be the case in a flight system. The magnets will probably be designed to operate in series from one power supply. Another power supply with a midvoltage center tap will probably supply the cathode, buffer, and anode with power. If no control problems arise, it may even be possible to supply all power requirements (except control) in a series from one power supply or directly from the power source.

The MPD arc jet engine power requirements are shown as a function of specific impulse in Fig. 120.

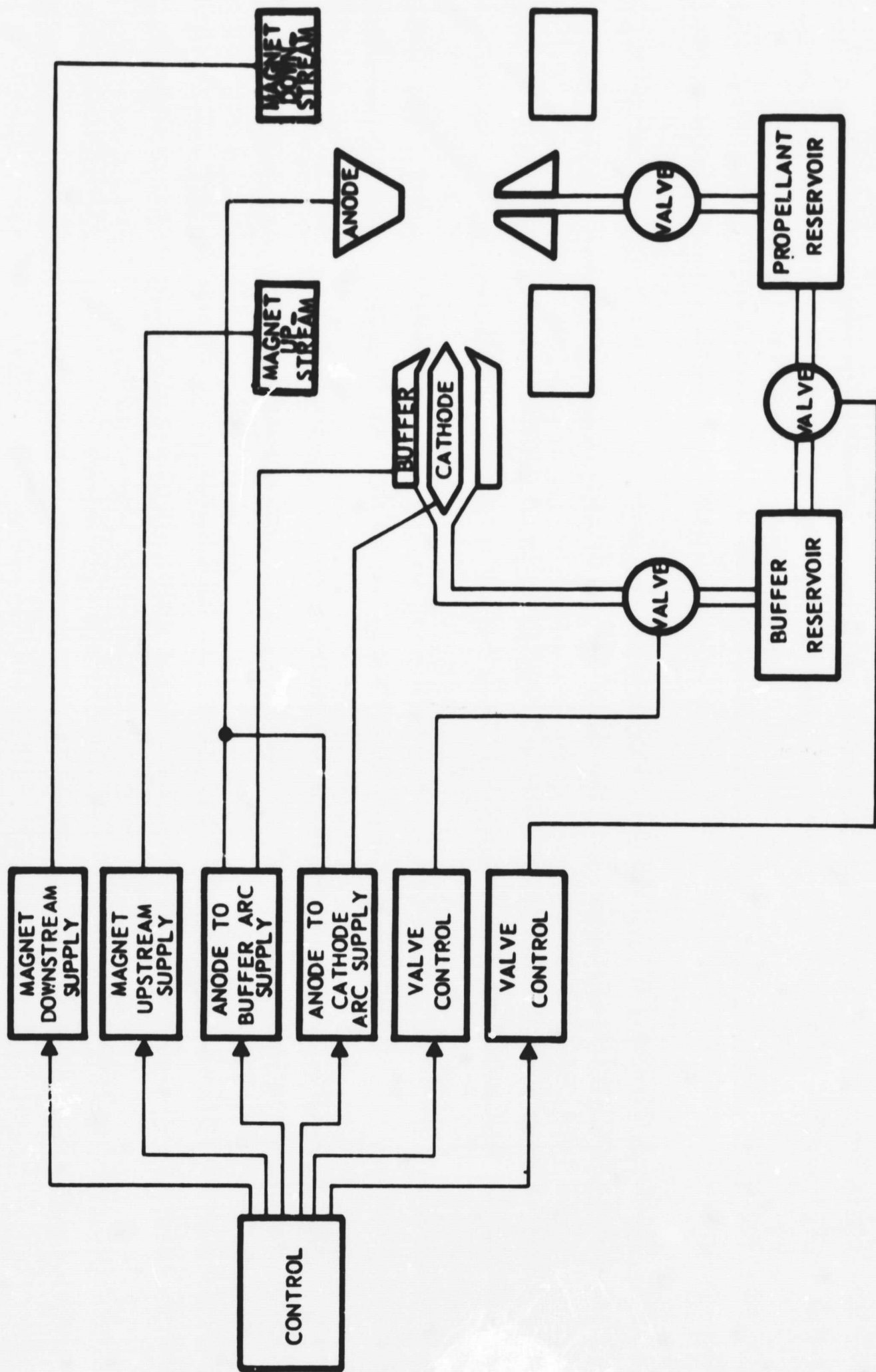


Figure 119. Block Diagram of MPD Arc Jet Power Supplies

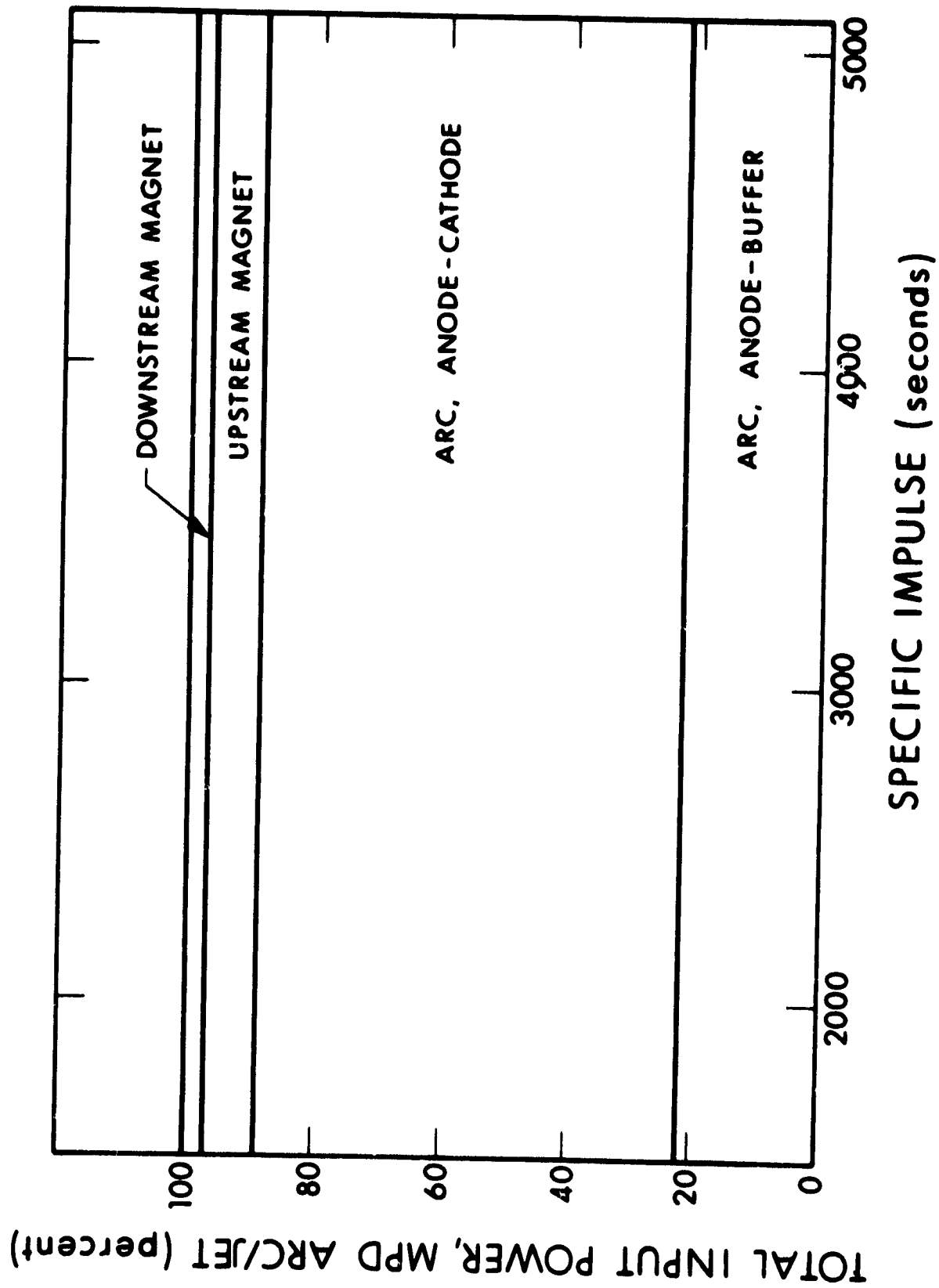


Figure 120. MPD Thruster Model IAC-3

Note that they are constant with respect to specific impulse. All changes in specific impulse, with constant power, are achieved by varying the propellant mass flow rate. This is why the flight MPD arc jet will have a wide range of throttling capability.

Figure 121 shows where the power supplies to the engine go. Since the bottom section of Fig. 121, beam kinetic power, is the only power turned into thrust, this is effectively a graph showing engine efficiency and losses vs specific impulse. When a high mass flow rate feed system is developed, the efficiency should rise substantially for 1500-3000 second specific impulses.

Presently, thruster control can be accomplished by seven external signals. The thruster control commands are delineated in Table XXIII. The feedback control system is discussed appropriately in the projected system development status (Section 2.5.6.3).

2.5.5.3 Discussion of the Experimental Program at EOS

The following statements are intended as a brief summary of the present status of our understanding of the physical processes which take place in an ALPHA engine. In the light of the controversy surrounding certain aspects of the device, the separate items are assigned to one or another category, according as whether the information has been conclusively established by experiment or else has been presumed or inferred from the results of actual measurements.

Power Balance

The beam power was repeatedly measured by means of a segmented calorimeter and also with a local calorimetric energy flux probe which had been built specifically for use in a condensible medium like lithium vapor. The results of these measurements consistently agreed with the difference

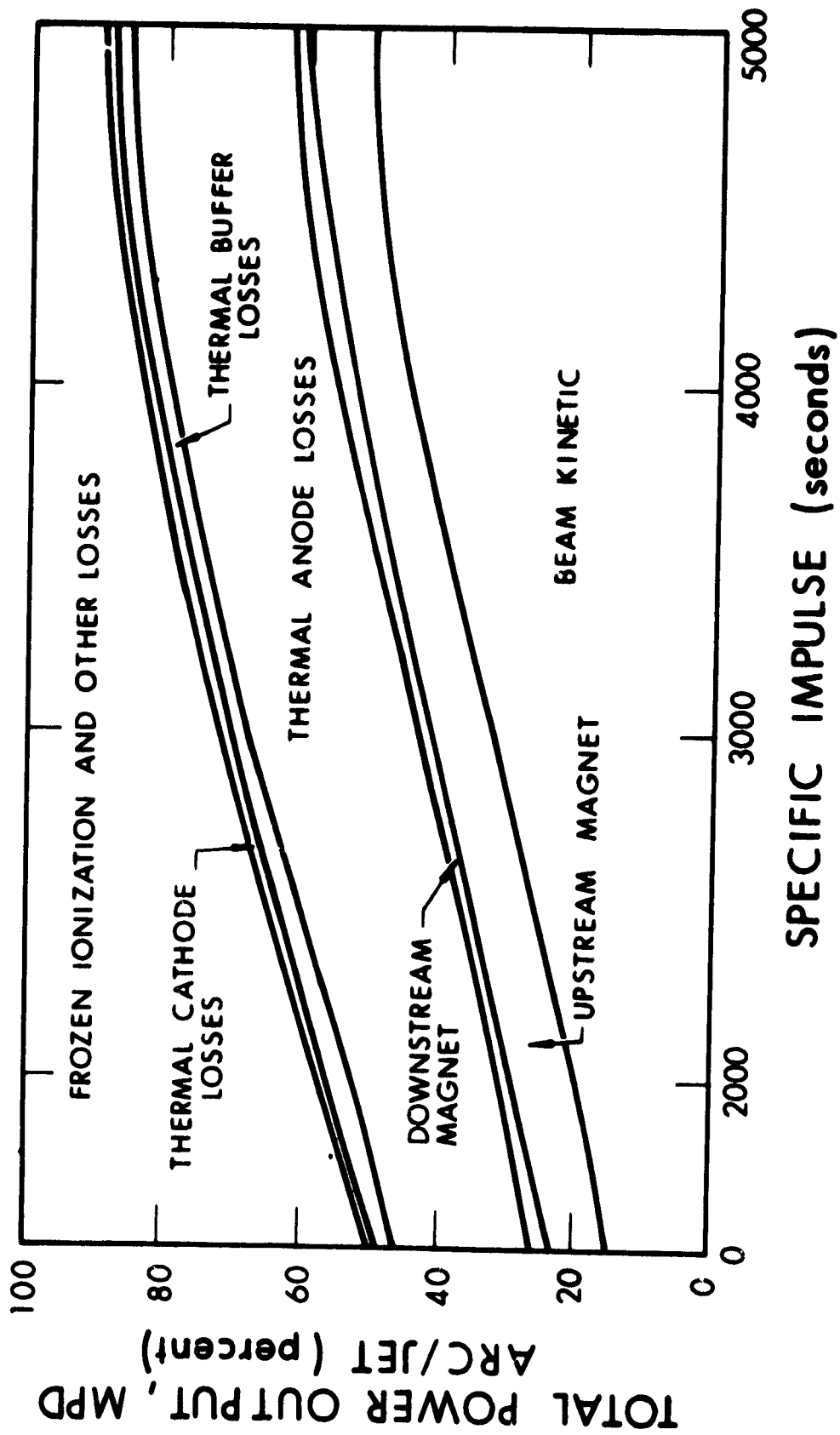


Figure 121. MPD Arc Jet Engine Power Requirements

TABLE XXIII
THRUSTER CONTROL COMMANDS

<u>COMMAND CHANNEL</u>	<u>DESCRIPTION</u>	<u>FUNCTION</u>
1	Magnet and lithium reservoir preheaters ON/OFF	Applies and shuts down on-board electrical power to solenoid and lithium tank preheaters prior to arc startup and prior to each restart
2	Magnet current ON/OFF	Energizes and de-energizes solenoids
3	Buffer gas ON/OFF	Initiates and terminates flow of hydrogen buffer gas
4	Liquid lithium feed valve OPEN/CLOSED	Starts and stops capillary force-actuated flow of liquid lithium
5	Driver gas pressurization ON/OFF	Starts and stops gas pressure-actuated flow of liquid lithium
6	Anode-cathode arc ON/OFF	Starts and stops anode-cathode arc current
7	Anode-buffer arc ON/OFF	Starts and stops anode-buffer (i.e., anode-to-ionizing electrode) arc current

between that arc power input and the electrode losses, the latter having been determined from the temperature rises in the various water cooling loops.

Average Particle Velocity in the Exhaust Beam

The lithium ion velocity measured by an optical phototracer technique agrees within experimental error with the average velocity computed by dividing the thrust by the mass flow rate. This procedure was repeated with sodium as the primary propellant, and once again good agreement was obtained.

Extended Current Loops in the Exhaust Beam

Hall current probe measurements (made during a sodium run) have indicated that at least half of the total arc current flows through the cathode jet as far as 8 inches downstream of the electrodes. When the background pressure in the vacuum chamber was relatively high, no loop current could be detected. As the tank pressure was reduced, the loop current rose to an asymptotic value.

Existence of Hall Currents

At a distance of several inches downstream of the face of the magnet housing the axial magnetic field strength on the centerline was found to increase by 5 to 10% when the arc was extinguished. The existence of Hall currents in the exhaust beam is thus conclusively established, since no other effect can account for the observed diamagnetism of the plasma.

Ion Rotation in the Cathode Jet

Spectroscopic Doppler shift measurements have indicated that the ions in the cathode jet were rotating.

Multiple Ionization

Spectral lines from the lithium ion (Li II) have been observed in the cathode jet, indicating that some double ionization of the lithium ion does exist.

Entrainment

Data reported when the tank pressure was less than 10^{-3} torr is considered to be reliable. Conversely, data obtained when the tank pressure exceeded this value must be considered suspect. This is particularly true of the high efficiency points ($\eta_0 > 60\%$) reported in Ref. 2-25.

Acceleration Mechanisms

Reasonable correlation with experimental data exists by assuming that the thrust is produced primarily by the acceleration of the ions through the potential drop between the anode and the exhaust beam. In some cases (especially with sodium propellant) some degree of double ionization must be invoked to account for the magnitude of the thrust observed.

Anomalous Performance

Many measurements exist where the thrust is greater than that which could be obtained by accelerating singly ionized particles across the anode-to-plasma potential difference. At the present time, it is felt that this can best be explained by multiple ionization, rather than by electron collisions.

2.5.5.4 Present Design Problems

Most of the remaining design problems are associated with future tasks, such as radiation-cooling and optimizing the configuration of the magnets or embarking upon a systematic weight reduction campaign. At the present time, only two important design problems may be said to exist, and even these have to do with extracting higher performance from an engine which now functions comparatively well; they are certainly not in the nature of problems which impede acceptable performance. The first of these is the question of how to further increase both the thrust and thermal efficiencies. This means getting an even larger fraction of the arc power into the form of kinetic beam power, while reducing the frozen losses and the power losses to the electrodes. Since the problem of maintaining adequately high potentials now appears to have been solved, the effort now must focus on their optimum utilization, i.e., for acceleration of ions rather than for multiple ionization. To accomplish this, it will be necessary somehow to further refine the internal geometry of the arc head, since the changes made in the independent variables \dot{m} , I_{arc} and B during tests of each configuration tended to quickly establish an upper limit for the performance of that configuration. All attempts to exceed the "intrinsic" maximum efficiency for any particular thruster (by increasing the anode-to-exhaust beam potential) appeared to lead instead to an increase in the degree of second ionization, and hence to a corresponding increase in the frozen flow losses.

The design philosophy which has been followed in the past has been to attempt to separate as much as possible the ionization processes from the acceleration processes, so that the latter could be subject to voltages greatly exceeding those prevailing in the latter. Closely related to this idea is the fact that virtually all of the losses can be associated with electron current. Hence, the electron current, as well as the potential drop across which it flows, must be reduced to

as low a value as possible. Since it is virtually impossible to promote functional separation between the ionization and acceleration processes without simultaneously introducing some spatial separation between the regions where each process is dominant, it is easy to understand how the idea for an "isolated anode configuration" ("IAC") arose. Actually, the design considerations leading to the IAC were more complex. The key point, however, is that the philosophy responsible for this development was so fruitful that the chief design problem at the present time is how to construct a thruster which embodies the same ideas, but carries them even further.

The other design problem is how to achieve greater flexibility in the propellant feed system, so as to permit higher mass flow rates and also to realize the full potential capability of the ALPHA thruster for throttling. The limitation on both of these is imposed by the coupling of the propellant mass flow rate to the arc current via the fraction of the power lost to the anode which is conducted into the vaporizer and utilized for propellant vaporization. This coupling is one of the key features of the present gas-actuated feed system. Among its advantages are the regenerative economies it affords, the fact that it facilitates radiation cooling of the anode, and of course, its mechanical simplicity. The problem at hand, then, is how to effect a de-coupling, or at least a relaxation of the constraints imposed by the coupling, without sacrificing these advantages. As mentioned earlier, the maximum propellant mass flow rate attainable in the present feed system is considered adequate for test purposes. It is possible, however, that future tests will indicate the need for still higher values of \dot{m} . If not, then a systematic attempt to solve the aforementioned problem by modifying the feed system design will probably have to await the projected incorporation of provisions for zero-gravity operation.

2.5.5.5 Areas of Uncertainty

Certain aspects of ground-based experiments on plasma thrusters in general and on MPD arc jets in particular are conducive to misinterpretation and erroneous measurements. These types of subtleties have plagued the industry since its inception. The resulting atmosphere of contested claims and of retractions of published data has given rise to a great deal of confusion amongst the proponents of competitive devices. This situation has had the inevitable effect of eroding the confidence of the various contracting agencies or else, in certain instances, inspiring the question of how an existing confidence level could logically be maintained. Against this background of justifiable skepticism it is disquieting, to say the least, to consider the ALPHA engine. Without exception, every other research group which has reported measurements of thruster efficiency anywhere near as high as those routinely recorded for ALPHA has, sooner or later, been forced to admit to serious errors in experimental procedure or in the interpretation of results. Indeed, "measurements" of efficiencies exceeding 100% were not uncommon; the latter at least had the merit of alerting the investigators to the existence of spurious effects in the laboratory, such as mass entrainment and extraneous current paths through vacuum chamber walls. What makes the ALPHA laboratory test results particularly suspect in some quarters is the inability of most other groups to duplicate the performance claimed. A noteworthy exception, however, is the work recently reported by Seikel (Ref. 2-30). Measurements using a thruster supplied by EOS were made in the NASA/Lewis facility. These results corroborate prior EOS findings.

Numerous arguments exist and have in the past been invoked to explain why the technical approach followed by EOS (especially with regard to propellant choice and thruster geometry) is responsible for the relatively high performance measured, and that the measurements themselves are indeed accurate. Conversely, the reasons for the failure of other groups

to reliably measure such performance has also been the subject of much consideration and discussion. These arguments will not be reproduced here. What is germane, however, is the fact that future plans affecting the development and application of ALPHA must be conditioned by the skepticism of some responsible observers. Nothing short of a flight test is ever likely to convince these skeptics that the thrust measurements made in the laboratory do not include any significant spurious effects attributable to the lack of a space environment.

Mass Entrainment

The extent to which entrainment effects in vacuum chamber tests of the thruster have been influencing laboratory measurements can be decisively ascertained only by means of a flight test. Experiments have been performed which indicate that the background pressure, so long as it is maintained below one micron (10^{-3} torr), has no discernible effect upon thruster performance. However, regardless of the vacuum chamber used, one cannot entirely discount the possibility that some type of entrainment still exists. Charged particles near the tank walls, for example, could conceivably approach and interact with the exhaust beam by travelling up magnetic flux lines. Once entrained, such particles may:

- a. Be accelerated along with the injected gas from the thruster;
- b. Increase the charged particle density in the exhaust beam, thereby causing the current distribution in the test chamber to be different from that in space;
- c. Cause the flow and diffusion of neutral propellant atoms to differ from the case without entrainment;
- d. Contribute to the rate of recombination of the ions and electrons downstream of the discharge region, thereby helping the propellant to escape the magnetic field in the test chamber sooner than it would in space.

Wall Effects

The problem of wall effects is in many ways similar to that of mass entrainment. Despite numerous precautions in the laboratory, it is possible that spurious current paths (via the tank walls) can distort performance measurements. In the near future it is planned to conduct several thruster tests in the new EOS/USAF Environmental Test Facility. Since this vacuum chamber is 22' x 35', such tests should reduce the probability of spurious wall effects even below that for past tests in much smaller tanks. The latter probability is felt to be very small, but here again, as with mass entrainment, no vacuum chamber of practical size is ever likely to be universally considered sufficiently large to completely preclude all possibility of wall effects.

RF Noise Interference

A simple experiment was conducted in the laboratory to obtain some qualitative information on the rf noise generated by the thruster. This was done in order to get a preliminary estimate of the potential seriousness of the interference problem. Four antennas were placed in various locations and orientations within the vacuum chamber, and the response was monitored on a VHF detector. Throughout the range from 10 to 500 MHz, this preliminary test indicated that the rf noise generated by the thruster is extremely small. Some additional results were obtained for frequencies below 1 MHz by displaying the arc voltage on an oscilloscope. As with the VHF detector, no significant change in the noise level over that of the background (i.e., no arc) was observed. The ripple of the dc power supply was orders of magnitude larger than any other signal seen on the scope, but far below radio frequencies. However, these test results may be misleading, since it is possible that the metal vacuum tank may affect the results. The tank is part iron and is 6' in diameter by 14' long. Also, there is a frequency band from 1 to 10 MHz which has not been examined. There is

a tendency to get more noise in the low frequencies when the thruster is operated on hydrogen instead of lithium, but a similar test has not been conducted for UHF. Due to these uncertainties, the results must be considered tentative. Thus, although it appears unlikely that thruster-generated RFI would pose a significant problem for space communications, this must be verified by further laboratory tests and, of course, a flight test.

Propellant Deposition

It has been observed in laboratory tests that any surface at moderate temperature which is directly exposed to the exhaust beam of the thruster will be coated with lithium. Conversely, it has been repeatedly and consistently observed that no appreciable lithium deposition occurs on other surfaces (of the thruster itself, as well as of the vacuum tank walls) so long as these surfaces are neither directly exposed to the beam nor intercept magnetic flux lines passing through or near the cathode jet. It is natural to conclude from these observations that no serious problems of propellant deposition on optics, temperature control surfaces, solar panels, etc, of a spacecraft with an ALPHA-type engine are likely to be encountered, provided certain simple precautions are taken with regard to the orientation of such surfaces. Once again, however, some residual doubt (at least) must remain until an actual flight test can be performed.

Zero-Gravity Feed

Zero-gravity feed systems have already been developed for cesium in conjunction with ion engines. No great technological innovations will be required to develop a lithium unit of comparable capacity and feed rate. Indeed, the transition from the system currently in use to a true zero-gravity device will probably require less engineering effort

than that which accompanied the transition from the earlier bellows-type system to the present gas-actuated one (see Subsection 2.5.4.2). Nevertheless, certain design problems do exist. These are mostly connected with the fact that a lithium feed system must be kept at higher temperatures than a cesium system. The melting and boiling points of lithium, for example, are 179 and 1317 deg C, respectively, compared with corresponding values of 29 and 670 deg C for cesium. It is important to note, however, that even in its present configuration, only a small part of the lithium feed system (comprising the vaporizer) is maintained at temperatures above 200 - 300 deg C. Moreover, very little of the heat supplied to the vaporizer actually represents an intrinsic power loss. Starting as waste anode heat which would otherwise necessitate provision for extra cooling, the thermal energy is transferred by conduction to the vaporizer, where it serves to pre-heat the propellant to its vaporization temperature.

As mentioned in Subsection 2.5.5.1 above, the zero-gravity version of the lithium feed system is likely to retain at least some utilization of gas pressure to supplement capillary forces and thereby permit relatively high mass flow rates.

2.5.6 PROJECTED DEVELOPMENT OF THE MPD ARC JET ENGINE AND SYSTEM

2.5 6.1 Projected MPD Arc Jet Description

Electrode Assembly

The ALPHA thruster electrode assembly consists of the anode, cathode and buffer, together with supporting structure. Most of these components have more than one function. The anode serves also as the lithium vapor injector. The buffer serves as the ionizing electrode and is maintained at a potential intermediate between that of the cathode and that of the anode. The annular region between the cathode and the buffer serves as the hydrogen injector. And finally, the supporting structure serves not only to mount and support the electrodes with respect to each other and with respect to the magnets, but it also serves three additional functions as well: first, to electrically insulate the cathode from the buffer; second, in its role as a "plasma isolator," to electrically insulate each portion of the upstream plasma from the radially adjacent annuli; and third, to reflect back-scattered neutrals and those ions which have gyrated about magnetic flux lines in the upstream direction.

Future designs of the electrode assembly will incorporate each of the foregoing features and will be completely radiation cooled.

Radiator System

The radiator system for the thruster includes some or all of the following items:

- a. Anode radiator
- b. Cathode radiator
- c. Buffer radiator
- d. Magnet radiators
- e. All conduction and convection paths between each radiator and the corresponding component

It excludes the power supply radiator (if any), which must be considered part of the powerplant package.

Most of the simplifications that can be envisaged at the present time will probably be embodied in the design of the radiator system for a flight model. The cathode and buffer radiators, for example, could be combined into a single unit with the help of a material like beryllium oxide, which is a good thermal conductor but also a good electrical insulator. Furthermore, it will probably not be difficult to dispense with the need for separate magnet radiators, and to rely instead upon radiation into space directly from the outer surfaces of the magnets themselves. Finally, it appears that, at the thruster power levels below 4 MW, no convective heat transfer will be required. It is possible, however, that heat pipe technology may be utilized even for microthruster applications, if this can prove significant in magnet power or mass.

Further study in the near future should settle this question. Indeed, it is anticipated that all of the design problems associated with radiation cooling the entire thruster will have been solved by mid-1968 for all power levels below 20 kW.

Magnet System

As in the case of the radiation cooling problem, it is expected that within the next two years much experience will have been accumulated designing, fabricating and testing flight-optimized magnets. In the process, the following questions will have to be answered:

- a. What is the optimum magnetic field distribution?
- b. Should electromagnets or permanent magnets, or some combination of these, be used to produce the requisite field distribution?
- c. What are the optimum materials and configurations for each type of system?

The answer to the first question is currently being sought in the laboratory. The remaining questions have already been partially answered on a contingency basis, and no special difficulties are foreseen in these areas.

Feed System

The engineering development work on the feed system will be concentrated in the following areas:

- a. Zero-gravity lithium feed
- b. Lithium flow metering
- c. Hydrogen plumbing

The design philosophy of the zero-g lithium feed will be to retain as much as possible of the present gas-actuated laboratory model version. One will attempt, therefore, simply to replace the gravity-operated "collector" by a comparable component which makes use of capillary forces instead. Once collected, the molten lithium would be forced from the reservoir into the vaporizer by pressure forces, exactly as

is done at the present time, except that hydrogen from the buffer gas supply tank, rather than argon, would be used for pressurization.

Metering of the lithium vapor flow by means of a calibrated sonic orifice, as is now done, will almost certainly be carried over to a flight model. This would be adequate for most thruster applications. It may not, however, be adequate for purposes of preliminary flight testing because it does not permit reliable measurement of instantaneous flow rates and also because a backup device would be highly desirable in view of the great importance of accurate flow rate measurements to the determination of thruster performance in a space environment. Most of the effort on an alternate lithium flow meter will be directed toward the development of an electromagnetic instrument designed to detect the minute currents induced by the flow of liquid lithium across magnetic flux lines.

The difficulty with hydrogen plumbing arises from the somewhat conflicting requirements of maximum reliability and maximum utilization (in the sense of multipurpose design). The existence aboard a spacecraft of a bottle of high-pressure hydrogen for some particular purpose provides the designer with an irresistible challenge to try to make this gas supply serve as many other useful functions as possible. Thus, it is natural to specify the use of hydrogen for pressurization of the lithium reservoir as well as for buffering the cathode. But additional possibilities exist which require careful investigation. The same gas supply, for example, could be used in a cold gas attitude control system for the spacecraft, or perhaps even for convective cooling of certain components such as batteries or magnets. The tradeoff between plumbing simplicity on the one hand and overall system simplification due to multiple functions on the other will be established early in any flight application program.

2.5.6.2 Projected Thruster Performance

Numerical predictions of projected thruster performance are especially risky in a program evolving as rapidly as ALPHA. It is therefore remarkable that Fig. 122, still accurately represents, not only the present performance status, but the best available projection as well. This figure was originally drawn very early in 1966 and was later incorporated into Ref. 2-31. It illustrates, in a rather simplified form, both a summary of achievements up to that time and an extrapolation extending several years into the future.

Figure 123 shows the minimum anticipated performance for a flight test model ALPHA thruster. It was drawn in April 1967, and at that time represented a projection of "nominal," rather than pessimistic performance.

2.5.6.3 Projected System Development Status

Figures 124 through 126 are a variety of simplified functional block diagrams of different ALPHA systems (represented symbolically by the two thrusters in the diagram).

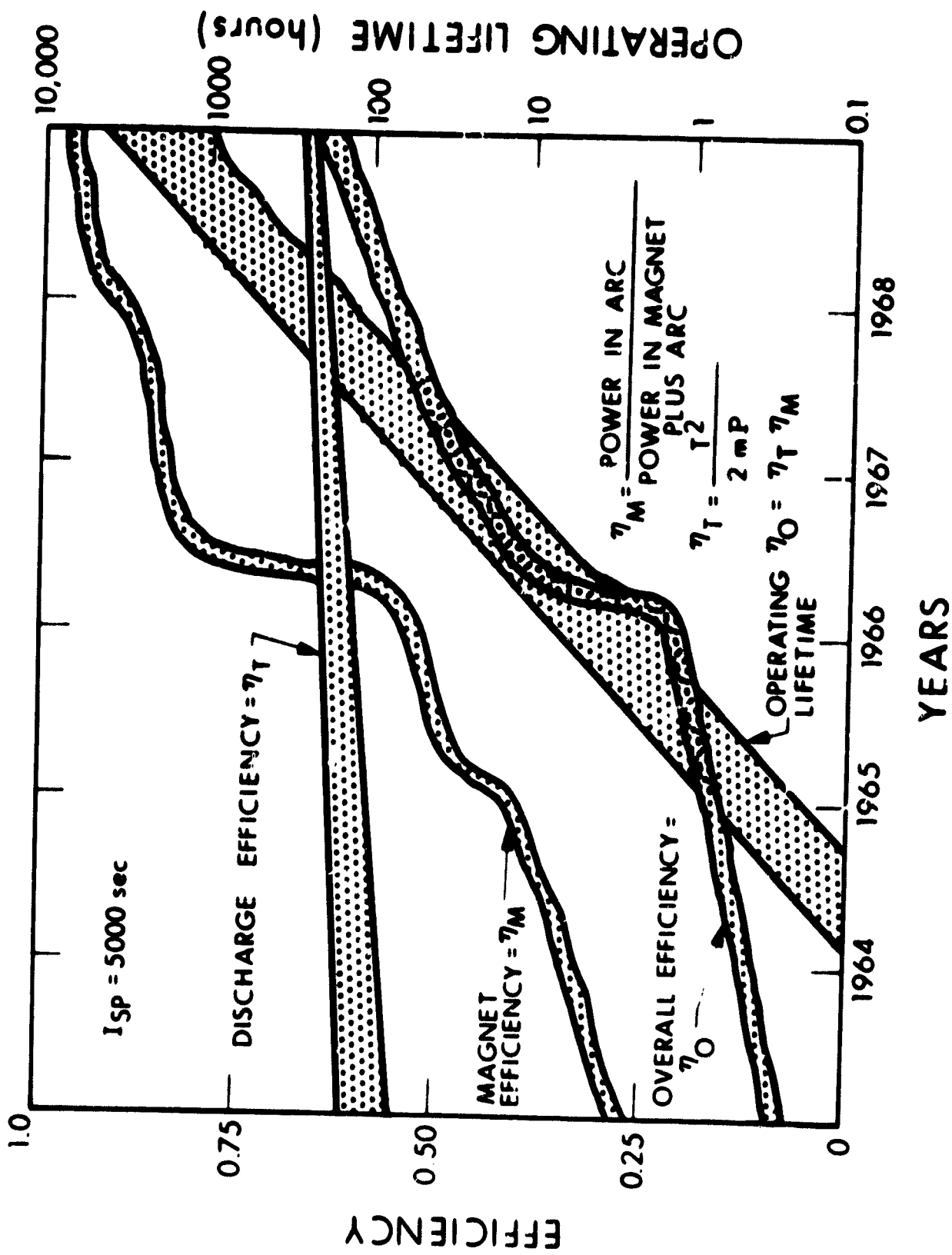


Figure 122. Improvements in Efficiency and Operating Lifetime of ALPHA

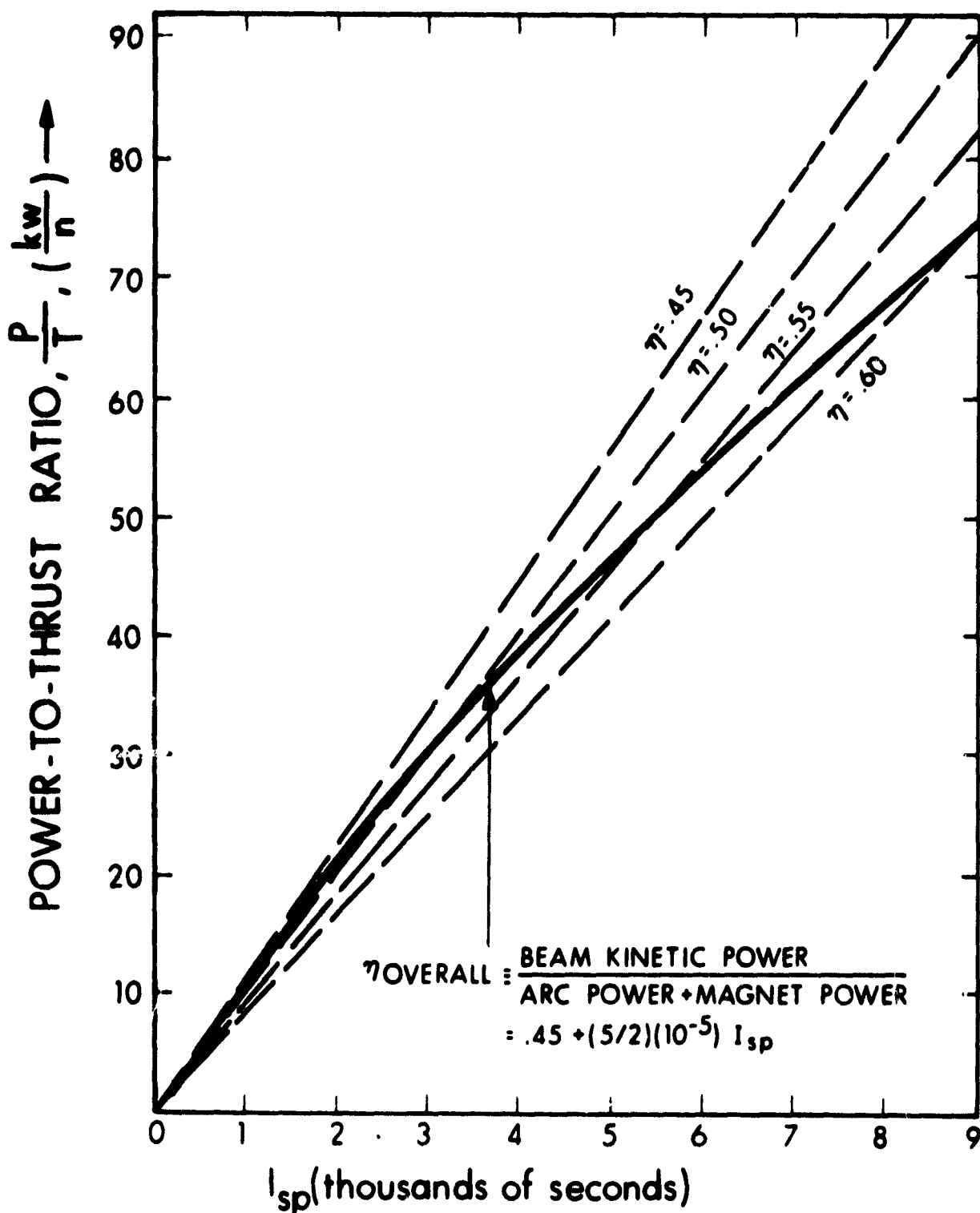


Figure 123. Projected Minimum Performance of a Flight Test Model ALPHA Thruster

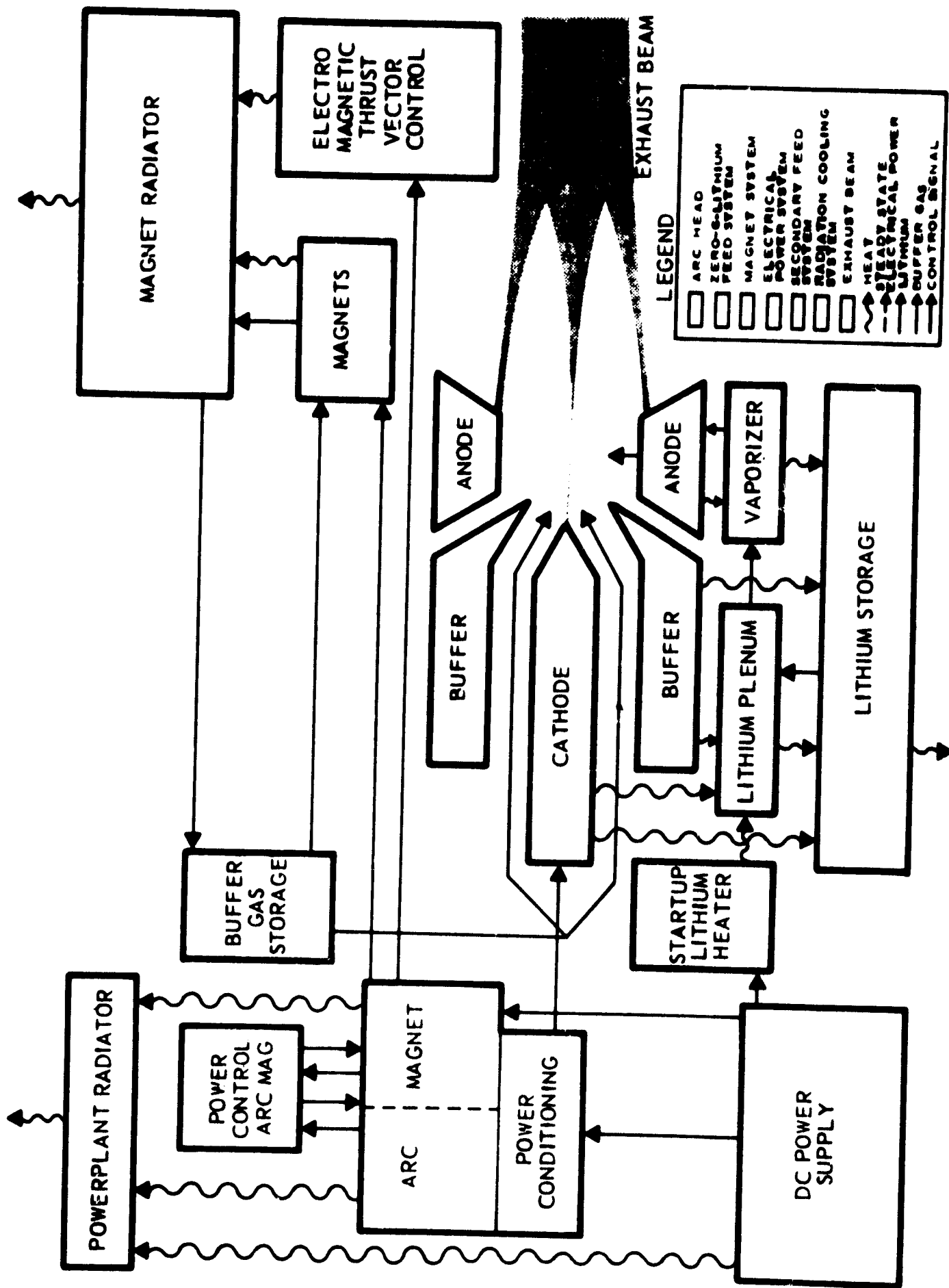


Figure 125. ALPHA System Block Diagram - 2

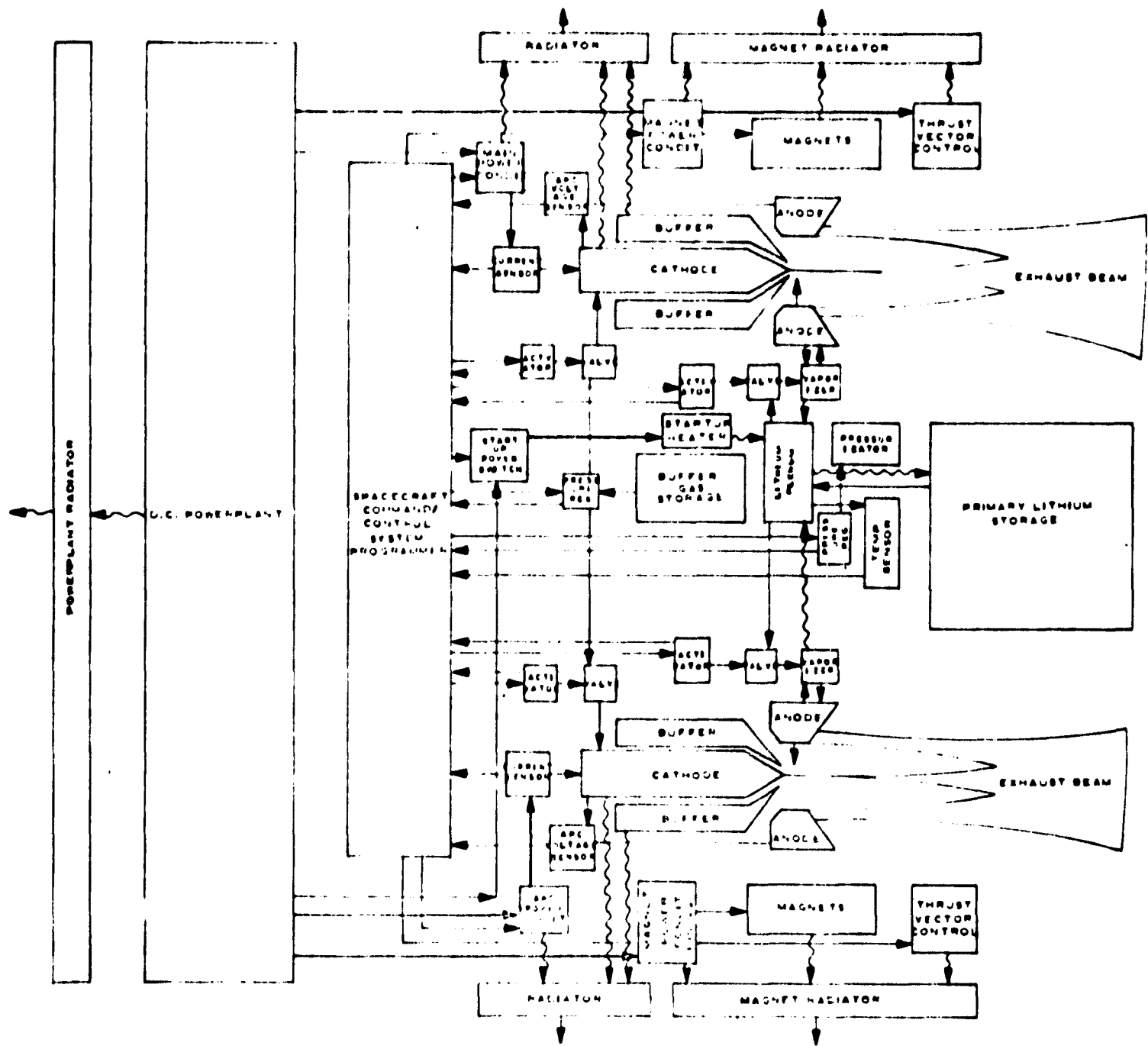


Figure 126. A A System Block Diagram - 3

2.6 REFERENCES AND BIBLIOGRAPHY FOR SECTION 2

2.6.1 REFERENCES

- 2-1. Preston, H., Thomas, Journal British Interplanetary Soc. 11, 173, (1952)
- 2-2. Schultz, R. D., Branson, L. K., "Charged-Colloid Propulsion System" Aerojet Report No. 1738 (Dec. 1959) Aerojet-General Corp. Azusa, Calif.

Schultz, Robert D. and Wiech, Raymond E. Jr., "Electrical Propulsion with Colloidal Materials," Paper - AGARD Combustion and Propulsion Panel - Technical Meeting on "Advanced Propulsion Techniques" - Pasadena, California 24-26, Aug. 1960
- 2-3. Hunter, Robert E. "Theoretical Consideration of Nonuniformly Charged Expellant Beams," ARL Tech. Note 60-138, Aeronautic Research Laboratory Air Force Research Division (Oct. 1960)
- 2-4. Hendricks, Charles D. Jr., "Charged Droplet Experiments," J. of Colloid Science 17, 249-259 (1962)
- 2-5. Cohen, E., "Research on the Electrostatic Generation and Acceleration of Submicron-size Particles" ARL-32-88 - WPAFB, May 1963
- 2-6. Cohen, E. and Huberman, M. N., "Research on Charged Particle Electrostatic Thrusters," Tech. Report AFAPL-TE-66-94, WPAFB, Sept. 1966
- 2-7. Hoffman, M. M., "Formation of Uniformly Charged Conducting Droplets and Possible Propulsion Applications," LA-2549-Physics-TID-4500, 16th Ed. Los Alamos Sci. Lab. (Sept. 1961)
- 2-8. Gignoux, Dominique, Einbinder, Harvey, Anton, Hermann, "Nozzle for Colloidal Propulsion Analytical Investigation," Cosmic, Inc. Report No. 19 (August 1961)
- 2-9. Gignoux, D and Anton, H., "Investigation of Charged Colloid Beams for Electrostatic Propulsion," NASA CR-54702/Cosmic, Inc. Report No. 165 (May 1967)
- 2-10. Hunter, R. E. and Wineland, S. H., "Exploration of the Feasibility of an Electrodeless Colloid Thruster Concept", U.S.A. Air Force Sixth Int. Symposium on Space Technology and Science, Tokyo, Japan (29 Nov. - 4 Dec. 1965)

- 2-11. Foldin, Daniel S. and Kvitek, George L., "An Analysis of Particle Formation Efficiency in a Colloid Thruster," AIAA Paper No. 66-253 AIAA Fifth Elec. Prop. Conf. - San Diego, Cal. (March 7-9 1966)
- 2-12. Beynon, J. C., Cohen, E., Goldin, D. S., Huberman, M. N., Kidd, P. W., Zafran, S., "Present Status of Colloid Microthruster Technology," AIAA Paper No. 67-531 - AIAA Elec. Prop. and Plasmadynamics Conf. - Colo. Spr. Sept. 11-13, 1967
- Huberman, M. N., Cohen, Ernest, "Research on Charged Particle Electrostatic Thrusters," Tech. Report AFAPL-TR-67-115, TRW Systems Sept. 1967
- 2-13. Kidd, P. W., "Parametric Studies of a Single Needle Colloid Thruster," AIAA Paper No. 67-530, AIAA Elec. Prop. and Plasmadynamics Conf. - Colo. Springs, Colorado, Sept. 11-13, 1967
- Kidd, P. W., "Research on the Bipolar Thruster," Tech. Report AFAPL-TR-67-110 TRW Systems - Sept. 1967
- 2-14. Perel, J. et al, "Electrodeless Particle Thruster," Tech. Report AFAPL-TR-67-106, EOS, Oct. 1967
- 2-15. Perel, J., Bates, T., Mahoney, J., Moore, R. D., and Yahiku, A. Y., "Research on a Charged Particle Bipolar Thruster," AIAA Paper No. 67-728 EOS - AIAA Elec. Prop. and Plasmadynamics Conference Sept. 11-13, 1967
- 2-16. S. H. Wineland, W. C. Burson, and R. E. Hunter, "The Electrohydrodynamic Generation of Charged Droplet Beams," Technical Report AFAPL-TR-66-72
- 2-17. Worlock, R. M., Ramirez, Peter, Ernstene, M. P. and Beasley, W. E., "A Contact Ion Microthruster System," AIAA Paper No. 67-80, January 1967
- 2-18. Anderson, J. R., and Thompson, S. A., "Development and Long-Life Performance of Ion Engines for Satellite Control," AIAA Paper No. 66-234, March 1966
- 2-19. Sohl, G., Fosnight, V. V., Goldner, S. J., and Speiser, R. C., "Cesium Electron Bombardment Ion Microthrusters," AIAA Paper No. 67-81, January 1967
- 2-20. Anderson, J. R., and Cybulski, R. J., "Status and Application of Low Thrust Electric Propulsion Systems," AIAA Paper No. 66-578 June 1966

- 2-21. G. L. Cann, S. T. Nelson, R. L. Harder, and P. F. Jacobs, "Magnetoplasmadynamic Thrustor Research," Technical Report No. EOS 7223-IR-1, November 1967.
- 2-22. G. L. Cann, R. A. Moore, R. L. Harder, and P. F. Jacobs, "High Specific Impulse Thermal Arc Jet Thrustor Technology," AFAPL-TR-65-48, Part II, January 1967.
- 2-23. A. Ducati, Giannini Scientific Corp., private communication.
- 2-24. P. Lindquist, AF/APL, private communication.
- 2-25. R. A. Moore, G. L. Cann, and L. R. Gallagher, "High Specific Impulse Thermal Arc Jet Thrustor Technology," AFAPL-TR-65-48, Part I, June 1965.
- 2-26. P. F. Jacobs, G. L. Cann, and R. L. Harder, "Diagnostic Measurements in ALPHA (ALkali Plasma Hall Accelerator)," NASA CR-72233, Final Report on Contract NAS3-8902, August 1966.
- 2-27. G. L. Cann, S. T. Nelson, R. L. Harder, and C. B. Shepard, Jr., "High Specific Impulse Thermal Arc Jet Thrustor Technology," Interim Report No. 3 on Contract AF 33(615)-1579, February 1967.
- 2-28. S. T. Nelson, G. L. Cann, and R. L. Harder, "High Specific Impulse Thermal Arc Jet Thrustor Technology," Part III, June 1967.
- 2-29. G. L. Cann, R. A. Moore, P. F. Jacobs, and L. R. Gallagher, "High Specific Impulse Thermal Arc Jet Thrustor Technology," Interim Report No. 2 on Contract AF 33(615)-1579, September 1965.
- 2-30. G. Seikel, private communication.
- 2-31. S. T. Nelson, "ALPHA," EOS Brochure No. EP 1-001 A, Electro-Optical Systems, Inc., 1966.

2.6.2 BIBLIOGRAPHY FOR SECTION 2.2

Feed System

1. Pawlik, E. V., and Wenger, N. C., "Performance Evaluation of a Mercury Propellant Feed System for a Flight Model Ion Engine," NASA TN-D-1213, June 1962
2. Mickelsen, W. R., "NASA Research on Heavy Particle Electrostatic Thrusters," AIAA Preprint No. 64-15, 1964.
3. Milder, N. L., "Fragmentation of Anthracene in an Electron-Bombardment Ion Source," NASA TN-D-2592, 1964.
4. Reader, P. D., "Experimental Effects of Propellant-Introduction Mode on Electron-Bombardment Ion Rocket Performance," NASA TN-D-2587, 1964.
5. Byers, D. C., Kerlake, W. R., and Grabman, J., "Experimental Investigation of Heavy-Molecule Propellants in an Electron-Bombardment Thruster," NASA TN-D-2401, 1964.
6. Dugan, J. V., Jr., "Some Theoretical Bases for Selection of Molecular Ion Propellants and a Survey of Molecular Plasma Collision Processes," NASA TN-D-1185, February 1964.
7. Montgomery, K. M., "Porous Matrix Phase Separator Evaluation," TRW-TAPCO Final Report, NASA CR-54152, NAS3-2518, TRW ER-6116, 18 September 1964.
8. Montgomery, K. M., "Propellant Flow Meter for Ion Rocket Systems," TRW-TAPCO Final Report, NASA CR-54070, TRW ER-5923, NAS3-2515, 15 June 1964.
9. Lawler, P. J., and Montgomery, K. M., "Research and Development of Propellant Feed Systems for Ion Engines," TRW-TAPCO Final Report, NASA CR-51, NAS8-2525, TRW, May 1964.
10. Masek, T. D., Kerrisk, D. J., "Zero-Gravity Feed System for Mercury Ion Engines," JPL Report 37-33, June 1965.
11. Kerrisk, D. J., and Masek, T. D., "A Zero-Gravity Mercury Propellant Feed System," AIAA Paper No. 66-250, 5th AIAA Elec. Prop. Conf., San Diego, 7-9 March 1966.
12. Stover, J. B., "Electric Breakdown and Arcing in Experimental Ion Engine Systems," AIAA Paper No. 63-057, March 1963.
13. Nakanishi, S., and Pawlik, E. V., "Preliminary Experimental Operation of High-Voltage Isolation Device for Propellant System of an Ion Rocket," NASA TM-X-1026, 1964.

14. Stover, J. B., "Effect of Thrustor Arcing on Ion Rocket System Design," AIAA Paper No. 64-682, NASA TM-X-52045, August 1964.
15. Nakanishi, S., "Experimental Investigation of a High-Voltage Isolation Device for Ion Thrustor Propellant Feed," NASA TN-D-3535, August 1966.

Ionization

1. Mirels, H., and Rosenbaum, B. M., "Analysis of One-Dimensional Ion Rocket with Grid Neutralization," NASA TN-D-266, 1960.
2. Wehner, G. K., and Rosenberg, D., "Mercury Ion Beam Sputtering of Metals at Energies of 4 to 15 keV," Jour. Appl. Phys., Vol. 32, No. 5, May 1961, pp. 887-890.
3. Kaufman, H. R., "The Neutralization of Ion Rocket Beams," NASA TN-D-1055, August 1961.
4. Kemp, R. F., Sellen, J. M., Jr., and Pawlik, E. V., "Beam Neutralization Tests of a Flight-Model Electron-Bombardment Engine," ARS Paper No. 266-62, November 1962.
5. Kemp, R. F., Sellen, J. M., Jr., and Pawlik, E. V., "Neutralizer Tests on a Flight-Model Electron-Bombardment Thrustor," NASA TN-D-1733, 1963.
6. Sirois, W., "Cathode Development Studies for Arc and Bombardment-Type Ion Engines," NASA Contract NAS3-3563, IPC Report 34TR-073, Final Report, April 1963.
7. Eckhardt, W. O., et al., "A New Cathode for Mercury Electron-Bombardment Thrustors," AIAA Paper No. 64-690, August 1964.
8. Milder, N. L., and Kerslake, W. R., "Evaluation of Filament Deterioration in Electron-Bombardment Ion Sources," NASA Tech. Note TN-D-2173, 1964.
9. Kerslake, W. R., "Cathode Durability in the Mercury Electron-Bombardment Ion Thrustor," AIAA Paper No. 64-683, NASA TM-X-52037, 1964.
10. Sellen, J. M., Jr., and Kemp, R. F., "Observations of Neutralized Ion Thrust Beams in the 25-Meter NASA Testing Chamber; Investigations of Ion Beam Diagnostics," Section III, TRW 8603-6037-SU-000, TRW Systems, July 1964.
11. Sirois, W., "Cathode Lifetime Studies," IPC Final Report, NASA CR-54109, NAS3-3563, 31 August 1964.
12. Wadhwa, R. P., Brauch, D. F., and Buneman, O., "Two-Dimensional Experiments (Computer) on Ion-Beam Neutralization," AIAA Paper No. 64-698, 4th AIAA Elec. Prop. Conf., Philadelphia, 31 August - 2 September 1964.

13. Kerslake, W. R., "Preliminary Operation of Oxide-Coated Brush Cathodes in Electron-Bombardment Ion Thrusters," NASA TM-X-1105, 1965.
14. Sellen, J. M., Jr., and Cybulski, R. J., "Environmental Effects on Laboratory and In-Flight Performance of Neutralization Systems," AIAA Paper No. 65-70, 2nd AIAA Aerosp. Sci. Meeting, New York City, 25-27 January 1965.
15. EOS, "Program for the Exploratory Development of a Contact Ionization Thruster," EOS Final Report, AFAPL-TR-65-68, Contract AF 33(615)-1530, May 1965.
16. Eckhardt, W. O., et al, "4000-Hour Life Test of a Liquid-Mercury Cathode in a 20-Cm. LeRC Ion Thruster," HRL Special Report, NASA Contract NAS3-6262, November 1966.
17. Eckhardt, W. O., Hagen, G., Snyder, J. A., and Knechtli, R. C., "High-Temperature Liquid-Mercury Cathodes for Ion Thrusters," HRL, NASA CR-81690, NASw-1404, QPR-1, 30 November 1966.
18. King, H. J., Eckhardt, W. O., Ward, W., and Knechtli, R. C., "Electron-Bombardment Thrusters Using Liquid-Mercury Cathodes," AIAA Paper No. 66-232, 5th AIAA Elec. Prop. Conf., San Diego, 7-9 March 1966.
19. Kerslake, W. R., "Oxide-Cathode Durability in Mercury Electron-Bombardment Ion Thruster," NASA TN-D-3818, February 1967.
20. Ward, J. W. and King, H. J., "Mercury Hollow-Cathode Plasma Bridge Neutralizer," AIAA Paper No. 67-671, AIAA Elec. Prop. and Plasmadyn. Conf. Colorado Springs, 11-13 September 1967.
21. Rawlin, V. K. and Pawlik, E. V., "A Mercury Plasma-Bridge Neutralizer," AIAA Paper No. 67-670, AIAA Elec. Prop. and Plasmadyn. Conf. Colorado Springs, 11-13 September 1967.
22. Hall, D. F., Kemp, R. F., and Shelton, H., "Mercury Discharge Devices and Technology," AIAA Paper No. 67-669, AIAA Elec. Prop. and Plasmadyn. Conf., Colorado Springs, 11-13 September 1967.
23. Reader, P. D. and Pawlik, E. V., "Cathode Durability Tests in Mercury, Electron-Bombardment Ion Thrusters," NASA TN-D-4055, 1967.
24. Frohlich, H., "A High Current Source for Ion and Electron Beams," Nucleonic, Vol. 1, No. 5, 1959, p. 183.
25. Nablo, S. V., "Demonstration of Ion Thrust Using the Duoplasmatron Arc-Type Source," Final Report, U. S. Army Contract No. DA-19-020-ORD-4969, September 1960.
26. Kaufman, H. R., "One-Dimensional Analysis of Ion Rockets," NASA TN-D-261, 1960.

27. Kerrisk, D. J., "Arc-Type Ion Sources for Electrical Propulsion," WPAFB, ASD Tech. Note 61-4, May 1961.
28. Kaufman, H. R., "Electron Diffusion in a Turbulent Plasma," NASA TN-D-1324, 1962.
29. Strickfaden, W. D., and Geiler, K. L., "Probe Measurements of the Discharge in an Operating Electron-Bombardment Engine," AIAA Paper No. 63056, NASA CR-50623, 1963.
30. Reader, P. D., "Ion Rocket with a Permanent Magnet," *Astronautics and Aerospace Engrg.*, Vol. 1, No. 9, Oct, 1963, pp. 83, AIAA Paper 63-031, March 1963.
31. Domitz, S., "Experimental Evaluation of a Direct-Current Low-Pressure Plasma Source," NASA Tech. Note TN-D-1659, 1963.
32. Kohlberg, I., "Analytic Considerations Related to the Lewis-Type Bombardment Ion Engine," AIAA Paper No. 63030-3-63, AIAA Elec. Prop. Conf., Colorado Springs, 11-13 March 1963, NASA Contract NAS8-1684.
33. Wasserbauer, J. F., "A 5-Centimeter-Diameter Electron-Bombardment Thrustor with Permanent Magnets," NASA TN-D-2072, 1964.
34. Cooper, D. W., and Kuhns, P. W., "Measurement of Ion and Electron Densities of Electron-Bombardment Ion Thrustor Beam," NASA TN-D-3761, December 1966.
35. Cohen, A. J., "Onset of Anomalous Diffusion in Electron-Bombardment Ion Thrusters," NASA TN-D-3731, November 1966.
36. McNeill, P. C., "An Experimental Bombardment Ion Source," AGARD, Phys. and Techn. of Ion Motors, 1966, pp. 207-222.
37. Kohlberg, I., and Nablo, S., "Physical Phenomena in Bombardment Ion Sources," AGARD, Phys. and Techn. of Ion Motors, 1966, pp. 155-206.
38. Loeb, H., "State of Development of the Geissen Ion Engine," presented at Symp. on Elec. Space Motion, Sonenberg, West Germany, 24 February 1966.
39. Knauer, W., Hagen, G., Gallagher, R., and Stack, E., "Investigation of the Discharge in Electron-Bombardment Thrusters," AIAA Paper No. 66-244, 5th AIAA Elec. Prop. Conf., San Diego, 7-9 March 1966, NAS3-7114.
40. Bechtal, R. T., "Discharge Chamber Optimization of the SERT II Thruster," AIAA Paper No. 67-668, AIAA Elec. Prop. and Plasmadyn. Conf., Colorado Springs, 11-13 September 1967.

Acceleration

1. Baldwin, L. V., and Sandborn, V. A., "Theory and Application of Hot-Wire Calorimetry for Measurement of Beam Power," Prog. in Astron. and Rocketry, Vol. 5 - Electrostatic Propulsion, 1961, pp. 425-446.
2. Kerslake, W. R., "Accelerator Grid Tests on an Electron-Bombardment Ion Rocket," NASA Tech. Note TN-D-1168, 1962.
3. Lockwood, D. L., Mickelsen, W. R., and Hamza, V., "Analytic Space Charge Flow and Theoretical Electrostatic Rocket Engine Performance," ARS Paper No. 2400-62, 1962.
4. Hamza, V., and Richley, E. A., "Numerical Solution of Two-Dimensional Poisson Equations: Theory and Application to Electrostatic Ion Engine Analysis," NASA TN-D-1323, 1962.
5. Stuart, R. V., and Wehner, G. K., "Sputtering Yields at Very Low Bombarding Ion Energies," Jour. Appl. Phys., Vol. 33, No. 7, July 1962, pp. 2345-52.
6. Kerslake, W. R., "Charge-Exchange Effects on the Accelerator Impingement of an Electron-Bombardment Ion Rocket," NASA Tech. Note TN-D-1657, 1963.
7. Kerslake, W. R., and Pawlik, E. V., "Additional Studies of Screen and Accelerator Grids for Electron-Bombardment Ion Thrusters," NASA Tech. Note TN-D-1411, 1963.
8. Domitz, S., and Pawlik, E. V., "Beam Current Measuring Device for Ion Engine Research," AIAA Jour., Vol. 1, No. 3, March 1963, pp. 712-713.
9. Mickelsen, W. R., "Theoretical Performance of Electrostatic Thrusters with Analytic Space-Charge Flows," NASA TR-R-174, 1963.
10. Hyman, J., Jr., Buckey, C. R., Eckhardt, W. O., and Knechtli, R. C., "Research Investigation of Ion Beam Formation from Electron-Bombardment Ion Sources," NASA Contract NAS3-2511, HRL Final Report, April 1963.
11. Hamza, V., "Numerical Solution of Axially Symmetric Poisson Equation; Theory and Application to Ion Thruster Analysis," NASA TN-D-1711, 1963.
12. Hamza, V., and Richley, E. A., "Numerical Evaluation of Ion Thruster Optics," NASA TN-D-1665, 1963.
13. Stuart, R. V., and Wehner, G. K., "Sputtering Yields," Gen. Mills Annual Report 2480, AD-424612, Contract NONR-1589(15), 15 November 1963.

14. Richley, E. A., and Mickelsen, W. R., "Effects of Molecular Flow in Plasma Generation and Some Analyses of Space Charge Flow in Ion Acceleration," AIAA Paper No. 64-7, Aerosp. Sci. Meeting, New York City, 20-22 January 1964.
15. Trolinger, J. D., Shipp, J. I., and Lennert, A. E., "Basic Processes of Ion Beam Termination," AEDC-TDR-64-105, AD-603905, Contract AF 40(600)-1000, August 1964.
16. King, H. J., "Research on Problems of Ion Beam Formation from Electron-Bombardment Ion Sources," HRL Summary Report, NASA CR-54143, NAS3-4118, HRL-4118-S, 18 August 1964.
17. Wadhwa, R. P., and Kooyers, G., "Analysis of Electron-Ion Mixing in Ion Engines," Litton Final Report, NASA CR-54033, NAS3-2503, 31 March 1964.
18. Pawlik, E. V., Margosian, P. M., and Staggs, J. F., "A Technique for Obtaining Plasma Sheath Configurations and Ion Optics for an Electron-Bombardment Ion Thrustor," NASA TN-D-2804, 1965.
19. Staggs, J. F., "An Electrolytic Tank for Two-Dimensional Analysis of Electrostatic Thrustor Optics," NASA TN-D-2803, 1965.
20. Wadhwa, R. P., and Brauch, D. F., "Analysis of Electron-Ion Mixing in Ion Engines," Final Report, Litton, NASA CR-54419, NAS3-5757, 20 July 1965.
21. Kerrisk, D. J., and Masek, T. D., "Nonuniformity and Grid Erosion in an Electron-Bombardment Ion Engine," AIAA Paper No. 65-688, 4th AIAA Elec. Prop. Conf., Philadelphia, 31 August - 2 September 1965.
22. Bussi, G., and Filippi, F., "Electrostatic Propulsion by Positive and Negative Ions," AGARD, Phys. and Techn. of Ion Motors, 1966, pp. 319-342.
23. Bonnal, J. F., Giacomini, J., Mainfray, G., Manus, C., Morellec, J., et al, "Physics of Synthetic Plasma Beams," AGARD, Phys. and Techn. of Ion Motors, 1966, pp. 215-278
24. Slattery, J. C., Friichtenicht, J. F., and Hansen, D. O., "Ion Engine Arcing Induced by Meteoroids," AIAA Paper No. 66-205, 5th AIAA Elec. Prop. Conf., San Diego, 7-9 March 1966.
25. Worlock, R. M., "Program to Develop and Demonstrate Methods to Deflect Beam for Ion Thrustor," Final Report, EOS, NASA CR-72091, NAS3-7936, 26 June 1966.
26. Smith, H. P. Jr., et al, "Investigation of Kilovolt Ion Sputtering," Univ. of Calif., QPR, NASA CR-72012, 31 October 1966.
27. Staggs, J. F., Gula, W. P., and Kerlake, W. R., "The Distribution of Neutral Atoms and Charge-Exchange Ions Down Stream of an Ion Thrustor," NASA TM-X-52259, presented at 5th AIAA Space Sci. Meeting, New York City, 23-27 January 1967.

28. Margosian, P. M., "Preliminary Tests of Insulated Accelerator Grid for Electron-Bombardment Thrustor," NASA TM-X-1342, February 1967.
29. Pawlik, E. V. and Reader, P. D., "Accelerator Grid Durability Tests of Mercury, Electron-Bombardment Ion Thrusters," NASA TN-D-4054, 1967.
30. Staggs, J. F., Gula, W. P., and Kevslake, W. R., "Distribution of Neutral Atoms and Charge-Exchange Loss Downstream of an Ion Thruster," AIAA Paper No. 67-82, 5th AIAA Aerosp. SCI. Mtg., New York City, 23-26 January 1967.

Power and Control

1. Reader, P. D., and Finke, R. C., "An Electron-Bombardment Ion Rocket Operated on Alternating Current Supplies," NASA TN-D-1457, December 1962.
2. Molitor, J. H., and Kaplan, M. H., "Optimization of Ion Engine Control Systems for Synchronous Satellites," AIAA Paper No. 63-273, AIAA Summer Meeting, Los Angeles, 17-20 June 1963.
3. Nakanishi, S., Pawlik, E. V., and Baur, C. W., "Experimental Evaluation of Steady-State Control Properties of an Electron-Bombardment Ion Thrustor," NASA TN-D-2171, February 1964.
4. Kotnik, J. T., and Sater, B. L., "Power Conditioning Requirements for Ion Rockets," presented at IEEE Int'l. Conf. on Aerospace Electrotech., Phoenix, 19-25 April 1964, NASA TM-X-51450.
5. Powell, J. D., McGarrell, P. H., and Hawersaat, W. H., "Power Conditioning Development for Ion Engines," AIAA Paper No. 64-764, 3rd Biennial Aerosp. Pwr. Sys. Conf., Philadelphia, 1-4 September 1964.
6. Worlock, R. M., et al, "Development of Automatic Control Systems for Electron-Bombardment and Contact Ion Engines," AIAA Paper No. 64-504, 1st AIAA Ann. Meeting, 29 June - 2 July 1964.
7. Work, G. A., and Heron, B. G., "Power Conditioning Systems for Ion Engines," AIAA Paper No. 64-681, 4th AIAA Elec. Prop. Conf., Philadelphia, 31 August - 2 September 1964.
8. Moore, E. T., Wilson, T. G., and McIntire, J. N., "Development of a 1.6 kW 2000 Volt High-Frequency DC-DC Converter for Ion Thrusters Using a Modulator Design for Inductive Energy Pumping Technique for Conversion, Regulation, and Protection," Summary Report, Wilmore Elec. Co., NASA CR-54408, NAS3-6264, 8 December 1965.
9. Molitor, J. H. et al, "Reliability Analyses of Modular Power Conditioning and Control Systems for Ion Engines," Final Report, JPL Contract 951144, NASA CR-80516, October 1966.

10. Molitor, J. H., et al, "Development and Test of an Ion Engine System Employing Modular Power Conditioning," Final Report, JPL Contract 951144, NASA CR-80515, August 1966.
11. HRL, "Reliability Analyses of Modular Power Conditioning and Control Systems for Ion Engines," HRL Final Report, NASA CR-80516, NAS7-100, JPL 951144, October 1966.
12. HRL, "Development and Test of an Ion Engine System Employing Modular Power Conditioning," HRL Final Report, NASA CR-80515, NAS7-100, JPL 951144, August 1966.
13. Davis, J. J., "Advanced Power Conditioning for an Ion Propulsion System," 3rd Space Congr., Cocoa Beach, 7-10 March 1966.

Facilities - Test

1. Mickelsen, W. R., and Childs, J. H., "Theoretical Analysis of Ultrahigh Vacuum Condensers," Rev. Sci. Inst., Vol. 29, No. 10, October 1958, pp. 871-873.
2. Grobman, J. S., "A Technique for Cryopumping Hydrogen," NASA TN-D-863, June 1961.
3. Richley, E. A., and Cybulski, R. J., "High Vacuum Condenser Design: Experimental Effects from Cesium and Mercury Ion Beams," NASA TN-D-1217, 1962.
4. Richley, E. A., "NASA Electrostatic Thrustor Instrumentation and Research," NASA TM-X-51766, presented at OSU Seminar on Expt'l Techniques on High-Speed Aerodynamics and Gas Dynamics, July 1963.
5. Hubach, R. A., "Analytical and Experimental Studies to Develop Ion Engine Ground Testing Techniques," AEDC-TDR-63-245, AD-423226, NAS5-517, HRL, AF 40(600)-948, November 1963.
6. Carta, D. G., "Problems of Millipound Thrust; the 'Hansen Suspension'," AIAA Paper No. 63034-63, AIAA Elec. Prop. Conf., Colorado Springs, 11-13 March 1963.
7. Wössner, H., "Vacuum Engineering and Space Simulation," VDI Zeitschrift, Vol. 106, No. 1, October 1964, pp. 1389-1392.
8. Finke, R. C., Holmes, A. D., and Keller, T. A., "Space Environment Facility for Electric Propulsion Systems Research," NASA-TN-D-2774, 1965.
9. Maslowski, E. A., "Experimental Data on Pumping of Mercury Ion Beams by Liquid Nitrogen-Cooled Condensers," NASA TN-D-3231, January 1966.

Clustering - Scaling

1. Reader, P. D., "Experimental Effects of Scaling on the Performance of Ion Rockets Employing Electron-Bombardment Ion Sources," ARS Paper No. 61-87-1781; also published in ARS Jour., May 1962.
2. Levoy, M., "Dual Electric-Nuclear Engine," AIAA Jour., Vol. 1, No. 6, 1963, pp. 1298-1302.
3. Pawlik, E. V., "An Experimental Evaluation of Array of Three Electron-Bombardment Ion Thrusters," NASA TN-D-2597, 1964.
4. Rossa, L. G., "A Parametric Study of Constant Thrust, Electrically-Propelled Mars and Venus Orbiting Probes," NASA TN-D-2154, 1964.
5. Pawlik, E. V., and Nakanishi, S., "Experimental Evaluation of Size Effects on Steady-State Control Properties of Electron-Bombardment Ion Thrusters," NASA TN-D-2470, 1964.
6. Reader, P. D., "Experimental Performance of a 50-Centimeter-Diameter Electron-Bombardment Ion Rocket," AIAA Paper No. 64-689, NASA TM-X-52042, 1964.
7. Reader, P. D., and Mickelsen, W. R., "Experimental Systems Studies of Large Modules and Arrays of Electrostatic Thrusters," AIAA Preprint No. 64-503, NASA TM-X-52019, June 1964.
8. Reader, P. D., "The Operation of an Electron-Bombardment Ion Source with Various Gases," Presented at Int'l. Conf. on Electron and Ion Beam Sci. and Tech., Toronto, Canada, 5-6 May 1964, NASA TM-X-52006.
9. Molitor, J. H., Pinckney, K. R., and Selieger, R. L., "Effects of Reliability Considerations on the Design of Electric Thruster Arrays," AIAA Paper No. 65-68, 2nd AIAA Aerosp. Sci. Meeting, New York City, 25-27 January 1965.
10. Geis, J. W., "Millipound-Thrust Electric Propulsion," Technical Report AFAPL-TR-66-65, September 1966.
11. Margosian, P. M., and Kerslake, W. R., "Experimental Evaluation of a Two-Directional Electron-Bombardment Ion Thruster," AIAA Paper No. 66-248, 5th AIAA Elec. Prop. Conf., San Diego, 7-9 March 1966.
12. Sohl, G., Fosnight, V. V., Goldner, S. J., and Speiser, R. C., "Cesium Electron-Bombardment Ion Microthrusters," AIAA Paper No. 67-81, 5th AIAA Aerosp. Sci. Meeting, New York City, 23-26 January 1967.
13. Maskek, T. D., and Womack, J. R., "Experimental Studies with a Clustered Ion Engine System," AIAA Paper No. 67-698, AIAA Elec. Prop. and Plasmadyn. Conf., Colorado Springs, 11-13 September 1967.
14. Wasserbauer, J. F., "A 5-Centimeter Diameter, Electron-Bombardment Thruster with Permanent Magnets," NASA TN-D-3628, 1966.

System Performance

1. Kaufman, H. R., and Reader, P. D., "Experimental Performance of Ion Rockets Employing Electron-Bombardment Ion Sources," ARS Paper No. 1374-60, November 1960.
2. Kaufman, H. R., and Reader, P. D., "Experimental Performance of Ion Rockets Employing Electron-Bombardment Ion Sources," Prog. in Astronautics and Rocketry, Vol. 5, 1961, pp. 3-20.
3. Kaufman, H. R., "An Ion Rocket with an Electron-Bombardment Ion Source," NASA TN-D-585, January 1961.
4. Elliot, D. G., and Molitor, J. H., "Thrust Unit Requirements for Electrically-Propelled Spacecraft," JPL Tech. Report No. 32-117, June 1961.
5. Reader, P. D., "Investigation of a 10-Centimeter Diameter Electron-Bombardment Ion Rocket," NASA Tech. Note TN-D-1168, 1962.
6. Milder, N. L., "Comparative Measurements of Singly and Doubly-Ionized Mercury Produced by Electron-Bombardment Ion Engines," NASA Tech. Note TN-D-1219, 1962.
7. Kaufman, H. R., "The Electron-Bombardment Ion Rocket," AFOSR Third Symp. on Adv. Prop. Concepts, Cincinnati, Ohio, October 1962.
8. Molitor, J. H., "Ion Propulsion for the Control of Stationary Satellites," ARS Paper No. 2666-62, presented at ARS 17th Annual Meeting, Los Angeles, 13-18 November 1962.
9. Kerrisk, D. J., "Potentialities of Electron-Bombardment Ion Engines for Electric Propulsion," JPL Tech. Report No. 32-301, June 1962.
10. Mickelsen, W. R., "Comparative Performance of Electrostatic Rocket Engines," IAS Paper No. 62-74, New York City, January 1962.
11. Kaufman, H. R., "The Electron-Bombardment Ion Rocket," 3rd AFRSR Symp. on Adv. Prop. Concepts, Cincinnati, 2-4 October 1962, Paper E-1862.
12. Shattuck, R. D., and Dennington, R. J., "Status and Future Engineering Problems of Electric Propulsion Systems," AIAA 2nd Manned Space Flight Meeting, Dallas, 22-24 April 1963.
13. Doughman, C. L., and Stump, F. C., "The Effect of System Parameters on Space Electric Power System Weights," AIAA Paper No. 63-243, AIAA Summer Meeting, Los Angeles 17-20 June 1963.
14. Kohlberg, I., "Analytic Considerations Relating to the Lewis-Type Bombardment Ion Engine," AIAA Paper No. 63030-B-63, 1963.
15. King, H. J., and Quintal, B. S., "Studies of a Lewis-Type Bombardment Ion Engine," AIAA Paper No. 63030-A-63, 1963, Colorado Springs, 11-13 March 1963.

16. AID, "Electrostatic Rocket Development; Comprehensive Report on Soviet Periodical Literature," AID-P-63-121, AD-429317, 10 December 1963.
17. Mickelsen, W. R., "Effect of Thrustor Characteristics on Electric Spacecraft Missions," AIAA Paper No. 64-676, NASA TM-X-52041, August 1964.
18. Kaufman, H. R., "Electrostatic Thrusters," New Scientist, April 1964.
19. Stuhlinger, E., "Electric Propulsion in 1964 -- A Status Review," AIAA Paper No. 64-524, 1st AIAA Annual Meeting, Washington, D.C., 29 June - 2 July 1964.
20. Eckert, A. C., Coerdts, R. J., Moffett, M. B., and Mueller, M. W., "Investigation, Testing, and Development of an Electron-Bombardment Ion Engine System," TRW-TAPCO, NASA CR-54148, NAS3-5745, TRW Report ER-6291, 15 December 1964.
21. Kaufman, H. R., "Electrostatic Thrusters," NASA TM-X-51747, 8 April 1964.
22. Mickelsen, W. R., "Electric Propulsion," NASA TM-X-51742, 1964.
23. Eckert, A. C., Bond, A. F., Coerdts, R. J., and Mueller, M. W., "Electron-Bombardment Ion Engine Development," TRW-TAPCO Final Report, NASA CR-54082, NAS3-2522, TRW-ER-5805, February 1964.
24. Shelton, R. D., Potter, R. A., Lacy, L., and Stuhlinger, E., "Evaluation and Analysis of Thrust Units for Power-Limited Propulsion Systems," NASA RP-241, AIAA Jour., Vol. 2, No. 4, 1964, presented at ARS Elec. Prop. Conf., Berkeley, 1964, ARS 2436-62.
25. Forrester, A. T., and Eilenberg, S. L., "Ion Rockets," Int'l Sci. and Tech., January 1964, pp. 52, 53, 56-61.
26. Kaufman, H. R., "Performance Correlation for Electron-Bombardment Ion Sources," NASA TN-D-3041, 1965.
27. Sohl, G., et al, "Ion Rocket System Research and Development," Final Report, NASA CR-54323, NAS3-5250, 30 December 1965.
28. Cox, A. L., "A Comparative Analysis of the Performance Capabilities of Various Types of Electrostatic Propulsion Engines," Brown Engrg. Co., Report No. R-136, February 1965.
29. Brewer, G. R., "Progress in Ion Propulsion," Flight International, Vol. 87, 8 April 1965, pp. 526-528.
30. Brewer, G. R., "Physical Electronic Phenomena in Ion Propulsion Engines," IEEE Spectrum, Vol. 2, August 1965, pp. 65-79.
31. Geis, J. W., "Research and Development of Electric Propulsion," Conf. on Civilian and Military Uses of Aerospace, New York City, 11-14 January 1965, New York Acad. of Sci., Vol. 134, 22 November 1965, pp. 317-341.

32. Floch, Y. L., and Labbe', J., "Some Experimental Results Obtained with a Mercury Ion Accelerator," *La Recherche Aerospatiale*, November-December 1965, pp. 31-39.
33. Anderson, J. R., and Work, G. A., "The Capabilities of Microthrust Electric Propulsion," AIAA Prop. Joint Specialist Conf., New York City, 1965.
34. Reader, P. D., "Durability Tests of Mercury Electron-Bombardment Ion Thrusters," AIAA Paper No. 66-231, March 1966.
35. Eilenberg, S. L., Caplinger, E., and Worlock, R. M., "Applications and Characteristics of Ion Thrusters in the Micro to Millipound Range," AIAA Paper No. 66-212, 1966.
36. Worlock, R. M., Caplinger, E., and Eilenberg, S. L., "Characteristics of Micropound Range Ion Thrusters," AIAA Paper No. 66-217, March 1966.
37. Speiser, R. C., "Technology and Development of Bombardment Ion Engines," AGARD, Phys. and Tech. of Ion Motors, 1966, pp. 255-272.
38. Bonnal, J. F., Coron, J., Mainfray, G., Manus, C., and Spiess, G., "Research on Ionic Propulsion," AGARD, Phys. and Tech. of Ion Motors, 1966, pp. 273-303.
39. Moeckel, W. E., "Promises and Potentialities of Electric Propulsion Status of Thruster Performance," NASA TM-X-52241, 3rd Ann. Meeting and Techn. Display, AIAA, Boston, 29 November - 2 December 1966.
40. Kerslake, W. R., Wasserbauer, J. F., and Margosian, P. M., "A Mercury Electron-Bombardment Ion Thruster Suitable for Spacecraft Station Keeping and Attitude Control," NASA TM-X-52163, presented at AIAA 5th Elec. Prop. Meeting, San Diego, 7-9 March 1966, AIAA Paper No. 66-247.
41. Free, B. A., and Mickelsen, W. R., "Comparative Performance of Thrusters for Solar Electric Spacecraft," AIAA Paper No. 67-86, AIAA 5th Aerosp. Sci. Mtg., New York, 23-26 January 1967.
42. Kaufman, H. R., and Kerrisk, D. J., "Performance Capabilities of Mercury Electron-Bombardment Ion Thrusters," AIAA Joint Spec. Conf., Washington, D.C., July 1967.
43. Kerslake, W. R., Byers, D.C., and Staggs, J. F., "SERT II Experimental Thruster System," AIAA Paper No. 67-700, AIAA Elec. Prop. and Plasmady. Conf., Colorado Springs 11-13 September 1967.
44. Eckhardt, W. D., King, H. J., Snyder, J. A., Ward, J. W., Myers, W. D., and Knechtli, R. C., "4000-Hour Life Test of a Liquid-Mercury Cathode in a 20-cm Ion Thruster," NASA Contract NAS3-6262, HRL Special Report, October 1966.

Flight System

1. Toms, R. S. H., "Study to Determine Flight Test Objectives for Ion Propulsion Systems," NASA CR-82019, NAS8-1545, PR-1, 22 May 1961.
2. Kemp, R. F., Sellen, J. M., Jr., and Pawlik, E. V., "Beam Neutralization Tests of a Flight-Model Electron-Bombardment Engine," ARS Paper No. 2663-62, November 1962.
3. Childs, J. H., and Cybulski, R. J., "Flight Tests and Early Missions for Electric Propulsion Systems," ARS Paper No. 2653-62, presented at ARS 17th Annual Meeting, Los Angeles, 13-18 November 1962.
4. Gold, H., "Spacecraft for Ion Thrustor Flight Tests," presented at Nat'l Aeronautics Mtg. and Production Forum, New York City, NASA TM-X-52008 27-30 April 1964.
5. Gold, H., Rulis, R. J., Maruna, F. A., and Hawersaat, W. H., "Description and Operation of Spacecraft in SERT I Ion Thrustor Flight Test," NASA TM-X-53050, 1964.
6. NASA, "NASA to Launch SERT I Spacecraft," NASA News Release No. 64-167, 14 July 1964.
7. Cybulski, R. J., Shellhammer, D. M., Lovell, R. R., Domino, E. J., and Kotnik, J. T., "Results from SERT I Ion Rocket Flight Test," NASA TN-D-2718, 1965.
8. RCA, "Development of the SERT I Spacecraft," Summary Report, NASA CR-54243, NAS8-2449, 1 February 1966.
9. King, H. J., Pinckney, K. R., Knauer, W., Molitor, J. H., Muldoon, W. J., and Kovar, D. G., "The Development and Testing of a Lightweight Flight-Prototype Engine System," AIAA Paper No. 66-216, 5th AIAA Elec. Prop. Conf., San Diego, 7-9 March 1966.

Mission

1. Stuhlinger, E., "The Flight Path of an Electrically-Propelled Space Ship," Jet Propulsion, Vol. 27, No. 4, p. 410, April, 1957.
2. Moeckel, W. E., "Fast Interplanetary Missions with Low-Thrust Propulsion Systems," Lewis Research Center, Cleveland, NASA Tech. Report R-79, 1960.
3. Melbourne, W. G., "Interplanetary Trajectories and Payload Capabilities of Advanced Propulsion Vehicles," Jet Propulsion Lab. Tech. Report TR32-68, Pasadena, Calif., March 1961.

4. Koerner, T. W., and Paulson, J. J., "Nuclear-Electric Power for Space Missions," Jet Propulsion Lab. Report TR34-230, Pasadena, Calif., January 1961.
5. Edelbaum, T. N., "The Use of High and Low Thrust Propulsion in Combination for Space Missions," J. Astronaut. Sci., Vol. 9, No. 2, 1962, pp. 49-62.
6. NASA, "Electric Propulsion for Spacecraft," NASA SP-22, December 1962.
7. Childs, J. H., and Cybulski, R. J., "Flight Tests and Early Missions for Electric Propulsion Systems," ARS Paper No. 2653-62, presented at ARS 17th Annual Meeting, Los Angeles, 13-18 November 1962.
8. Downey, J. A., III, Fields, S. A., and Stuhlinger, E., "Performance Comparison Between Variable Thrust and Constant Thrust Electric Propulsion Systems for Mars Flyby and Earth Escape Missions," NASA Tech. Memo X-50122, July 1963.
9. Dennington, R. J., LeGray, W. J., and Shattuck, R. D., "Electric Propulsion for Manned Missions," Proc., AIAA and NASA Conf. on Engrg. Problems of Manned Interplanetary Exploration, Palo Alto, Calif., 30 September - 1 October 1963, AIAA, pp. 145-159.
10. Kaufman, H. R., "The Electron-Bombardment Ion Rocket," Adv. Prop. Concepts, Vol. 1, 1963, pp. 3-17.
11. Mickelson, W. R., Kaufman, H. R., "Electrostatic Thrusters for Space Propulsion, Present and Future," NASA RP-318, NASA TM-X-51710, presented at Brit. Interplanetary Soc. Symp. on Adv. Prop. Systems, London, 9 October 1963.
12. Zimmerman, A. V., MacKay, J. S., and Rossa, L. G., "Optimum Low-Acceleration Trajectories for Interplanetary Transfer," NASA TN TN-D-1456, January 1963.
13. Stuhlinger, E., "Ion Propulsion for Space Flight," McGraw-Hill Book Co., New York, 1964.
14. Stuhlinger, E., "Electric Propulsion - 1964," Astronautics and Aeronautics, Part 1, p. 26, August 1964.
15. Mickelsen, W. R., and Kaufman, H. R., "Status of Electrostatic Thrusters for Space Propulsion," NASA TN-D-2172, 1964.
16. Brown, D. W., "Low Thrust Orbit Raising in Continuous Sunlight," NASA TN-D-2072, 1964.
17. Kaufman, H. R., "Electric Propulsion for Spacecraft," New Scientist, Vol. 23, 1964, pp. 263-265, NASA-RP-290, 1964.
18. Soufl, R. V., "Study of Station Keeping Using Low Thrust (Ion) Engines," Aerosp. Corp., TDR-269(4504-20)-1, SSD-TDR-63-374, AD-431841, 8 January 1964.

19. Errard, J. C., "Perspective on Aerospace Propulsion Systems," NASA TM-X-52073, 1965.
20. Mickelsen, W. R., and Mackay, J. S., "Interplanetary Flight with Electric Propulsion," *Astronautics and Aeronautics*, Vol. 3, No. 1, January 1965, pp. 44-49.
21. Strack, W. C., "Combined High-Low Thrust Propulsion for the Close Solar Probe Mission," NASA TN-D-3145, 1965.
22. Brown, H., "Application of Nuclear-Electric Propulsion to Manned Mars Missions," AIAA Paper No. 65-414, July, 1965.
23. HAC, "Solar-Powered Electric Propulsion Spacecraft Study," Final Report, HRL, NASA CR-71185, NAS7-100, JPL 951144, December 1965.
24. Mackay, J. S., et al, "Manned Mars Landing Missions Using Electric Propulsion," Lewis Research Center, Cleveland, NASA Tech. Note TN-D-3194, January 1966.
25. Goodman, M., "Advanced Low-Thrust Propulsion Systems for Station Keeping and Stability Control of the NASA Manned Orbital Research Laboratory (MORL): Resistojets and Radioisotope Jets," AIAA Paper No. 66-226, March 1966.
26. Molitor, J. H., Berman, D., Seliger, R. L., and Olson, R. N., "Design of a Solar-Electric Propulsion System for Interplanetary Spacecraft," AIAA Paper No. 66-214, March, 1966.
27. Ritchie, D., Toms, R., and Menetrey, W., "Potentials of Solar Power for Electric Propulsion," AIAA Paper No. 66-210, March 1966.
28. Stearns, J. W., and Kerrisk, D. J., "Solar-Powered Electric Propulsion Systems -- Engineering and Applications," AIAA Paper No. 66-567, March 1966.
29. Surugue, J., Fabri, J., and Grives, E. L., "The Potentialities of Electric Propulsion in the Near Future," presented at 17th Annual Int'l. Astron. Congr., Madrid, 15-19 October 1966, TP-394.
30. Molitor, J. H., "Application of Ion Thrust Motors in Attitude and Position Control of Satellites," AGARD, Phys. and Techn. of Ion Motors, 1966, pp. 393-422.
31. Toms, R. S. H., Waddell, R. L., and Fine, S. B., "Feasibility Study of an Ion-Propelled Mars Orbiter/Lander Spacecraft with Solar Photovoltaic Power," EOS Final Report, AFAPL-TR-66-109, Vols. I, II, III, 1966.
32. Molitor, J. H., Berman, D., Seliger, R. L., and Olson, R. N., "Design of a Solar-Electric Propulsion System for Interplanetary Spacecraft," AIAA Paper No. 66-214, 5th Elec Prop. Conf., San Diego, 7-9 March 1966.

33. Evvard, J. C., "Non-Chemical Space Propulsion," Lewis Research Center, Cleveland, NASA Tech. Memo TM-X-52267, January, 1967, Conf. on Non-Chemical Prop., AIAA and Catholic U of A, Washington, D.C., 12 January 1967.
34. Friend, E., and Hoyer, S., "Ion Engine Spacecraft Design and Mission Analysis," AIAA 5th Aerospace Sciences Meeting, AIAA Paper No. 67-87, New York, 23-26 January 1967.
35. Shukay, T. R., "Power and Weight Requirements for Ion Engine Systems as Functions of Mission Requirements," AIAA Jour., Vol. 4, No. 5, May 1967, pp. 615-620.
36. Meissinger, H. F., Park, R. A., and Hunter, K. M., "A 3 kW Solar Electric Spacecraft for Multiple Interplanetary Missions," AIAA Paper No. 67-711, AIAA Elec. Prop. and Plasmadyn. Conf., Colorado Springs, 11-13 September 1967.
37. Brewer, G. R. and Molitor, J. H., "Timetable for Ion Propulsion," Space and Aeronautics, June 1967.
38. Keislake, W. R., Wasserbauer, J. F., and Margosian, P. M., "A Mercury Electron-Bombardment Ion Thruster Suitable for Spacecraft Station Keeping and Attitude Control," AIAA Paper No. 66-247, AIAA Fifth Elec. Prop. Mtg., San Diego, 7-9 March 1966 also NASA TM-X-52163, 1965.
39. Kerrisk, D. J. and Kaufmann, H. R., "Electric Propulsion Systems for Primary Spacecraft Propulsion," AIAA Paper No. 67-424, AIAA Joint Spec. Conf., Washington, D.C., July 1967.

SECTION 3
POWER CONDITIONING AND CONTROL

3.1 POWER CONDITIONING ELECTRONICS

The power conditioning electronics has to provide both the steady-state and the transient electrical interface between the power source and the thruster. The principal functions which the power conditioning electronics may have to perform in order to provide these interfaces include:

- Dc-to-ac inversion
- Voltage transformation
- Rectification
- On-off power control
- Analog power, voltage, and current control
- Overload control
- Current-limiting
- Filtering (input and output)
- Isolation

Subsystem block diagrams for these functions where the prime source of power is dc are provided in Fig. 127. There can be many variations of these block diagrams, dependent on the type of input power, thruster requirements, and, in the case of a dc powerplant, the design approach for the dc-ac inversion function. Input and output filtering requirements are also dependent on the design of the dc-ac inverter. Figure 128 is a typical block diagram of the power conditioning electronics when the prime source of power is ac. The ac power source eliminates the need of a dc-ac inverter.

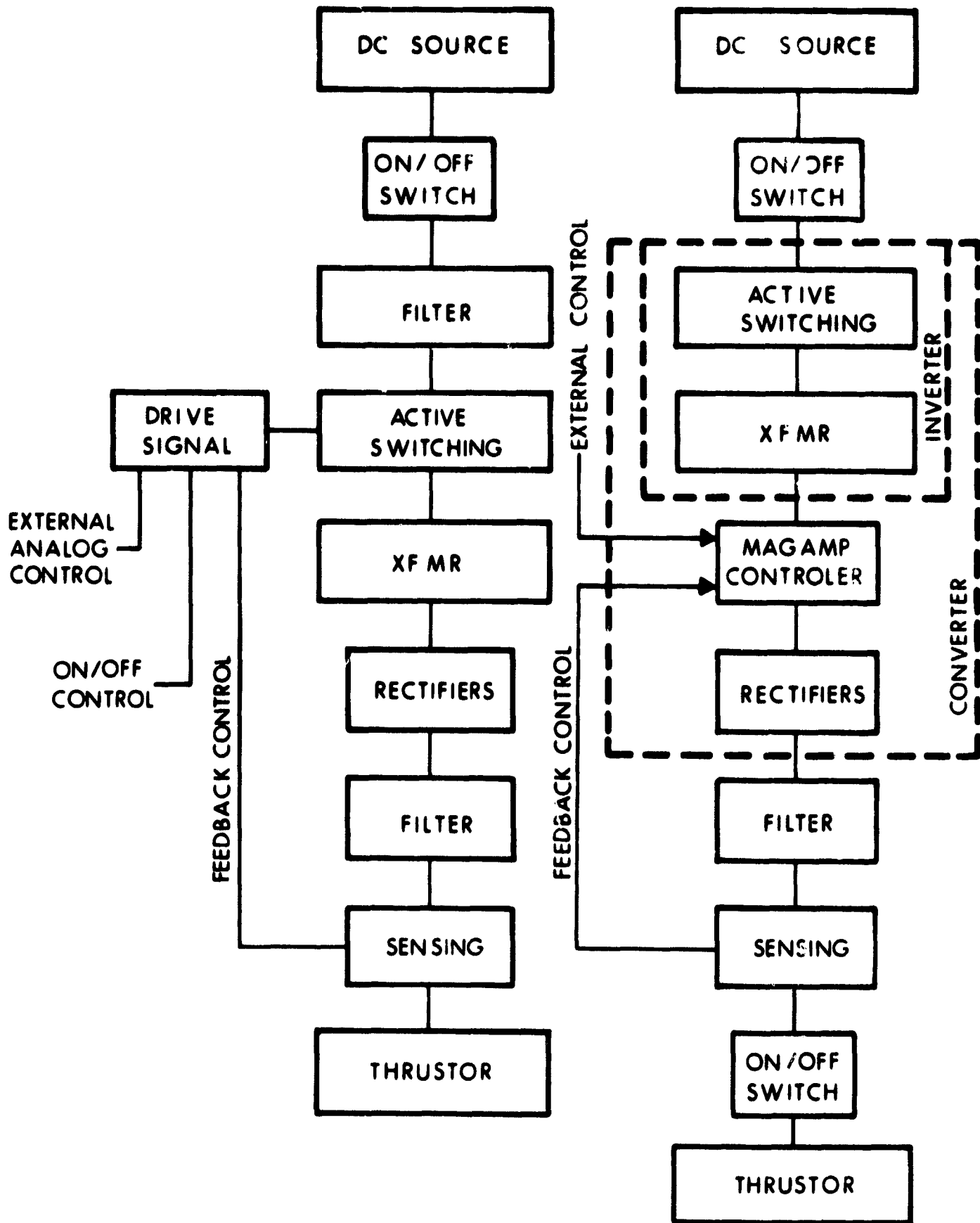


Figure 127. Block Diagrams of Power Conditioning Electronics for DC Power Source

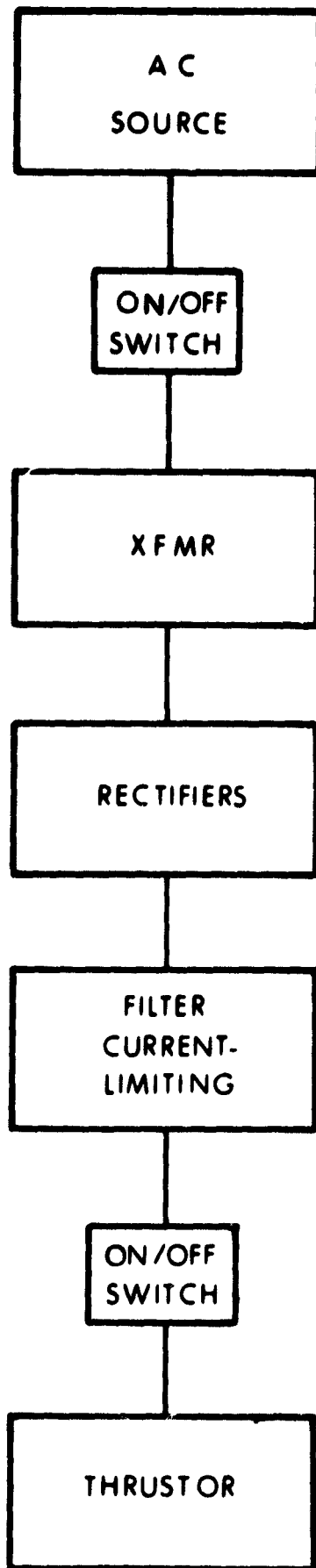


Figure 128. Block Diagram of Power Conditioning Electronics for AC Power Source

3.1.1 INVERTER-CONVERTER CIRCUIT DESIGN

The dc-ac inversion function requires the use of switching devices which have the ability to interrupt current flow in a controlled on-off operation. By using two or more such devices, the ac waveform required for magnetic transformation can be generated at power levels governed by the switching element capabilities. Figure 129 shows the basic approach to the inversion function. The desirable operating characteristics of the switching element include:

Negligible turnon and turnoff times as compared to the operating frequency

Negligible forward drop in the on state (low saturation resistance)

Resistance in the off state approaching that of an open circuit

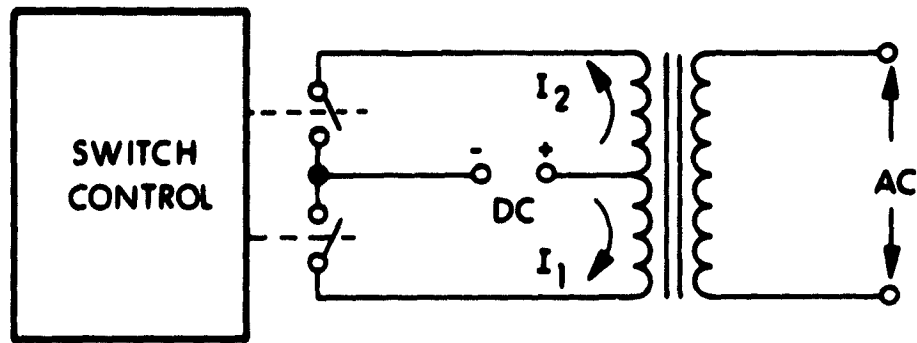
Negligible control power as compared to the inversion power level

Complete control of the switching operation

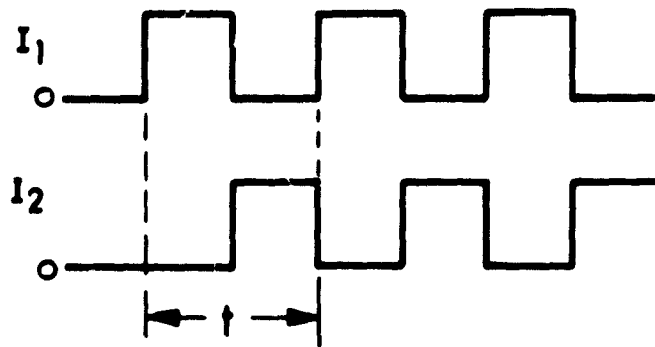
3.1.1.1 Basic Design Considerations

There are many devices that can be used for active switching. Unfortunately, most do not provide the desirable operating characteristics. Transistors, silicon controlled rectifiers, and thyratrons are the only active switching elements that can be considered for static power inverters at the present time.

SCR's and thyratrons have been used primarily as the active switch in high power (> 500W) inverter development to date. The ability to switch power at both high current and high voltage levels without series-parallel hybrid schemes of the active element has been their chief advantage relative to the power transistor. Available SCR's, for example, can switch currents as high as 1000A at up to 700V. The thyatron has an additional advantage of high tolerance to both nuclear radiation and high temperature operation.



a. CIRCUIT CONFIGURATION



b. IDEAL CURRENT WAVEFORMS WHERE τ IS THE RESULTING AC PERIOD

Figure 129. Basic Inverter Operation Diagram and Output Waveform

From the standpoint of inverter design, the transistor has two distinct and inherent operational advantages: the first involves the finite switching times for the devices which places an upper limit on the inverter switching frequency. As the switching times of the active switch become a significant portion of the switching period ($t = 1/f$), the inverter efficiency decreases rapidly. Increased switching frequencies, however, result in significant reductions in magnetic component mass.

The typical range of turnon and turnoff times for transistors, SCR's and thyratrons is shown in Fig. 130. As shown, the turnon characteristics for the three devices are relatively competitive. From the standpoint of turnoff times, however, the SCR requires a much longer time. Transistor inverters, on the other hand, have been fabricated with switching frequencies as high as 200 kHz at an efficiency greater than 85 percent. Thyratrons limit efficient inverter operation to a switching frequency of less than 1.5 kHz. Inverters utilizing SCR's can be efficiently designed for switching frequencies ranging from 3 to 4 kHz. The effect of switching frequency on magnetic component mass is illustrated in Fig. 131 for the output transformer. The choice of operating frequency involves, then, a tradeoff between the merits of low magnetic component mass and inverter circuit efficiency.

The second advantage of the transistor involves the indirect control that the base signal exercises over forward current. Unlike transistors, turnoff for SCR's and thyratrons cannot be accomplished through action of the control gate. Turnon for SCR's and thyratrons, however, does not require a gating signal for the duration of on-time ($t/2$) but only a pulse of sufficient width to turn on the SCR.

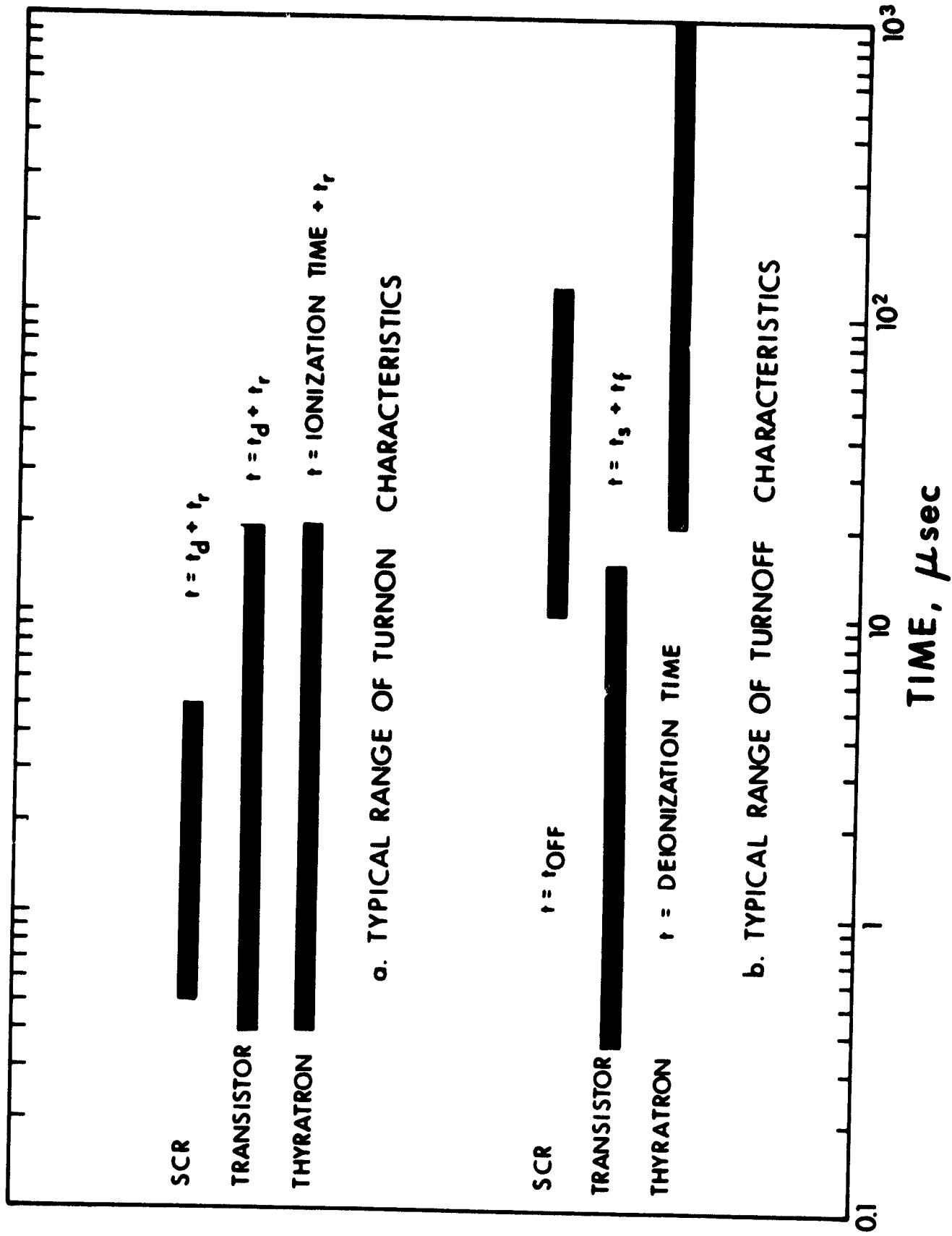


Figure 130. Comparison of Component ON-OFF Switching Characteristics

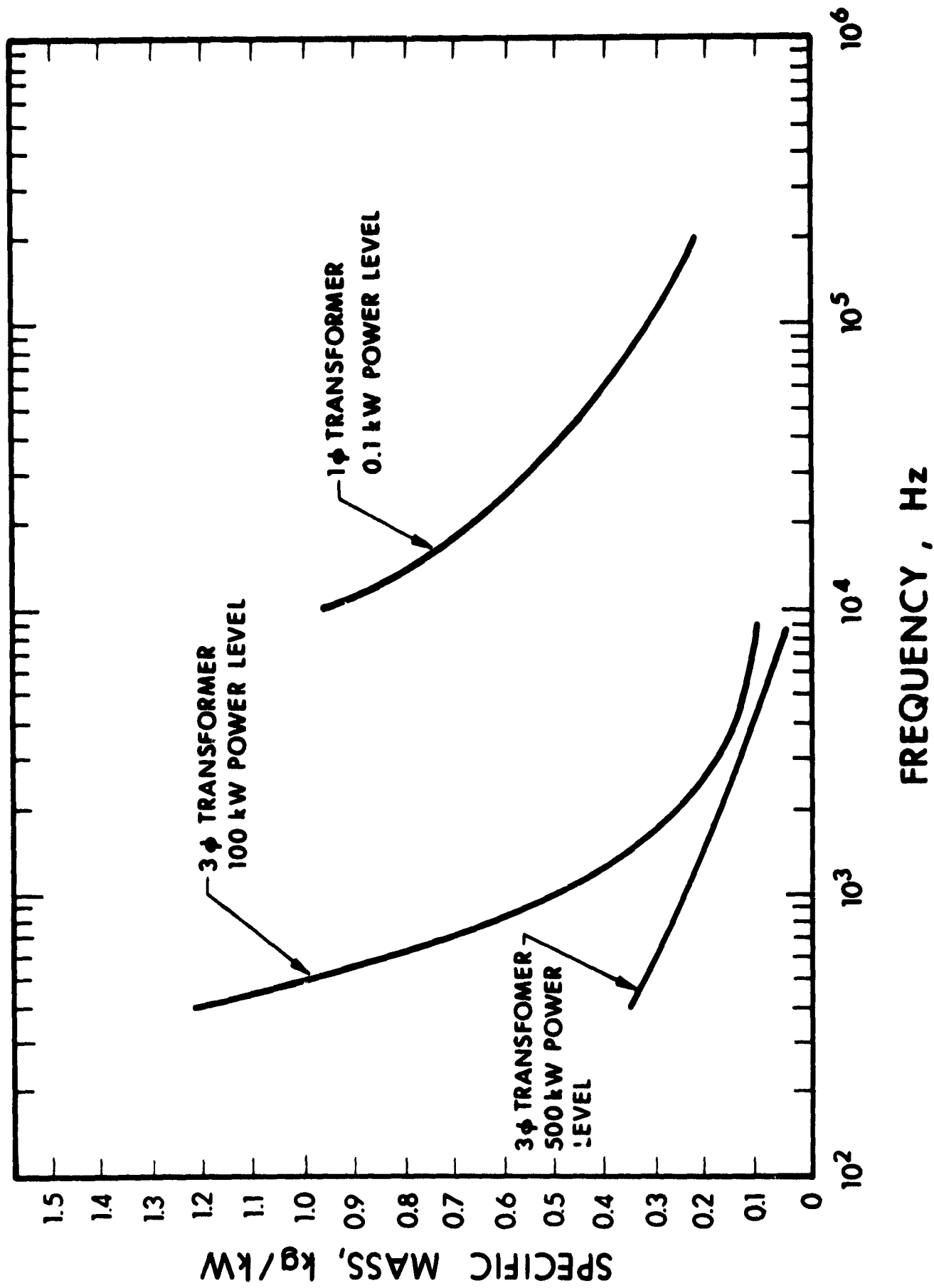


Figure 131. Transformer α versus Operating Frequency

The disadvantages to circuits requiring direct turnoff commutation as compared to the indirect high gain control in transistor circuits are in the areas of mass, reliability, and efficiency. In addition to the reliability consideration of operating time, care must be exercised to prevent mistriggering of SCR's by external interference. This interference may come from many sources including other SCR's, and will act on either the gate or anode to cause possible circuit malfunction.

Inverter circuits are typically arranged in either a push-pull or bridge configuration. The bridge configuration has the advantage of operation at up to twice the input voltage level used for push-pull arrangements. In addition, both circuits may acquire their timing from a self-excited or driven mode.

3.1.1.2 Single-Phase Transistor Inverters

The relative advantages and disadvantages of the two timing modes for transistor inverters include:

1. Self-excited timing

a. Advantages

- (1) Simplicity
- (2) Switches conduct alternately, minimizing the possibility of source shorting periods
- (3) Some inherent overload protection (this results from loss of gain in the feedback loop)
- (4) High efficiency at low power levels

b. Disadvantages

- (1) Operating frequency varies with changes in load input voltage or environmental conditions
- (2) Possible high transient spikes
- (3) Possible starting problems under loaded conditions

2. Driven timing

a. Advantages

- (1) Stable operating frequency
- (2) Reduced starting and transient problems
- (3) Turnoff accomplished by removal of timing waveform
- (4) Readily adaptable to pulsewidth modulation techniques
- (5) High efficiency at high power levels

b. Disadvantages

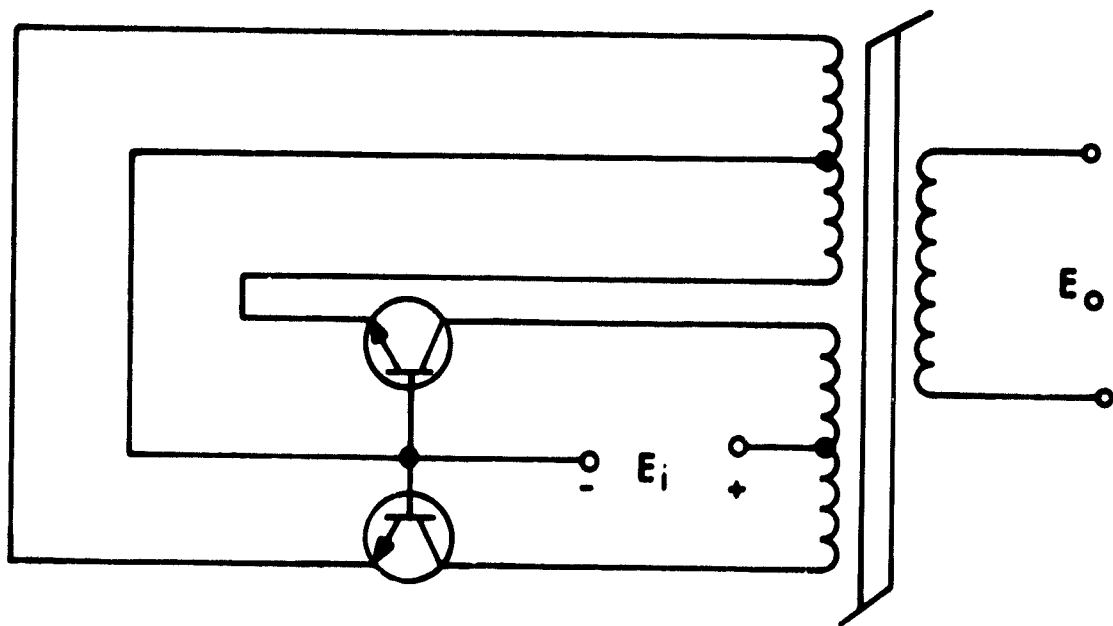
- (1) Requires more circuitry and components than self-excited approach
- (2) Requires careful selection of timing waveform or circuit design to avoid source-shortening periods due to active switch storage times
- (3) Requires additional overload protection circuitry

At the present time modularized power conditioning systems for ion thrusters as large as 5 kW could be fabricated with self-excited inverters. The driven approach would be required above the 4 kW level for higher efficiency.

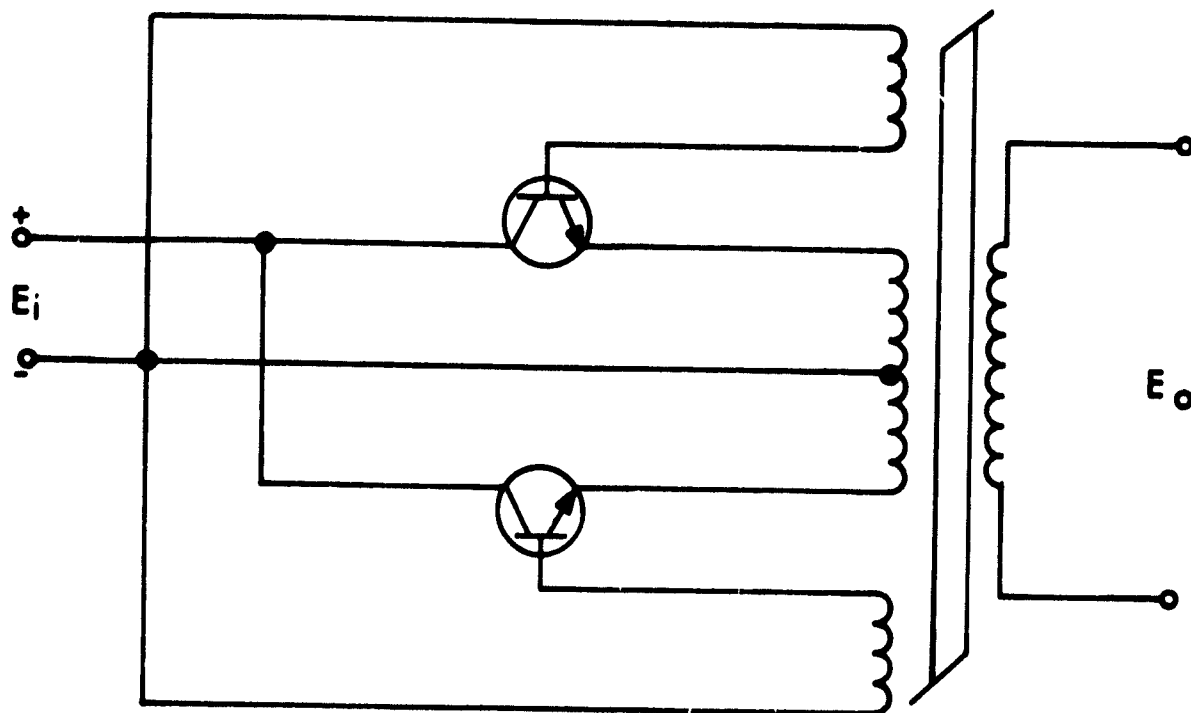
Basic Push-Pull Self-Excited Inverters

In a self-excited inverter, two transistors alternately conduct, switching the dc input voltage across half the primary, causing flux in the core to be cycled between positive and negative saturation. The circuits of Fig. 132 show two basic transistor inverters.

Assume one of the transistors is switched into the saturated condition. The collector current rises linearly until the transformer core (square hysteresis loop material) saturates. At core saturation, the rate of change of flux, which until now has been relatively constant, will be reduced suddenly, causing a reduction in the induced voltages. The sharpness of this change will depend on the squareness of the hysteresis



(a) COMMON BASE



(b) COMMON COLLECTOR

Figure 132. Common Base and Common Collector Self-Excited Push-Pull Inverters

loop. The decrease in induced drive voltages causes the conducting transistor to come out of saturation and turn off. Simultaneously, a small reverse change in flux ϕ causes a reversal of transformer voltages, and serves to switch the second transistor on, thus completing the cycle.

The frequency of operation can be set by the choice of the magnetic core parameters, the primary turns, and the input voltage. If the voltage drop across the transistor and winding resistance is assumed to be negligible, the frequency of operation is given by

$$f = \frac{E_{in}}{4 \frac{n}{2} \phi_m}$$

where E_{in} is the input voltage, n is the number of turns in the transformer primary, and ϕ is the transformer flux. The best efficiency is obtained when the power drawn by the load is very nearly equal to the maximum output that may be obtained, and when the feedback winding is matched to the input impedance of the transistor. The circuit is inherently safe from overloads in that it switches off if the loading becomes too heavy; the transistors will not conduct again until the fault has been cleared.

There are several versions of the basic push-pull circuit.

Common Base Circuit - The common base circuit is shown in Fig. 132(a). Its major advantage is that with low input voltages, somewhat faster switching times may be obtained in the configuration. The major disadvantage is that the base-to-emitter winding on the transformer must carry the total collector current.

Common Collector Circuit - This circuit, shown in Fig. 132(b) required a drive winding with a slightly higher number of turns than the primary (emitter-to-emitter winding). This circuit has

an advantage with respect to transistor cooling when used in a system that has the negative side of the dc power supply grounded to the vehicle system ground. The collectors of most transistors are mounted directly on the transistor base plate, and in this type system the transistor can be attached directly to a cold plate without electrical insulators.

Common Emitter Circuit - Two versions of the common emitter circuit are illustrated in Fig. 133. The starting circuit is the basic difference between these two inverters. (Starting circuits were not included in Fig. 132.) This circuit eliminates the drive problems in the common base and common collector circuits, and is frequently used in low power inverter design.

Improved Self-Excited Push-Pull Inverter

There have been many modifications made to the basic common emitter transistor inverter shown in Fig. 133(a). The modifications have been made primarily to eliminate high collector current spikes during commutation, which are a direct result of the finite storage effects in the transistor. During the storage period, while the transistor on one side of the circuit begins to conduct, the transistor on the other side remains on; thus the two simultaneous collector currents produce magnetic fluxes that buck each other, thus producing the high current spikes. The collector current is determined to a first approximation by the base current times β . The collector-to-emitter voltage V_{ce} is at its maximum at this time; therefore, transistor dissipation is extremely high until the stored charge is cleared in the opposing transistor. Since the storage time is directly proportional to overdrive, these losses are even greater at reduced loads than at rated loads. Increased switching

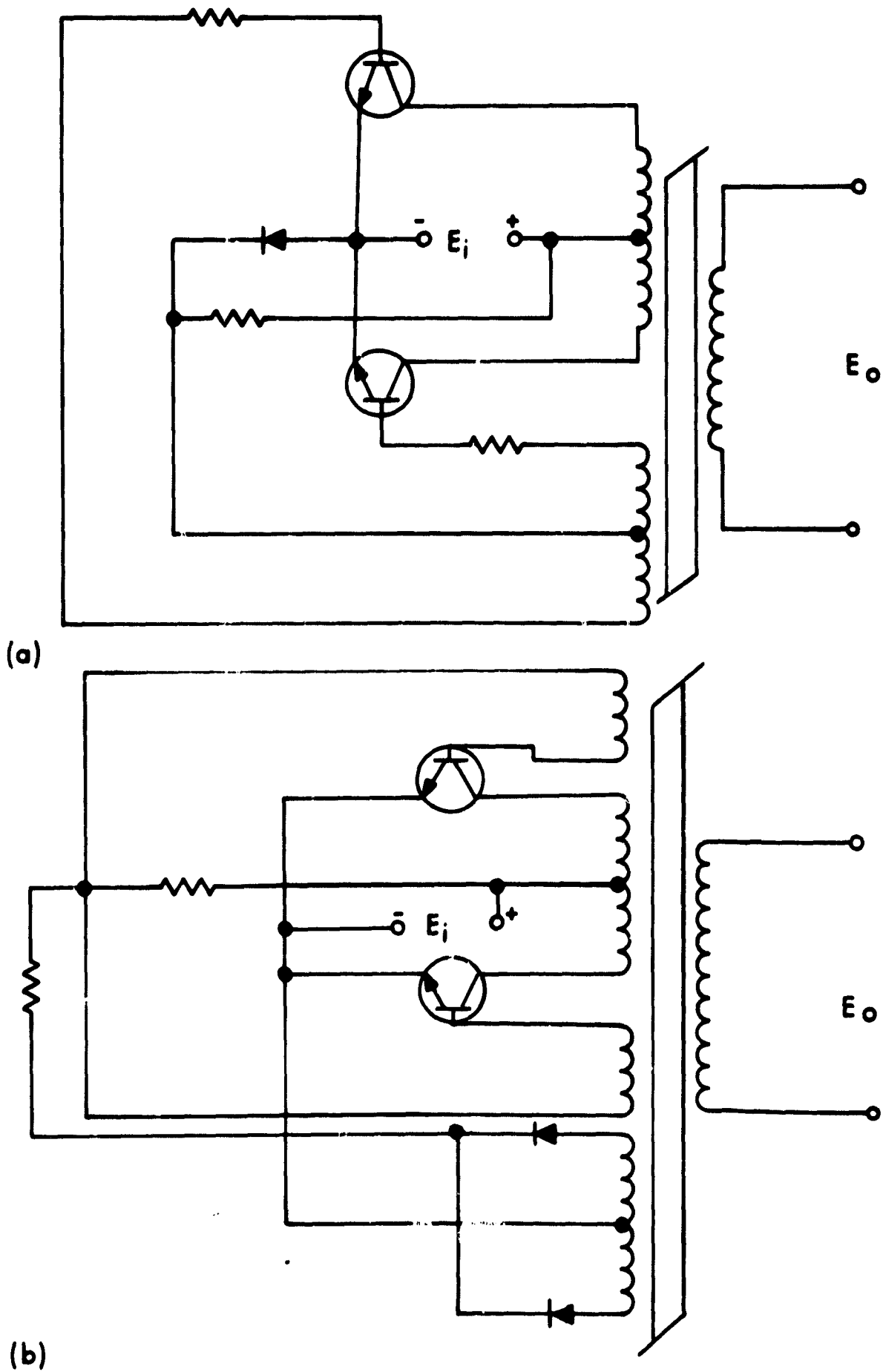


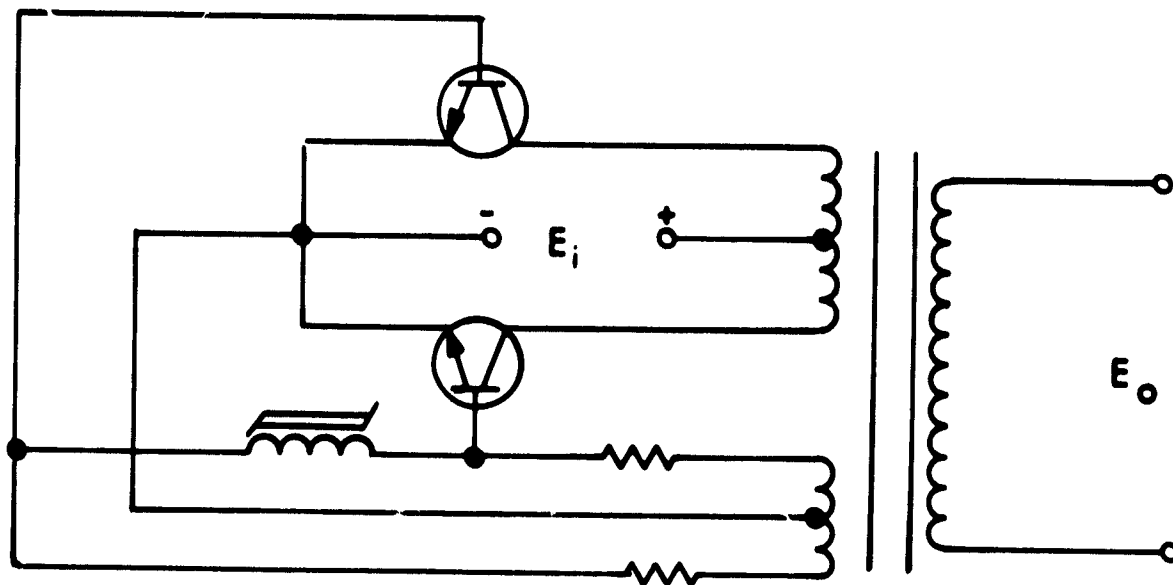
Figure 133. Common Emitter Self-Excited Push-Pull Inverters

frequency also increases the average losses due to the storage effects. The net result is transistor degradation, lower efficiency and reduced inverter operating life. The high collector currents also cause excessive voltage spikes at switchover which could destroy the transistor. The voltage spikes are a result of the stored energy from the inductance of the circuit leads and leakage flux of the transformer.

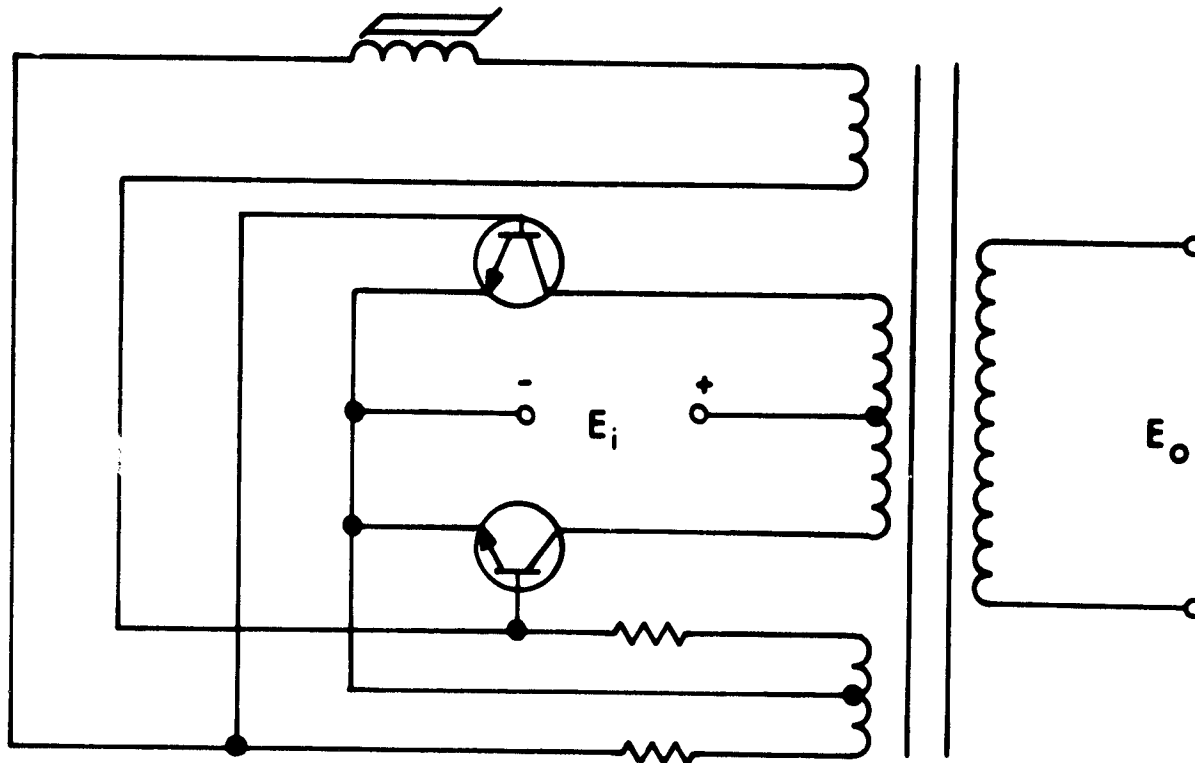
Several modified common emitter inverters that compensate for storage effects are shown in Fig. 134. In these circuits, the saturable output transformer has been replaced with a linear or nonsaturating transformer. The timing is provided by the saturable inductor in the base circuit.

The modified Jensen inverter shown in Fig. 135 is probably the most commonly used self-excited push-pull power inverter. In this circuit, a saturable base drive transformer (T1) controls the inverter switching operation at base-circuit power levels, and the linear output transformer couples the output to the load as in Fig. 134. Because the core material of the output transformer (T2) is not allowed to saturate, the peak collector current of the transistors in the inverter is determined principally by the value of the load impedance. This feature makes possible high circuit efficiency. Operation is as follows:

Because of a small inherent unbalance in the circuit, one of the transistors, say Q1, initially conducts more heavily than the other. The resulting increase in the voltage across the primary of T2 is applied to the primary of T1 in series with the feedback resistor, R_{fb} . The secondary windings of T1 are connected so that Q2 is reverse-biased and driven to cutoff, while Q1 is driven into saturation. As T1 saturates, the rapidly increasing primary current causes a greater voltage drop across feedback resistor R_{fb} . This increase in voltage across R_{fb} reduces the voltage applied to the primary of T1; thus the drive input



(a) BASIC SATURABLE BASE INDUCTOR INVERTER



(b) MODIFIED SATURABLE BASE INDUCTOR INVERTER

Figure 134. Modified Common Emitter Self-Excited Push-Pull Inverter

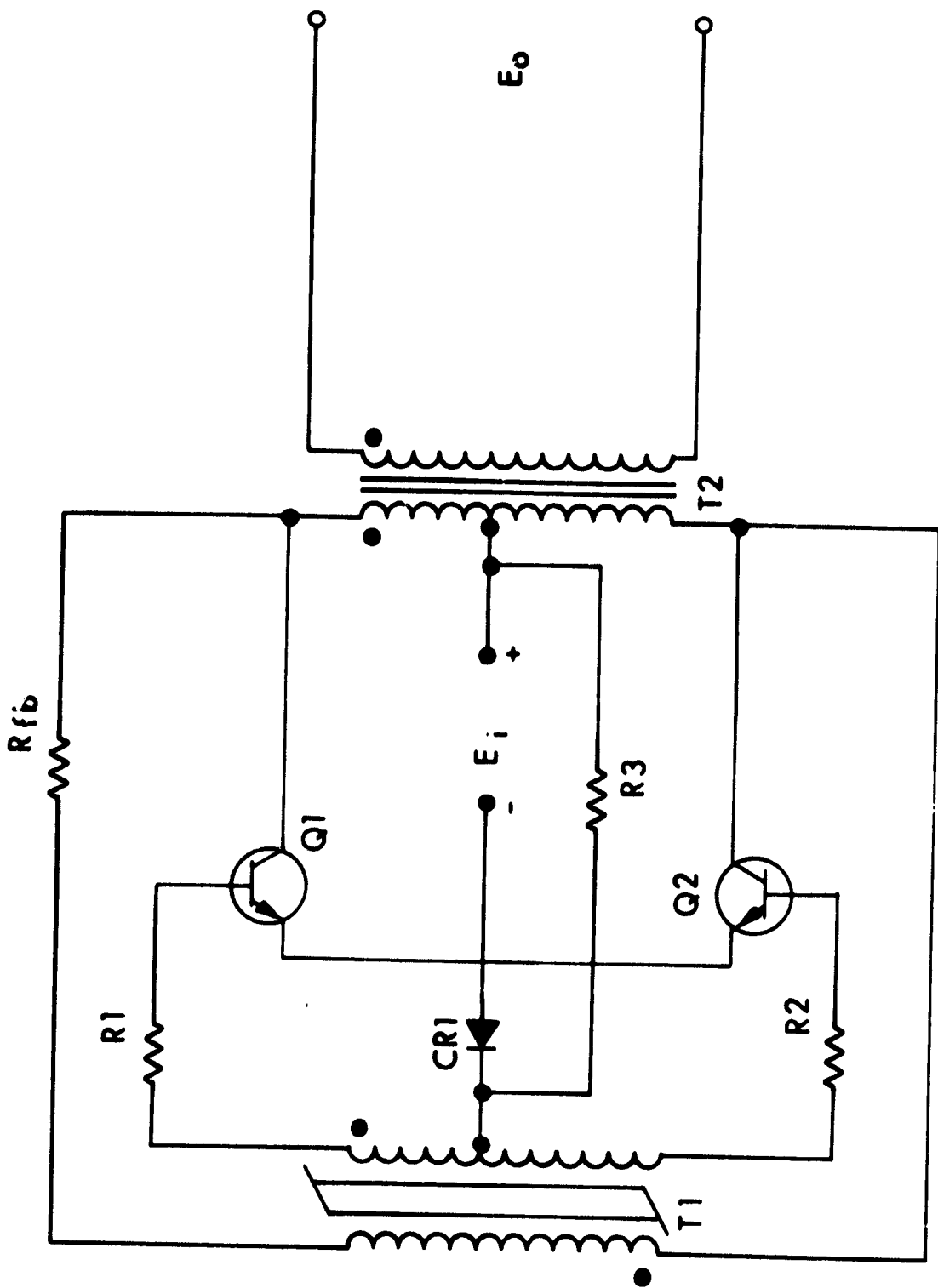


Figure 135. Modified Jensen Type Self-Excited Push-Pull Inverter

and ultimately the collector current of Q1 are decreased. The decrease in the collector current of Q1 causes a reversal of the polarities of the voltages across all the transformer windings. Transistor Q1, therefore, is rapidly driven to cutoff, and Q2 is allowed to conduct. The inverter operates in this state until saturation of T1 in the opposite direction. The cycle is repeated at a frequency determined by the design of T1 and the value of resistor R_{fb} . The external base resistor (R1) reduces the effect of the transistor base-to-emitter voltage, V_{be} , on the operation of the circuit. These stabilizing resistors are needed because V_{be} varies among individual transistors with temperature and operating time.

To insure that the inverter starts oscillating after power has been applied to the circuit, an initial drive signal is provided by the R3/CR1 network (one of many starting circuits that can be used). There are several methods that can also be employed for on-off inverter control. These include: (1) on-off control of the input power and (2) shorting the transistor bases to ground. The latter method has proved very effective in providing overload control or short-circuit protection for the inverter.

At high power levels, low closed-loop transistor gain can result in significant reductions in circuit efficiency. Low gain may also prevent the inverter from sustaining oscillations with aging or changes in environmental conditions. In a self-excited push-pull inverter this can be solved in part, by additional inverter stages. Figure 136 illustrates a two-stage push-pull self-excited inverter that compensates for storage-time effects.

Driven Push-Pull Inverter

Efficient (> 80 percent) self-excited push-pull inverter operation is presently limited to about 1 kW of power with available power transistors.

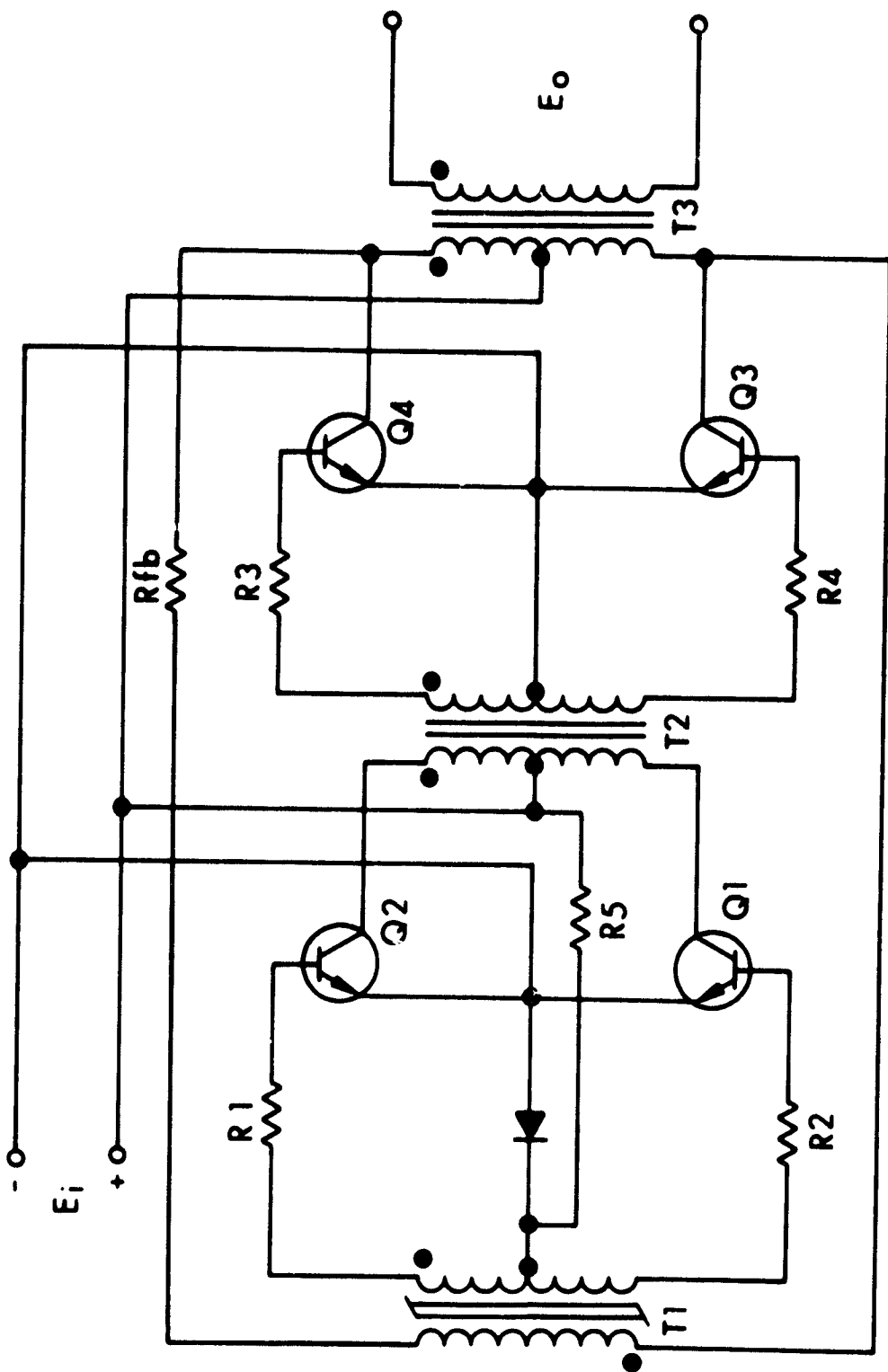
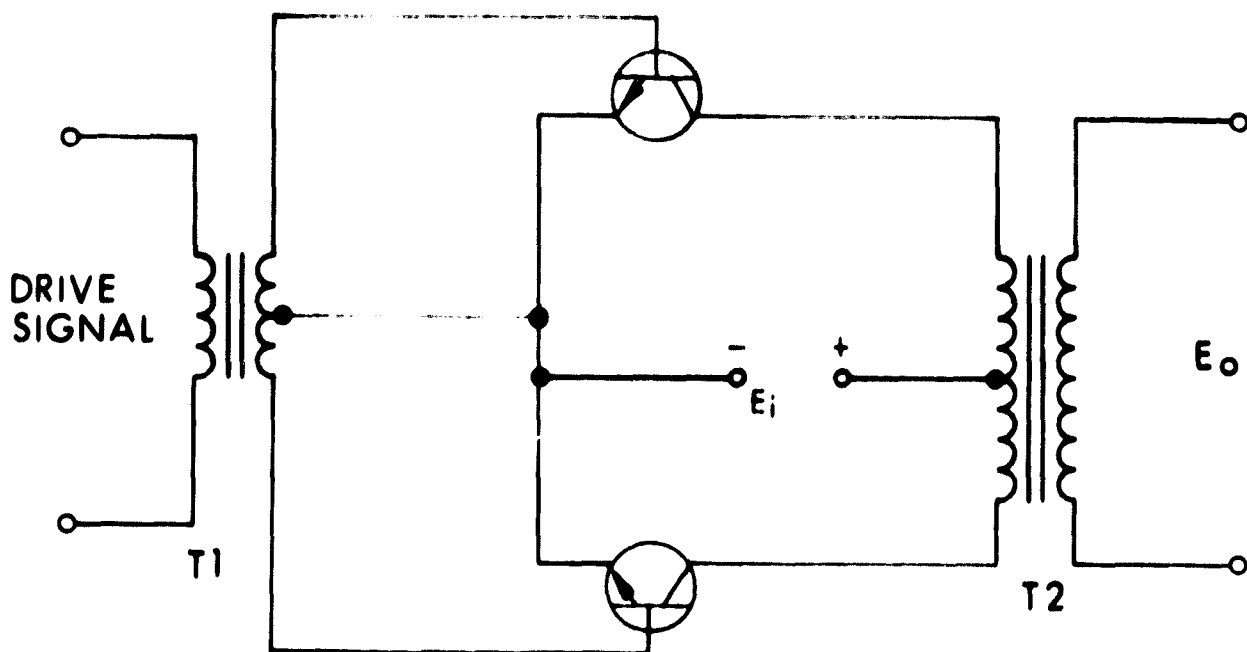


Figure 136. Two-Stage Self-Excited Push-Pull Inverter

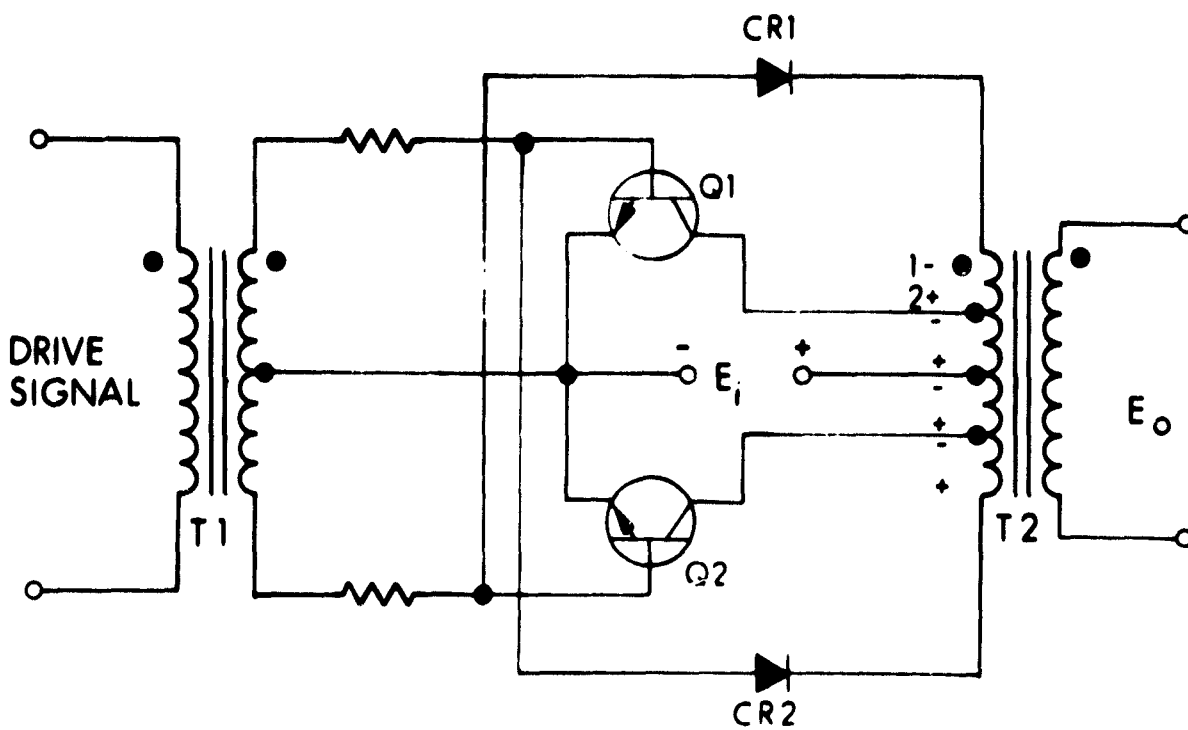
This is due to both the low closed-loop transistor gains and the power switching capabilities of the transistor. To increase both the power handling capability and the efficiency at higher power levels, driven inverters can be used. The basic push-pull or parallel inverter power stage is shown in Fig. 137(a). To further increase the power handling capabilities of this single power stage, a number of different hybrid series-parallel schemes can be employed. Two or more push-pull power stages, for example, can be paralleled by wiring their output transformer secondaries in series. This effectively parallels the transistors, and currents are balanced without dissipative compensation elements. Multiphase inverter systems, such as that shown in Fig. 138, are another example where isolated drive timing signals are required.

In addition to increasing the power handling capabilities and efficiency of an inverter system, the driven type of inverter offers several advantages that can exclude the use of self-excited inverters. As previously mentioned, these advantages include: (1) faster switching in the power stage, (2) regulation by pulsewidth modulation of the drive signals at any power level, and (3) an operating frequency that is insensitive to load, input voltage, and environmental variations.

The basic parallel inverter power stage shown in Fig. 137(a) is subject to the same current spike problems that occur in the basic common emitter circuits shown in Fig. 133 as a result of the transistor storage effects. Storage time compensation in the driven inverter stage can be provided in a number of ways. The circuit shown in Fig. 137(b) is one approach which prevents forward bias from being applied to one transistor while the other is in the storage time transitional period. The polarities shown in Fig. 137(b) exist after base drive has reversed but before storage time has allowed the conducting transistor to turn off. Reverse bias is applied to Q1 but forward bias is shunted from Q2 through CR1, winding 1-2, and the collector-emitter circuit of Q1 to the return of the drive winding. When Q1 starts turning off and



(a) BASIC PARALLEL INVERTER



(b) INVERTER WITH COMPENSATION FOR STORAGE TIME

Figure 137. Push-Pull Inverter Power Stage

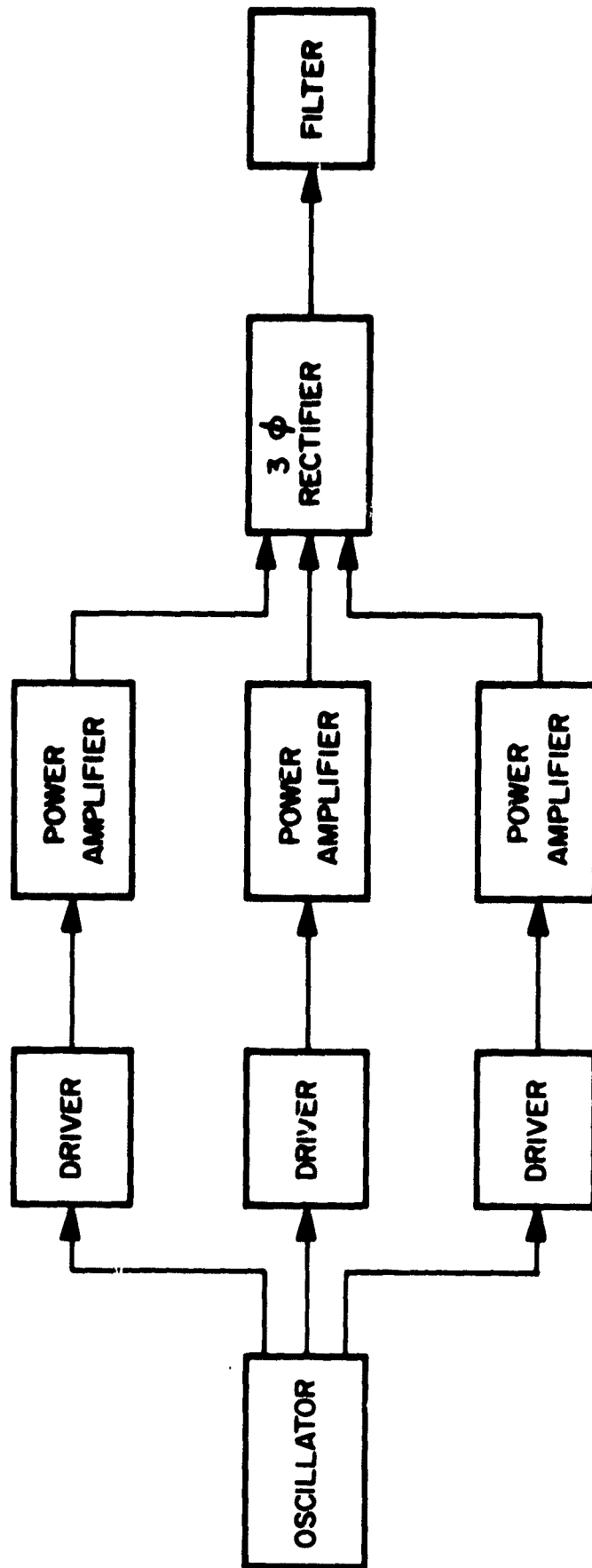


Figure 138. Polyphase DC-DC Converter Block Diagram

applied to Q1 but forward bias is shunted from Q2 through CR1, winding 1-2, and the collector-emitter circuit of Q1 to the return of the drive winding. When Q1 starts turning off and the emitter-to-collector voltage exceeds the bias winding voltage, forward bias is applied to Q2 and the next cycle of operation begins. The bias windings are necessary to overcome the forward drop of the diodes. The feedback rectifiers will automatically compensate for storage time regardless of load or environmental variations.

Self-Excited Bridge Inverter

In applications where the dc powerplant voltage approaches half the breakdown voltage ratings of the transistor, the push-pull inverter cannot be used. (This can be overcome if series transistor switches are used but due to the problems of compensation this technique is not recommended.) Each transistor in the push-pull inverter is subjected to twice the supply voltage during the time it is in cutoff. This is caused by the voltage induced in one-half of the transformer primary by the half that is conducting and is series-aiding to the powerplant voltage. Fast-switching transistors that are capable of switching currents above 10 amperes limit push-pull operation at the present time to about 50 volts.

To overcome the 50V input limitation, a bridge inverter such as that shown in Fig. 139 can be used. Neglecting transient effects, this circuit doubles the push-pull inverter voltage limitation without any compensation circuitry. In the bridge inverter Q1 and Q4 conduct simultaneously on alternate half-cycles while Q2 and Q3 conduct on the other half-cycle. Like the push-pull inverter (Fig. 136) the timing and storage compensation are provided by the saturable base drive transformer and feedback circuit. Initial oscillations are ensured by R1, R2, and CR1.

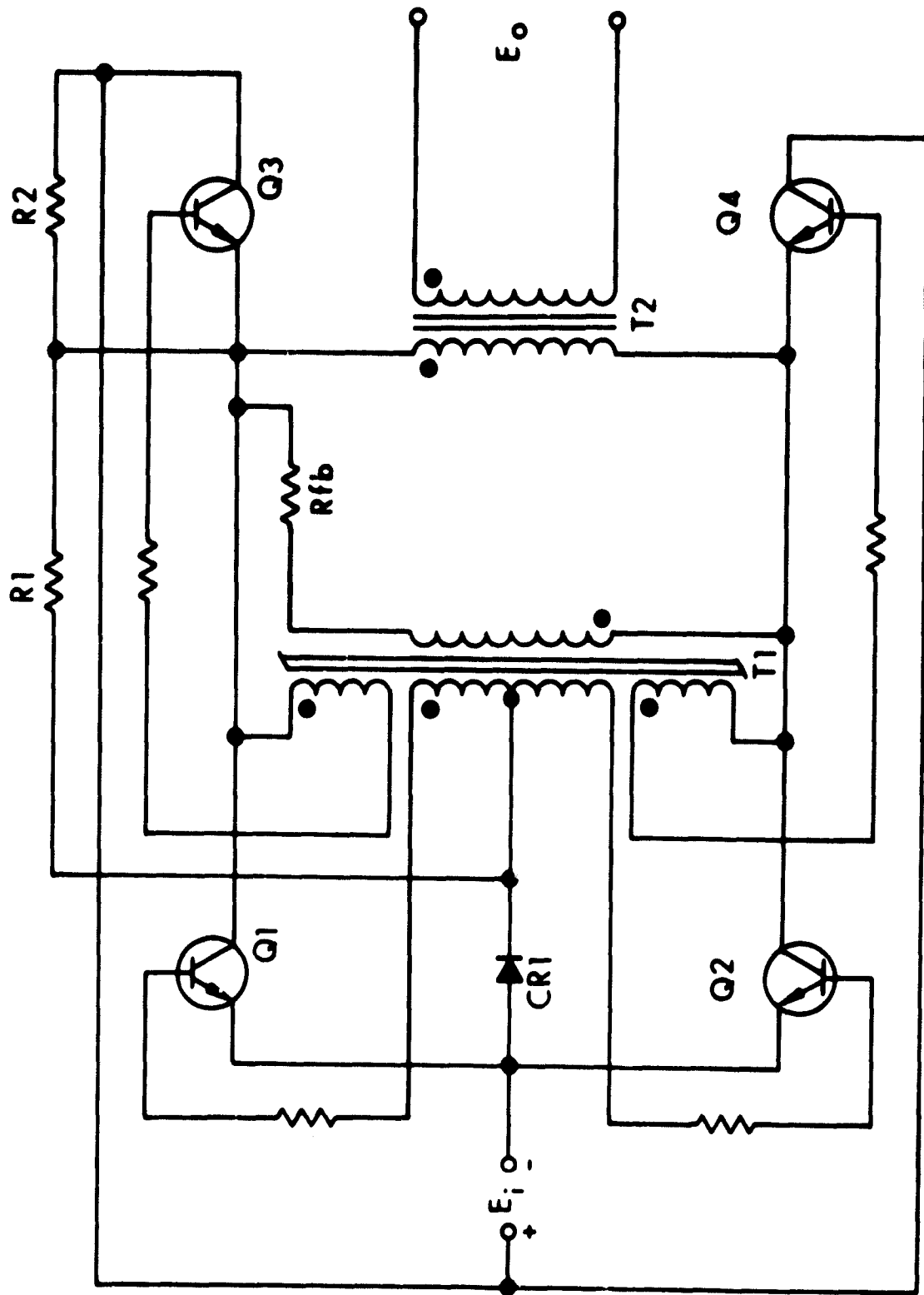


Figure 139. Modified Jensen Self-Excited Bridge Inverter

If the transistor closed-loop gain is too low to provide efficient operation, a two-stage inverter such as that shown in Fig. 140 could be used. This circuit utilizes both push-pull and bridge inverter operation. The power stage utilizes the bridge configuration due to the breakdown voltage ratings of the principal power transistors. Since medium power transistors are available with breakdown voltage ratings as high as 500V a push-pull drive circuit can be used. This inverter circuit also provides compensation for storage effects with feedback from the output transformer back to the saturable base drive transformer.

Driven Bridge Inverter

The basic driven bridge inverter power stage is shown in Fig. 141. At the higher input voltage levels the driven bridge inverter would be used instead of the parallel inverter power stage for the same reasons as discussed previously. Utilizing available transistors, a driven bridge inverter could be fabricated for at least 4 kW of power conditioning with 4 power transistors at about 90 percent efficiency.

3.1.1.3 Single-Phase Controlled Rectifier Inverters

In order to commutate on an SCR or thyatron switching device, a suitable means of reducing the anode current for a sufficient amount of time must be employed. The actual turnoff can be accomplished by using a variety of methods which include at least one of the following provisions:

- Reversal of current
- Auxiliary circuit interruption
- Diversion of anode current
- Anode reverse-biasing

Since the active switches are not ideal elements, other considerations may result in the incorporation of additional components necessary to

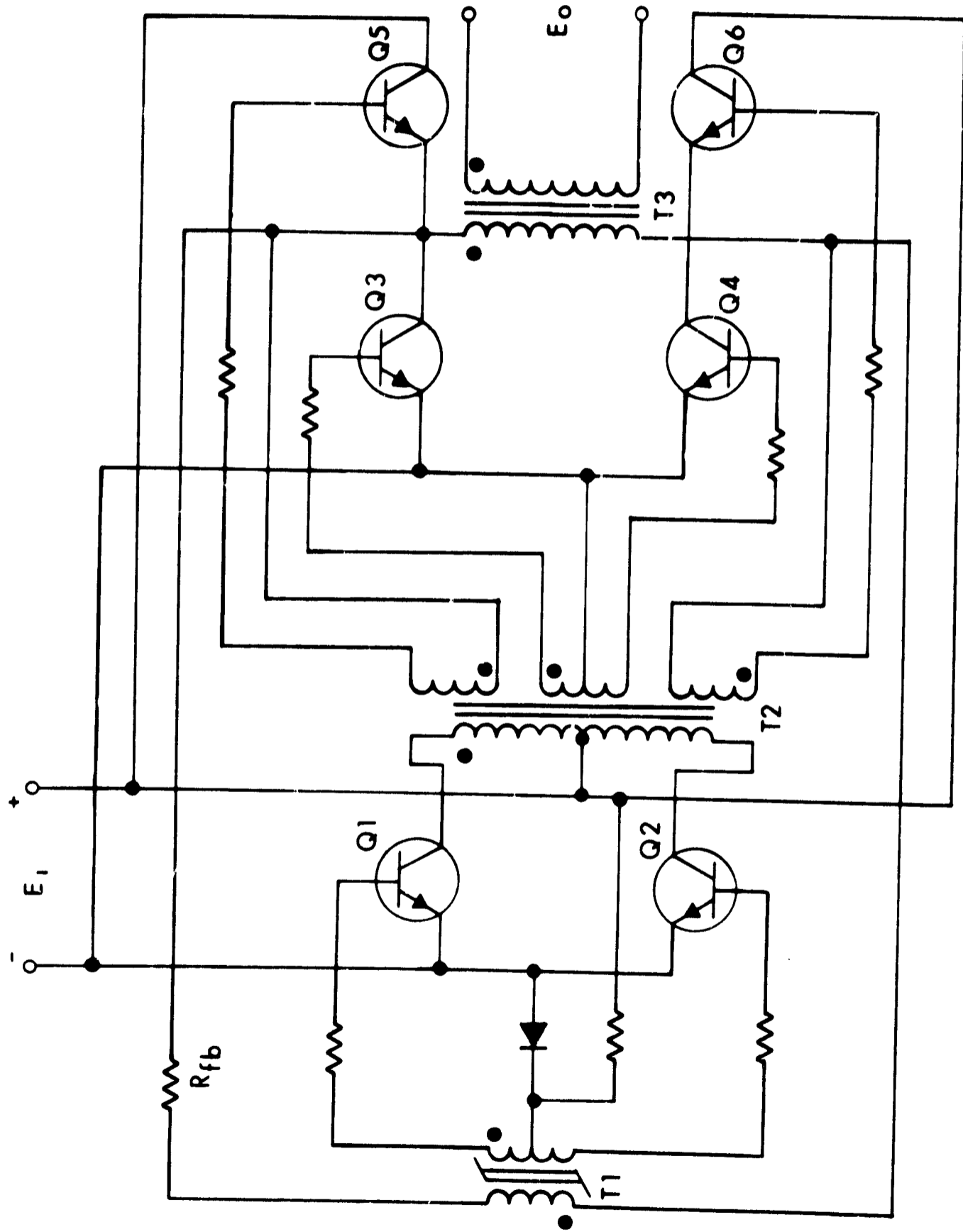


Figure 140. Two-Stage Self-Excited Hybrid Inverter

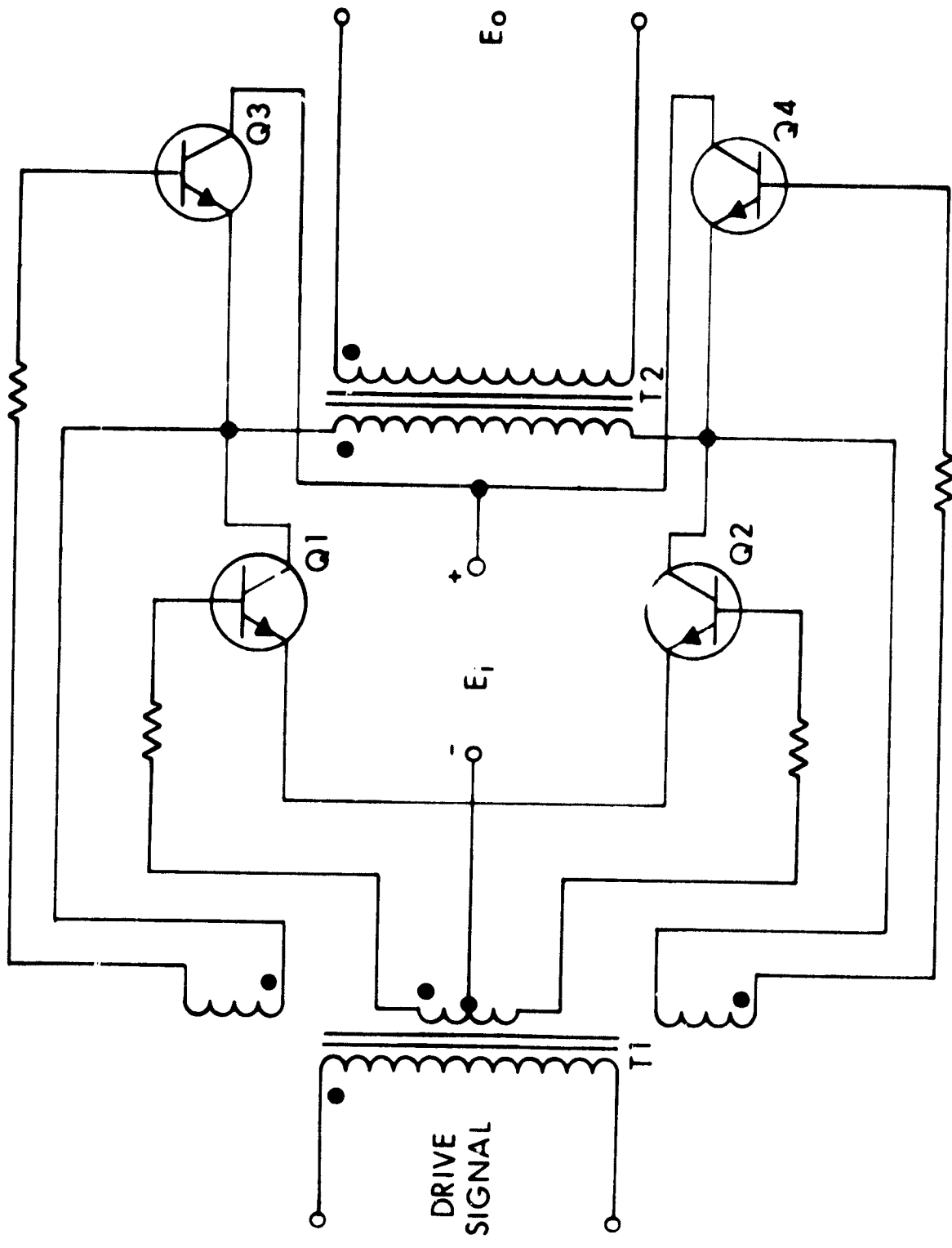


Figure 141. Basic Bridge Inverter Power Stage

limit voltage overshoots, rates of voltage change, and rates of current change. Thus, in general, the functions of commutation become:

The reduction of forward current to zero in the previously conducting active component

The delay of forward voltage reapplication to the previously conducting active component until it has gained its forward blocking capability

The control of forward current buildup in the active component presently being turned on

The commutation of controlled rectifiers in inverter circuits can be accomplished by using one of our general methods. From the standpoint of basic commutation in the inverter, the relative advantages and disadvantages of these commutation techniques include:

1. Parallel Capacitor Commutated

a. Advantages

- (1) Simplicity
- (2) Cathodes of controlled rectifiers are at ground potential
- (3) Commutating network can be placed on transformer secondary

b. Disadvantages

- (1) Large kVA rating required for commutating capacitor to handle inductive loads reliably
- (2) Poor voltage regulation
- (3) Circuit can only be turned off by removing input dc power
- (4) Care must be exercised to insure reliable starting
- (5) Commutation may fail at high load power factors

2. Impulse Commutated

a. Advantages

- (1) The loss of gating signals does not necessarily result in commutation failure
- (2) Circuits are well adapted to voltage control techniques
- (3) Circuits can be used to reverse power flow if desired
- (4) High efficiency
- (5) Low regulation
- (6) Load power factor variations do not require changes in the commutation components or result in commutation failure

2. Impulse Commutated (cont.)
 - (7) The values of L and C for commutation are smaller than in the parallel inverter
 - b. Disadvantages
 - (1) Circuit can only be turned off by removing input dc power
 - (2) Large input filter capacitor is usually required at the inverter input terminals
3. Series Capacitor Commutated
 - a. Advantage - The gating excitation may be interrupted to stop inverter operation
 - b. Disadvantages
 - (1) Operating frequency changes with load variations
 - (2) Output voltage changes with load variations
 - (3) Very light loads may cause commutation failure
4. Harmonic Commutated
 - a. Advantages
 - (1) Permits operation over the full 360 degrees of phase control
 - (2) Supplements commutation of polyphase systems
 - (3) Provides power factor improvement and increased regulation
 - b. Disadvantages
 - (1) Requires a fixed harmonic voltage source or other stabilization scheme for operation over a wide load range
 - (2) Possibility exists of commutation failure under light load conditions with internally produced harmonic voltage

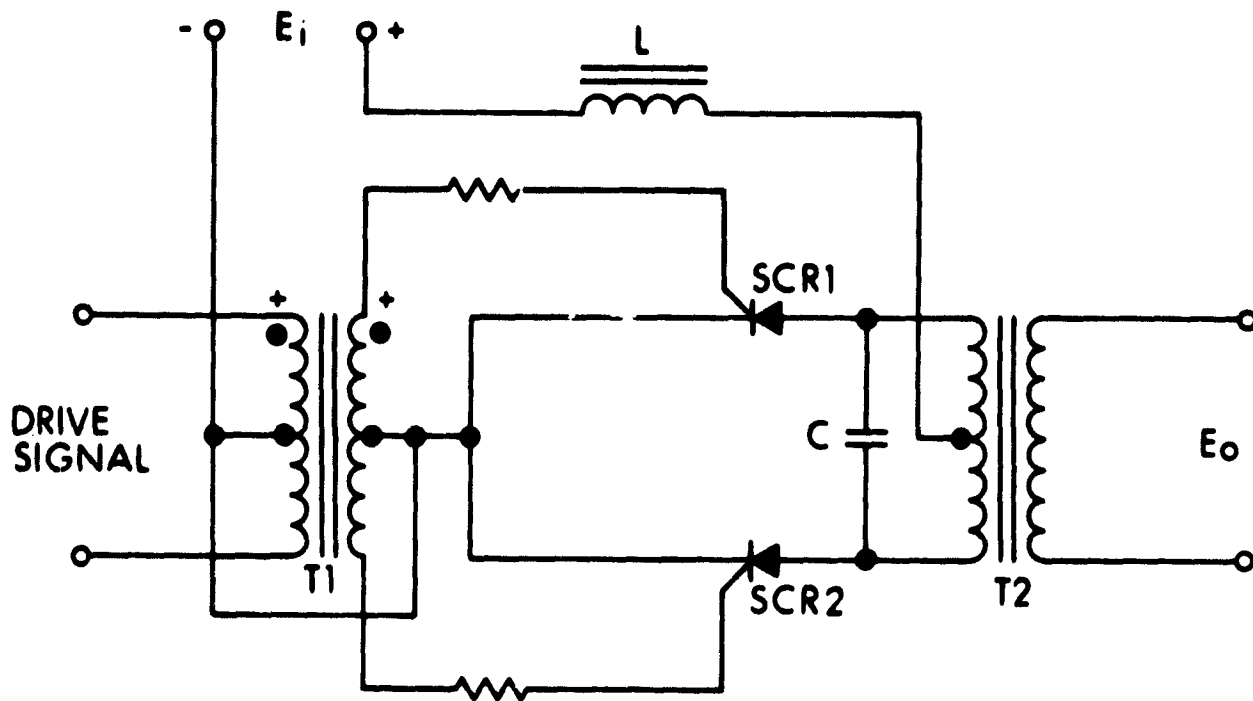
For most electric propulsion power conditioning requirements the impulse commutated inverter is the recommended design approach for controlled rectifier inverters. At low input voltages or high temperature inverter operation with constant load, however, the parallel capacitor commutated inverter should be considered.

Parallel Capacitor Commutated Push-Pull Inverter

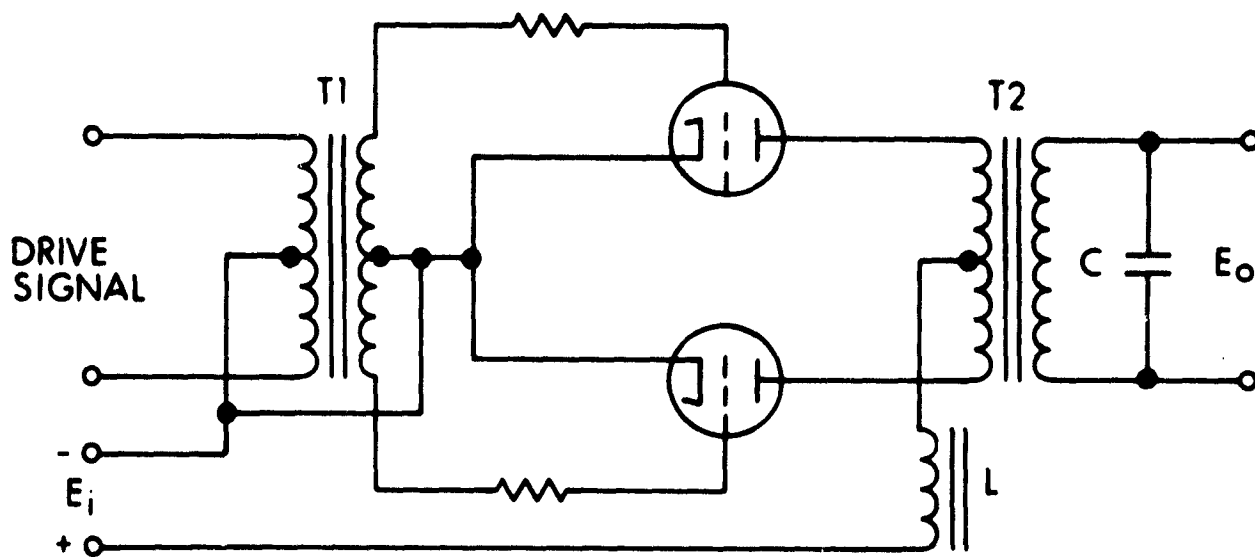
The parallel capacitor commutated inverter circuit is illustrated in Fig. 142(a). This circuit represents one of the earliest inverter design approaches utilizing controlled rectifiers. It is commonly referred to as the parallel inverter and has been successfully used in many applications. Commutation of the conducting SCR is accomplished by the commutating capacitor (C). This capacitor can be placed on the primary or the secondary side of the transformer. With SCR 1 conducting, the operation of the circuit is as follows:

A firing pulse is applied to the gate of SCR 2. SCR 2 rapidly turns on and the anode voltage falls to nearly ground potential (+1V). Since the capacitor was charged to twice the supply voltage (positive at SCR 2 side) the voltage at the anode of SCR 1 is about twice the supply voltage below ground potential (less the SCR 2 drop). Note that at this point the voltage across the transformer has not yet changed in polarity. The capacitor discharges through the transformer into the load, and at the same time is being charged in the reverse direction by the supply voltage. Thus, the discharge rate is faster than the RLC time constant alone. The time that the anode of SCR 1 is held below ground level must be as long or longer than the turnoff time of the SCR. The voltage waveform across the transformer (and load) is the same as the capacitor voltage waveform. SCR 2 is now conducting and SCR 1 is off. A firing pulse is applied to the gate of SCR 1 and the commutation process repeats in the reverse direction.

Voltage and current waveforms for the parallel inverter are shown in Fig. 143. A variety of waveforms can exist at the load depending upon inverter component values and load characteristics. As previously mentioned, the commutating capacitor can be placed on the secondary side of the transformer or split between primary and secondary. Figure 142(b) is a thyatron inverter with the commutating capacitor across the transformer secondary winding. There are two advantages with the capacitor on the secondary. In the case of a stepup transformer the size of the capacitor can be reduced by the square of the turns ratio.

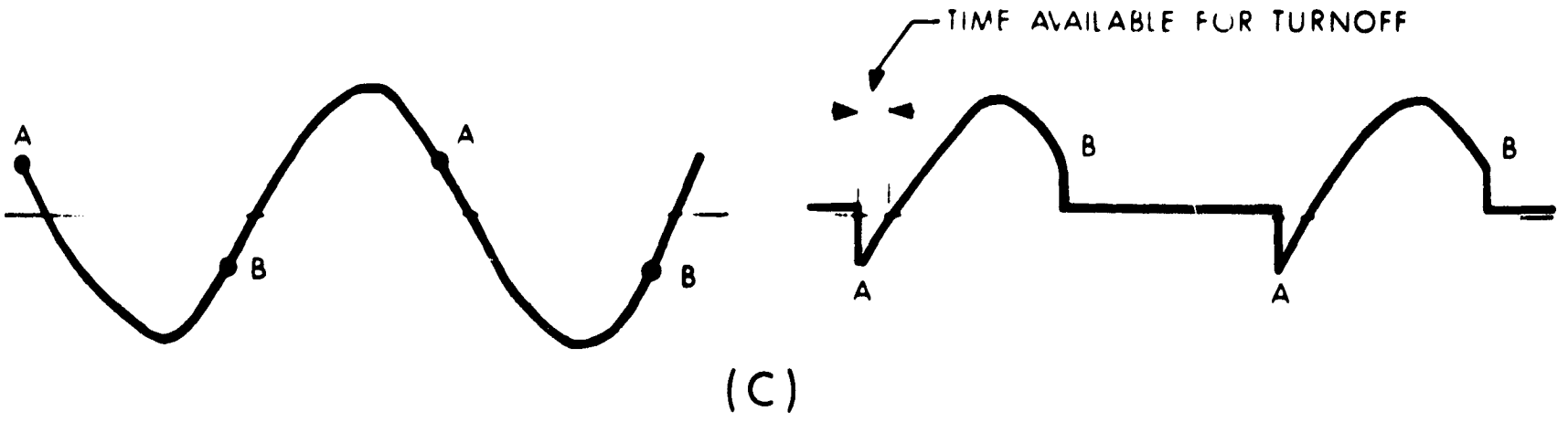
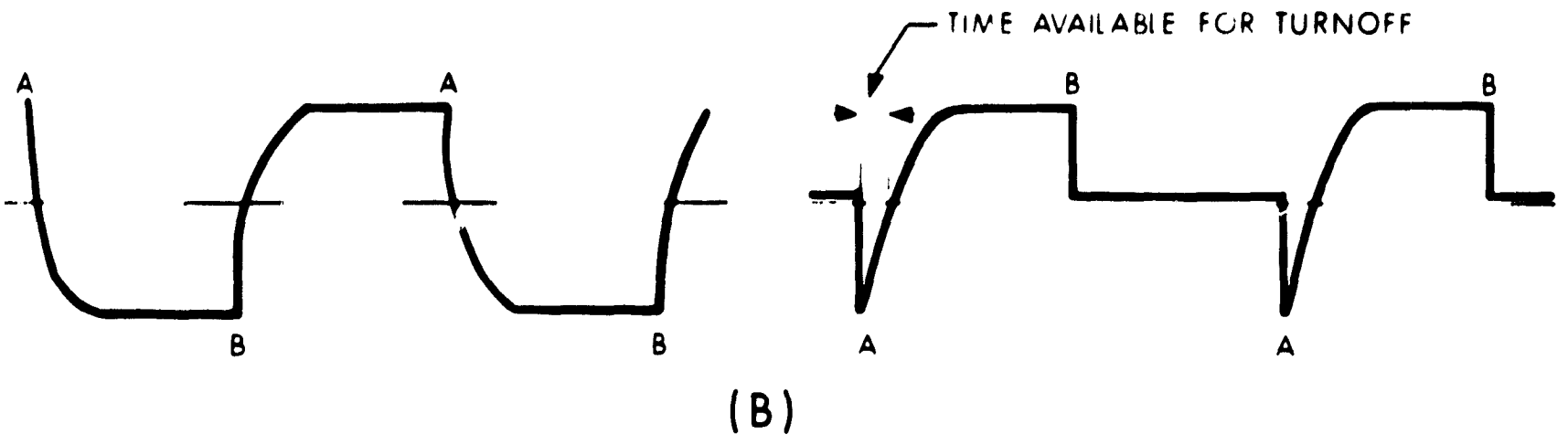
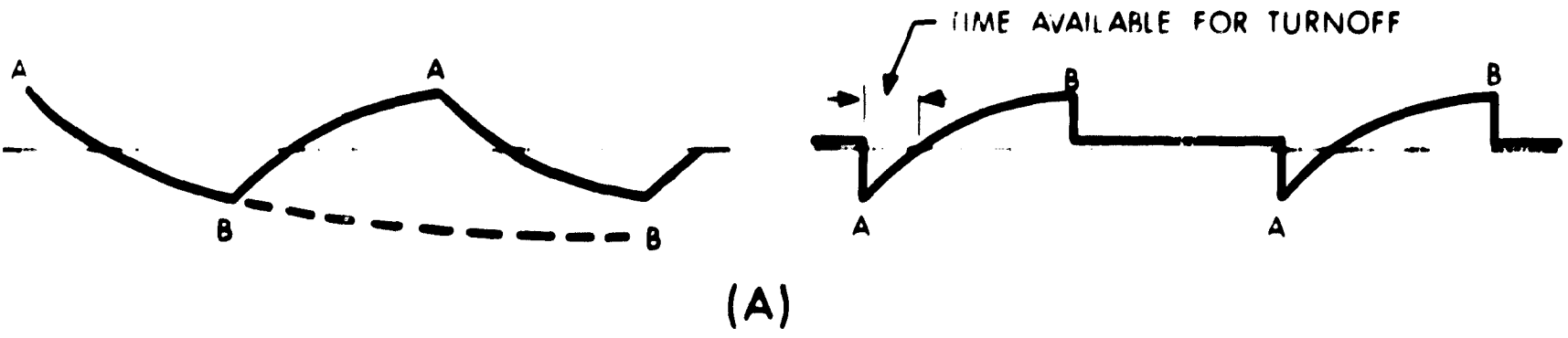


(a) BASIC SCR INVERTER



(b) HIGH TEMPERATURE THYRATRON INVERTER

Figure 142. Parallel Capacitor Commutated Inverters



LOAD WAVEFORM

ANODE VOLTAGE WAVEFORM

A- LIGHT RESISTANCE LOAD
 B- HEAVY RESISTANCE LOAD
 C- PARTIALLY INDUCTIVE LOAD

Figure 143. Parallel Inverter Waveforms

For high temperature thyatron operation this approach also allows the capacitor to be placed out of the hot zone.

The inductance (L) serves as a ballast to prevent excessive current flow during switching. During the switching interval, high currents can flow in the primary to the commutating capacitor and to the anode of the SCR which has been turned on. If this current is not limited, the charging time for the capacitor will be very short and the SCR to be turned off will not be reverse-biased long enough for turnoff to occur.

Another type of parallel inverter is shown in Fig. 144. This is known as a counter-emf inverter. An external voltage is applied to the commutation transformer at the same instant that the grid trigger voltage is applied to the opposite tube to reverse the voltage on the conducting thyatron. Detailed operation of this circuit was not found in the literature and several problem areas can be seen. The commutating transformer, for example, must handle large currents with extremely low dc drop and be able to supply over twice the supply voltage to reverse-bias the thyatron. The driving power required for commutation appears to be extremely high with this circuit.

Impulse Commutated Push-Pull Inverter

The basic impulse commutated inverter is illustrated in Fig. 145. This design approach is basically the parallel inverter with a different or improved mode of commutation. Like the parallel inverter the switching frequency of the inverter is determined by the frequency of the gate drive signal. The commutation is also initiated by alternately gating each SCR on successive half-cycles. The actual commutation or turnoff of the conducting SCR in this circuit is provided by the L-C resonate circuit as opposed to only the commutating capacitor in Fig. 142. L and C1 are selected to resonate at a frequency that develops a pulse of sufficient width to turn off the conducting SCR. The inductor also serves as a ballast to limit the current flow during switching.

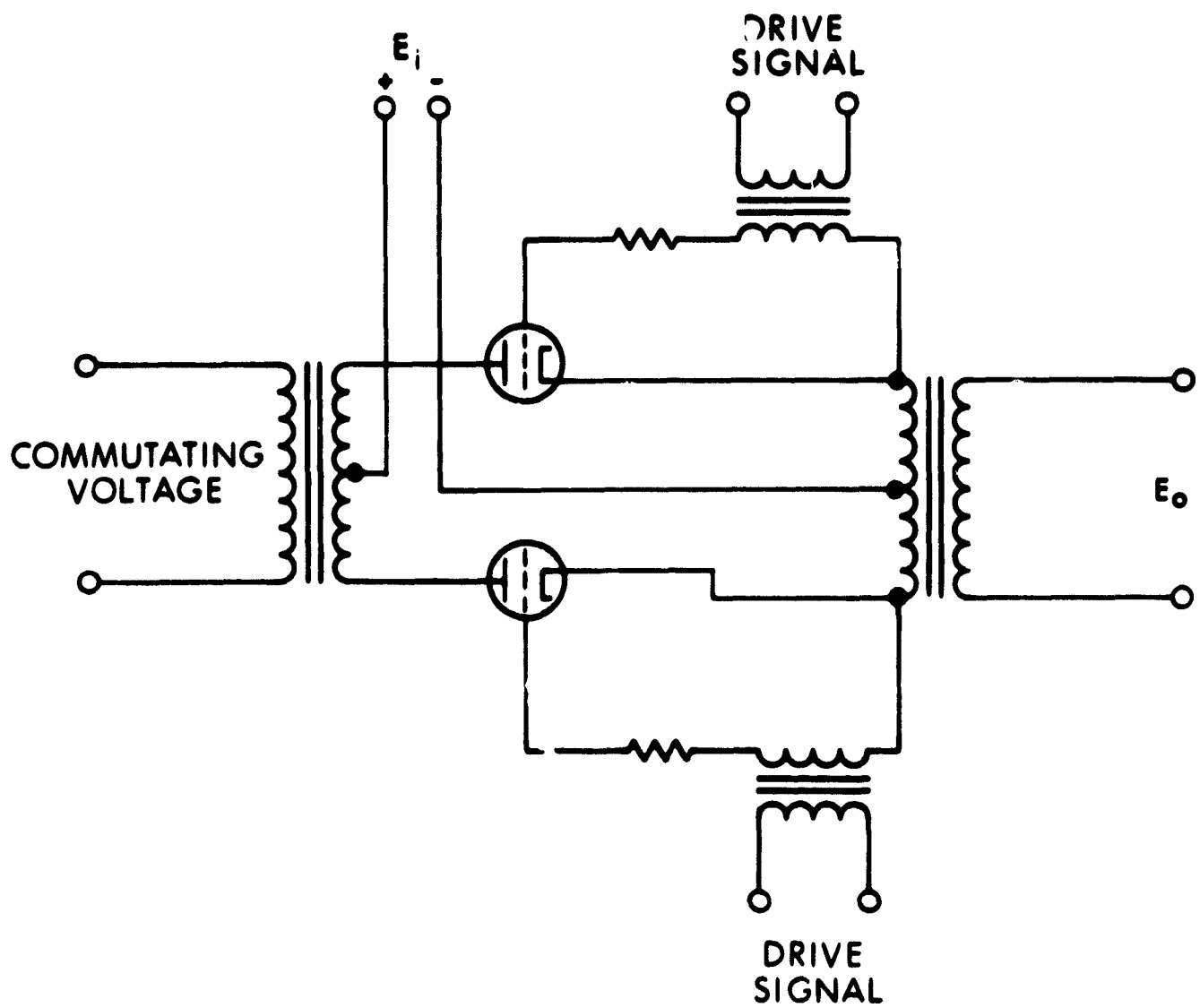


Figure 144. Counter EMF Parallel Inverter

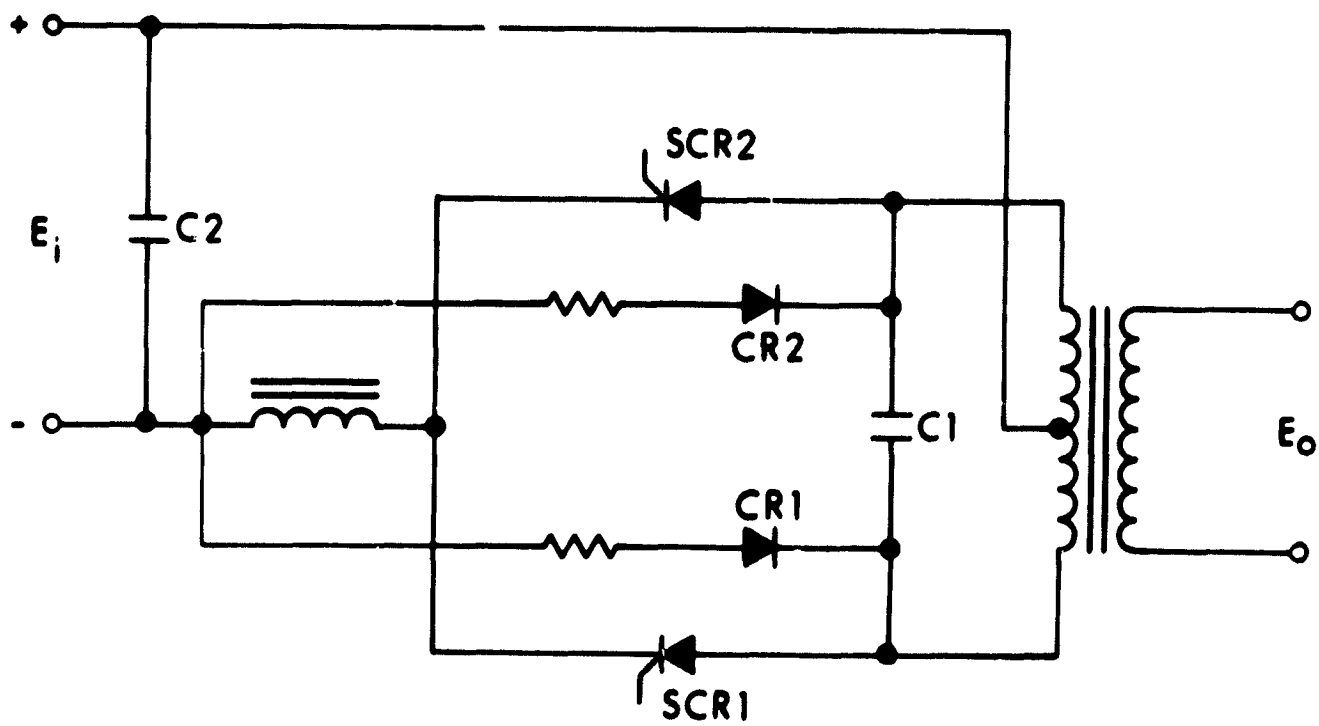
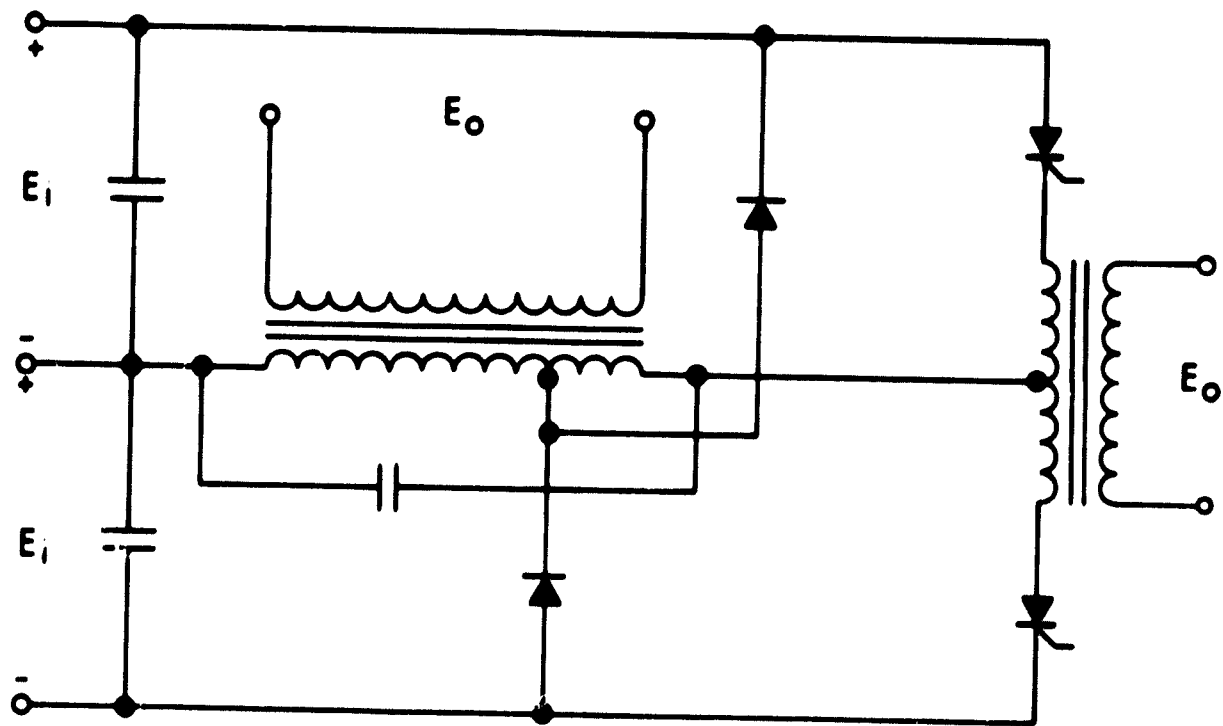


Figure 145. Basic Push-Pull Impulse Commutated Inverter

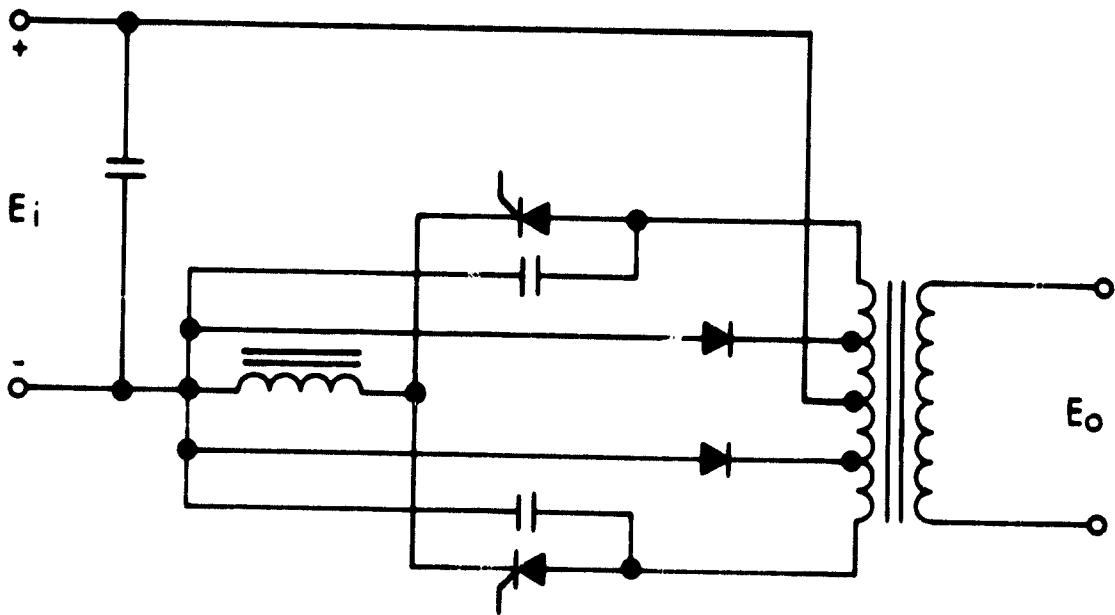
The rectifiers shown in Fig. 145 serve several purposes that result in the many advantages of the impulse commutated inverter. By providing a feedback path for trapped energy, the diodes limit the rise in voltage across either half of the transformer primary during switching. This maintains a square wave output voltage and permits the use of SCRs that have a lower breakdown voltage rating. By placing the feedback rectifiers on the ends of the primary winding as shown in Fig. 145 the energy that is fed back is dissipated in the inverter. This is eliminated by placing the diode cathodes at a tap and removing the series resistors as illustrated in Fig. 146. In this configuration the energy that is trapped in the commutating inductor or in a capacitive or inductive load is fed back to the source. The feedback path to the source increases the inverter efficiency and eliminates the need for a large commutating capacitor when the load is largely inductive. In the parallel inverter, the commutating capacitor becomes prohibitively large with inductive loads. The small value of commutating capacitance in the impulse commutated inverter also insures starting under no-load conditions. The minimum value of commutating capacitance required in the impulse commutated inverter can be approximated by:

$$C1 \geq \frac{t_{off} I}{E}$$

The need of a large input filter capacitor (C2) is the principal disadvantage of this design approach. This capacitor must be placed at the input terminals of the inverter to minimize the effects of transmission line inductance on switching characteristics. The size of this capacitor is dependent on the magnitude of trapped energy that is fed back during each half-cycle and the limitations on the rise in source voltage from the energy feedback. One of many modifications to the basic push-pull circuit is shown in Fig. 146(a). This circuit can be used as a basic building block for polyphase bridge inverters.



(a)



(b)

Figure 146. Modified Push-Pull Impulse Commutated Inverters

The need of a center tapped dc supply or a neutral point established by a pair of large capacitors is one disadvantage of this circuit.

Unlike push-pull transistor inverters that are driven, the impulse commutated push-pull inverter cannot be pulse-width modulated for voltage control or regulation due to the commutation requirements. Figure 147 illustrates a design approach for output voltage control using two push-pull inverters with outputs wired in series. Output voltage or power control is obtained in this circuit by phase-shifting the drive signal of one inverter with respect to the other. Maximum output is obtained when the drive signals to each inverter are in phase.

Series Capacitor Commutated Inverter

The chief advantage of a series capacitor commutated inverter is its ability to produce a very nearly sinusoidal output waveform when supplying a relatively fixed load. Since sine wave excitation is not required in electric propulsion power conditioning equipment, the series capacitor commutated circuits do not appear to have any practical value.

Harmonic Commutated Inverter

The six-phase double way harmonic commutated inverter is one of many harmonic commutated inverter design approaches. Like the series capacitor commutated inverter, this design approach does not appear to have any worthwhile application in power conditioning equipment for electric propulsion.

Impulse Commutated Bridge Inverters

The conventional single-phase bridge inverter utilizing impulse commutation is illustrated in Fig. 148(a). The basic operation of

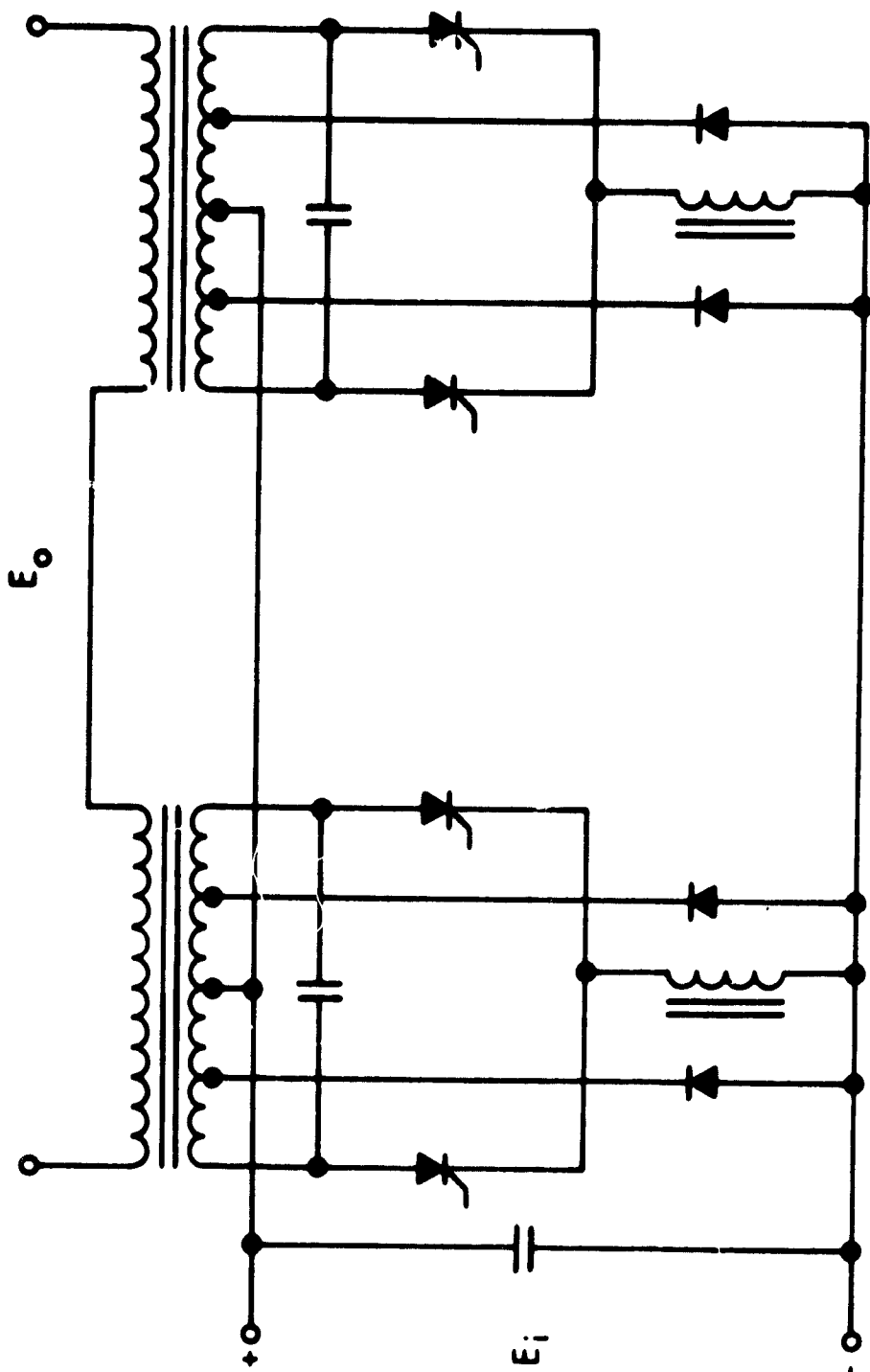
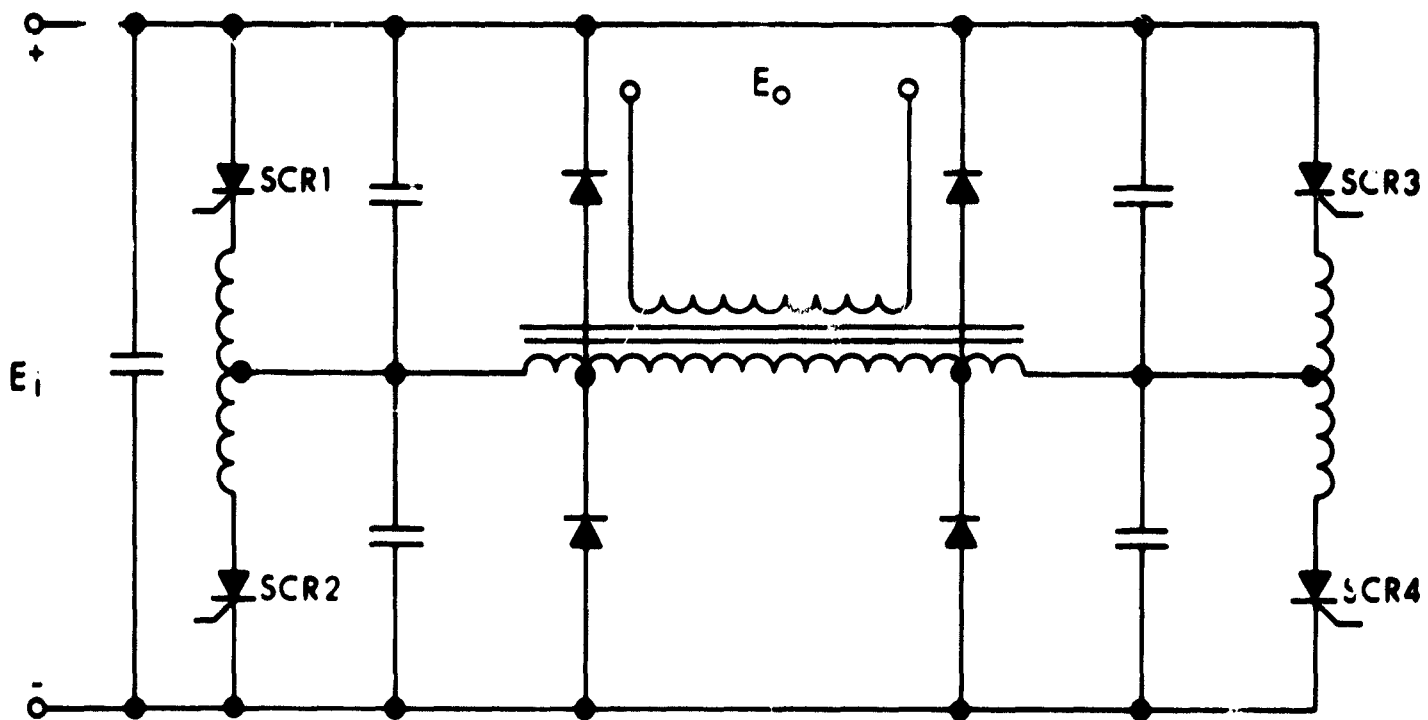
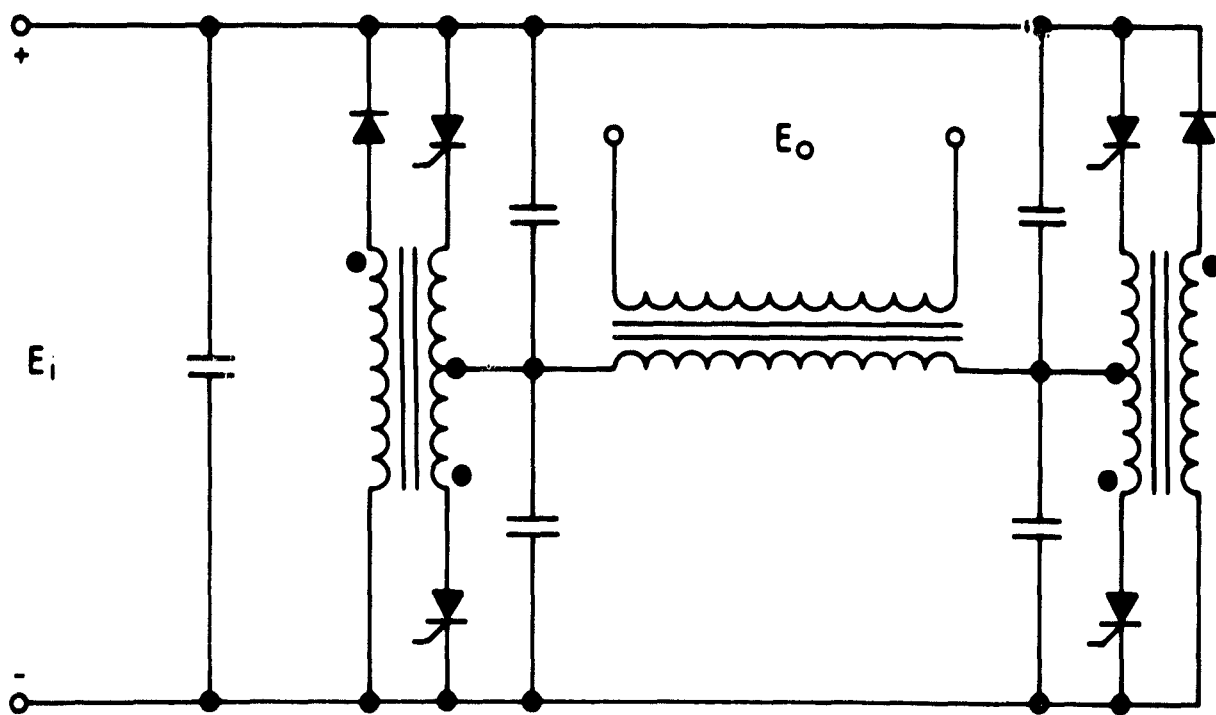


Figure 147. Push-Pull Inverter Circuit for Output Control



(a) CONVENTIONAL BRIDGE INVERTER CIRCUIT



(b) MODIFIED BRIDGE INVERTER CIRCUIT

Figure 148. Impulse Commutated Bridge Inverters

this inverter is similar to the push-pull circuit. It provides high efficiency, low regulation, and tolerance to a wide range of power factors with the same commutating components. The bridge inverter has two distinct advantages relative to push-pull operation. The first advantage is the inherent ability to operate reliably at higher input voltages. The ability to operate at twice the input voltage also doubles the power capability over that for the single-phase push-pull circuits. The second and perhaps more important advantage is the provision for pulsewidth modulation without the need of additional inverter circuits. Voltage control and inversion can be accomplished simultaneously with but one output transformer. Commutation is provided by SCR 1 and SCR 2 conducting simultaneously on alternate half-cycles with SCR 4 and SCR 3, respectively. Pulsewidth modulation or voltage control can be provided by time-delaying the drive signals on one side of the bridge with respect to the other side. The phase-shifting drive circuitry for the bridge inverter is identical to that for Fig. 147.

A modification to the basic bridge inverter is shown in Fig. 148(b). In this circuit the feedback of trapped energy is provided by commutating transformers which eliminate two feedback diodes.

3.1.1.4 Liquid-Metal JXB Inverter

The feasibility of using the liquid-metal JXB switch as the active switching element in low voltage, high current dc-ac inverters was examined. The principal advantages of this device are its insensitivity to nuclear radiation and its capability for operation in a thermal environment as high as 600°C.

Several different operational configurations using mercury have been fabricated and tested by various organizations. The results of this work indicate that there are many operational problems involved with this device. These include:

Severe low frequency limitations

High magnetic field requirements

Subject to erratic operation during periods of high shock and vibration

Projected lifetime and reliability are low as a result of packaging requirements

Even though the JXB switch exhibits some environmental and electrical advantages, it appears that the problem areas will not be improved enough for this device to be used effectively in future space power conditioning systems.

3.1.2 VOLTAGE TRANSFORMATION

Transformation of the powerplant voltage to the nominal voltage levels required by an electric thruster is usually provided by the power transformer which also provides isolation between the source and load. If isolation is not required, a dc input voltage can be stepped down by pulsewidth modulation of a series switch between the source and the load. At low power levels this approach is more efficient than transformation provided by a single static inverter. Since high voltage isolation is required for most of the auxiliary thruster supplies, the series switch approach is at present limited to control system power requirements. The voltage doubler circuit shown in Fig. 149 is commonly used for high stepup voltage, low power requirements. The V- supply for the contact ion thruster would be the principal application. The voltage doubler circuit improves the output waveform by reducing the stray transformer capacitance that results from high stepup turns ratios.

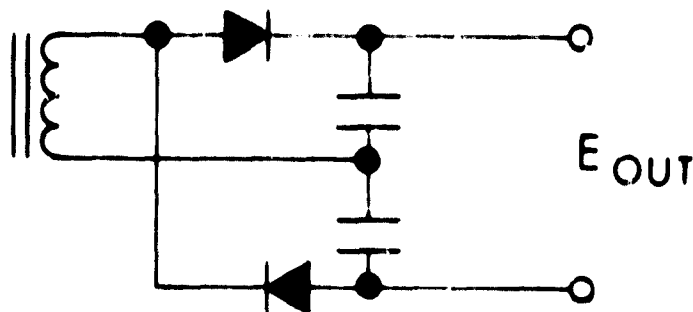
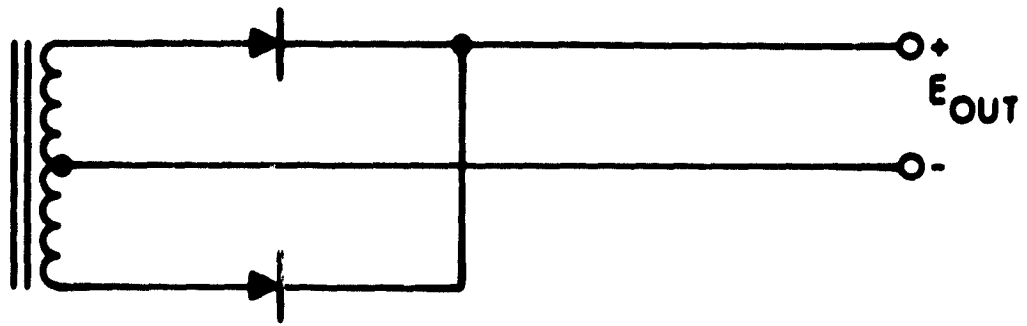


Figure 149. Voltage Doubler Circuit

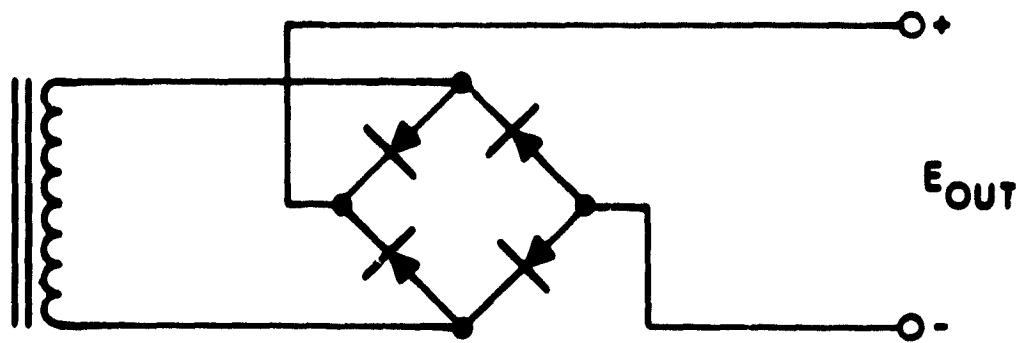
3.1.3 RECTIFICATION

The principal input power requirements for electric thrusters involve a dc voltage requirement. This requires rectification of the alternating waveform (sine, square or quasi-square) after transformation to the desired input voltage level has been accomplished. The standard power rectification circuits are illustrated in Fig. 150 for single-phase and polyphase power.

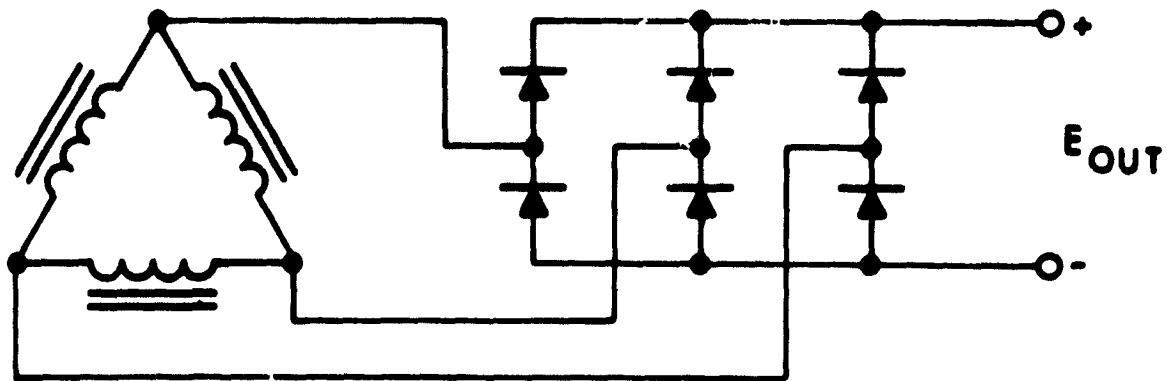
The peak inverse voltage (PIV) rating required for each diode is the principal difference between the two single-phase circuits. The diodes in Fig. 150(a) require a PIV rating that is at least twice the peak output voltage; the PIV ratings are halved in the bridge circuit. The resultant ripple voltage and ripple frequency for each circuit is identical. The application of either the single-phase center-tapped or bridge circuit is dependent on several design considerations. The considerations include rectifier circuit efficiency, system design, PIV ratings of available diodes, transformer size and efficiency, and the impedance characteristics reflected to the transformer primary.



a. SINGLE-PHASE



b. SINGLE-PHASE BRIDGE



c. THREE-PHASE

Figure 150. Typical Full-Wave Rectifier Circuits

The centertap circuit is necessary in low voltage ($< 50V$) rectification due to efficiency considerations. The rectifier losses are doubled in the bridge circuit since twice as many diodes are required. At voltages higher than half the PIV rating of available diodes the bridge circuit is necessary. For single semiconductor diodes, the maximum PIV rating can range from 600 to 1200 volts depending on the switching speed and forward current capability of the device. Selection of the optimum circuit for rectification in the intermediate voltage range involves several tradeoffs. The individual inverters in a multiple inverter system using bridge rectifiers, for example, do not require synchronization when their outputs are wired in series. The multiple inverter approach not only reduces the switching requirements for the active switches but also the PIV ratings required for the output rectifiers. Another important design tradeoff involves rectifier efficiency versus output transformer size and, hence, efficiency. A smaller output transformer can be fabricated with bridge rectification since the number of secondary turns required for the centertap circuit is halved.

There are numerous hybrid rectification design approaches that can be implemented in addition to the standard circuits shown in Fig. 150. Output control or regulation, for example, can be coupled with rectification by replacing the diodes with either transistors or SCRs. In many applications, the voltage or current requirements exceed the maximum ratings of available diodes. In these applications, series-parallel diode arrangements must be provided. Series-parallel schemes have the disadvantage of requiring dissipative networks for equal current or voltage division across the diodes. This is especially critical during transient or switching periods. In high voltage applications compensation can be minimized by using a series of silicon avalanche diodes. Voltage division for these diodes can be accomplished by shunting each diode with a capacitor only. These diodes recover if the PIV rating is exceeded during transient conditions.

The polyphase rectifier circuit for a delta-connected transformer secondary shown in Fig. 150(c) results in a lower ripple voltage and a higher ripple frequency that is obtained with the single-phase circuits. Like the bridge circuit, the polyphase full wave rectifier circuits can be wired in series without inverter synchronization.

3.1.4 POWER AND VOLTAGE CONTROL

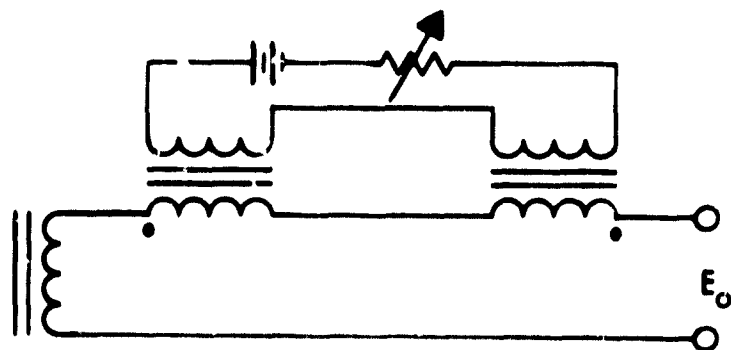
Analog or on-off control of the voltage or power to the thruster can be accomplished by:

- Input power conditioning control elements
- Internal power conditioning (inverter) control
- Output power conditioning control elements

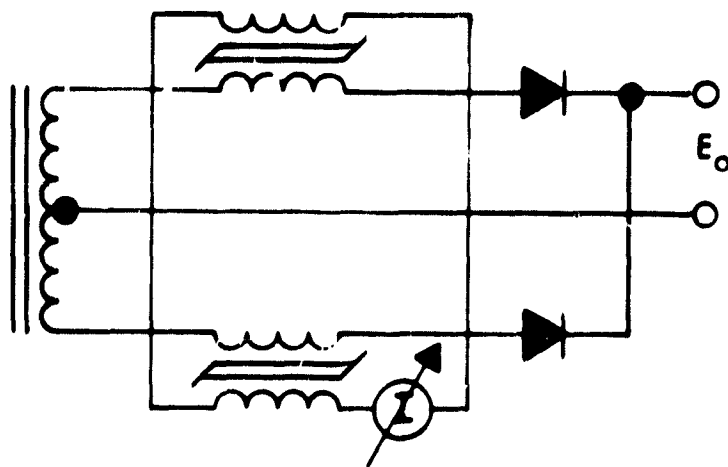
Input or output ac control can be provided with saturable reactors, magnetic amplifiers, or SCRs. Transistor circuits provide input and output dc control. Device choice along with the relative system position is primarily dependent upon efficiency considerations.

The basic electrical schematic for the magnetic devices are illustrated in Fig. 151. By virtue of the controllable impedance offered by the magnetic device, the output power can be controlled. This involves primarily control of the commutation angle by externally controlling the volt-seconds required for the device to saturate. Until saturation the device exhibits essentially an infinite impedance. After saturation, a short circuit is essentially provided.

The simple saturable reactor circuit, of which there are many variations, has been used for many years in a wide number of applications. It offers a rugged design approach, high degree of linearity, and tolerance to a wide range of environmental conditions. Gate control of the



(a) SATURABLE REACTOR



(b) MAGNETIC AMPLIFIER

Figure 151. Magnetic Control Circuits

alternating input power is a direct function of the control winding power; output power increases with an increase in control power. The power gain in a saturable reactor is limited to a range from 10 to 100. This results in relatively low circuit efficiency which limits the application of saturable reactors to primarily high temperature and low voltage circuits in space power systems.

The magnetic amplifier, or magamp, is differentiated from the saturable reactor by the addition of rectifiers which prevents demagnetization of the core by the alternating input voltage. With the rectifiers and square-loop core material, the magamp can provide gain and efficiency characteristics that are considerably higher than the saturable reactor characteristics in most applications. Low voltage applications are the exception due to the diode losses. The control winding current is inversely related to the output gate power in a magamp; increases in control current increase the volt-seconds required for core saturation.

Silicon controlled rectifiers, like the magnetic devices, also control power and voltage by controlling the commutation angle. The application of these devices, however, can result in erratic operation due to the high susceptibility of turnon characteristics to transients.

3.1.4.1 Input and Output Control

In applications where turboalternator voltages are stepped up to meet the engine requirements, voltage or power control with a magnetic amplifier on the power transformer secondary would be preferred. For stepdown applications that involve only one supply per power transformer, primary control could be more efficient than secondary control. The

arc supply for the cesium electron-bombardment thruster is the principal example of a primary control application. In supplies that require analog control or regulation, on-off control as well as current-limiting can be provided with the same control element. In supplies that only require on-off control and current-limiting, control provided by a magamp could be more advantageous than the series combination of a current-limiting choke and contactor. This approach is recommended for the ion engine high voltage supplies, for example, since the magamp diodes have been provided by the rectification requirements.

In the case of a dc powerplant, control of the inverter output voltage can be provided by controlling the inverter input voltage. Series and shunt transistor regulators as well as the switching types can be employed for input voltage control. These control techniques, while being well known and reliable, are not especially recommended for electric propulsion power conditioning applications due to efficiency considerations. They are used primarily in low power, high stepup voltage applications where secondary control cannot be provided effectively due to insulation requirements. Control of the thruster power or voltage can also be provided in the inverter output circuit using the same techniques employed with the turboalternator powerplant. In single-phase push-pull SCR and selfexcited transistor inverters, voltage or power control in the output circuits is essential.

3.1.4.2 Internal Inverter Control

Nondissipative control of the inverter output can be provided by phase-shifting or pulsewidth modulating lowlevel inverter drive signals. Driven push-pull and bridge transistor inverters use the pulsewidth modulation techniques. Output control in the SCR bridge inverter can be provided by pulsewidth modulating or phase-shifting one pair of

drive signals. On-off control can be provided by gating the drive signals.

Modulation or the phase-shifting of drive signals can be accomplished in a number of ways. The reference oscillator or multivibrator is the first and common stage to all design approaches. For pulsewidth modulated drive signals, the multivibrator output can be coupled to a voltage-controlled monostable multivibrator. The output of the multivibrator in turn is coupled to the drive amplifiers for the power stage of the inverter. The duty cycle of the multivibrator is controlled by the output voltage of a differential amplifier that compares the inverter output voltage with a signal voltage. In applications that require phase-shifting between pairs of drive signals, one pair of drive signals would be coupled directly from the multivibrator to the drive amplifier. The other pair of drive signals are obtained from the same multivibrator but are phase-delayed prior to drive-amplifier coupling. A magnetic amplifier can be used for the phase delay by controlling the bias current which in turn would be controlled by a differential amplifier.

3.1.5 FILTERING

Filtering is an important and integral part of the design of almost all power conditioning equipment. The design of this function, however, is frequently neglected until the overall system design approach for the power conditioning electronics, particularly the inversion and regulation schemes and, hence, the critical active components, have been selected. With the advent of extremely large power conditioning systems for electric propulsion it is imperative that filter design tradeoffs be made with the various inversion and regulation design schemes in the initial system and circuit design phases. It is also extremely important that source and load characteristics or requirements relative to filtering be accurately defined and that unnecessary

requirements not be imposed for the sake of uncertainty. In addition to the always inherent system design considerations of minimizing the specific mass and maximizing the efficiency, there are other factors that must be examined closely which are especially relative to filtering requirements when optimizing the overall system. These include volume, temperature, and electrical constraints.

The filter requirements for power conditioning equipment can be classified into three general areas. These areas are:

- Input filtering (energy storage)
- Output filtering
- Suppression of radio frequency interference

3.1.5.1 Input Filtering

The input filter interface for dc-ac inversion or dc-dc conversion equipment, when required, usually consists of a capacitor shunted across the input power terminals. A choke input L-C filter is also used where additional filtering over that provided by only a capacitor is required.

The input filter may perform one or several functions as the interface between the power source and the power conditioning equipment. These functions include energy storage, stiffening source characteristics in the case of a "soft" source, and the reduction of ripple and switching spikes on the bus bar.

Filter functional requirements, the design approach, and the electrical characteristic requirements of the components (L and C) are primarily dependent on:

- Overall power conditioning system design approach
- Power source or power conversion equipment characteristics

Dc-ac inversion scheme
Regulation scheme
Load requirements and characteristics
Switching frequency
Active power conditioning component characteristics

Since the design of an optimum power conditioning system is a result of many design approach iterations of the different power conditioning functions required, it is difficult to analyze the total effect of each of the previous factors on filtering requirements. Optimizing any single power conditioning function does not necessarily result in optimization of the system. The general trends in filtering requirements and penalties as a function of each of these factors can be identified for both circuit and system design tradeoff studies.

The switching characteristics of an impulse-commutated inverter, for example, requires an energy pulse for commutation. This energy is eventually trapped in the commutating inductor and can be either dissipated in the inverter or returned to the source. If the source and transmission line impedances are negligible and the source is able to receive electrical energy as well as supply it, the stored energy would be delivered back to the source. These characteristics are not available in applicable electric propulsion powerplant systems. For high efficiency, an input filter (energy storage capacitor) is required between the powerplant and the power conditioning inverter. To minimize any effects of transmission line inductance on inverter switching characteristics, it is imperative that the filter capacitor be physically located at the inverter input terminals. These requirements result in thermal limitations on the application of the inverter. Presently available capacitors, especially energy storage types, are limited to 125°C operation and usually require derating above 85°C. The size of the filter capacitor for the impulse-commutated inverter is dependent on:

Load power factor (e.g., feedback rectifiers allow energy that is stored in a capacitive or an inductive load to be fed back to the filter circuit rather than dissipated in the circuit)

The load power requirements, controlled rectifier switching times, and energy trapped in commutating inductor

Limitations on rise in source voltage after commutation

Capacitor ripple current limitations

Increases in any of these factors will increase the size of the filter capacitor. Since the loads for ion engines are primarily resistive, the power factor consideration can be eliminated. There is always some leakage inductance in the power transformer, however, which is also another energy storage consideration for the filter. One of the most important considerations that involves the size of the filter capacitor is the variation of trapped energy in the commutating inductor with load variations from the initial design point. The maximum value of trapped energy in the commutating inductor occurs under no-load conditions. Due to the relatively slow response of an ion engine and the no-load modes that can occur during its operation, it is important that the input filter capacitor be sized according to the no-load trapped energy in the commutating inductor.

In other controlled rectifier and transistor inverter design approaches, an input filter capacitor would be used primarily to filter out the ripple on the transmission line resulting from inverter commutation. Where fast switching frequencies are employed, an input filter capacitor might be needed to minimize the effect of transmission line inductance or power source characteristics on the inverter switching characteristics.

From the standpoint of weight and power loss considerations, use of input filter chokes or L-C filters is usually avoided. There is also the adverse effect of input inductance on switching characteristics that must be considered as mentioned previously for the transmission line. To meet filtering requirements not met by a shunt capacitor, or to limit supply current during commutation, there are some situations where an input choke is necessary. The parallel-commutated controlled rectifier inverter is an example where current-limiting is needed due to short-circuit conditions during commutation. Current-limiting may also be necessary due to load or output filter capacitance. For the ion engine, the load effects can be neglected since the power factor is nearly equal to one. The effect of the output filter, especially a simple shunt capacitor or pi network filter, cannot be neglected in an analysis of input current-limiting requirements. Increasing the capacitance of these output filters to meet load filtering requirements results in increased capacitor charging currents after commutation. Excessively high charging current requirements can result in active switch degradation or even failure without some type of current-limiting. Although this condition is usually avoided in output filter design, the magnitude of charging currents relative to active switch ratings should be checked for compatibility and current-limiting requirements. Voltage regulation employing the high efficiency pulsewidth modulation techniques is an application where the choke of an L-C filter could be required for filtering rather than current-limiting.

3.1.5.2 Output Filtering

There are generally two classes of output filtering requirements involved with power conditioning equipment. The first involves wave shaping where sinusoidal voltages are required. Since ion thrusters do not require a sinusoidal voltage, this class of filtering can be neglected. The second class of filtering involves lowering the ripple factor after the inverter output has been rectified. For ion thrusters, this involves primarily the V+ and V- supplies. (Other requirements, for example, can include the electromagnet and arc supplies for the electron-bombardment thruster.)

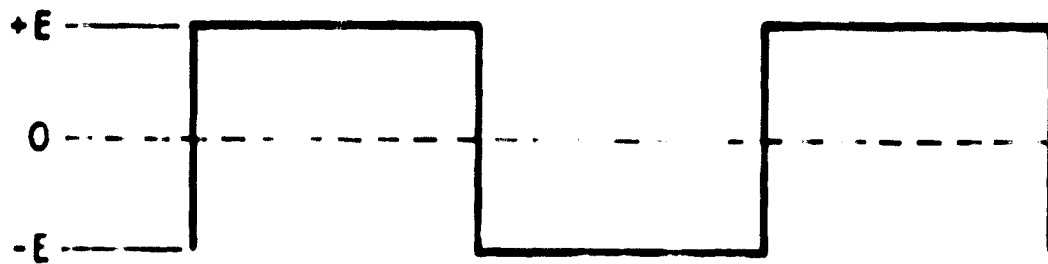
Neglecting half-wave rectification, the ripple that is present on the output voltage after rectification and before any filtering or high efficiency regulation scheme is added can be attributed to one or several sources. These include: (1) unbalanced secondary winding on the output power transformer, (2) unbalance in the rectifier circuit, (3) finite switching times inherent in active components required for commutation and rectification, and (4) the effect of stray or circuit inductance and capacitance on switching characteristics. The first, second and fourth sources of ripple can usually be reduced during dc-dc converter design to a point where they will have a negligible effect relative to the ripple produced by the turnon and turnoff times of the active components. This primary source of output ripple produces the input transmission line ripple as discussed previously. Figure 152 compares the output voltage waveforms, before and after rectification, for active components having both ideal switching characteristics ($t_r = t_f = 0$) and finite switching characteristics ($t_r = \tau_1$; $t_f = \tau_2$). The filter has the function, then, of transforming (b) to as close to (a) as is required by the load. For the ion engine V+ and V- supplies the ripple should be less than 3 percent.

There are four basic output filter design approaches that can be used for filtering the rectified voltage shown in Fig. 152(b).

These are:

- a. R-C filter
- b. L-C filter
- c. Pi filter
- d. Cascaded L-section filter

These filters are illustrated in Fig. 153 with fullwave rectification. The pi and cascaded L-section filters are extensions of the L-C

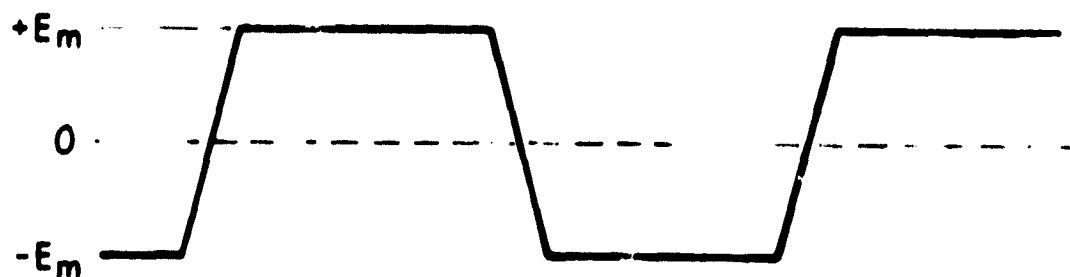


(a) INVERTER OUTPUT

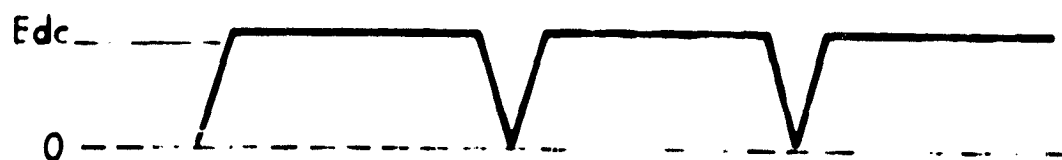


(b) RECTIFIED OUTPUT

(a) Inverter And Rectifier Output Voltage Waveforms With Ideal Switching Characteristics ($t_r = t_f = 0$)



(a) INVERTER OUTPUT



(b) RECTIFIED OUTPUT

(b) Inverter And Rectifier Output Voltage Waveforms With Finite Switching Characteristics ($t_r = \tau_1$; $t_f = \tau_2$)

Figure 152. Inverter Output Waveforms

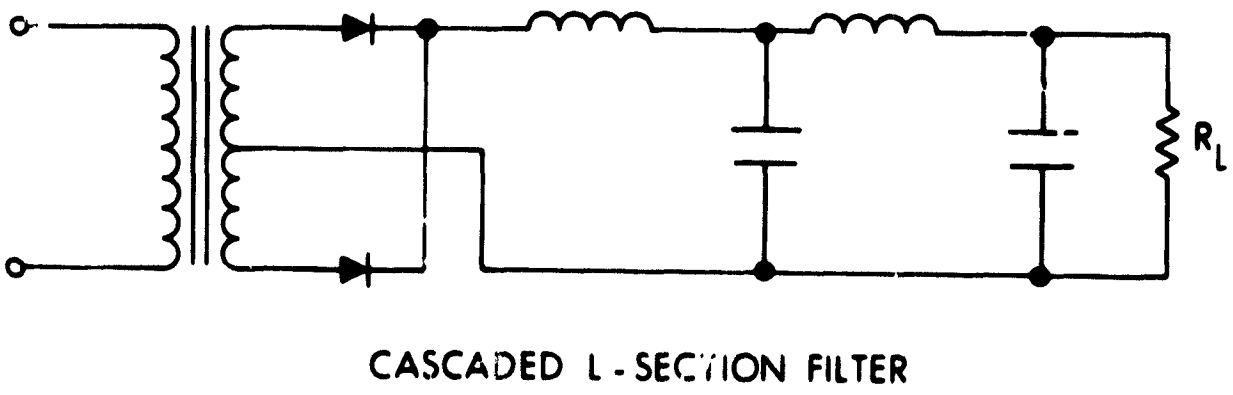
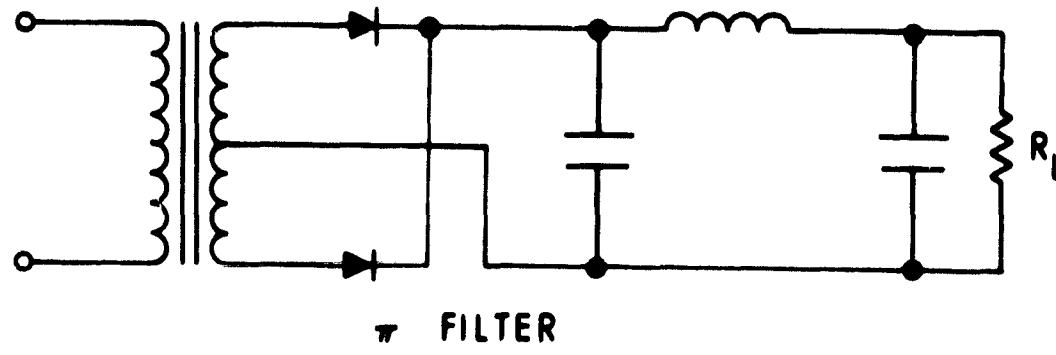
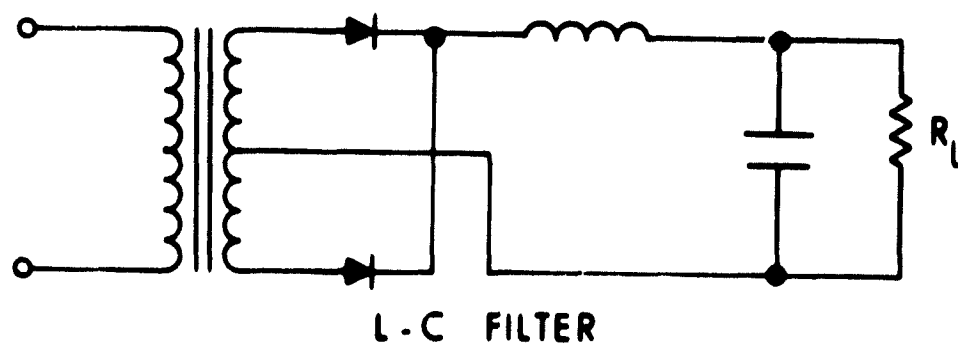
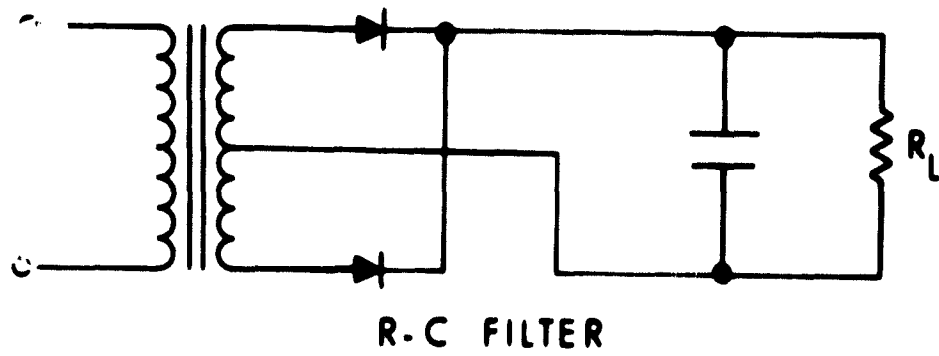
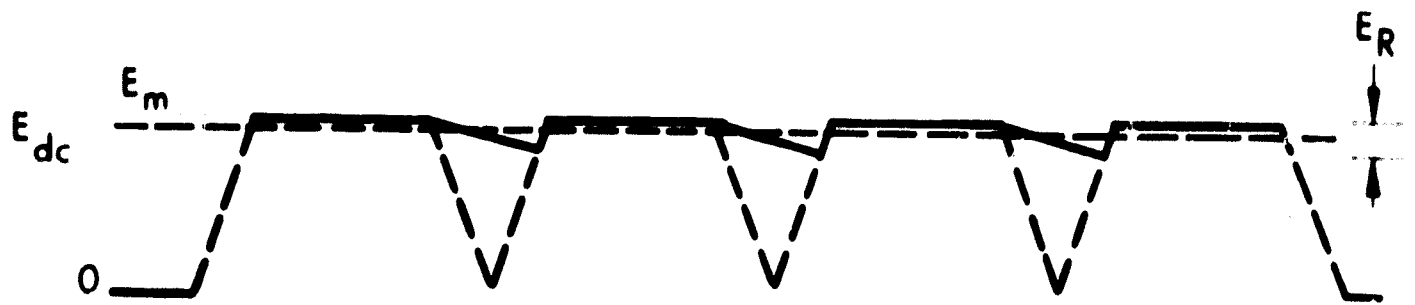


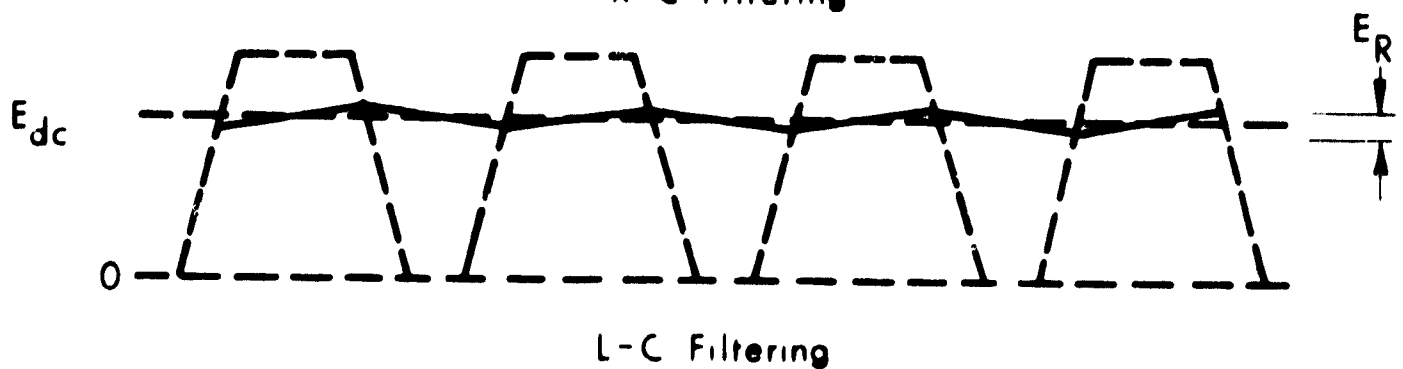
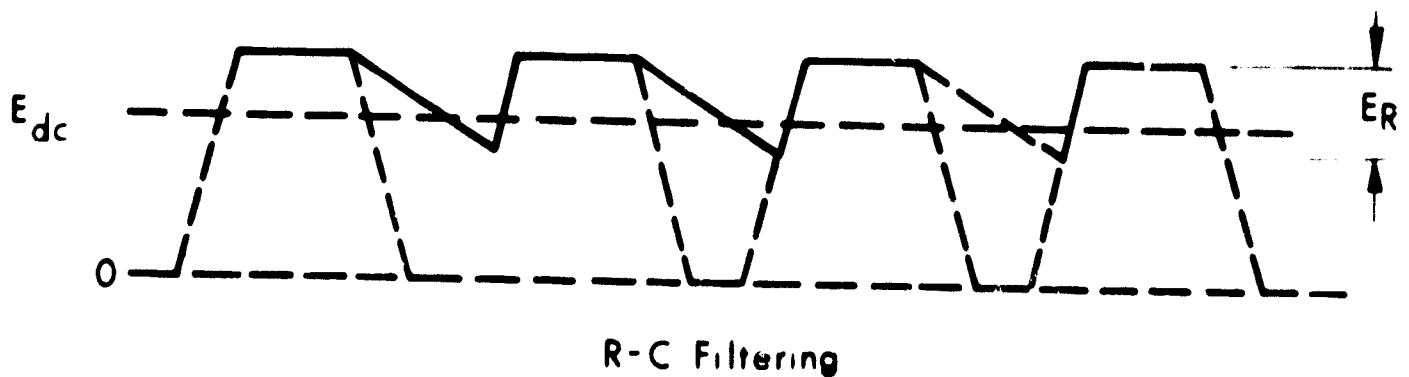
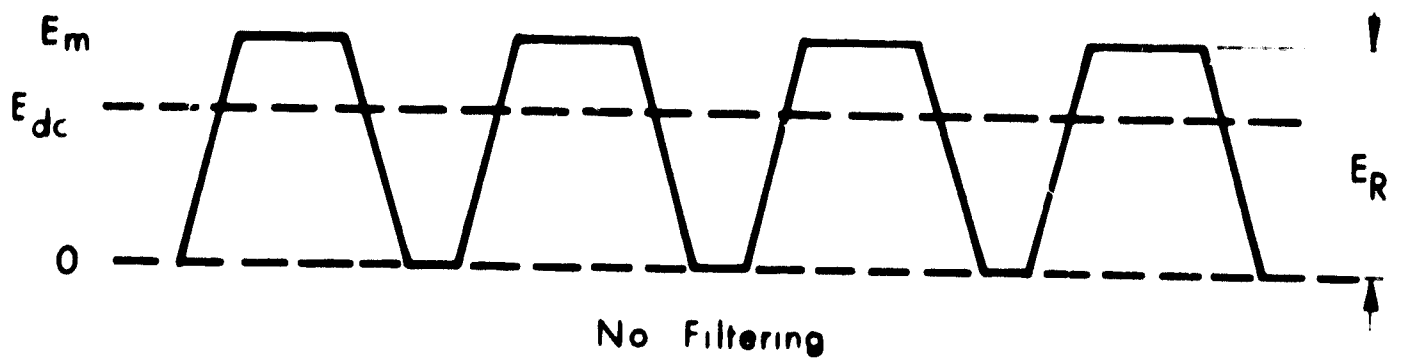
Figure 153. Power Conditioning Output Filter Networks

filter and are used where the ripple requirements are too severe for the single L-section filter. For the 3 percent ion engine requirements, the R-C or L-C filter should provide sufficient attenuation for most power conditioning design approaches. The use of either filter is primarily dependent on regulation techniques and active component switching times.

With an R-C filter, both the charging and the discharging paths for the capacitor must be examined. Assuming that the charging currents are not high enough to damage the active components and the charging time is short compared to $1/2t$, where the switching frequency $f = 1/t$, the output voltage using R-C filtering is illustrated in Fig. 154(a). The value of C required to meet the R-C filtering requirements is proportional to the switching times t_r and t_f and inversely proportional to R. In the charging circuit there will be some series impedance (R_s). As R_s/R_L decreases, or ωRLC increases, the peak charging current increases. For a fixed R_s/R_L there will be a maximum ωRLC then that cannot be exceeded without damaging the active components. As a first approximation, the charging currents can be calculated with the impedance of the capacitor at the desired switching frequency. If the charging currents resulting from the capacitance calculated to meet filtering requirements exceeds the active component ratings, additional series impedance must be added to the capacitor charging circuit. This can be accomplished by replacing the R-C filter with the L-C type. In addition to limiting the charging current, the L-C filter will improve the regulation and ripple factor characteristics of the R-C filter with a smaller value of C. The disadvantages associated with the L-C filter are the added voltage drops and power losses in the inductor.



(a) Unmodulated dc-dc Converter Output With R-C Filtering



(b) Pulse Width Modulated dc-dc Converter Output With R-C And L-C Filtering

Figure 154. Voltage Waveforms, Filtered and Unfiltered

When pulsewidth modulation techniques are employed for high efficiency regulation an L-C filter must be used. Figure 154(b) illustrates various pulsewidth modulated waveforms after rectification. The purpose of utilizing pulsewidth modulation techniques in either the inverter or the rectifier circuits is to maintain efficiently a constant dc output voltage with changes in input voltage, load, or other circuit parameters. With E_m changes and thus cycle changes it is obvious that the R-C filter cannot perform the required filtering. In addition to requiring an excessively large capacitor, the capacitor in the R-C filter always charges to E_m .

In the L-C filter, the capacitor performs the function of shunting alternating components of current past the load. To do this the capacitor reactance is usually smaller than the load impedance of $C > 1/\omega RL$. To reduce the ripple shunted by the capacitor, the reactance of the capacitor should also be much lower than the reactance of the inductor or $C \gg 1/\omega^2 L$. As the switching frequency increases or the load decreases C and L will decrease. Decreasing the duty cycle or the difference between E_m and E_{dc} will also decrease the size of these components. Since a positive voltage transient will appear at the output of the regulator when the load current is suddenly decreased, and will be maximum when the load current is switched from full to no-load, the L-C ratio should be minimized within practical limits. The maximum output voltage can be calculated with the following expression:

$$V_o (\text{max}) = V_o^2 + \frac{L I_o^2}{C}^{1/2}$$

This neglects any losses in the output filter.

Even though the inverter and regulator design approaches affect both the input and the output filter design and resulting component values considerably, an even greater effect can be realized by the overall system design approach. Utilizing a modularized dc-dc converter approach, for example, with eight modules delivering the required $V+$ power, the switching ripple without filtering could be theoretically 12.5 percent of the resulting output voltage. This would reduce not only the output filter requirements but the input filter requirements of the single inverter. The 12.5 percent figure assumes that none of the eight modules is commutating at the same time. For realistic filtering requirements the probability of two or more modules switching at the same time must be determined.

3.2 CONVERTERS

In static converter design, a fundamental tradeoff exists between weight and efficiency. For example, as the frequency is increased the weight of the converter may be decreased mainly because of the reduction in weight of the magnetic and filtering components. However, as the switching frequency is increased, the efficiency of the circuit is reduced because of increased transistor switching losses. In the frequency range of interest here, the transformer losses actually decreased as the switching frequency was increased, but the increasing transistor switching losses more than cancel this effect. The transformer losses decrease because of reduced copper losses and because at higher switching frequencies the transformer may be operated at a low flux density without the penalty of a large number of primary turns.

Transistor losses are a function of switching time and it is therefore desirable to use as fast a switching device as is possible. However, as the required output power level is increased, large power transistors must be used and these are typically characterized by inherently slower switching speeds than those of the lower power class. The result is that conventional, large power converters are usually operated at low switching frequencies and have relatively high efficiencies, but are very bulky and extremely heavy.

The modular approach utilizes extremely fast switching transistors in the light to medium power level, together with highly efficient magnetic materials, to produce extremely lightweight, highly efficient, and highly reliable high frequency power converter modules. These modules can then be used as "building blocks" to assembly larger power systems that are much smaller, weight considerably less, and are as efficient as a conventional power converter.

Before the design of the high frequency converters could be initiated, considerable attention was given to the following areas:

- a. Second breakdown effects
- b. Storage time effects
- c. Fast switching power transistors
- d. Fast recovery rectifiers
- e. Transformer designs
- f. Circuit selection

3.2.1 SECOND-BREAKDOWN EFFECTS

Second breakdown is a factor that must be considered in the design of high speed, high power converters. In general, second breakdown is a condition in a junction transistor that causes the output impedance to change instantaneously from a large positive value to a negative value and then a final small positive value. In some respects, second breakdown appears similar to a normal avalanche breakdown, either collector-to-base (BV_{CBO}) or collector-to-emitter $V_{CE(SUS)}$. There are however, two major differences: (1) the second breakdown final limiting voltage is always in the 5 to 30 volt range, while BV_{CBO} and $V_{CE(SUS)}$ usually have much higher limiting values, and (2) second breakdown is energy dependent while BV_{CBO} and $V_{CE(SUS)}$ are independent of energy to a first order approximation.

Physically, second breakdown is a local thermal runaway effect induced by severe current concentrations. These concentrations can result from biasing conditions, excessive transverse base fields and defects in the base region or junctions or both. It can be found to some degree in all junction transistors. In many transistors, primarily small signal and low frequency power types, the maximum steady state dissipation rating limits the voltage-current product to something less than critical value necessary to produce second breakdown. Results show that transistors with higher frequency

behavior is attributed to a narrower, active base spacing, which increases the severity of transverse base fields, amplifies biasing effects and raises the defect level relative to the greater tolerances required.

If the on time of the transistor is decreased or the frequency of operation is increased, the critical voltage-current product necessary to produce second breakdown becomes greater. This condition results from the fact that the rate of localized heating is governed not only by current concentration, but by the thermal time constant of the semiconductor material; therefore high frequency, high power transistors can safely handle large power dissipation without incurring second breakdown in high speed switching circuits.

High frequency, high power transistors are rated for second breakdown in two ways; (1) a safe operating range curve for forward-bias drive conditions, with time as the running variable, and (2) a safe operating range curve showing second breakdown energy as a function of reverse-bias voltage and inductances. Forward bias second breakdown can be analyzed as follows: During the turnon time the transistor is subjected to high dissipation in the active region. A plot of the experimentally determined load line superimposed on the transistor safe operating region curve for the appropriate time duration, t_{ON} , will determine whether the circuit is operating in the safe operating region for second breakdown.

3.2.2 STORAGE TIME EFFECTS

As operating frequency increases, limiting factors such as power dissipation, core loss, frequency response and storage effect become more severe on converter operation. At high frequencies, the most severe limiting factor is the storage time effect. Figure 155 shows a typical two transformer converter circuit. During the storage period, while the transistor on one side of the push-pull circuit begins to conduct, the transistor on the other side remains on; thus

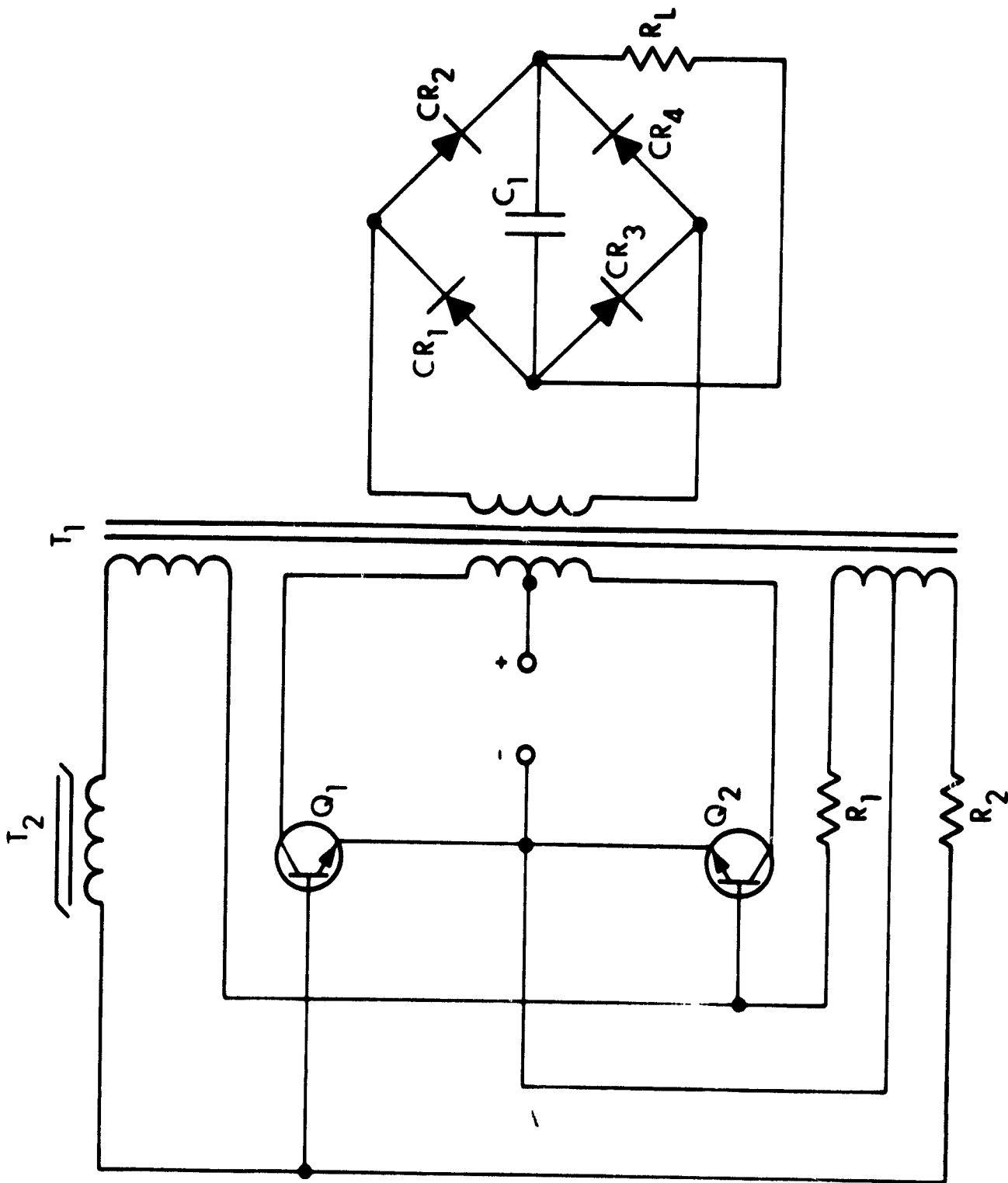


Figure 155. Typical Two-Transformer Converter

the two simultaneous collector currents cause magnetic fluxes that oppose each other. Therefore high current spikes are produced.

The collector current is determined to a first approximation by the base current times beta. The collector-to-emitter voltage (V_{CE}) is at its maximum at this time, therefore transistor dissipation is extremely high until the stored charge is cleared in the opposite transistor. Since the storage time is directly proportional to overdrive, these losses are greater at lighter loads than at rated loads of the converter.

The high collector currents also cause excessive voltage spikes at switchover which could destroy the transistors. The voltage spikes are a result of the stored energy from the inductance of the circuit leads and leakage flux of the transformer.

It is imperative that the transistors of high frequency converters should have low thermal resistances and fast switching characteristics.

The converter transformer should have low core loss and low leakage inductance.

Converter circuits that receive their drive or are synchronized from a separate driver or inverter stage are also subject to the same problems. Figure 156 shows a converter circuit which provides compensation for storage time. The circuit prevents forward bias from being applied to one transistor while the other transistor is on. The polarities shown exist after base drive has reversed but before storage time has allowed the on transistor to turn off. Reverse bias is applied to Q1 but forward bias is shunted from Q2 through CR2, winding 1-2 and the collector-emitter circuit of Q1 to the return of the drive winding. When Q1 starts turning off and the emitter-collector voltage exceeds the bias winding voltage, forward bias is

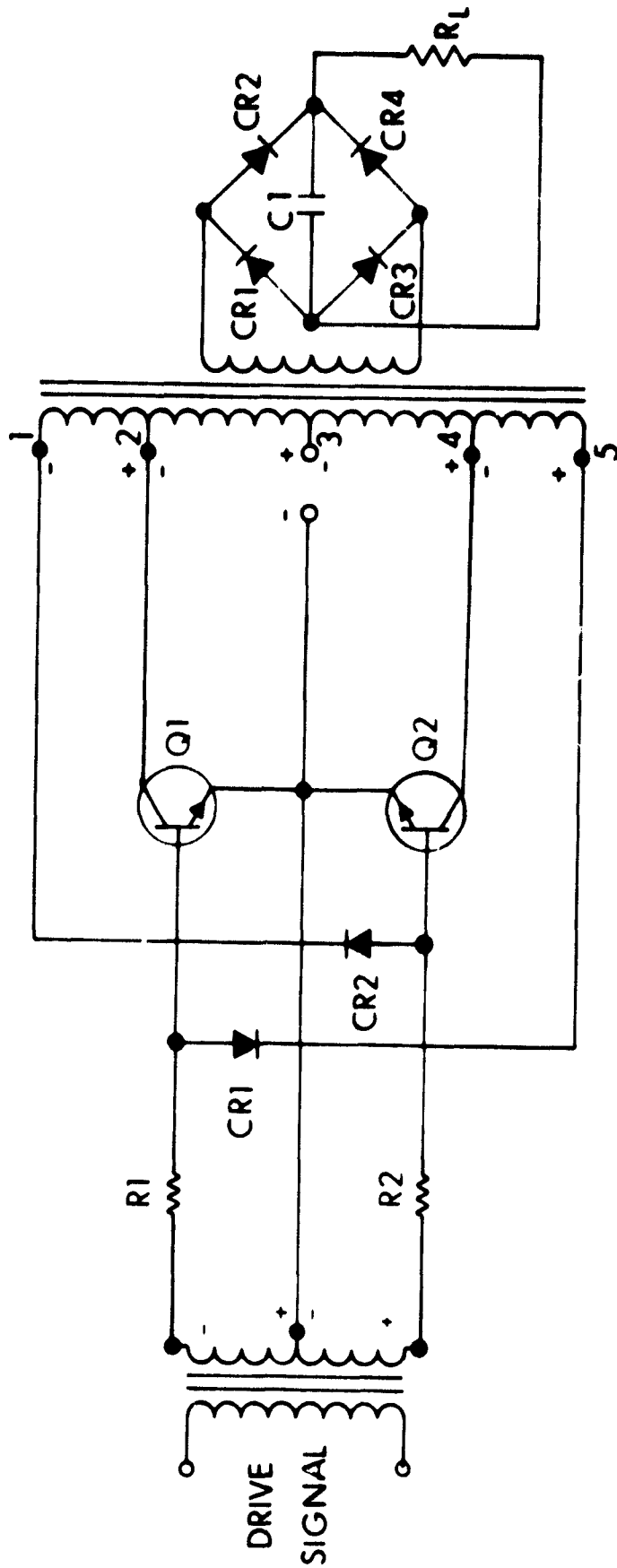


Figure 156. Converter with Compensation for Storage Tube

applied to Q2 and the next cycle of operation begins. The bias windings are necessary to overcome the forward drop of the diodes.

The converter circuit that was selected for the Mars Orbiter program is shown in Fig. 157. This circuit was selected for several reasons. First because of its simplicity and secondly because the converter circuit compensates for storage time without any modifications. Transformer T1 is a saturating type which determines the frequency of operation. T2 is the output transformer and does not saturate. When T1 saturates, base drive for both transistors falls to zero until the "on" transistor starts turning off. Stored energy in the core is then released which forward biases the opposite transistor, thus starting the next half cycle of operation.

The methods discussed automatically compensate for storage time regardless of load or environmental conditions. There are other means to accomplish the same end, but most of them do not adjust for changing load or temperature.

3.2.3 TRANSISTORS CONSIDERATIONS

In order to design efficient high frequency converters, fast switching power transistors are necessary. A survey of state-of-the-art power switching transistors was made early in the program. During the evaluation phase, the several manufacturers were contacted. The results of the examination are given in Table XXIV. Here the parameters which are essential for an initial selection are listed - current and voltage ratings and switching times.

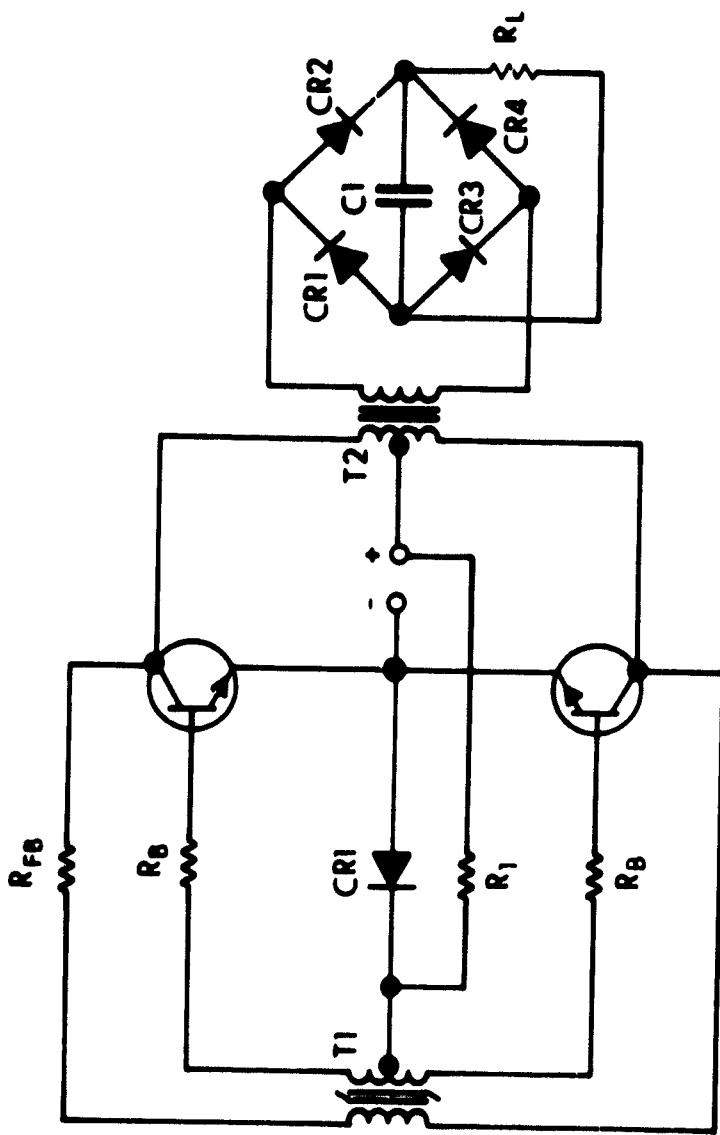


Figure 157. Basic DC-DC Converter

TABLE XXIV
SILICON SWITCHING POWER
TRANSISTORS

Type	Mfg.	BV _{CBO}		V _{CEO}	I _C (Max)		I _B (Max)		Thermal Res. °C/W	Junct. T. (Max) °C	Nominal Switching Times		
		V	V		A	A	A	A			t _r	t _f	t _s
2N3442	RCA	160	140	140	10	7	7	1.5	200	1.0	1.0	1.0	
2N3773	RCA	160	140	140	16	4	4	1.17	200	1.0	1.0	1.0	
2N3363	RCA	150	90	90	25	10	10	1.5	200	1.0	0.5	1.5	1.5
TA2669A	RCA	150	90	90	20	10	10	1.25	200	0.5	0.5	1.5	1.5
SHT8923	Solitron	140	120	120	90	20	20	0.5	200	0.06	0.7	0.8	0.8
SDT8805	Solitron	300	300	300	20			1.0	200				
2N3151	Solitron	150	150	150	70	15	15	0.33	200	0.5	0.4	0.6	0.6
2N3079	Delco	200	200	200	10	2	2	0.5-0.7	150	3	2	3.3	3.3
2N3080	Delco	300	300	300	10	2	2	0.5-0.7	150	3	2	3.3	3.3
DTS431	Delco	400	400	400	5	2	2	0.5-0.7	150	0.4	0.35	0.45	0.45
2N2583	Delco	500	325	325	10	2	2	0.5-0.7	150	2.1	1.0	2.2	2.2
2N2580	Delco	400	325	325	10			0.7	150	1.5		3.2	3.2
2N2761	West.	250	250	250	30	7.5	7.5	0.5	175	3.0	9.0	-	-
2N2742	West.	200	200	200	20	7.5	7.5	0.5	175	5.0	13.0	-	-
164-30	West	315	300	300	20	7.5	7.5		175	6.0	12.0	-	-
2N1016E	Silicon T.	250	250	250	7.5	5.0	5.0	0.1	200	0.2	0.5	2.0	2.0
STC2501	Silicon T.	150	150	150	150	15	15	0.33	200	.10	4	16	16

The maximum collector current, the dissipation, and the heat sink thermal resistance of the power transistors can be approximated on the basis of the following conditions:

The maximum collector current is given approximately by

$$I_C = \frac{P_{OUT}/\eta}{V_S - V_{CE(SAT)}}$$

where

- V_S is the supply voltage
- $V_{CE(SAT)}$ is the collector-to-emitter saturation voltage
- P_{OUT} is the output power
- η is the desired efficiency of the output transformer

The transistor dissipation can be approximated as follows (base dissipation was neglected here):

$$P_D = \frac{T_1}{T} V_{CE(SAT)} I_C + 2 I_{CEX} V_S + \frac{t_{on} + t_f}{T} \frac{V_S I_C}{3}$$

where

- V_S is the supply voltage
- $V_{CE(SAT)}$ is the transistor saturation voltage
- I_C is the collector current
- I_{CEX} is the collector current with the base reverse-biased
- t_{on} is the transistor turn on time
- t_f is the transistor fall time
- T_1 is $1/2 (T - (t_{on} + t_f))$
- T is the period

The equation above is used only as a guide for the first stages of design; the exact dissipation is determined experimentally.

3.2.4 RECTIFIER CONSIDERATIONS

The rectifier circuits of the high frequency converters were an important design consideration. At high switching frequencies fast recovery silicon rectifiers are necessary if the converter efficiency is to be optimized.

At low frequencies, the losses normally associated with rectifier diodes are due to the forward voltage drop during the conduction cycle and to the reset current pulse leakage current. Normally, the largest percentage of the losses are attributed to the forward conduction characteristics.

Diodes with recovery times in the 10 to 20 microsecond region may have excellent loss characteristics up to 1 kHz. At the higher frequencies, the rectification efficiency is increasingly impaired and heat losses increase as a direct result of the increased recovery losses. To minimize the rectifier recovery losses, fast recovery rectifiers with recovery times of a few hundred nanoseconds are required in the output rectifier circuit of the converter. Several current fast recovery diodes are listed in Table XXV.

3.2.5 TRANSFORMER CONSIDERATIONS

In the design of efficient high frequency converters, the transformer design is a very important consideration. Losses that could perhaps be neglected at lower frequencies become predominant at high frequencies.

Practical transformers can be designed quite efficiently using Hi-Mu-80 and Supermalloy magnetic materials at switching frequencies up to 10kHz.

TABLE XXV
SILICON RECTIFIER DIODES
FAST RECOVERY TYPES

Assumed Operating Conditions - 250 Volts - 1A

DIODE TYPE	PIV	MAX CURRENT	FORWARD DROP (1A)	RECOVERY TIME (Max)
Unitrode UTR 52	500	2A (1A at 100°C)	1.1	400 nsec
Unitrode UTR 3350	500	3A (1.5A at 100°C)	1.0	350 nsec
Motorola IN4937	600	1A (100°C)	1.2	0.2 μsec
MR836	600	3A (100°C)	1.1	0.2 μsec
MR846	600	3A (100°C)	1.4	1 μsec
West. IN3903	<u>400</u>	20A	0.7	0.2 μsec
IN5007	600	1A (40°C)	1.1	0.120 μsec
IN3883	<u>400</u>	6A (140°C)	0.95	0.200 μsec
T. I. IN3883	<u>400</u>	8A (140°C)	1.0	0.200 μsec
IN3913	<u>400</u>	30A (100°C)	1.4 (30A)	0.200 μsec

These materials exhibit reasonable losses in this frequency range. The optimum tape thickness for this frequency range is 1/2 mil, but the stacking factor is quite poor in this size. An additional factor is the fact that most magnetic material manufacturers will not guarantee the characteristics of core materials of 1/2 mil or less. With operating frequencies up to 10 kHz, 1 mil tape wound cores may be used very effectively and efficiently.

Some ferrite cores offer certain advantages over tape wound cores in the frequency range above 50 kHz. The major disadvantages of ferrite core materials are low curie temperature, low maximum flux density and considerable variance of maximum flux density with temperature. The advantages that this core material offers are the many different core configurations that are available, their low cost, and above all they exhibit low losses at frequencies extending into the RF spectrum.

At frequencies beyond 10 kHz the skin effect starts to become significant. For example, at 50 kHz a transformer can have more skin effect wire loss than the measured wire loss. Since Litz wire is not available in the large wire sizes that are required for power conversion, the alternative is to use parallel windings of smaller diameter wire which equal the cross-sectional area of the desired wire size.

The problems of leakage inductance and interwinding capacitance are also factors that affect the design of the transformer. For low voltage windings, the scarcity of turns on the transformer and leakage inductance can cause very poor coupling between windings and this can result in poor load regulation. Higher voltage windings are hindered by interwinding capacitance which causes increased losses in both the transformer and in the power transistors. The combination of both can cause spurious oscillations that can appreciably disrupt circuit operation.

The core of a transformer is selected on the basis of power handling requirements, frequency, and temperature of operation. Temperature is an important consideration in the selection of a ferrite core because the curie temperature for many ferrites is quite low. Magnetization is zero above the curie temperature. Another important consideration in the selection of core material is the desired transformer efficiency. The efficiency can be used to obtain an approximation for the magnetic power to be dissipated. The necessary volume of core material can then be estimated on the basis of the value of magnetic power and the core loss factor for the selected material at the operating frequency. The core loss factor is determined from the core-material data furnished by the manufacturer.

In the design of the transformer, the curie temperature must be considered together with the variation of flux-density as a function of temperature and the desired operating value of flux density, B. For the base-drive transformer, a temperature rise results in a decrease in flux density and an ultimate increase in operating frequency. The ambient temperature and the maximum operating core temperature are used to compute the maximum permissible temperature rise, ΔT . A second estimate of the volume of core material must then be made on the basis of the magnetic power to be dissipated and the temperature rises according to $3.2 \text{ mW/cm}^3 \text{ } ^\circ\text{C}$. This volume should be compared with the volume selected above on the basis of core losses. The final volume should satisfy both requirements.

The output power transformer is designed to satisfy the following familiar equation:

$$N_P = \frac{V_S \times 10^8}{4 \text{ FAB}}$$

where

- V_S is the source voltage in volts
- F is the operating frequency in cps
- A is the transformer core area in cm^2
- B is the flux density in gaussses

In the design of the output transformer for high frequency converters, excessive primary turns should be avoided to minimize power dissipation, to insure that the transformer can be fabricated using the proper wire size and the relatively small cores that are usually employed, and to insure that the leakage inductance effects are minimized. Good balance and close coupling between primaries can be achieved by means of bifilar windings. The flux density for the output transformer is determined by the usual compromise: The selected wire size on the basis of a 50 percent duty cycle must be large enough so that power dissipation will be low. If the wire size is inadequate, dissipation will be appreciable and a high transformer core temperature will result.

The design of the base-drive transformer is quite different from that of the output transformer. When the driver transformer saturates, a sharp drop in the applied primary voltage must be produced. The magnetizing current must then increase from a small value to one that is comparable to the primary current. The following equation may be used to arrive at the number of primary turns because of the saturation requirement:

$$H_S = \frac{1.26 N_P I_m}{l}$$

where

- H_S is the value of magnetizing field strength at saturation in oersteds
- N_P is the number of primary turns
- I_m is the value of magnetizing current at saturation in amperes
- l is the length of magnetic path in centimeters

The equation presented above together with the basic transformer equation must both be satisfied for the proper design of the base drive transformer.

3.2.6 CIRCUIT SELECTION

The circuit suitable for high frequency operation was selected for several reasons. The circuit is shown in Fig. 158. The paragraphs that follow will describe its operation and point out reasons for its selection.

In the circuit, a saturable base-drive transformer T1 controls the converter switching operation at base-circuit power levels, and a linear output transformer couples the output to the load. Because the core material of the output transformer, T2, isn't allowed to saturate, the peak collector currents of the transistor in the inverter are determined principally by the value of the load impedance. This feature makes possible high circuit efficiency. Operation of the circuit is as follows:

Because of a small inherent unbalance in the circuit, one of the transistors, say Q1, initially conducts more heavily than the other. The resulting increase in the voltage across the primary of the output transformer T2 is applied to the primary of the base-drive transformer T1 in series with the feedback resistor, R_{FB} . The secondary windings of transformers T1 are connected so that transistor Q2 is reversed biased and driven to cutoff while transistor Q1 is driven into saturation. As transformer T1 saturates, the rapidly increasing

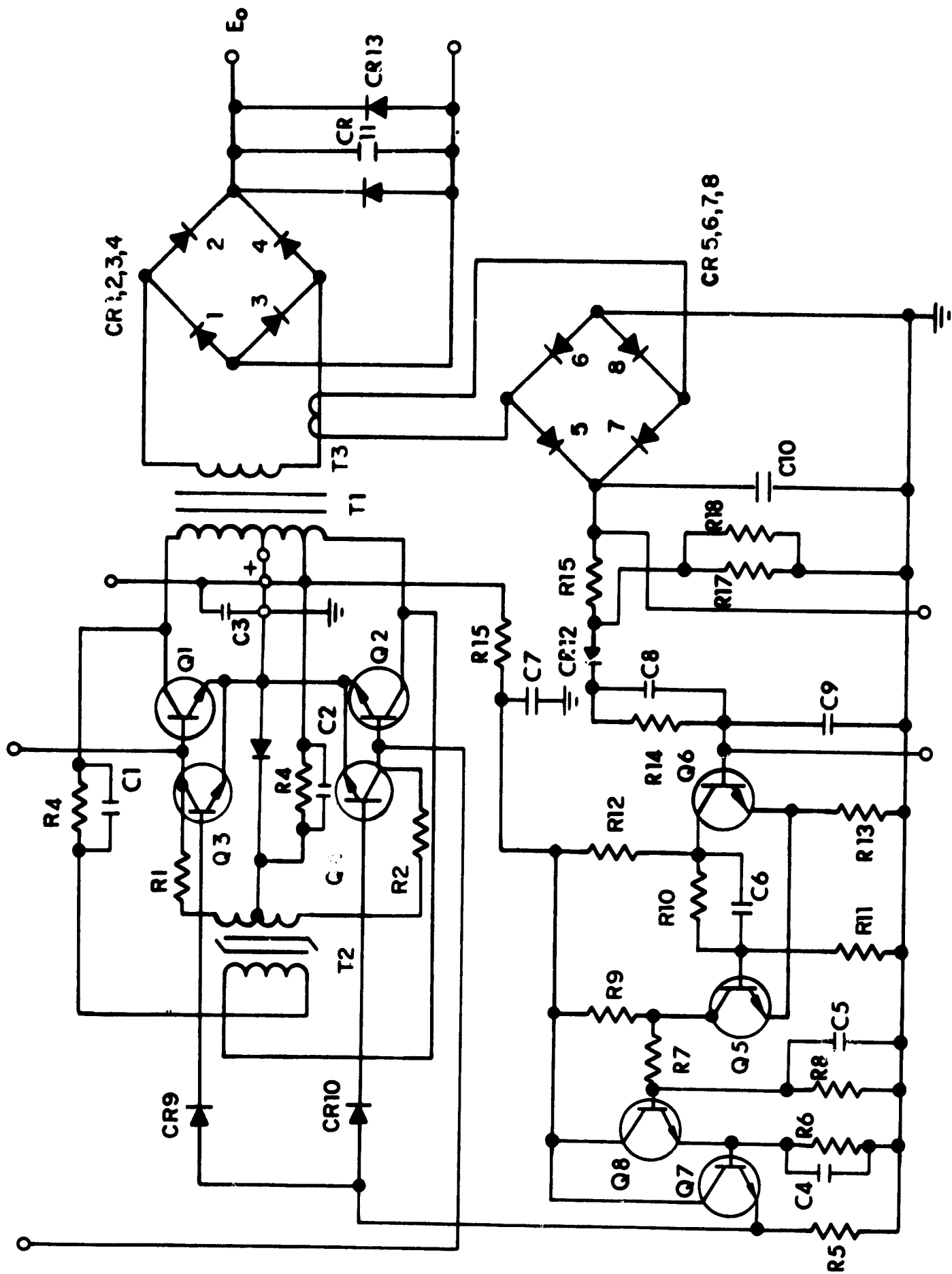


Figure 158. Diagram of Selected Circuit

primary current causes a greater voltage drop across feed-back resistor R_{FB} . This increase in voltage across R_{FB} reduces the voltage applied to the primary of transformer T1; thus the drive input and ultimately the collector current of transistor Q1 are decreased.

The decrease in the collector current of transistor Q1 causes a reversal of the polarities of the voltages across all the transformer windings. Transistor Q1, therefore, is rapidly driven to cutoff, and transistor Q2 is then allowed to conduct. The inverter operates in this state until the saturation of transformer T1 in the opposite direction is reached. The circuit then switches to the initial state and the cycle is repeated at a frequency determined by the design of transformer T1 and the value of feedback resistor R_{FB} .

The external base resistors, R_B , reduce the effect of the transistor base-to-emitter voltage, V_{BE} , on the operation of the circuit. These stabilizing resistors are needed because V_{BE} varies among individual transistors with temperature and operating time.

The collector current in each transistor must rise to a value equal to the load current plus the magnetization current of transformers T1 and T2 and the feedback current to produce the required drive. Because the output transformer is not allowed to saturate, the magnetization current is only a small fraction of the load current. In the switching operation, transistor Q1 will continue to conduct after the drive is removed because of the excessive charge that was stored in the base during saturation. However, transistor Q2 will not conduct until the core of transformer T1 has been reverse-magnetized and current has been injected into the base of transistor Q2. In the single transformer converter, both transistors conduct heavily during the switching. In the two-transformer circuit, neither transistor conducts during the switching time and thus very low power supply impedance is not necessary for fast switching.

The energy stored in the output transformer by its magnetizing current is sufficient to assure a smooth change-over from one transistor to the other with no possibility of the converter oscillations stopping.

Operation of the high frequency converter is relatively insensitive to small system variations that may result in a slight over-loading of the circuit. Under such conditions, the base power losses will increase but these losses are so small that a slight increase in them will not noticeably affect circuit performance. The amount of energy stored in the output transformer will also be increased. Although this increase will result in a greater transient dissipation, the converter switching will still be smooth. Because the output transformer is not saturated, the collector currents are always determined by the circuit load impedance and not by small system variations.

A practical design of a high frequency converter should include a means of initially biasing the transistors into conduction to assure that the circuit will be started reliably. Such biasing networks can be readily added to the inverter, and are much more dependable than just assuming that the circuit unbalance will immediately shock the converter into oscillation.

3.2.7 OVERLOAD AND SHORT CIRCUIT PROTECTION

Ion engines are subject to arcing quite frequently and, if adequate protection is not provided, the power conditioning subsystem can easily be destroyed. It was for this reason that the basic module was provided with overload and short circuit protection. In the event of an overload or short circuit condition it was desirable to

shut down the oscillator circuit for as long as the overload or arc persisted. Upon removal of the overload or short circuit, the converter circuit would automatically return to its normal mode of operation.

The current overloads are sensed by current transformer T3. The output voltage from the current transformer is proportional to the current flowing in the primary winding. This output voltage is rectified by the full-wave bridge circuit composed of CR5, CR6, CR7, and CR8. Filtering of the output voltage is provided by capacitor C10. A near constant impedance is provided by a resistor network composed of R15 and R17. A portion of the rectified voltage is then used to drive a level detector circuit (Schmitt trigger) composed of Q5 and Q6. The output from the level detector circuit is then coupled to an emitter following circuit (Q8), which in turn drives the output transistor (Q7). The output stage of the overload circuit provides sufficient drive to saturate transistors Q3 and Q4 which serve to short out the base drive to the power switching transistors Q1 and Q2. When the base drive to the oscillator transistors is removed, the oscillator ceases to function for a prescribed period of time (the off time is determined by the amount of overload).

After the predetermined off time, the oscillator circuit attempts to start again and if the overload or short circuit is still present the oscillator circuit shuts down again. The converter circuit will cycle on and off until the overload or short circuit is removed from the output terminals. Upon removal of the overload or short circuit, the converter will automatically return to its normal mode of operation.

3.3 50 kHz CONVERTER DESIGN

To illustrate specific designs of high frequency modular converters, the following material is abstracted from the results of a previous program (NAS3-7926). In that program several configurations and operating frequencies were examined. The investigation of the 50 kHz, 100 watt design is reported here in detail.

Five converter circuits were designed, breadboarded and tested. Each circuit utilized a different output transformer with a different volt/turn ratio. The efficiency as a function of output power is shown in Fig. 159. Variations in efficiency occurred below and above the 100 watt level. At the 100 watt level the efficiencies were almost the same, approximately 89 percent.

The component weights for the circuits breadboarded and tested are listed below:

<u>Circuit (No.)</u>	<u>Weight (grams)</u>
1	89.1
2	90.2
3	92.4
4	100.4
5	96.5

Circuit No. 2, shown in Fig. 160, was selected as the representative circuit at the 40 kHz switching frequency. This circuit was then subjected to further performance tests.

Figure 161 shows the variation of output voltage as a function of input voltage at constant power and at constant load.

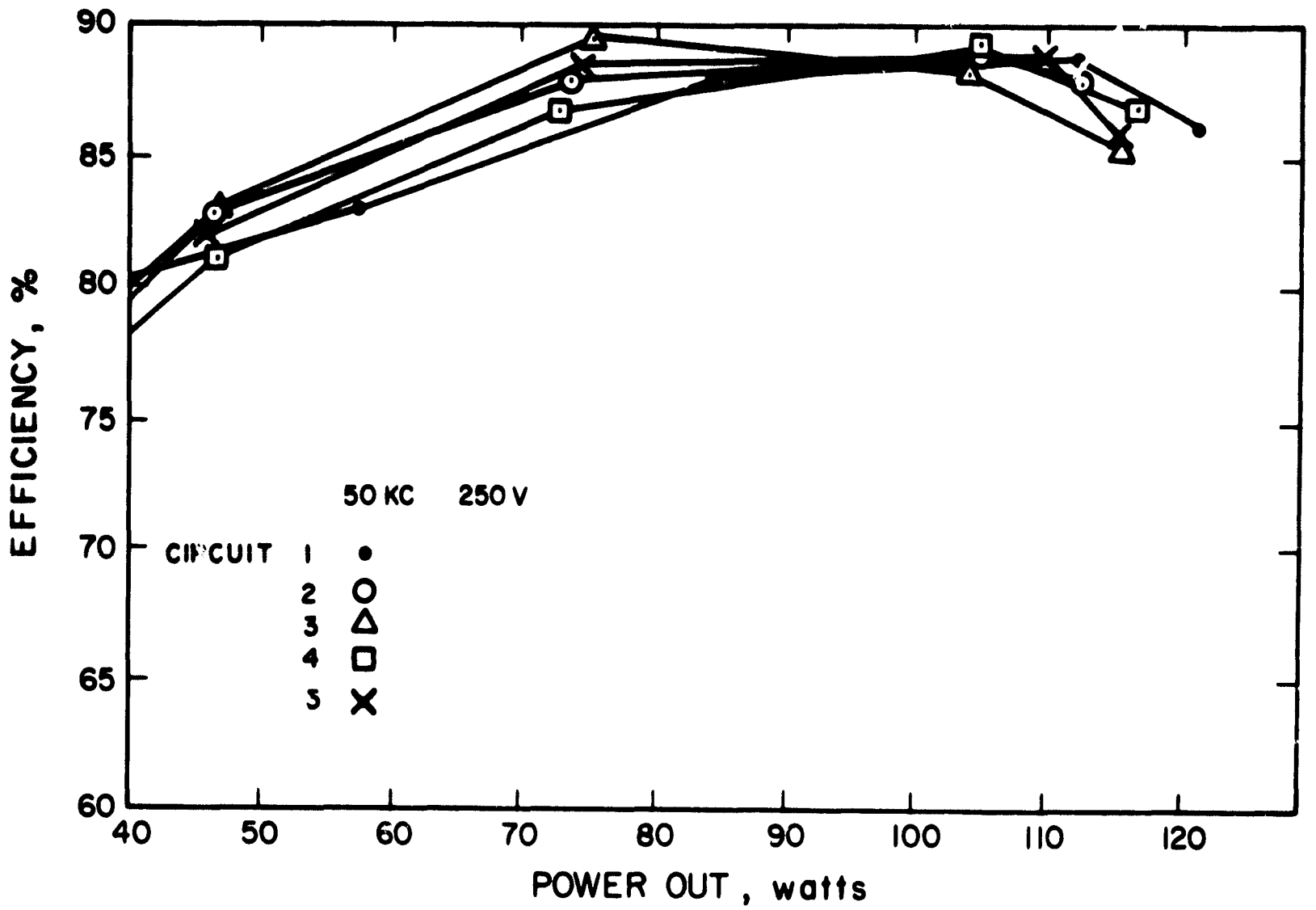


Figure 159. Efficiency versus Power Output

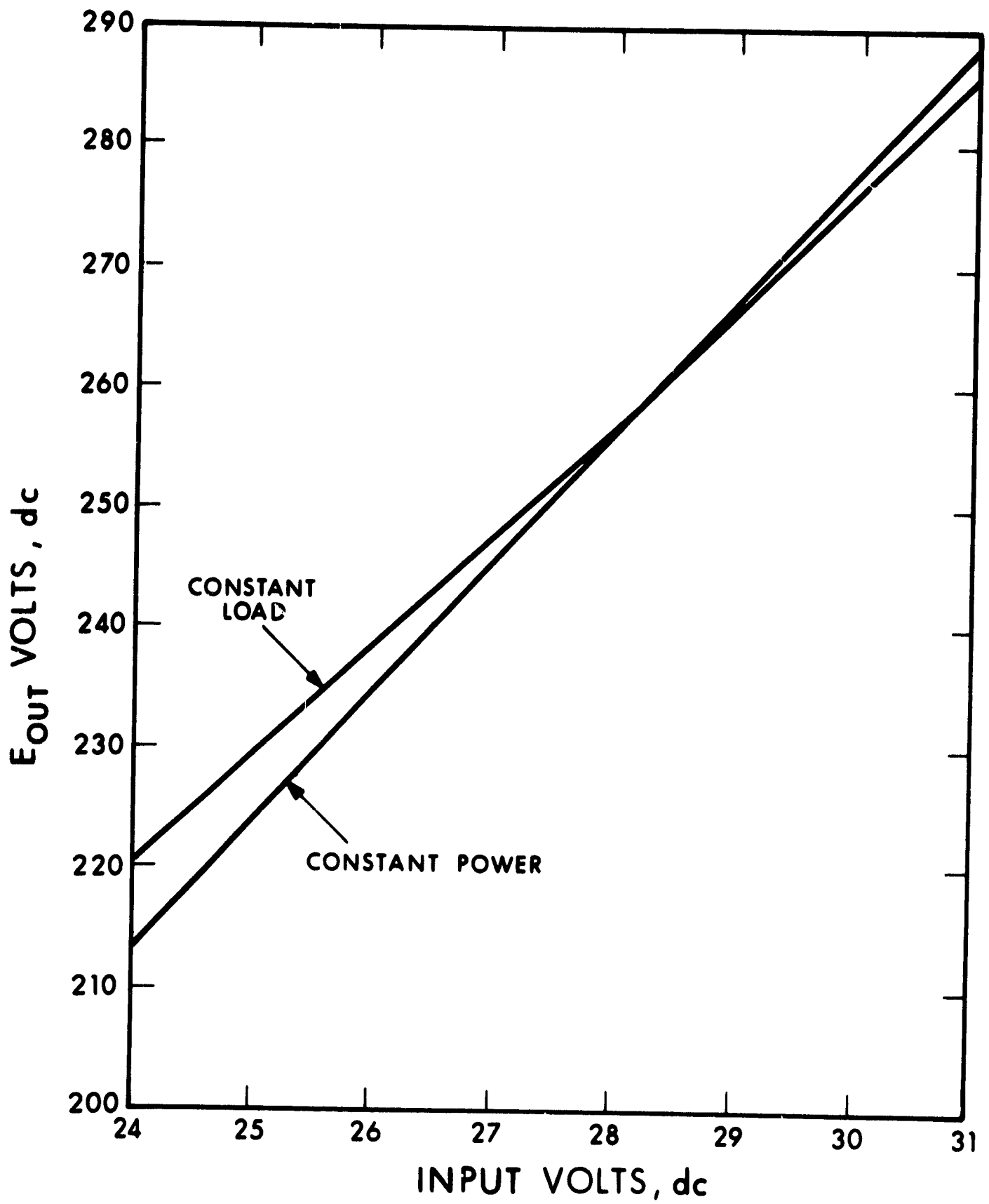


Figure 161. Output Voltage versus Input Voltage at 50 kHz

Figure 162 shows the variation of output voltage as a function of output power.

Figure 163 shows the change in efficiency of the 50 kHz module as a function of temperature at 100 watts output.

Figure 164 shows the switching frequency variation as a function of ambient temperature for temperature variations from -50°C to $+130^{\circ}\text{C}$.

The table below shows a breakdown of the component weights for the 50 kHz module.

COMPONENT WEIGHT

<u>Significant Components</u>	<u>Weight (grams)</u>
Output transformer	40.20
Driver Transformer	2.75
Current Transformer	2.85
Output Filter Capacitor	12.85
Output Power Transistors (2)	8.45
<u>Basic DC-DC Converter Circuit</u>	
Total Components	73.6 (or 2.59 oz)
<u>Complete Module No. 1 Circuit with Overload and Short Circuit Protection</u>	
Total Components	91.2 (or 3.21 oz)

The results of similar studies at other frequencies resulted in system component weights of 131 grams at 10 kHz and 34 grams at 200 kHz and efficiencies of 93 percent and 87 percent. The three 100 watt converters are shown in Figure 165.

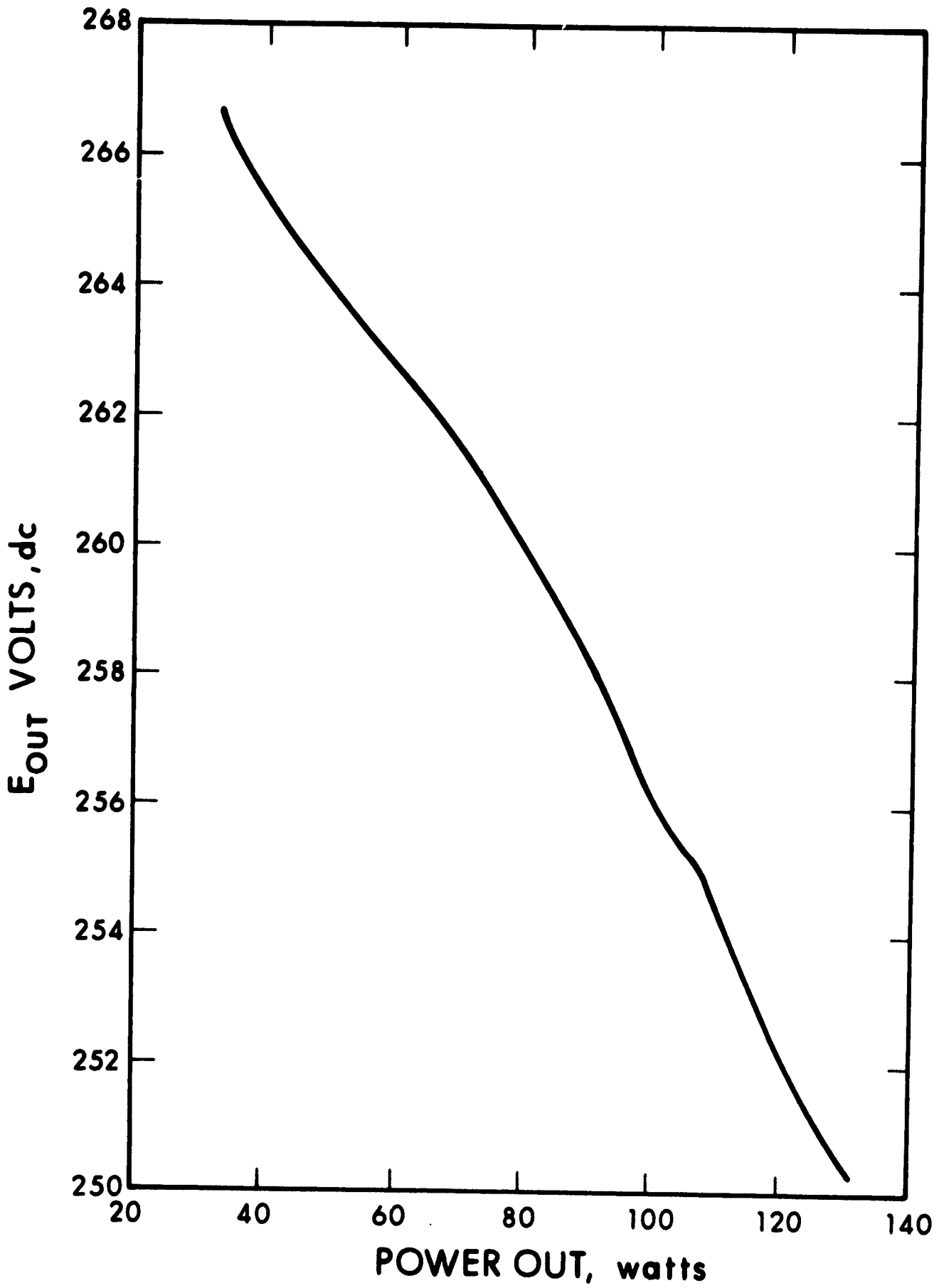


Figure 162. Output Voltage versus Output Power at 50 kHz

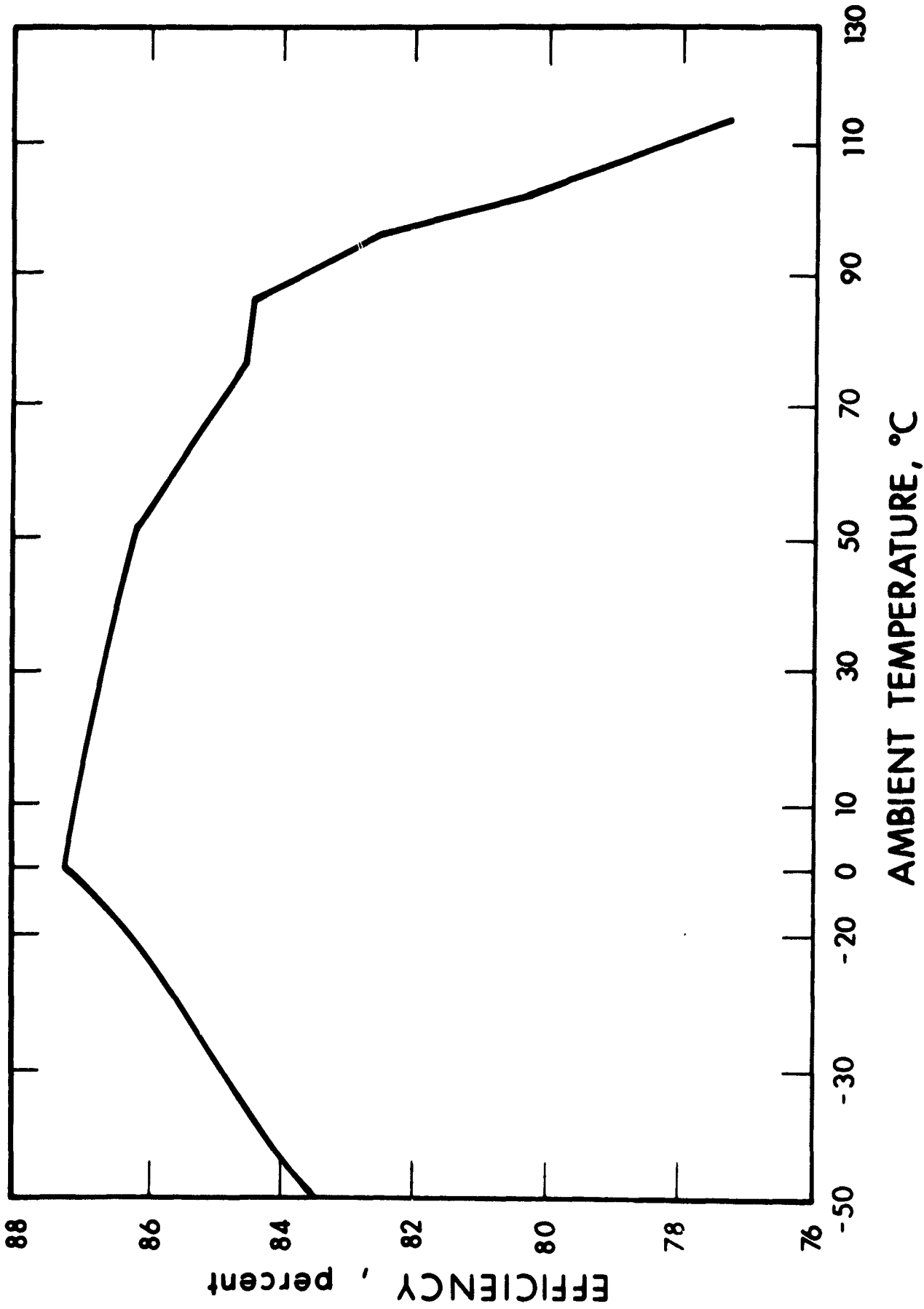


Figure 163. Efficiency versus Temperature at 100 Watts Output

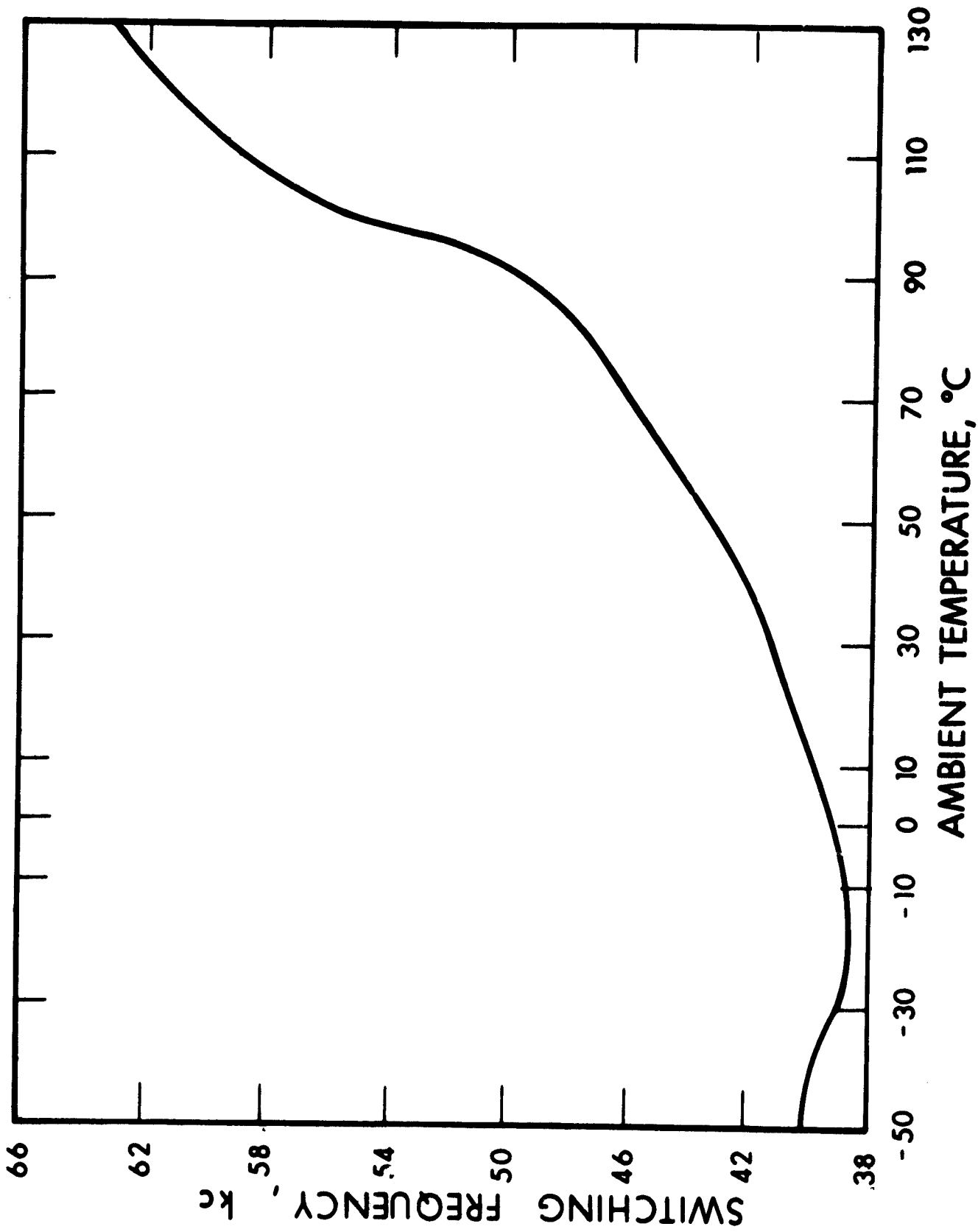
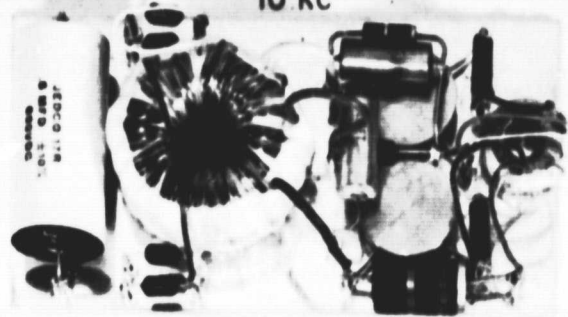
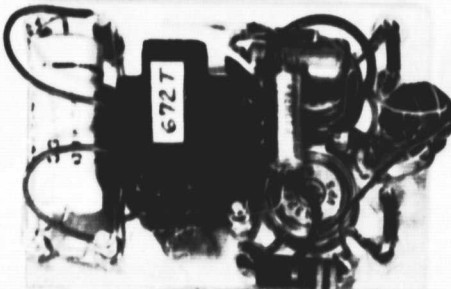
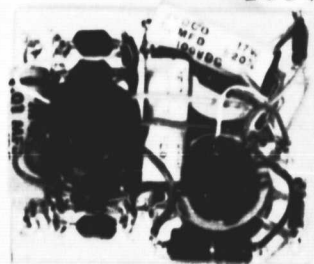


Figure 164. Switching Frequency versus Temperature

(NOMINAL 100 WATT MODULES)		
MODULE	CONV EFF AT 100W OUT	COMPONENT WEIGHT
<p>10 KC</p> 	93%	131 GRAMS OR 4.62 OZ.
<p>50 KC</p> 	90%	91.2 GRAMS OR 3.21 OZ.
<p>200 KC</p> 	87%	34.4 GRAMS OR 1.21 OZ.

ELECTRO OPTICAL SYSTEMS, INC.
A Subsidiary of Xerox Corporation

Figure 165. High Frequency DC-DC Converters